Imperial College London

NC 3Rs National Centre for the Replacement Refinement & Reduction of Animals in Research

Galleria mellonella: an infection model for the *Mycobacterium tuberculosis* complex

Masanori Asai, *M.Res.*, *BSc.* (*Hons*.)

DEPARTMENT OF INFECTIOUS DISEASE
IMPERIAL COLLEGE LONDON

A THESIS SUBMITTED IN FULFILMENT OF
THE DOCTOR OF PHILOSOPHY DEGREE
MARCH 2022

Statement of Originality

I hereby declare that the work presented in this thesis is my own original research, completed in accordance with the regulations of Imperial College London. I confirm that all sources of information cited in my work has been fully acknowledged throughout the thesis and, where appropriate, permission for the reproduction of figures and tables were acquired.

Copyright Declaration

The copyright of this thesis rests with the author. Unless otherwise indicated, its contents are licensed under a Creative Commons Attribution-Non Commercial-No Derivatives 4.0 International Licence (CC BY-NC-ND).

Under this licence, you may copy and redistribute the material in any medium or format on the condition that; you credit the author, do not use it for commercial purposes and do not distribute modified versions of the work.

When reusing or sharing this work, ensure you make the licence terms clear to others by naming the licence and linking to the licence text.

Please seek permission from the copyright holder for uses of this work that are not included in this licence or permitted under UK Copyright Law.

Acknowledgements

To my supervisors, Professor Paul Langford, Dr. Sandra Newton, Dr. Brian Robertson and Dr. Yanwen Li, I am extremely grateful to have not one but four incredible supervisors. Thank you all for your continued support, encouragement, patience and inspiration throughout my Ph.D., your insights into science and life have helped to not only develop my professional skills but also helped tremendously for my personal growth. I truly could not have asked for a better team of supervisors for this journey, thank you.

I would like to acknowledge my collaborators, Dr. John Spiropoulos and Dr. William Cooley at the Animal and Plant Health Agency (UK), for their work on histopathological and transmission microscopy analysis over the course of this project, the images you have captured have been stunning and your professional insights have been invaluable to the success of this project. I would also like to express my gratitude to Dr. Gerard Sheehan and Professor Kevin Kavanagh at Maynooth University, for the success and output of our collaborative proteomic project, without your insight and generosity this would not have been possible.

I share my deepest appreciations to everyone in the Section of Paediatric Infectious Disease at the Department of Infectious Disease, Imperial College London (ICL), with special acknowledgement to Dr. Fadil Bidmos, Dr. Janine Bosse, Dr. Victoria Wright, Oliver Stringer and Oliver Powell, I would also like to extend this acknowledgement to Dr. Nitya Krishnan at the MRC Center for Molecular Bacteriology and Infection (CMBI) (ICL), for their insight, guidance and motivating discussions over the course of this project.

I am thankful for the works by lab managers at ICL, Dr. Nadia Khan, Sena Plevnik, Lesley Rawlinson, and Dr. Sharron Stubbs, for continuing to ensure that the lab operates smoothly and safely throughout the year. I would also like to thank Dr. Jessica Rowley and Dr. Ana Ferreira Da Silva at the CMBI and Stephen Rothery at the ICL Facility for Imaging by Light Microscopy, for their assistance with the microscopy work.

I would like to acknowledge my research funder the National Centre for the Replacement, Refinement and Reduction of Animals in Research (NC3Rs, UK), for supporting this project. I am extremely grateful for this opportunity to have engaged in and contributed to the global 3Rs movement in research. I am also grateful to my host institute, ICL, for providing the facilities and professional training opportunity over the course of this project.

To my friends, partner and family, over the course of this project, you have all helped me to ride the peaks and troughs of research, navigate challenges in life, and supported me in ways words cannot describe. To my parents, thank you for believing in me, for always standing by my side, and supporting me over the years. I am truly grateful and blessed to have you all in my life; I could not have done this without you all. This Thesis is dedicated to all of you.

Abstract

Tuberculosis (TB), caused by *Mycobacterium tuberculosis* (*MTB*), is a leading cause of global infectious disease mortality. Advancement in TB research relies heavily on the use of animal infection models. However, all models have their limitations serving as bottlenecks in research, underlining the need for alternatives. This thesis describes the characterisation of an infection model for the *MTB* complex (MTBC) in *Galleria mellonella* (*Gm*) – the greater wax moth. Time-kill assays of *Gm* challenged with *Mycobacterium bovis* BCG (BCG), double auxotrophic *MTB* (SAMTB), or *MTB* (H37Rv) demonstrated that *Gm* can differentiate virulence between members of the MTBC, with establishment of a persistent (BCG) or proliferative (SAMTB and H37Rv) infection. A *Gm*-MTBC microscopy interaction study revealed internalisation of mycobacteria by phagocytic haemocytes (analogous to mammalian neutrophils and macrophages) as early as 1 hour post-infection. A non-replicative bacilli phenotype (lipid accumulation) was observed only in BCG infection. A histological study of infected *Gm* identified the formation of granuloma-like structures, containing non-replicative bacilli (loss of Ziehl-Neelsen-staining for SAMTB and H37Rv alone). The utility of *Gm* as a screen for antimycobacterial drug toxicity/efficacy and comparative *MTB* virulence was demonstrated using clinically relevant compounds, and isogenic *MTB* mutants (Δ*phoP* and Δ*dosR*), respectively. Proteomic and gene expression analysis of BCG infected *Gm*, identified immune responses indicative of phagocytosis, formation of granuloma-like structures, and secretion of antimicrobial peptides. Furthermore, proof-of-concept models of *ex vivo* granuloma-like structures and real-time *in vivo* drug screening are presented. These results indicate that *Gm* is a viable alternative infection model for TB being capable of mimicking critical aspects of the disease, and can be used to assess comparative *MTB* virulence, and as

a low-medium throughput antimycobacterial drug screen. The adoption and continued development of this model has the potential to substantially reduce/replace the use of animals in TB research.

TABLE OF CONTENTS

STATEMENT OF ORIGINALITY **2**

COPYRIGHT DECLARATION **2**

ACKNOWLEDGEMENTS **3**

ABSTRACT **5**

TABLE OF CONTENTS **7**

ABBREVIATIONS **10**

LIST OF TABLES **14**

LIST OF FIGURES **15**

LIST OF PUBLICATIONS AND PRESENTATIONS **18**

CHAPTER 1 ..... **20**

1.1 TUBERCULOSIS **21**
1.1.1 TUBERCULOSIS – HISTORICAL CONTEXT 21
1.1.2 TUBERCULOSIS: CURRENT STATE OF AFFAIRS 25
1.1.3 MYCOBACTERIUM TUBERCULOSIS COMPLEX 26
1.1.4 MYCOBACTERIUM TUBERCULOSIS 26
1.1.5 PATHOGENESIS OF TUBERCULOSIS 27
1.1.6 TREATMENT OF TUBERCULOSIS 31
1.2 ANIMAL MODELS OF TUBERCULOSIS **32**
1.2.1 MOUSE MODEL OF TB 33
1.2.2 GUINEA PIG MODEL OF TB 34
1.2.3 RABBIT MODEL OF TB 35
1.2.4 NHP MODEL OF TB 36
1.2.5 ZEBRAFISH MODEL OF TB 37
1.2.6 FRUIT FLY MODEL OF TB 39
1.2.7 THE 3RS AND ANIMALS IN EXPERIMENTATION 40
1.3 *GALLERIA MELLONELLA* **42**
1.3.1 GALLERIA MELLONELLA AS AN INFECTION MODEL 43
1.4 INSECT INNATE IMMUNE SYSTEM **46**
1.4.1 ANATOMICAL AND PHYSIOLOGICAL BARRIERS 46
1.4.2 INNATE IMMUNITY: CELLULAR RESPONSES 48
1.4.3 INNATE IMMUNITY: HUMORAL RESPONSES 50
1.5 *GALLERIA MELLONELLA* AS AN INFECTION MODEL FOR MYCOBACTERIA **54**
1.6 SUMMARY **56**
1.7 HYPOTHESIS **58**
1.8 AIMS **58**

CHAPTER 2 60

2.1 MATERIALS 61
2.1.1 MATERIALS USED IN THIS STUDY 61
2.2 METHODS 62
2.2.1 MYCOBACTERIAL STRAINS AND CULTURE CONDITIONS 62
2.2.2 ACQUISITION AND MAINTENANCE OF GALLERIA MELLONELLA 64
2.2.3 PREPARATION OF MYCOBACTERIAL INOCULA FOR GALLERIA MELLONELLA INFECTION 64
2.2.4 INJECTION OF GALLERIA MELLONELLA WITH MYCOBACTERIA INOCULA 65
2.2.5 ASSESSMENT OF MYCOBACTERIAL VIRULENCE IN GALLERIA MELLONELLA 68
2.2.6 MEASUREMENT OF IN VIVO MYCOBACTERIAL SURVIVAL IN GALLERIA MELLONELLA 68
2.2.7 PREPARATION OF ANTIMYCOBACTERIAL COMPOUNDS 69
2.2.8 EVALUATION OF ANTIMYCOBACTERIAL COMPOUND TOXICITY IN GALLERIA MELLONELLA 70
2.2.9 MINIMUM INHIBITORY CONCENTRATION ASSAY 70
2.2.10 *TREATMENT OF INFECTED GALLERIA MELLONELLA WITH ANTIMYCOBACTERIAL COMPOUNDS* 71
2.2.11 IN VIVO LIVE IMAGING OF FLUORBCG IN GALLERIA MELLONELLA 72
2.2.12 TRANSMISSION ELECTRON MICROSCOPY OF GALLERIA MELLONELLA HAEMOCYTES 73
2.2.13 HISTOPATHOLOGY OF GALLERIA MELLONELLA 74
2.2.14 GALLERIA MELLONELLA HAEMOLYMPH SMEAR SLIDES 74
2.2.15 CONFOCAL FLUORESCENCE MICROSCOPY OF GALLERIA MELLONELLA HAEMOCYTES 75
2.2.16 EX VIVO MODEL OF GALLERIA MELLONELLA – MYCOBACTERIA GRANULOMA-LIKE STRUCTURE 76
2.2.17 TOTAL HAEMOCYTE COUNT 77
2.2.18 QUANTIFICATION OF GALLERIA MELLONELLA WEIGHT-LOSS FOLLOWING INFECTION 78
2.2.19 LABEL FREE QUANTITATIVE PROTEOMIC OF GALLERIA MELLONELLA HAEMOLYMPH 78
2.2.20 ANALYSIS OF GALLERIA MELLONELLA CELL FREE HAEMOLYMPH PROTEOMIC DATA 80
2.2.21 GENE EXPRESSION ANALYSIS OF GALLERIA MELLONELLA INNATE IMMUNE RESPONSE 81
2.2.22 STATISTICAL ANALYSIS AND DATA VISUALISATION 83

CHAPTER 3 84

3.1 INTRODUCTION 85
3.2 RESULTS AND DISCUSSION 87
3.2.1 ASSESSMENT OF BCG LUX VIRULENCE IN GALLERIA MELLONELLA 87
3.2.2 SURVIVAL OF BCG LUX WITHIN GALLERIA MELLONELLA FOLLOWING INFECTION 93
3.2.3 INTERACTION OF BCG LUX WITH GALLERIA MELLONELLA HAEMOCYTES 97
3.2.4 BCG LUX INFECTION IS SYSTEMIC IN GALLERIA MELLONELLA 102
3.2.5 GALLERIA MELLONELLA FORMS GRANULOMA-LIKE STRUCTURES IN RESPONSE TO BCG LUX INFECTION 105
3.3 CONCLUSION 109

CHAPTER 4 111

4.1 INTRODUCTION 112
4.2 RESULTS AND DISCUSSION 115
4.2.1 ASSESSMENT OF SAMTB LUX VIRULENCE IN GALLERIA MELLONELLA 115
4.2.2. PROLIFERATION OF SAMTB LUX WITHIN GALLERIA MELLONELLA FOLLOWING INFECTION 118
4.2.3 INTERACTIONS OF SAMTB LUX WITH GALLERIA MELLONELLA HAEMOCYTES 121
4.2.4 SAMTB LUX INDUCES THE FORMATION OF GRANULOMA-LIKE STRUCTURES IN GALLERIA MELLONELLA 125
4.2.5 GRANULOMA-LIKE STRUCTURES CAN BE MODELLED EX VIVO USING SAMTB INFECTED GALLERIA MELLONELLA HAEMOCYTES 130
4.3 CONCLUSION 134

CHAPTER 5 137

5.1 INTRODUCTION 138
5.2 RESULTS AND DISCUSSION 141
5.2.1 H37RV IS MORE VIRULENT THAN BCG LUX AND SAMTB LUX 141
5.2.2 PROLIFERATION OF H37RV WITHIN GALLERIA MELLONELLA FOLLOWING INFECTION 144
5.2.3 INTERACTION OF H37RV WITH GALLERIA MELLONELLA HAEMOCYTES 150
5.2.4 H37RV INDUCES THE FORMATION OF GRANULOMA-LIKE STRUCTURES IN GALLERIA MELLONELLA 152
5.2.5 GALLERIA MELLONELLA CAN BE USED TO DISTINGUISH RELATIVE VIRULENCE OF H37RV MUTANTS 158
5.3 CONCLUSION 163

CHAPTER 6 165

6.1 INTRODUCTION 166
6.2 RESULTS AND DISCUSSION 170
6.2.1 CLINICALLY RELEVANT ANTIMYCOBACTERIAL COMPOUNDS ARE NON-TOXIC IN GALLERIA MELLONELLA 170
6.2.2 TREATMENT OF INFECTED GALLERIA MELLONELLA IMPROVES LARVAL SURVIVAL OUTCOME 171
6.2.3 ANTIMYCOBACTERIAL TREATMENT REDUCES MYCOBACTERIAL BURDEN IN GALLERIA MELLONELLA 177
6.2.4 CHANGES TO ANTIMYCOBACTERIAL BURDEN FOLLOWING REPEATED OR COMBINATION THERAPY 188
6.2.5 LIVE GALLERIA MELLONELLA – MYCOBACTERIUM TUBERCULOSIS COMPLEX FLUORESCENCE IMAGING AS A SCREEN FOR DRUG EFFICACY 193
6.3 CONCLUSION 195

CHAPTER 7 197

7.1 INTRODUCTION 198
7.2 RESULTS AND DISCUSSION 201
7.2.1 BCG LUX INFECTION INDUCES DIVERSE CHANGES IN THE GALLERIA MELLONELLA PROTEOME 201
7.2.2 BCG LUX INDUCES THE PRODUCTION OF KEY INNATE IMMUNE FACTORS IN GALLERIA MELLONELLA 211
7.2.3 BCG LUX PROTEIN EXPRESSION IN GALLERIA MELLONELLA SUGGESTS ADAPTATION TO INTRACELLULAR STRESS AND SURVIVAL 218
7.2.4 LOW DOSE BCG LUX INFECTION PROTECTS GALLERIA MELLONELLA AGAINST HIGH DOSE INFECTION 222
7.2.5 INNATE IMMUNE GENE EXPRESSION BY GALLERIA MELLONELLA FOLLOWING BCG LUX INFECTION 226
7.2.6 GALLERIA MELLONELLA PROTEINS DO NOT CROSS-REACT WITH HUMAN INNATE IMMUNE ANTIBODIES USED IN THE ISOPLEXIS HUMAN INNATE PANEL 230
7.3 CONCLUSION 231

CHAPTER 8: CONCLUSIONS AND FUTURE PERSPECTIVES 234

CHAPTER 9: REFERENCES 244

APPENDIX 281

SUPPLEMENTARY FIGURES 282
SUPPLEMENTARY TABLES 286
PUBLICATIONS 295
PERMISSION SUMMARY TABLE FOR THIRD PARTY COPYRIGHT WORK 352
LETTERS OF PERMISSION 353

Abbreviations

3Rs	Replace, refine, and reduce the use of animals in research
Abs	Antibodies
ADC	Albumin dextrose catalase
AMPs	Antimicrobial peptides
AMR	Antimicrobial resistance
ANOVA	Analysis of variance
apoLp-III	Apolipophorin-III
ATBI	Active TB infection
BCG	Bacille Calmette Guérin
BCG *lux*	*Mycobacterium bovis* BCG *lux*
BDQ	Bedaquiline
cDNA	Complementary DNA
CFP-10	10-kDa culture filtrate protein
CFU	Colony forming units
CL	Containment level
COVID	Coronavirus
Ct	Cycle threshold
DAMPs	Damage associated molecular patterns
DAPI	4',6-diamidino-2-phenylindole
DMSO	Dimethyl sulfoxide
DTT	Dithiothreitol
EDTA	Ethylenediaminetetraacetic acid
EGF	Epidermal growth factor
ESAT-6	6-kDa early secreted antigenic target
ETH	Ethambutol
FDR	False discovery rate
FITC	Fluorescein isothiocyanate
FluorBCG	*Mycobacterium bovis* BCG Δ*panCD* (Psmyc Turbo635asv-YFP)
$FMNH_2$	Flavin mononucleotide
Gm	*Galleria mellonella*
GM-CSF	Granulocyte-macrophage colony-stimulating factor
h	Hours
H&E	Haematoxylin and eosin
hCAP-18	Human cationic antimicrobial peptide-18
HCL	Hydrochloric acid
Hdd11	Putative defence protein gene 11
HIV	Human immunodeficiency virus
HPLC	High performance liquid chromatography
HT	Heat treated
HYG	Hygromycin

IAA	Iodoacetamide
ICL	Imperial College London
IL	Interleukin
ILI	Intracytosolic lipid inclusion
Imd	Immune deficiency
IMPI	Insect metalloproteinase inhibitor
INF	Interferon
INH	Isoniazid
IP	Induced protein
IPS	Insect physiological saline
JAK-STAT	Janus Kinase-signal transducer and activator of transcription
KAN	Kanamycin
KCl	Potassium chloride
LD	Lipid droplets
leu	Leucine
LFQ	Label-free quantitation
LPS	Lipopolysaccharide
LTA	Lipoteichoic acid
LTBI	Latent TB infection
MCP-1	Monocyte chemoattractant protein 1
MDR	Multi-drug resistant
MIC	Minimum inhibitory concentration
min	Minutes
MIP	Macrophage inflammatory protein
MMPs	Matrix metalloproteinases
MNGCs	Multi-nucleated giant cells
MOX	Moxifloxacin
MS	Mass spectrometry
MTB	*Mycobacterium tuberculosis*
MTBC	MTB complex
NaCl	Sodium chloride
NETs	Neutrophil extracellular traps
NHPs	Non-human primates
NF_kB	Nuclear factor kappa B
NTM	Non-tuberculous mycobacteria
Nude	Congenitally athymic nu/nu
OADC	Oleic albumin dextrose catalase
OD	Optical density
PAMPs	Pathogen associated molecular patterns
Pan	Pantothenate
PAS	para-aminosalicylate
PBMCs	Peripheral blood mononuclear cells
PBS	Phosphate buffered saline

PBS-T	PBS-Tween 80 (0.05%)
PCA	Principal component analysis
PCR	Polymerase chain reaction
PD	Pharmacodynamic
PDGF	Platelet derived growth factor
PDIMs	Phthiocerol dimycocerosates
PGLs	Phenolic glycolipids
PGRPs	Peptidoglycan recognition proteins
PIP	Piperacillin
PK	Pharmacokinetic
PO	Phenoloxidase
POA	Pyrazinoic acid
PPAE	Prophenol oxidase activating enzyme
ppm	Part per million
PPO	Pro-phenoloxidase
PRRs	Pattern recognition receptors
PT	Point of treatment
PTU	N-Phenylthiourea
PZA	Pyrazinamide
qPCR	Quantitative PCR
REM	RIF, ETH and MOX
RIF	Rifampicin
RLU	Relative light units
RPM	Revolutions per minute
RT	Reverse transcription
RT-qPCR	Reverse transcription quantitative PCR
SAMTB	*MTB* H37Rv Δ*leuD* Δ*panCD*
SAMTB *lux*	*MTB* H37Rv Δ*leuD* Δ*panCD lux*
SCID	Severe combined immunodeficient
SD	Standard deviation
Serpin	Serine protease inhibitor
SM	Streptomycin
SSDA	Statistical significant and differentially abundant
TA	Toxin-antitoxin
TAG	Triacyl-glycerol
TB	Tuberculosis
TEM	Transmission electron microscopy
THC	Total haemocyte count
TIMPs	Tissue inhibitors of MMPs
TNF	Tumour necrosis factor
VEGF	Vascular endothelial growth factor
WHO	World Health Organization
WT	Wild-type

XDR	Extensively drug resistant
YFP	Yellow fluorescent protein
ZN	Ziehl-Neelsen
ΔΔCt	Comparative Ct
FMNH2	Flavin mononucleotide
g	Centrifugal force

List of Tables

Table 1.1. Similarities between insect (haemocytes) and mammalian (neutrophils) innate immunity.

Table 2.1. *G. mellonella* innate immune gene primers used in this project.

Table 6.1. *In vitro* (broth microdilution) MIC of clinical antimycobacterial compounds.

Table 7.1. SSDA proteins of interest identified in the haemolymph of BCG *lux* infected *G. mellonella* at 4 h post-infection.

Table 7.2. SSDA proteins of interest identified in the haemolymph of BCG *lux* infected *G. mellonella* at 48 h post-infection.

Table 7.3. SSDA proteins of interest identified in the haemolymph of BCG *lux* infected *G. mellonella* at 168 h post-infection.

Table 7.4. BCG *lux* proteins detectable in the haemolymph of infected *G. mellonella.*

Table 7.5. SSDA proteins identified in the haemolymph of *G. mellonella* 48 h post-immunisation with a non-lethal dose of BCG *lux* (1 x 10^5 CFU).

List of Figures

Figure 1.1. Timeline history of tuberculosis events.

Figure 1.2. The pathogenesis of tuberculosis.

Figure 1.3. Proportion of most commonly used animals in tuberculosis research.

Figure 1.4. The number of *G. mellonella* publications available as of July 2021 on NCBI PubMed central using the search term "Galleria mellonella" between 2000-2021.

Figure 1.5. Advantages of using *G. mellonella* as a model organism.

Figure 1.6. The innate immune responses of *G. mellonella*.

Figure 2.1. Infection of *G. mellonella* using a microsyringe.

Figure 3.1. Assessment of BCG *lux* virulence in *G. mellonella*.

Figure 3.2. Physical changes to *G. mellonella* following infection with BCG *lux.*

Figure 3.3. Impact of experimental procedures and BCG *lux* viability on *G. mellonella* survival.

Figure 3.4. Optimisation of *G. mellonella* homogenate recovery from lysing matrix tubes.

Figure 3.5. *In vivo* correlation of BCG *lux* luminescence and CFU in *G. mellonella*.

Figure 3.6. Survival of BCG *lux* within *G. mellonella* using luminescence as a measure of relative mycobacterial abundance.

Figure 3.7. Ziehl-Neelsen stain of *G. mellonella* haemocytes infected with BCG *lux*.

Figure 3.8. Transmission electron microscopy of *G. mellonella* haemocytes infected with BCG *lux*.

Figure 3.9. Dissemination of amaranth dye in *G. mellonella*.

Figure 3.10. Dissemination of FluorBCG in *G. mellonella.*

Figure 3.11. Histological sections of *G. mellonella* infected with BCG *lux* over a two-week time course.

Figure 3.12. Development of granuloma-like structures in *G. mellonella* infected with BCG *lux*.

Figure 4.1. Assessment of SAMTB *lux* virulence in *G. mellonella*.

Figure 4.2. Physical changes to *G. mellonella* following infection with SAMTB *lux.*

Figure 4.3. *In vivo* correlation of SAMTB *lux* luminescence and CFU in *G. mellonella* over a one-week time course.

Figure 4.4. Survival of SAMTB *lux* within *G. mellonella* using luminescence as a measure of relative abundance.

Figure 4.5. Growth inhibition of SAMTB *lux* in presence and absence of pantothenate and leucine.

Figure 4.6. Association of SAMTB *lux* with *G. mellonella* haemocytes.

Figure 4.7. Transmission electron microscopy of SAMTB *lux* infected *G. mellonella* haemocytes.

Figure 4.8. Histological sections of *G. mellonella* infected SAMTB *lux* over a one-week time course.

Figure 4.9. Development of granuloma-like structures in *G. mellonella* infected with SAMTB *lux*.

Figure 4.10. Cultivated *ex vivo G. mellonella* haemocytes of SAMTB *lux* infected larvae develop granuloma like structures.

Figure 4.11. Cultivated *ex vivo* SAMTB *lux* granuloma-like structure resembles multinucleate giant cells.

Figure 5.1. Assessment of H37Rv virulence in *G. mellonella*.

Figure 5.2. Comparison of H37Rv, BCG *lux* and SAMTB *lux* virulence in *G. mellonella*.

Figure 5.3. Melanisation of *G. mellonella* larvae following H37Rv infection.

Figure 5.4. Survival of H37Rv within *G. mellonella*.

Figure 5.5. Changes in the number of circulating haemocytes following infection with H37Rv.

Figure 5.6. Mortality of *G. mellonella* correlates with *in vivo* H37Rv proliferation and suppression of circulating haemocytes.

Figure 5.7. Transmission electron microscopy of H37Rv infected *G. mellonella* haemocytes.

Figure 5.8. Histological sections of *G. mellonella* infected H37Rv over a 192 h time course.

Figure 5.9. Haematoxylin & eosin images of unique granuloma-like structure found in *G. mellonella* infected with H37Rv.

Figure 5.10. Development of granuloma-like structures in *G. mellonella* infected with H37Rv.

Figure 5.11. Assessment of H37Rv Δ*phoP* virulence in *G. mellonella.*

Figure 5.12. Assessment of H37Rv Δ*dosR* virulence in *G. mellonella*.

Figure 6.1. Survival of *G. mellonella* infected with BCG *lux* or SAMTB *lux,* following treatment with first or second-line antimycobacterial compounds.

Figure 6.2. Survival of *G. mellonella* infected with H37Rv, following treatment with first-line antimycobacterial compounds.

Figure 6.3. Reduction of BCG *lux* bioluminescence in *G. mellonella* following treatment with first or second-line antimycobacterial compounds.

Figure 6.4. Reduction of SAMTB *lux* bioluminescence in *G. mellonella* following treatment with first or second-line antimycobacterial compounds.

Figure 6.5. Reduction of SAMTB *lux* bioluminescence in *G. mellonella* is highly associated with treatment dose.

Figure 6.6. Survival of *G. mellonella* infected with H37Rv*,* following treatment with first-line antimycobacterial compounds.

Figure 6.7. Reduction of *in vivo* H37Rv burden in *G. mellonella* following treatment with first-line antimycobacterial compounds.

Figure 6.8. Reduction of BCG *lux* and SAMTB *lux* bioluminescence in *G. mellonella* following treatment with a combination of first and second-line antimycobacterial compounds.

Figure 6.9. Reduction of BCG *lux* and SAMTB *lux* bioluminescence in *G. mellonella* following mono or dual treatment with INH or RIF.

Figure 6.10. Demonstration of *G. mellonella* - FluorBCG as a live screen for drug screening.

Figure 7.1: PCA of haemolymph proteomes generated from BCG *lux* infected *G. mellonella*.

Figure 7.2: Volcano plot of SSDA proteins detected in BCG *lux* infected *G. mellonella* over a 168 h time course.

Figure 7.3: The effect of immune priming on survival of BCG *lux* infected *G. mellonella*.

Figure 7.4: PCA of haemolymph proteomes generated from BCG *lux* infected *G. mellonella*.

List of Publications and Presentations

The work presented in this thesis has been published as peer-reviewed journal articles.

1. Li Y, Spiropoulos J, Cooley W, Kahara JS, Gladdstone CA, Asai M, Bossé JT, Robertson BD, Newton SM, Langford PR (2018) *Galleria mellonella* – a novel infection model for the *Mycobacterium tuberculosis* complex. *Virulence* 9(1), 1126 -1137.

2. Asai M, Li Y, Khara JS, Gladstone CA, Robertson BD, Langford PR, Newton SM (2019) Use of the invertebrate *Galleria mellonella* as an infection model to study the *Mycobacterium tuberculosis* complex. *Journal of Visualized Experiments* (148), e59703.

3. Asai M, Li Y, Khara JS, Robertson BD, Langford PR, Newton SM (2019) *Galleria mellonella*: An infection model for screening compounds against the *Mycobacterium tuberculosis* complex. *Frontiers in Microbiology* 10, 2630.

4. Asai M, Li Y, Spiropoulos J, Cooley W, Everest D, Robertson BD, Langford PR, Newton SM. (2020) A novel biosafety level 2 compliant tuberculosis infection model using a Δ*leuD*Δ*panCD* double auxotroph of *Mycobacterium tuberculosis* H37Rv and *Galleria mellonella*. *Virulence* 11(1), 811-824.

5. Asai M, Sheehan G, Li Y, Robertson BD, Kavanagh K, Langford PR, Newton SM (2021) Innate immune responses of *Galleria mellonella* to *Mycobacterium bovis* BCG challenge identified using proteomic and molecular approaches. *Frontiers in Cellular and Infection Microbiology* 11, 619981

The work presented in this thesis was presented at the following conferences

1. Asai M, Li Y, Robertson BD, Langford PR, Newton SM *Galleria mellonella*: a novel infection model for *Mycobacterium tuberculosis*. Acid Fast Club Summer Meeting. St Andrews, UK. July 2019. Oral Presentation.

2. Asai M, Li Y, Khara JS, Robertson BD, Langford PR, Newton SM. *Galleria mellonella*: a novel infection model for screening potential anti-mycobacterial compounds against members of the *Mycobacterium tuberculosis* complex. The Microbiology Society Annual Conference. Belfast, UK. January 2019. Poster Presentation.

3. Asai M, Li Y, Khara JS, Robertson BD, Langford PR, Newton SM. *Galleria mellonella*: a novel infection model for screening potential anti-mycobacterial compounds against members of the *Mycobacterium tuberculosis* complex. Keystone Symposia. Banff, Canada. March 2021. Poster Presentation.

4. Asai M, Li Y, Spiropoulos J, Cooley W, Everest D, Robertson BD, Langford PR, Newton SM. A novel biosafety level 2 compliant tuberculosis infection model using a Δ*leuD*Δ*panCD* double auxotroph of *Mycobacterium tuberculosis* H37Rv and *Galleria mellonella.* Pan-London 3Rs symposium (Virtual). London, UK. March 2021. Poster and Video Presentation.

5. Asai M, Li Y, Robertson BD, Langford PR, Newton SM. Comprehensive characterisation of *Galleria mellonella* as a model for *Mycobacterium tuberculosis* H37Rv. Acid Fast Club Winter 2022 Meeting (Virtual). London, UK. January 2022. Oral Presentation.

Chapter 1
Introduction

1.1 Tuberculosis

Tuberculosis (TB) is a bacterial infectious disease caused by *Mycobacterium tuberculosis* (*MTB*) (World Health Organization [WHO], 2020). Despite the common misconception that TB is a "disease of the past", it is one of the top ten global causes of death and the leading bacterial cause of death from a single infectious agent (WHO, 2020). In 2020, the WHO reported an estimated 1.4 million deaths and 10 million novel TB cases in 2019 alone (WHO, 2020). It is undeniable that *MTB* is one of the most successful human pathogens in existence, whose impact continues to cause substantial damage to global health security.

1.1.1 Tuberculosis – historical context

TB is an ancient disease recognised since antiquity (Figure 1.1) and referred to throughout history by many aliases such as phthisis, tabes, schachepheth, king's evil, consumption, and white plague (Barberis et al., 2017). Historical records show that the TB referred to as "the white plague" was the source of substantial hardship in the mid-18th to early-19th century in North America and Europe (Murray, 2004). This epidemic was brought on by the societal changes of the industrial revolution (increase in population density, poor hygiene, and poverty), propagating the explosive spread of TB (Glaziou et al., 2018). At its peak, TB was responsible for one in four deaths in Europe and North America (Murray, 2004; Glaziou et al., 2018). The burden of TB steadily declined over the 19th and 20th centuries with improvements in socioeconomics, the establishment of public health systems, and recognition that TB is an infectious disease (Murray, 2004).

The German physician Robert Koch revolutionised TB research in 1882 by proving that the disease is infectious in origin and identifying the causative biological agent as the "tubercle bacillus" (Koch, 1882; Blevins & Bronze, 2010). Medical innovation continued in the 19th century with the discovery of X-rays by Wilhelm Konrad Röntgen in 1895. X-ray imaging enabled faster diagnosis of TB by visualising chest abnormalities (Posner, 1971). Thus, clinicians were able to more accurately diagnose individuals with TB due to their knowledge of TB being a pulmonary disease, in addition to X-ray imaging as a tool. Another scientific innovation occurred at the turn of the 20th century, where Albert Calmette and Camille Guérin successfully developed the first and only licenced TB vaccine to date based on *Mycobacterium bovis*, the causative agent of bovine TB. Calmette and Guérin applied Louis Pasteur's principle of attenuation, serially passaging cultures of *M. bovis*, which resulted in an attenuated *M. bovis* strain now referred to as Bacille Calmette Guérin (BCG) (Sakula, 1983). Public vaccination using BCG began on a small scale in 1921, and since then countless millions have been vaccinated, with BCG quickly becoming one of the world's most commonly used vaccines (Dockrell & Smith, 2017).

Substantial development in TB treatment was made in 1944 by the discovery of streptomycin (SM) and para-aminosalicylate sodium (PAS-sodium or para-amino salts) by Selman Waksman and Jörgen Lehmann, respectively (Iseman, 2002). SM and PAS were the first clinically utilised antimycobacterial compounds and helped to significantly improve the survival outcomes of individuals afflicted by TB (Iseman, 2002). Soon after, the British Medical Research Council commissioned the use of SM and PAS as a combination drug regimen, which proved to be more efficacious and served as the foundation for the multi-drug regimens currently used to treat TB (Iseman, 2002). In addition to the improvement in socio-economic and general

hygiene, these significant advancements in basic research, diagnosis and treatment, helped to rapidly reduce the number of TB incidence and mortality rates in the mid-20th century (Murray, 2004). However, as research funding dwindled with the focus of the pharmaceutical industry shifting into more profitable segments of medicine, antimicrobial compounds and vaccine research progress diminished (Fogel, 2015). In the present day, the disparities between high-income and low-income countries have led to a situation where TB is rare in high-income countries, but a substantial burden to health in low-income countries, and has led to a misconception that TB is a disease of the past (Keshavjee & Farmer, 2012).

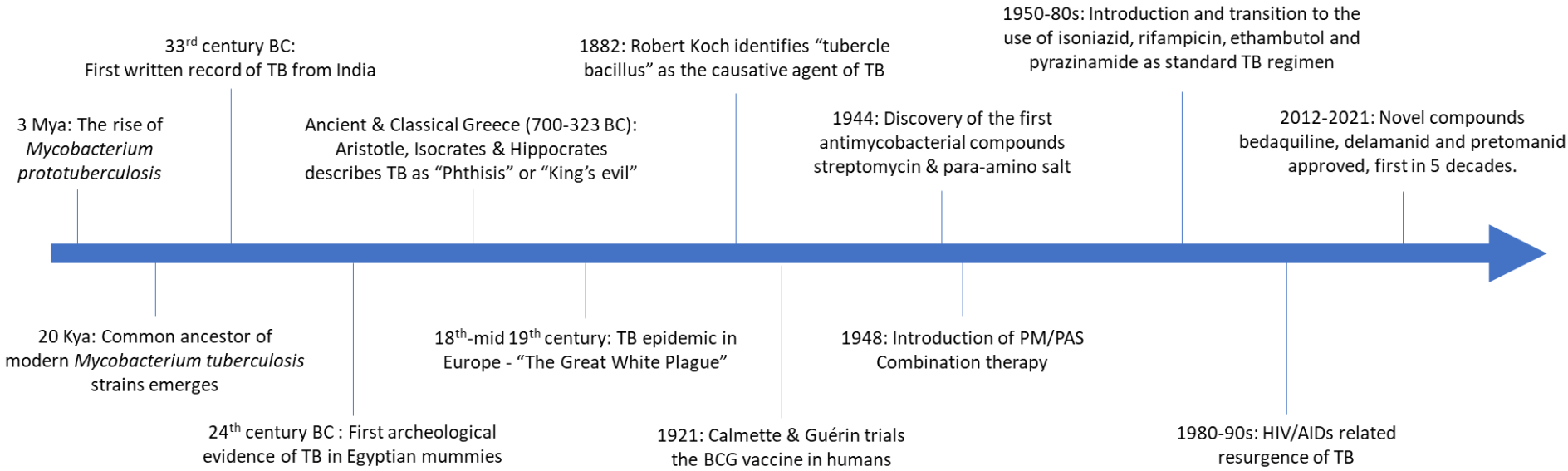


Figure 1.1: Timeline history of tuberculosis events.

1.1.2 Tuberculosis: current state of affairs

TB was declared a global emergency by the WHO in 1993 and efforts are now underway to end the global TB epidemic by 2035 via the "End TB strategy" (WHO, 2020). As a disease, TB disproportionately affects those living in low and middle-income regions e.g., Africa, South-East Asia, South America, Russia and Eastern Europe (Reid et al., 2019). In these regions, medical care is below the WHO universal care standards, making diagnosis, treatment and application of preventative measures challenging (WHO, 2020). The WHO estimates that a quarter of the world's population is currently infected with *MTB*. The majority are believed to have latent TB infection (LTBI), a clinical definition for individuals who are asymptomatic and non-contagious carriers of *MTB* (WHO, 2020). Amongst those latently infected, 5-10% will develop symptomatic and contagious active TB infection (ATBI), serving as a large reservoir for future transmission (WHO, 2018).

The progress to end the global TB epidemic has been slow, with the first of the WHO's milestones in 2020 being missed by a substantial margin due to economic, scientific, and societal roadblocks (WHO, 2020). These issues, as for many bacterial infectious diseases, are further complicated by the rise and spread of multi/extensively drug-resistant (MDR/XDR) *MTB* strains, which pose substantial challenges to global health security (O'Neill, 2016). A report on antimicrobial resistance (AMR) commissioned by the Wellcome Trust and the UK Department of Health, highlighted that with the lack of substantial interventions and research output, 75 million deaths could be attributable to MDR/XDR TB alone between 2015 and 2050 (O'Neill, 2016). Furthermore, due to the coronavirus (COVID)-19 pandemic, the disruption of TB surveillance and continuity of care in the endemic region could contribute to an additional 1.4 million deaths between 2020 and 2025 (WHO, 2020). This clearly underlines the need for

substantial global efforts to stay ahead of this disease in order to successfully end the global TB epidemic by 2030 (WHO, 2020).

1.1.3 Mycobacterium tuberculosis complex

MTB and other mycobacterial species, e.g., *M. bovis*, *Mycobacterium africanum, Mycobacterium microti, Mycobacterium mungi, Mycobacterium canetti, Mycobacterium caprae, Mycobacterium orygis* and *Mycobacterium pinnipedii,* are collectively known as the *Mycobacterium tuberculosis* complex (MTBC) (Kanabalan et al., 2021). The MTBC is a collection of genetically similar (>99.9%) mycobacteria species capable of causing TB in humans or TB-like disease in animals (Lekko et al., 2020). Members of the MTBC share a common ancestor known as *Mycobacterium prototuberculosis,* estimated to be 3 million years old (Uren et al., 2020). Early East African humanoids were infected with *M. prototuberculosis*, which differentiated into the early MTBC 35,000 years ago. The success of *MTB* as a human pathogen is attributable to millennia of co-evolution with humans, selecting for highly adapted tuberculous bacilli (Uren et al., 2020).

1.1.4 Mycobacterium tuberculosis

MTB is an aerobic to facultative anaerobe, prototroph and facultative intracellular pathogen (Cook et al., 2009; Gengenbacher & Kaufmann, 2012; Eoh & Rhee, 2013). Humans are the only known natural reservoir of *MTB*, with no known environmental reservoirs (Sousa et al., 2020). The non-motile and non-sporulating *MTB* bacilli are 1.5-4 μm in length and 0.3-0.5 μm in width (Cook et al., 2009). *MTB* replicates slowly, dividing every ~20 hours (h) in laboratory media under logarithmic growth (Talbot & Raffa, 2014). The colonies of *MTB* on agar are typically small, white and dry with irregular and protruding outlines (Asmar & Drancourt,

2015). *MTB* is Gram-neutral and cannot be distinguished from other bacteria using Gram-staining (Hinson et al., 1981). The mycobacterial cell wall does not retain the Gram-stain (crystal violet/ safranin) due to its unique cell wall containing mycolic acid (Talip et al., 2013). Instead, acid-based staining (e.g., Ziehl-Neelsen [ZN]) can be used to distinguish mycobacteria based on their ability to resist decolourisation by acids, classifying mycobacteria as acid-fast (Laga et al., 2014). The mycobacterial cell wall is thick, waxy, lipid-rich and hydrophobic, and consequently *MTB* is intrinsically resistant to large varieties of antibiotics and tolerant to chemical and dehydration damage (Alahari et al., 2007; Gygli et al., 2017). The genome of *MTB* is GC rich and 4.4 Mb in size, containing approximately ~4000 genes (Jiang et al., 2015; Meehan et al., 2019). Unlike most bacteria, where drug-resistant mutants arise due to horizontal gene transfer, spontaneous mutations in the chromosomal genes are the predominant cause of resistance in *MTB* (Yuan et al., 2021).

1.1.5 Pathogenesis of tuberculosis

Infection occurs when aerosolised *MTB* are transmitted from individuals with active pulmonary TB (Pai et al., 2016). *MTB* bacilli are inhaled into the lung alveoli via the respiratory tract and are immediately phagocytosed by the macrophages and neutrophils. These myeloid cells attack *MTB* bacilli using oxidative burst, proteolytic enzymes, antimicrobial peptides (AMPs), neutrophil extracellular traps (NETs) and by inducing apoptosis (Borkute et al., 2021). Alveolar macrophages phagocytose apoptotic and necrotic neutrophils, in addition to non-cell associated bacilli which become contained in a phagosome (Pai et al., 2016; Borkute et al., 2021). In most cases, *MTB* is eliminated by the host production of reactive oxygen and nitrogen species and hydrolytic enzymes following phagolysosomal fusion in neutrophils and macrophages (Fogel, 2015). However, *MTB* has the capacity to evade the host immune system

through a series of evolutionary adaptations, which includes inhibition of phagolysosome maturation and acidification, and resistance to reactive species (Zhai et al., 2019). Any surviving *MTB* escapes the phagosome and accesses the cytosol of neutrophils and macrophages, inducing the production of cytokines and chemokines, leading to the recruitment of additional immune cells to the site of infection (Bussi & Gutierrez, 2019). The nutrient rich intracellular environment provides a haven for *MTB* to replicate, which ultimately leads to the induction of macrophage cell death. Necrosis further enhances mycobacterial replication. *MTB* disseminates to the surrounding areas and further infects recruited phagocytes (Bussi & Gutierrez, 2019). Infected immune cells begin to aggregate and are centrally compartmentalised by phagocytes to form multicellular structures known as granulomas (Figure 1.2) (Cambier et al., 2014; Pai et al., 2016).

The foundations of a granuloma rely on innate immune cells and are further reinforced by adaptive immune cells following T cell priming by dendritic cells, allowing granuloma maturation (Pagán & Ramakrishnan, 2018). The structural integrity of granulomas is maintained by the equilibrium between the loss and recruitment of immune cells. In a healthy individual, this equilibrium is maintained, and a mature homeostatic or protective granuloma is formed (Ehlers & Schaible, 2013). Under such conditions, *MTB* switches from a replicating to a non-replicating and dormant (viable but metabolically inactive) phenotype, which is induced by hypoxic conditions within the granuloma, leading to LTBI. However, in an individual with a compromised immune system (e.g., ageing, auto-immune disease, co-infection [human immunodeficiency virus (HIV)], chronic disease, cancer, chemotherapy), dysregulation of the equilibrium may occur over time, leading to reactivation of LTBI (Ehlers & Schaible, 2013). While the hypoxic condition of granulomas may suggest an unfavourable

growth condition, a recent study has shown that *MTB* can induce their vascularisation, creating favourable conditions for mycobacterial replication (Uusi-Mäkelä & Rämet, 2018). Furthermore, central necrosis of granulomas provides a nutrient-rich environment for accelerated growth (Pagán & Ramakrishnan, 2018). Reactivated *MTB* can disseminate within the host, which, if undetected, can lead to extrapulmonary TB infection (e.g., meningitis, miliary, and osteomyelitis) (Pai et al., 2016).

While it is clear that granulomas are a hallmark of human TB infection and integral to the success of *MTB* as a human pathogen, the mechanisms underlying formation and maintenance of protective/homeostatic vs transmissive granuloma or necrotic/non-necrotic granulomas, remains unclear. However, it is evident that the progression of disease relies heavily on host immune status and the virulence of the infecting strain (Lerner et al., 2015; Pagán & Ramakrishnan, 2018).

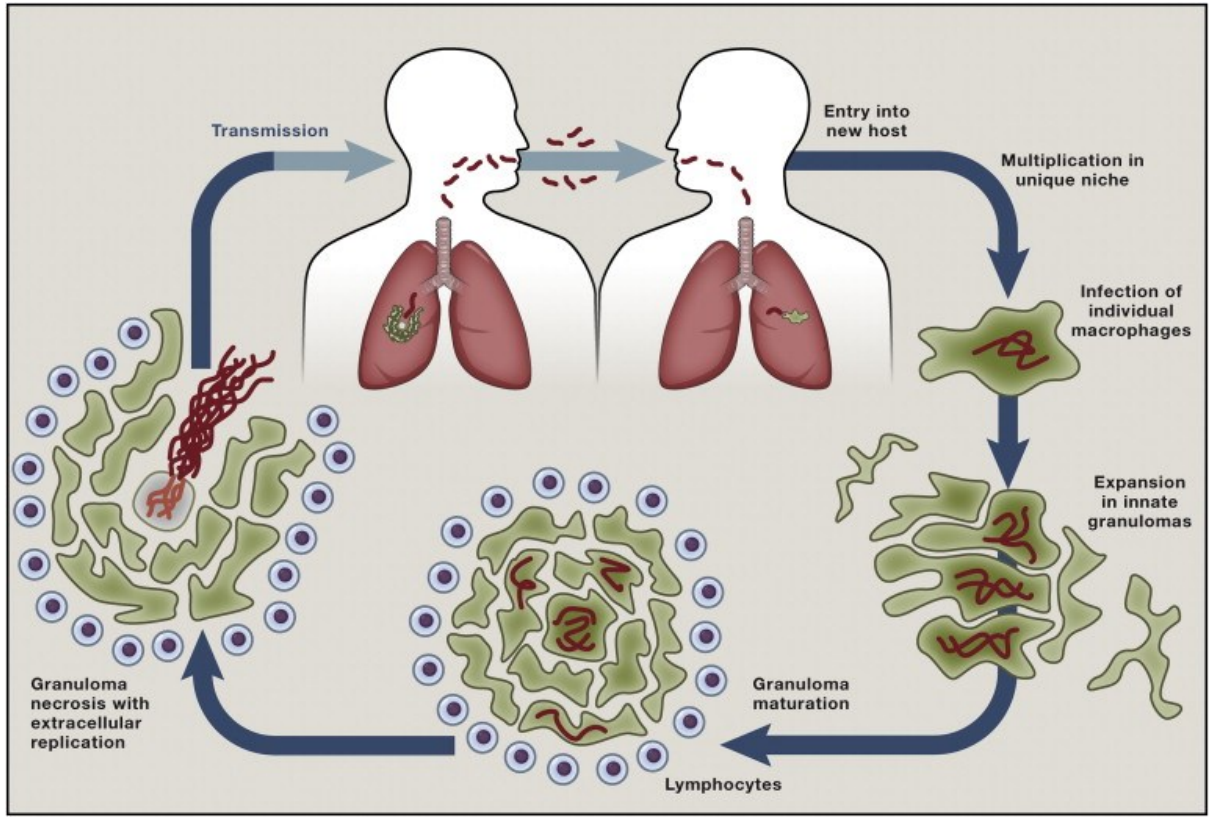


Figure 1.2: The pathogenesis of tuberculosis. *MTB* bacilli are transmitted by individuals with symptomatic and contagious ATBI. Healthy individuals inhale the aerosolised bacilli. In the lung, alveolar macrophages phagocytose the bacilli and initiate intra-cellular immune effector mechanisms to clear the infection. *MTB* evades these mechanisms; replicates and induces macrophage cell death. This initiates the formation of the granuloma through the recruitment of healthy phagocytes via chemokines and cytokines. The granuloma matures with the addition of adaptive immune cells (T cells and B cells). Only 5-10% of individuals with LTBI will go on to develop ATBI in their lifetime. Reproduced from Cambier et al., 2014, with permission from Elsevier Inc.

1.1.6 Treatment of tuberculosis

Before the discovery of SM and PAS, effective treatment for TB was non-existent. Infected individuals in isolation were offered fresh air and sunlight as standard care in sanatoriums (Masten, 1935). Currently, effective treatment is available as a cocktail of antimycobacterial drugs, typically consisting of isoniazid (INH), rifampicin (RIF), ethambutol (ETH) and pyrazinamide (PZA) for drug-sensitive TB cases (WHO, 2017). However, typical treatment regimens are long (> six months) and associated with unpleasant toxic side effects (Tweed et al., 2018). Nevertheless, the use of multidrug chemotherapy is preferential as treatment: 1) rapidly reduces mycobacterial load, limiting disease morbidity, mortality and transmission; 2) targets the persistent (drug tolerant and/or highly host immune resistant) mycobacterial population and reduces the risk of relapse; and 3) minimises the risk of drug-resistance (Lee et al., 2020). Despite these efforts, MDR and XDR-TB are a source of substantial global burden, and responsible for high levels (43%) of treatment failure (WHO, 2020). Due to the limited advancement in TB drug discovery, only three novel compounds: bedaquiline, delamanid and pretomanid, have been developed and approved for clinical use in the past four decades (Tiberi et al., 2018). To fulfil the WHO “End TB Strategy” goals, drugs and treatment regimens that are safer, more efficacious and efficient are urgently needed. As of August 2020, there are 22 antimycobacterial compounds and 16 TB regimens in phases 1, 2 and 3 clinical trials, including 13 novel compounds (WHO, 2020).

1.2 Animal models of tuberculosis

Advancement in TB research has relied heavily on animal infection models, which has enabled researchers to understand the pathogenesis, disease progression and host-interactive biology of TB. Furthermore, animal models have played an integral role in evaluating drug and vaccine efficacy and toxicity before their use in human clinical trials. A literature analysis of the NCBI database revealed that approximately 35% of TB research articles cited the use of animal infection models in their studies (Zhan et al., 2017). Mice, guinea pigs, rabbits, non-human primate (NHP) and zebrafish are the most commonly used animals in TB research (Figure 1.3). Each model mimics one or more aspects of the TB disease, e.g., clinical signs, disease progression, pathology and immunological responses. However, each model has its biological limitations. Additionally, broader challenges associated with using animals in research must be overcome, such as ethical regulation, cost, time, care, and the need for specialised animal facilities. Therefore, no single model is a perfect model for all intended use.

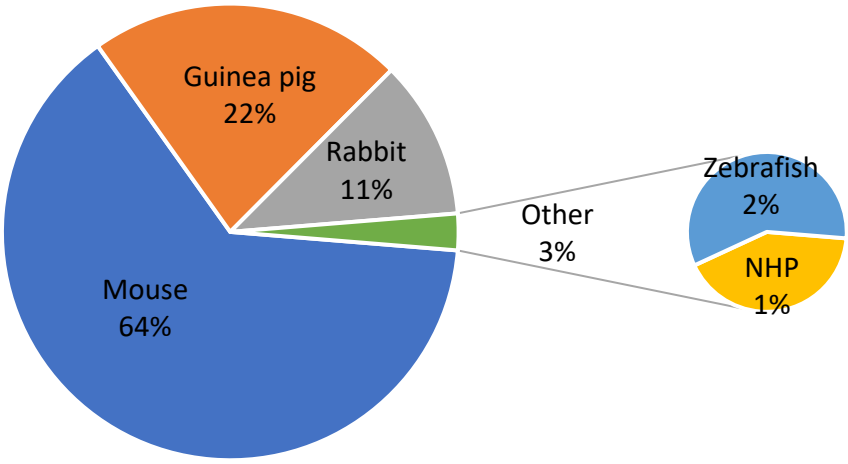


Figure 1.3: Proportion of most commonly used animals in tuberculosis research as of June 2021, determined using The NCBI PubMed database search between 1920-2021 for "Tuberculosis" AND "Mouse/Guinea pig/Rabbit/Zebrafish/NHP", representing 17014 research articles.

1.2.1 Mouse model of TB

Mice are the most popular animal used in TB research, owing to their small size, ease of handling and relatively inexpensive cost (Fonseca et al., 2017). As a widely used experimental animal, their physiology, immunology and genetics are extensively characterised (Bucsan et al., 2019). Mice (C57BL/6 or BALB/c) infected via the respiratory tract with an *MTB* dose of $1x10^3$ colony forming units (CFU), can develop a chronic pulmonary disease lasting ≥ six months (Yang et al., 2021). In addition to ATBI, LTBI can either be induced through drug or vaccine interventions or via the use of the spontaneous LTBI model (Lenaerts et al., 2004; Nuermberger et al., 2004). Historically, mouse models have provided a wealth of information on *MTB*-host immune interactions and played an integral role in identifying the role of T lymphocytes in protective immunity (Orme & Collins, 1983). Mice are among the most sophisticated animal model in research, with the availability of inbred and outbred strains, gene-knockouts and humanised mice, enabling more complex disease modelling and host-directed TB studies to be performed (Yang et al., 2021). Another appeal of this model is the large variety of immunological reagents available for use in functional assays (Zhan et al., 2017).

Despite its popularity, there are disadvantages to the use of mice as a model for TB. Disease progression in mice can vary widely on *MTB* infectious strain/dose and the strain of mouse used (Yang et al., 2021). Assessing the severity of the disease is challenging, as infected mice do not present with obvious clinical symptoms as seen in humans until the latter stages of infection (e.g., weight loss, coat quality and behavioural changes, and localised irritation and inflammation) (Bouté et al., 2017; Nemeth et al., 2020). The most widely used inbred strains, C57BL/6 and BALB/c do not develop granulomas as seen in humans. Instead, they form

diffused, non-caseating and non-necrotic lesions (Kramnik & Beamer, 2016). Mouse strains such as C3HeB/FeJ (Kramnik & Beamer, 2016), humanised (Calderon et al., 2013), B6J.C3-Sst1 (Kramnik & Beamer, 2016) and collaborative cross (Smith et al., 2016) can be used to mimic human-like granulomas (Yang et al., 2021). However, availability of specialised inbred or genetically altered strains can lead to bottlenecks due to regulatory issues and availability of mice due to generation time. Furthermore, alterations in the gene pool can result in adverse effects, such as intra/inter experimental reproducibility, significant changes in susceptibility to *MTB* and inability to manage bacterial load (Yang et al., 2021). While mouse LTBI models exist, challenges with reproducibility or variability between latency length, the intensity of relapse and predictor of recurrence remains an issue (Zhan et al., 2017).

1.2.2 Guinea pig model of TB

Compared to mice, guinea pigs are more susceptible to *MTB*, requiring a lower dose (20 to 50 CFU) to induce chronic pulmonary infection three weeks post-infection, before control of infection is lost 6-9 months post-infection (Clark et al., 2015). Unlike mice, guinea pigs develop both necrotic and non-necrotic granulomas, as seen in humans (Williams & Orme, 2016). Pathological analysis of caseous necrotic granulomas in guinea pigs revealed a hypoxic centre, similar to humans, but cavitation is rarely observed and only in selected *MTB* strains (Kato-Maeda et al., 2012). Guinea pigs have been used to study extrapulmonary infection such as TB meningitis, which showed dissemination of *MTB* in the central nervous system in a strain-dependent manner (Be et al., 2011). Guinea pigs have also been used to study the impact of co-morbidity factors such as type-2 diabetes (Podell et al., 2014). As a model organism, its larger size relative to mice, allows for greater quantity of biological materials to be retrieved from a single experiment increasing output when compared to mice. As with mice, guinea

pigs lack clear clinical manifestations of TB disease. Unlike mice, antibodies (Abs) specific for guinea pig immune components are limited. However, cross-reactive Abs designed for mice, gene expression and flow cytometric assays have been utilised and optimised for guinea pigs to overcome this limitation (Clark et al., 2015).

1.2.3 Rabbit model of TB

Rabbits are a popular non-rodent animal model due to their docile nature, which even allows for bleeding without the need for sedatives (Yang et al., 2021). As a host, rabbits are relatively resistant to *MTB* and are more susceptible to infection with *M. bovis* (Lurie, 1964). *MTB* infected rabbits can mimic pulmonary TB pathology similar to those in humans (including cavitary lesions) in an *MTB* strain and dose (<5 to 500 CFU) dependent manner (Lurie, 1964; Manabe et al., 2003, 2008; Tsenova et al., 2020). Rabbits can establish a chronic infection in 2-4 months post-infection. Prolonged incubation can lead to a controlled outcome for some rabbits, with residual paucibacillary lesions detected 5-6 months post-infection (Yang et al., 2021). LTBI established in a rabbit model can be reactivated using immune suppression treatment, making this model ideal to study co-morbidity factors such as HIV (Esteves et al., 2018). Rabbits have also been used to study extrapulmonary infections such as bone (Li et al., 2017) and meningeal TB (Tucker et al., 2016).

Compared to mice and guinea pigs, the larger size of rabbits makes them more expensive to maintain due to the need for a large housing facility. Similarly, rabbits lack apparent clinical symptoms of TB (Yang et al., 2021). In addition, the immunological toolbox and reagents available for rabbits are significantly limited as with guinea pigs (Zhan et al., 2017; Wagar et al., 2018; Entrican et al., 2020). However, generation of such a toolbox and reagents are

actively being undertaken (Peng et al., 2015). For applications such as drug screening, the larger size of rabbit requires similar treatment doses to the much larger NHPs, making it uneconomical for hard to synthesise candidate compounds (Yang et al., 2021).

1.2.4 NHP model of TB

NHPs such as rhesus and cynomolgus macaques are considered as the gold standard of animal models, owing to their anatomical, physiological and immunological similarities to humans (Foreman et al., 2017). NHPs are highly susceptible to *MTB* infection and can mimic the full spectrum of clinical and pathological manifestations of human TB infection (Scanga & Flynn, 2014). NHPs are used to study complex diseases states and are often used as screens for vaccine and drug efficacy. Complex immunological data can be generated by using human Abs, which are cross-reactive against NHPs, thereby providing essential translational information critical for predicting responses in humans (Flynn et al., 2015). Furthermore, the similarities of NHPs to humans are more representative of the human response when compared to other animal models (Yang et al., 2021). During the 1970s, TB researchers used the NHP model to study BCG vaccine efficacy and the host immune response, providing valuable insight required to create future vaccines (Peña & Ho, 2016). More recently, NHPs have been utilised to show that BCG vaccination via intravenous injection, as opposed to intradermal injection, can induce a more robust immune response providing hope for rejuvenating the use of the BCG vaccine (Darrah et al., 2020).

Despite these advantages, the use of NHPs in experiments has come under substantial ethical scrutiny from the public due to their similarities to humans and is a recurrent subject in legislative discussions (Carvalho et al., 2019). Furthermore, with practicality in mind, the use

of NHPs can be limiting as they are substantially larger than other models, require larger housing facilities, more intensive care, and are less readily available. As a result, the use of NHPs is associated with a substantial financial burden (Foreman et al., 2017). Transgenic or inbred lines of NHPs are challenging to generate due to the higher ethical consequences associated with this model organism (Coors et al., 2010; Zhao et al., 2019).

1.2.5 Zebrafish model of TB

The zebrafish (*Danio rerio*), native to South Asia, is a fresh water tropical fish marked with zebra-like stripes that run along the side of its body. Zebrafish are small, with larva being 1-2 mm and adults ~3 cm in size (Bouz & al Hasawi, 2018). Zebrafish are considered as a lower vertebrate model, which are animals possessing lower levels of sentience and are considered ethically more acceptable than the use of higher vertebrate model such as NHPs (Gunatilake, 2019). While zebrafish lack lungs, their physiology and pharmacology are still comparable to humans and translational for TB research (Bouz & al Hasawi, 2018), and the zebrafish genome contains at least one ortholog for ~70% of the human genome (Howe et al., 2013). The immune system of zebrafish is unique, where adaptive immunity develops only > 6 days post-fertilisation, enabling the study of innate immunity in isolation from adaptive immunity (van Leeuwen et al., 2015). As a TB model, the translucent zebrafish larva has been used to study the role of innate immunity in the formation of granulomas. Innate immunity can form early granulomas independently of adaptive immunity, which is required for maturation (Davis et al., 2002). The use of zebrafish as a drug screen is widespread in research (Takaki et al., 2012; Ordas et al., 2015; Dalton et al., 2017; Matty et al., 2019), typically involving infection with bioluminescent or fluorescent mycobacteria. Changes in luminescence or fluorescence are measured in response to treatment to determine drug efficacy more rapidly than traditional

models reliant on CFU enumeration. Zebrafish are genetically tractable and gene knockouts can be created to precisely study host immune factors (Cronan & Tobin, 2014; Bouz & al Hasawi, 2018).

However, there are drawbacks to the use of zebrafish as a model for TB. The greatest of which is the need for the use of a surrogate mycobacterial species to *MTB*. As a cold-blooded animal typically found in the ocean, zebrafish cannot be acclimated to 37 °C, making them an unsuitable host for *MTB* (Pype et al., 2015). As such, *Mycobacterium marinum*, a non-tuberculous mycobacterium (NTM) is used to study TB in zebrafish. *M. marinum* causes granulomatous disease in fish and is an opportunistic human pathogen capable of causing skin and soft tissue infection called fish handler's disease (Sette et al., 2015). Genetically, 85% of orthogonal coding sequences are shared between *MTB* and *M. marinum*, which is in contrast to the similarities of 99.95% between *MTB* and *M. bovis* (Garnier et al., 2003; Stinear et al., 2008). This variability between *MTB, M. bovis* and *M. marinum* may result in missed efficacy hits. Though, it is important to note that despite 99.95% similarity between *M. bovis* and *MTB*, 0.05% accounts for more than 2400 single nucleotide polymorphisms. Therefore, even between *M. bovis* and *MTB* an attrition to the hit rate is expected (Yuan & Sampson, 2018). Other disadvantages include the need for a specialised zebrafish aquaculture facility and trained personnel for rearing and maintenance (Avdesh et al., 2012). Additionally, while the small size of the zebrafish larva aids in drug throughput screening (typically carried out in a 96 well plate, where each well containing 1 larva, allowing in total for screening five compounds plus control, with a group sample size of n = 8), infection and treatment is often carried out using glass microcapillary injection needles, which require specialised equipment and training (Avdesh et al., 2012; Takaki et al., 2012).

1.2.6 Fruit fly model of TB

The fruit fly (*Drosophila melanogaster*) is an invertebrate model of TB (Franco & Olsson, 2014). As an invertebrate, the use of the fruit fly does not require oversight from ethical committees in most countries, making them extremely attractive as an alternative to vertebrate models (Kaito et al., 2020). However, as with zebrafish, the fruit fly cannot be incubated at 37 °C and is not a viable biological host for *MTB* and requires the use of *M. marinum* as a surrogate (Dionne et al., 2003). As an invertebrate, the fruit fly lacks adaptive immunity. Nonetheless its innate immune system is complex and is comparable to that seen in mammals (see 1.4). In this model, mycobacterial infection is characterised as a phagocytosis-dependent dissemination and induction of systemic disease (Dionne et al., 2003). As a genetically tractable model, fruit flies can be easily engineered to create knockout strains to test the role of specific host innate immune components (Dionne et al., 2003). For example, changes to the host metabolism following infection have been studied using mutant fruit flies, showing similar changes in energy reallocation as observed in humans (Dionne et al., 2006). Fruit flies have also been adopted to rapidly determine drug efficacy using fluorescent mycobacteria in a manner similar to zebrafish (Oh et al., 2013).

However, there are issues with the use of the fruit fly as a model for TB. Firstly, this invertebrate can be challenging to work for a number of reasons. During infection, fruit flies must be anesthetised using carbon dioxide gas to prevent escape. The injection of infectious material, requiring the use of a glass capillary needle operated under microscopy, makes the procedure as complex as traditional infection procedures (Ashburner & Roote, 2007) e.g., intratracheal injections in mice typically requiring anaesthesia or specialised 3D printed platforms (Cheng et al., 2017). Furthermore, the ability of flies to take flight is a biohazard

(infected or genetically modified) requiring considerable attention. Secondly, treatment is often carried out by allowing flies to graze on antibiotic infused food (Oh et al., 2013). Such a treatment method makes accurate dosing challenging and can increase inter-study variability. Thirdly, while most models discussed thus far are capable of mimicking aspects of granulomas, the hallmark of human TB, the fruit fly model is unable to develop any such structures following infection with *M. marinum* (Dionne et al., 2003).

1.2.7 The 3Rs and animals in experimentation

The ability of each model to reproduce aspects of TB disease can vary widely depending on the animals used. There appears to be a distinct correlation between increasing disease complexity observed in a TB model and the rise in non-biological factors (ethics, ease of use, cost and time). As a result, the most representative models are those which are considerably challenging both ethically and practically. Considering the ethical impacts, substantial efforts have been made globally to adopt the 3Rs (replace, refine and reduce) in animal experimentation in the past decade. Today, researchers are encouraged to consider the ethical implications of their work and how existing models can be refined or the numbers of animals used reduced. Equally, the use of lower vertebrate (e.g., zebrafish), invertebrate (e.g., fruit fly), organoids and computational models, which are all ethically more acceptable than traditional models, are considered favourable replacements. Taking these views on board, TB models such as zebrafish and fruit fly have gained attention owing to their reduced ethical burden. However, a non-mammalian TB infection model that is a viable host for *MTB*, lacking the need for any specialised equipment or facility, is economical, reproducible, allowing for medium-high throughput screening, and that which fits within the remit of the 3Rs, is yet to

be established. Ultimately, to successfully meet the End-TB strategy goals, such models are urgently needed to facilitate higher research output.

1.3 *Galleria mellonella*

Galleria mellonella (*Gm*) is a species of moth belonging to the *Pyralidae* family of the Lepidoptera order and is more commonly known as the greater wax moth. *Gm* can be found on most continents, often in bee and wasp hives as parasites causing bumblebee/wasp-galleriosis. This leads to substantial damage in the apiculture industry (Kwadha et al., 2017). The *Gm* life cycle takes up to 10 months, consisting of four stages: egg (3-30 days), caterpillar (28 days-6 months), pupae (1-9 weeks) and adult insect (12-21 days) (Kwadha et al., 2017). However, under optimal conditions, *Gm* can fully mature to adulthood in 40 days (Jorjão et al., 2018). Despite the industrial impact on apiculture, the *Gm* caterpillar (often referred to as waxworm or hereon as larvae) are bred commercially as live food for domestic reptiles and birds, and as fish bait (Pereira & Rossi, 2020). In science, *Gm* larvae have steadily gained attention in infectious disease and toxicology research (Cook & McArthur, 2013; Champion et al., 2016; Tsai et al., 2016; Killiny, 2018; Pereira et al., 2018; Jorjão et al., 2018; Cutuli et al., 2019; Dinh et al., 2021). Over 2000 *Gm* research articles have been registered on the NCBI PubMed database over the past two decades, with ~1000 published over the past 5 years (Figure 1.4).

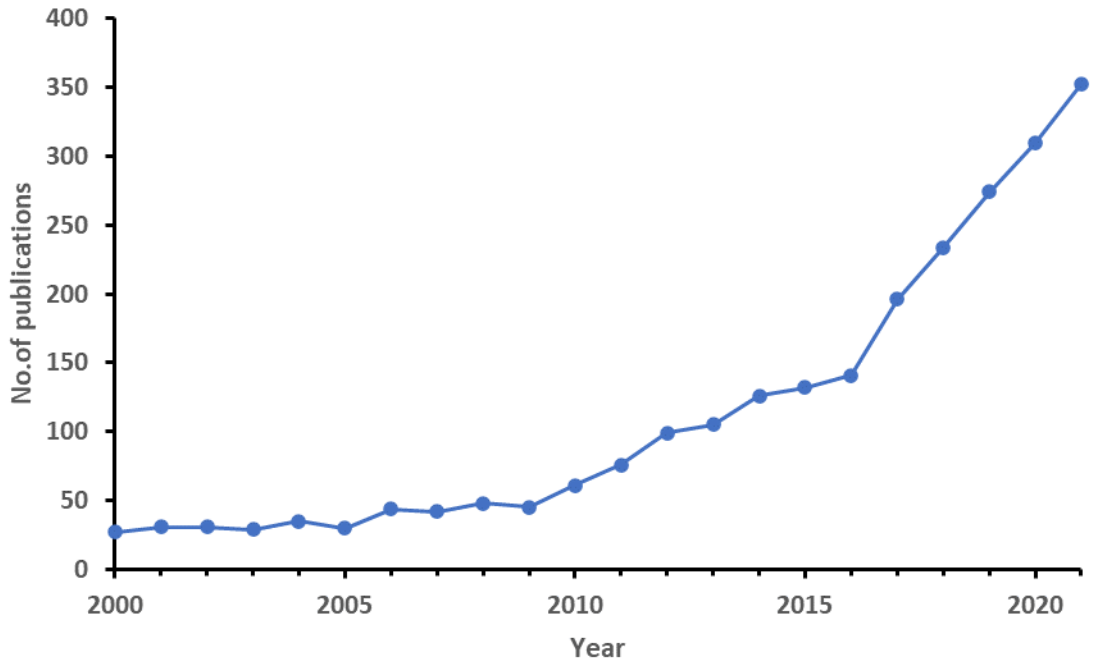


Figure 1.4: The number of *G. mellonella* publications available as of July 2021 on NCBI PubMed central using the search term "*Galleria mellonella*" between 2000-2021. Image represents a total of 2030 research articles. Publication number for 2021 is extrapolated based on the July 2021 data.

1.3.1 Galleria mellonella as an infection model

As an infection model, more than 65 bacterial and fungal pathogens have been studied using the *Gm* model, and the number of pathogens tested continues to increase each year (Dinh et al., 2021). *Gm* offers several desirable traits as a model organism (Figure 1.5), which include: 1) size (2-3 cm) allowing for easy handling and manipulation; 2) can be incubated at 37 °C mimicking the human physiological temperature; 3) highly economical (£1 = 30 larvae); 4) does not require specialised equipment for infection or facility for maintenance; 5) rapid and reproducible data generation; 6) ethically more acceptable and does not require ethics approval; and 7) has a complex innate immune system comparable to those in mammals. *Gm* has been used to assess comparative virulence of bacterial and fungal isolates (Card et al., 2016; Jønsson et al., 2017; Sousa et al., 2018; Durieux et al., 2021) and as a screen to determine efficacy and toxicity of novel drugs in over 37 research articles (Cutuli et al., 2019).

The response of *Gm* to infection has been studied using, qualitative observations such as changes in larval melanisation (see 1.4.3), histopathology and microscopy, as well as quantitative methods such as measurement of *Gm* survival, recovery of bacteria/fungi, measurement of innate immune cell density, transcriptomic and proteomic analysis (Pereira et al., 2018; Dinh et al., 2021).

Nevertheless, as a model *Gm* is in its infancy, and as such there are some limitations. For example, *Gm* lacks a publicly available, fully assembled and annotated genome (only a partial annotation is available on the NCBI database), limiting the generation of genetically modified *Gm*. Immunologically, *Gm* lacks commercially available immune reagents preventing complex functional innate immune assays from being carried out. However, a comprehensive *Gm* transcriptome and proteome database is available which has enabled genetic and immunological studies to be carried out despite such limitations (Vogel et al., 2011; Sheehan & Kavanagh, 2018; Dinh et al., 2021).

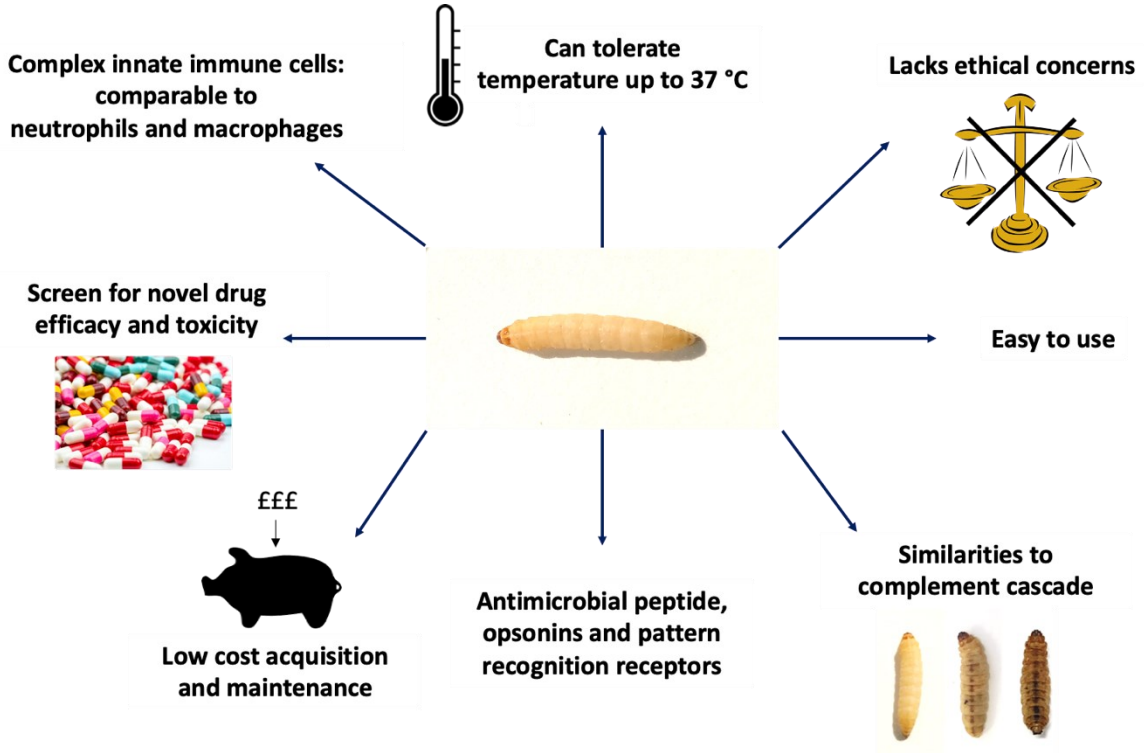


Figure 1.5: Advantages of using *G. mellonella* as a model organism. Reproduced from Asai et al., 2019.

1.4 Insect innate immune system

As with all invertebrate infection models, one inherent limitation of *Gm* is its lack of adaptive immunity (Hillyer, 2016). Nevertheless, the insect innate immune system is complex, functionally and structurally similar to those found in mammals, making invertebrate models the ideal candidates to study the virulence and mechanism of human pathogens, and host innate immune-pathogen interactions (Wojda, 2017).

1.4.1 Anatomical and physiological barriers

The first line of the insect defence system is its cuticle, a layer of chitin laced epithelium covering the insect body, which like mammalian skin, minimises the risk of infection or mechanical damage (Trevijano-Contador & Zaragoza, 2018). Physiological barriers such as low pH, low humidity, low nutrient availability and digestive enzymes in vital organs (trachea and gut) create an inherently challenging environment for pathogens to colonise (Wojda, 2017). When these barriers fail, insects engage the germ-line encoded cellular and humoral response of their innate immune system (Figure 1.6).

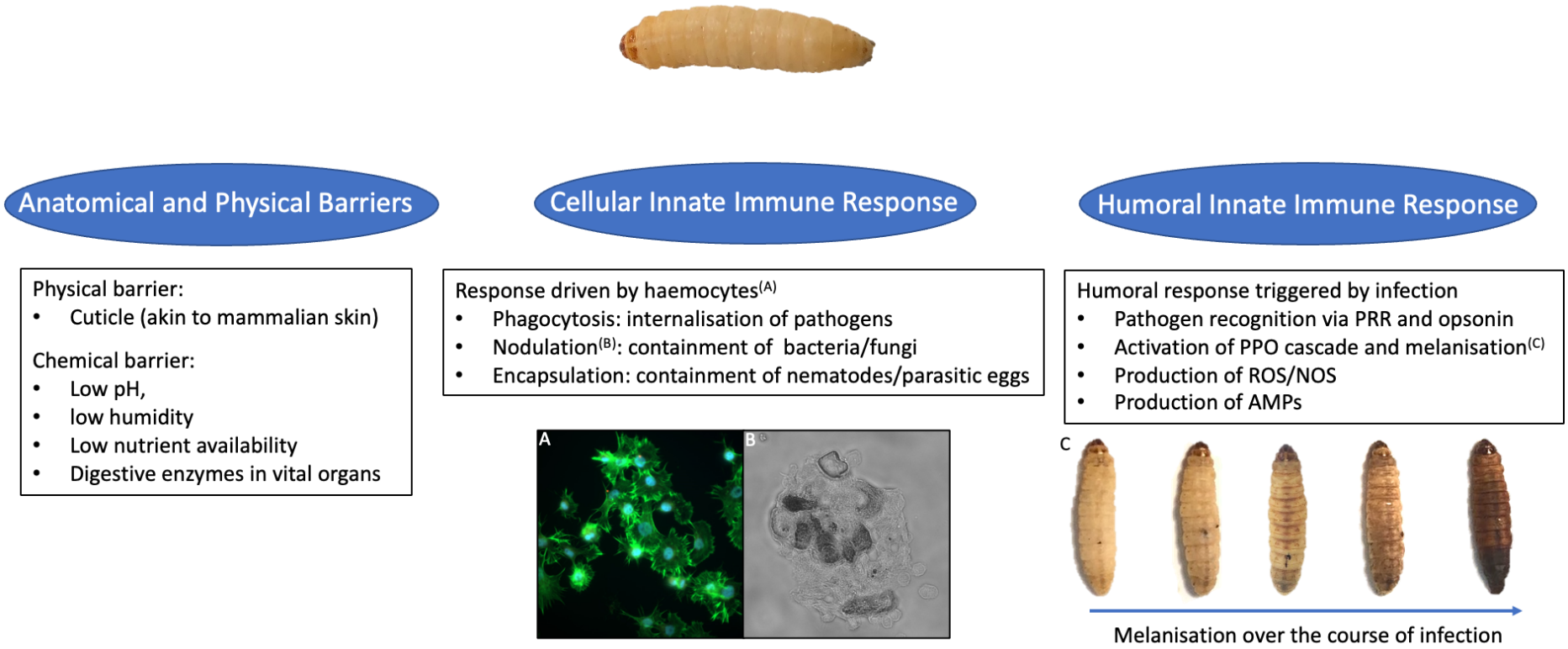


Figure 1.6 The innate immune responses of *G. mellonella*. An overview of *Gm* innate immune response. (A) Representative image of haemocytes under fluorescent microscopy, where nuclei are stained with 4',6-diamidino-2-phenylindole (DAPI, in blue) and cell membrane in fluorescein isothiocyanate (FITC, in green). (B) Representative image of haemocyte nodulation taken using differential interference contrast imaging. (C) larval melanisation monitored over the course of infection with mycobacteria.

1.4.2 Innate immunity: cellular responses

The cellular response relies on the activity of innate leukocyte-like cells known as haemocytes (Hillyer, 2016). Haemocytes are found in a plasma-like solution known as the haemolymph, which is pumped throughout the insect body via an open circulatory system known as the haemocoel (Hillyer, 2016). Unlike mammalian blood, the haemolymph does not take part in respiration, which is carried out by a complex respiratory tube network known as the trachea (Kavanagh & Reeves, 2004). Haemocytes are found in two active states, circulating or sessile (tissue and organ associated). In non-immune challenged insects, sessile haemocytes are the predominant active state. However, haemocytes can switch between the two active states dynamically (Leitão & Sucena, 2015). During infection or mechanical damage, the density of haemocytes tends to increase as sessile haemocytes switch to the circulating active state (Sigle & Hillyer, 2016; Sheehan & Kavanagh, 2018).

The cellular immune response can be separated into phagocytosis, cellular encapsulation and nodulation (Hillyer, 2016). Haemocytes are differentiated into sub-types and their function in cellular responses can vary depending on the insect species. In *Gm*, five sub-types of haemocytes have been identified: prohaemocytes, plasmatocytes, granulocytes, spherulocytes, and oenocytoids (Pereira et al., 2018). Prohaemocytes are progenitor cells that can differentiate into other sub-types. Plasmatocytes and granulocytes are phagocytic haemocytes, akin to neutrophils and macrophages, and the most common sub-types found in *Gm* and in most insect species (Bergin et al., 2005). Oenocytoids contain key components for melanisation (Hillyer, 2016). Spherulocytes are known transporter of cuticle components (Hillyer, 2016). In innate immunity, spherulocytes are speculated to contribute towards coagulation and clotting (Stączek et al., 2020).

Phagocytosis is a cellular mechanism which is highly conserved between invertebrate and mammalian cells (Kavanagh & Reeves, 2004). Phagocytosis is the internalisation of a small number of microbial targets, such as bacteria or fungi, by a single phagocytic cell. Phagocytosis is initiated upon recognition of pathogen associated molecular patterns (PAMPs) or damage associated molecular patterns (DAMPs) molecules by pattern recognition receptors (PRRs) (Sheehan et al., 2018b). Using PRRs such as apolipophorin and calrecticulin, *Gm* can differentiate classes of microbes which include bacteria (Gram-positive/negative), fungi and viruses (Pereira et al., 2018). Phagocytosed pathogens are neutralised by damage elicited by reactive species or hydrolytic enzymes within the phagosome (Kavanagh & Reeves, 2004; Bergin et al., 2005).

For pathogens that are too large for phagocytosis; nodulation or cellular encapsulation is utilised by insects (Hillyer, 2016). Nodulation and cellular encapsulation may also be induced, where phagocytosis fails to clear the pathogen (Jiravanichpaisal et al., 2006). Nodulation is used to contain large clusters of bacterial and fungal pathogens. Granulocytes attach to the microbial mass, degranulate and release plasmatocyte spreading peptides, which attract and aggregate plasmatocytes, forming the multi-cellular nodule. Nodule formation appears to be driven by eicosanoid-based signalling, is lectin-mediated, and the presence of extracellular matrix like protein, nodular (or putative defence protein Hdd 11 [Hdd11] in *Gm*), has been associated with the formation of nodules (Kavanagh & Reeves, 2004; Dubovskiy et al., 2016b; Hillyer, 2016). Cellular encapsulation is a process closely resembling nodulation and it is the formation of a smooth capsule surrounding large pathogens such as nematodes, protozoa and parasitoid eggs and larvae (Hillyer, 2016). Like nodule formation, cellular encapsulation

is driven by plasmatocytes and granulocytes, in a granulocyte dependent manner to form a multi-cellular capsule layer (Kavanagh & Reeves, 2004; Pereira et al., 2018). The formation of nodules and capsules are resource intensive processes and utilise large numbers of haemocytes, typically causing a reduction in the number of circulating haemocytes as a result of recruitment (Dubovskiy et al., 2016b). Both nodules and capsules, may be melanised to further contain the pathogen (Dubovskiy et al., 2016b). While it is clear haemocyte adhesion, spreading and degranulation play key roles in the formation of nodules and capsules, the precise mechanism of these cellular responses remains to be determined.

1.4.3 Innate immunity: humoral responses

The humoral arm of *Gm* innate immunity consists of PRRs and opsonin for recognition of pathogens, signalling pathways leading to production of humoral effectors such as AMPs, or induction of mechanisms such as generation of reactive species, haemolymph clotting, and melanisation. As such, cellular and humoral responses are interconnected and often occur concurrently.

The humoral response is activated by the binding of cell-surface PRRs and opsonins (circulating PRRs) to bacterial and fungal PAMPs, e.g., lipopolysaccharide (LPS), lipoteichoic acid (LTA), β-1, 3 glucan and fungal conidia (Tsai et al., 2016). In *Gm*, apolipophorin-III (apoLp-III), peptidoglycan recognition proteins (PGRPs), *Gm* cationic protein 8 and hemolin have been identified as PRRs and opsonins (Tsai et al., 2016). Activation of PRRs, initiates one of three innate immune signalling pathways found in insects: Toll, the immune deficiency (Imd) and the Janus Kinase-signal transducer and activator of transcription (JAK-STAT) pathways (Hillyer, 2016). The immune signalling pathways, receptors and effectors can vary widely depending

on the insect species and are generally poorly described in literature (Hillyer, 2016). However, Toll and Imd pathways are believed to be activated by Gram-positive bacteria/fungi and Gram-negative bacteria, respectively (Wrońska & Boguś, 2020). There are structural and functional similarities between mammalian interleukin (IL)-1 and *D. melanogaster* Toll receptors, activating nuclear factor kappa B (NF_kB) in mammals and NF_kB homologues in insects (Medzhitov et al., 1997). Additionally, insect PRR, apoLp-III functions similarly to mammalian apolipoprotein E and both enhance phagocytic activity (Whitten et al., 2004). Once activated, immune signalling pathways induce the production and secretion of AMPs in the haemocytes, the fat body (liver like organ), digestive tract, salivary glands, and the reproductive organ, in a pathogen dependent manner (Hillyer, 2016; Pereira & Rossi, 2020). AMPs are found in all classes of life and are a crucial component of innate immunity providing a broad spectrum of microbicidal activity. Twenty putative AMPs have been identified thus far in *Gm* (Pereira et al., 2018), amongst which the most notable and best characterised are lysozyme, gallerimycin, galiomicin, cecropins, cobatoxin, morcin and gloverins. The microbicidal mechanism of AMPs can vary ranging from membrane permeablisation to inhibition of DNA and protein synthesis (Wu et al., 2018).

Melanisation is an essential biological process in *Gm* necessary for anatomical and physiological maintenance such as cuticle hardening, wound healing and immunity (Wojda, 2017). Melanisation is a humoral mechanism that is initiated following pathogen recognition by the PRR, which induces a serine protease cascade system, that functions similarly to the complement cascade, called the pro-phenoloxidase (PPO) cascade (Wang et al., 2017). This cascade is responsible for converting tyrosine into melanin precursor, which is then cross-linked with haemolymph protein to form melanin. This conversion is reliant upon the

activation of PPO, secreted by oenocytoids, into phenoloxidase (PO) by the serine protease activated PPO activating enzyme (Nakhleh et al., 2017). Melanisation is often carried out at the site of nodulation or cellular encapsulation, where a layer of melanin is deposited around the pathogen, isolating the microbe from the nutrient rich haemolymph, causing starvation and asphyxiation, leading to death (Wojda et al., 2020). Furthermore, the PPO cascade produces reactive species as a biproduct of its enzymatic activity, inducing chemical damage to the pathogen. However, reactive species are cytotoxic, and the PPO cascade is tightly regulated by serine protease inhibitors (Hillyer, 2016). Reactive species are also induced in phagocytic haemocytes to neutralise the internalised pathogen. Homologous pathways for reactive species generation between mammalian neutrophil and insect haemocytes have also been identified (Browne et al., 2013). Most notable of which are the generation of superoxide via NADPH oxidase complex like pathways involving homologous proteins to $p47^{phox}$ and $p67^{phox}$ (Bergin et al., 2005; Renwick et al., 2007). In phagocytic haemocytes, reactive species are neutralised by antioxidant systems such as superoxide dismutase (SOD), glutathione-S-transferase and peroxidase to prevent cytotoxicity (Pereira et al., 2018).

Melanisation is often accompanied by haemolymph clotting, activated by the same serine protease cascade (Li et al., 2002). Upon activation, granulocytes release clotting factors, which alongside the soluble factors found in the haemolymph, causes haemocyte adhesion and haemolymph coagulation and subsequent melanisation (Pereira et al., 2018). Clotting may also be induced in the presence of extracellular nucleic acid released from damaged tissue or cells, which is likely to be a precautionary measure against infection (Nascimento et al., 2018). Whilst large scale clotting in mammals would lead to thrombosis, as insects have an open circulatory system, coagulation is a unique and important humoral response that is

capable of rapidly localising pathogens (Wojda et al., 2020). As highlighted in Section 1.4, there are clear differences between insect and mammalian innate immunity, including melanisation and coagulation. However, a substantial number of similarities also exist (Table 1.1).

Table 1.1. Similarities between insect (haemocytes) and mammalian (neutrophils) innate immunity

	Hemocytes	Neutrophils
Phagocytosis	Lectin-mediated	Lectin-mediated
ROS	O_2^-, H_2O_2, NO^-	O_2^-, H_2O_2, NO^-
Degranulation	Yes	Yes
AMPs	Peroxynectin, transferrin, lysozyme, defensin	MPO, transferrin, lysozyme, defensin
Receptors	TLRs, B-1,3-glucan, IL-IR	TLRs, B-1,3-glucan, IL-IR
Transcription factors	NFκB, IκB	NFκB, IκB
Cascades	IMD, JNK, JAK-STAT	IMD, JNK, JAK-STAT
Kinases	p38 MAPK, ERK, PKC, PKA	p38 MAPK, ERK, PKC, PKA
Neutrophil extracellular nets (NET)	NET-like structures present	NETs present

Reproduced from Browne et al., 2013, with permission from Taylor and Francis Group.

1.5 *Galleria mellonella* as an infection model for mycobacteria

Over the past two decades the use of *Gm* in mycobacteriology have been described but has been limited to that of NTM, which includes *Mycobacterium marinum*, *Mycobacterium fortuitum*, *Mycobacterium aurum*, *Mycobacterium abscessus*, *Mycobacterium kansasii*, and *Mycobacterium avium hominissuis* (Entwistle & Coote, 2018; Meir et al., 2018; Kirubakar et al., 2020). NTM are a group of environmentally ubiquitous mycobacteria that are opportunistic human pathogens and do not cause TB or leprosy (Johansen et al., 2020). Infections caused by NTM present with a wide variety of clinical manifestations ranging from skin/soft tissue infection to meningitis, with pulmonary infection being the most common (Ratnatunga et al., 2020). As with members of the MTBC, infections caused by NTM are difficult to diagnose due to their long incubation period, and they are intrinsically resistant to many antibiotics (Ratnatunga et al., 2020). Associated with high morbidity and mortality, NTM are a substantial burden to both immune competent and compromised individuals and are now regarded as emerging pathogens of interest (Johansen et al., 2020). The *Gm*-NTM models demonstrated that NTM can induce *Gm* larval mortality in a NTM dose-dependent manner. Meir, Grosfeld and Brakan, examined histopathological sections of *Gm* infected with *M. abscessus*, which revealed the presence of granuloma-like structures containing mycobacteria within the fat body (Meir et al., 2018). As a screen for antimycobacterial drugs, *Gm* infected with NTM responded to treatment with clinically recommended antimycobacterial compounds in a drug dose and NTM strain and species dependent manner (Entwistle & Coote, 2018; Meir et al., 2018). Infection of *Gm* with *Mycobacterium smegmatis,* a species of mycobacteria generally considered to be non-pathogenic, has also been described (Ignasiak & Maxwell, 2017).

The use of *Gm* as a model for *MTB*, *M. bovis* and *Mycobacterium avium* has previously been evaluated by Metalnikov, Cameron and Hollande in the 1920s and 1930s (Metalnikov, 1920; Hollande, 1930; Cameron, 1934). All three researchers reported that the tubercle bacilli were phagocytosed within minutes of infection and agreed that infection led to generation of nodules or granuloma-like structures, found throughout the larval cavity. However, all three mycobacterial species tested in *Gm* appear to be non-virulent having no ill effect on the larvae. Interestingly, Cameron compared the outcome of *Gm* infection with 28 other bacterial pathogens and reported conflicting results to those observed by Metalnikov (Cameron, 1934). Furthermore, both reported non-virulent outcomes for many of the bacteria tested which have since shown virulence in more recent studies including *M. avium*, *Vibrio cholerae*, *Streptococcus pyogenes*, *Streptococcus pneumoniae*, and *Shigella dysenteriae* (Cameron, 1934; Loh et al., 2013; Barnoy et al., 2017; Bokhari et al., 2017; Entwistle & Coote, 2018; Cools et al., 2019). While it is difficult to determine the root cause of this discrepancy between recent and past studies, it is not unreasonable to speculate that advancement in even the most basic tools, such as incubators, culture media, or improvements in bacterial strain cataloguing technology over the past century, may play a substantial role in the infectious outcome. Furthermore, mycobacteria are notoriously known to be influenced by media and growth conditions which may alter their virulence (Barnoy et al., 2017).

1.6 Summary

As discussed in this chapter, *MTB* is a highly adapted and a formidable foe of humans. Treatment of TB is becoming increasingly challenging with the rise and spread of MDR and XDR *MTB* strains, and the lack of clinically available novel antimycobacterial compounds. Therefore, without the concerted effort in TB research to develop novel treatments, preventative and diagnostic measures, TB will continue to be a substantial burden in endemic regions. Furthermore, increased migration of individuals from TB endemic to non-endemic region risks silent and potentially explosive propagation in less vigilant areas. Current research relies heavily on the use of traditional animal models that range from mice to NHPs. While these models have provided a wealth of information to our knowledge of TB, higher vertebrate models are associated with non-biological limitations, that can serve as a bottleneck to research output. To resolve these concerns, researchers have utilised 3Rs models which are ethically more acceptable, such as zebrafish and fruit flies. However, both models come with a biological limitation which requires the use of *M. marinum* as a surrogate for *MTB*, which could cause variability in expected outcomes. Thus, there is a clear need for a 3Rs model in TB research that lacks the need to use surrogacy for *MTB* and which is capable of replicating key aspects of TB disease, including the granuloma. *Gm* is a candidate to consider for such application and is a model organism with a proven track record, already validated using over 65 bacterial and fungal pathogens. *Gm* possesses innate immune cells with similar functions to neutrophils and macrophages and is capable of replicating granuloma-like structures (nodule/cellular encapsulation). Unlike zebrafish and the fruit fly models, *Gm* can be incubated at 37 °C and therefore can be used to study human pathogens under optimal physiological conditions. While studies in *Gm* have been conducted using NTM, members of the MTBC have not been examined in modern times (past five decades). While

studies examining the use of *Gm* with MTBC are available from the 1920s and 1930s, this needs to be re-evaluated using modern techniques. As such, to determine whether *Gm* is a viable host for MTBC, this thesis will first re-examine *Gm* as a host for MTBC by re-establishing, characterising and evaluating the use of *Gm* as an infection model for BCG. This proof-of-concept study will allow for additional *Gm*-MTBC infection models to be established, including an *MTB* model.

1.7 Hypothesis

Gm larvae can be used as a reproducible, low-cost and ethically more acceptable model to study TB, and as a platform for medium-high throughput screening of novel antimycobacterial agents, and for the assessment of comparative *MTB* virulence, thereby reducing and/or replacing the use of animals in TB research.

1.8 Aims

To test this hypothesis, the aims of the study are:

1 Re-evaluate and characterise the use of *Gm* as an infectious host for members of the MTBC using BCG as proof of concept.

2 Establish and characterise the use of *Gm-MTB* Δ*leuD*Δ*panCD* as a novel containment level (CL) 2 compliant infection model for *MTB.*

3 Establish and characterise the use of *Gm* in CL 3 as an infection model for *MTB* H37Rv and determine whether it can be used for comparative *MTB* virulence study.

4 Determine whether *Gm*-MTBC infection models can be used for low-medium throughput drug screening of antimycobacterial compounds.

5 Analyse the *Gm* innate immune response following infection with BCG using quantitative proteomic and gene expression methods.

This thesis addresses the Aims of this project as follows: in Chapter 3, the *Gm*-BCG infection model is established and characterised to re-examine Metalnikov, Hollande and Cameron's observations from the 1920s and 1930s, and conclusively determine whether MTBC, BCG as a surrogate for *MTB* in the first instance, is virulent in *Gm* (Aim 1). In Chapter 4, following definitive evidence that BCG is virulent in *Gm*, a novel CL2 *Gm* infection model for MTBC was

established and characterised, using a double auxotroph mutant of *MTB* with the aim to remove the limitation of the requirement for a CL3 facility and mitigate the need for BCG surrogacy (Aim 2). In Chapter 5, the *Gm* model was optimised for use with *MTB* H37Rv at CL3. Once established, the *Gm*-*MTB* H37Rv infection model was characterised, and its use as a platform for comparative virulence studies examined (Aim 3). In Chapter 6, the collective *Gm*-MTBC infection models established in this project, were examined for their capacity as a low-medium throughput screen for antimycobacterial compounds (Aim 4). In Chapter 7, the innate immune response of *Gm* to infection with BCG was analysed using quantitative proteomic and molecular methods, with the goal of providing a comprehensive immune database serving as a source of information for future studies (Aim 5). Finally in Chapter 8, the major findings of this project are summarised, and future prospects for *Gm* as a model for MTBC are discussed.

Chapter 2
Materials and Methods

2.1 Materials

2.1.1 Materials used in this study

Difco™ Middlebrook 7H9 nutrient broth, Difco™ Middlebrook 7H10 & 7H11 nutrient agar, BBL™ albumin dextrose catalase (ADC) and BBL™ oleic albumin dextrose catalase (OADC) mycobacterial growth supplements were purchased from Becton, Dickinson and Company (BD) (USA). Kanamycin (KAN), phosphate buffered saline (PBS), Tween® (polysorbate)-80, dimethyl sulfoxide (DMSO), glycerol, n-decyl aldehyde, AFB colour staining kit, haematoxylin, eosin, lithium carbonate, INH, RIF, ETH, PZA, moxifloxacin hydrochloride (MOX), bedaquiline (BDQ), piperacillin (PIP), sodium chloride (NaCl), potassium chloride (KCl), Tris hydrochloric acid (Tris-HCl), ethylenediaminetetraacetic acid (EDTA), sodium citrate, leucine (Leu), calcium pantothenate (Pan), dithiothreitol (DTT), iodoacetamide (IAA), 10% buffered formalin solution, amaranth, 10% buffered formalin, glutaraldehyde, FITC, N-Phenylthiourea (PTU), and C18 spin filters were bought from Sigma-Aldrich (USA). Grace's insect medium, gentamicin/amphotericin B, TRIzol™ reagent, ethanol (99.9%), paraffin wax, Countess™ Cell Counting Chamber Slides, SYBR™ gold and SlowFade™ Gold antifade mountant were acquired from Thermo Fisher Scientific (USA). 2- and 4-well Millicell EZ slide was obtained from Millipore (MA, USA). Custom polymerase chain reaction (PCR) primers (Table 2.1) were synthesised by Eurofins Genomics (DE). RNeasy, QuantiTect reverse transcription, and QuantiFast SYBR Green PCR kit were purchased from QIAGEN (Germany). *Gm* was purchased from LiveFoods Direct (UK). Lysis matrix S was purchased from MP Biomedical (USA), and hygromycin B (HYG) from Roche Diagnostics (USA). Sequence grade trypsin and ProteaseMax™ was obtained from Promega (USA), and Fast-Read 102® from VWR (UK). Osmium tetroxide, Araldite® epoxy, uranyl acetate, lead citrate was purchased from Electron Microscopy Sciences (USA).

2.2 Methods

2.2.1 Mycobacterial strains and culture conditions

The bioluminescent *M. bovis* BCG *lux,* referred hereon as BCG *lux*, created by transforming *M. bovis* BCG (Montreal strain) with the plasmid shuttle vector pSMT1, carrying the *luxAB* genes of *Vibrio harveyi* (Snewin et al., 1999), was kindly gifted by Prof. Douglas Young (Imperial College London [ICL], UK). *M. bovis* BCG Pasteur Δ*panCD* (Psmyc Turbo635asv-YFP), referred hereon as FluorBCG, was constructed by Dr Nitiya Krishnan (ICL, UK), by transforming *M. bovis* BCG Δ*panCD* (Pasteur strain) with the plasmid shuttle vector pCB22 (carrying complementation for the *ΔpanCD* auxotrophy). The plasmid was further modified to allow for the expression of both yellow fluorescence protein (YFP) (Mishra et al., 2017) and Turbo635asv (Blokpoel et al., 2003; Carroll et al., 2010) under an artificial operon driven by the Psmyc promoter (Ehrt et al., 2005). *MTB* H37Rv (TMC 102/ATCC 35837), known hereon as H37Rv, was purchased from ATCC (USA). H37Rv Δ*leuD*Δ*panCD* mutant (referred hereon as SAMTB) was generously donated by Professor William Jacobs Jr. (Albert Einstein College of Medicine, USA). SAMTB was transformed by Dr Samantha Sampson (ICL, UK) into an auto-luminescent mutant (referred hereon as SAMTB *lux*), using the plasmid construct pMV306, carrying the full *lux* operon of *Photorhabdus luminescens* (Andreu et al., 2010). H37Rv Δ*phoP* and complemented Δ*phoP* were kindly gifted by Prof. Carlos Martín (University of Zaragoza, ES). H37Rv Δ*dosR* and complement Δ*dosR* were gifted by Dr Sharon Kendall (Royal Veterinary College, UK).

All mycobacterial work in this project was carried out in CL2 (BCG *lux*, FluorBCG, and SAMTB *lux*) or CL3 (MTB H37Rv and MTB Δ*phoP*, Δ*dosR*, and their complemented mutants) in accordance with strict institutional and governmental guidelines. All liquid mycobacterial

cultures were grown in Middlebrook 7H9 broth supplemented with 10% ADC, 0.2 % glycerol and 0.05% Tween®-80. All solid mycobacterial cultures were grown on Middlebrook 7H11 agar, supplemented with 10% OADC and 0.5% glycerol. No additional changes were made to broth and agar formulations for *MTB* H37Rv, *MTB* H37Rv Δ*dosR* and Δ*dosR* complement and FluorBCG strains. For the growth of BCG *lux* and MTB H37Rv Δ*phoP*, broth and agar were further modified with the addition of HYG (50 μg/ml), for selection of pSMT1 and Δ*phoP*, respectively. For the growth of SAMTB *lux*, broth and agar were additionally supplemented with Leu (25 μg/ml) Pan (24 μg/ml), HYG (50 μg/ml) and KAN (20 μg/ml) to complement Δl*euD*Δ*panCD* double auxotrophy and select for pMV306. For the growth of *MTB* H37Rv Δ*phoP* complement HYG (50 μg/ml) and KAN (20 μg/ml) were added to the broth and agar to select for the complemented mutant. Mycobacterial cultures were grown to the mid-log growth phase, and aliquots of 25% glycerol stocks were prepared and maintained in a -80 °C freezer for use in experimentation.

For experimentation, frozen glycerol stocks of mycobacteria were defrosted and inoculated into Middlebrook 7H9 broth with appropriate modifications (as outlined above). The starting culture density was standardised to OD of 0.1 (BCG *lux* and SAMTB *lux*) or 0.01 (H37Rv) using a spectrophotometer and incubated at 37 °C in an orbital shaker (220 revolutions per minutes, RPM) until the mid-log growth phase, which typically correlated to an optical density $(OD)_{600}$ of 0.6-0.8. For BCG *lux* and SAMTB *lux*, bioluminescence (relative light unit, RLU/ml) was additionally utilised as a measure of relative growth, which was measured using a luminometer (Berthold Technologies, Germany). For non-auto luminescent BCG *lux*, 1% n-decyl aldehyde (v/v in ethanol) was added as the substrate for the emission of luminescence (see Chapter 3). No substrate is required for the auto luminescent SAMTB *lux*. The RLU:CFU

ratio in Middlebrook 7H9 broth cultures were 3:1 and 0.03:1 for BCG *lux* (**Supplementary Figure 2.1**) and SAMTB *lux* (**Supplementary Figure 2.2**), respectively. Growth curve of H37Rv in media was similarly provided (**Supplementary Figure 2.3**). For mycobacteria grown on solid media, mycobacterial culture was serially diluted ten-fold, and 10 µl of each dilution was plated onto Middlebrooks 7H11 agar with appropriate modifications (as outlined above). The inoculated plates were incubated at 37 °C in a static incubator with 5% carbon dioxide for 2-3 weeks.

2.2.2 Acquisition and maintenance of Galleria mellonella

Sixth (last) instar *Gm* larvae were purchased from Livefoods Direct (UK). Upon delivery, healthy larvae were selected based on their uniform cream colour, lack of melanisation, body mass (200-250 mg), size (approximately 2-3 cm), and motility (high levels of movement with the ability to right themselves when turned over). Dead larvae, which were defined as those that failed to respond to physical stimulation, or melanised larvae (discoloration of the cuticle) were discarded into a 50 ml conical bottom centrifuge tube and euthanised in a -80 °C freezer for 15 minutes (min). Healthy larvae were stored in the dark at 18 °C, inside a breathable plastic container (original packaging from Livefoods Direct) lined with wood chippings, for no more than one week prior to experimentation in order to preserve larval quality and minimise pupation. *Gm* were not fed at any point following their arrival to the lab.

2.2.3 Preparation of mycobacterial inocula for Galleria mellonella infection

Mycobacterial cultures were prepared for *Gm* infection. Mid-log growth phase culture was pelleted at 3000 g for 10 min at room temperature. The mycobacterial pellet was washed twice in PBS containing 0.05% polysorbate-80 (PBS-T), to dissipate any clumping of

mycobacteria (Tsukamura, 1991). Following the final wash, the mycobacterial pellet was resuspended to a desired CFU inocula in PBS-T, using OD and RLU (where available for BCG *lux* and SAMTB *lux*) as a relative measure for CFU. For inocula preparation, OD_{600} of 0.6, 1.5, 8 and 12, correlated to 1 x 10^8, 2 x 10^8, 1 x 10^9, and 2 x 10^9 CFU/ml, respectively. Whereas for bioluminescence, 3 x 10^9 and 4 x 10^7 RLU/ml correlated to 1 x 10^9 and 2 x 10^9 CFU/ml for BCG *lux* and SAMTB *lux*, respectively. Bioluminescence readings can be influenced by changes in temperature and oxygenation levels (Neilson et al., 1999; Roy, 2017), therefore where bioluminescent measurement of inocula were abnormal, if the culture grew to the expected OD_{600}, preparation of inocula proceeded using OD_{600} instead. In any case, inocula for each experiment were enumerated for their CFU to validate the infectious dose, and to screen for contaminants. Heat treated (HT) inocula were prepared from viable suspensions, which were incubated for 1 hour in a water bath set to 85 °C. Validation of HT was confirmed by CFU enumeration of pre- and post-heat treated cultures and measured after 3 weeks of incubation.

2.2.4 Injection of Galleria mellonella with mycobacteria inocula

Prior to the infection procedure, larvae were acclimatised to room temperature for 2 hours. Larvae were gently decontaminated with 70% ethanol, to minimise contamination from the cuticle microbiota of *Gm*. Acclimated and decontaminated larvae were then counted into a sterile Petri dish lined with a layer of filter paper. A platform for infection was constructed by taping a layer of filter paper on to a raised flat surface such as a Petri dish or a lid of a pipette tip box (**Figure 2.1A**). Each individual *Gm* was rolled onto its back and secured into position using tweezers, exposing the pro-leg (**Figure 2.1B**). Infection of the larva was carried out using a microsyringe (25-gauge, 25 µl capacity fixed needle syringe from SGE Analytical Science,

Australia or Hamilton Company, Germany), the tip of the needle being inserted 5-6 mm into the last-left proleg at a 10-20° angle to the horizontal plane, with 10 µl of inoculum being delivered (**Figure 2.1C**). Using the microsyringe, the injected larva was carefully transferred from the platform to a Petri dish lined with filter paper, stored inside a breathable cardboard box in the dark, and incubated at 37 °C over the time course of the particular experiment. When compared to traditional methods (Fuchs et al., 2010; Kavanagh & Fallon, 2010; Ramarao et al., 2012), *Gm* injection as described here, greatly minimises the proximity of the user's hand to the needle during the procedure, and substantially minimises the risk of needle stick injuries, without sacrificing injection through-put. The procedure was approved by the ICL safety unit.

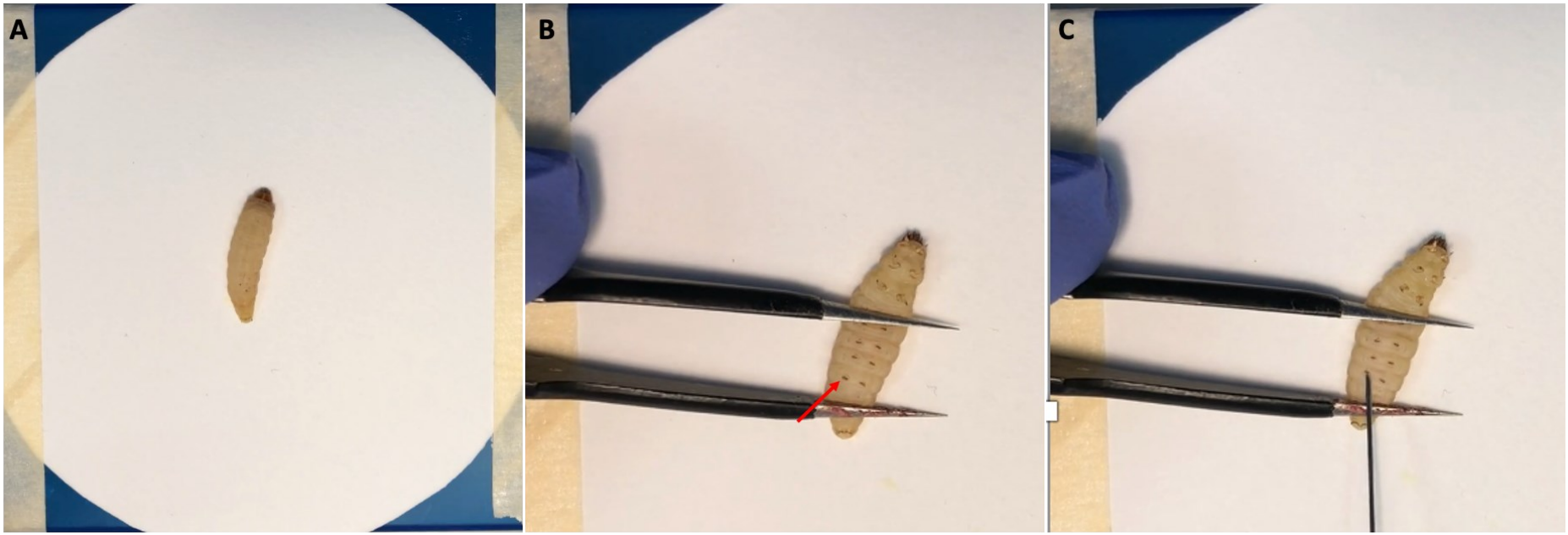


Figure 2.1: Infection of *Galleria mellonella* using a microsyringe. (A) injected platform consisting of a raised flat surface covered in filter paper for absorption of infectious material. (B) Larva is flipped onto its back to expose the pro-legs (red arrow), and secured into place using tweezers. (C) Larval infection takes place by injection of the mycobacterial inoculum into the haemocoel via the last-left pro-leg.

2.2.5 Assessment of mycobacterial virulence in Galleria mellonella

Survival assays were conducted to evaluate mycobacterial virulence in *Gm*. Larvae were infected with varying CFU doses, strains or species of mycobacteria, and the changes in larval survival outcome was recorded every 24 h over a 96 h time course for BCG *lux* and SAMTB *lux*, and a 192 h time course for H37Rv. Larvae were considered dead when they failed to respond to touch. In the event of pupation, larvae were discarded and counted as having survived. For controls, naïve (unmanipulated) larvae served as the larval quality control, larvae mock infected with PBS-T were used as the negative infection controls, and larvae pricked (to mimic needlestick injury) as technical controls. The outcome of the virulence assays was plotted as a Kaplan-Meir survival curve, and the significance of survival outcome was determined using the Mantle-Cox log-rank test between the relevant controls and experimental groups. Sample size ranged from 10 to 30 larvae per group, and at least two independent experiments were conducted. Specific samples and experimental repeats are outlined in each Chapters 3-5.

2.2.6 Measurement of in vivo mycobacterial survival in Galleria mellonella

Changes in *in vivo* mycobacterial load over the course of infection were determined by enumerating CFU or measuring bioluminescence (for BCG *lux* and SAMTB *lux*). Following infection, larvae were homogenised at 0, 24, 48, 72, 96, and 168 h post-infection for BCG *lux* and SAMTB *lux*, or at 0, 24, 48, 72, 96, 144, 168 and 192 h post-infection for H37Rv. At each time point, larvae were randomly selected and individually homogenised within a lysing matrix tube containing 800 µl of PBS-T and six 1/8-inch metal beads using the FastPrep-24™ 5G instrument (MP Biomedical, USA) or FastPrep F120 instrument (for use in CL3) (MP Biomedical, USA). Machine parameters for both homogenisers were set to 6.0 m/s for 1 min.

For CFU enumeration, serial ten-fold dilutions were prepared, and each dilution was plated onto Middlebrook 7H11 agar containing appropriate supplements, with further addition of PIP (10-20 µg/ml) to prevent growth of native *Gm* flora (Entwistle & Coote, 2018) (see Chapter 3). Inoculated agar plates were incubated at 37 °C in a static incubator with 5% carbon dioxide for 2-3 weeks. For measurement of bioluminescence, a larval homogenate was decanted into a luminometer tube, and any residual homogenate on the lysis matrix tube was washed off with a single volume of PBS-T (see Chapter 3). The bioluminescence of BCG *lux* or SAMTB *lux* within the homogenate was measured using a luminometer as described previously (2.2.1). The RLU:CFU ratio was determined to be 4:1 and 0.02:1 for BCG *lux* and SAMTB *lux*, respectively (see Chapters 3 and 4). For measurement of *in vivo* mycobacterial survival, four (H37Rv) or five (BCG *lux* and SAMTB *lux*) larvae were sacrificed at each time point and the experiment was repeated three times.

2.2.7 Preparation of antimycobacterial compounds

For treatment of *Gm* infected mycobacteria, clinically recommended antimycobacterial compounds were prepared in PBS at dosages recommended for the treatment of adult TB (WHO, 2010, 2014), scaled relative to the body/mass of the larva (200 mg). First-line antimycobacterial compounds: INH (5 mg/kg), RIF (10 mg/kg), ETH (15 mg/kg) and PZA (25 mg/kg); and second-line antimycobacterial compounds: MOX (6.7 mg/kg) and BDQ (5.7 mg/kg) were prepared. In comparison to dosages typically used in animals, these dosages were of similar magnitude to/or lower than those used in mice (Mourik et al., 2017; Lee et al., 2018). Additionally, combinations of antimycobacterial compounds INH/RIF, RIF/ETH, RIF/ETH/MOX (REM) were similarly prepared.

2.2.8 Evaluation of antimycobacterial compound toxicity in Galleria mellonella

Toxicity of antimycobacterial compounds were evaluated at doses up to 10x the dosage typically used for treatment of adult TB, relative to body/mass of *Gm*. Larvae were injected as similarly described in 2.2.4 with 10 µl of a given compound and toxicity, defined by larval mortality, reduction in motility and melanisation, was monitored every 24 h for 96 h. Toxicity was evaluated using a sample size of ten larvae per group and two independent experiments were conducted.

2.2.9 Minimum inhibitory concentration assay

Prior to the treatment of *Gm* infected with mycobacteria, the efficacy of INH, RIF, ETH, PZA, MOX, BDQ and PIP (see 2.2.6) against BCG *lux*, SAMTB *lux* and H37Rv were determined *in vitro* via broth dilution minimum inhibitory concentration (MIC) assays (Khara et al., 2020). Serial two-fold dilutions of compounds ranging from 16 to 0.125 µg/ml were prepared in Middlebrook 7H9 broth with appropriate supplements (minus selective antibiotics), and 100 µl of each dilution were seeded into wells of a 96 well plate in triplicates. These wells were further inoculated with 100 µl (OD_{600}: 0.1, 10^7 CFU/ml) of mid-log phase mycobacterial culture. The positive control was broth inoculated with mycobacteria alone, and the negative control was broth alone. The outer most wells of the 96 well plate were filled with sterile water to reduce edge effects. The plates were lidded (and sealed in CL3) and transferred to an airtight container lined with moist paper towels, to minimise evaporation. The plates were incubated on a rocking platform (20 RPM) for 1 week, before the turbidity of each well was measured (OD_{520}) using an VersaMax™ plate reader (Molecular Devices, UK) in CL2 and iMark™ Microplate Absorbance Reader (Bio-Rad Laboratories, USA) in CL3. The MIC was defined as the concentration of compounds required to inhibit growth of mycobacteria,

measurable via visual observation and spectrophotometry. The MICs were determined through two independent experiments.

2.2.10 *Treatment of infected Galleria mellonella with antimycobacterial compounds*

Efficacies of antimycobacterial compounds were evaluated in larvae infected with BCG *lux* (1 x 10^7 CFU), SAMTB *lux* (2 x 10^7 CFU) and H37Rv (2 x 10^6 CFU) (see Chapter 6). Treatment was administered via injection as similarly described in 2.2.4. For BCG *lux* and SAMTB *lux*, a single compound or combination of compounds were given 1 h post-infection, or for repeated dosing, a second dose was given 24 h post-infection. For H37Rv, treatment with a single compound was given 72 h post infection and no repeat dosing was carried out. Treated larvae were monitored over the course of 96 h (for BCG *lux* and SAMTB *lux*) or 120 h (for H37Rv) post-treatment, larval survival outcome and changes to *in vivo* mycobacterial survival, was used as a measure of treatment efficacy and were similarly assessed using methods described in 2.2.5 and 2.2.6. Infected larvae mock treated with PBS-T served as the no treatment control. The minimum sample size used for treatment efficacy studies was 20 larvae, and a minimum of two independent experiments were conducted, specific samples and experimental repeats are outlined in Chapter 6. Larval survival following treatment was plotted as a Kaplan-Meir survival curve, and the significance of treatment on larval survival outcome was determined using the Mantle-Cox log-rank test carried out between the no treatment control and the experimental groups. Changes in *in vivo* mycobacterial load were plotted as an XY line graph or a column chart, and the significance of treatment efficacy on reduction of *in vivo* mycobacterial load was determined using one-way analysis of variance (ANOVA) with Šídák multiple comparison, Kruskal-Wallis test with Dunn's multiple comparisons, or an unpaired t-test, as appropriate.

2.2.11 In vivo live imaging of FluorBCG in Galleria mellonella

The spread of injected fluids throughout the larval body was demonstrated by injecting larvae with 10 µl of 0.2% amaranth dye (w/v in PBS), as similarly described in 2.2.4. To better visualise the movement of the dye, larvae were immobilised on ice for 15 min prior to dye injection. The permeation of the dye throughout the larval cavity was captured using an iPhone X camera (Apple, USA) over 80 seconds as the effect of ice immobilisation began to wear off.

Furthermore, to determine whether injection with mycobacteria similarly led to systemic dissemination of the inocula within the larval body, larvae were infected with FluorBCG (2.5 x 10^6 CFU). As above, larvae were immobilised on ice for 15 min prior to injection of FluorBCG and the movement of the YFP expressing bacilli was video-recorded using a proprietary portable fluorescent imaging platform, provided courtesy of Dr Brian Robertson (ICL, UK). The imager was comprised of lighting unit consisting of a green and amber light emitting diode with filter units for YFP and Turbo-365 selection, which was attached to a D5300 camera (Nikon, JP), on an imaging platform. The default camera settings for video were used. For assessment of disease progression (formation of infection foci, see Chapter 3), ice immobilised infected larvae were photographed at 72 h and 168 h post-infection, using camera settings of ISO 400 and shutter speed of 1/30.

The *Gm*-FluorBCG model was also evaluated as a drug screen in a pilot study (see Chapter 6). Larvae were infected with FluorBCG (5 x 10^6 CFU) and were treated (as described in 2.2.10) with a 10 µl dose of either INH (10 mg/kg) or RIF (20 mg/kg) 1 h post-infection and incubated

at 37 °C for 120 h. Changes in YFP fluorescence were measured and qualitatively analysed against infected larvae mock treated with PBS-T.

2.2.12 Transmission electron microscopy of Galleria mellonella haemocytes

Transmission electron microscopy (TEM) was utilised to visualise the haemocyte-mycobacteria intracellular interaction. Infected larvae (n = 10, per time point) were punctured between the head and the thorax using a 30-gauge needle, and haemolymph (containing haemocytes) were pooled (approximately 40 µl/larva) into a 2 ml reaction tube containing ice cold PBS and centrifuged at 800 g for 10 min at 4 °C. Haemolymph were collected at the following time points: 24, 48, 72, 96, 144 and 336 h post-infection for BCG *lux,* at 1, 24, 96 and 168 h post-infection for SAMTB *lux*, and 1, 24, 96, 144 and 192 h post infection for H37Rv. The pelleted haemocytes were resuspended in ice cold 3% glutaraldehyde (v/v in PBS), fixed for 10 min, pelleted at 800 g for 10 min and stored at 4 °C prior to processing by Dr William Cooley at the Animal and Plant Health Agency (APHA, Weybridge, Surrey, UK) for TEM. Fixed haemocytes from naïve larvae and mycobacteria were used as controls. The fixed pelleted cells were subsequently post-treated with 1% osmium tetroxide (v/v in phosphate buffer), dehydrated in a graded series of ethanol: 30%, 50%, 70%, 90% and 100%, embedded in Araldite epoxy resin, and sliced into ultra-thin sections (70-90 nm). Samples were mounted onto a grid, stained with 0.5% uranyl acetate (w/v in water) and 3% lead citrate (w/v in water) on EM AC20 (Leica Microsystems, DE), and examined on a Tecnai bioTWIN transmission electron microscope (FEI company, USA). Images were captured using AMT advantage V701 software (Deben, UK) and AMTXR60 camera (Deben, UK).

2.2.13 Histopathology of Galleria mellonella

Histopathology of infected larvae was undertaken to visualise the progression of disease and the formation of granuloma-like structures. A minimum of three larvae were randomly selected at each timepoint and were fixed by injecting 100 µl of 10% buffered formalin and stored in 10% buffered formalin. Larvae were fixed at the following time points: 24, 72, 96, 168 and 336 h post-infection for BCG *lux,* at 24, 48, 96 and 168 h post-infection for SAMTB *lux*, and 24, 48, 96, 144 and 192 h post infection for H37Rv. Naïve larvae were fixed and stored as the control. Fixed larvae were processed by Dr John Spiropoulos at the APHA (UK). Each larva was cut in half along the dorsal line and processed for histology using Sakura Tissue-Tek VIP (Sakura, USA). Processed larvae were embedded in paraffin wax using the Histostar™ Embedding Center (Fischer Scientific, USA), and 4 µm thickness tissue sections were produced using an RM2135 microtome (Leica Biosystems, DE). Sections were mounted onto a glass slide for haematoxylin and eosin (H&E) or ZN, stained using the Varistain V24-4 Automatic Slide Stainer (Thermo Scientific, USA) and examined using an Eclipse 80i light microscope (Nikon, JP), where images were captured using a DS-Ri1 camera (Nikon, JP) via the NIS-Element Basic Research imaging software (Nikon, JP).

2.2.14 Galleria mellonella haemolymph smear slides

For simple visualisation of haemocyte-mycobacterial interaction, haemolymph was extracted from BCG *lux* (1 x 10^7 CFU) infected larvae (n = 3, per time point) at 24 and 96 h post-infection (see Chapter 3). Haemolymph was bled (approximately 40 µl/larva) from the larva via needle puncture (30-gauge) of the soft tissue between the head and the thorax and pooled into an ice-cold reaction tube containing 3 µl of PTU (5 mg/ml). A drop (10 µl) of haemolymph was placed onto a glass slide mixed with 10 µl ice cold PBS and smeared across the slide in a single

smooth motion using another glass slide at a 45° angle. Smears were dried in a heated oven set to 45 °C and ZN stained using the AFB colour staining kit on a stain rack, following the manufacturers guidelines. Smear slides were analysed by Dr John Spiropoulos using the Eclipse 80i light microscope (Nikon, JP), and images were captured using NIS-Element Basic Research imaging software and a DS-Ri1 camera (Nikon, JP).

2.2.15 Confocal fluorescence microscopy of Galleria mellonella haemocytes

Taking a fluorescent approach to visualising haemocyte-mycobacterial interaction, haemolymph (approximately 40 µl/larva) was harvested from SAMTB *lux* (2 x 10^7 CFU) infected larvae (n = 3, per time point) at 1 and 168 h post-infection, pooled into 700 µl of ice-cold PBS containing 3 µl of PTU (5 mg/ml) to minimise melanisation and coagulation (Sheehan & Kavanagh, 2018). The cell suspension was mixed and 200 µl seeded into wells of a 4-well Millicell® EZ SLIDE (culture slide) and further layered with 200 µl of PBS. The cells were left to stand at room temperature for 30 min to allow for cell adhesion. Non-adherent cells were washed off with two volumes of PBS, adherent cells fixed with 10% buffered formalin for 15 min and washed twice more with PBS.

Fixed slides were stained for mycobacteria using SYBR™ Gold as described previously (Ryan et al., 2014), where SYBR™ Gold was found to selectively stain mycobacterial DNA and RNA. Compared to conventional fluorescent stains such as auramine-O, SYBR Gold is more sensitive, as DNA/RNA bound dye increases signal intensity by > 1000-fold, which substantially reduces background noise and improves the signal to noise ratio (Ryan et al., 2014). SYBR™ Gold was diluted 1:1000 in a staining solution, prepared by combining phenol crystal (8 g), glycerine (60 ml), isopropanol (14 ml), and sterile water (26 ml). The slides were

flooded with the staining solution, lightly covered with Parafilm™, heated in an oven at 65 °C for 5 min, and cooled to room temperature for 1 min. The Parafilm was removed, slides were washed with acid-alcohol (0.5% HCL in 70% isopropanol) for 3 min and washed with water. Two drops of SlowFade™ Gold Antifade Mountant, containing 4',6-diamidino-2-phenylindole (DAPI), was applied to counterstain the haemocyte nuclei. The coverslip was applied, and the edges were sealed using clear nail varnish. The prepared slides were examined on a SP8 inverted fluorescent confocal microscope (Leica Microsystems, DE) using the LAS X software and the integrated camera (Leica Microsystems, Germany) at the ICL Facility for Imaging by Light Microscopy (FILM).

2.2.16 Ex vivo model of Galleria mellonella – mycobacteria granuloma-like structure

For the formation of *ex vivo* granuloma-like structures, haemolymph (approximately 40 µl/larva) was harvested from SAMTB *lux* (1 x 10^6 or 2 x 10^7 CFU) infected larvae (n = 5, per time point) at 24, 48, 72 and 96 h post-infection, pooled into a 1.5 ml reaction tube containing 900 µl of ice-cold insect physiological saline (IPS: NaCl [150, mM], KCl [5 mM], Tris HCl [100 mM], EDTA [10 mM], and sodium citrate [30 mM] in sterile water adjusted to pH 6.9), preserving cell viability and minimising melanisation and coagulation (Fuchs et al., 2010, 2018). The cell suspension was mixed and centrifuged at 800 g for 10 min at 4 °C. The supernatant was discarded, and the pellet was resuspended in another volume of ice-cold IPS and pelleted once more. The pelleted haemocytes were resuspended in 500 µl of IPS, and 10 µl of this cell suspension was mixed 1:1 with 0.4% trypan blue dye (to determine cell viability) and loaded into a Countess™ Cell Counting Chamber Slide for automated cell counting using the Countess™ Automated Cell Counter (Thermo Fisher, USA).

The cell suspension was adjusted to 10^5 cells/ml, using Grace's insect media supplemented with amphotericin B (0.25 μg/ml), gentamycin (10 μg/ml), PTU (1 μg/ml) and PIP (20 μg/ml), and 1 ml of the suspension was seeded into wells of a 24-well plate or 2-well Millicell® EZ SLIDE. Each well containing cell suspension was further layered with 500 μl of supplemented Grace's medium. Haemocytes extracted from PBS mock infected larvae and media alone served as cell and media controls, respectively. The 24-well plates or culture slides were transferred into a vented plastic box, lined with moist paper towels to minimise evaporation, and incubated at 37 °C in a rocking incubator (10 RPM) for one week. For maintenance, haemocyte cultures were inspected every 24 h for contamination, and 750 μl (50% total volume) of media was replaced every 24 h. After 1 week of incubation the cell culture was fixed with 10% buffered formalin for 15 min, washed twice with 1.5 ml of PBS, and processed as previously described for ZN (see 2.2.14) and SYBR gold staining (see 2.2.15). Brightfield culture images were taken on an IMT-2 inverted microscope (Olympus, Japan) with attached LabCam adapter (LabCam, USA) using an iPhone X camera (Apple, USA), and ZN stained images were acquired on an Eclipse E200 light microscope (Nikon, Japan) with attached LabCam adapter using an iPhone X camera. SYBR Gold images were obtained on an Axio Observer 7 (Zeiss, Germany), using the integrated camera and ZEN Blue software, at the ICL Facility for Imaging by Light Microscopy (FILM).

2.2.17 Total haemocyte count

The total haemocyte count (THC) was measured to determine the changes in the number of circulating haemocytes following infection with H37Rv. At each timepoint, 0, 24, 48, 72, 96, 144, 168 and 192 h post-infection, larvae (n = 4) were bled as described in 2.2.12 and pooled into 1.5 ml reaction tubes containing ice cold IPS. A uniform cell suspension was obtained by

mixing, and 10 µl loaded into wells of FAST READ 102® counting chambers. Cell counts were taken from four non-adjacent squares within a grid consisting of 10 squares. Viability was not measured. THC of PBS-T mock infected and naïve larvae were measured as controls. THC/ml/larva were calculated using the equation bellow:

$$THC = \left(\left(\frac{\sum cells\ counted\ in\ N\ squares}{N} \right) \times dilution\ factor\ x\ 10^4 \right) \div X\ Gm$$

N = number of squares counted, X = number of larvae bled, dilution factor was 20.

2.2.18 Quantification of Galleria mellonella weight-loss following infection

Changes to larval body mass following infection with BCG *lux* or SAMTB *lux* were evaluated (see Chapter 4), as individuals with TB are known to suffer from severe weight loss. Larvae (n = 5, per group) were infected with either BCG *lux* (1 x 10^7 CFU) or SAMTB *lux* (2 x 10^7 CFU), and changes to the larval body mass were measured individually using a Secura™ Analytical Balance (Sartorius AG, Germany) every 48 h over a 96 h time course. For each larva, the percentage change in mass relative to that at 0 h was calculated. Weight loss of infected larvae was compared against control naïve PBS-T mock infected larvae. Weight loss was presented as a column chart and significance was determined using one-way ANOVA with Šídák multiple comparison.

2.2.19 Label free quantitative proteomic of Galleria mellonella haemolymph

To better characterise the innate immune response of *Gm* to infection with BCG *lux*, proteomic analysis was undertaken (see Chapter 7). Haemolymph was harvested from BCG *lux* infected (1 x 10^7 or 1 x 10^5 CFU) larvae (n = 10, per time point) at 4, 48, and 168 h post-

infection as previously described (see Chapter 7). Haemolymph (approximately 60 µl/larva) was pooled into sterile 1.5 ml reaction tubes on ice, containing 5 µl of PTU (5 mg/ml) to prevent melanisation. Haemolymph was centrifuged at 10000 g for 10 min to pellet the haemocytes and 30 µl of the cell free haemolymph was carefully aspirated and transferred into a fresh 1.5 ml reaction tube containing 270 µl of PBS. The cell-free haemolymph of naïve larvae was collected as the control. For each time point, three independent samples were collected. Cell free haemolymph samples were stored in a -80 °C freezer before shipment to Dr. Gerard Sheehan and Prof. Kevin Kavanagh at Maynooth University, Ireland, for further processing as described previously (Sheehan & Kavanagh, 2018; Sheehan et al., 2018a, 2019, 2020b, 2021).

Proteins found within the cell free haemolymph (75 µg) were measured via Bradford assay (BSA standards [100 – 1500 µg/ml]), were acetone precipitated, quantified with Qubit® (Thermo Fisher, USA), reduced with DTT (200 mM), alkylated with IAA (1 M) and digested overnight at 37 °C with sequencing grade trypsin and ProteaseMax, at a trypsin:protein ratio of 1:40. Digested peptides were treated with trifluoracetic acid to acidify the sample and deactivate trypsin and purified on a C18 Spin filter. One micro gram of purified peptide mixture was loaded onto a Q-Exactive™ liquid chromatography mass spectrometer (LC-MS) system (Thermo Fisher, USA) connected to a Dionex™ Ultimate 3000 high performance liquid chromatography (HPLC) system (Thermo Fisher, USA). Peptides were separated using a Biobasic C18 Picofrit™ column (100 mm length, 75 mm internal diameter) (Thermo Fisher, USA), on an increasing acetonitrile gradient, using a 65 min reverse phase gradient (250 nL/min). All data were acquired with the mass spectrometer running under automatic data

dependent switching mode. A high-resolution mass spectrometry (MS) scan (2000 – 3000 Da) was performed on the Orbitrap to identify the 15 most intense ions prior to MS/MS.

2.2.20 Analysis of Galleria mellonella cell free haemolymph proteomic data

The protein signatures detected in 2.2.19 were annotated using the Andromeda search engine in MaxQuant (version 1.2.2.5; http://maxquant.net/maxquant), correlated against the six-frame translation of expressed sequence tag contigs of *Gm, Hyalophora cecropia*, *Manduca sexta*, and *Bombyx mori* (Vogel et al., 2011; Cox et al., 2011), as well as to those of *M. bovis* BCG (Brosch et al., 2007). In this analysis the following search parameters were used: first and second peptide search tolerance were 20 parts per million (ppm) and 4.4 ppm respectively, carbamidomethylation of cysteine was set as fixed modification, oxidation of methionines and acetylation of N-terminals were set as variable modifications with a maximum of 2 missed cleaved sites. False discovery rate (FDR) was set to 1% for both peptide and protein and FDR was estimated based on a search against target-decoy data base. For identification, peptide required a minimum length of seven amino acid and required more than one unique peptide for each protein. The MS data generated in 2.2.19 and the MaxQuant search output files were deposited to the proteomeXchange consortium via the Proteomic Identification Database (PRIDE) partner repository with the identifier PXD015250.

Perseus (v 1.5.5.3; http://maxquant.net/perseus) was used for data processing, statistical analysis, and graph generation. Label-free quantitation (LFQ) signal intensities were $\log_2$ transformed and one-way ANOVA and t-tests with B+H multiple testing correction were conducted between the control (naïve) and each of the time points (4, 48 and 168 h post-infection) for both 10^5 and 10^7 CFU BCG *lux* samples. A p value of 0.05 was used as the cut-off

for statistical significance and Benjamini-Hochberg correction was applied for FDR. Non-existent or low abundance protein (i.e., those detected but not present in all datasets) were included in analysis of total differentially expressed groups, following imputation of the zero-value, using number close to the lowest value of the range of proteins detected, plus or minus the standard deviation (SD).

2.2.21 Gene expression analysis of Galleria mellonella innate immune response

Changes in gene expression following infection with BCG *lux* was studied in a selection of innate immune genes (see Chapter 7) using the two-step reverse transcriptase (RT) quantitative polymerase chain reaction (qPCR). Larvae infected with either 10^5 and 10^7 CFU of BCG *lux* (n = 5, per time point) were randomly selected at 4, 48 and 168 h post-infection, and individually homogenised in a lysing matrix tube containing 900 µl of TRIzol ™ reagent and six 1/8 inch metal beads, as described in 2.2.6. RNA from the larval homogenates was extracted using a RNeasy mini kit. RNA of naïve larvae was also extracted as the baseline control for gene expression. RNA of five larvae were pooled, quantified and quality checked (A260/280 and A260/230 values: > 1.8 and >1.5, respectively) on a Nanodrop (Thermo Scientific, USA). One micro gram of RNA was treated to remove genomic DNA, and reverse transcribed into complementary DNA (cDNA) using a QuantiTect® reverse transcription kit.

q-PCR was carried out using the QuantiFast SYBR® Green PCR kit on a StepOne Plus real-time PCR system (Thermo Scientific, USA), targeting *Gm* innate immune genes using the primers listed in **Table 2.1**. Primer sequences for *gloverin, cecropin, hemolin, insect metalloproteinase inhibitor (IMPI)*, and *ubiquitin* were obtained from published papers (Dubovskiy et al., 2016a; Lange et al., 2018b). The primer sequences for *Hdd11* were designed using NCBI RefSeq of

Gm Hdd11 (NCBI accession number: XM_031907851) as template, and primer specificity was evaluated using NCBI primer-BLAST against the available *Gm* scaffold genome (NCBI accession number: GCF_003640425.2). All PCR amplicons were analysed via agarose gel electrophoresis and staining, giving a single product band, confirming their specificity (data not shown). The identities of the PCR amplicons were confirmed through sequencing, which returned the expected products (**Table 2.1**). Changes in gene expression were determined via the comparative cycle threshold (ΔΔCt) method, using gene expression in naïve larvae as the baseline and *ubiquitin* as the house keeping gene (Lange et al., 2018b). Gene expression was determined in three independent experiments, each RT-qPCR was run in triplicate with no-template controls.

Table 2.1. *G. mellonella* innate immune gene primers used in this project

Gene	Primer sequence (5'-3')	Matched NCBI ascension number for PCR amplicon sequences
Gloverin F	GTGTTGAGCCCGTATGGGAA[1]	XM_026909162
Gloverin R	CCGTGCATCTGCTTGCTAAC[1]	
Cecropin F	CTGTTCGTGTTCGCTTGTGT[1]	XM_026898304
Cecropin R	GTAGCTGCTTCGCCTACCAC[1]	
Hemolin F	CTCCCTCACGGAGGACAAAC[1]	XM_026893524
Hemolin R	GCCACGCACATGTATTCACC[1]	
IMPI F	TAGTAAGCAGTAGCATAGTCC[2]	XM_031913565
IMPI R	GCCATCTTCACAGTAGCA[2]	
Hdd11 F	TCGGCTTGTGAGTTCGTTGT[*]	XM_031907851
Hdd11 R	GGCACTAGAAGGAGCACCAC[*]	
Ubiquitin F	TCAATGCAAGTAGTCCGGTTC[1]	XM_026892927
Ubiquitin R	CCAGTCTGCTGCTGATAAACC[1]	

F: forward R: reverse. 1: Lange et al., 2018b 2: Dubovskiy et al., 2016b *: This project

2.2.22 Statistical analysis and data visualisation

Statistical analysis and data visualisation was carried out on Prism (GraphPad Software, USA) unless otherwise stated. Selection as to use parametric or non-parametric tests was chosen based on normality of data. All XY line graph and/or column charts represent the mean and the SD of the mean. The following p-values: 0.05, 0.01, 0.001, 0.0001, not significant, corresponds to the following annotations: *, **, ***, ****, ns, respectively.

Chapter 3
Re-evaluation of *G. mellonella* as a host for members of the *M. tuberculosis* complex using *M. bovis* BCG *lux*

3.1 Introduction

As discussed in Chapter 1, the use of *Gm* as an infection model for bacterial and fungal pathogens has become increasingly popular over the past two decades, with over 65 *Gm*-pathogen models described thus far (Dinh et al., 2021). The appeal of G*m* as a host is driven by the practicality of this insect model (e.g., economical, ease of use and reduced ethical implications). Traditional animal infection models (e.g., mice, guinea pigs, and NHPs) bottleneck TB research, and are costly, time consuming, low throughput and ethically challenging. To achieve the WHO's end TB strategic goal by 2035 (WHO, 2020), novel TB infection models such as *Gm*, that can overcome the practical limitations of traditional animal models, hold substantial value to increase the output and throughput of TB research.

Gm has been adopted by NTM researchers over the past five years, with *M. marinum*, *M. fortuitum*, *M. aurum*, *M. abscessus*, *M. kansasii*, and *M. avium hominissuis* being reported as virulent in *Gm* (Entwistle & Coote, 2018; Meir et al., 2018; Kirubakar et al., 2020). Between 1920 and 1930, Metalnikov, Cameron and Hollande independently tested *Gm* as an infectious disease model using a number of bacterial pathogens including *MTB*, *M. bovis* and *M. avium*. These early *Gm*-mycobacteria studies all reported rapid internalisation and localisation of mycobacteria leading to containment and persistence in granuloma-like structures or killing through melanisation. While reports of persistence or killing of mycobacteria in *Gm* was a heated debate among scientists, they all concluded that mycobacteria could not cause virulent infection in *Gm*, despite its virulence in humans (Metalnikov, 1920; Hollande, 1930; Cameron, 1934). However, examination of other bacteria screened and reported as avirulent in *Gm* by Cameron and Metalnikov (see literature review Chapter 1) and studies conducted more recently (2000s onwards), resulted in considerable levels of disagreement. Many

bacterial species, previously reported as avirulent, were in fact virulent in *Gm*. These included: *M. smegmatis M. avium*, *V. cholerae*, *S. pyogenes*, *S. pneumoniae*, and *S. dysenteriae* (Cameron, 1934; Loh et al., 2013; Barnoy et al., 2017; Ignasiak & Maxwell, 2017; Bokhari et al., 2017; Entwistle & Coote, 2018; Cools et al., 2019). It is unclear why such widespread discrepancy has occurred between past and present studies. Nevertheless, it is clear that a re-evaluation of *Gm* as a candidate model to study virulent TB infection is warranted under these circumstances.

In this Chapter, *Gm* was re-evaluated as a model host for MTBC, via a proof-of-concept study utilising BCG *lux* as a surrogate for *MTB*. BCG *lux* was selected as surrogate as BCG is considered a standard surrogate amongst TB researchers and can easily be handled under CL2 conditions, minimising the biosafety risks associated with CL3 (Altaf et al., 2010; Harris et al., 2014; Turner et al., 2015; Yuan & Sampson, 2018; Painter et al., 2020). BCG *lux* has been genetically modified to be bioluminescent, and emitted light has been used as a measure for relative mycobacterial load (Snewin et al., 1999; Kampmann et al., 2000, 2004, 2006; Tena et al., 2003; Martineau et al., 2007a; Martineau et al., 2007b; Newton et al., 2008; Andreu et al., 2010; Newton et al., 2011; von Both et al., 2018). Application of luminescence measurement in *Gm* was optimised as part of this proof-of-concept work. I hypothesised that, based on recent *Gm* studies involving NTM, early *M. bovis* infection of *Gm* was incorrectly classified as avirulent. I therefore anticipated that BCG *lux* infection would be virulent for *Gm*.

3.2 Results and Discussion

3.2.1 Assessment of BCG lux virulence in Galleria mellonella

The virulence of BCG *lux* in *Gm* was assessed over a 96 h time course by recording survival of *Gm* larva following injection of a range (10^5 to 10^7 CFU) of BCG *lux* inocula (**Figure 3.1**). BCG *lux* was virulent in *Gm*, with larval survival decreasing as the BCG *lux* inoculum increased. Infection of *Gm* with 2 x 10^7 CFU of BCG *lux* resulted in 98% mortality over 96 h, whereas infection with 10^{5-6} CFU of BCG *lux* resulted in a non-lethal infection with 100% survival. The $LD_{50,}$ which is the infectious dose required to achieve ~50% killing over a desired period of observation, was 1 x 10^7 CFU at 96 h. All *Gm* infected with a dose >10^6 CFU of BCG *lux* displayed signs of sickness (melanisation, reduced motility and visible wasting) which increased in severity over time (**Figure 3.2**). The duration of the time course (96 h) was chosen based on the rate of *Gm* pupation (**Figure 3.2**), as the control groups (naïve and PBS) began to pupate, entering their next stage of life, around this time, with ~10 % and 30 % of the control group populations pupating at 96 and 168 h, respectively. As *Gm* are an environmental pest, pupae were euthanised by freezing and disposed of in an appropriate manner. Where *Gm* pupation was unavoidable during the study period, pupae were discarded and recorded as having survived.

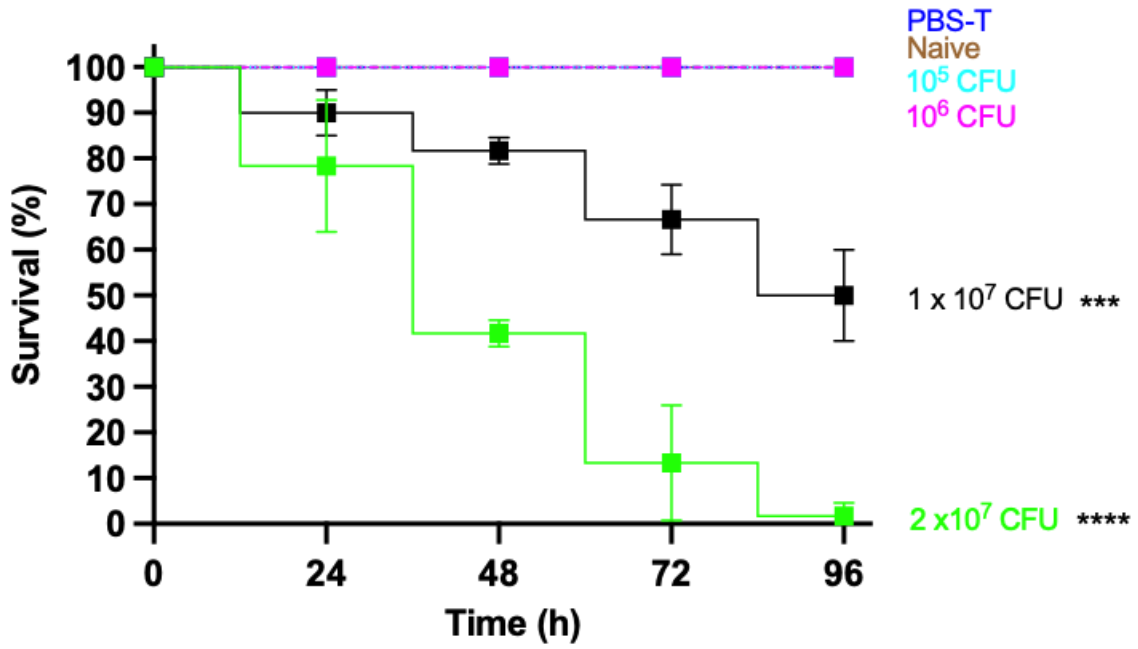


Figure 3.1: Assessment of BCG *lux* virulence in *G. mellonella*. Larvae were infected with corresponding doses of BCG *lux*. Mock infection (PBS-T) and unmanipulated (naïve) *Gm* were included as control groups. Larvae were incubated in the dark at 37 °C following infection, and larval survival monitored every 24 h for 96 h. Plotted are the means of three independent experiments, and the error bars represent the SD of the means. Sample size per experiment was n = 20 for BCG $10^{6\text{-}7}$ CFU, n = 10 for BCG *lux* 10^5 CFU and the control groups (Naïve and PBS-T) n = 10. Mantle-Cox log-rank test with Bonferroni's correction against PBS-T where *** ($p < 0.001$) and **** ($p < 0.0001$). Adapted from Li et al., 2018.



Figure 3.2: Physical changes to *G. mellonella* following infection with BCG *lux*. Larvae were infected with 1 x 10^7 CFU of BCG *lux* and melanisation (darkening of larval body) were monitored every 24 h over a 96 h time course. Healthy control larva and larva that have undergone pupation are represented by 0 h and pupa, respectively.

The effect of experimental procedures (i.e., needlestick injury, “pricking” or injection of PBS-T) on the survival outcome of *Gm* was examined as controls (**Figure 3.3**). The experimental procedures did not influence *Gm* survival. While it is evident that virulence of BCG *lux* in *Gm* is dependent on the infectious dose, it is unclear if this is dependent on the active production of virulence factors by live BCG *lux*, a response to cell surface virulence factors, or the sheer abundance of injected bacilli. Therefore, in order to assess these parameters, *Gm* were infected with heat-treated BCG *lux* at a virulent dose (1 x 10^7 CFU). HT BCG *lux* did not cause lethal effects in *Gm*, with 100% survival following 96 h incubation (**Figure 3.3**). Furthermore, infected larvae showed no signs of melanisation, were active and some pupated thereby indicating that the virulence of BCG *lux is* dependent on the viability of the inoculum. Taken together, these results indicate that like other pathogens previously found to be avirulent by Cameron and Metalnikov, wild-type (WT) *M. bovis,* a member of the MTBC complex, likely can cause virulent infection in *Gm* (Metalnikov, 1920; Cameron, 1934).

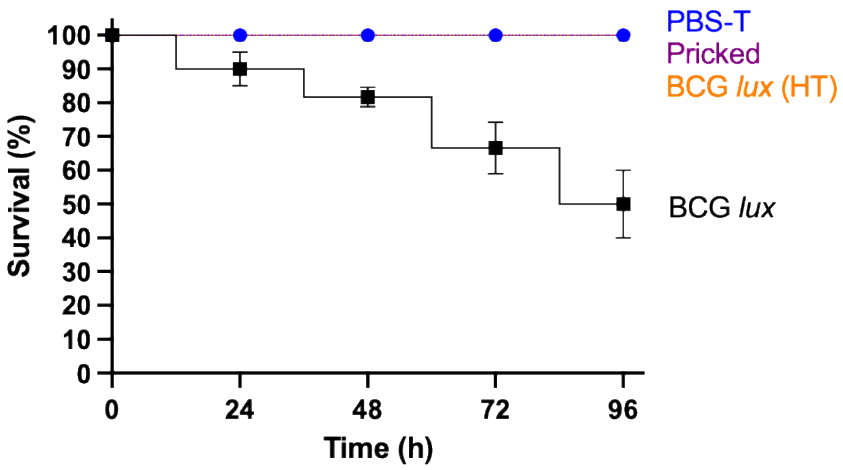


Figure 3.3: Impact of experimental procedures and BCG *lux* viability on *G. mellonella* survival. The effects of needlestick injury (pricked), injection of PBS-T and the viability of BCG *lux* (using HT inocula, 1 x 10^7 CFU) on larval survival was measured over 96 h. Plotted are the means of three independent repeats, and error bars represent the SD of the means. BCG *lux* (1 x 10^7 CFU) was used as a virulent control. Sample size per experiment was n = 10 for pricked and PBS-T groups, and n = 20 for BCG *lux* (LD_{50} and HT). Mantle-Cox log-rank test with Bonferroni's correction revealed no statistical difference between the PBS-T and HT infected larvae.

A closer inspection of Cameron's methodology identified the potential source of the discrepancies in the observed virulence (Cameron, 1934). Cameron cultured, *MTB*, *M. bovis* and *M. avium* on Dorset's egg medium, Petroff's medium and Kobayashi's medium respectively. Incubated medium was dissolved into sterile Ringer's solution to prepare a mycobacterial inoculum of 2 x 10^9 CFU/ml. For injection, 20 µl of this suspension equating to 4 x 10^7 CFU, were injected into larvae. Infected larvae suffered no adverse effects, progressing into adult moths (Cameron, 1934), despite being infected with double the dose required to achieve near 100% killing in 96 h, as presented in this Chapter. If such practice was standard at the time, Metalnikov and Hollande could have similarly prepared their inoculum directly from colonies grown on the medium or from specimens (e.g., Guinea pig lungs), without carrying out broth sub-culturing. Mycobacterial colonies found on solid medium are predominantly represented by bacilli in stationary phase of bacterial growth. Log growth

phase bacilli only represents a small sub-set of this population, in the outer rims of the colonies. Preparation of inoculum directly from metabolically dormant, starving or dying bacteria, would not properly represent the virulent phenotype of pathogenic mycobacteria. Therefore, it is likely that the virulence of inoculum prepared by Cameron and others more closely resembles infection of *Gm* with lower doses of BCG *lux* (10^{5-6} CFU), which similarly led to non-lethal infection as presented in this Chapter. In support of this hypothesis, larvae infected with 10^5 CFU of BCG *lux* showed no ill effect and pupated but ZN stain of a haemocyte smear slide prepared 96 h post-infection showed the presence of BCG *lux* bacilli in the haemolymph. These data are in-line with observations made by all three authors (Metalnikov, 1920; Hollande, 1930; Cameron, 1934).

Moreover, the pathogenicity of BCG *lux* and *M. bovis* used by early studies in *Gm* is perplexing, as the attenuated BCG *lux* was more virulent than the pathogenically superior "mother" *M. bovis* isolate. Nevertheless, as a vaccine strain, a level of virulence is retained by BCG to induce an immunogenic reaction in the host. Currently more than 20 BCG strains are available (Ritz & Curtis, 2009). All vaccine strains commonly lack the RD1 region, which encodes for the ESAT-6 secretion system (ESX-1) (Type VII secretion system) and virulence factors, the 6-kDa early secreted antigenic targets (ESAT-6) and the 10-kDa culture filtrate protein (CFP-10) (Mostowy et al., 2003; Etna et al., 2015; Ly & Liu, 2020). *MTB* synthesise the virulence factors ESAT-6 and CFP-10, which are secreted by ESX-1 to induces cytolysis of the infected host cells, disseminating mycobacteria to the surrounding environment, thereby promoting progression of the disease (Hsu et al., 2003). The deletion of RD1 is believed to be the crucial element in the attenuation of virulent *M. bovis* to BCG by Calmette and Guérin. A comparative virulence study of 13 BCG strains, identified BCG Montréal (also known as Frappier), as one of the most

virulent in severe combined immunodeficiency (SCID) mice (Zhang et al., 2016). The virulence of BCG is likely attributable to phthiocerol dimycocerosates (PDIMs) and phenolic glycolipids (PGLs) (Liu et al., 2009). Antigenic protein MPB83 is secreted by BCG Montréal, but in trace levels due to mutation of the regulatory gene *sigK*; however, the precise function of MPB83 remains unknown (Charlet et al., 2005). PDIMs mediate mycobacteria receptor dependent phagocytosis (Astarie-Dequeker et al., 2009), regulates cell wall permeability (Camacho et al., 2001) and protects mycobacteria from nitric oxide stress in macrophages (Rousseau et al., 2004). PDIMs also contribute to phagosomal escape and induce host cell autophagy (Quigley et al., 2017). PGLs can enhance macrophage recruitment and invasion (Tabouret et al., 2010; Cambier et al., 2013). Furthermore, duplication of regulatory genes, *sigH* and *whiB1* in BCG, which are critical for management of oxidative and nitric oxide stress repose (Zhang et al., 2016), may enhance the ability of BCG *lux* to survive the harsh intracellular conditions and enter non-replicative state (Brosch et al., 2007).

Comparison of the BCG *lux* virulence reported here against published NTM-*Gm* data (Entwistle & Coote, 2018; Meir et al., 2018) was challenging due to the difference in mycobacterial species, strains, CFU inocula and differences in virulence of species and strains used. In Entwistle and Coote's study, *Gm* infection with *M. fortuitum* at 1 x 10^7 CFU, lead to 0% survival over 96 h (Entwistle & Coote, 2018); in contrast using BCG *lux* at equivalent dose, infection led to 50% survival. Such difference in *Gm* survival between BCG *lux* and *M. fortuitum* infected larvae are likely influenced by differences in virulence mechanisms and the rate of bacterial growth (Entwistle & Coote, 2018). Reflecting on the faster growth of NTM, virulent inocula were typically 2-3 log CFU lower than with BCG *lux* (Entwistle & Coote, 2018; Meir et al., 2018; Kirubakar et al., 2020). *M. abscessus* survived best in *Gm,* with growth of

3.5 log CFU reported following infection with 10^3 CFU and 6 days of incubation (Meir et al., 2018). *M. fortuitum* required higher inocula CFU as the innate immune response was capable of eliminating a large proportion of injected mycobacteria (Entwistle & Coote, 2018).

3.2.2 Survival of BCG lux within Galleria mellonella following infection

To further evaluate *Gm* as a host for mycobacteria, survival of BCG *lux* (1 x 10^7 CFU) within *Gm* was monitored over a two-week time course. The changes in BCG *lux* load *in vivo* were determined at various time points (0, 24, 48, 72, 96, 168 and 366 h) through luminescence measurement of BCG *lux* found in the *Gm* homogenate (n = 5 per time point). The luminescent property of BCG *lux* originates from the inclusion of the plasmid, pSMT1, carrying the *V. harveyi luxAB* gene (Snewin et al., 1999). Light emission is dependent on the enzymatic conversion of co-factor, reduced flavin mononucleotide ($FMNH_2$) to flavin mononucleotide (FMN) by the bacterial luciferase (LuxAB), catalysed by the addition of decanal (aldehyde) as substrate (Brodl et al., 2018). The co-factor $FMNH_2$ is produced only in viable or metabolically active cells, thereby availability of $FMNH_2$ reduces with dead or metabolically inactive cells (Snewin et al., 1999). Application of luminescence as a measure of viable bacteria has been previously confirmed using both the *in vitro* (cell lines) and *in vivo* (mouse) infection models (Snewin et al., 1999; Kampmann et al., 2004; Newton et al., 2011).

First, optimisation of recovery of *Gm* homogenate was carried out to ensure all essential material were recovered from the lysis matrix. When the crude homogenate was decanted, the residue of the homogenate was retained within the tube (**Figure 3.4A**). Pipetting the remaining crude homogenate was not feasible as larger debris often led to blockage of the pipette tip. Washing of the lysing matrix tube was required, to consistently recover maximal

quantity of samples. Sample recovery was assessed using *Gm* homogenate prepared from larvae infected with 1 x 10^6 CFU of BCG *lux*. Recovery efficacy between single or double washing, using 1 ml of PBS-T at each step was assessed. A single wash was sufficient to recover the remaining residue from the tube, with no significant improvement seen in recovered luminescence with additional washing steps (**Figure 3.4B**). Similarly, inclusion or exclusion of metal beads made no significant impact on measured luminescence. A baseline background luminescence emitted by the larva, averaged at 7 x 10^3 RLU/ml (ranging from 5 - 8 x 10^3 RLU/ml [n = 5]).

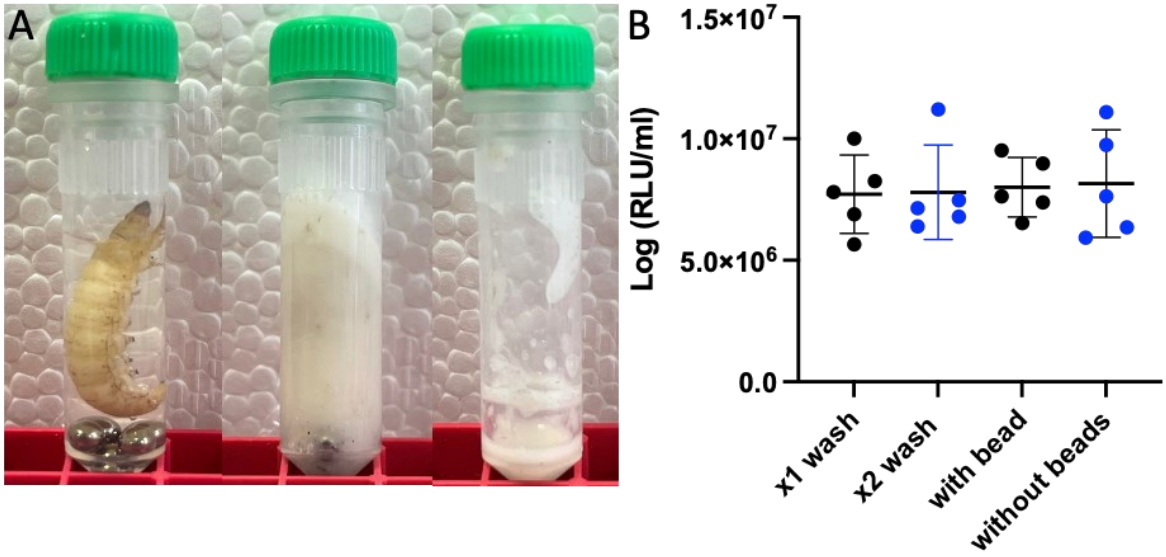


Figure 3.4: Optimisation of *G. mellonella* homogenate recovery from lysing matrix tubes. Larvae infected with 1 x 10^6 CFU of BCG *lux* were homogenised in lysing matrix tubes (n = 5 per group), and the luminescence (RLU) of the homogenate was measured. (A) Larvae were homogenised in PBS-T and six 1/8" steel beads, homogenates were decanted, and lysing matrix tubes were washed once or twice each with 1 ml of PBS-T to recover residual homogenate. Images show larva at pre- and post-homogenisation and the residual homogenate left within the lysing matrix tube following sample decantation. (B) RLU of total homogenate was measured following either one or two PBS-T washing steps. Plotted are the means and the SD of the means from a single independent experiment. Non-parametric Mann-Whitney test between x1 and x2 wash, and beads and without beads, indicated no significant difference.

To give context to the BCG *lux* luminescence data, the correlation between RLU and CFU in *Gm* was determined. Four time points, reflecting early (0 and 24 h), mid (96 h) and late (168 h) stage infection were chosen retrospectively for CFU enumeration, based on changes to BCG *lux* luminescent activity over the two-week time course (**Figure 3.6**). Infected (1 x 10^7 CFU) larvae were homogenised (n = 4, per time point), and 10 μl of crude homogenates were plated onto Middlebrook 7H11 agar for CFU enumeration; and the luminescence of the remaining homogenate was determined. However, contamination was detected on the agar plate after overnight incubation, which originated from the native *Gm* flora. Entwistle and Coote reported similar observations in their *Gm*-NTM study. PIP was found to inhibit the growth of the *Gm* flora, without effecting the growth of NTM (Entwistle & Coote, 2018), however the concentration of PIP used was not reported in their publication.

The susceptibility of BCG *lux* to PIP was determined via MIC assay to assess feasibility of its use to enumerate BCG *lux* from the *Gm* homogenate. PIP was tested at concentrations between 1280 μg/ml and 10 μg/ml in a two-fold serial dilution. BCG *lux* was highly tolerant of PIP with a defined MIC of 160 μg/ml. Middlebrook 7H11 agar containing 1, 10, and 20 μg/ml of PIP was prepared to determine an inhibitory concentration for *Gm* flora. *Gm* homogenates of naïve larva were plated (10 μl) and incubated overnight. Agar containing 10 and 20 μg/ml of PIP successfully inhibited the *Gm* flora, whereas 1 μg/ml failed to inhibit the growth. As a result, Middlebrook 7H11 agar containing 10 μg/ml was chosen as the optimal concentration and CFU of BCG *lux* were successfully enumerated without contamination at 0, 24, 96 and 168 h post-infection. The average RLU:CFU ratio *in vivo* was 4:1, ranging from 2:1 to 5:1 (**Figure 3.5**). This was in line with the *in vitro* (Middlebrook 7H9 broth) RLU:CFU ratio of 3:1. These findings confirm that luminescence, proportionately and more importantly relatively, reflects

the changes in viable BCG *lux in vivo*, over the course of infection. Luminescence measurement as relative output of CFU, is an established *in vivo* methodology and has been applied to *M. abscessus* and *Enterococcus faecalis Gm* infection models in the past (La Rosa et al., 2013; Meir, Grosfeld and Barkan, 2018).

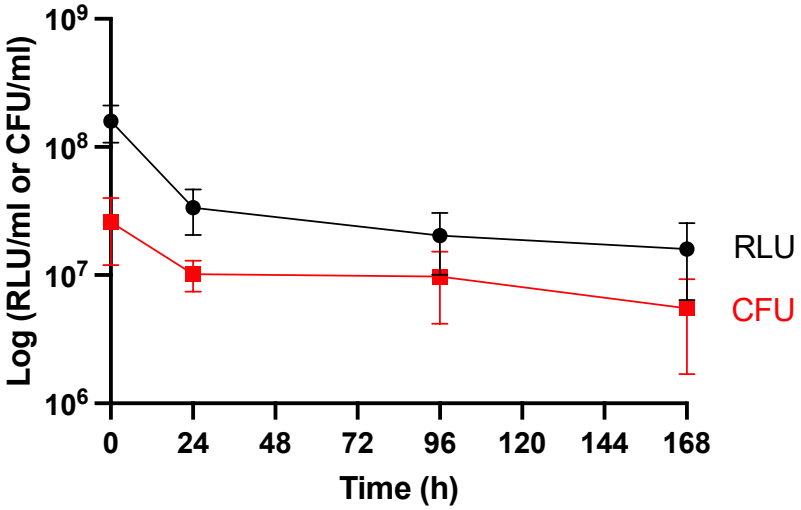


Figure 3.5: *In vivo* correlation of BCG *lux* luminescence and CFU in *G. mellonella*. Larvae (n = 30) were infected with 1 x 10^7 CFU of BCG *lux* and CFU and luminescence (RLU) measurements were taken at 0, 24, 96 and 168 h post-infection to determine RLU:CFU ratio (n = 4, per time point). Plotted are the means of two independent experiments, and the SD of the means. Adapted from Asai et al., 2019a.

Homogenates of BCG *lux* (1 x 10^7 CFU) infected larvae, prepared using the optimised method, revealed that luciferase activity could be detected throughout the two-week time course (**Figure 3.6**). Once injected, the luminescence of BCG *lux* rapidly declined within the first 72 h of infection (~0.70 log RLU). The luminescence of BCG *lux* continued to decline steadily between 72 h and 336 h post-infection (~0.25 log RLU), levelling off into a plateau. Overall, approximately 1 log RLU unit reduction was recorded over two-weeks. These results indicate a strong initial response from the innate immune system of *Gm* to clearly eliminate BCG *lux*, leading to a substantial reduction in luminescence. However, *Gm* was unable to fully clear the

infection, and BCG *lux* establishes a persistent infection, as indicated by the plateau in luminescence. Batch variability in starting luminescence was detected (**Figure 3.5 and 3.6**) despite standardised preparation of inocula (consistent RLU measurement *in vitro*, OD and CFU of inocula checked) and no changes in virulence were observed between periods of experimentation. Changes were likely caused by variability in BCG *lux* (stocks and media) and *Gm* quality. These data were not discouraging as the trend in luminescence was consistent (Chapter 2.2.3).

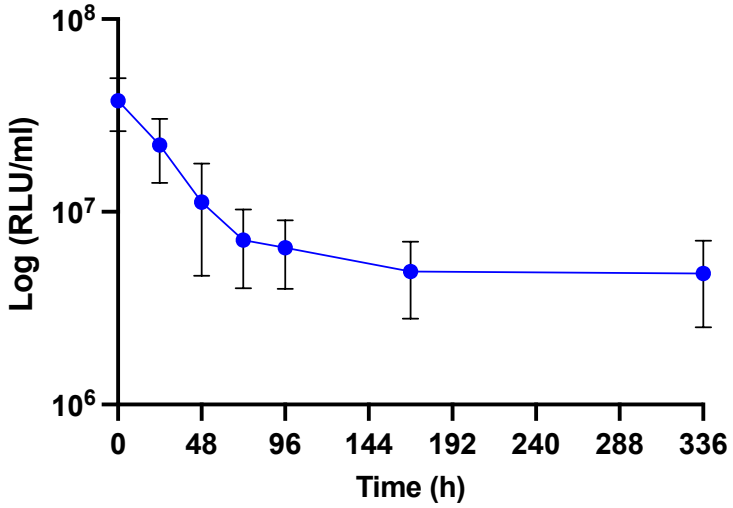


Figure 3.6: Survival of BCG *lux* within *G. mellonella* using luminescence as a measure of relative mycobacterial abundance. Larvae (n = 30) were infected with 1 x 10^7 CFU of BCG *lux*. The luminescence (RLU) of BCG *lux* within the *Gm* homogenate was measured to determine the relative abundance of BCG *lux* over the two-week time course. At each time point, n = 5 were sacrificed. Plotted are the means of three independent experiments, and the error bars represent the SD of the means. Adapted from Li et al., 2018.

3.2.3 Interaction of BCG lux with Galleria mellonella haemocytes

Co-localisation of BCG *lux* bacilli with circulating haemocytes were visualised under standard light microscopy. Infected larvae were bled for their haemocytes at 24 h and 96 h post-infection (n = 3 per time point). Smear slides were prepared and ZN stained, visualising both the haemocytes and BCG *lux* bacilli (**Figure 3.7**). At 24 h post-infection, individual bacilli or

clusters of BCG *lux* bacilli co-localised with *Gm* haemocytes (**Figure 3.7A**). It was not possible to confirm internalisation of BCG *lux* by the haemocytes using standard light microscopy. By 96 h post-infection aggregates of haemocytes (~ 15 cells in a single 2D visual plane) were observed by microscopy, which co-localised with a large cluster of BCG *lux*, running along the whole length of aggregated haemocytes (**Figure 3.7B**).

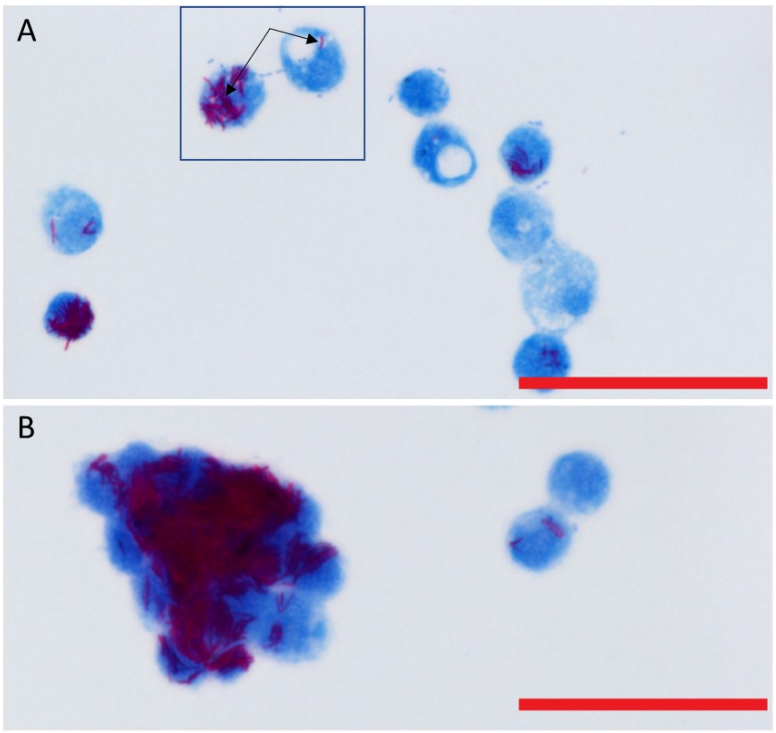


Figure 3.7: Ziehl-Neelsen stain of *G. mellonella* haemocytes infected with BCG *lux*. Larvae were infected with 1x10^7 CFU of BCG *lux* and bled for haemocytes at 24 h (A) and 96 h (B) post-infection. Haemocyte smear slides were prepared and stained using ZN staining. (A) At 24 h post-infection haemocytes (boxed) co-localised with individual or small clusters of bacilli (arrows). (B) By 96 h post-infection aggregates of haemocytes co-localised with large clusters of bacilli were observed. Scale bars represent 50 μm. Adapted from Li et al., 2018.

The co-localisation of BCG *lux* bacilli and *Gm* haemocytes was further characterised using TEM (**Figure 3.8**). Samples for TEM were collected from infected (1 x 10^7 CFU) larvae at 24, 48, 72, 96, 144 and 366 h post-infection (n = 10, per time-point). BCG *lux* inoculum and haemocytes of naïve larva were examined as controls (n = 10). *Gm* haemocytes contained ultrastructurally

internalised bacilli at 24 h post-infection (**Figure 3.8A**), which was lacking from the naïve haemocyte control (**Figure 3.8I**). Over the course of two-weeks, intracellular aggregates of bacilli typically associated with granulomas were present, indicating that BCG *lux* invaded and/or were phagocytosed by haemocytes (**Figure 3.8A-G**). TEM data supports co-localisation of BCG *lux* bacilli with the haemocytes as seen in **Figure 3.7**, and is suggestive of internalised bacilli. Furthermore, TEM detected accumulation of what appears to be lipid material within the BCG *lux* bacilli from 48 h post-infection onwards, which was absent in the BCG *lux* bacilli control (**Figure 3.8D-H**)**.**

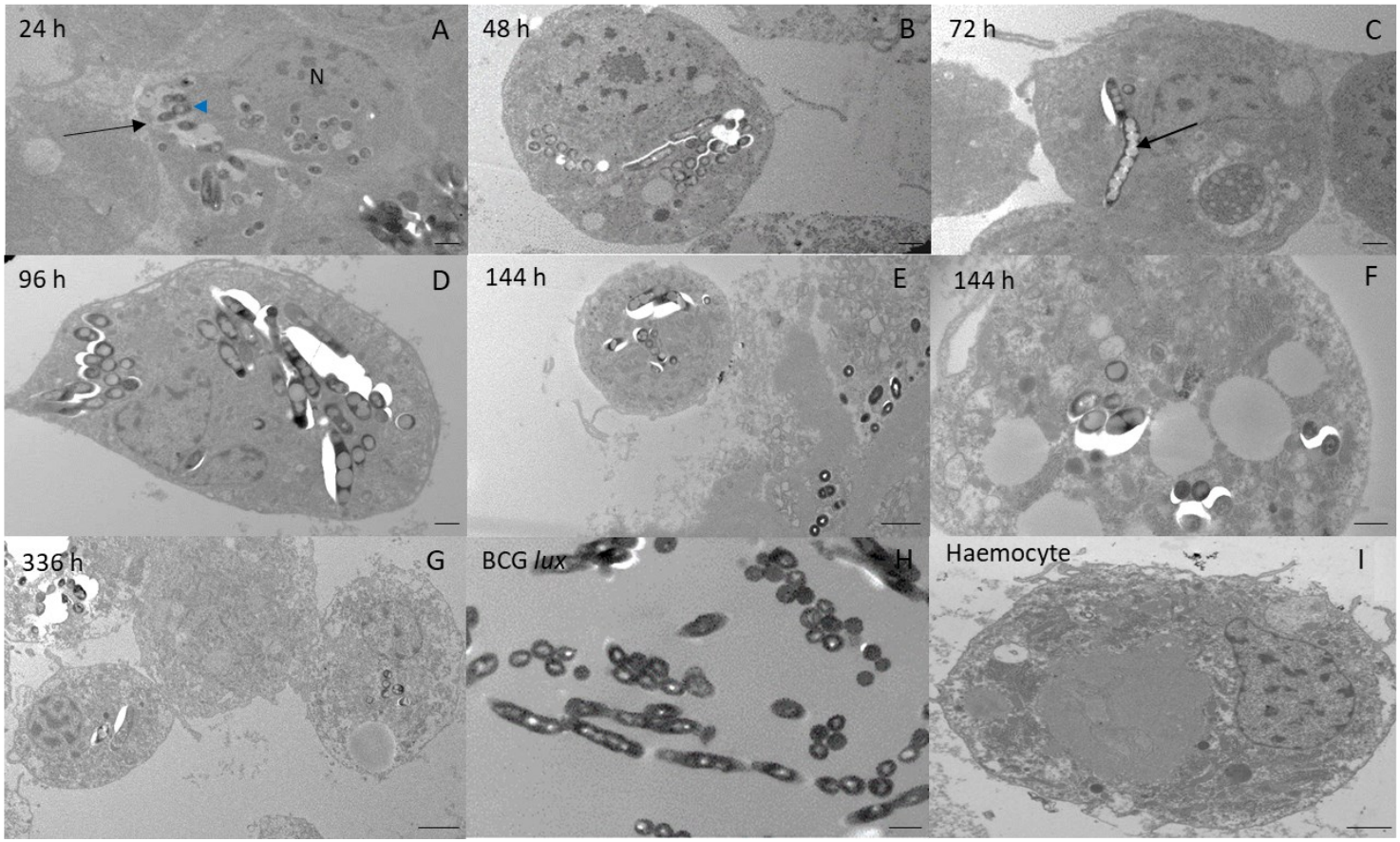


Figure 3.8: Transmission electron microscopy of *G. mellonella* haemocytes infected with BCG *lux*. Larvae infected with BCG *lux* (1 x 10^7 CFU) were bled (n = 10) at 24 h (A), 48 h (B), 72 h (C), 96 h (D), 144 h (E, F) and 336 h (G) post-infection. BCG *lux* inoculum (H) and haemocytes of naïve (uninfected) larva were provided as controls. By 24 h (A) post-infection, internalisation of BCG *lux* (blue arrowhead) by haemocyte (black arrow, N = nucleus) was observed. Single and aggregates of intracellular BCG *lux* were observed throughout the two week time course (A-G), from 72 h (D) post-infection onwards, accumulating lipids (black arrow) typically associated with non-replicating and persistent mycobacteria. These images are representative of *Gm*-BCG *lux* interaction at a given time point. Scale bar represents 500 nm (A-D, F, H-I) and 2 µm (E, G). N = nucleus. Adapted from Li et al., 2018.

The observed accumulation of lipid material within the bacilli over time was of particular interest, as the formation of intracytosolic lipid inclusions (ILI) primarily formed of triacyl-glycerol (TAG), has previously been reported amongst *MTB* located inside lipid rich foamy macrophages of human granulomas (Peyron et al., 2008; Russell et al., 2009). Such a phenotype is considered a hallmark of persistent and non-replicating mycobacteria in LTBI (Santucci et al., 2016). *MTB* has been reported to accumulate large quantities of TAG in response to multiple combination of stress factors such as acidic, hypoxic, and or nutrient limitations (Deb et al., 2009). It is speculated that *MTB* metabolises the TAG accumulated in the ILI, as a source of carbon and energy during the non-replicating and persistent phase of infection through unknown mechanisms (Daniel et al., 2011). While a number of key and essential enzymes for TAG biosynthesis in mycobacteria have been identified, further research is required to fully understand lipid metabolism, biosynthesis, and regulation in mycobacteria (Asis et al., 2021). The ILI formation by BCG *lux* in the *Gm* model, with optimisation, could lead to the establishment of a non-replicative persistent or dormant TB infection model, which would be a desirable addition as a more accessible alternative to the complex and costly pre-existing animal models (Santucci et al., 2016).

During infection, BCG *lux* likely acquired lipids or an intermediate from the host. The insect fat body (analogous to the human liver) is a multicellular tissue responsible for the synthesis, transport, accumulation and release of proteins, lipids, and carbohydrates (Skowronek et al., 2021); and is the most probable source of lipid material for BCG *lux* ILI formation. The activation of the innate immune response induces the synthesis and secretion of diglycerides into the haemolymph by the fat body, which accumulate as cytoplasmic lipid droplets (LD) within the haemocytes as seen in **Figure 3.8** (Péan et al., 2017; Skowronek et al., 2021).

In the fruit fly model, *M. marinum* infection led to the accumulation of cytoplasmic LD within the haemocytes and co-localisation of lipids with the internalised bacilli. This response was mediated by a *upd3* (IL-6 like cytokine) repression of *Atg2* (Péan et al., 2017). *Atg2* is a regulator of triglyceride synthesis, where overexpression altered accumulation of cytoplasmic LD, leading to a reduction in the number of viable *M. marinum* bacilli and co-localisation of bacilli with cytoplasmic LD. These observations were further validated in IL-6 treated BCG *lux* and SAMTB infected THP-1 and primary human macrophages, respectively (Péan et al., 2017). Treated cell-lines displayed increased mycobacterial survival outcome and cytoplasmic LD accumulation. This result indicates that mycobacteria appear to exploit host immunity in a similar manner between mammals and insects, to induce a more favourable intracellular environment for survival. Unfortunately, further investigations in *Gm* are limited by the lack of reagents and tools necessary to carry out equivalent experiments (e.g., lack of transgenic mutant). However, based on Pean's work, it's likely that BCG *lux* utilises similar mechanisms to form ILI in *Gm* and improve survival outcome.

3.2.4 BCG lux infection is systemic in Galleria mellonella

While infection of *Gm* is carried out via injection, the progression of infection from the site of injection is unknown. Based on the changes in appearance of the *Gm* larva (**Figure 3.2**) and the presence of mycobacterial bacilli in the haemolymph (**Figure 3.7**), a systemic infection of the whole larva was suspected. In order to assess the dissemination of inoculum from the point of injection, mock infection using 10 μl of amaranth dye (0.2%) was carried out on larva anesthetised on ice to decrease the rate of haemolymph circulation within the haemocoel (**Figure 3.9**). Amaranth (0.2%) was non-toxic to *Gm* and is typically metabolised in 24-48 h,

based on observed reversal to a healthy cream colour and lack of mortality 96 h post-injection. At the point of injection, the amaranth dye is localised at the site of injection (0 seconds post-injection). The dye begins to radiate from the site of injection with improvements in haemocoel circulation as the effect of ice immobilisation starts to wain off (20 seconds post-injection onwards). Full dissemination of the dye is achieved 80 seconds post-injection. In the absence of anesthetisation, near immediate distribution of the dye was achieved.

However, the movement of non-toxic amaranth dye within the haemocoel may not accurately represent the interaction between virulent *BCG lux* and *Gm*. Immune responses such as coagulation, may act to rapidly contain the inoculum at the site of injection minimising initial dissemination of the mycobacterial bacilli within the haemocoel. Therefore, using a combination of fluorescent BCG (FluorBCG), expressing YFP and Turbo635asv, the movement of FluorBCG (2.5 x 10^6 CFU) in *Gm* was monitored over 168 h using a proprietary handheld fluorescence camera (courtesy of Dr Brian Robertson, ICL). To minimise movement during imaging, *Gm* were anesthetised on ice.

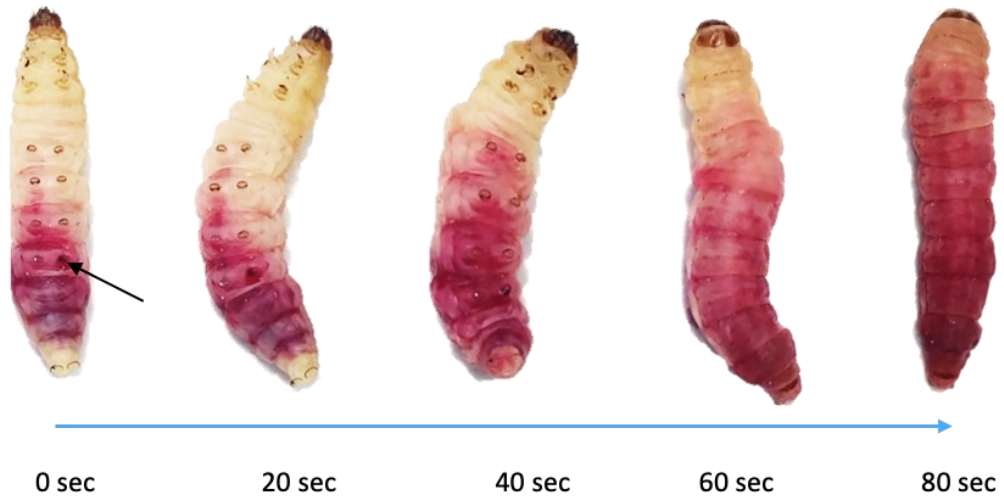


Figure 3.9: Dissemination of amaranth dye in *G. mellonella*. Anesthetised larvae were injected with 10 μl of 0.2% amaranth dye, via the last left proleg (indicated by the black arrow, 0 second post-injection) and the movement of the dye within the larval cavity was monitored over an 80 second time course.

At the point of infection, movement of FluorBCG from the terminal segment (area near the site of injection) was visualised through the dorsal vessel of the haemocoel (**Figure 3.10A**). Foci of infection were established throughout the larval body over the course of 168 h (**Figure 3.10B**). As the infection progressed, foci became more pronounced with reduction in the diffusion of YFP signal throughout the larval body, suggesting that FluorBCG were contained more tightly over time. While full dissemination of FluorBCG was achieved, foci were more densely packed towards the terminal segment of the larva, nearer to the site of injection. Quantification of FluorBCG in *Gm* was not carried out, as the purpose of this experiment was to simply demonstrate the dissemination of mycobacteria in *Gm* using fluorescence.

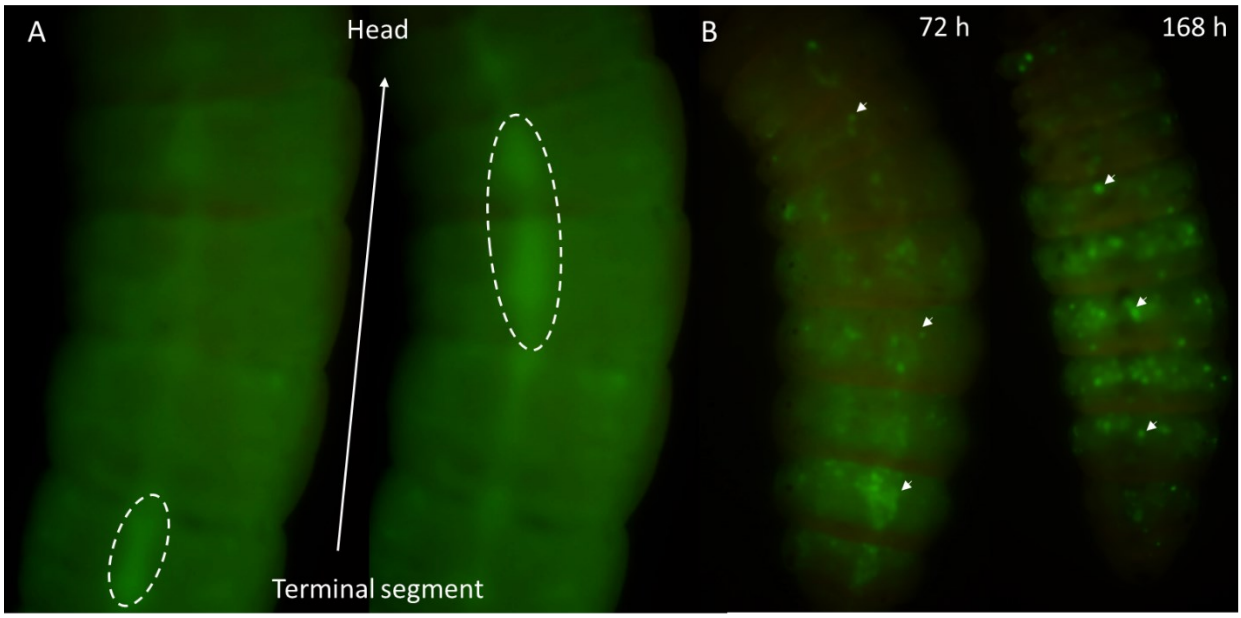


Figure 3.10: Dissemination of FluorBCG in *G. mellonella.* Larvae were infected with 2.5 x 10^6 CFU of FluorBCG. (A) The movement of FluorBCG (highlighted by the dotted lines), from terminal segment (site of injection) to the head of the larva via the dorsal vessel of the haemocoel immediately following injection. (B) Systemic dissemination of FluorBCG is represented by foci of infection throughout the larva (highlighted by the white arrow heads), which increases in definition and intensity as infection becomes more compartmentalised over time. Panel A represent the same larva over time. Panel B is a representative of larvae at a given time point.

3.2.5 Galleria mellonella forms granuloma-like structures in response to BCG lux infection

To further characterise the *Gm*-BCG *lux* interaction, ZN and H&E histopathological sections of infected larvae (1 x 10^7 CFU) were prepared over a two-week time course. As early as 24 h post-infection, granuloma-like structures containing both loose (**Figure 3.11A**) and densely packed bacilli were identified (**Figure 3.11E**). As the infection progressed (72 h [**Figure 3.11B**], 96 h [**Figure 3.11C**] and 336 h [**Figure 3.11D**] post-infection), granuloma-like structures became more organised. The appearance of ZN stained mycobacteria changed over time from individual bacilli (**Figure 3.11A**) to indistinguishable amorphous acid-fast material (**Figure 3.11C, D**), indicating mycobacterial degradation, which appears to have radiated from the centre of the structure (**Figure 3.11C**).

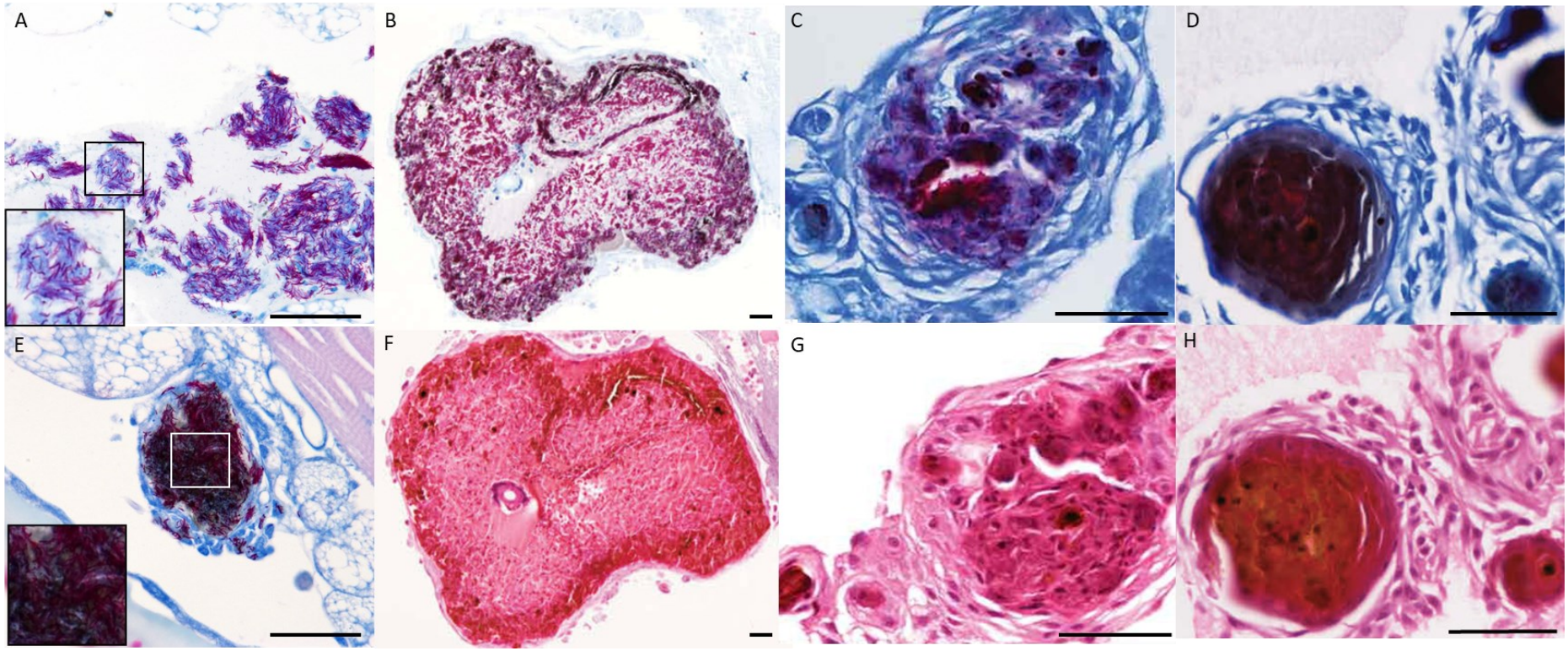


Figure 3.11: Histological sections of *G. mellonella* infected with BCG *lux* over a two-week time course. BCG lux (1 x 10^7 CFU) infected larval tissue sections (n = 3, per time point) were stained with ZN, (A-E) or H&E, (F-H). At 24 h post-infection, granuloma-like structures with loosely (A, magnification provided [black insert]) or tightly (E, magnification provided [white insert]) aggregated BCG *lux* bacilli were formed. As infection progressed (72 h [B, F], 96 h [C, G] and 336 h [D, H]) these became more organised, with *Gm* cells surrounding infected cells. ZN stain (C, D) showed staining of amorphous acid-fast material indicating mycobacterial degradation. The formation of granuloma-like structures was associated with host cell necrosis, as indicated by the differential staining of *Gm* cell nucleus (F-G). Scale bars represents 50 µm (A-H). Adapted from Li et al., 2018.

The H&E stains (**Figure 3.11F-H)** corresponding to the ZN stains (**Figure 3.11B-D**), shows *Gm* cells have undergone necrosis in areas associated with the presence of BCG *lux* bacilli, as indicated by the deeper stain and/or the lack of nuclear staining. These granuloma-like structures increased in size and numbers over the course of infection, distributed throughout the larval body (**Figure 3.12**), as previously indicated by the dissemination of FluorBCG (**Figure 3.10B**). Similarly, granuloma-like structures were more abundant towards the terminal segment of the larva (**Figure 3.12, 168h**).

The granuloma-like structures identified here, closely resemble the multi-cellular structures described by Cameron as "nodules" in *MTB* infected *Gm* (Cameron, 1934). Generally, the formation of granuloma-like structures or nodules are thought to be a generic and non-specific response of plasmatocytes and granulocytes, designed to isolate non-host material (Gandhe et al., 2007; Hillyer, 2016). Furthermore, granuloma-like structures and nodules have been reported in other *Gm*-bacterial (e.g., *M. abscessus, E. coli* and *C. perfringens*) and fungal (e.g., *C. albicans* and *A. fumigatus*) models, supporting the idea that such responses are broad and non-specific (Perdoni et al., 2014; Sheehan et al., 2018a; Kay et al., 2019; Chen & Keddie, 2021). Nevertheless, the ability of *Gm* to reproduce granuloma-like structures is beneficial for modelling granulomatous disease such as those caused by MTBC and *M. mycetomatis* (Kloezen et al., 2015; Sheehan et al., 2020b). Furthermore, as the invertebrate innate immune system is capable of distinguishing pathogen class and selectively synthesising AMPs, the induction of pathogen-specific variation in structural composition of granuloma-like structures or "nodules" cannot be ruled out.

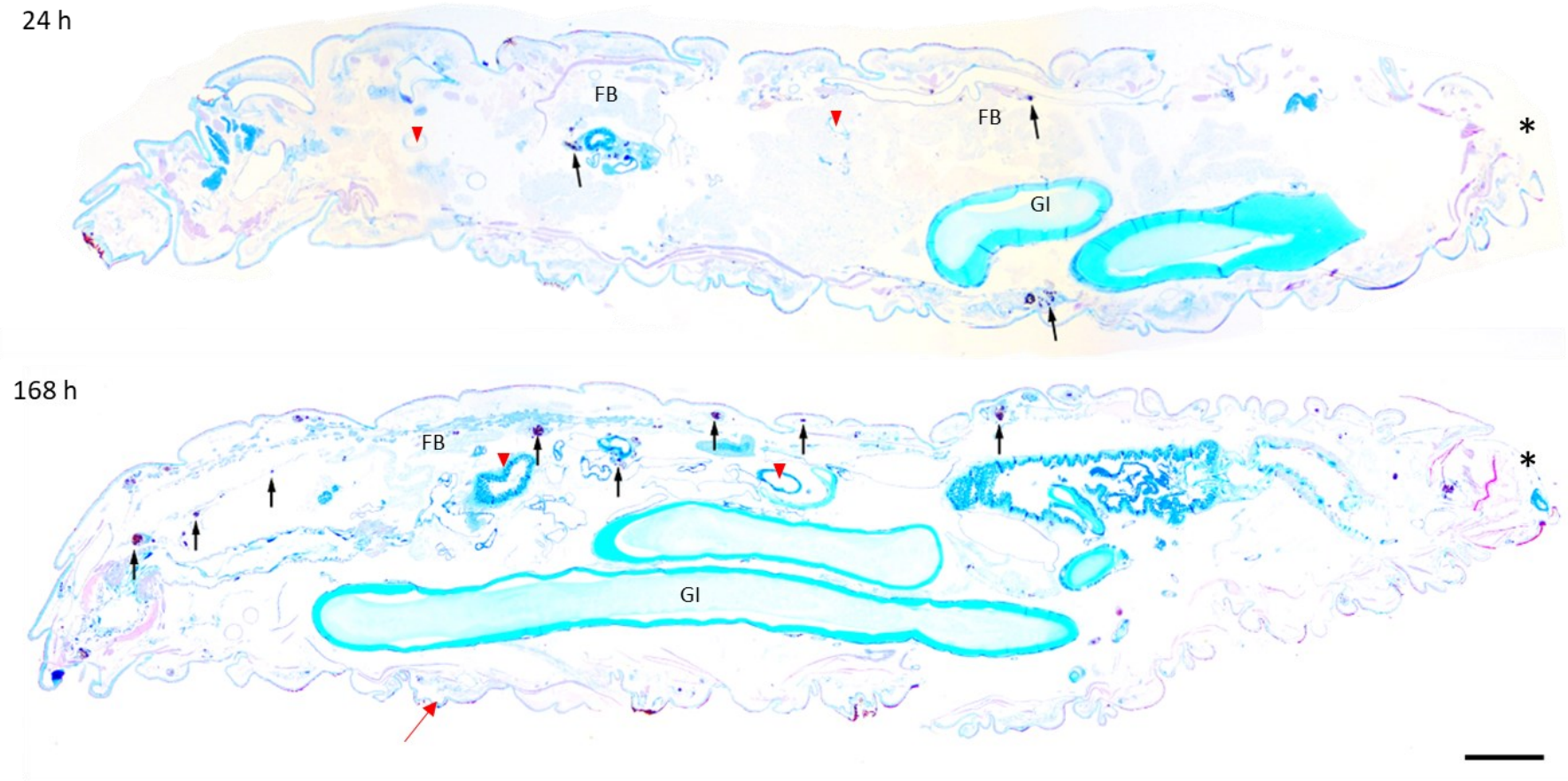


Figure 3.12: Development of granuloma-like structures in *G. mellonella* infected with BCG *lux*. Sagittal cross-section of larva infected with BCG *lux* (1 x 10^7 CFU) at 24 h and 168 h post-infection. Granuloma-like structures (black arrows) can be found throughout the larval body, typically associated with the fat body (FB), in increasing frequency and in size, over the course of infection. GI represents gastrointestinal tract, downward triangle (red) indicates trachea, * signifies the head and red arrow indicates site of injection. Scale bars indicate 1000 µm.

3.3 Conclusion

In this Chapter, *Gm* was re-evaluated as a model host to study infection with members of the MTBC following reports that they were avirulent in this model by Metalnikov, Hollande and Cameron in early *Gm* research conducted in the 1920s and 1930s. Such evaluation was warranted as inconsistencies were apparent amongst past (1920s and 1930s) and present (2000s onwards) virulence data a number of bacterial pathogens.

This proof-of-concept study demonstrated that BCG *lux,* a member of the MTBC complex, can cause virulent infection in *Gm*, in a mycobacterial dose and viability dependent manner. Observations of this study contradicted reports of avirulent infection at four times the dose required to induce 50% mortality in this study (Cameron, 1934). Differences in mycobacterial inoculum (log phase vs stationary) preparation were possible causes of this discrepancy. Injection of mycobacteria led to rapid dissemination throughout the larval body causing systemic infection. The luminescence of BCG *lux* measured from the larval homogenate was an accurate and reproducible measure of mycobacterial viability in *Gm*. The luminescence (RLU) and CFU of BCG *lux* growing within *Gm* correlated. BCG *lux* establish a non-replicative but persistent infection in *Gm* over the course of two-weeks. Co-localisation and internalisation of BCG *lux* was visualised through microscopy, where internalised BCG *lux* formed ILI over time, taking on a non-replicative phenotype typically observed in the foamy macrophage of human granuloma. Granuloma-like structures were formed over the course of infection in increasing frequency and improved organisation over the course of two-weeks. Host necrosis and mycobacterial degradation was present within such structures.

In conclusion, with the exception of virulence, general observations were in-line with those reported by early studies and those of *Gm*-NTM studies. The results presented in this Chapter gave convincing evidence to warrant further investigation of the use of *Gm* as host for *MTB* (Chapter 4 and 5), application of this model system as a screen for antimycobacterial drug efficacy (Chapter 6), and characterisation of host and mycobacterial responses (Chapter 7). Furthermore, the *Gm*-BCG *lux* model enables the study of TB disease using a member of the MTBC, under CL2 conditions. The practical and economic advantages offered by *Gm* combined with its biological capacity to mimic many features desirable for the study of TB, is greatly appealing to the mycobacterial research community, particularly those lacking specialised facilities and equipment.

Chapter 4
Establishment and characterisation of a novel *G. mellonella* containment level 2 compliant tuberculosis infection model using *M. tuberculosis* H37Rv Δ*leuD*Δ*panCD*

4.1 Introduction

In Chapter 3, using the attenuated BCG vaccine strain of *M. bovis*, a proof-of-concept *Gm*-BCG *lux* infection model was established and characterised. BCG *lux* caused a virulent infection leading to larval mortality in a mycobacteria dose dependent manner. BCG *lux* established a persistent infection and switched to a non-replicative state indicated by the formation of ILI, typically observed in foamy macrophages of human granuloma. Furthermore, *Gm* developed granuloma-like structures throughout the larval body in response to infection with BCG *lux*; a hallmark of human TB infection. Despite the genetic similarities between *M. bovis* and *MTB* (>99.9% similarities), the virulence of BCG greatly differs from pathogenic members of the MTBC, primarily due to the lack of RD1 (Pym et al., 2002). RD1 of pathogenic mycobacteria encodes for key virulence factors (ESAT-6 and CFP-10) and secretory system (ESX-1) and is required for the optimal egress of mycobacteria from infected host cells (Liu et al., 2009). Deletion of RD1 in *MTB* have been shown to induce BCG like attenuation (Lewis et al., 2003). Therefore, the pathogenicity and host-pathogen interaction observed in the *Gm*-BCG *lux* infection model may not accurately represent those of *Gm* and *MTB*.

The appeal of BCG is its recognised status as a standard surrogate for *MTB* (Chapter 3) and its reduced biohazardous risk, enabling work to be carried out at CL2 (Yuan & Sampson, 2018). However, despite its associated risks, the use of *MTB* is preferred over surrogate mycobacteria such as BCG, *M. smegmatis* and *M. marinum* (Tobin & Ramakrishnan, 2008; Turner et al., 2015), as the data generated using *MTB* are considered more clinically relevant. Over the past two decades, several attenuated strains of *MTB* have been generated (Hondalus et al., 2000; Sambandamurthy et al., 2002, 2005; Sampson et al., 2004, 2011; Derrick et al., 2007; Clemmensen et al., 2017; Kar et al., 2017; Bahal et al., 2018), with the aim of

overcoming the safety limitations of *MTB* WT (CL3), while simultaneously reducing the need to utilise surrogates for *MTB*. The double auxotroph, Δ*leuD*Δ*panCD MTB* (SAMTB) is one such attenuated strain.

SAMTB was originally produced as a candidate live attenuated MTB vaccine and was created from the most commonly used laboratory strain, H37Rv (Sampson et al., 2004; Mouton et al., 2019). WT H37Rv was attenuated via deletion of two essential genes, Δ*leuD* and Δ*panCD*, which inhibit the growth of SAMTB in the absence of supplementary amino acids, Pan and Leu (Sampson et al., 2004; Mouton et al., 2019). This attenuation has been rigorously tested under both *in vitro* and *in vivo* conditions (Sampson et al., 2004, 2011), leading to its CL2 compliance designation. As a strain, SAMTB retains many of the desirable features of *MTB* WT (Mouton et al., 2019). The growth of SAMTB *in vitro* (culture) and within macrophages was comparable to *MTB* WT. SAMTB displayed a similar drug response profile to *MTB* WT and induced comparable or slightly higher immunogenic responses in peripheral blood mononuclear cells (PBMCs). However, proteomic analysis identified that SAMTB was more inclined to enter a heightened level of stress when compared to WT. Proteomic signatures of SAMTB associated with acidic, oxidative and/or nitrosative stress was upregulated during growth under physiological or acidic conditions (Mouton et al., 2019).

This Chapter describes the establishment and characterisation of a novel SAMTB-*Gm* model of infection. This model provides the necessary information to determine the similarities and differences between the virulence of two different members of the MTBC, *M. bovis* (BCG) and MTB (SAMTB) in *Gm*. As with BCG *lux*, a strain of SAMTB that has been genetically modified with a bioluminescence reporter plasmid (SAMTB *lux*) was used to rapidly quantify *in vivo*

mycobacterial abundance. I hypothesised that possession of key virulence factors, which are lacking in BCG (RD1), will lead to a more virulent (lethal) and proliferative infection in *Gm* when challenged with SAMTB. The rationale was that the successful establishment of a *Gm*-SAMTB *lux* infection model would provide advantages over BCG in terms of biology, whilst retaining CL2 usability.

4.2 Results and Discussion

4.2.1 Assessment of SAMTB lux virulence in Galleria mellonella

Gm larvae were infected with varying inocula (10^5-10^8 CFU) of SAMTB *lux* and larval survival was monitored over a 96 h time course (**Figure 4.1**). Larvae infected with SAMTB *lux* led to a virulent and lethal infection in a mycobacterial dose-dependent manner. *Gm* infected with 5 x 10^7 and 1 x 10^8 CFU led to a highly virulent outcome of 12 % and 0 % survival, 96 h post-infection, respectively. The LD_{50} dose at 96 h was calculated as 2.5 x 10^7 CFU. Infection with 1 x 10^6 and 1 x 10^7 CFU of SAMTB *lux* caused an avirulent (defined as non-lethal) infection with 100% survival over 96 h. Pricked and naïve controls were indifferent to the PBS control (data not shown). As with BCG *lux*, virulence of SAMTB *lux* was dependent on the viability of inocula; HT SAMTB *lux* (2 x 10^7 CFU) did not cause a lethal infection. Physiological changes to the larvae were observed when challenged with a virulent inoculum (2 x 10^7 CFU) causing reduced larval motility, melanisation (**Figure 4.2A**) and wasting (**Figure 4.2B**), over the course of 96 h. Wasting of infected larvae were individually measured at 48 h and 96 h post infection (**Figure 4.2B**). Weight loss was more substantial in larvae infected with SAMTB *lux* at both 48 h ($p < 0.01$) and 168 h ($p < 0.001$) post-infection, when compared to the mock infected PBS control. Larvae infected with BCG *lux* (1 x 10^7 CFU) led to substantially higher levels of weight loss when compared to the larvae infected with SAMTB *lux* (48 h: $p < 0.0001$, 96 h: $p < 0.0001$).

The virulence of SAMTB *lux* (2 x 10^7 CFU) was of similar magnitude to BCG *lux* (1 x 10^7 CFU) at 96 h post infection with larval survival of 63% and 50%, respectively. This was comparable to observations made in SCID mice challenged with BCG and SAMTB (Guleria et al., 1996; Sampson et al., 2004). Infection of SCID mice with BCG (1 x 10^6 CFU) led to a virulent and lethal infection (Guleria et al., 1996). In contrast mice challenged with 3 x 10^4 CFU SAMTB,

which is four times the lethal dose of WT, led to avirulent and non-lethal infection (Sampson et al., 2004). This indicates that in SCID mice, BCG is more virulent than SAMTB, similar to what is observed in *Gm*. However, this is a comparison of data from two separate mice studies and thereby must be interpreted with caution. The difference in lethality of SAMTB infection outcome between *Gm* and the SCID mice are likely due to differences in infectious dose and host immune competence. While SCID mice are severely immune compromised, lacking functional B and T cells (Guleria et al., 1996), their remaining immune system remains more robust than that of *the Gm* (Browne et al., 2013; Sheehan et al., 2018b). As such, *Gm* appears to be more sensitive to virulent bacteria than SCID, leading to the recorded mortality.

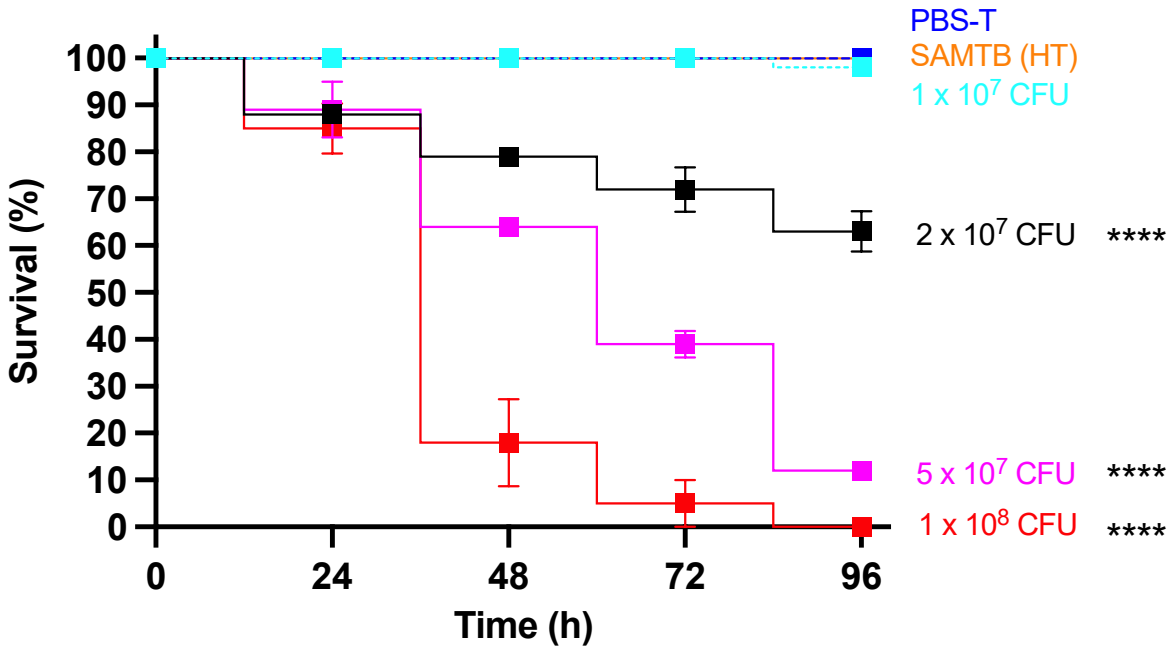


Figure 4.1: Assessment of SAMTB *lux* virulence in *G. mellonella*. Larvae were infected with varying doses of SAMTB *lux*. Mock infection (PBS-T) was included as control. Larvae were incubated in the dark at 37 °C following infection, and larval survival were monitored every 24 h for 96 h. Plotted are the means of three independent experiments, and the error bars represent the SD of the means. Sample size per experimental group was n = 30. For statistical test, Mantle-Cox log-rank test with Bonferroni's correction were conducted between infectious dose and PBS-T, where **** ($p < 0.0001$). Adapted from Asai et al., 2020.

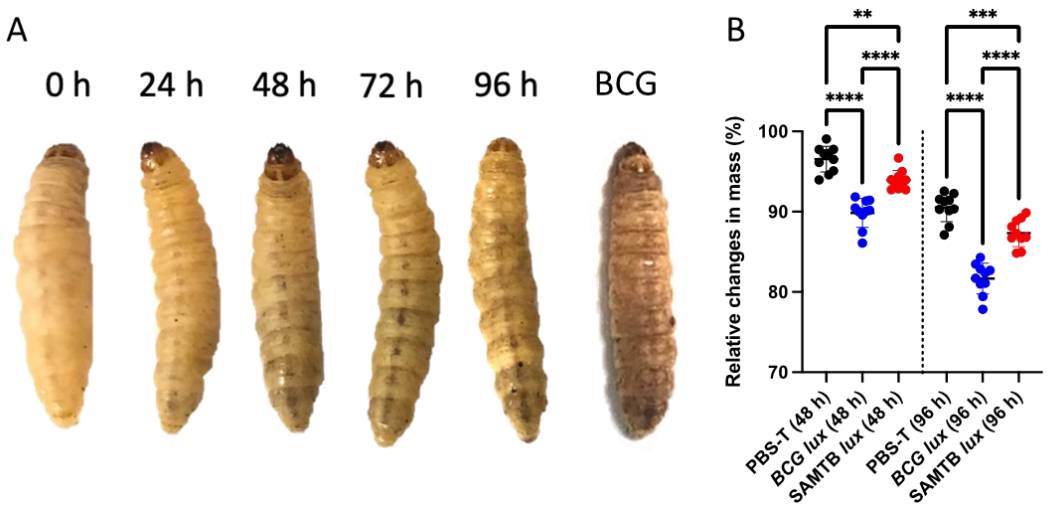


Figure 4.2: Physical changes to *G. mellonella* following infection with SAMTB *lux*. Larvae were infected with 2 x 10^7 CFU of SAMTB *lux* and (A) melanisation (darkening of larval body) were monitored every 24 h over a 96 h time course. A representative *Gm* larva is shown for each time point (0 h = uninfected healthy). A BCG *lux* infected larva at 96 h is represented as (BCG) for comparison. (B) Wasting of *Gm* following infection with SAMTB *lux* (2 x 10^7 CFU) or BCG *lux* (1 x 10^7 CFU) was monitored 48 h and 96 h post-infection. Changes in larval mass are represented as percentage relative to larval mass at t = 0 h. Data represent two independent repeats each with n = 5 larva. One-way ANOVA with Šídák multiple comparison was carried out, where ** ($p < 0.01$), *** ($p < 0.001$) and **** ($p < 0.0001$).

Individuals with TB, typically show signs of heavy weight loss and reduction in muscular mass known as the metabolic wasting syndrome (Ding et al., 2020). Wasting is a key aspect of the disease and has been reproduced in mice (Bouté et al., 2017) and zebrafish (Sridevi et al., 2014) TB models. Ding *et al*. (2020) compared the metabolic changes between mice, zebrafish and human TB infection using MS, and identified 10 metabolites (out of 89 identified) which consistently declined in abundance in all three models, despite the highly diverse set of vertebrate hosts examined (Ding et al., 2020). This indicates that regardless of variabilities in metabolic rate, size, body temperature and developmental stages presented in the three hosts, similar mechanisms may be utilised for TB induced wasting. As such, a future study to explore the changes in *Gm* metabolites during infection is warranted, further enabling the comparison of wasting related metabolites against invertebrate and vertebrate host. The

substantial loss of larval mass in BCG *lux* infected larvae, may reflect the more virulent (although marginal: 50% vs 63% larval survival outcome of BCG *lux* and SAMTB *lux*, respectively) nature of the infection. This may indicate a greater induction of the host immune response, such as the synthesis and secretion of AMP, and mobilisation of lipids and carbohydrate by the fat body (Skowronek et al., 2021), in larvae infected with BCG *lux,* leading to higher energy expenditure and thereby weight loss.

4.2.2. Proliferation of SAMTB lux within Galleria mellonella following infection

The luminescence of SAMTB *lux* was used as a relative measure for *in vivo* mycobacterial load. Unlike BCG *lux,* SAMTB *lux* was transformed using the more stable, chromosomally integrating pMV306 plasmid vector carrying the full *lux* operon of *Photorhabdus luminescens* (Andreu et al., 2010). The possession of a full *lux* operon results in auto-luminescence, i.e., emission of light without the requirement for additional substrate (decanal). To determine the correlation between luminescence (RLU) and CFU, larval homogenates were plated for CFU and measured for RLU at 0, 24, 96 and 168 h post-infection (**Figure 4.3**). These four time points were chosen based on changes in larval bioluminescence over a one-week time course (**Figure 4.4**). The susceptibility of SAMTB *lux* to PIP was determined using a MIC assay at concentrations between 1280 μg/ml and 10 μg/ml in a two-fold serial dilution. SAMTB *lux* was similarly resistant to PIP as BCG *lux* with an MIC of 160 μg/ml when plated on PIP infused agar plates as described previously (Chapter 3). The average RLU:CFU ratio *in vivo* was determined to be 0.02:1, ranging from 0.01 and 0.04 (**Figure 4.3**). This was comparable to a 0.03:1 ratio determined for *in vitro* cultured bacteria. Variability in SAMTB *lux* luminescence (**Figures 4.3 and 4.4**) was measurable due to batch effect. Similar precautions were taken with inocula prepared via standardised methods as stated in Chapter 3 (consistent RLU

measurement *in vitro*, OD and CFU of inocula checked), and trends in luminescence and virulence were monitored between periods of experimentation (Chapter 2.2.3).

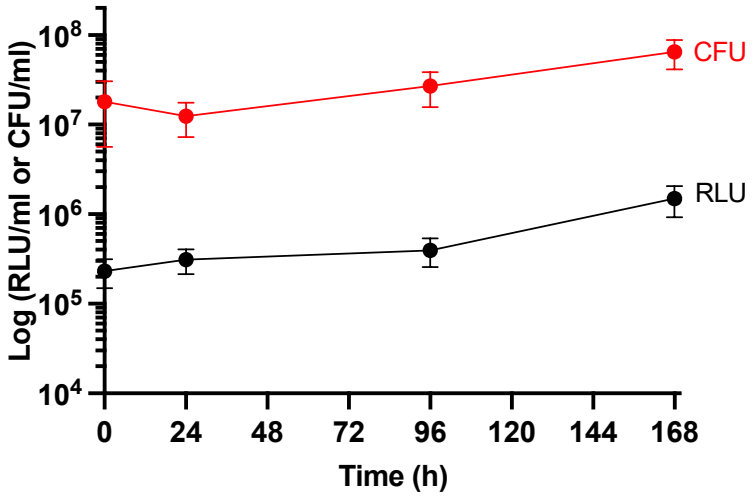


Figure 4.3: *In vivo* correlation of SAMTB *lux* luminescence and CFU in *G. mellonella* over a one-week time course. Larvae were infected with 1 x 10^7 CFU of SAMTB *lux* and CFU and RLU measurements were taken at 0, 24, 96 and 168 h post-infection (n = 4, per time point). Plotted are the means of two independent experiments, and the SD of the means. Adapted from Asai et al., 2020.

The survival of SAMTB *lux* (2 x 10^7 CFU) in *Gm* was monitored over a one-week time course. Following infection, a moderate rise in luminescence was detected between 0 and 24 h (~0.25 log RLU); luminescence continued to rise gradually between 24 and 96 h (~0.10 log RLU); before a substantial rise between 96 and 168 h post-infection (~0.40 log RLU). Overall, a rise in approximately 0.75 log RLU was detected over the one-week time course resulting in mycobacterial proliferation, measurable by both luminescence (**Figure 4.4**) and CFU (**Figure 4.3**). This finding contrasts with that of BCG *lux* infection, which established a non-replicative but persistent infection in the larva.

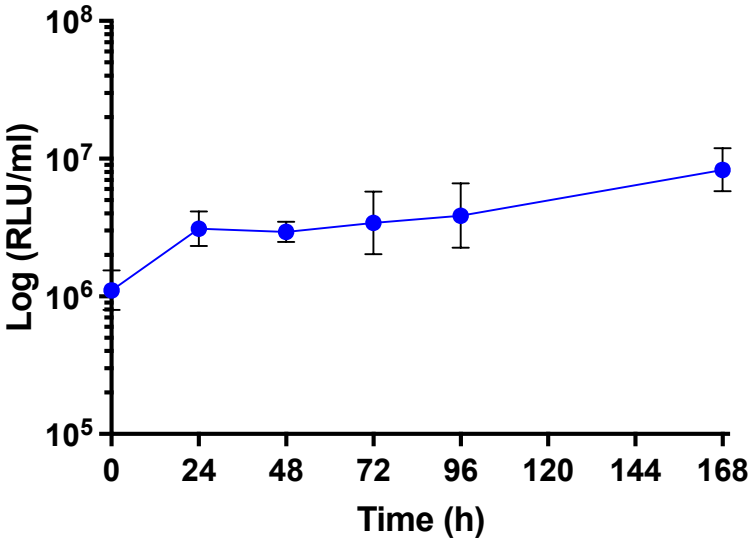


Figure 4.4: Survival of SAMTB *lux* within *G. mellonella* using luminescence as a measure of relative abundance. Larvae (n = 30) were infected with 2 x 10^7 CFU of SAMTB *lux*. The luminescence (RLU) of SAMTB *lux* within the GM homogenates was measured to determine the relative abundance of SAMTB *lux* over the one-week time course. At each time point, n = 4 were sacrificed. Plotted are the means of three independent experiments, and the error bars represents the SD of the means. Reproduced from Asai et al., 2020.

The growth of SAMTB *lux* in *Gm*, contradicted the reports of growth inhibition in the mice, guinea pigs and NHPs models (Hondalus et al., 2000; Sampson et al., 2004, 2011). In the first instance, cultures of SAMTB *lux* were prepared in the presence and absence of Leu and Pan (**Figure 4.5**), demonstrating that the Δ*leuD*ΔP*anCD* autotrophy was still in effect. Discrepancies seen in mice, guinea pigs, and NHPs, likely originate from the inability of SAMTB *lux* to access host Leu and Pan. A nutritional analysis of *Gm* revealed that commercial live food *Gm* contained of 10.8 g/kg and 32.8 mg/kg of Leu and Pan, respectively (Finke, 2015). Furthermore, high Leu content was further confirmed by a study of *Gm* metabolome which revealed that Leu comprises 4.91% of the total metabolome detected, however the proportion of Pan was not reported (Killiny, 2018). While larvae are not fed in the lab, it appears that residual quantities of Leu and Pan are sufficient for SAMTB *lux* growth *in vivo.* Therefore, the availability of these nutrients likely reflects the moderate rise in luminescence

at 24 h post-infection as SAMTB *lux* metabolism adjusts to the fresh nutrient rich environment.

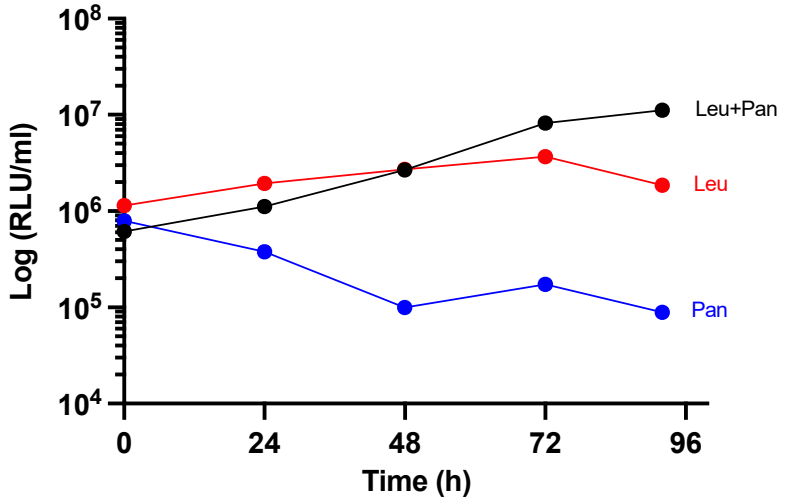


Figure 4.5: Growth inhibition of SAMTB *lux* in presence and absence of pantothenate and leucine. The luminescence (RLU) of SAMTB *lux* grown in Middlebrook 7H9 was monitored every 24 h for 96 h in presence of both Pan and Leu (black) or in absence of Leu (blue) or Pan (red). The growth of SAMTB *lux* relied on the addition of both Pan and Leu.

4.2.3 Interactions of SAMTB lux with Galleria mellonella haemocytes

Confocal microscopy was undertaken on *Gm* haemocytes extracted from SAMTB *lux* infected larvae at 1 h and 168 h post-infection. Early association of SAMTB *lux* bacilli with individual haemocytes were detected 1 h post infection (**Figure 4.6A**). By 168 h post-infection, large aggregates of haemocytes (~55 µm in diameter) resembling an early-stage granuloma-like structure were observed (**Figure 4.6B**). In this structure, healthy haemocytes appear to aggregate and surround infected and melanised haemocytes, containing large aggregates of bacilli. Phagocytosis of SAMTB *lux* bacilli was confirmed at 1 h post-infection via TEM (**Figure 4.7A**), where there is also evidence of phagocytosis associated membrane invaginations (**Figure 4.7B**). Internalised SAMTB bacilli increased between 24 h (**Figure 4.7C**) and 96 h (**Figure 4.7D**) post-infection, however visualisation became challenging due to insufficient

resin penetration surrounding the bacilli and causing breakage (represented by hollow or white holes in the background). At 168 h post-infection, uninfected haemocytes adhered to two infected haemocytes containing large masses of proliferating SAMTB *lux* (**Figure 4.7E**), which is comparable to **Figure 4.6B**.

Unlike, infection with BCG *lux,* intracellular SAMTB *lux* lacked development of pronounced ILI, reflecting the active and proliferative nature of the infection. Furthermore, the number of bacilli found within the haemocytes appeared to increase over time when compared to BCG *lux* infection. This likely reflects the higher abundance of circulating bacilli following intracellular replication and dissemination of SAMTB *lux* into the haemocoel. Moreover, the lack of distinguished ILI in SAMTB *lux* infected haemocytes, when compared to BCG *lux,* supports the hypothesis that weight loss may be influenced by the differences in induced levels of immune response. The induction of immune response is supported by the observation in the fruit fly TB model (*M. marinum*), where infection led to the secretion of lipids from the insect fat body, which accumulated within the haemocytes and co-localised with intracellular bacilli (Péan et al., 2017). A measurement of Nile red lipid stain intensity in BCG *lux* and SAMTB *lux* infected haemocytes correlated with measured weight loss, may indication similar lipid-bacilli association in *Gm*.

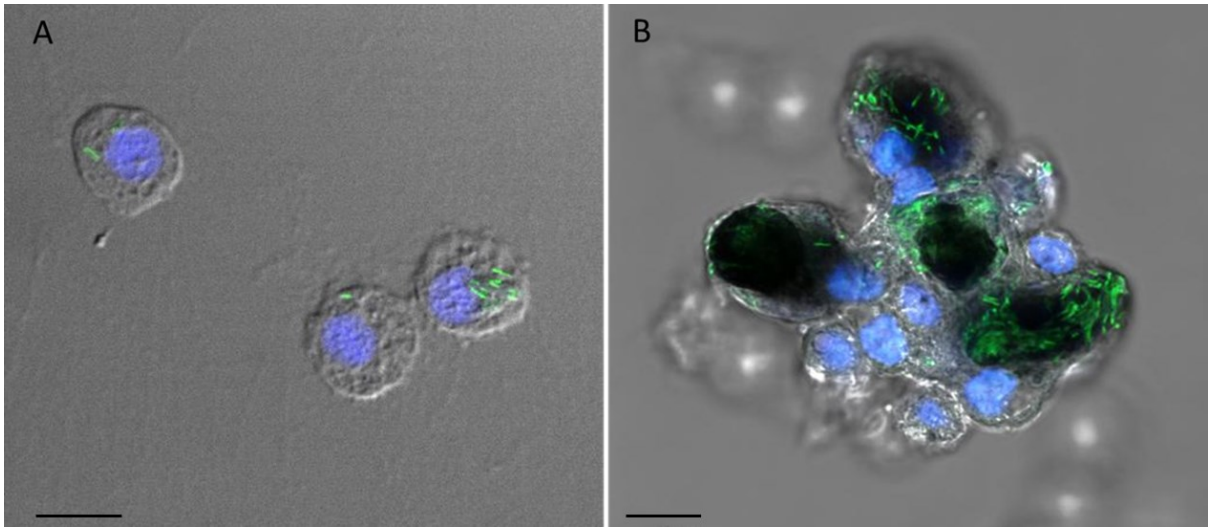


Figure 4.6: Association of SAMTB *lux* with *G. mellonella* haemocytes. The interaction of SAMTB *lux* bacilli with *Gm* haemocytes characterised using fluorescent confocal microscopy. Haemocytes were extracted from infected larvae (2 x 10^7 CFU). One hour post-infection (A), early association of SAMTB *lux* bacilli (in green) with individual haemocytes (blue) were visualised. By 168 h post-infection (B), healthy haemocytes aggregated to surround infected and melanised haemocytes containing large clusters of individually distinguishable bacilli. Presented are the superimposed images of DAPI nucleus staining (blue), SYBR gold mycobacteria staining (green) and differential interference contrast imaging. Scale bars represent 10 µm. Reproduced from Asai et al., 2020.

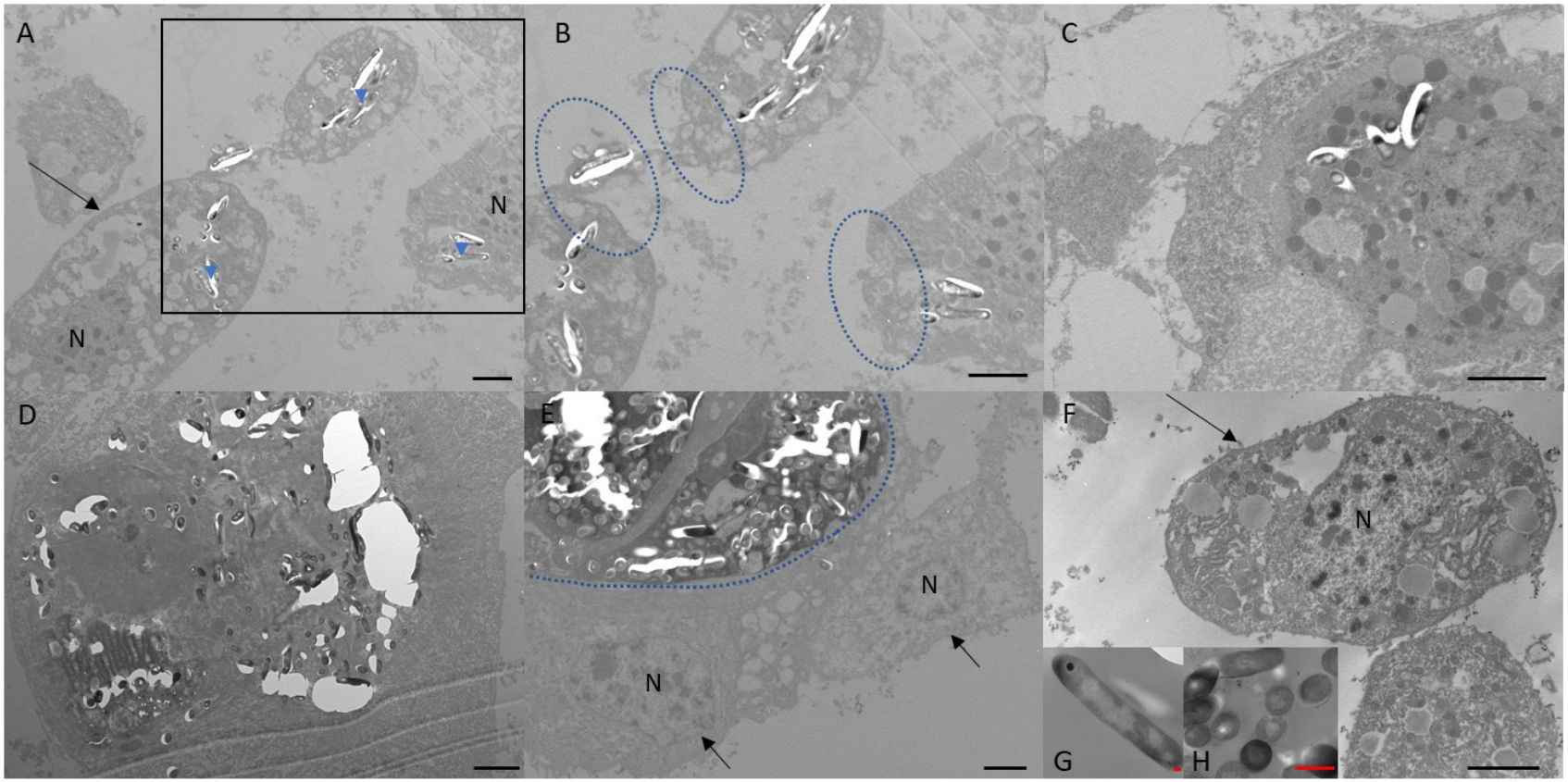


Figure 4.7: Transmission electron microscopy of SAMTB *lux* infected *G. mellonella* haemocytes. Larvae infected with SAMTB *lux* (2 x 10^7 CFU) were bled (n = 10, per time point) at 1 h (A, B), 24 h (C), 96 h (D), and 168 h (E) post-infection. Haemocytes of naïve (uninfected) larvae (F) and SAMTB bacilli in varying geometric orientations (G, H) were provided as controls. As early as 1 h post-infection (A), internalisation of SAMTB *lux* bacilli (blue arrowhead) by haemocytes (black arrow) occurred. (B) Magnified region of A (boxed), highlights membrane invaginations (blue dotted area), often associated with phagocytosis. Increase in abundance of intracellular SAMTB *lux was* seen over the course of infection (24 h [C], 96 h [D] and 168 h [E]). By 168 h (E) post-infection, aggregation of healthy haemocytes surrounding heavily infected haemocytes (highlighted in blue) were identified, representing early granuloma-like structures. N = nucleus. Scale bars represent 2 µm for A-F, 100 nm for G and 500 nm for H. Adapted from Asai et al., 2020.

4.2.4 SAMTB lux induces the formation of granuloma-like structures in Galleria mellonella

Histological sections of SAMTB *lux* (2 x 10^7 CFU) infected larvae were prepared and stained with H&E and ZN. As early as 24 h post-infection, foci of localised SAMTB *lux* bacilli surrounded by *Gm* cells and organised as granuloma-like structures, were identified (**Figure 4.8A-D**). The arrangement of bacilli within these foci varied, ranging from scattered individually distinguishable bacilli to dense clusters of indistinguishable amorphous acid-fast material. Corresponding H&E stain of these regions identified central host cell necrosis, evident from the deeper staining and the lack of nucleus staining (**Figure 4.8B, D**). The morphology of the granuloma-like structures varied over the course of infection, such as those containing a mixture of densely packed mass with high ZN staining and individually identifiable bacilli (**Figure 4.8E, F**), exclusively densely packed mass with high ZN staining (**Figure 4.8G, H**), or those disseminating prolific individually distinguishable extracellular bacilli (**Figure 4.8L**). Some of the densely packed structures at one-week post infection did not stain with ZN (**Figure 4.8J, K**). Infiltration of host organs, such as the GI tract, by bacilli was also identified, although the host reaction to such an event was not visually evident (**Figure 4.8M**). At all stages of infection, extracellular bacilli were identified in the haemolymph of the ZN stained section. Systemic infection by SAMTB *lux* was confirmed by sagittal section of the whole larva (**Figure 4.9**). At 24 h post-infection, granuloma-like structures were identifiable, but were scarce throughout the body (**Figure 4.9, 24 h**). By one-week post-infection, granuloma-like structures were visibly more abundant, larger in size and found ubiquitously throughout the body (**Figure 4.9, 168 h**). Foci were most developed and abundant towards the terminal segment of the larva, closer to the site of injection, as with BCG *lux* infection.

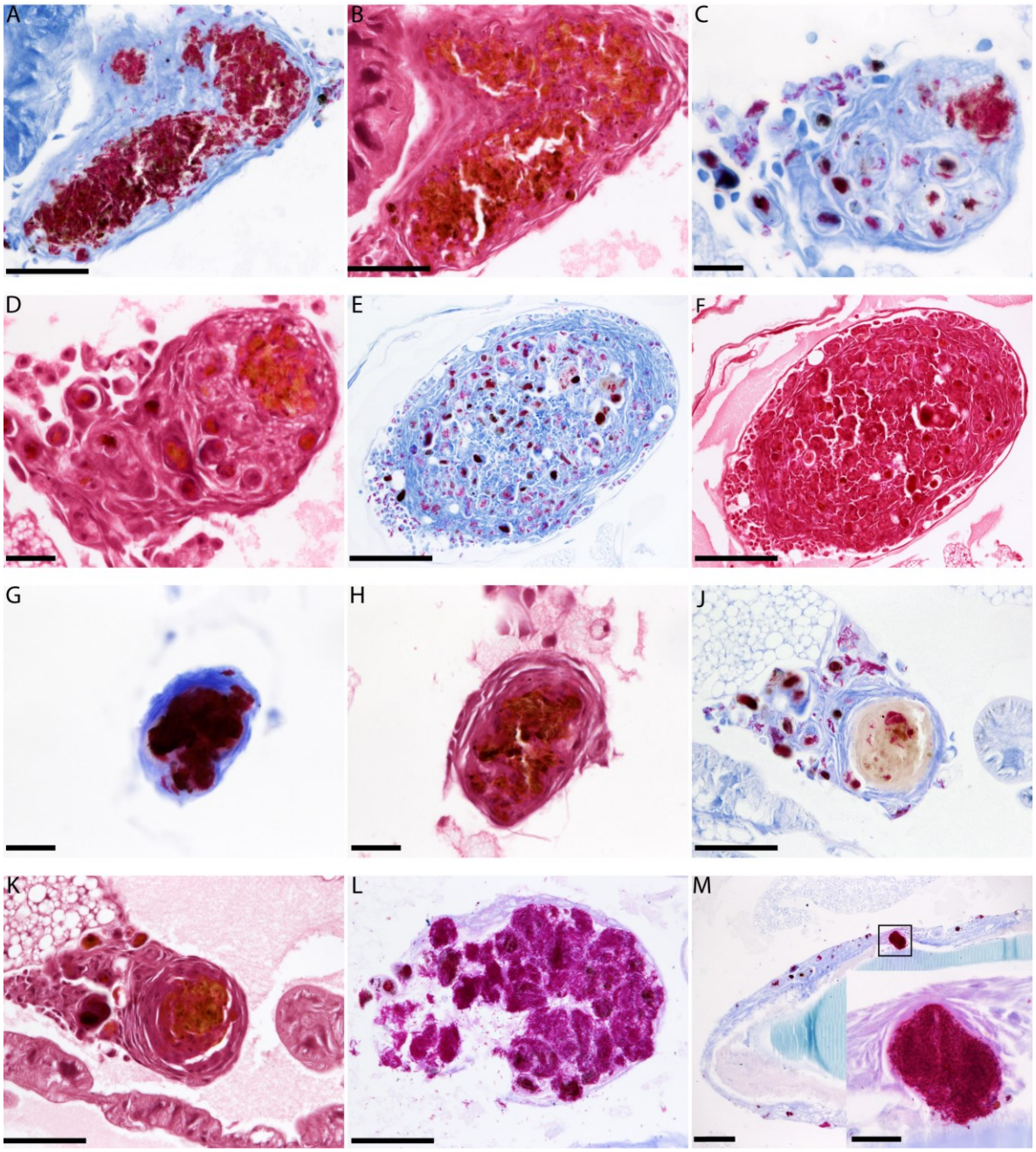


Figure 4.8: Histological sections of *G. mellonella* infected SAMTB *lux* over a one-week time course. Tissues sections were prepared from larvae (n = 3, per time point) infected with SAMTB *lux* (2 x 10^7 CFU) and stained with ZN (A, C, E, G, J, L, M) or H&E (B, D, F, H, K). Composition of granuloma-like structures varied over time: 24 h (A-D), 48 h (G, H) 168 h (E, F, J-M), containing mixture of densely packed mass with high ZN staining and individually distinct bacilli (E), exclusively densely packed mass with high ZN staining (G), or those disseminating prolific individually identifiable bacilli (L). Late granuloma-like structure indicated loss in acid-fastness (168 h: J, K). H&E stains indicates cell necrosis through cellular fragmentation, loss/fading nucleus staining, and loss of eosinophilia were observed specially in the area associated with densely packed acid-fast materials. (M) *Gm* organs (light blue area, GI tract) were invaded by proliferating bacilli (magnified inset panel in M). Scale bars represents 50 µm for A, B, J, K and L; 20 µm for C, D, G, H, and M (inset); 100 µm for E, F, and M. Reproduced from Asai et al., 2020.

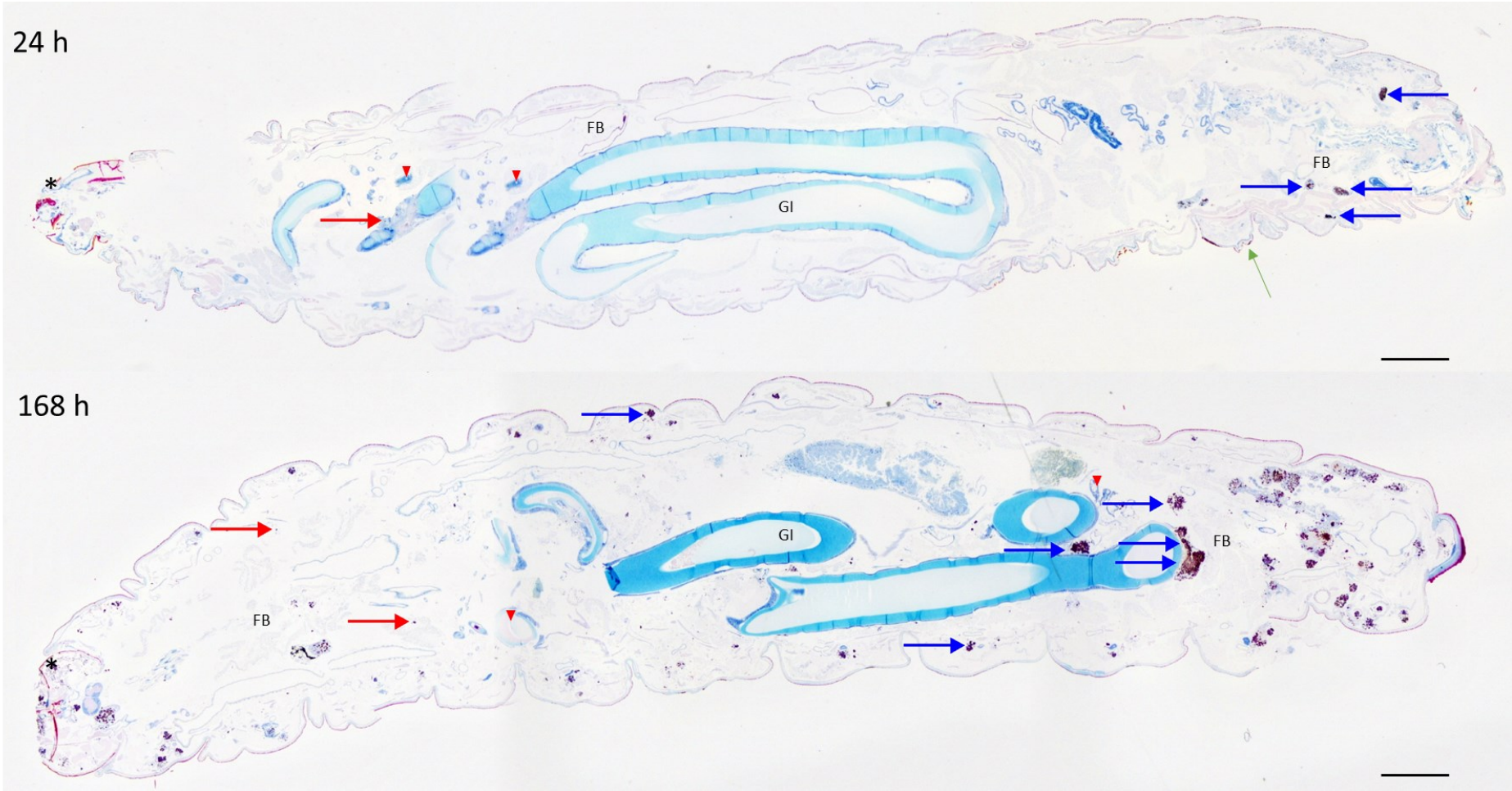


Figure 4.9: Development of granuloma-like structures in *G. mellonella* infected with SAMTB *lux*. Sagittal cross-section of larva infected with SAMTB *lux* (2 x 10^7 CFU) at 24 h and 168 h post-infection. Granuloma-like structures (red and blue arrows) can be found throughout the larval body, typically associated with the fat body (FB), in increasing frequency and size, over the course of infection. GI represents gastrointestinal tract; downward triangle (red) indicates trachea; blue arrows indicate granuloma-like structures resembling those of Figure 4.8A, C, E and L; and red arrow indicates structures resembling Figure 4.8G. * signifies the head and green arrow indicates site of injection. Scale bars indicate 1000 µm. Adapted from Asai et al., 2020.

As with BCG *lux* infection, granuloma-like structures were found throughout the larval body. However, the bacilli found within these structures differed greatly between the two models. In the BCG *lux* model, bacilli transitioned from individual bacilli to densely packed acid-fast material that retained its affinity to stain with carbol-fuchsin, indicating possible mycobacterial degradation (**Figure 3.11**). In contrast, in the SAMTB *lux* model, both replicating and degrading mycobacteria were identified throughout the 168 h time course (**Figure 4.8**). Furthermore, granuloma-like structures containing loosely packed proliferating bacilli were identified at 168 h post-infection, which disseminated and likely contributed to progression of the disease. Such observations indicate that these structures are actively utilised by SAMTB *lux* as a haven for replication. Dissemination of actively replicating bacilli support the abundance of intracellular bacilli over the course of infection (**Figure 4.7**), lacking a non-replicative phenotype (ILI) previously visualised in the BCG *lux* model.

While observations support that SAMTB *lux* infection is proliferative in *Gm*, the histopathology image of late granuloma-like structure at 168 h post-infection (**Figure 4.8J**) indicate a possible switch from replicating to a non-replicating phenotype in select granuloma-like structures. Acid-fastness is unique to mycobacteria due to their lipid-rich cell wall structure. However, under certain circumstances, acid-fastness can be lost, a phenomenon referred commonly as the “Koch paradox”(Vilchèze & Kremer, 2017). Loss of acid-fastness was first confirmed as a mycobacterial phenotype in bacilli recovered from lesions of caseous or miliary TB (Mallassez & Vignal, 1883). Acid-fast negative bacilli, grown in culture media can infect animals causing TB, confirming their origin as tuberculous mycobacteria (Miller, 1932). It was found that the switching of mycobacterial phenotype from active to non-replicative dormant or persistent bacilli, altered the composition of the mycolic

cell wall through regulation of *kasB*, encoding one of two ß-ketoacyl-ACP synthases responsible for the terminal elongation of mycolic acid biosynthesis. (Bhatt et al., 2007). Loss of acid-fastness has been associated with the shortening of lipid chains which are found in the mycolic wall, as a consequence of stress induced regulation of *kasB*, leading to a loss in biochemical ability to retain the ZN primary dye (Bhatt et al., 2007).

As described in Chapter 3, the accumulation of TAG as cytosolic ILI in *MTB* can be an indicator of non-replicative bacilli. The observations of ILI and loss of acid-fastness are often co-founding amongst bacilli which are in a dormant or persistent state (Vilchèze & Kremer, 2017). Although loss of acid-fastness was identified in SAMTB *lux* infected *Gm*, ILI was not observed in abundance in intracellular bacilli using TEM examination at any given time point. In contrast, while BCG *lux* accumulated ILI, acid-fastness was not lost in the *Gm* model. Structurally in the SAMTB *lux* model, granuloma-like structures containing acid-fast negative bacilli appeared to be well organised and were unlikely to be the source of proliferative bacilli compared to other structures present in the model (**Figure 4.8L**). Thus, persistent or dormant bacilli likely made up a small sub-population within the larvae, unlikely to be detected amongst the more prominent proliferative bacilli released from the granuloma-like structures. Furthermore, while ILI is often associated with persistence or a dormant state, studies indicate that *MTB* utilise the stored TAG in the ILI during nutrient deprivation whereas it may actively and preferentially utilise TAG within the intracellular environment as source of energy (Jackson et al., 1989; Deb et al., 2009). Moreover, the ILI formation may be enhanced in BCG *lux*, owing to the inability to induce cell lysis via RD1 associated virulence factors (Liu et al., 2009). As a result, BCG *lux* bacilli are perhaps more sensitive to stress factors such as hypoxia or oxidative stress, triggering the accumulation of ILI more readily than *MTB*. Whilst

the predisposition of SAMTB *lux* to express a stress response was noted by Mouton and colleagues, such factors did not appear to influence the growth of SAMTB *lux* in the larvae (Mouton et al., 2019).

To counter the effects of loss of acid-fastness, a dual fluorescence staining approach utilising auramine-O (*MTB*) and lipophilic Nile red (lipid accumulation) along with polyclonal anti-mycobacterial serum for immune fluorescence imaging is recommended (Seiler et al., 2003; Kapoor et al., 2013; Vilchèze & Kremer, 2017). Combination of these stains will indicate loss of acid-fastness over time (auramine-O), accumulation of ILI (Nile red) and confirmation of acid-fast negative mycobacteria (polyclonal anti-mycobacterial serum). If additional time and funding were available, *Gm* histological sections of BCG *lux* and SAMTB *lux* at varying time points could be stained to further characterise the capacity of these model systems (*Gm*-BCG *lux*/SAMTB *lux*) to replicate dormant or persistent infection.

4.2.5 Granuloma-like structures can be modelled ex vivo using SAMTB infected Galleria mellonella haemocytes

An *ex vivo Gm* haemocyte model of granuloma-like structures was developed as a proof-of-concept pilot study. Haemocytes were extracted from PBS or SAMTB *lux* (1 x 10^6 and 2 x 10^7 CFU) infected larvae at 24, 48, 72, 96 h post-infection (n = 5, time-point). Haemocytes (10^5 cells/ml) were seeded into 24 well culture plates and incubated for one week at 37 °C in a rocking incubator, where the culture medium was changed every 24 h. The viability of extracted haemocytes ranged from 82-90% for the PBS and 69-90 % for SAMTB infected, where a higher infectious dose led to a greater decline in cell viability. Haemocytes proliferated and formed granuloma-like structures in an infection dose-dependent manner

(**Figure 4.10**). PBS controls did not induce cell proliferation. ZN staining identified that these *ex vivo* granuloma-like structures contained large quantities of SAMTB *lux* bacilli (**Figure 4.11A-B**). While viability of cultured cells was not determined for this pilot study, seeding with higher numbers of haemocytes lead to cell death as was identified through severe melanisation or detachment from the culture plate surface. While further viability assessment will be conducted in future studies, this may be difficult by conventional measures (e.g., using single cell suspensions in trypan blue) due to the formation of granuloma-like structures.

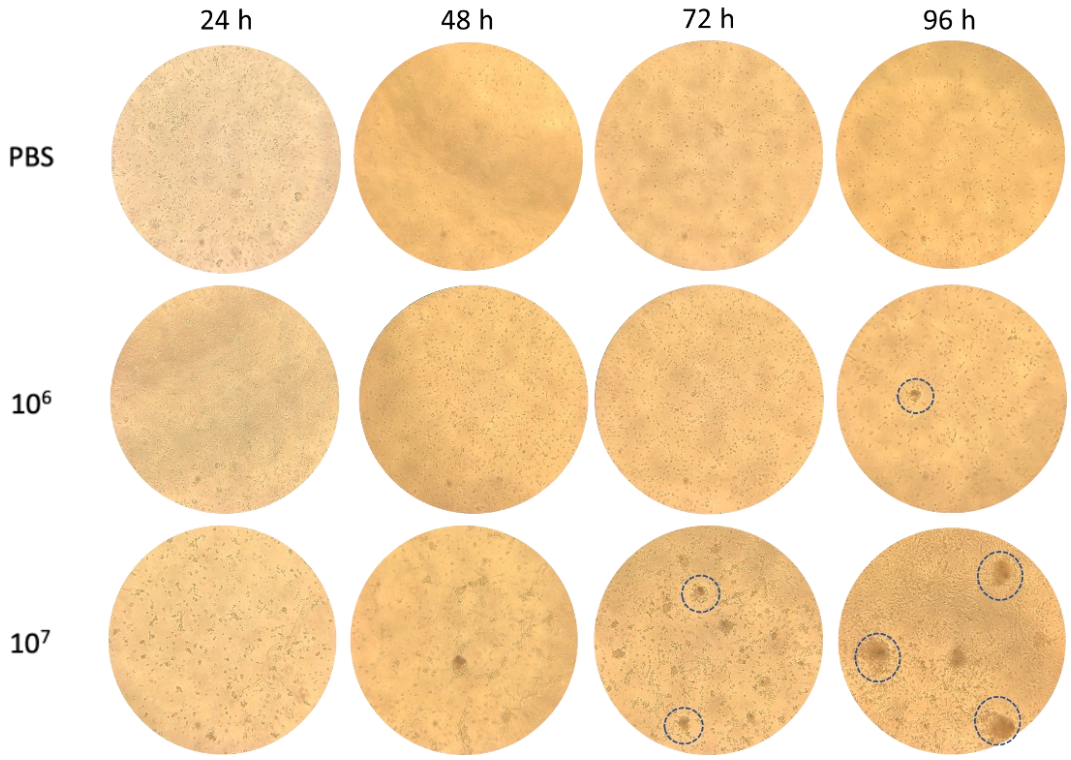


Figure 4.10: Cultivated *ex vivo G. mellonella* haemocytes of SAMTB *lux* infected larvae develop granuloma like structures. Haemocytes (10^5 cell/ml) were bled from SAMTB *lux* (1 x 10^6 or 2 x 10^7 CFU) or PBS infected larvae (n = 5, time point) at 24 h, 48 h, 72 h, and 96 h post-infection and incubated for one-week at 37 °C in a rocking incubator. Formation of granuloma-like structures were identified in haemocytes extracted from SAMTB *lux* infected larvae only. Images were taken using a standard light microscope at 10x magnification.

The highlighted structures in **Figure 4.10** were reproduced in culture slide chambers for ease of imaging, revealing large structures of fused haemocytes, indicated by indistinguishable

outlines of individual cells or nucleus DAPI staining (**Figure 4.11C**). These structures contained large quantities of SAMTB *lux* and appeared to be attracting nearby healthy uninfected haemocytes. Furthermore, the structures are highly comparable to multinucleate giant cells (MNGCs), also known as Langhans giant cells, and resemble those developed *in vitro* using PBMCs (Lay et al., 2007; Shrivastava & Bagchi, 2013).

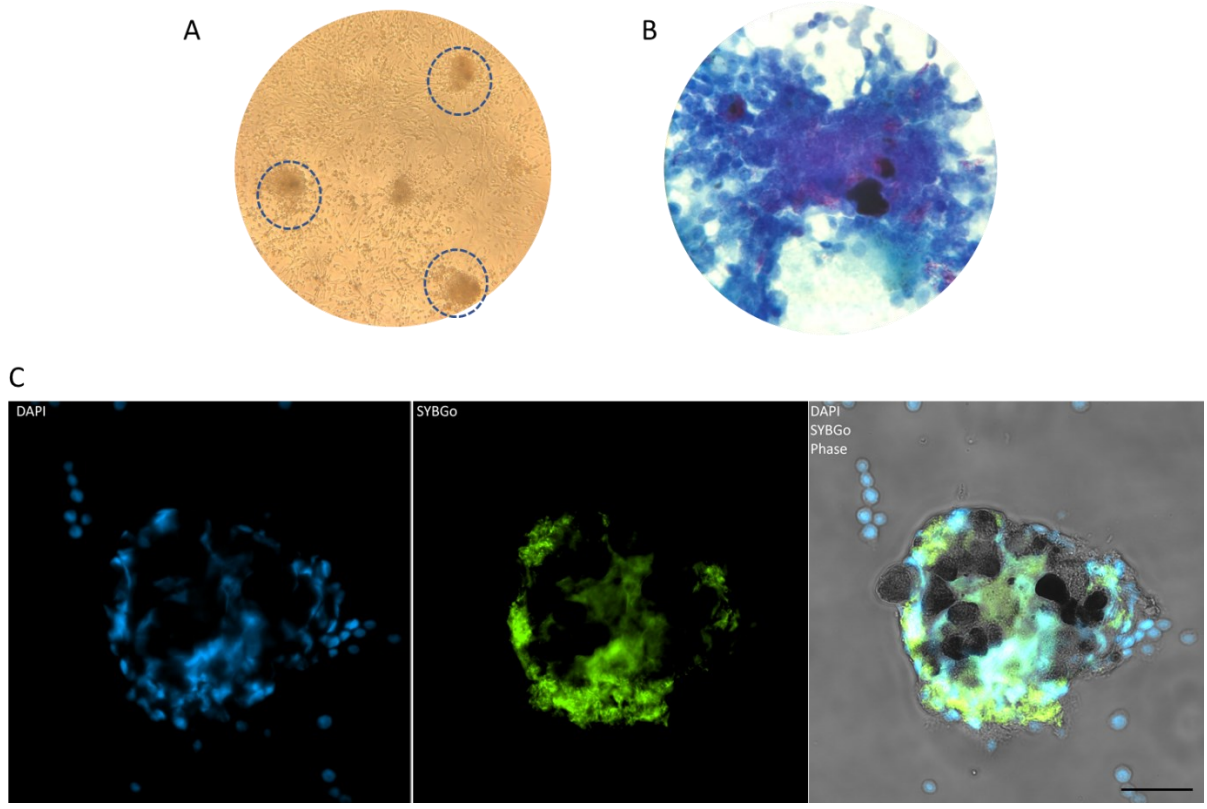


Figure 4.11: Cultivated *ex vivo* SAMTB *lux* granuloma-like structure resembles multinucleate giant cells. (A) Image (10x magnification) of *ex vivo* granuloma-like structure from 10^7 CFU infection extracted 96 h post-infection (as seen in Figure 4.10). (B) ZN staining (100x magnification) of an *ex vivo* granuloma-like structure, showing a large mass of SAMTB *lux* bacilli contained by aggregates of multiple haemocytes. (C) Fluorescent wide-field microscopy of an *ex vivo* granuloma-like structure cultivated on a cell chamber slide. Fused haemocytes were identified through individually indistinguishable cellular margins (phase) and nucleus (DAPI, blue), closely resembling MNGCs. Large numbers of SAMTB *lux* (SYBR gold, green) are associated with the granuloma-like structure. Scale bar represents 50 µm.

Additionally, similar formations of cell aggregates resembling MNGCs have similarly been reported in the innate immune *M. marinum* larval zebrafish model of TB (Davis et al., 2002).

These observations, in two unique models (*Gm* and zebrafish), indicate that the formation/initiation of granuloma or granuloma-like structures can occur in the absence of adaptive immunity. However, for maintenance of these structures adaptive immunity is essential (Davis et al., 2002). This is indicated by the high numbers of bacilli found within the *ex vivo* structure (**Figure 4.11C**) which will likely lead to loss of structural integrity without continuous recruitment of haemocytes and/or immune effectors to regulate intracellular mycobacterial replication. Nevertheless, the development of granuloma-like structures in *Gm* and specificity (generic or pathogen) remains unclear and is a subject of future investigation once the necessary tools and reagents are developed for *Gm* as previously stated in Chapter 3.

4.3 Conclusion

The aim of this Chapter was to determine if *MTB* induced a more virulent (lethal) infection in *Gm*, when compared to BCG, which lacks RD1. To maintain the accessibility of the model, as presented with BCG *lux* in Chapter 3, the use of a double auxotroph of *MTB* H37Rv (SAMTB *lux*) was explored. I hypothesised that SAMTB *lux* would induce a more virulent infection in *Gm* due to its retention of RD1. However, the virulence of SAMTB *lux* was of similar magnitude to BCG *lux.* Examination of prior animal studies (mice, guinea pigs and NHPs) with SAMTB similarly indicated marginally reduced virulence when compared to infection with BCG. However, SAMTB *lux* was able to proliferate within *Gm*, unlike in animal models or BCG *lux* in *Gm*. A study into the nutritional value of *Gm* (Finke, 2015) identified that the larvae contained high level of Leu and Pan, which were likely less abundant or inaccessible in other models. The availability of host Leu and Pan would have enabled SAMTB *lux* to bypass the limitations induced by the Δ*leuD* and Δ*panCD* deletions, leading to growth.

TEM confirmed that SAMTB *lux* bacilli were found within circulating haemocytes at all time points, with the numbers generally increasing over time. However, unlike infection with BCG *lux,* SAMTB *lux* bacilli did not accumulate visibly distinctive levels of cytosolic ILI. This may be associated with a lower rate of fat body activation by SAMTB *lux* compared to BCG *lux* leading to lower abundance of freely available host lipids for the formation of mycobacterial ILI. The abundance of ILI in BCG *lux* infection may indicate higher levels of fat body activation and thereby energy expenditure leading to greater weight loss. As with BCG *lux,* formation of granuloma-like structures by SAMTB *lux* was found throughout the larval body in increasing number and size as the infection progressed. In comparison to BCG *lux* infection, the state of SAMTB *lux* found within the granuloma-like structures greatly varied with a mixture of

proliferative and degenerating bacilli at all time points. Interestingly despite the lack of ILI accumulation in TEM examined bacilli, a number of late (168 h post-infection) granuloma-like structures lost their acid-fastness. Such a phenomenon, referred to as Koch's paradox, has typically been associated with persistent or dormant bacilli, and indicates that perhaps a select sub-population of SAMTB *lux* may have switched from active to persistent or dormant infection.

To better understand the formation of granuloma-like structures in *Gm*, the feasibility of an *ex vivo* model was assessed. Granuloma-like structures could be formed *ex vivo* in a SAMTB *lux* dose-dependent manner. Microscopy examination confirmed aggregations of haemocytes around a central mass of SAMTB *lux* in an organised to semi-organised manner. The appearance of the structures closely resembled that of MNGCs formed in *in vitro* human PBMCs and *in vivo* in zebrafish TB models. While this pilot model requires additional work, the initial observation is of interest and further work will be carried out, but it is beyond the scope of this project.

Thus far this project has established two *Gm*-MTBC infection models using BCG *lux* and *SAMTB lux*. Based on the attenuated response of SAMTB *lux* seen in this Chapter, infection of *Gm* using *MTB* WT under CL3 conditions is warranted (Chapter 5). This must be carried out to determine whether the susceptibility of *Gm* to members of MTBC is relates to pathogenicity and virulence and not a generic response to infectious dose, which was initially anticipated to be demonstrated by comparing the SAMTB *lux* and BCG *lux* models. Furthermore, a characterisation of an *MTB* WT model would be essential as some research will be limited to

CL3 conditions, such as the screening of null and loss-of-function mutants of *MTB* or clinical isolates.

Chapter 5
Establishment and characterisation of *G. mellonella* as a host for *M. tuberculosis* H37Rv

5.1 Introduction

Animal infection models have played a crucial role in our understating of TB pathogenesis, disease progression and host-*MTB* interaction. Functional screening of *MTB* virulence in animals, in tandem with genetic analysis and *in vitro* studies, have helped us to identify key mechanisms of disease, leading to new targets for biomarkers, therapeutics, and preventative measures (Dhar & McKinney, 2010; Gonzalo-Asensio et al., 2014; Lavin et al., 2021; Koyuncu et al., 2021). The use of animals has been essential for determining relative lethality and virulence of clinical isolates (Mourik et al., 2019; Vinogradova et al., 2021; Fursov et al., 2021); and to confirm strain attenuation for the creation of candidate live vaccines (Martin et al., 2006; Waters et al., 2009). To date, a wide range of animals has been characterised as hosts for mycobacterial infection, each with their benefits and limitations. In any novel model, identifying key strengths and weaknesses are vital for model adoption.

Thus far, two CL2 compliant *Gm*-TB infection models, BCG *lux* (Chapter 3) and SAMTB *lux* (Chapter 4), have been established and characterised. As previously discussed, BCG *lux* and SAMTB *lux* are attenuated strains of their pathogenic progenitor *M. bovis* and *MTB* H37Rv, respectively. In *Gm*, higher levels of lethality were anticipated for SAMTB *lux*, as it possesses RD1, which encodes key mycobacterial virulence factors, and is lacking in BCG *lux* (Liu et al., 2009). However, the virulence of SAMTB *lux* in *Gm* was of similar magnitude to BCG *lux*, over a 96 h time course. In animals (mice and guinea pigs), BCG was more virulent (lethal) than SAMTB (Guleria et al., 1996; Sampson et al., 2004). This severe attenuation of SAMTB was attributed to the lack of *in vivo* replication observed in mice and guinea pigs. However, in contrast to these observations, SAMTB *lux* was capable of replicating in *Gm*, likely due to the availability of host Leu and Pan leading to the bypass of auxotrophy. It is unclear whether the

growth of SAMTB *lux* in *Gm* results in WT phenotypic properties, including virulence, as no other *in vivo* model has shown replicative infection.

My observations in *Gm* (Chapters 3 and 4) raised questions as to the susceptibility and sensitivity of *Gm* to members of the MTBC. Is the virulence of SAMTB *lux* in *Gm* equivalent to WT and simply indistinguishable from BCG *lux?* Is the observed larval mortality to mycobacterial infection a generic response to different inocula? Or is the virulence of SAMTB *lux* lower than BCG *lux* purely due its double auxotrophic phenotype and independent of *in vivo* replication in *Gm*? The answers to such questions were potentially answerable through infection studies of *Gm* larvae with WT *MTB* H37Rv (referred here on as H37Rv). Moreover, to fully evaluate *Gm* as a host for MTBC, establishment and characterisation of a *Gm*-H37Rv model was essential and timely, since I had received feedback and requests for such data from the scientific community, following the presentation of the BCG *lux* and SAMTB *lux* models. In addition, work with H37Rv would allow screening of functional mutations in a WT background, a widespread practice within the *MTB* community (e.g., to identify potential targets for novel antimycobacterial agents), where the use of surrogate mycobacterial species or attenuated strains are not always suitable.

As a strain, *MTB* H37Rv originates from the clinical isolate H37, which was isolated from a TB patient at the Trudeau Institute (New York, USA) in 1905 (Kubica et al., 1972). The H37 isolate later evolved into the high and low virulence H37Rv and H37Ra strains, respectively (Oatway & Steenken, 1936). The widespread use of H37Rv, along with its phenotypic similarities with the tubercle bacilli originally described by Robert Koch, led to it becoming the most commonly used strain in TB research (O'Toole & Gautam, 2017). In this Chapter, a *Gm*-H37Rv model was

established and characterised to fully evaluate this insect model as host for the members of MTBC. Furthermore, comparative virulence studies of WT and isogenic mutants attenuated for infection in mammalian hosts were carried out to determine the utility of the *Gm*-H37Rv model.

5.2 Results and Discussion

5.2.1 H37Rv is more virulent than BCG lux and SAMTB lux

In view of constructive comments from the TB researching community, in particular those on the comparatively short infection times, the study period for H37Rv was extended from the 96 h, previously used for BCG *lux* and SAMTB *lux* models, to 192 h. This allowed for a longer incubation, and the use of a lower infectious dose, which more closely represented the chronic nature of TB infection.

As before, larvae were first challenged with varying number of CFUs to determine H37Rv virulence (lethality). Like BCG *lux* and SAMTB *lux,* larval mortality positively correlated with a larger inoculum (**Figure 5.1**). Over a 192 h time course, the LD_{50} dose of H37Rv was determined to be 2 x 10^6 CFU. The virulence was dependent on viability of the inocula as demonstrated using HT H37Rv (2 x 10^6 CFU). To compare virulence of H37Rv with BCG *lux* and SAMTB *lux,* larvae were challenged with 10^6 and 10^7 CFU, and observed over 96 h and 192 h, respectively, to reflect both the original and revised experimental designs. In infections with 10^7 CFU monitored over 96 h, H37Rv was more virulent with only 30% larval survival, when compared to the 50% and 54% survival of BCG *lux* (1 x 10^7 CFU) and SAMTB *lux* (2 x 10^7 CFU), respectively (**Figure 5.2**). Similarly, in larvae infected with 10^6 CFU and monitored over 192 h, H37Rv was the most virulent, with only 46 % survival compared to SAMTB *lux* (77%) or BCG *lux* (93%) survival (**Figure 5.2**). These observations confirmed that *Gm* is sensitive to differences in mycobacterial virulence as demonstrated using three independent mycobacterial models examined under two different CFU doses and time courses. Interestingly, in contrast to observations in Chapter 4, at a lower infectious dose of 10^6 CFU but over a longer time period, SAMTB *lux* was more lethal than BCG *lux* by 16%. Which

indicates that perhaps at an infectious dose of 10^7 CFU, the activated *Gm* immunity cannot differentiate the virulence between BCG *lux* and SAMTB *lux*, and there was a broad benefit to adjusting the infectious dose and infection time.

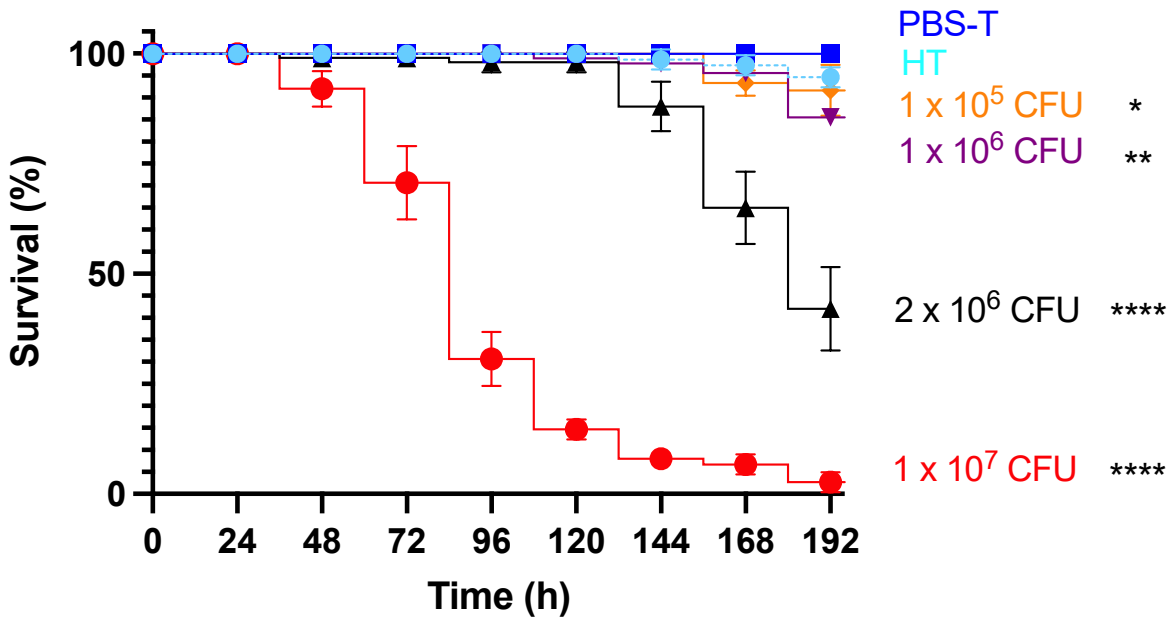


Figure 5.1: Assessment of H37Rv virulence in *G. mellonella*. Larvae were infected with varying doses of *MTB* H37Rv. Mock infection (PBS-T) was included as control. Larvae were also challenged with non-viable HT H37Rv (2 x 10^6 CFU). Larvae were incubated in the dark at 37 °C following infection, and larval survival were monitored every 24 h for 192 h. Plotted are the means of three independent experiments, and the error bars represent the SD of the means. Sample size per experiment was n = 25. Mantle-Cox log-rank with Bonferroni's correction was carried out against PBS-T, where * ($p < 0.05$), ** ($p < 0.01$), **** ($p < 0.0001$).

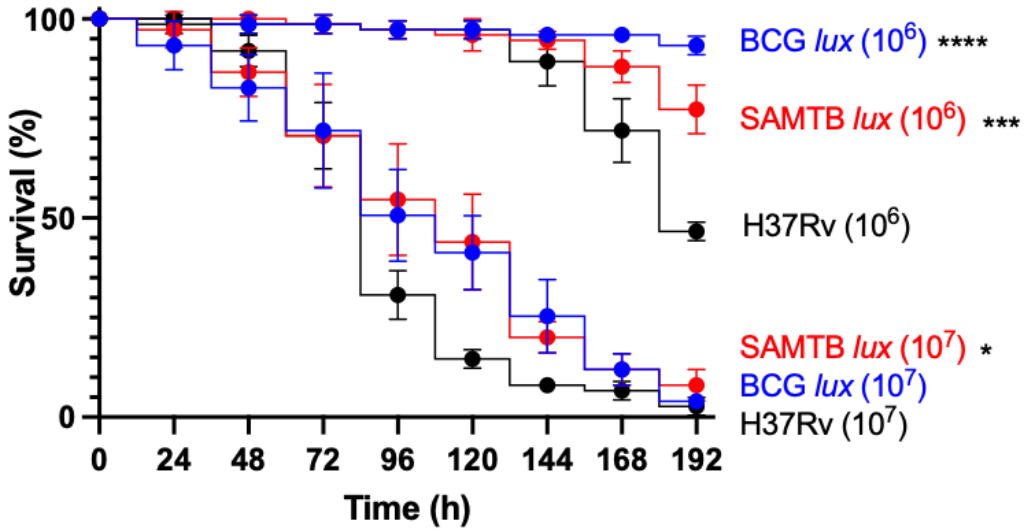


Figure 5.2: Comparison of H37Rv, BCG *lux* and SAMTB *lux* virulence in *G. mellonella*. Larvae were infected with 10^6 or 10^7 CFU of either H37Rv, BCG *lux* or SAMTB *lux*. Larvae were incubated in the dark at 37 °C following infection, and larval survival were monitored every 24 h for 192 h. Plotted are the means of three independent experiments, and the error bars represent the SD of the means. Sample size per experiment was n = 25. Mantle-Cox log-rank test with Bonferroni's correction was carried out against H37Rv within the respective CFU dose groups of BCG *lux or* SAMTB *lux*, where * ($p < 0.05$), *** ($p < 0.001$), **** ($p < 0.0001$).

Observation of infected larvae over 192 h revealed that those challenged with 10^6 CFU of H37Rv, appeared to be more active over the first 120 h of infection, when compared to those infected with a higher CFU inocula, indicating that the period of incubation prior to symptomatic infection is longer in larvae infected with lower CFU inoculum. In support of these observations, the rate of melanisation was substantially slower in larvae challenged with 10^6 CFU of H37Rv (**Figure 5.3**) and the levels of systemic melanisation were different to those observed in BCG *lux* and SAMTB *lux* infection. Diffused localised areas with melanisation were first identified at 96 h post-infection and became more visually distinct as speckles of granuloma-like structures identifiable through the larval cuticle.

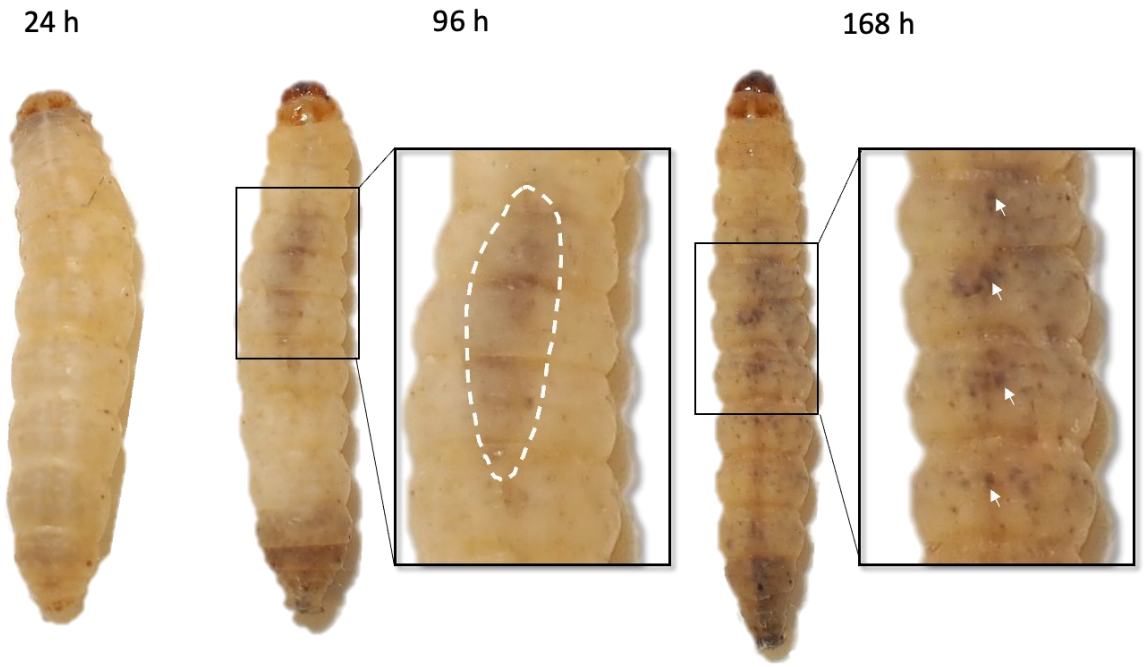


Figure 5.3: Melanisation of *G. mellonella* larvae following H37Rv infection. Changes in larval appearance was monitored at 24 h, 96 h and 168 h following infection with 2 x 10^6 CFU of H37Rv. Magnified (boxed) area highlights (white dotted) the development of a large sub-cuticle structure, which are typically found along the dorsal vessel of the haemocoel. Over time, these structures became more distinct becoming visually distinguishable speckles.

5.2.2 Proliferation of H37Rv within Galleria mellonella following infection

Unlike BCG *lux* and SAMTB *lux*, H37Rv has not been engineered to fluoresce, therefore changes in H37Rv load were measured using CFU enumeration. The MIC of PIP was determined to be 320 μg/ml for H37Rv, similar to that determined previously for BCG *lux* and SAMTB *lux*. Together with observations from the NTM study (Entwistle & Coote, 2018), strong resistance to PIP seems to be a common trait amongst different mycobacterial species. 7H11 plates containing 20 μg/ml of PIP were used for CFU enumeration. The survival of H37Rv (2 x 10^6 CFU) in *Gm* (n = 4 larvae per time point) was measured every 24 h over 192 h except for 120 h post-infection. Following infection, a substantial rise of ~0.90 log CFU was recorded between 0 and 96 h post-infection. The growth rate declined considerably between 96 h and

192 h post-infection with a minor rise of ~0.20 log CFU. Over a 192 h time course, H37Rv grew by ~1.1 log CFU in *Gm* larvae (**Figure 5.4**).

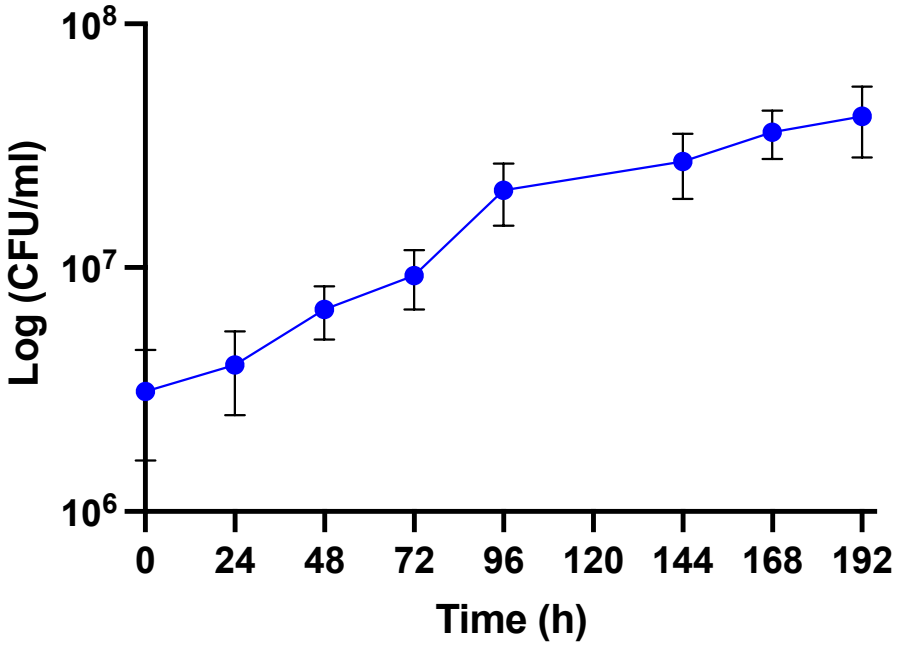


Figure 5.4: Survival of H37Rv within *G. mellonella*. Larvae (n = 25) were infected with 2 x 10^6 CFU of H37Rv. CFU were enumerated from the *Gm* homogenate in order to measure the changes in *in vivo* H37Rv load over a 192 h time course. Plotted are the means of three independent experiments, and the error bars represents the SD of the means.

Comparison of H37Rv and SAMTB *lux* survival in *Gm* is limited by the lack of *in vivo* SAMTB *lux* 10^6 CFU infection data. Evaluation of H37Rv and SAMTB *lux* 10^7 CFU survival data (**Figure 4.3**) found that H37Rv replicated twice as much in *Gm* when compared to SAMTB *lux* over a 168 h time course (~ 1 log CFU and ~0.5 log CFU, respectively). Typically, the rate of bacterial growth *in vivo* positively correlates with the infectious dose (Leggett et al., 2017). Therefore, given the higher infectious dose of SAMTB *lux*, growth that is similar to or above that of H37Rv was anticipated. While host Leu and Pan were likely available to SAMTB *lux*, the abundance of these amino acids may not have been sufficient for an optimal level of growth. Furthermore, the growth of SAMTB *lux* may be restricted under intracellular conditions due to the increased

sensitivity of SAMTB *lux* to intracellular stimuli, leading to preferential expression of the mycobacterial stress response (Mouton et al., 2019).

In a traditional animal TB infection model (mice and guinea pigs), the mycobacterial load *in vivo* is anticipated to plateau and/or reduce over the course of infection (Manca et al., 1999; Yam et al., 2009; Wang et al., 2019b), following the engagement of adaptive immunity. In contrast to traditional models, as an invertebrate, *Gm* solely relies on the innate immune response. Therefore, H37Rv, which lacks auxotrophic impairment or virulence attenuation, was predicted to replicate to higher levels than BCG *lux* or SAMTB *lux*. Indeed, the rate and overall load of H37Rv recovered were substantial higher than BCG *lux* or SAMTB *lux*. However, a decline in the rate of replication was observed between 96 h and 192 h post-infection (**Figure 5.4**), likely reflecting the containment of bacilli in the granuloma-like structures and the bactericidal activity observed within such structures as reported in the two prior models (Chapters 3 and 4). Similarly, the decline in growth of H37Rv correlates with the progression of larval melanisation, indicating increasing levels of bactericidal activity. However, in absence of adaptive immunity, these structures fail to contain or adequately limit the growth of H37Rv, ultimately leading to containment failure and further disease progression. This is supported by the changes to the number of circulating haemocytes found in *Gm* following H37Rv infection (**Figure 5.5**).

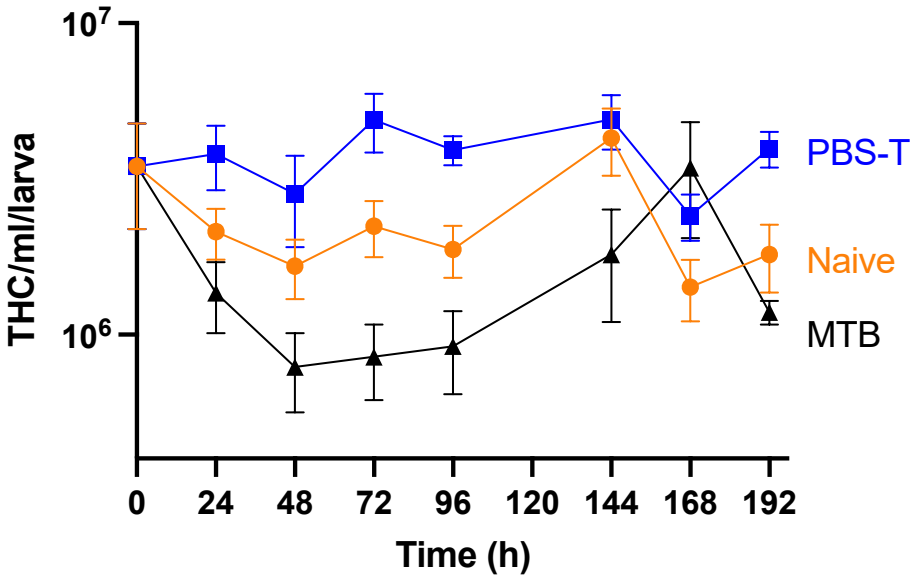


Figure 5.5: Changes in the number of circulating haemocytes following infection with H37Rv. The total haemocyte count (THC) was measured from the haemolymph of n = 4 larvae (per time point) following injection of H37Rv or PBS-T, over a 192 h time course. THC measurement of naïve larvae were included as absolute control. Plotted are the means of three independent experiments, and the error bars represents the SD of the means.

The number of circulating haemocytes declined following infection until 48 h post-infection; haemocytes are actively recruited from the circulation into sessile states as they form the granuloma-like structures throughout the larval body. Between 48 h and 96 h post-infection, levels of circulating haemocytes remain low, reflecting the successful containment of H37Rv within the granuloma-like structures. However, there is a surge in the number of circulating haemocytes between 96 h and 168 h post-infection, which suggests that H37Rv and haemocytes are released back into the haemolymph following containment failure. By 192 h post-infection, the number of haemocytes declines once again. At all-time points, with exception of 168 h post-infection, the number of circulating haemocytes remains below that of the naïve and PBS-T treated larvae, indicating recruitment to sites of H37Rv containment/infection. Longitudinal changes in haemocyte count were not taken for BCG *lux*

or SAMTB *lux* due to time constraints and will be examined in future work. The haemocyte data was overlaid with larval survival and changes to *in vivo* H37Rv CFU (**Figure 5.6**).

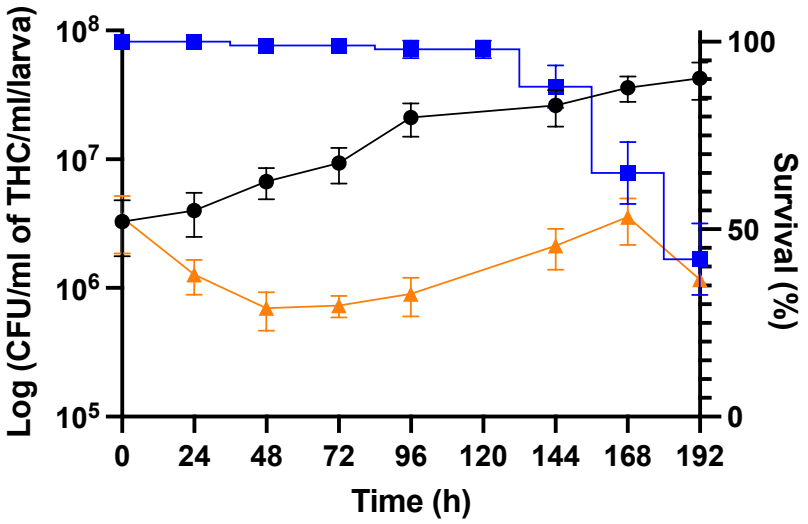


Figure 5.6: Mortality of *G. mellonella* correlates with *in vivo* H37Rv proliferation and suppression of circulating haemocytes. This plot represents a culmination of data presented in Figures 5.1, 5.4 and 5.5. All data represent infection carried out with 2 x 10^6 CFU of H37Rv. CFU/ml in black, THC/ml/larva in orange, and larval survival in blue.

As visualised in **Figure 5.6**, larval mortality and *in vivo* H37Rv replication correlates with changes in the number of circulating haemocytes over the course of infection. Most interestingly, the increase in larval mortality appears to positively correlate with recovery of circulating haemocytes to t = 0 h levels and to the reduced but continued *in vivo* replication from 96 h post-infection onwards (**Figure 5.6**).

In other *Gm* studies, larval mortality typically correlates positively with *in vivo* microbial replication as demonstrated with NTM (Entwistle & Coote, 2018; Meir et al., 2018), *Shigella* spp. (Barnoy et al., 2017), and *C. albicans* (Sheehan & Kavanagh, 2018). However, correlation between changes in haemocyte count with larval mortality or *in vivo* microbial load are more

variable. For example, in *C. albicans* infection of *Gm*, there is an overall decline in the number of circulating haemocytes (Sheehan & Kavanagh, 2018). Whereas NTM (*M. fortuitum* and *M. marinum*) infection led to a rise in the number of circulating *Gm* haemocytes (Entwistle & Coote, 2018). Furthermore, *Gm* haemocyte counts are not consistently reported in all published studies, likely due to the wide variety of anticoagulant reagents used causing high levels of variability between studies. These reagents - which include PBS (Lapointe et al., 2012), 2-mercaptoethanol supplemented PBS (Sheehan & Kavanagh, 2018), Grace's insect medium (Wrońska & Boguś, 2020), and insect physiological saline (Entwistle & Coote, 2018) are all used to prevent coagulation of haemolymph and create a single cell suspension. Therefore, effective comparison of haemocyte counts with other studies is challenging and should be interpreted with caution.

5.2.3 Interaction of H37Rv with Galleria mellonella haemocytes

As with the SAMTB *lux* infection (Chapter 4), TEM of *Gm* haemocytes extracted from infected larvae (2 x 10^6 CFU) at 1 h, 24 h, 96h, and 192 h post-infection, confirmed the presence of H37Rv bacilli over the course of the 192 h (**Figure 5.7**). H37Rv bacilli were rapidly internalised by phagocytic haemocytes 1 h post-infection (**Figure 5.7A**). Despite infection of *Gm* with a dose ten-fold less than that used for SAMTB *lux,* large clusters of haemocytes in a granuloma-like structure containing H37Rv bacilli can be observed as early as 24 h post-infection (**Figure 5.7B**). Such multi-cellular structures, where outlines of individual cells could not easily be distinguished, were the most predominant amongst *Gm* infected with H37Rv (**Figure 5.7B-D**). By 192 h post-infection, necrotic haemocytes were visualised, which lacked cell membrane integrity, leaking intracellular material and bacilli into the surrounding environment (**Figure 5.7E**). Internalised bacilli reflected the proliferative nature of H37Rv infection (as with SAMTB *lux)* and lacked pronounced accumulation of ILI, indicating that bacilli found in circulation are metabolically active, and do not appear to have traits indicating physiological stress.

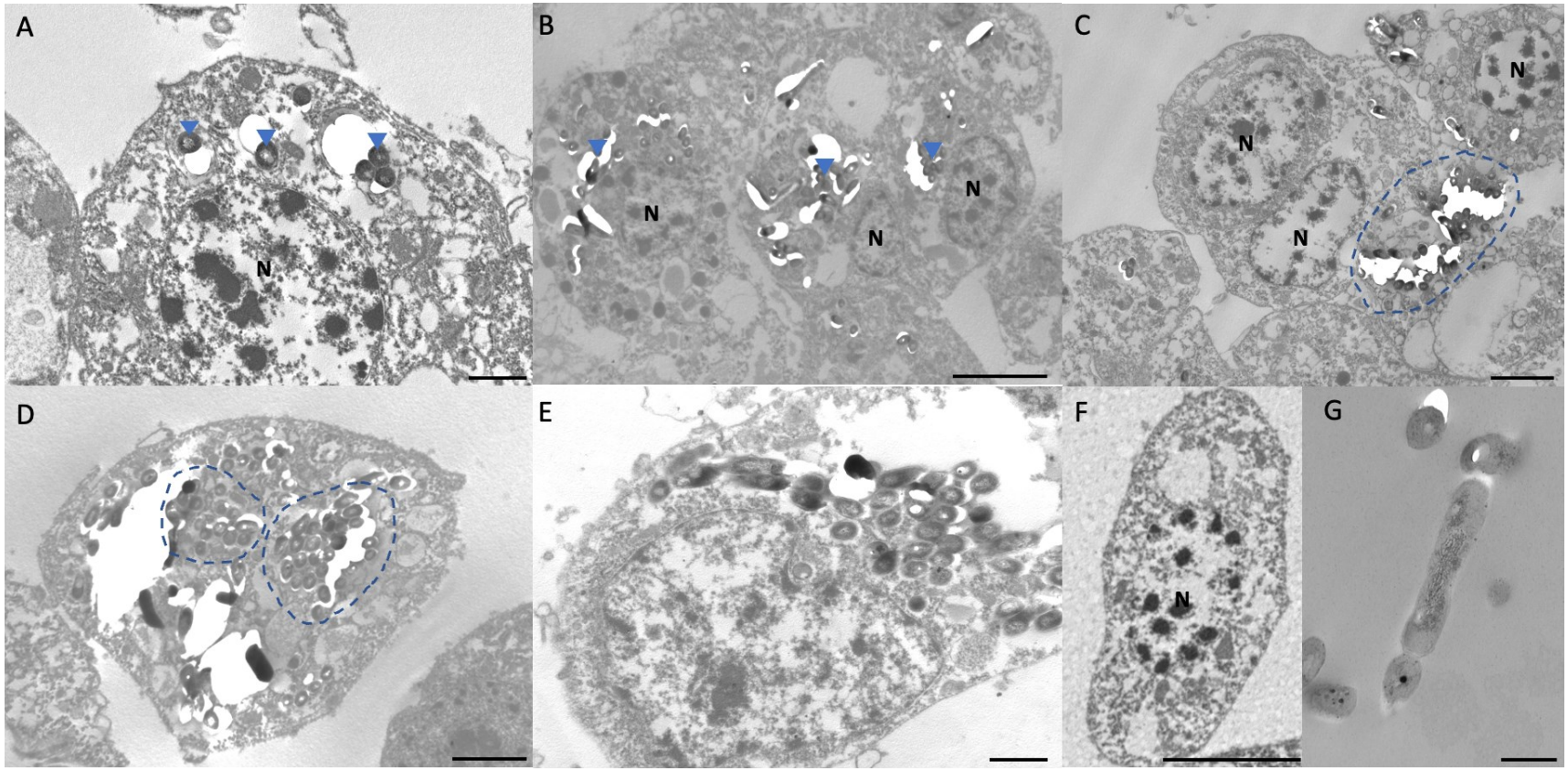


Figure 5.7: Transmission electron microscopy of H37Rv infected *G. mellonella* haemocytes. Larvae infected with H37Rv (2 x 10^6 CFU) were bled (n = 10, per time point) at 1 h (A), 24 h (B), 96 h (C), 144 h (D) and 192 h (E) post-infection. Haemocytes of naïve (uninfected) larvae (F) and H37Rv bacilli (G) were provided as controls. (A) As early as 1 h post-infection, internalisation of H37Rv bacilli (blue arrowheads) by haemocytes was observed. (B) Aggregates of haemocytes at 24 h post-infection containing small clusters of H37Rv bacilli (blue arrowheads). (C) At 96 h post-infection, early granuloma-like haemocyte aggregates surrounding a central mass of mycobacteria (highlighted in blue) were observed. The abundance of intracellular H37Rv was observed over the course of infection, with individual haemocytes containing large aggregations of bacilli by 144 h post-infection (D, highlighted in blue). (E) By 192 h post-infection, haemocytes were mainly necrotic, with loss of cell integrity and leakage of intracellular materials and bacilli. N = nucleus. Scale bars represent 1 µm: A,E, 2 µm: C,D, 4µm: B,F and 400 nm: G.

5.2.4 H37Rv induces the formation of granuloma-like structures in Galleria mellonella

Histological sections were prepared from *Gm* larvae infected with H37Rv (2 x 10^6 CFU) which were stained with ZN or H&E. As early as 24 h post-infection, granuloma-like structures containing clusters of individually distinguishable bacilli and dense ZN reactive material were observed (**Figure 5.8A**). Dense masses of ZN reactive material likely signify, leakage of acid-fast material due to host directed degradation of mycobacterial bacilli. A corresponding H&E staining of these structures confirm arrangement of host cells and ZN reactive areas corresponds with deeper staining as well as pockets lacking eosinophilia (**Figure 5.8B**). Beyond the initial point of containment at 24 h post-infection, granuloma-like structures at 48 h post-infection (**Figure 5.8C**) primarily consisted of host cells containing small numbers of mycobacteria. Arrangement of host cells at 48 h post-infection lacked complexity in comparison to those structures previously observed at similar time points of BGC *lux* and SAMTB *lux* infection as indicated by H&E staining (**Figure 5.8D**). This likely reflects the lower infectious dose of H37Rv, and the level of immune response induced.

Over time, as H37Rv replicated within the larvae, the cellular arrangement of the granuloma-like structures became more complex (**Figure 5.8E-L**). By 144 h post infection, well organised granuloma-like structures containing large clusters of ZN reactive bacilli can be identified (**Figure 5.8E**). Within the same structure, brown/black masses were visualised, which may represent melanisation of residual mycobacterial material. The corresponding H&E stain (**Figure 5.8F**) shows a complex arrangement of host cells forming a clear border around the infected host cells. Furthermore, as before, deeply ZN reactive regions correspond with stronger H&E staining and pockets with loss of eosinophilia. Areas associated with large clusters of individually distinguishable bacilli stained as circular eosinophilic areas with a

central spongy loss in eosinophilia (**Figure 5.8F and 5.9A**). By 192 h post-infection, granuloma-like structures containing foci of dense ZN-reactive mass which was losing its ZN staining and changing colour, ranging from black (likely melanisation), to deep red, dark brown and grey masses (**Figure 5.8G**). As with other larger foci, strong H&E staining co-localised with areas of intense ZN staining (**Figure 5.8H**). At the same time point (192 h post-infection), bacterial foci predominantly lacking ZN staining were visualised as a large grey mass (**Figure 5.8I**), which was also found with SAMTB *lux* infection (Chapter 4). Such structures losing ZN reactivity were observed as early as 96 h post-infection in H37Rv infected larvae (**Figure 5.8K**). With H&E staining, both acid-fast negative structures at 96 h and 192 h post-infection (**Figure 5.8J and L**) appear to be largely indistinguishable from those previous H&E stains of ZN reactive structures (**Figure 5.8H**)**.** However, within the foci of ZN negative granuloma-like structures, cell nuclei were more easily visualised (**Figure 5.9C**) in comparison to foci with dense masses of ZN reactive material (**Figure 5.9B**). The lack of more obvious nuclei in H&E-stained ZN reactive masses, may be an indication of high levels of host necrosis producing cellular debris. Whereas in ZN negative foci, changes in host-pathogen interaction may have prevented extensive levels of host cell necrosis.

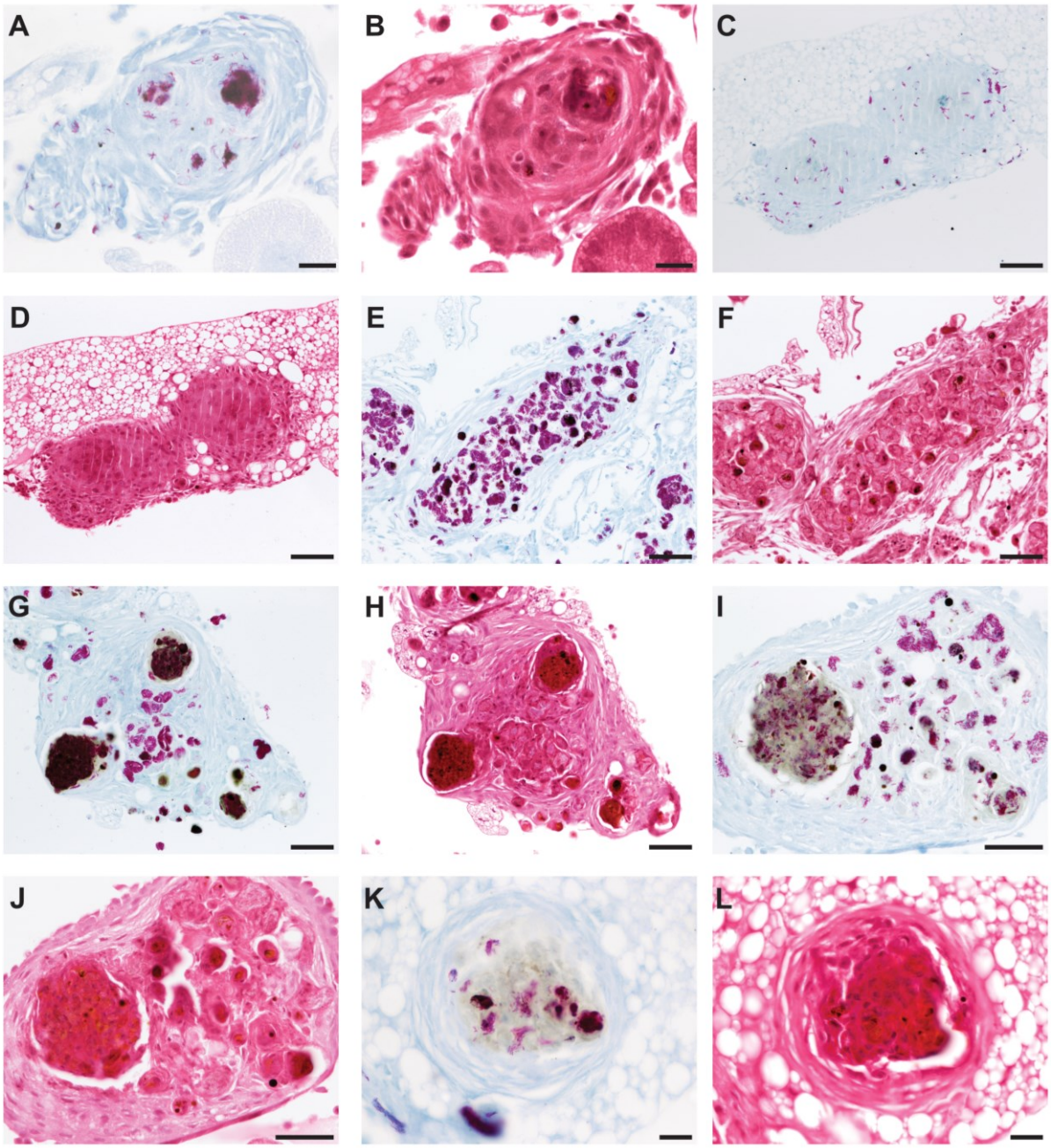


Figure 5.8: Histological sections of *G. mellonella* infected H37Rv over a 192 h time course. Tissues sections were prepared from larvae (n = 3, per time point) infected with H37Rv (2 x 10^6 CFU) and stained with ZN (A, C, E, G, I, and K) or H&E (B, D, F, H, J, and L). Composition of granuloma-like structures varied over time: 24 h (A, B), 48 h (C, D), 144 h (E, F) 192 h (G-J) and 96 h (K, L), with mixtures of individually distinct clusters of bacilli of varying size and densely packed masses of highly ZN reactive material. Loss in ZN affinity was observed in structures 96 h post-infection onwards (G, I, K). H&E staining indicates cell necrosis through cellular fragmentation, loss/fading of nuclear staining, and loss of eosinophilia (pockets lacking staining) were observed specially in the areas associated with densely packed ZN reactive materials. Scale bars represents 20 µm for A, B, K, and L; 100 µm for C- H; 50 µm for I and J.

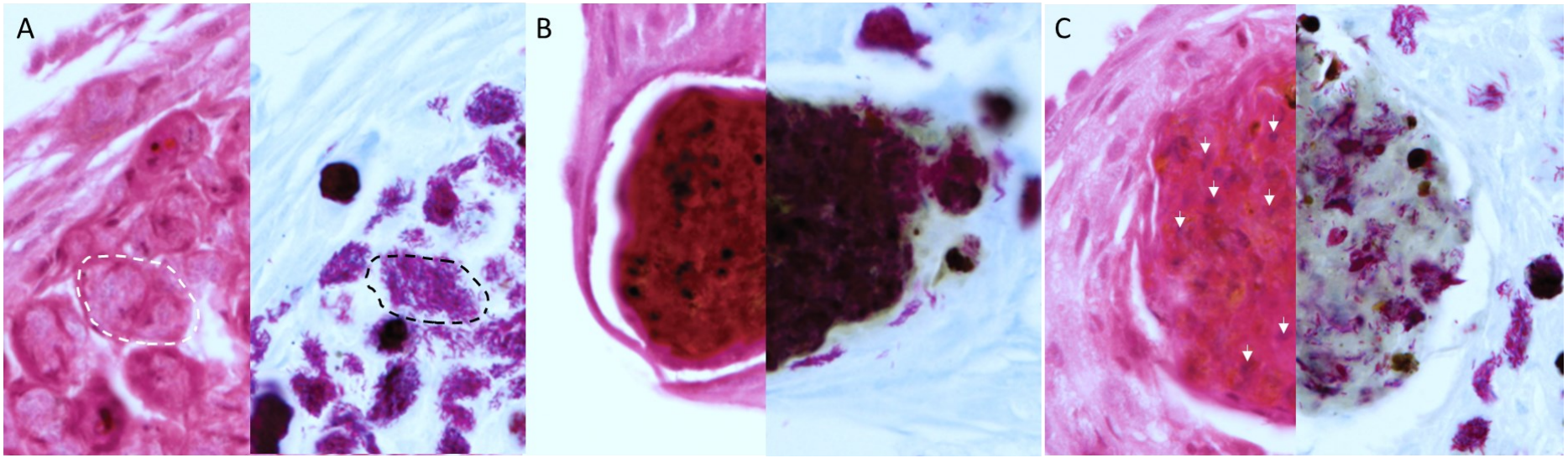


Figure 5.9: Haematoxylin & eosin images of unique granuloma-like structure found in *G. mellonella* infected with H37Rv. Magnified images of H&E stains presented previously as Figure 5.8G-J, highlighting key areas of interest. (A) Under ZN staining, large collections of individually distinct H37Rv bacilli were observed (right, highlighted in black). Under H&E, these structures stain as a clearly defined circular area with a spongy pocket with a loss in eosinophilia (left, highlighted in white). (B) Granuloma-like structure containing dense ZN reactive material (right, ZN stain), with little loss in ZN reactivity. Structure is stained deep red under H&E, indicating high levels of host cell necrosis. (C) Granuloma-like structure associated with predominant loss of ZN reactivity (right, ZN stain). In contrast to (B), the granuloma-like structure did not stain as intensely with H&E, and host cell nuclei can be distinguished in the stain (as highlighted by the white arrows); likely indicating that the level of host cell necrosis is low despite the presence of mycobacterial mass.

Based on these histopathology images, loss of acid-fastness cannot be attributed to a specific state of infection (early, mid, or late). However, based on the Koch paradox (as previously stated in Chapter 4), such entities could represent late-stage granuloma-like structures where bacilli have undergone physiological changes to adapt and survive under granulomatous conditions (Vilchèze & Kremer, 2017). The use of a lower infectious dose of H37Rv, relative to BCG *lux* and SAMTB *lux,* resulted in greater variability and visualisation of capsulation and maturation of granuloma-like structures over the course of infection. It is unclear whether formation of host capsular structures is induced by the host, mycobacteria, or both. Based on current knowledge of insect innate immunity, it is likely that growth of such structures is mediated by a cellular process known as nodulation, which is primarily triggered through recognition of pathogens and mediated via phagocytosis (Dubovskiy et al., 2016b). Over time, the growing nodule is likely reinforced through encapsulation of the structure, which is typically reserved for larger invading pathogens such as nematodes and wasp eggs (Dubovskiy et al., 2016b; Hillyer, 2016; Jung et al., 2019). The growth of granuloma-like structures is most evident in the sagittal whole larva section of infected *Gm* over the course of infection (**Figure 5.10**).

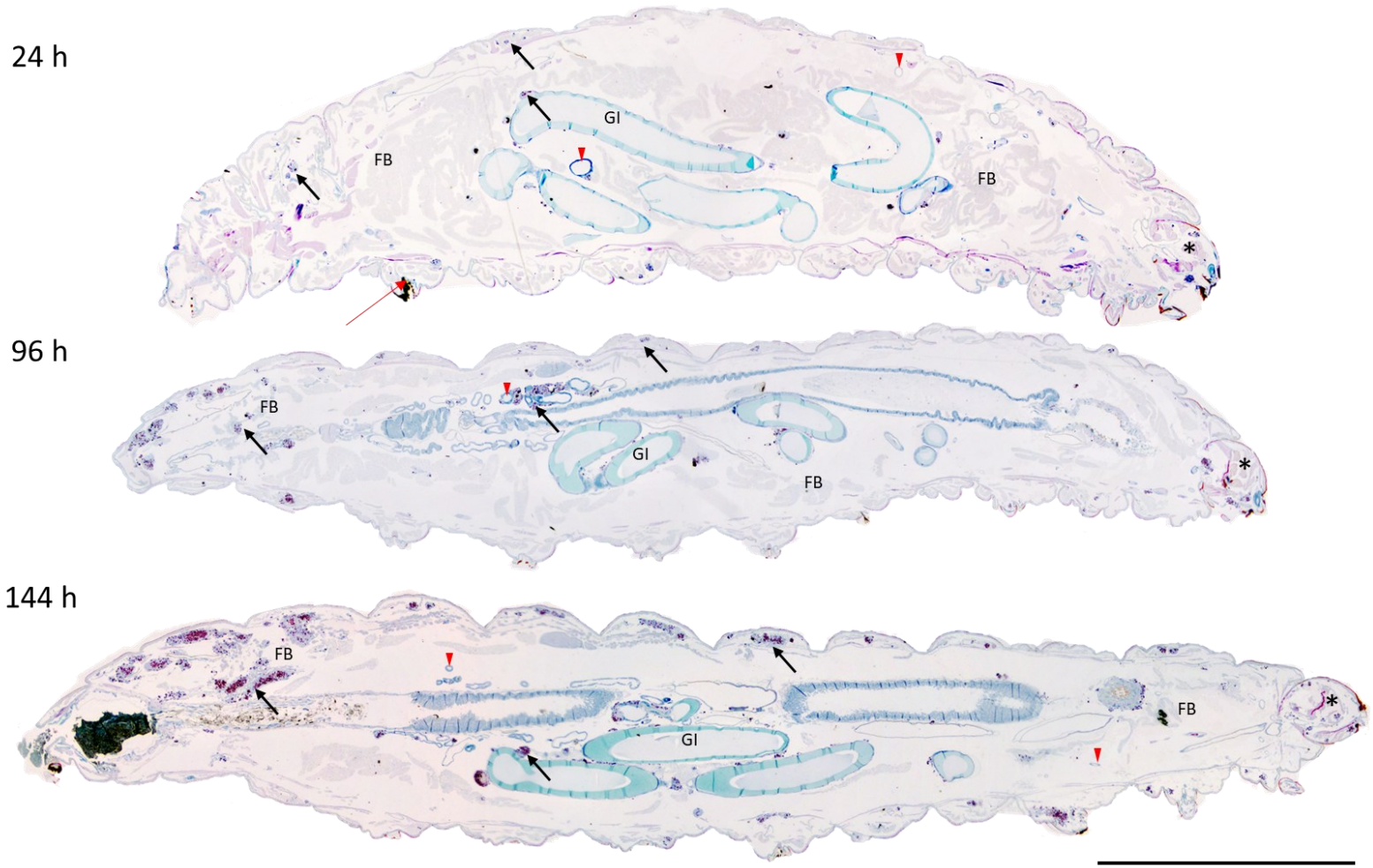


Figure 5.10: Development of granuloma-like structures in *G. mellonella* infected with H37Rv. Sagittal cross-section of larva infected with H37Rv WT (2 x 10^6 CFU) at 24 h, 96 h and 144 h post-infection. Granuloma-like structures (arrows) can be found throughout the larval body, increasing in size and frequency over the course of infection. GI: gastrointestinal tract; red downward triangle: trachea; *: head; red arrow: site of injection; Scale bars: 1000 µm.

5.2.5 Galleria mellonella can be used to distinguish relative virulence of H37Rv mutants

To assess the use of *Gm* as a screen for comparative *MTB* virulence, two mutants of H37Rv: Δ*phoP* and Δ*dosR*, were selected for screening compared to H37Rv WT and their complemented strains. Both strains were chosen based on their attenuated phenotypes in mammalian models (Pérez et al., 2001; Gonzalo-Asensio et al., 2008; Converse et al., 2009; Gautam et al., 2015). The *phoP* gene is part of the PhoPR two-component regulatory system. PhoP has been widely associated with regulation of *MTB* virulence, metabolism, and the stress response (Gonzalo-Asensio et al., 2008). The relevance of PhoP in virulence regulation was one of the key reasons for its selection as one of the two critical knockout mutations to generate the candidate live attenuated TB vaccine, MTBVAC (Broset et al., 2015; Aguilo et al., 2016). The *dosR* gene (also known as *devR*) is part of the DosRST two-component regulatory system (Zheng et al., 2016). The induction of the DosR pathway is activated by intracellular stimuli such as nitric oxide, carbon monoxide and hypoxia. The DosR regulon modulates mycobacterial metabolism into a non-replicative dormant, persistent, and latent state (Zheng et al., 2020). Therefore, infection of *Gm* with either Δ*phoP* and Δ*dosR* is anticipated to result in an attenuated (less lethal) outcome when compared to WT, due to the impact these genes have on the fitness of *MTB*.

In *Gm*, the lethality (virulence) of Δ*phoP* (2 x 10^6 CFU) was substantially attenuated compared to the WT (2 x 10^6 CFU), with larval survival of 93% and 48%, respectively, at 192 h (**Figure 5.11**). Virulence was restored to near WT levels (58% survival) when larvae were challenged with 2 x 10^6 CFU of the Δ*phoP* complemented strain (**Figure 5.11**). The results were in-line with those in SCID mice, where the Δ*phoP* mutant was avirulent (non-lethal) over a course of 250 days. Infection of SCID mice with the complemented strain restored virulence to the WT

level (Martin et al., 2006). While changes to *in vivo* CFU were not undertaken in *Gm*, prior studies in BALB/C mice (Pérez et al., 2001; Gonzalo-Asensio et al., 2008), indicated that *phoP* deletion impaired mycobacterial replication *in vivo,* but persistence of mycobacteria was reported despite this growth impairment.

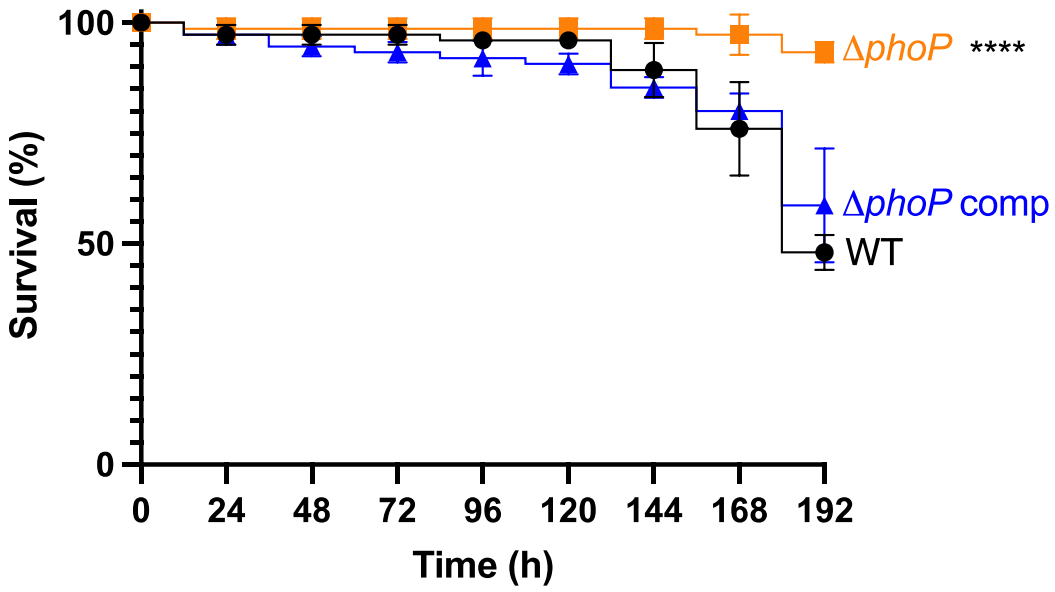


Figure 5.11: Assessment of H37Rv Δ*phoP* virulence in *G. mellonella*. Larvae were infected with 2 x 10^6 CFU of H37Rv: WT, Δ*phoP* or Δ*phoP* complemented strain (Δ*phoP* comp). Larvae were incubated in the dark at 37 °C following infection, and larval survival were monitored every 24 h for 192 h. Plotted are the means of three independent experiments, and the error bars represent the SD of the means. Sample size per experiment was n = 25. Mantle-Cox log-rank test with Bonferroni's correction was carried out against WT, **** ($p < 0.0001$).

One of the key effects of Δ*phoP* mutation is believed to be the prevention of ESAT-6 secretion by ESX-1. This was demonstrated though immunoblots of WT and Δ*phoP* culture filtrate and cell lysates, which showed that deletion of *phoP* lead to inhibition of secretion but not the production of ESAT-6 (Frigui et al., 2008; Kumar et al., 2016b). As discussed in Chapters 3 and 4, ESAT-6 is a key virulence factor with membranolytic activity that prevents phagosomal maturation and facilitates egress of bacilli from infected cells, thereby promoting further

propagation of mycobacteria (Simeone et al., 2021). This inability of the Δ*phoP* mutant to secret ESAT-6, functionally attenuated the virulence of H37Rv to similar levels of BCG (**Figures 5.2 and 5.11**), which naturally lacks RD1 that encodes ESAT-6 and ESX-1 (Liu et al., 2009). A transcriptional study of Δ*phoP,* identified significant changes in transcriptional regulation amongst 78 genes, representing ~2% of the total *MTB* genome, of which 11 genes were associated with RD1 (Gonzalo-Asensio et al., 2008). In addition to the membranolytic activity, a comprehensive study of ESAT-6 and ESX-1 identified that the loss of RD1 can reduce uptake of mycobacteria by phagocytes *in vitro* (Brodin et al., 2006). Such reduction in phagosomal uptake will work against the survival of an intracellular pathogen such as *MTB*. Additionally, the transcriptional studies identified that PhoP regulates other key stress factors associated with hypoxia, persistence, and lipid metabolism (Gonzalo-Asensio et al., 2008). Moreover, of the 78 genes regulated by PhoP, 48 genes were differentially regulated under intracellular conditions in THP1 (Fontán et al., 2008), murine bone marrow-derived macrophages (Schnappinger et al., 2003; Rohde et al., 2007), human dendritic cells and macrophages (Tailleux et al., 2008), highlighting the importance of PhoP during intracellular survival.

In *Gm*, the lethality (virulence) of Δ*dosR* (2 x 10^6 CFU) increased substantially when compared to the WT (2 x 10^6 CFU), with larval survival of 30% and 53%, respectively (**Figure 5.12**). Larval infection with the complemented Δ*dosR* strain (2 x 10^6 CFU) increased survival to 62%, i.e., restoring virulence to the WT level (**Figure 5.12**). In comparison to prior animal studies, the hyper-virulence of Δ*dosR* observed in *Gm,* contradicted the majority consensus of attenuated or indifferent infectious outcome in NHPs (Mehra et al., 2015), C57BL/6, BALB/C and C3HeB/FeJ mice (Converse et al., 2009; Gautam et al., 2015), guinea pigs (Malhotra et al.,

2004) and rabbits (Converse et al., 2009). However, hyper-virulence observed in *Gm* agreed with that reported in SCID mice infected with Δ*dosR* (Parish et al., 2003).

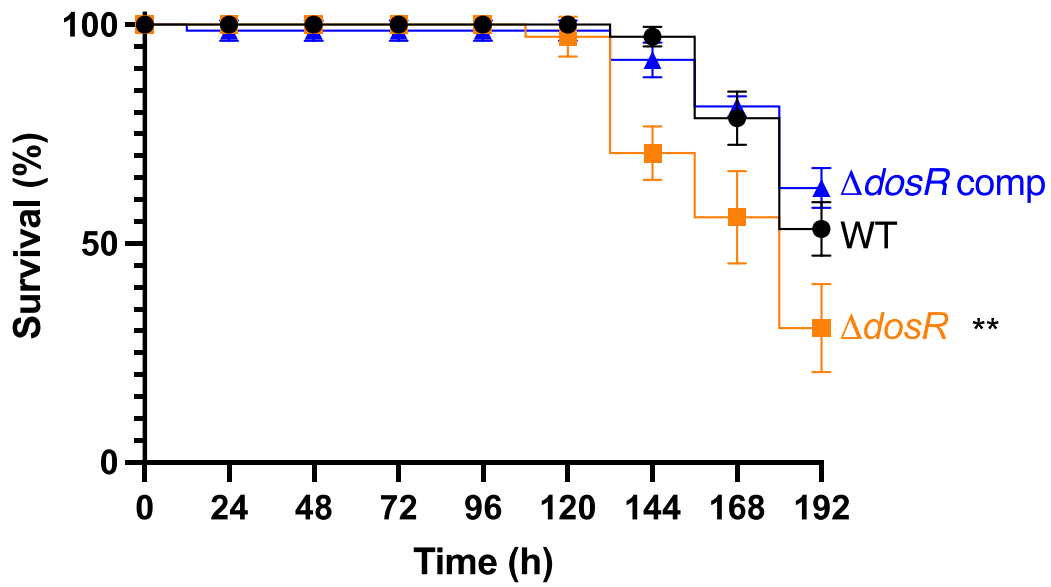


Figure 5.12: Assessment of H37Rv Δ*dosR* virulence in *G. mellonella*. Larvae were infected with 2 x 10^6 CFU of *MTB* H37Rv: WT, Δ*dosR* or the Δ*dosR* complemented strain (Δ*dosR* comp). Larvae were incubated in the dark at 37 °C following infection, and larval survival were monitored every 24 h for 192 h. Plotted are the means of three independent experiments, and the error bars represent the SD of the means. Sample size per experiment was n = 25. Mantle-Cox log-rank test with Bonferroni's correction was carried out against WT, ** ($P < 0.001$).

One possible explanation for the discrepancy between hyper-virulent, attenuated and indifferent outcome following infection with the Δ*dosR* mutant could be associated with the host capacity to develop hypoxic granulomas. For example, hypoxic granulomas do not develop in some mouse models (e.g., C57/BL6) (Rustad et al., 2008). Indeed, *dosR* mutants are attenuated in models where hypoxic granuloma do develop such as in NHPs, rabbits, guinea pigs and C3HeB/FeJ mice (Malhotra et al., 2004; Converse et al., 2009; Gautam et al., 2015). Hyper-virulence maybe due to the severely immunocompromised state of SCID mice (Parish et al., 2003). Authors also studied the phenotype of hyper-virulence Δ*dosR* mutant in

immunocompetent DBA mice, reporting a substantial rise in Δ*dosR* load (~8-10 fold) during the acute phase of infection when compared to the WT, prior to the induction of adaptive immunity (Parish et al., 2003). Additionally, infection of interferon (INF)-γ activated macrophages with Δ*dosR* led to replication and consistently higher levels of mycobacterial load over time when compared to the WT (Parish et al., 2003).

Interpretation of Δ*dosR* hyper-virulence in *Gm* is limited due to our current knowledge of the pathophysiology (e.g., cellular composition, gaseous composition, and pH) of granuloma-like structures. Furthermore, it is important to highlight that the significance of DosR on hypoxic response is currently a topic of continued debate, with studies highlighting the influence of other two-component systems, e.g., PhoPR (Gonzalo-Asensio et al., 2008) or that the hypoxic stress response can be induced independent of DosR (Rustad et al., 2008). However, based on cautious interpretation of the available data for Δ*dosR* infections, the outcome of hyper-virulence in *Gm* is most likely the result of enhanced and unregulated multiplication of Δ*dosR* in *Gm,* as seen in SCID mice. Future studies are required to define the pathophysiology of the granuloma-like structures so that the role of DosR in *Gm* infection can be identified.

The comparative virulence data in *Gm* for Δ*phop* and Δ*dosR* mutants of *MTB* demonstrates that this simple insect model is capable of distinguishing changes in mycobacterial virulence. While observations of the Δ*dosR* mutant differed from the majority published consensus, reversion to WT virulence was a promising indication that observed virulence was caused by the introduced mutation. Future studies of *MTB* WT and known attenuated mutant pairs will potentially enhance uptake of the *Gm*-H37Rv infection model, and also give insights into both bacterial and host interactive biology.

5.3 Conclusion

In this Chapter, a CL3 *Gm-MTB* H37Rv infection model was established and characterised. In response to feedback from the TB research community, the model included a substantially (ten-fold) lower inoculum and an extended study window of 192 h from 92 h. As hypothesised, *Gm* challenged with H37Rv resulted in a more virulent (lethal) infection when compared to that caused by BCG *lux* or SAMTB *lux,* as described in Chapters 3 and 4. Following infection, H37Rv proliferated over the course of 192 h, while the rate of replication declined after 92 h post-infection. Changes in the rate of replication likely reflected increasing bactericidal activity which correlates with increasing severity of larval melanisation and abundance of circulating haemocytes.

TEM confirmed the presence of H37Rv bacilli over the course of infection similar to that observed with BCG *lux* and SAMTB *lux.* As with SAMTB *lux*, the number of bacilli found within haemocytes increased over time and these bacilli lacked obvious accumulation of ILI, reflecting the proliferative nature of the infection. Overall, the development of granuloma-like structures appeared to be more gradual than BCG *lux* and SAMTB *lux* models, likely because of the lower infectious dose used for H37Rv infection. ZN negative granuloma-like structures became more frequent beyond 96 h post-infection. These structures were previously identified in the SAMTB *lux* but not in BCG *lux* infection model, and I speculate they are a potential indicator of a non-replicative sub-population. These ZN negative granuloma-like structures appeared to be better organised than those containing dense ZN positive material or individually distinct proliferative bacilli.

The use of *Gm* as a screen for comparative MTB virulence was examined and demonstrated using two *MTB* H37Rv mutants Δ*phop* and Δ*dosR*. Both strains exhibited substantial differences in virulence (lethality) when compared to WT. Virulence reverted to near WT levels for both strains following complementation of the deleted genes. For the Δ*phop* mutant, attenuation in *Gm* was in-line with those previously reported in mice (Martin et al., 2006). However, comparison of *Gm*-Δ*dosR* infection was more complex with various reported degrees of virulence ranging from hyper-virulent, no effect, and avirulent. In *Gm*, survival of Δ*dosR* was in-line with that of hyper-virulence seen in SCID mice infection (Parish et al., 2003). While screening of additional mutants is required, the results generated in this Chapter are encouraging and supports the application of *Gm* as a cheap, ethically more acceptable comparative screen for mycobacterial virulence.

Interpreting the results presented in this Chapter together with those presented previously in the BCG *lux* and SAMTB *lux* Chapters, has successfully addressed the concerns surrounding the susceptibility and sensitivity of *Gm* as an infection model for members of the MTBC.

Chapter 6
The use of *G. mellonella* – *M. tuberculosis* complex infection models as screens for antimycobacterial compounds

6.1 Introduction

AMR is a significant threat to global health security, with a projection of 10 million deaths by 2050, overtaking the death toll of cancer (O'Neill, 2016). Not only would AMR make "simple" infections more deadly, but it will also prevent our capacity to practice modern medicine such as cancer treatment and major surgery, owing to the risk of surgical or nosocomial infection (Chandler, 2019). As with other infectious diseases, TB treatment is becoming increasingly challenging (Knight et al., 2019), with roughly a third of all TB deaths being attributable to AMR (Dheda et al., 2017). The current available arsenal of antimycobacterial compounds used to treat TB is limited (Mizrahi & Warner, 2019), and continues to dwindle with the rise of *MTB* isolates possessing resistance to the last line antimycobacterial compounds: delamanid and bedaquiline (Polsfuss et al., 2019; Nimmo et al., 2020; Nguyen et al., 2020). While the drug discovery and development pipeline continue to expand, research and trials take several years and billions of dollars before completion and deployment in the clinic (WHO, 2020). As a result, only three compounds (delamanid, bedaquiline and pretomanid) has been approved for the clinic in the past 50 years (WHO, 2020).

Animal models are a vital component of the drug discovery and development pipeline (Zhan et al., 2017). Their use has provided researchers with insight into the pathogenesis and progression of diseases, helping to unravel novel mechanisms and targets for developing novel therapeutics (Zhan et al., 2017). Additionally, *in vivo* screening of candidate compounds is essential for generating crucial safety and efficacy data and is a prerequisite before clinical trials in humans (Singh & Seed, 2021). However, animal models are among the most significant bottlenecks within the pipeline due to their biological limitations (capacity to

mimic aspects of disease), financial sustainability, ethical regulation, and research throughput (Tsai et al., 2016).

The selection of candidate compounds for *in vivo* screening is informed by toxicology and efficacy data derived using *in vitro* studies. However, *in vitro* efficacy does not necessarily translate to *in vivo* efficacy, as compounds may be degraded and deactivated by the host (Tsai et al., 2016). Similarly, compounds with low *in vitro* efficacy may have higher *in vivo* efficacy, such as those which modulate host immune responses (Bergman et al., 2020). Furthermore, some animal models are biologically more prone to intra- and inter-experimental variability, the effect of which is amplified by the limited sample size due to ethical regulations (Fitts, 2011; Zhan et al., 2017). As a result of these challenges, not all candidate compounds are taken forward for *in vivo* testing and contributes to compound attrition within the pipeline. However, attrition can be minimised by adopting alternative infection models as a pre-screen between *in vitro* and *in vivo* studies using traditional animal models.

Alternative infection models (e.g., insect and fish) are ethically more acceptable and economical alternatives to traditional animal models, capable of mimicking key aspects of the disease (van Leeuwen et al., 2015; Tsai et al., 2016). Despite their relative simplicity, these models can produce biologically insightful data, owing to their complex and evolutionarily conserved biological systems (Dionne et al., 2003; van Leeuwen et al., 2015; Dinh et al., 2021). The efficacy and toxicity data generated in these models could more accurately infer potential *in vivo* activities when compared to the use of *in vitro* screening alone (Tzelepis et al., 2013; Tsai et al., 2016; Jijie et al., 2021). Furthermore, using these models as a pre-screen can significantly reduce the number of animals used and/or prevent unnecessary usage of animals

in drug screening studies. Simultaneously, adopting an alternative infection model as a pre-screen would also substantially increase the number of candidate compounds screened in a biological system. Therefore, alternative models can minimise the rate of attrition between *in vitro* and *in vivo* screening and ensure maximum screening output.

Gm is an ideal candidate for use as a pre-screen, with its physiological characteristics representing those seen in traditional animal models and humans (Cutuli et al., 2019). For example, unlike the fruit fly and zebrafish larva, *Gm* can be incubated at 37 °C thus more accurately representing human physiological conditions to mimic disease (Tsai et al., 2016). The size of *Gm* is more convenient for handling during infection and treatment procedures, allowing for easy and precise dosing, when compared to the much smaller fruit fly and zebrafish larva (Oh et al., 2013; Tsai et al., 2016; Dalton et al., 2017). According to an extensive literature review by Cutuli et al., between 2016 to 2018, 37 research articles highlighted the use of novel antibacterial therapeutic and/or strategies against 14 different bacteria genera in *Gm* (Cutuli et al., 2019). Similarly, the use of *Gm* as a model for toxicity screening is becoming increasingly popular (Ignasiak & Maxwell, 2017; Coates et al., 2019; Wijesinghe et al., 2020; Cé et al., 2020; Moya-Andérico et al., 2021; Rigotto Caruso et al., 2021). Such an increase in uptake over a short period, underlines the popularity, traction and validation of the use of *Gm* as a pre-screen for candidate compounds.

In this Chapter, the *Gm*-MTBC (BCG *lux,* SAMTB *lux* and H37RV) models established in this project were evaluated as screens for antimycobacterial compounds using clinically relevant first- and second-line drugs. The data presented here demonstrate the application of *Gm* within the TB drug development and discovery pipeline under CL2 and CL3 environments. The

data generated highlights the potential of the *Gm*-MTBC models as a highly cost-effective and time-efficient drug screening system, with potential for low-medium throughput application.

6.2 Results and Discussion

6.2.1 Clinically relevant antimycobacterial compounds are non-toxic in Galleria mellonella

First- (INH, RIF, ETH, PZA) and second-line (MOX and BDQ) antimycobacterial compounds, clinically used for the treatment of TB, were screened for toxicity in *Gm* before their efficacy evaluation. Toxicity was evaluated at the clinically recommended dosage for treatment of adult TB infection, as outlined by the WHO (WHO, 2010). The recommended dosages were: INH (5 mg/kg), RIF (10 mg/kg), ETH (15 mg/kg), PZA (25 mg/kg), MOX (6.7 mg/kg) and BDQ (5.7 mg/kg). Treatment dosages were scaled relative to the body mass of the larva (200 mg). Naïve (unmanipulated) larvae were injected with a single dose of an antimycobacterial compound, and toxicity (melanisation, reduction in motility and death) was monitored every 24 h for 96 h. Larvae injected with PBS-T was the control.

All compounds were evaluated for additional toxicity at 0.1x and 10x the clinically recommended dosage, except for BDQ, which was only assessed at 0.1x due to the high purchasing cost of BDQ. All compounds, at any given dosage, lacked toxicity in *Gm* (i.e., no larval mortality, no reduction in larval motility, and lacked melanisation). These observations indicate that clinically relevant compounds are safe for use in *Gm* and can be further evaluated for antimycobacterial activity in infected larvae.

The MIC of INH, RIF, PZA, ETH, MOX and BDQ, were determined for BCG *lux,* SAMTB *lux* and H37Rv at one-week as a reference for *in vitro* efficacy (**Table 6.1**). The MIC was defined as the minimum concentration required to inhibit the growth of mycobacteria. All drugs showed inhibitory activity as anticipated. The lack of inhibition by PZA was expected since it is widely

known to lack *in vitro* activity under typical culturing conditions (Tarshis & Weed, 1953; Zhang et al., 2013b).

Table 6.1. *In vitro* (broth microdilution) MIC of clinical antimycobacterial compounds

	MIC (µg/ml)					
	INH	RIF	ETH	PZA	MOX	BDQ
BCG *lux*	0.25	< 0.125	1	> 16	< 0.125	N/D
SAMTB *lux*	0.25	< 0.125	0.5	> 16	0.25	< 0.125
H37Rv	0.5	< 0.125	2	>16	N/D	N/D

MIC was determined using 10^6 CFU of mycobacteria seeded into wells of a 96-well plate, each containing antimycobacterial compounds at various dilutions in Middlebrook 7H9 broth. Plates were incubated at 37 °C for one week, and the turbidity of each well was measured using a plate reader (520 nm). N/D: not defined.

6.2.2 Treatment of infected Galleria mellonella improves larval survival outcome

The efficacy of first- and second-line antimycobacterial compounds in improving survival of *Gm* infected with BCG *lux* (1 x 10^7 CFU) and SAMTB *lux* (2 x 10^7 CFU) was determined. At 1 h post-infection larvae were injected with a single dose of a given antimycobacterial compound at the clinically recommended dosages, relative to *Gm* body mass, as previously described for toxicity testing. Larval survival was monitored every 24 h for 96 h following treatment. Infected larvae treated with PBS-T were used as the control.

All antimycobacterial treatments, with exception to ETH significantly improved the survival outcome of BCG *lux* infected larvae (INH, RIF, MOX and PZA: $p < 0.0001$) over the 96 h time course when compared to the control (**Figure 6.1A**). Treatment with RIF or INH was the most efficacious, with 100% and 95% survival, respectively. Moderate improvement in survival

outcome was observed for MOX and PZA (82.5% and 75%, respectively). While ETH had the lowest survival outcome of 45 %, treatment led to considerable improvements relative to the survival of the control (22.5%), supporting trend in improvements.

SAMTB *lux* infected larvae were similarly tested, where only RIF ($P < 0.0001$) and INH ($P < 0.0001$) treatment led to significant improvements in larval survival outcome over 96 h when compared to the control (**Figure 6.1B**). As with BCG *lux* infection, treatment with RIF or INH was the most efficacious, with 100% and 90% survival, respectively. Despite a lack of significance, a moderate improvement in survival was observed for MOX (67.5%), supporting trend in improvement. Survival outcome was substantially lower for PZA, BDQ and ETH (52.5%, 47.5% and 45%, respectively); similar to the survival of the control at 45%. BDQ was not evaluated in the BCG *lux* model due to time constraints but will be tested in future studies.

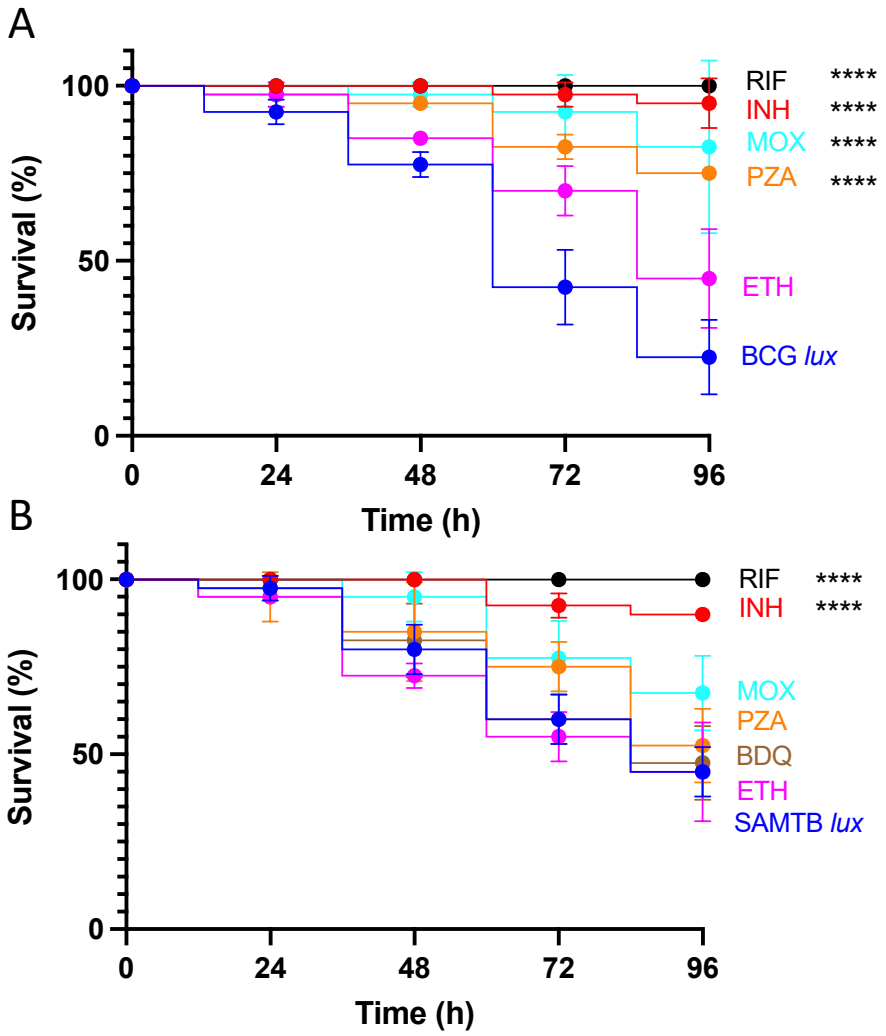


Figure 6.1: Survival of *G. mellonella* infected with BCG *lux* or SAMTB *lux,* following treatment with first- or second-line antimycobacterial compounds. Larvae (n = 20, per treatment group) were infected with either (A) BCG *lux* (1 x 10^7 CFU) or (B) SAMTB *lux* (2 x 10^7 CFU) and treated with a single dose INH (5 mg/kg), RIF (10 mg/kg), ETH (15 mg/kg), PZA (25 mg/kg), MOX (6.7 mg/kg) or BDQ (5.7 mg/kg), given 1 h post-infection. Infected larvae treated with PBS-T were used as the control. Larvae were monitored every 24 h for 96 h. Plotted are the means of two independent experiments, and the error bars represent the SD of the means. For statistical analysis, Mantle-Cox log-rank test with Bonferroni's correction, between treatment groups and the control were carried out: **** ($P < 0.0001$). BCG *lux* data adapted from Asai et al., 2019b.

The efficacy of clinically relevant antimycobacterial compounds was similarly assessed in the CL3 *Gm*-H37Rv infection model. As previously addressed in Chapter 5, alterations were made to this model's design, including reducing the infectious dose from 10^7 CFU to 10^6 CFU and extending the study's time frame from 96 h to 192 h. These changes enabled a prolonged

incubation of 72 h compared to 1 h incubation used for BCG *lux* and SAMTB *lux* infected larvae before treatment. This change in the length of incubation was made in response to concerns (reviewers' comments) that 1 h may not be sufficient for mycobacteria to be internalised by haemocytes. However, ZN, TEM and confocal microscopy images confirmed bacilli association with and internalisation by phagocytic haemocytes as early as 1 h post-infection for the BCG *lux* and SAMTB *lux* models. Furthermore, rapid treatment following infection (15 min-2 hours) is a common practice in the *Gm* models (Peleg et al., 2009; Krezdorn et al., 2014; Tsai et al., 2016; Entwistle & Coote, 2018; Meir et al., 2018; Tkhilaishvili et al., 2020; Grygorcewicz et al., 2020; Thieme et al., 2020; Petronio et al., 2020), which reflects their design for rapid determination of drug efficacy.

In the H37Rv model, RIF and INH were the only efficacious treatment that led to significant improvements ($P < 0.0001$) in larval survival (96% and 93.3%, respectively) over the 192 h time course (**Figure 6.2**). Treatment efficacy of PZA and ETH was low with 50.6% and 37.3% survival, respectively, which was indifferent to the control survival of 41.3%. Second-line antibiotics were not evaluated due to time constraints but will be tested in future studies.

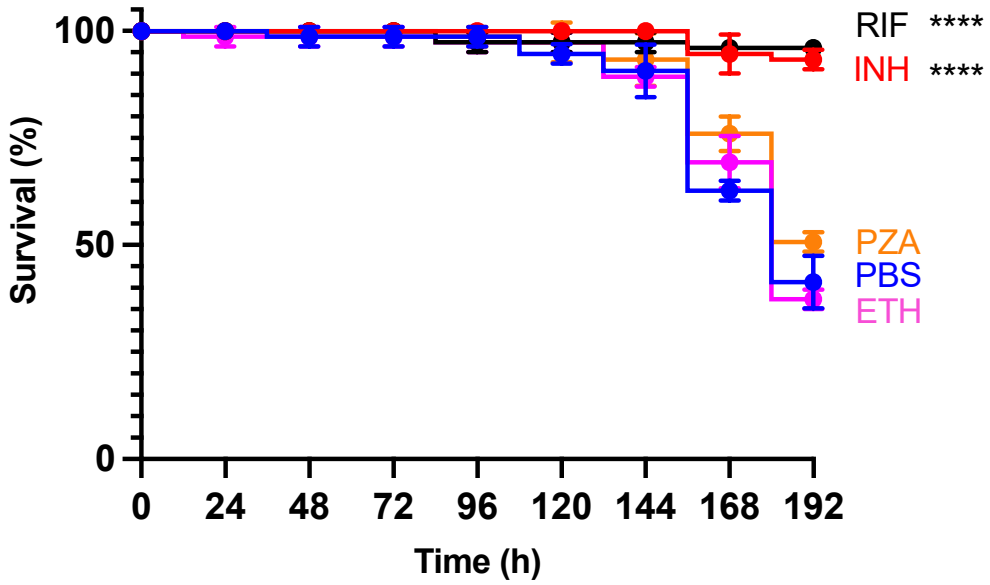


Figure 6.2: Survival of *G. mellonella* infected with H37Rv, following treatment with first-line antimycobacterial compounds. Larvae (n = 25, per treatment group) were infected with H37Rv (2 x 10^7 CFU) and treated with a dose of INH (5 mg/kg), RIF (10 mg/kg), ETH (15 mg/kg), or PZA (25 mg/kg). Infected larvae treated with PBS-T were used as the control. Larvae were monitored every 24 h for 192 h. Treatment was administered via injection 72 h post-infection. Plotted are the means of three independent experiments, and the error bars represent the SD of the means. Mantle-Cox log-rank test with Bonferroni's correction was carried out between the treatment groups and the control: **** ($P < 0.0001$).

Comparison of four first-line antimycobacterial compounds evaluated in all three *Gm*-MTBC models indicates a trend in treatment efficacy of RIF > INH > PZA > ETH. However, in both the SAMTB *lux* and H37Rv models, survival of PZA and ETH treated larvae were not statistically different from control groups. MOX moderately improved survival outcomes in the BCG *lux* and SAMTB *lux* models: INH > MOX > PZA. Treatment of SAMTB *lux* with BDQ did not improve survival outcomes compared to the control, indicating that the "second-line" compounds do not necessarily signify better efficacy for treatment outcomes in *Gm*. The improved survival outcome of PZA treated BCG *lux* infected larvae was surprising as BGC *lux* is intrinsically resistant to PZA (Ritz et al., 2009). A further discussion of PZA activity is given later in this Chapter.

The variance in treatment outcome between the three models likely reflects the replicative state of mycobacteria in these models, i.e., non-replicative (BCG *lux*) vs replicative (SAMTB *lux* and H37Rv). Therefore, the efficacy of compounds screened against BCG *lux* should be interpreted with caution, taking into account the non-replicative and naturally declining activity of BCG *lux* in *Gm* over the 96 h time course (**Figure 3.6**).

Intriguingly, the survival of the controls was lower for SAMTB *lux* (45% vs 63% est. [Chapter 4]) and substantially lower (22.5% vs 50% est. [Chapter 3]) for BCG *lux* than anticipated. However, for H37Rv, little to no variability was reported between the control in this study and Chapter 5 (41.3% vs 42%, respectively). The observed variance in BCG *lux and SAMTB lux* studies could result from trauma of repeat injection at the point of infection and during treatment, which was carried out in a short period (1 h). Repeated injection could have overstimulated the larval immune response in response to injury (Hillyer, 2016), leading to a higher mortality outcome. In the case of the H37Rv model, the extended incubation period between infection and treatment (72 h vs 1 h post-infection, for H37Rv and BCG *lux*/SAMTB *lux*, respectively), combined with a reduction in infectious dose, could have reduced the activation of injection associated immune responses. To evaluate whether injection trauma alone could have induced adverse outcomes, naïve larvae mock-infected and treated with PBS-T 1 h post-infection were monitored over 96 h. However, no adverse effects on larval health were observed.

Furthermore, other *Gm* studies that have carried out repeated injections (as many as three) have similarly not reported any adverse effect on larval mortality outcome due to treatment

(Peleg et al., 2009; Krezdorn et al., 2014; Tsai et al., 2016; Entwistle & Coote, 2018; Tkhilaishvili et al., 2020; Grygorcewicz et al., 2020; Thieme et al., 2020; Petronio et al., 2020). Additional injection-associated complications, such as puncturing the gut or contamination from the cuticle, were considered a potential cause of increased mortality. However, based on experience, such occurrences lead to rapid and noticeable changes to larval phenotype (severe melanisation and liquefication of larvae) and death within 24 h, which was not observed in our untreated infection control. Therefore, it is likely that this variability between survival of the control group in this chapter and those prior, is due to batch effects associated with the condition of the *Gm* (seasonal temperature effect during transport) and/or the mycobacteria culture condition (medium quality and bacilli clumping).

6.2.3 Antimycobacterial treatment reduces mycobacterial burden in Galleria mellonella

The efficacy of first- and second-line antimycobacterial compounds in *Gm* was further evaluated by measuring changes to the *in vivo* mycobacterial burden following treatment. For BCG *lux* and SAMTB *lux,* bioluminescent measurement of the larval homogenate was used to rapidly quantify relative changes in *in vivo* mycobacterial burden as previously carried out in Chapters 3 and 4. For H37Rv, only the CFU was enumerated, as carried out in Chapter 5. Infected larvae treated with PBS-T was used as the control.

In larvae infected with BCG *lux*, all treatments showed a trend in mycobacterial bioluminescence reduction over the 96 h time course (**Figure 6.3A, B**). INH was the most effective and only compound to significantly reduce BCG *lux* bioluminescence ($p < 0.0001$), reducing the mean bioluminescence by 94.1%, relative to the control at 96 h (**Figure 6.3B**). Treatment with RIF, MOX and ETH did not lead to a significant reduction in bioluminescence

following treatment (**Figure 6.3A**). However, by 96 h, BCG lux bioluminescence declined moderately for RIF, MOX and ETH: 64.7%, 61.8 and 60.4%, respectively, relative to the control (**Figure 6.3B**). PZA was the least effective compound with no more than 26.5% reduction in mean bioluminescence at any time point over the 96 h time course (**Figure 6.3A, B**).

Overall, the non-replicative persistent nature of the BCG *lux* infection in *Gm* was not conducive to differentiating subtle differences in drug efficacies, as bioluminescence naturally declined over time. The bioluminescence measurement of PZA treated larvae was more in line with the PZA resistant nature of BCG *lux*. However, PZA remains perplexing, as despite the lack of substantial changes to *in vivo* BCG *lux* burden, survival outcome of PZA treated larvae improved significantly over the control (**Figure 6.1A**).

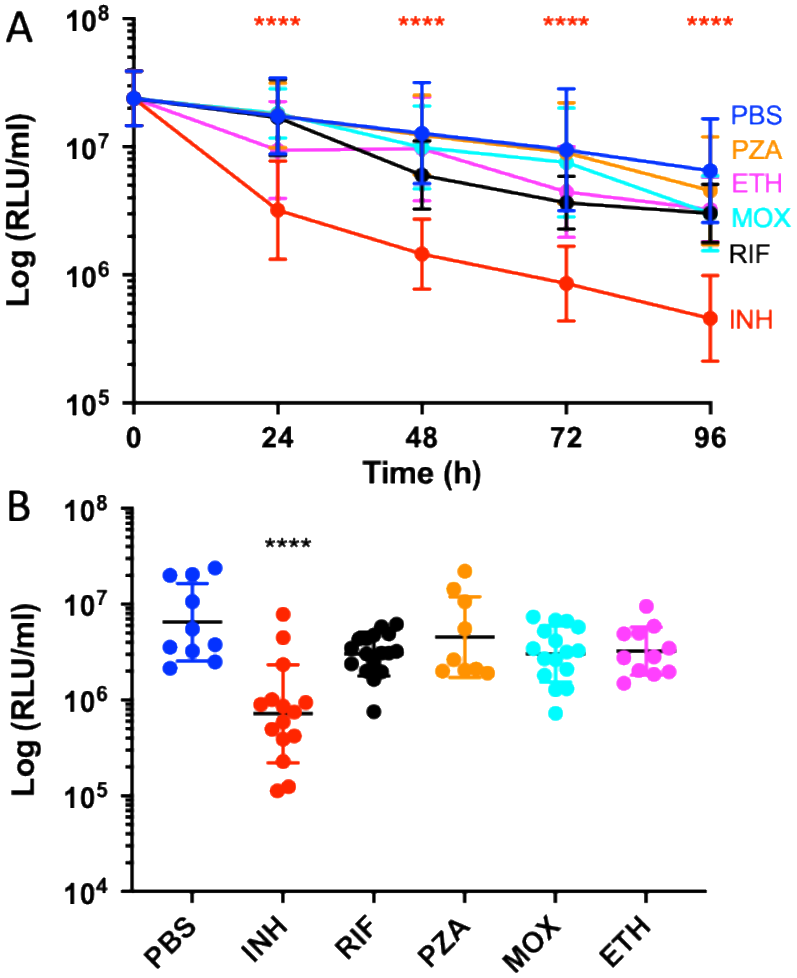


Figure 6.3: Reduction of BCG *lux* bioluminescence in *G. mellonella* following treatment with first or second-line antimycobacterial compounds. Larvae (n = 30, per treatment group) were infected with BCG *lux* (1 x 10^7 CFU) and treated with a single dose of INH (5 mg/kg), RIF (10 mg/kg), ETH (15 mg/kg), PZA (25 mg/kg) or MOX (6.7 mg/kg). Infected larvae treated with PBS-T were used as the control. Four larvae were individually homogenised from each group, every 24 h, for 96 h. (A) Changes in BCG *lux* bioluminescence over the 96 h time course. (B) Changes in BCG *lux* bioluminescence at the 96 h endpoint. Plotted are the means of three independent experiments, and error bars represents the SD of the means. Kruskal-Wallis test with Dunn's multiple comparisons was carried out against the control: **** ($p < 0.0001$). In (A), the colour of the asterisk corresponds to the relevant treatment groups. Reproduced from Asai et al., 2019b.

The effect of treatment on *in vivo* SAMTB *lux* bioluminescence was similarly assessed (**Figure 6.4**). At 96 h, INH or RIF treatment significantly reduced ($p < 0.0001$) the mean mycobacterial bioluminescence by 99.7% and 98.6%, respectively, relative to the control (**Figure 6.4A, C**). Treatment with MOX led to a substantial but non-significant reduction in the mean

bioluminescence of 76.4%, relative to the control at 96 h (**Figure 6.4C**). ETH, and BDQ treatment resulted in a more subtle reduction in the mean bioluminescence of 26.4% and 32.4%, respectively, relative to the control at 96 h (**Figure 6.4C**). Whereas treatment with PZA led to non-significant increased in mean bioluminescence by 9% relative to the control at 96 h (**Figure 6.4C**)

SAMTB *lux* infected larvae were similarly treated with MOX, PZA or ETH prepared at 10x the recommended clinical dosage to evaluate whether a higher concentration would improve efficacy. As previously indicated, BDQ was limited to the clinically recommended dosage due to material shortage. A significant improvement in the reduction of SAMTB *lux* bioluminescence was observed for MOX and ETH at 10 x dosage, over the 96 h time course (**Figure 6.4B**). The reduction in the mean bioluminescence relative to the control at 96 h was 97.4% ($p < 0.0001$) and 89.1% ($p < 0.05$) for MOX and ETH, respectively (**Figure 6.4 C**). While treatment with a higher dose of PZA improved efficacy, the reduction in bioluminescence relative to control at 96 h post-infection remained non-significant (52.2% and 26.4% for 10x and 1x dosage, respectively). The lack of PZA activity in SAMTB *lux* was anticipated as the deleted *panD* gene encodes aspartate decarboxylase, a known target of PZA (Gopal et al., 2017).

To further assess the effects of compound dosing on treatment efficacy, the most active compounds, INH and RIF, were each screened at three different doses: 1x, 0.1x and 0.01X, relative to their clinically recommended dosage. Treatment led to apparent improvements in the bioluminescence reducing activity, which correlated with a rise in treatment dosage (**Figure 6.5**). Taken together, these observations highlight that the *Gm* model is sensitive to

drug dosage, and any novel compound requires testing at a range of concentrations to identify optimal dosage.

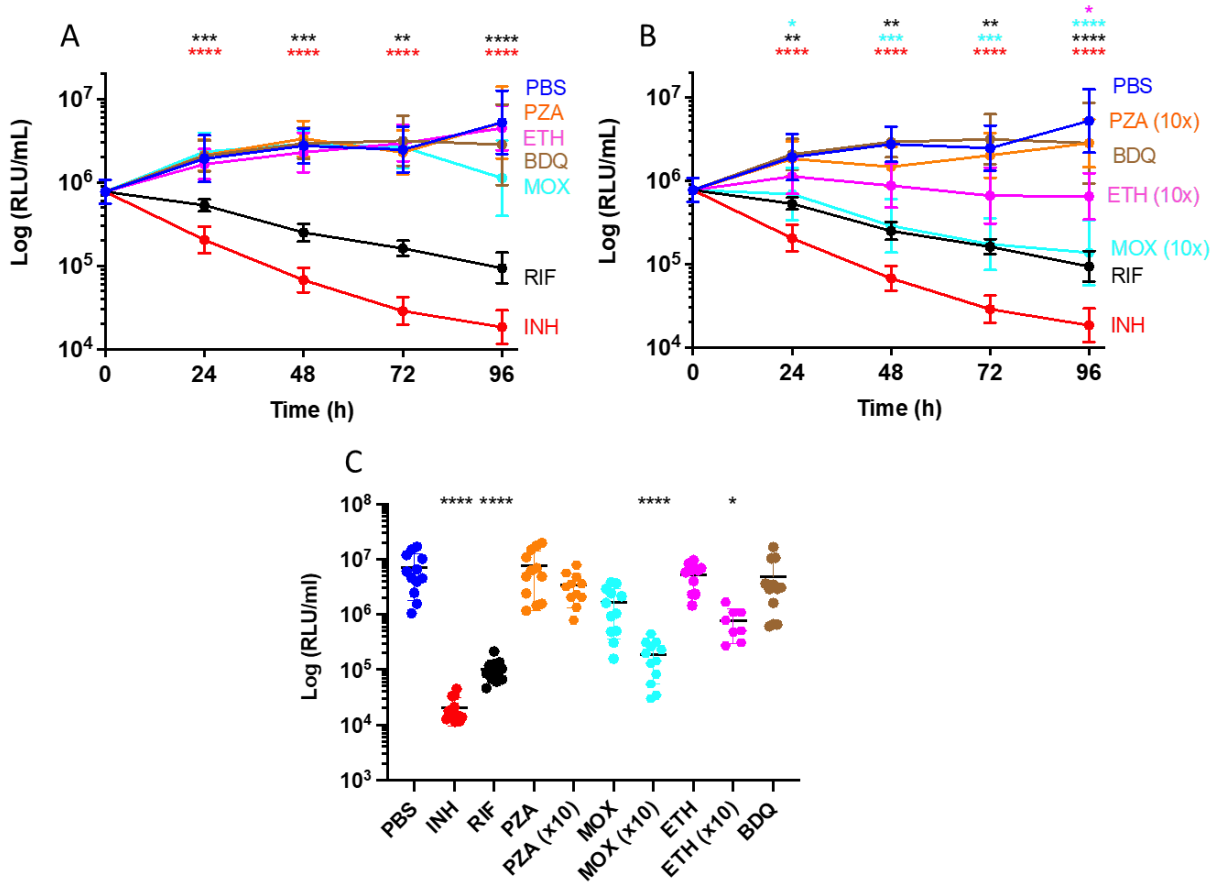


Figure 6.4: Reduction of SAMTB *lux* bioluminescence in *G. mellonella* following treatment with first or second-line antimycobacterial compounds. Larvae (n = 30, per treatment group) were infected with SAMTB *lux* (2 x 10^7 CFU) and treated with a single dose of INH (5 mg/kg), RIF (10 mg/kg), ETH (15 mg/kg), PZA (25 mg/kg), MOX (6.7 mg/kg), BDQ (5.7 mg/kg), ETH (10x, 150 mg/kg), PZA (10x, 250 mg/kg), or MOX (10x, 67 mg/kg). Infected larvae treated with PBS-T was used as the control. Four larvae were individually homogenised from each group, every 24 h, over 96 h. (A) Change in SAMTB *lux* bioluminescence over the 96 h time course. (B) Change in SAMTB *lux* bioluminescence over the 96 h time course using ETH, PZA and MOX at 10x clinically recommended dosage. (C) Changes in SAMTB *lux* bioluminescence at the 96 h endpoint. Plotted are the means of three independent experiments, and error bars represent the SD of the means. Kruskal-Wallis test with Dunn's multiple comparisons was carried out against the control: * ($p < 0.05$), ** ($p < 0.01$), *** ($P < 0.001$) and **** ($p < 0.0001$). In (A) and (B), the colour of the asterisk correlates to the treatment groups. Reproduced from Asai et al., 2020.

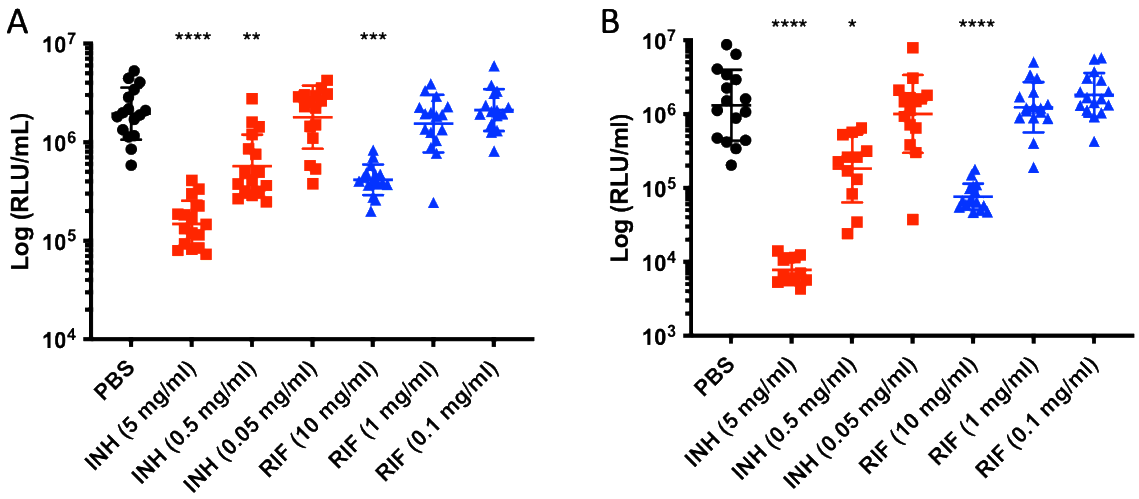


Figure 6.5: Reduction of SAMTB *lux* bioluminescence in *G. mellonella* is highly associated with treatment dose. Larvae (n = 30, per treatment group) were infected with 2 x 10^7 CFU of SAMTB *lux* and treated with a single dose of INH (5 mg/kg, 0.5 mg/kg or 0.05 mg/kg) or RIF (10 mg/kg, 1 mg/kg or 0.1 mg/kg). Infected, PBS-T treated larvae were used as the control. Four larvae were individually homogenised from each group, every 24 h, over 96 h. (A) SAMTB *lux* bioluminescence at 24 h post-infection. (B) SAMTB *lux* bioluminescence at 96 h post-infection. Plotted are the means of two independent experiments, and the error bars represent the SD of the means. Kruskal-Wallis test with Dunn's multiple comparison was carried out against the control: * ($p < 0.05$), ** ($p < 0.01$), *** ($P < 0.001$) and **** ($p < 0.0001$). Reproduced from Asai et al., 2020.

While the bioluminescent properties of BCG *lux* and SAMTB *lux* enables a rapid assessment of relative drug efficacy, ideal for a cost and time-efficient pre-screen model, bioluminescence reflects only their metabolic activity and not viability (Andreu et al., 2010). Therefore, bioluminescence cannot be used to determine the mechanism of antimycobacterial action (i.e., bactericidal or bacteriostatic). As such, any initial screening using bioluminescence should be followed up with CFU enumeration. In the case of this project, the activity of the core compounds (INH, RIF, PZA and ETH) were examined in the H37Rv model using CFU enumeration.

For the *Gm*-H37Rv infection model, CFU was measured at 72 h, as reference (point of treatment, PT) for determining relative growth between 72 h and 192 h post-infection; and at 192 h to assess treatment efficacy. As with treatment survival outcome, only the core first line antimycobacterial compounds were examined against H37Rv. ETH and PZA were used at 10x the clinical recommended dosage following observations of improved efficacy in the SAMTB *lux* model. To note, despite trend in improvement, treatment with ETH (10x) did not significantly improve larval survival (61.3%) at 192 h, relative to the control (**Figure 6.6**). However, considerable improvements were observed over treatment with ETH (1x) (37.3%). PZA (10x) treatment did not improve larval survival (50.6%), with negligible differences in efficacy over PZA (1x) (50.6%).

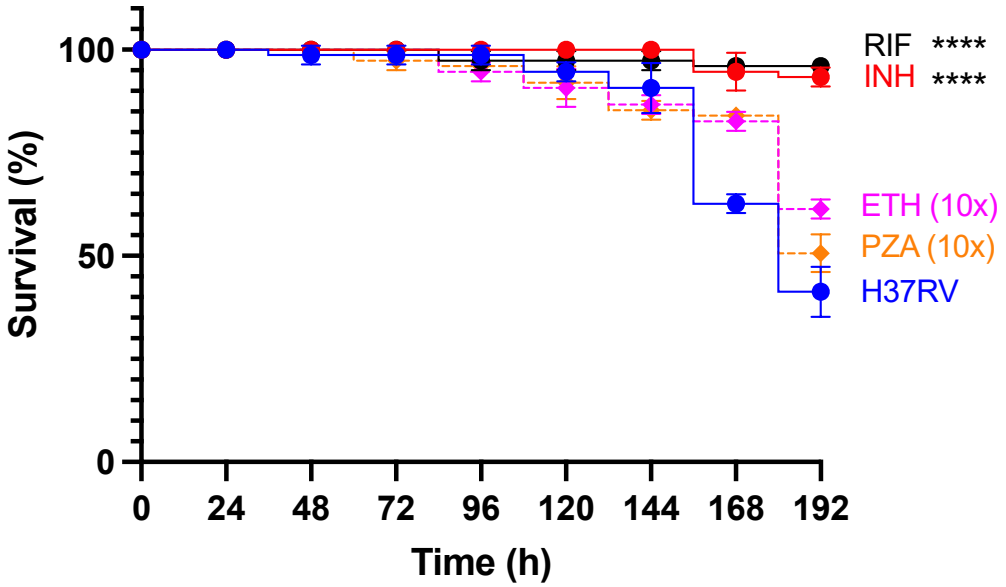


Figure 6.6: Survival of *G. mellonella* infected with H37Rv, following treatment with first-line antimycobacterial compounds. Larvae (n = 25, per treatment group) were infected with either H37Rv (2 x 10^6 CFU) and treated with a single dose of either INH (5 mg/kg), RIF (10 mg/kg), ETH (150 mg/kg), or PZA (250 mg/kg), given 72 h post-infection. Larvae infected and mock-treated with PBS-T was used as the control. Larvae were monitored every 24 h over a 192 h time course. Plotted are the means of three independent experiments, and the error bars represent the SD of the means. For statistical analysis, Mantle-Cox log-rank test with Bonferroni's correction between treatment groups and the control were carried out: **** ($P < 0.0001$).

In the H37Rv model, all compounds, except for PZA showed significant reduction ($p < 0.0001$) in mycobacterial burden (**Figure 6.7**). As with the treatment of SAMTB *lux* and BCG *lux*, INH and RIF were the most efficacious, leading to 99.6% (1.3×10^5 CFU) or 96.1% (1.2×10^6 CFU) reduction in CFU relative to the PBS control (3.2×10^7 CFU) at 192 h post-infection. ETH (10x) treatment led to a 76.4% (7.6×10^6 CFU) reduction in CFU compared to the control. PZA (10X) had little to no activity, with only a 12.7% (2.8×10^7 CFU) reduction in CFU relative to the control.

The following compound activity was deduced by using CFU enumerated from the larval homogenate at PT: (2.4×10^6 CFU) and from the control (PBS-T: 3.2×10^7 CFU) as references. INH shows an evident bactericidal activity as recovered CFU are significantly lower ($p < 0.0001$, unpaired t-test) than the PT. Bactericidal activity of RIF was significantly lower ($p < 0.01$, unpaired t-test) than PT but less substantial than INH. The broader spread in recovered CFU may indicate that the efficacy of RIF degrades over the course of treatment. While ETH reduced the mycobacterial burden by 76.4%, relative to the control, a significant level of growth ($p < 0.001$) was measured over PT. This indicates that the activity of ETH is likely bacteriostatic rather than bactericidal. The mycobacterial burden of larvae treated with PZA was not statistically different from control H37Rv.

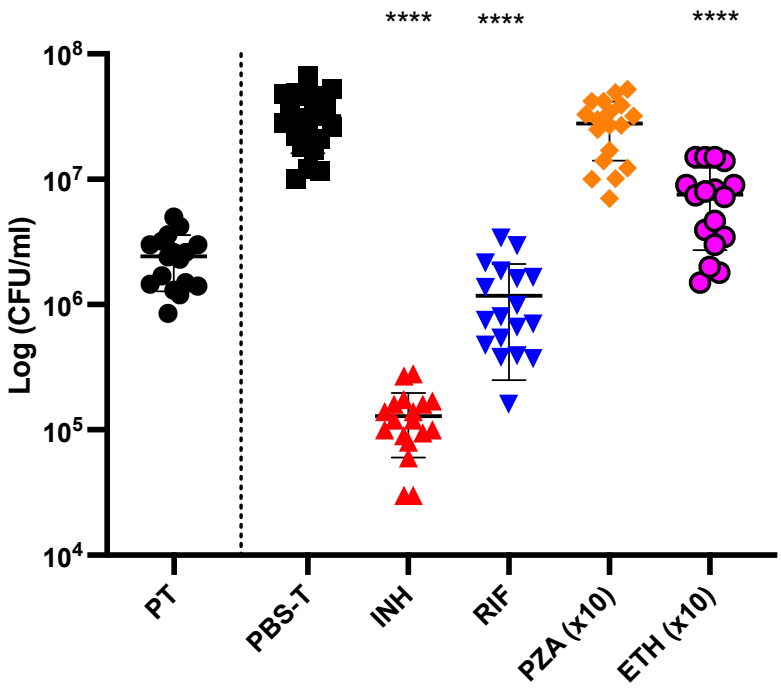


Figure 6.7: Reduction of *in vivo* H37Rv burden in *G. mellonella* following treatment with first-line antimycobacterial compounds. Larvae (n = 25, per treatment group) were infected with 2 x 10^6 CFU of H37Rv and treated with a single dose of INH (5 mg/kg), RIF (10 mg/kg), ETH (150 mg/kg), or PZA (250 mg/kg). Infected, PBS-T treated larvae were used as the control. CFU at the point of treatment (PT) was measured as a reference. Four larvae were individually homogenised from each group at 192 h post-infection and plated for CFU enumeration. Plotted are the means of five independent experiment, and error bars represents the SD of the means. One-way ANOVA test with Holm-Šídák multiple comparisons was carried out against the control (PBS): **** ($p < 0.0001$).

Overall, treatment efficacy as measured via larval survival outcome and changes to *in vivo* mycobacterial burden agree in all three *Gm* models. RIF and INH treatment were the most efficacious compounds, which is in line with those previously reported in C3HeB/FeJ and C3H mouse models (Nikonenko et al., 2004; Driver et al., 2012). Despite improved survival outcomes (significant or trend) using ETH, MOX or RIF (BCG *lux*), and ETH, MOX and BDQ (SAMTB *lux*) at the recommended clinical dosage (1x) and inhibitory activity *in vitro*, these compounds lacked any substantial activity in reducing *in vivo* mycobacterial bioluminescence. For ETH and MOX, this is likely a dosing issue as significant improvement in efficacy was observed when utilised at 10x recommended clinical dosage. When larvae were treated with

ETH (10x), a bacteriostatic effect was observed from the bioluminescence measurements of SAMTB *lux* and the hindered growth of H37Rv. These observations align with the bacteriostatic activity of ETH reported *in vitro* and *in vivo* (BALB/C mouse) models (Zhang et al., 2012; Zimmerman et al., 2017). MOX (10x) showed a similar level of reduction in bioluminescence to RIF in the SAMTB *lux* model, indicating a potential bactericidal activity, which was the mode of action reported in the C3H mouse model (Nikonenko et al., 2004).

For PZA, the lack of antimycobacterial activity can be attributed to several potential reasons. As briefly mentioned previously, BCG is intrinsically resistant to PZA due to the deletion of the *pncA* gene, which encodes for the enzyme pyrazinamidase. This enzyme is essential for the conversion of the "pro-drug" PZA into its active form, pyrazinoic acid (POA) (Ritz et al., 2009). The lack of efficacy against SAMTB *lux* is due to the deletion of the *panD* gene, which encodes aspartate decarboxylase, a key target of POA (Gopal et al., 2017; Mouton et al., 2019). However, as H37Rv possesses both the *pncA and panD* genes, PZA was anticipated to be efficacious *in vivo.*

Classically, PZA is known to be most efficacious against slow-growing or non-growing mycobacteria (Zhang et al., 2003). Its antimycobacterial activity is most potent in its active form POA, further enhanced when protonated in an acidic environment (Zhang et al., 2003). As a result, the antimycobacterial activity of PZA/POA is potentiated under intracellular conditions, under the influence of low-pH, nutrient deprivation, and hypoxia (McDermott & Tompsett, 1954; Wade & Zhang, 2004; Peterson et al., 2015). It is a possibility that sufficient levels of stress were not reached in *Gm* larvae for optimal activation of PZA to POA. However,

an indication that such intracellular conditions may be replicated in *Gm* is evident from my observations of ILI accumulations and loss of acid-fastness, as described in Chapter 3-5.

Additionally, a study conducted by Via et al., demonstrated that PZA could be converted into POA by the host (Via et al., 2015). If *Gm* can convert PZA to POA, some level of efficacy would be expected in the H37Rv model. If PZA conversion to POA takes place, one of the key targets of PZA/POA would be PanD (aspartate decarboxylase), a vital driver of the Pan biosynthesis pathway. Pan is crucial for the synthesis of coenzyme A, which is responsible for metabolic processes such as fatty acid synthesis and production of ATP (Zhang et al., 2013a; Gopal et al., 2017; Ragunathan et al., 2021). While POA may inhibit the biosynthesis of Pan in H37Rv, this inhibitory activity is likely bypassed through access to the host Pan, which is found in abundance (32.8 mg/kg) within the larvae (Finke, 2015).

PZA (1x) marginally improved larval survival outcome in all three models (**Figures 6.1 and 6.6**), and a second mechanism of PZA/POA may contribute to this outcome. Gopal et al. proposed that POA is incorporated into the PDIM synthesis pathway in place of the native acyl groups, disrupting PDIM synthesis, which leads to anti-virulence activity (Gopal et al., 2016). Gopal et al. further hypothesised that impairment in PDIM induced by PZA/POA then modulates the host immune system and potentiates PncA driven PanD associated antimycobacterial activity (Gopal et al., 2016). However, in the *Gm* models, lacking the impact of the inhibitory effect of PanD, the marginal improvements in survival outcome likely reflect the reduction in mycobacterial virulence due to PDIM synthesis disruption. It is unlikely that *Gm* would be able to reap the benefits of the immune modulatory activity of PZA/POA as congenitally athymic

nu/nu (nude) mice, lacking functional adaptive immunity, were unable to survive infection by *MTB* despite being treated with PZA (Almeida et al., 2014).

6.2.4 Changes to antimycobacterial burden following repeated or combination therapy

Treatment of TB is often delivered as a cocktail of antimycobacterial compounds. Therefore, combinations of antimycobacterial compounds were similarly assessed in larvae infected with BCG *lux* and SAMTB *lux*. The following combinations of compounds were evaluated in the two models using compounds at the clinically recommended dosages: INH+RIF, RIF+ETH, and REM (RIF, ETH and MOX). For the SAMTB *lux* infection model, the use of INH was omitted as further improvement will reduce levels of bioluminescence to the limit of detection (10^3 RLU). PZA was omitted for further analysis due to the lack of activity, as addressed earlier in this Chapter.

Treatment of BCG *lux* infected larvae using combinations of antimycobacterial compounds (INH+RIF, RIF+ETH or REM) significantly improved efficacy at both 24 h (**Figure 6.8A**) and 96 h (**Figure 6.8B**) when compared to their use alone for RIF (24 h: $p < 0.05$ and 96 h: $p < 0.05$), ETH (24 h: < 0.05 and 96 h: $p < 0.001$), and MOX (24 h: $p < 0.0001$ and 96 h: $p < 0.001$). However, no combinations made improvements over the use of INH or RIF alone at any given time point. Similarly, for treatment of SAMTB *lux,* no combinations evaluated led to significant improvements in efficacy over the use of RIF alone at any time point (**Figure 6.8B and D**). These observations indicate that any improvements in combination therapy reflect the potent activity of INH or RIF and are not an indication of synergistic activity. These experiments were carried out to demonstrate that a combination of compounds can be screened in *Gm* as utilised in the clinic as the gold standard of treatment. The lack of improvements in efficacy was not surprising given that combination treatments are used to minimise the development

of drug-resistance and the lengthy course of treatment, but not for their synergistic activity (WHO, 2010).

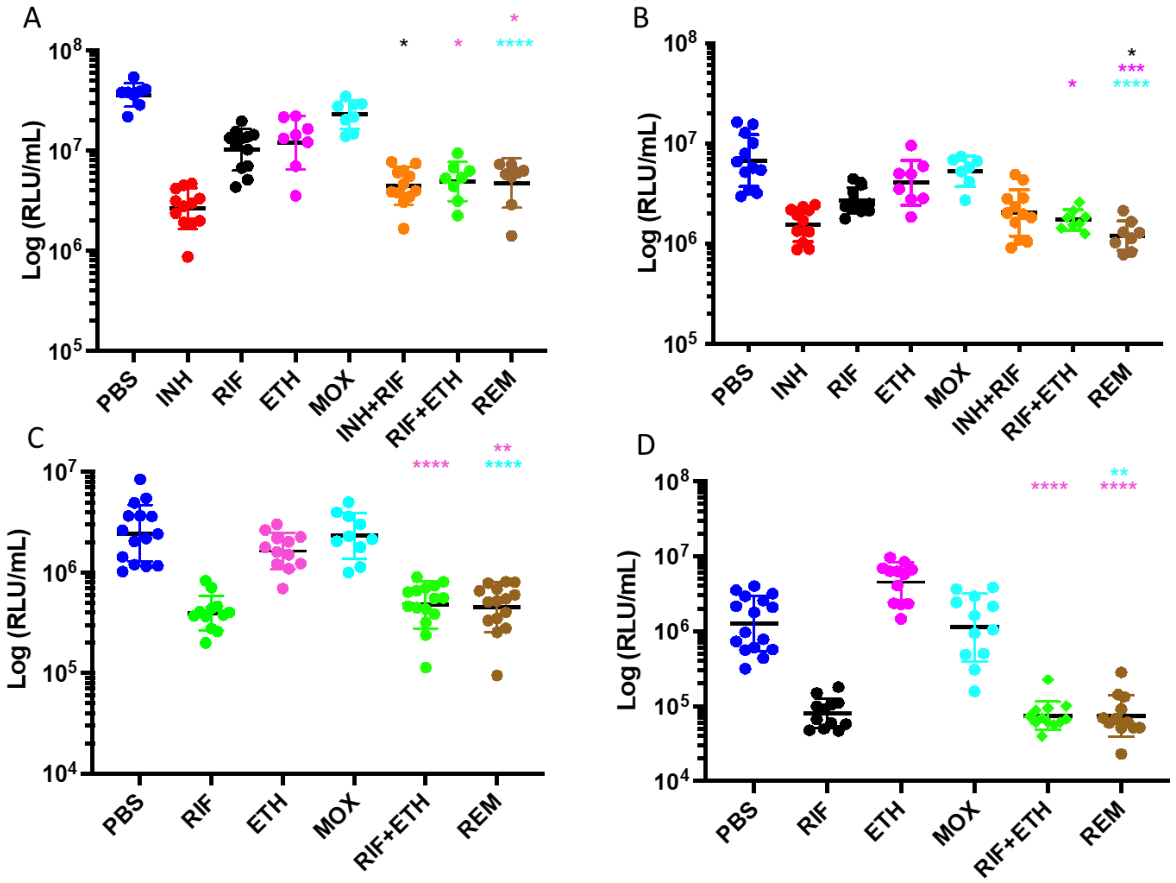


Figure 6.8: Reduction of BCG *lux* and SAMTB *lux* bioluminescence in *G. mellonella* following treatment with a combination of first and second-line antimycobacterial compounds. Larvae (n = 30, per treatment group) were infected with BCG lux (1 x 10^7 CFU, A and B) or SAMTB *lux* (2 x 10^7 CFU, C and D) and treated with a single dose of INH (5 mg/kg), RIF (10 mg/kg), ETH (15 mg/kg), MOX (6.7 mg/kg), INH+RIF (5 and 10 mg/kg, respectively), RIF+ETH (10 and 15 mg/kg, respectively) or RIF, ETH and MOX (REM, 10, 15 and 6.7 mg/kg, respectively). Infected, PBS-T treated larvae were used as the control. Four larvae were individually homogenised from each group, every at (A and C) 24 h and (B and D) 96 h. Plotted are the means of 2 or more independent experiments, and the error bars represent the SD of the means. Kruskal-Wallis test with Dunn's multiple comparisons was carried out between the combination and their respective mono compound treatment: * ($p < 0.05$), ** ($p < 0.01$), *** ($p < 0.001$) and **** ($p < 0.0001$). The colour of asterisks correlates to the statistically relevant mono compound treatment groups. Adapted from Asai et al., 2020, 2019b.

Furthermore, during TB treatment, antimycobacterial compounds are often administered over six months or more as repeated doses. Therefore, the effect of repeated dosing on *in vivo* mycobacterial burden were evaluated using BCG *lux* or SAMTB *lux* (RIF only) infected larvae. INH or RIF treatment was administered as mono or dual dosage. The use of INH and RIF were chosen based on observations that they were the most efficacious compound in *Gm.* For treatment, larvae were infected and treated 1 h post-infection for mono dosing and 1 h and 24 h post-infection for dual dosing.

In larvae infected with BCG *lux*, dual INH dosing led to significant improvement in treatment efficacy over single INH dosing ($p < 0.01$), with moderate (53.9%) improvement in reduction of mycobacterial bioluminescence at 96 h post-infection (**Figure 6.9A**). Dual RIF dosing did not significantly improve treatment efficacy, but a trend in reduction was observed (**Figure 6.9A**). Only a minor (17.7%) improvement in mycobacterial bioluminescence reduction was observed at 96 h post-infection. Similarly, for SAMTB *lux* infected larvae*,* dual RIF dosing did not significantly improve drug efficacy over single dosing (**Figure 6.9B**), while a trend in improvement was observed. Improvements in bioluminescence reduction were minor (23.3%) at 96 h post-infection.

Pharmacokinetic (PK) and pharmacodynamic (PD) of antimycobacterial compounds examined in this Chapter are currently undetermined in *Gm*. Thus, the half-life of INH and RIF in the larva may not be sufficient to show any benefit of repeated dosing over a 96 h time course. Therefore, in a future study, the impact of repeated dosing should be evaluated in the H37Rv model, with spaced dosing at 48 h and 96 h post-infection, over a 192 h time course. Such a change will allow the compound to degrade over time, creating a scenario where meaningful

data are more likely to be observed. In humans, drug metabolism is typically carried out by the liver and/or are excreted in urine. Drug metabolism in insects may possibly be carried out in the fat body (akin to the liver) (Skowronek et al., 2021), and/or be passed through the digestive system as frass (Arrese & Soulages, 2010; Engel & Moran, 2013). Based on the degradation and detoxification of insecticides, metabolism of compounds in insects are likely driven by enzymatic activities (Wilkinson & Brattsten, 1972). The lack of defined PK/PD for antibacterial and antifungal compounds is a widespread issue and is currently one of the key limitations of the *Gm* model. However, in recent years a small number of studies have defined PK/PD in *Gm* for a selection of compounds (Thomas et al., 2013; Forastiero et al., 2015; Astvad et al., 2017; Maurer et al., 2019), using HPLC based assays and well diffusion assays. However, these studies have only defined PK/PD of compounds found circulating in the haemolymph and omit any possible retention within the tissues. While the definition of PK/PD for antimycobacterial compounds in *Gm* was beyond the scope of this extensive project, future work will aim to address this to enable better comparison against existing model systems.

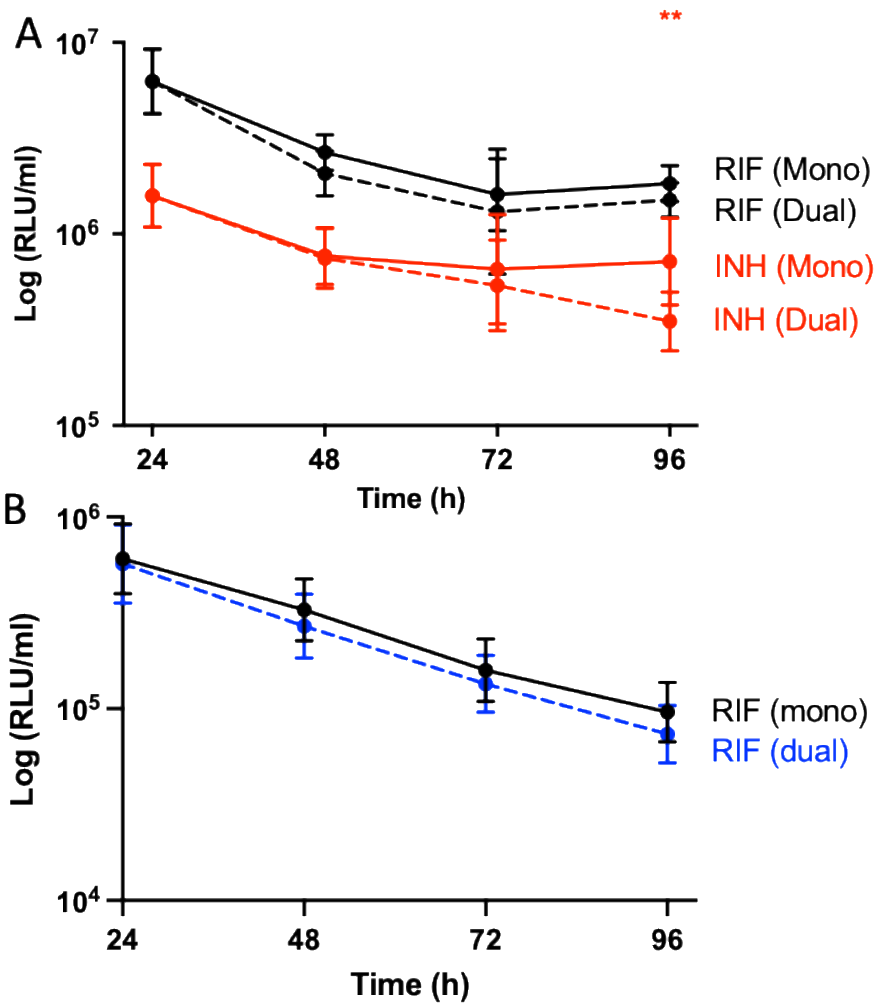


Figure 6.9: Figure 6.8 Reduction of BCG *lux* and SAMTB *lux* bioluminescence in *G. mellonella* following mono or dual treatment with INH or RIF. Larvae (n = 30, per treatment group) were infected with (A) BCG *lux* (1 x 10^6 CFU) or (B) SAMTB *lux* (2 x 10^7 CFU). Changes to mycobacterial bioluminescence were measured every 24 h for 96 h following infection. Plotted are the means of three independent experiments, and the error bars represent the SD of the mean. A t-test was carried out for statistical analysis between the respective mono and dual treatment pairs at each time point: ** ($P < 0.01$). Adapted from Asai et al., 2020, 2019b.

6.2.5 Live Galleria mellonella – Mycobacterium tuberculosis complex fluorescence imaging as a screen for drug efficacy

As a proof of concept, the feasibility of using *Gm* infected with FluorBCG as a drug screening system was evaluated using the proprietary handheld fluorescence camera (courtesy of Dr Brian Robertson, ICL). Larvae were infected with 5 x 10^6 CFU of FluorBCG and treated using either INH or RIF at 2x clinically recommended dosage, given 1 h post-infection. Larvae were incubated for 120 h rather than 96 h to account for the dissipation of the YFP signal. Unlike bioluminescence measurement, which directly correlates to metabolic activity and thus viable bacilli, YFP is not directly linked to the viability of bacilli and thus can persist following death. Treatment efficacy was defined as a reduction in YFP signal at the 120 h endpoint. Only a visual assessment was made to determine treatment efficacy for this pilot experiment, and accurate fluorescence measurements were not taken.

Treated larvae showed a substantial and visibly distinguishable reduction in FluorBCG YFP signal compared to the PBS-T control (**Figure 6.10**). Treatment with RIF appeared to be the most effective, with less frequent and smaller foci of infection than in INH treated larvae. A dose of 2x clinically recommended dosage was used as efficacy was not visibly at 1x dosage. However, developing an image analysis pipeline would enable accurate measurements of subtle differences in fluorescence.



Figure 6.10: Demonstration of *G. mellonella* - FluorBCG as a live screen for drug screening. Larvae infected with 5 x 10^6 CFU of FluorBCG were treated with a single dose of INH (10 mg/kg) or RIF (20 mg/kg), 1 h post-infection. Larvae were incubated for 120 h, and FluorBCG YFP signal was visualised to determine drug efficacy using visual comparison against the PBS-T treated infection control.

The use of a drug screening system where efficacy can be monitored within the same larva throughout the treatment study is highly desirable. This allows for the generation of highly accurate data compared to methodologies that rely on sacrificing larvae for homogenisation. Similar live imaging methodology has already been adopted for the *Gm* model using a complex and expensive IVIS imaging system to measure *in vivo* bioluminescence (Meir et al., 2018). In contrast to such a system, the proprietary handheld fluorescence camera is much cheaper and easier to operate and provides a substantially improved image resolution. Therefore, future work will further optimise this live, non-destructive sampling, drug screening model.

6.3 Conclusion

In this Chapter, using the three *Gm*-MTBC models established in this project, their application as a toxicity and efficacy screen for antimycobacterial compounds were evaluated using a selection of clinically recommended compounds.

First- and second-line antimycobacterial compounds were non-toxic in *Gm* at concentrations as high as 10x recommended clinical dosage. Treatment of BCG *lux,* SAMTB *lux* or H37RV infected larvae using a single compound type, at the recommended clinical dosage for adult TB infection, improved larval survival outcome compared to the PBS-T treated control. For improvement in survival outcome, the order of drug efficacy was RIF > INH > PZA > ETH or MOX > BDQ for first- and second-line compounds, respectively. Changes in the model design, as seen between BCG *lux*/SAMTB *lux* and H37Rv, (i.e., infection dose or treatment duration), did not appear to have an impact on overall treatment efficacy. Changes to *in vivo* mycobacterial burden were measured using bioluminescence (BCG *lux* and SAMTB *lux*) and CFU (H37Rv) following treatment. INH and RIF were the most potent compound with substantial activity in all three models. ETH and MOX showed significant activity at only 10x the clinically recommended dosage. PZA was the least active, lacking substantial activity at any given point even at 10x clinically recommended dosage. This inactivity of PZA likely reflects many factors: 1) the resistance of mycobacteria BCG *lux* and SAMTB *lux* to PZA, 2) bypassing of the POA inhibition of Pan biosynthesis through the use of host Pan, 3) the potential lack of sufficient mycobacteria driven of conversion of PZA to POA due to insufficient intracellular stress. The activity of the compounds in *Gm* (bactericidal or bacteriostatic) were deduced in the H37Rv model using CFU measurement, which was in agreement with activity reported in animal models. Treatment of infected larvae (BCG *lux* and SAMTB *lux*) with a

combination of compounds or repeat dosing did not improve the efficacy of the compounds. Finally, the use of *Gm*-FluorBCG as a live fluorescence *in vivo* screen for drug efficacy was demonstrated as a proof-of-concept experiment, with treated larvae demonstrating a clear reduction in FluorBCG YFP fluorescence flowing treatment.

Overall, this work demonstrates that the *Gm*-MTBC models established in this project can successfully be used to determine the toxicity and efficacy of compounds, which are comparable to those seen in other animal models. However, there are clear limitations, including the absence of standardised screening methodology (Cutuli et al., 2019) and the lack of data PK/PD in *Gm* for relevant compounds, both making crucial comparisons between *Gm* and against pre-existing models challenging.

Chapter 7
Characterising the innate immune responses of *G. mellonella* to *M. bovis* BCG *lux* infection

7.1 Introduction

The *Gm* innate immune system is complex, and functionally and anatomically comparable to mammals. The *Gm* immune response can be broadly separated into three categories: anatomical and physiological barriers, cellular responses, and humoral responses (Wojda, 2017).

The cellular immune response is primarily driven by two of the six haemocytes identified in *Gm*, plasmatocytes and granulocytes, which are vital for microbial clearance via phagocytosis, nodulation, and encapsulation (Pereira et al., 2018). The humoral immune system differentiates pathogens by detecting a diverse range of PAMPs/DAMPs using a wide variety of PRRs in its possession (Hillyer, 2016). Thus far, 65 PRRs genes have been identified in tobacco worms, a close relative of *Gm* (Hillyer, 2016). The abundance of PRRs in invertebrates are believed to be an evolutionary mechanism to compensate for the lack of an adaptive immune response (Flajnik and Kasahara, 2009; Wang et al., 2019). The PRRs activate one of three immune signalling pathways identified in insects: Toll, Imd and JAK-STAT (Hillyer, 2016), which initiates immune pathways, leading to the production and secretion of defence proteins e.g., AMPs, proteins, enzymes, and radicals (Wojda, 2017).

Melanisation is a crucial antimicrobial mechanism driven by the PPO cascade (Nakhleh et al., 2017), which is often compared to the mammalian complement cascade as both processes rely on an enzymatic cascade following pathogen recognition leading to the production of cytotoxic and opsonic molecules (Nakhleh et al., 2017). However, they differ in their final stages, with the PPO cascade terminating with the deposition of melanin to encase the

pathogens, whereas the complement cascade induces cell lysis via the membrane attack complex (Sheehan et al., 2018b).

Despite lacking adaptive immunity, improvements in survival outcome were reported for insects immunised with non-lethal or deactivated pathogens, prior to infection with a lethal dose (Eleftherianos et al., 2006; Bergin et al., 2006; Pham et al., 2007; Mikonranta et al., 2014; Wu et al., 2014; Sheehan et al., 2021). Adaptive-like immune response was first described by Metalnikov in 1927, who immunised larvae with HT *Vibrio cholerae*, and reared 12 generations of *Gm* from the immunised group, where each iteration led to increased protection against *V. cholerae* (Metalnikov, 1928). However, Clay later disputed the claim that *Gm* can induce inheritable adaptive-like immunity (Clay, 1935). Instead, adaptive-like immune response, began to be interpreted more as a "priming" or "training" of innate immunity, as it was described as "rapid in development and short in duration" (Chadwick, 1967). Now popularly termed as "innate immune priming", such phenomenon continues to be a topic of debate to this day and research is on-going (Cooper & Eleftherianos, 2017; Sheehan et al., 2020a). Immune priming appears to be heavily influenced by the insect type and immunisation agent used, leading to large variability in observed protective effects (Cooper & Eleftherianos, 2017). Unravelling the precise mechanism behind immune priming has the potential to transform our current understanding of immunity.

The use of insects as model organisms continues to grow with increasing interest from the scientific community, and as a result the world of insect immunology is developing at a substantial pace. However, our ability to conveniently study the innate immune system of *Gm* is hindered by the lack of a fully annotated genome, availability of transgenic mutants, and

commercially accessible Abs. Nevertheless, researchers have applied transcriptomic and proteomic approaches to comprehensively characterise and provide informative details of the *Gm* immune response to infection (Vogel et al., 2011; Sheehan & Kavanagh, 2018; Dinh et al., 2021).

In previous Chapters (3-5), *Gm*-MTBC models were shown to mimic vital aspects of TB disease, such as internalisation of mycobacteria, formation of granuloma-like structures, and bacterial progression to non-replicative phenotypes, e.g., ILI with BCG *lux*, and loss of acid fastness with SAMTB *lux* and H37Rv, respectively. In this Chapter, the innate immune response of *Gm* to BCG *lux* is characterised using proteomic and transcriptomic (gene expression) approaches. These data complement observations recorded in the previous Chapters and provided data for comparison with immune responses induced in other *Gm* infection models, traditional TB models and in humans. A proteomic approach was also used study immune priming in the *Gm*-BCG *lux* model.

7.2 Results and Discussion

7.2.1 BCG lux infection induces diverse changes in the Galleria mellonella proteome

The changes in *Gm* innate immunity in response to BCG *lux* (1 x 10^7 CFU) were measured and quantified using LFQ proteomics of the cell-free haemolymph extracted from larvae at 4 h, 48 h and 168 h post-infection. These time points were chosen to reflect early, mid, and late-stage infection in *Gm*, based on histological and TEM observations as reported in Chapter 3. The proteomes generated at each time point were compared against the uninfected naïve control at 0 h. In total, 185 proteins were identified, of which 104 were detectable at all time points. In total, there were 146 statistically significant (ANOVA, $p < 0.05$) and differentially abundant (> ± 1.5x fold) (SSDA) proteins identified. There were 6, 54, and 86 SSDAs at 4 h, 48 h, and 168 h post-infection, respectively. Proteins absent or in low abundance were included in the analysis but were expressed as an imputation of the zero value, calculated relative to the lowest value of proteins detected ±SD. Principal component analysis (PCA) of the generated proteomes revealed a clear and distinguishable clustering of replicates at each time point (**Figure 7.1**). SSDA proteins detected throughout infection were visualised as a volcano plot (**Figure 7.2**). All SSDA proteins identified are listed in Supplementary Tables 7.1 – 7.6.

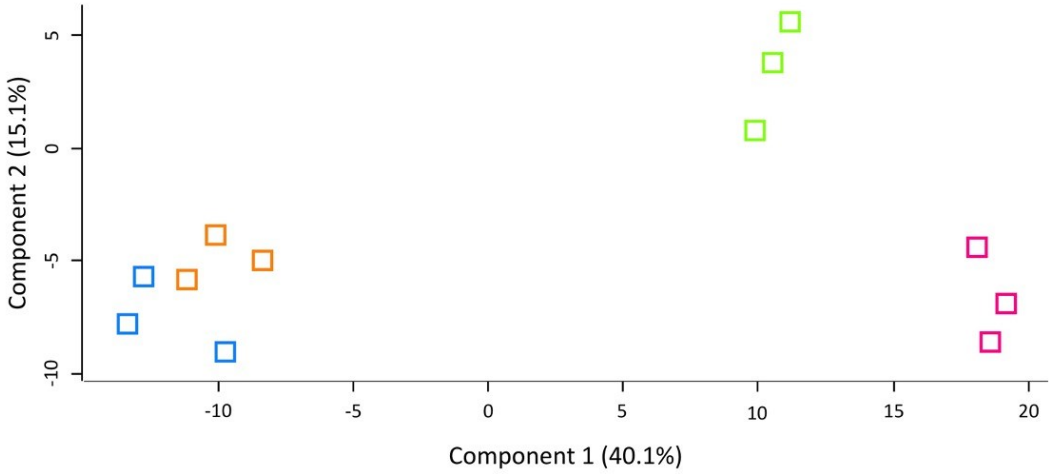


Figure 7.1: PCA of haemolymph proteomes generated from BCG *lux* infected *G. mellonella*. Proteomes generated from the cell-free haemolymph at 0 h (blue), 4 h (orange), 48 h (green) and 168 h (pink) post-infection showed clear grouping between experimental repeats and distinction between the time points. Plotted are PCA generated from three independent repeats, with each repeat consisting of n = 10 larvae (60 μl/larva). Reproduced from Asai et al., 2021.

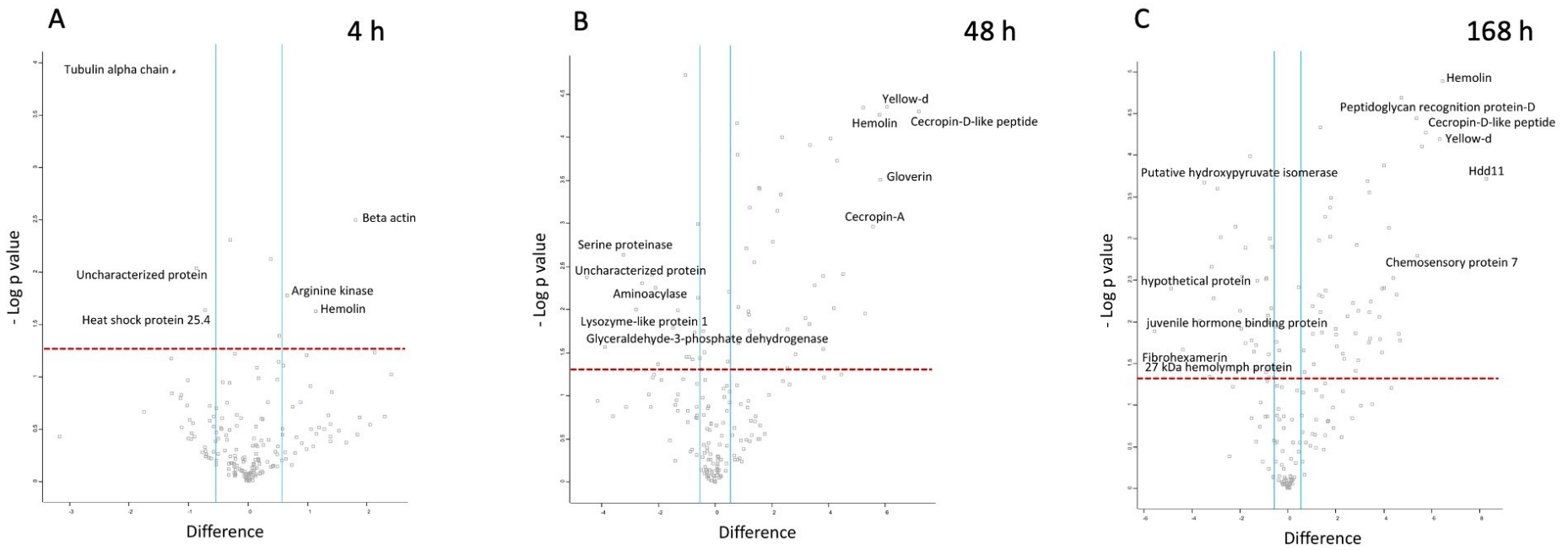


Figure 7.2: Volcano plot of SSDA proteins detected in BCG *lux* infected *G. mellonella* over a 168 h time course. Volcano plots were generated from the haemolymph proteome of larvae infected with BCG *lux* (1 x 10^7 CFU) at (A) 4 h, (B) 48 h and (C) 168 h post-infection. The plot represents differences in protein abundance (-log 2 mean intensity) and the significance of the difference ($p < 0.05$, two-sided-test), all compared to the control. Proteins above the horizontal red line are considered statistically significant, and those to the right or left of the vertical blue lines are considered differentially abundant (> ± 1.5x fold). The plots are generated from post-imputed data of three independent experiments, with each repeat generated from pooled haemolymph of n = 10 larvae (60 µl/larva). Reproduced from Asai et al., 2021.

Table 7.1: SSDA proteins of interest identified in the haemolymph of BCG *lux* infected *G. mellonella* at 4 h post-infection

p value	Fold change	GI number	Protein name	Peptides	Sequence coverage [%]	Score
0.003166	3.5	157927723	Beta actin	11	54.1	277.07
0.023588	2.2	186703381	Hemolin	7	50.7	323.31
0.009208	1.8	229002332	Protein associated with transcription activator MBF2	3	14.5	114.37
0.02304	1.7	169646838	Heat shock protein 25.4	13	48	237.16

Red: signifies an increase in protein abundance. Green: signifies a decline in protein Abundance. Protein abundance was calculated relative to their abundance in the uninfected naïve control at t = 0 h.

Table 7.2: SSDA proteins of interest identified in the haemolymph of BCG *lux* infected *G. mellonella* at 48 h post-infection

p value	Fold change	GI Number	Protein names	Peptides	Sequence coverage [%]	Score
4.97E-05	145.3	156630481	Cecropin-D-like peptide	2	14.5	46.071
0.000311	56.3	110649240	Gloverin	2	28.8	18.817
5.49E-05	55.7	186703381	Hemolin	7	50.7	323.31
0.001092	47.5	116087	Cecropin-A	1	8.5	9.783
0.011076	39.1	23208535	Peptidoglycan recognition-like protein B	13	34	231.94
0.009535	18.3	74873244	Hdd11	9	60.7	323.31
0.000104	16.8	154240658	Peptidoglycan recognition protein-D	7	22	120.85
0.004092	14.1	45594226	Serpin-4B	4	70	68.718
0.028322	14.0	56718390	Prophenol oxidase activating enzyme 3	17	42.1	210.04

0.005167	11.5	33860163	IMPI protein	8	33.2	67.368
0.000123	10.1	112983994	Peptidoglycan recognition protein	13	57.9	306.89
0.016888	5.9	226342884	Serpin-11	13	39.2	166.87
0.000461	5.0	157927723	Beta actin	11	54.1	277.07
0.000708	4.6	183979237	Transgelin	6	21.1	169.94
0.001639	4.1	52782700	Beta-1,3-glucan recognition protein	2	12.7	43.006
0.0004	3.0	157704337	Hdd1	6	56.9	146.94
0.010426	2.3	27733415	Serpin 3a	11	12.8	243.76
0.004211	23.0	229002332	Protein associated with transcription activator MBF2	3	14.5	114.37
0.0273	14.7	109119903	GAPDH	13	51.2	192.01
0.002301	9.4	121308868	Serine proteinase	9	25.4	96.748

0.023861	4.7	145286562	Lysozyme-like protein 1	3	9.2	48.058
1.90E-05	2.1	153791206	Scolexin	15	28.2	323.31
0.03539	1.9	46396271	27 kDa hemolymph protein	13	59.6	323.31

Red: signifies an increase in protein abundance. Green: signifies a decline in protein abundance. Protein abundance was calculated relative to their abundance in the uninfected naïve control at t = 0 h.

Table 7.3: SSDA proteins of interest identified in the haemolymph of BCG *lux* infected *G. mellonella* at 168 h post-infection

p value	Fold Change	GI Number	Protein Name	Peptides	Sequence coverage [%]	Score
0.00019	310.1	74873244	Hdd11	9	60.7	323.31
1.30E-05	87.8	186703381	Hemolin	7	50.7	323.31
5.38E-05	54.4	156630481	Cecropin-D-like peptide	2	14.5	46.071
3.60E-05	41.1	154240658	Peptidoglycan recognition protein-D	7	22	120.85
2.05E-05	26.6	183979237	Transgelin	6	21.1	169.94
0.016753	25.6	23208535	Peptidoglycan recognition-like protein B	13	34	231.94
0.01404	24.6	56718390	Prophenol oxidase activating enzyme 3	17	42.1	210.04
0.002981	20.9	45594226	Serpin-4B	4	70	68.718
0.000752	18.6	157927723	Beta actin	11	54.1	277.07
0.0039	16.3	116087	Cecropin-A	1	8.5	9.783

0.003987	15.1	226342884	Serpin-11	13	39.2	166.87
0.016175	14.3	23208546	Heat shock 23	6	25.6	52.216
0.005683	11.0	33860163	IMPI protein	8	33.2	67.368
0.007629	10.7	112702923	Peptidoglycan-recognition protein-LB	2	60.5	41.555
0.000281	10.7	112983994	Peptidoglycan recognition protein	13	57.9	306.89
0.015931	10.8	4090964	Hdd1	9	14.4	102.23
0.017641	10.3	156254836	Serpin-2	8	23.6	91.985
0.007352	7.6	110649240	Gloverin	2	28.8	18.817
0.007705	2.6	27733415	Serpin 3a	11	12.8	243.76
0.004825	2.5	52782700	Beta-1,3-glucan recognition protein	2	14.5	39.877
0.006553	2.0	162462783	Heat shock protein 25.4	6	12	51.116
0.003962	29.2	229002332	Protein associated with transcription activator MBF2	3	14.5	114.37

0.045961	9.6	46396271	27 kDa hemolymph protein	8	24.7	78.91
0.002178	9.1	121308868	Serine proteinase	9	25.4	96.748
0.000253	7.7	112983816	GAPDH	8	38.8	67.248
0.003107	1.9	153791206	Scolexin	15	28.2	323.31
0.00101	1.7	2498144	Apolipophorins Alt. Apolipophorin II/Apolipophorin I	12	85.9	323.31

Red: signifies an increase in protein abundance. Green: signifies a decline in protein abundance. Protein abundance was calculated relative to their abundance in the uninfected naïve control at t = 0 h.

7.2.2 BCG lux induces the production of key innate immune factors in Galleria mellonella

7.2.2.1 Pathogen recognition and phagocytosis associated protein

Hemolin is a member of the immunoglobulin superfamily (Eleftherianos et al., 2007), and was found in increasing abundance over the course of infection (4 h: +2.2 fold, 48 h: +55.7 fold, and 168 h: +87.8 fold, relative to the control). Hemolin is a pathogen-induced, non-self-targeting opsonin, which tags and binds microbes to haemocytes and enhances phagocytic activity (Aathmanathan et al., 2018). Hemolin also acts in tandem with PRRs to promote phagocytosis and haemocyte aggregation following the detection of a broad range of microbial factors such as LPS and LTA of Gram-negative and -positive bacteria, as well as β-1,3-glucan of fungi (Yu & Kanost, 2002; Eleftherianos et al., 2007; Jung et al., 2019). However, its interaction with the unique structural properties of the mycobacterial cell wall has not yet been described and this, to my knowledge, is the first study to investigate the innate immune response of *Gm* to mycobacteria using modern molecular biological methodologies. Based on the known binding to LTA (Yu & Kanost, 2002), I speculate that *Gm* hemolin may recognise the non-canonical type V LTA, lipoglycan, found within the mycobacterial cell wall (Mishra et al., 2011). Future studies will evaluate the possible interaction between the two factors.

Hemolin structurally resembles the vertebrate axon surface protein, axion 1, and possesses cell-adhesion properties similar to neural cell adhesion molecules (Aathmanathan et al., 2018). The consistent and increasing expression of hemolin and its cell-to-cell adhesive properties, likely contributes to the development of granuloma-like structures during infection (Lapointe et al., 2012), which may be further enhanced by mycobacterial factors such as PDIMs and PGLs (Ly & Liu, 2020). Furthermore, mycobacteria can leverage the wide variety of adhesion molecules expressed on the surface of their cell membrane to promote

adherence to the host cell and induce phagocytosis (Bisht & Meena, 2019). Hemolin likely enhances the ability of mycobacteria to gain entry to host cells facilitating infection.

The proteomic analysis did not identify novel PRR proteins associated with mycobacterial recognition. However, PGRPs and β-1,3-glucan recognition protein were detected in abundance relative to the control from 48 h post-infection onwards. This was surprising as these PRRs are typically associated with Gram-positive bacteria and fungi, respectively (Pereira et al., 2018). It is unlikely that the synthesis and secretion of these recognition proteins are in response to a secondary infection, owing to the lack of observed deviation from the expected survival outcome or mycobacterial load. As such, I hypothesise that the abundance of these recognition proteins could be a generic priming response in anticipation of a secondary infection.

Actin are essential proteins found in the eukaryotic cell cytoskeleton responsible for a wide range of functions, including motility, cell division, endocytosis, intracellular trafficking, chromatin remodelling, DNA repair and transcriptional regulation (Gupta et al., 2020). During cytoskeletal remodelling events (e.g., cell motility or phagocytosis), globular actin (G-actin) is converted into filamentous actin (F-actin), directed by the serum response factor signalling pathway transcriptionally regulated by β-actin (Caron & Hall, 1998; Bunnell et al., 2011). Studies into defective cytoskeletal regulation identified that a mutation in β-actin leads to an increased susceptibility to infection (Cuvertino et al., 2017), and impaired neutrophil function leading to a reduction in ROS production and rate of G- to F-actin polymerisation (Nunoi et al., 1999). In *Gm*, an abundance of β-actin was detected 4 h post-infection (+3.5 fold relative to the control), likely indicating that infection with BCG *lux* triggers the induction of a

cytoskeletal remodelling event, as haemocytes are mobilised, and phagocytosis of mycobacteria occurs (Rougerie et al., 2013). In support of this observation, fluorescence microscopy conducted on primary murine epithelial and lung cells by Alaridah *et al.*, showed that the presence of mycobacteria leads to upregulation of actin distribution (Alaridah et al., 2017).

7.2.2.2 Granuloma-like structures and tissue modulating protein

A key advantage of this insect model is its capacity to mimic the formation of granuloma-like structures. Following the initial stage of infection, the level of β-actin continued to increase over the course of infection (48 h: +5.0 fold, and 168 h: +18.6 fold relative to the control). In zebrafish larvae infected with *M. marinum,* high levels of actin cytoskeletal rearrangement were reported within granulomatous macrophages (Cronan et al., 2016). Therefore, it is probable that the continuously rising abundance of β-actin in *Gm,* reflects the development and maintenance of granuloma-like structures. The detection of β-actin in abundance within the cell-free haemolymph indicates that proteins are released from necrotic and/or lytic haemocytes, as β-actin are typically found in the cytoplasm. This was anticipated as the maintenance and formation of the granulomas typically involves sustaining the equilibrium between live and dead cells (Cronan et al., 2018).

A known protein associated with the formation of granuloma-like structures is Hdd11, which facilitates the cross-linking of pathogen and haemocytes during nodulation/formation of granuloma-like structures (Gandhe et al., 2007; Sheehan et al., 2020b). The abundance of Hdd11 increased over time (4 h: not detected, 48 h: +18.3 fold and 168 h: +310.1 fold relative to the control). This echoed the histological data presented in Chapters 3-5, where the

number of granuloma-like structures increased in abundance and size over the infection course. Similarly, when the fungal granulomatous disease, mycetoma was modelled in *Gm*, a substantial increase in the abundance of Hdd11 was observed over the course of infection (Sheehan et al., 2020b). However, the level of detected Hdd11 detected was 42% higher in the mycetoma model compared to the BCG *lux*. While a comparison between induction of immune response between different diseases is challenging, such variation in Hdd11 levels is likely the result of differences in pathogenicity between *M. mycetomatis* and the attenuated BCG *lux*.

In humans, the development of granulomas is modulated by matrix metalloproteinases (MMPs), which are involved in tissue remodelling during granuloma formation and maintenance via enzymatic degradation of tissue and extracellular proteins (Davis & Ramakrishnan, 2009). The destructive activity of MMPs is regulated by tissue inhibitors of MMPs (TIMPs), maintaining the homeostatic balance of live and dead cells required for structural integrity of granulomas (Parasa et al., 2017). In *Gm*, infection with BCG *lux* led to increased abundance (4 h: +11.5 fold and 168h: +11.0 fold) of IMPI protein. IMPIs lacks structural resemblance to vertebrate TIMPs (Vilcinskas & Wedde, 2002) and do not inhibit the activity of host MMPs, as their primary function is to inhibit microbial metalloproteinases (Wedde et al., 2007). While MMPs and TIMPS are yet to be identified in *Gm*, their presence in fruit flies has been confirmed, indicating a high likelihood that similar molecules exist in *Gm* (Vilcinskas & Wedde, 2002). However, another function of IMPIs has been reported as a regulator of larval metamorphosis and, thus, could indirectly influence the formation of granuloma-like structures in the host tissue (Wedde et al., 2007).

7.2.2.3 Prophenoloxidase cascade and melanisation associated proteins

Larval melanisation following infection with MTBC was reported in all three models established in this project. Many immune proteins associated with the serine protease PPO cascade, responsible for melanisation, were identified in the proteomes generated from BCG *lux* infected larvae. These proteins were found in abundance at 48 h (Prophenol oxidase activating enzyme 3 (PPAE): +14.0 fold, serine protease inhibitor (serpin)-3a: +2.3 fold, serpin-4B: +14.1 fold, and serpin-11: +5.9 fold) and 168 h (PPAE 3: +26.6 fold, serpin-2: +10.3 fold, serpin-3a: +2.6 fold, serpin-4B: +20.9 fold, serpin-11: +15.1 fold), but not at 4h post-infection.

PPAE is one of the terminal serine proteases in the PPO cascade, responsible for converting PPO into the active PO (Lu et al., 2014). PO catalyses the process of melanisation, by converting the tyrosine and quinones into melanin and produce toxic by-products such as reactive oxygen and cytotoxic quinones (Nappi & Christensen, 2005). As a result of these toxic by-products, an unregulated reaction can lead to a detrimental effect on the host health, and thus the PPO cascade is negatively regulated by a series of serpins and serine proteinases, which acts to limit the speed and extent of the melanisation (Lu et al., 2014).

In comparison to *Gm* proteomes generated from *S. aureus* (Sheehan et al., 2019), where PPO cascade associated proteins were detectable as early as 6 h post-infection, BCG *lux* failed to induce a similar response at 4 h post-infection. Such differences likely reflect the higher level of pathogenicity in *Gm* observed with *S. aureus* (90% mortality using 2 x 10^6 CFU inocula after 48 h time course) and the rapid growth of *S. aureus*, relative to the attenuated and slow-growing BCG *lux*. This slow-growing nature of BCG *lux* likely resulted in a controlled host modulation of the PPO cascade at early stages of infection. However, as the infection

progressed, PPO cascade activity continues to rise as BCG *lux* persists within the larva, and a corresponding acceleration in rate of larval melanisation was observed.

7.2.2.4 Antimicrobial peptides

AMPs (also known as host defence peptides) are ubiquitous innate immune effectors found in prokaryotes and eukaryotes, secreted constitutively, or induced in response to external factors such as pathogen detection (Lei et al., 2019). Structurally AMPs are typically composed of amino acids arranged as short chains (typically 15 to 50 amino acids), which fold to create a secondary structure: α--helical, β-stranded, β-hairpin/loop or extended conformation (Wu et al., 2018). The antimicrobial activity of AMPs is believed to be primarily driven by permeablisation, destabilisation and lysis of the microbial cell membrane (Wu et al., 2018). Some AMPs have been reported to translocate the microbial cell membrane and disrupt intracellular activity such as DNA and protein biosynthesis through interaction with enzymes and DNA (Le et al., 2017). While the precise mechanism behind the antimicrobial activity of AMPs remains unclear, like traditional antimicrobial compounds, efficacy appears to be dependent on target microbe and the concentration of AMP used (Le et al., 2017; Wu et al., 2018).

In *Gm* infected with BCG *lux* a rise in abundance of cecropin A, cecropin-D-like protein and gloverin were detectable at 48 h and 168 h post-infection, when compared to the control. SSDA AMPs were not detectable at 4 h post-infection. Cecropins are a group of AMPs, typically 31-39 residues in length, with an α-helical motif capable of inducing membrane-lytic activity via pore formation and are described to possess broad-spectrum activity against both Gram-positive and -negative bacteria as well as fungi (Yi et al., 2014; Wu et al., 2018; Zdybicka-

Barabas et al., 2019). Gloverin is a larger (14 kDa) glycine rich AMP, exclusive to the insect order of Lepidoptera (Yi et al., 2014). As a broad-spectrum AMP, (active against both Gram-positive and -negative and fungal pathogens), gloverin inhibits microbial cell membrane protein biosynthesis and increases permeability (Yi et al., 2014). In reflection of their broad-spectrum antimicrobial activity both cecropins and gloverin were detected in *Gm* infected with *S. aureus* (Sheehan et al., 2019), *A. fumigatus* (Sheehan et al., 2018) and *M. mycetomatis* (Sheehan et al., 2020b) at varying degrees of abundance.

Cecropin A, cecropin-D-like protein and gloverin can be synthetically synthesised (Lin et al., 2019; Kalsy et al., 2020; Correa et al., 2014b, 2014a), and have been tested against several bacterial and fungal pathogens: *Acinetobacter baumanii*, *Salmonella typhimurium*, *P. aureginosa*, *E. coli*, *S. aureus*, *C. albicans*, *Malassezia obtuse*, *Malassaezia sloofiae* (Lin et al., 2019; Cytryńska et al., 2007; Oñate-Garzón et al., 2017; Kalsy et al., 2020; Lee et al., 2013; Lee et al., 2015). However, the antimicrobial activities of cecropins and gloverin on mycobacteria are yet to be determined. Recently, a recombinant hybrid peptide comprised of cecropin A and magainin-2 was created based on broad-spectrum membrane-lytic activity with minimal cytotoxicity to eukaryotic cells (Yue et al., 2020). This *in vitro* synthesised hybrid peptide showed promising antimycobacterial activity against BCG, although the activity of cecropin A alone was not reported (Yue et al., 2020).

A leading AMP-based TB treatment is driven by the human cationic antimicrobial peptide-18 (hCAP-18). During infection, hCAP-18 is proteolytically cleaved into cathelin and LL-37. The activated α-helical LL-37, possessing bactericidal and immunomodulatory activity, enhances phagocytosis, regulates the inflammatory response, cell recruitment and autophagy, while

simultaneously inducing bactericidal effects (membrane-lytic) activity within the phagosome (Torres-Juarez et al., 2015). Insect derived cecropin A, which is similarly α-helical, has been demonstrated to display immune-modulatory (anti-inflammatory) activity, suppressing nitrite production, tumour necrosis factor (TNF)-α and IL-1β (Lee et al., 2015). Therefore, if cecropin A could similarly regulate phagocytosis and autophagy, as with LL-37, such activity would also be a reasonable explanation for the abundance of β-actin following infection.

7.2.3 BCG lux protein expression in Galleria mellonella suggests adaptation to intracellular stress and survival

BCG *lux* derived proteins were identified in the cell-free haemolymph of infected *Gm* (**Table 7.4, Supplementary Table 7.7**). Unlike *Gm* protein expression, quantification was not possible as BCG *lux* lacked the control to determine relative abundance. Therefore, the data are presented for qualitative interpretation alone. The detection of BCG *lux* proteins was challenging as those from *Gm* considerably outnumbered those derived from BCG *lux*.

Table 7.4: BCG *lux* proteins detectable in the haemolymph of infected *G. mellonella*

LFQ Intensity Value			Uniprot Identifier	Protein Name
4 h BCG	48 h BCG	168 h BCG		
6.46E+08	0	0	A0A0H3M2K9	Ribonuclease VapC
2.94E+07	0	0	A1KFW3	2,3-bisphosphoglycerate-dependent phosphoglycerate mutase
1.05E+07	0	0	A0A0H3MJ06	Diacylglycerol O-acyltransferase
8.85E+06	0	0	A1KNQ0	Adenosylhomocysteinase
0	2.96E+08	0	A0A0H3MDY6	Diacylglycerol O-acyltransferase
0	8.04E+07	0	A0A0H3M719	Molybdopterin
0	2.31E+07	0	A0A0H3M8U8	Acyl-CoA dehydrogenase (FadE23)
0	9.24E+06	0	A0A0H3MB41	Protein associated with Decaprenyl diphosphate synthase-like superfamily

No protein of interest was detected at 168 h post-infection.

At 4 h post-infection, VapC, belonging to the VapBC type II toxin-antitoxin (TA) system was detected. This TA system is essential for intracellular survival and metabolic regulation during infection and are induced in response to intracellular stress, drug treatment, and nutrient deprivation (Ramage et al., 2009; Sharrock et al., 2018). In mice and guinea pigs infected with a Δ*vapC* mutant, growth attenuation and host immunomodulating activity were identified, where suppression of innate immune response was lower in the Δ*vapC* mutant (Agarwal et al., 2020).

Both 2,3-bisphosphoglycerate-dependent phosphoglycerate mutase and adenosylhomocysteinase were also detected at 4 h post-infection. The 2,3-bisphosphoglycerate-dependent phosphoglycerate mutase is associated with glucogenesis and differentially induced following oxidative stress and is associated with the mycobacterial antioxidant defence system (Hillion et al., 2017). Adenosylhomocysteinase has been associated with methylation in many cellular processes (e.g., DNA replication and repair, methionine metabolism, polyamine, and phospholipid biosynthesis), and is essential for *in vitro* growth. Adenosylhomocysteinase has been found to be upregulated *in vitro* in cultures of clinical isolates and *in vivo* within lung tissue of MTB infected mice (Dubnau et al., 2005; Singhal et al., 2012).

At both 4 h and 48 h post-infection, diacylglycerol O-acyltransferase was detected, which is also induced under intracellular stress and nutrient deprivation and facilitates the accumulation of triacylglycerol in *MTB*, leading to the formation of ILI and induction of the non-replicative phenotype (Sirakova et al., 2006). *MTB* mutants lacking diacylglycerol O-acyltransferase were unable to develop ILI when stimulated, and WT ILI formation was

recovered upon complementation (Sirakova et al., 2006). The detection of diacylglycerol O-acyltransferase protein agrees with the observed ILI accumulation in BCG *lux* during infection, as found in the TEM images (Chapter 3).

At 48 h post-infection, molybdopterin, acyl-CoA dehydrogenase and decaprenyl diphosphate synthase-associated protein were detected. Molybdopterin is involved in molybdenum cofactor biosynthesis (Wang et al., 2013), is essential for the operation of mycobacterial nitroreductase, and has been shown to participate in hypoxia and nitric oxide stress responses (Williams et al., 2011). Acyl-CoA dehydrogenase is a key enzyme involved in energy generation, lipid biosynthesis and cholesterol degradation (Beites et al., 2021). Acyl-CoA dehydrogenase is induced following cell envelope damage caused by oxidative and nitrosative stress (Voskuil et al., 2011), and following antimycobacterial treatment (INH and ETH) which targets cell wall synthesis (Wilson et al., 1999; Voskuil, 2013). Decaprenyl diphosphate synthase-associated protein is typically involved in cell wall synthesis (Kaur et al., 2004). The induction of decaprenyl diphosphate synthase under intracellular stress has been shown to thicken the mycobacterial cell wall (Ghazaei, 2018).

These detectable BCG lux proteins likely originate from live BCG *lux* found circulating within the haemolymph or from dead and decaying BCG *lux*. The detected proteins indicate that BCG *lux* undergoes similar intracellular adaptations within *Gm* haemocytes comparable to those previously described in traditional TB infection models. Future studies will generate proteomes for *Gm*-infected with SAMTB *lux* and H37Rv.

7.2.4 Low dose BCG lux infection protects Galleria mellonella against high dose infection

Immune priming in the *Gm*-BCG *lux* model was examined by immunising larvae with a non-lethal dose of BCG *lux* (1 x 10^5 CFU) or PBS-T, 48 h prior to infection with a lethal dose of BCG *lux* (2 x 10^7 CFU). Immunisation outcome was measured over 96 h following the infection with the lethal dose of BCG *lux* (**Figure 7.3**). Over the 96 h time course, immunisation led to a significant improvement ($p < 0.0001$) in the larval survival outcome, with a final survival of 30 % and 3 % for immunised and non-immunised larvae, respectively.

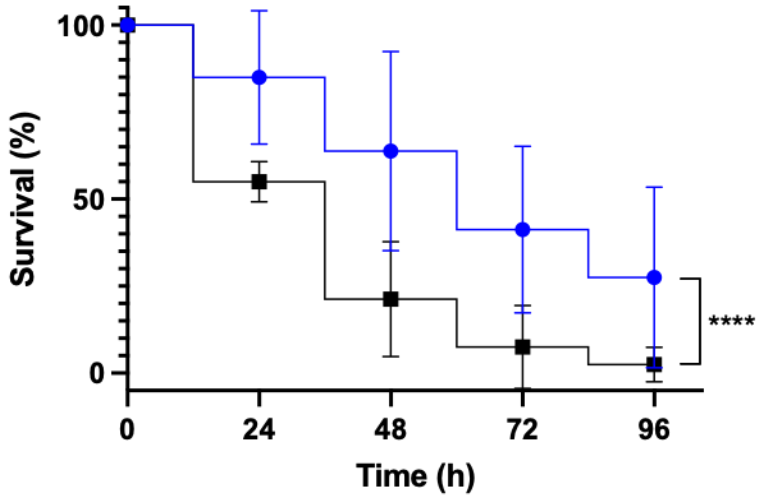


Figure 7.3: The effect of immune priming on survival of BCG *lux* infected *G. mellonella*. Larvae (n=10, per group) were immunised with either non-lethal (1 x 10^5 CFU, blue) or PBS-T (black), 48 h prior to infection with a lethal dose of BCG *lux* (2 x 10^7 CFU). Priming efficacy was measured over the course of the 96 h time course. Plotted are the means of three independent experiments, and the error bars represent the SD of the means. Log-rank Mantle-Cox test was carried out for statistical analysis: **** ($p < 0.0001$).

The observed improvement in survival for those immunised with BCG *lux* indicates that the priming response is specific to the introduction of the bacterium and not a generic response to the injection procedure or delivery of foreign fluids as demonstrated by the PBS-T control. Observations with BCG *lux* immunised larvae are in line with those previously reported in insect-bacterial/fungal infection models (Bergin et al., 2006; Pham et al., 2007; Sheehan et

al., 2020; Sadd & Schmid-Hempel, 2006). However, immunisation introduced a substantial level of variability as indicated by the SD (**Figure 7.3**). The precise source of such variability is not known. Speculatively, such variability may be introduced as a result of individual responses to immunisation, influenced by larval health or proximity to pupation.

Proteomic analysis of *Gm* cell-free haemolymph prepared from larvae infected with 1 x 10^5 CFU at 48 h post-immunisation was carried out to identify any immune effectors which may act to protect the larvae from lethal BCG *lux* infection at the point of infection (**Figure 7.4, Table 7.5, Supplementary Table 7.8 – 7.9**).

Table 7.5: SSDA proteins identified in the haemolymph of *G. mellonella* 48 h post-immunisation with a non-lethal dose of BCG *lux* (1 x 10^5 CFU).

p value	Fold Change	GI Number	Protein Name	Peptides	Sequence coverage [%]	Score
0.018523	25.7	23208535	Peptidoglycan recognition-like protein B	13	34	231.94
0.024315	13.8	15214063	Lysozyme (Alt. 1,4-beta-N-acetylmuramidase)	3	13.3	24.686
0.013977	8.7	116087	Cecropin-A (Alt. Cecropin-C)	1	8.5	9.783
0.002902	5.6	112983994	Peptidoglycan recognition protein	13	57.9	306.89
0.016571	4.1	186703381	Hemolin	7	50.7	323.31
0.000989	49.4	2498144	Apolipophorins (Alt. Apolipophorin II/Apolipophorin I)	3	22.1	21.829
0.033365	9.3	109119903	GAPDH	13	51.2	192.01

Red: signifies an increase in protein abundance. Green: signifies a decline in protein abundance.

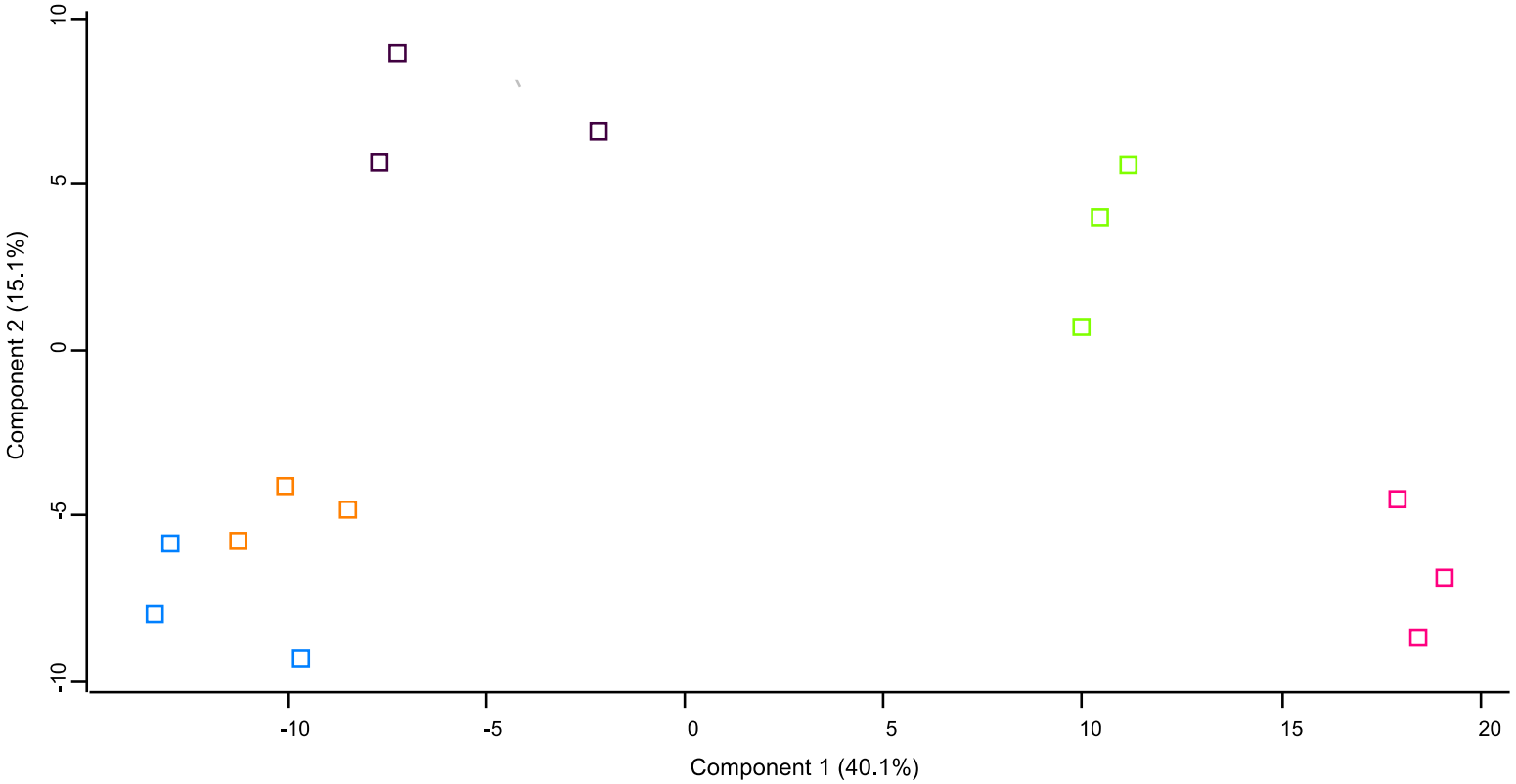


Figure 7.4: PCA of haemolymph proteomes generated from BCG *lux* infected *G. mellonella*. Proteomes generated from the cell-free haemolymph at 0 h (blue), 4 h (orange), 48 h (green), 168 h (pink) and 48 h post-immunisation (black) showed clear grouping between experimental repeat and distinction between the time points. Plotted are PCA generated from three independent repeats, with each repeat consisting of n = 10 larvae (60 µl/larva).

The proteomic profile of larvae at 48 h post immunisation was distinct from that of the control or any of the non-immunised proteomes (**Figure 7.4**). As for the SSDA proteins detected (**Table 7.5**), with the exception of hemolin, all proteins were previously absent at 4 h post-infection (**Table 7.1**).

Hemolin was detectable at levels ~2 fold higher than previously detected at 4 h post-infection, indicating that phagocytic activity is likely enhanced following immunisation (Aathmanathan et al., 2018). While peptidoglycan recognition-like protein B and peptidoglycan recognition protein were detected at an elevated level following immunisation, it is unclear whether such PRRs will have the capacity to detect and amplify innate immune activity in response to mycobacteria. The abundance of cecropin A in the haemolymph and improvements in survival of immunised larvae indicates that, perhaps, cecropin A does possess antimycobacterial activity even in absence of modification (Yue et al., 2020). Previously only a reduction in lysosomal abundance was detectable at 48 h post-infection (**Table 7.2**). However, in immunised larvae, lysosome was detectable at 10 fold higher abundance relative to the naïve control. At low abundance < 500 μg/ml, BCG is typically resistant to lysosomal activity, however at concentrations > 1000 μg/ml, BCG becomes more sensitive to lysosomal activity (Kanetsuna, 1980). While the precise availability of lysozyme in *Gm* is unknown, the presence of lysozyme at the point of infection could enhance the innate immune response against a lethal dose of BCG *lux*. The observed protective effect thereby likely originates from the combined activity of hemolin, cecropin A and lysozyme present at the point of infection, enhancing the capacity of the larval immune response to combat BCG *lux*.

7.2.5 Innate immune gene expression by Galleria mellonella following BCG lux infection

The *Gm* innate immune response to BCG *lux* was similarly investigated by measurement of gene expression by two-step RT-qPCR. Larvae were infected with either high (1 x 10^7 CFU) or low (1 x 10^5 CFU) doses of BCG *lux* and cDNA prepared from whole larval extracted RNA. Relative gene expression was quantified via ΔΔCT using naïve larvae as the control and ubiquitin as the house keeping gene (Dubovskiy et al., 2016a; Lange et al., 2018b). The genes for quantification were selected based on their significance, as previously described in this Chapter; *gloverin*, *cecropin*, *hemolin*, *Hdd11* and *IMPI*.

Irrespective of the infectious dose, all infections with BCG *lux* led to the induction of all innate immune genes examined (**Figure 7.3**). For all five genes quantified, high dose infection led to statistically significant expression (*gloverin*, *cecropin*, *hemolin* and *Hdd11*) or suppression of (*IMPI*) when compared to low dose infection (**Supplementary Figure 7.1**). In both high and low dose BCG *lux* infection, all genes showed a clear but not statistically significant trend in gradual reduction of gene expression over the course of infection, with the expression of genes being the highest at 4 h post-infection (**Figure 7.3**). This trend in reduction of gene expression was similarly observed in *Gm* infected with the Gram-negative bacterium *Riemerella anatipestifer* (Liu et al., 2019).

When comparing the *Gm*-BCG *lux* innate immune gene expression with the generated proteomic data, the correlation between protein presence and mRNA gene expression improved over the course of infection. However, abundance was largely not in agreement with only two genes (*gloverin* and *cecropin*) examined, in agreement with the proteome data

for abundance between 48 h and 168 h post-infection. Comparison at 4 h post-infection was not possible as, with exception of hemolin, no other examined protein was detected.

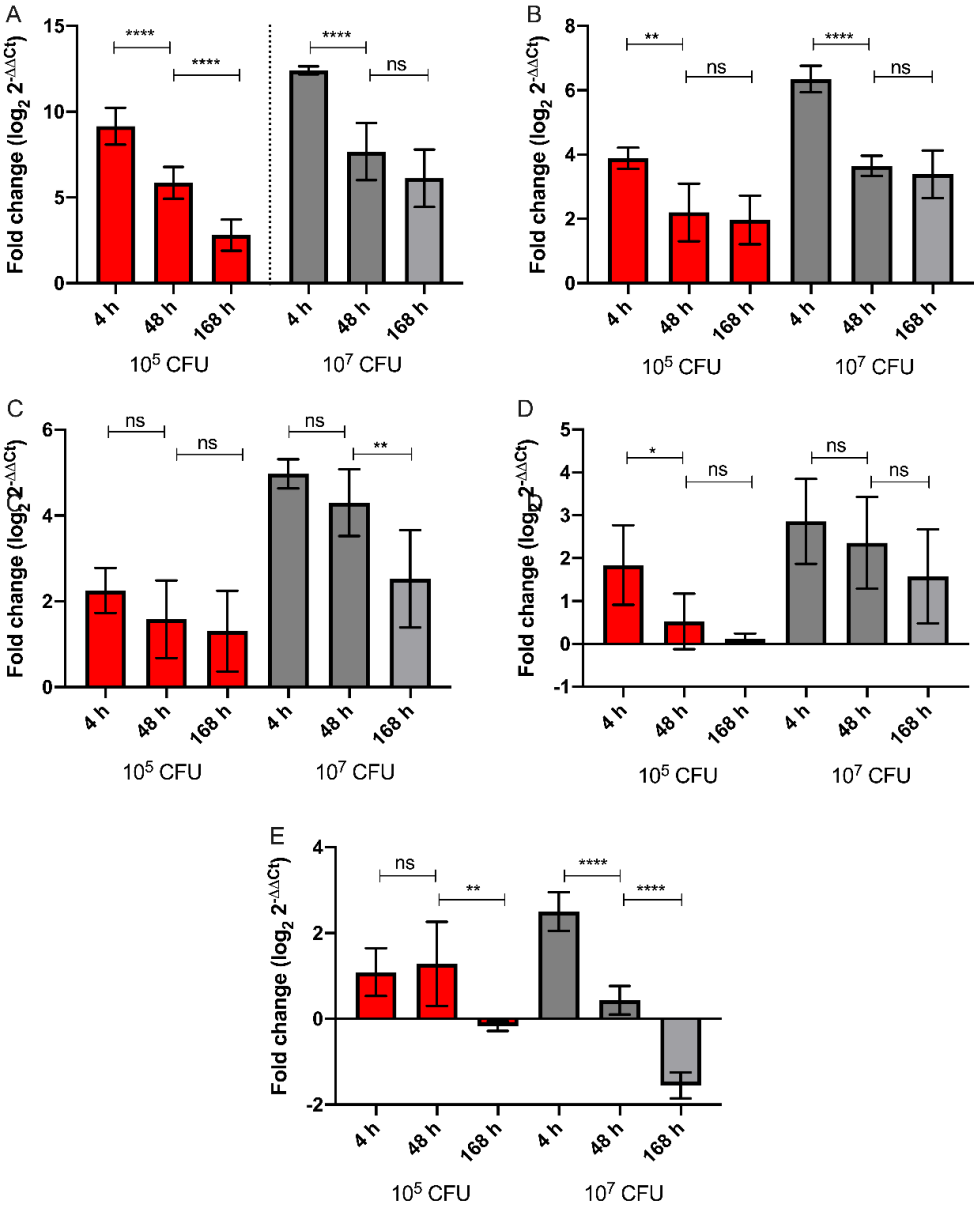


Figure 7.3 Level of *G. mellonella* innate immune gene expression following infection with low or high dose of BCG *lux*. Relative gene expression of (A) *gloverin*, (B) *cecropin*, (C) *hemolin*, (D), *Hdd11* and (E) *IMPI* was measured by qPCR (ΔΔCT) using naïve larvae as control and ubiquitin as the house keeping gene. Plotted are the mean of three independent repeats, each consisting of three technical repeats. Error bars represent the SD. Level of gene expression between each time point within respective doses were conducted using Mann-Whitney U-test: * ($p < 0.05$), ** ($p < 0.01$), and **** ($p < 0.0001$). Reproduced from Asai et al 2021.

The disparities between gene expression and proteome datasets maybe due to the source of the extracted RNA. While the proteomic data relied on proteins present within the cell-free haemolymph, RNA was prepared from whole larvae, thereby incorporating mRNA present in the haemolymph, haemocytes, and the tissues. It is unknown whether the genes studied here, are expressed locally or globally. Gene expression studies of a wide variety of organisms from humans (Sonawane et al., 2017), *M. sexta* (Cao & Jiang, 2017) and *Ceracris nigricornis* Walker (Yuan et al., 2019), all underlined the importance of recognising the contribution of tissue specific gene expression. Regarding tissue specific gene expression, the agreement between gene expression and protein abundance for AMPs: gloverin and cecropin, could be attributable to the primary synthesis and secretion of AMPs by the fat body, which constitutes a large proportion of the larval body mass (Huan et al., 2020).

Comprehensive developmental studies of fruit flies (Becker et al., 2018) and blister beetles (Li et al., 2014) using both transcriptomic and proteomic approaches, identified low correlation between gene expression and protein abundance (20-34%). Translational delay was considered a factor for the variability, where gene induction and protein synthesis could be influenced by mRNA state, downstream gene regulation, post-transcriptional modification and/or availability of biosynthetic material (Liu et al., 2016). To account for such delay in protein expression, a time shift between mRNA and protein measurement was introduced. When a Spearman correlation coefficient was calculated with this revised parameter, only a marginal improvement was observed in subset of fruit fly mRNA-protein pairs: 11.4 % and 13.8%, pre- and post-adjustments respectively. (Becker et al., 2018). While improvements can be made, there are limitations to the comparison of these two Omics approaches, where correlation generally declines with a rise in biological complexity i.e., prokaryotes to

eukaryotes (Gygi et al., 1999; de Sousa Abreu et al., 2009; Schwanhüusser et al., 2011; Kumar et al., 2016a). Comparison becomes further challenging when considering that abundance of protein per gene is relative to translational efficiency and protein stability (Vogel et al., 2010). For example, deep proteomic and transcriptomic analysis of 29 human tissues identified that the number of proteins synthesised per transcript was an order of magnitude higher for a selection of transcripts (Wang et al., 2019).

As the number of genes tested in this study was relatively small, further study will be required for a more comprehensive comparison between proteomic and transcriptomic data in *Gm*. Nevertheless, to my knowledge, this is the first comparative study to examine both transcriptomic and proteomic data in *Gm*.

For the purpose of identifying the innate immune responses activated following infection, as gene expression and presence of protein are in moderate agreement as the infection progresses, RT-qPCR-based gene expression study is a more economical approach to study *Gm* innate immunity when compared to proteomics. However, proteomics is a more accurate representation of the state of innate immunity at the point of interest, as it detects the presence/absence of the functional proteins which is responsible for engaging in the innate immune activity. In future studies, the transcriptomic response of BCG *lux* during *Gm* infection will similarly be evaluated.

7.2.6 Galleria mellonella proteins do not cross-react with human innate immune antibodies used in the Isoplexis human innate panel

Previously, anti-mouse monoclonal and anti-human polyclonal Abs generated for heat-shock proteins, IL-1α and TNF-α have been reported to cross-react in *Gm* (Wittwer et al., 1999; Wrońska & Boguś, 2020). Therefore, a multiplexed proteomic approach was taken to determine whether, any *Gm* proteins would cross react with any of the 19 monoclonal human innate immune Abs (epidermal growth factor [EGF], granulocyte-macrophage colony-stimulating factor [GM-CSF], Granzyme B, IFN-γ, IL-1β, IL-4, IL-6, IL-7, IL-8, IL-10, IL-15, induced protein [IP]-10, monocyte chemoattractant protein [MCP]-1, macrophage inflammatory protein [MIP]-1α, MIP-1β, platelet derived growth factor [PDGF]-BB, sCD137, TNF-α, vascular endothelial growth factor [VEGF]), available from Isoplexis (USA). However, likely due to their monoclonal nature, no cross-reactivity was detectable using such an approach.

7.3 Conclusion

In this Chapter, using proteomics and transcriptomics (gene expression) approaches, I have demonstrated that *Gm* initiates a large and diverse set of innate immune responses in response to BCG *lux*, which dynamically changes over the course of infection.

Within the larvae infected with BCG *lux,* a total of 146 SSDA proteins were detected relative to the control. Amongst these proteins, hemolin and beta-actin were of particular interest due to their potential involvement in phagocytosis and granuloma-like structure formation. Hdd11 previously described in the fungal granulomatous disease, mycetoma (Sheehan et al., 2020b), was similarly identified with increasing abundance in correlation with the development of granuloma-like structures in response to BCG *lux*. A number of proteins associated with the PPO cascade were identified, which when compared to *Gm* infected with a more pathogenic and fast-growing *S. aureus* strain (Sheehan et al, 2019), indicated that BCG *lux* induced mild PPO cascade activation following infection, which gradually worsened over the course of infection. These observations (Hdd11 and PPO cascade) were all in agreement with the phenotypic observations reported in Chapter 3. AMPs, cecropins and gloverin were identified in the proteome of BCG *lux* infected larvae. While antimycobacterial activity of both AMPs are unknown, hybrid synthetic cecropin A has been reported to be effective against BCG (Yue et al., 2020). Furthermore, cecropin A, may share similar immune-modulatory activity to LL-37 used for human TB therapy due to structural (α-helical) and functional (immunomodulatory) similarities (Lee et al., 2015; Torres-Juarez et al., 2015). Unfortunately, no BCG *lux* specific response was detected in this study, likely implying that PRRs and opsonins already characterised in *Gm* may interact with aspects of the unique mycobacterial wall via currently unknown mechanisms.

A few BCG *lux* proteins were identified, although relative quantification was not possible, these proteins largely represented those associated with intracellular adaptation and survival. The detection of diacylglycerol O-acyltransferase, required for the formation of ILI (Sirakova et al., 2006), is in line with cytosolic lipid accumulation within intracellular BCG *lux* bacilli, as visualised in the TEM presented in Chapter 3. Detection of these proteins indicates that *Gm* is under intracellular stress as is found in other infection models.

Immune priming was evaluated in *Gm*, where following immunisation with a non-lethal dose of BCG *lux* (1 x 10^5 CFU) or PBS-T, substantial improvements in larval survival were observed. Proteomic analysis of immunised *Gm* identified a number of proteins which may induce protective effects. Hemolin, cecropin A and lysozyme detected in increased abundance likely contributed to an enhanced antimicrobial effect driven by increased phagocytic activity and granuloma-like structure formation driven by hemolin, speculative cecropin A activity based on activity of the hybrid AMP, and lysosomal activity.

The innate immune response of *Gm* to low (1 x 10^5 CFU) and high (1 x 10^7 CFU) doses of BCG *lux* was similarly quantified via transcriptomics (gene expression) using qPCR (ΔΔCT). All five genes selected (*gloverin*, *cecropin*, *hemolin*, *Hdd11* and *IMPI*) were induced in response to either dose of BCG *lux,* where level of gene induction was consistently higher amongst larvae infected with the higher dose of BCG *lux*. Regardless of the dose, following initial induction, all genes showed a trend in declining levels of expression. Overall gene expression and protein abundance correlated poorly. However, protein presence showed moderate correlation with gene expression from 48 h post-infection onward. Comparison between transcriptomic and proteomic data must be carried out with caution, as the source RNA (from whole larvae vs

protein from haemolymph) and biological factors (e.g., translational delay), can contribute to high levels of variability.

Lacking the commercial availability of *Gm* Abs, transcriptomic and proteomic approaches are currently the only methodology to comprehensively examine the *Gm* innate immune system. However, as annotation of the *Gm* genome improves over time, I anticipate that the study of *Gm* innate immune system will become more easier and more accessible. Future studies will focus on the response of BCG *lux* to the *Gm* innate immune response using both Omics approaches. I will also expand the proteomic database by generating proteomes for *Gm*-SAMTB *lux* and H37Rv, reflecting both the host and pathogen.

Chapter 8
Conclusions
and future perspectives

The overall aim of this project was to evaluate the use of *Gm* as a 3Rs model to study *MTB* infection. Over the course of this project, I tested the hypothesis that *Gm* larvae can be used as a reproducible, low-cost, and ethically more acceptable model to study TB; in particular one that can be used as a platform for medium-high throughput screening of novel antimycobacterial agents, and for the assessment of comparative *MTB* virulence, thereby reducing and/or replacing the use of animals in TB research.

Early research by Metalnikov, Cameron and Hollande, reported that *MTB*, *M. bovis* and *M. avium*, were unable to cause a virulent (lethal) infection in *Gm*. Recently, other pathogens reported by Metalnikov, Cameron and Hollande, as avirulent have recently been re-evaluated as virulent. In Chapter 3, *Gm* was re-evaluated as a host for the MTBC using BCG *lux*. The lethality of BCG *lux* in *Gm* was demonstrated using a CFU inoculum that was one fourth originally used by Cameron, and the rate of larval mortality positively correlated with a rise in CFU infectious dose. Measurement of *in vivo* BCG *lux* burden revealed establishment of a persistent and non-replicative infection. Such observations were supported by the formation of ILI in BCG *lux* internalised by circulating haemocytes, a phenotype typically associated with non-replicative bacilli. Following infection, host cells surrounded the BCG *lux* bacilli, to form a multi-cellular structure resembling a granuloma. Such granuloma-like structures increased in number and size with the progression of infection. BCG *lux* within these structures stained deeply as a large individually indistinguishable ZN-positive mass indicative of mycobacterial degradation, and host cells showed evidence of necrosis by H&E staining. These findings highlighted the potential of *Gm* as a promising TB infection model warranting further investigation.

In Chapter 4, a novel CL2 compliant *MTB* infection model was established using *Gm* and SAMTB *lux*. In comparison to BCG *lux,* SAMTB *lux* was anticipated to be more virulent as it retained the RD1 region, which is lacking in BCG *lux* and known to be essential for mycobacterial virulence. SAMTB *lux* established a proliferative infection in *Gm*, owing to the availability of host Leu and Pan to bypass the double auxotrophy. However, its virulence was of similar magnitude to BCG *lux,* indicating virulence may be influenced by the double auxotrophy despite the availability of nutrients. ILI formation was lacking in intracellular SAMTB *lux* bacilli, reflecting the proliferative nature of the infection. The abundance of granuloma-like structures was more apparent in SAMTB *lux* infection, which contained masses of individually distinguishable and brightly ZN-reactive bacilli, indicative of metabolically active and replicating bacilli. Intriguingly, during the late stage of infection (168 h) granuloma-like structures containing large masses of SAMTB *lux*, lost their ability to stain with ZN. This phenomenon, known as 'Koch's paradox', has previously been associated with both dormant and persistent phenotypes, indicating the possible existence of a sub-population of SAMTB *lux* in this model. In addition, exploiting the interaction between *Gm*-SAMTB *lux,* a pilot proof-of-concept *ex vivo* model of granuloma-like structures was developed; in future work this will be used to better understand their induction and development. Based on the "attenuation" of SAMTB *lux* in *Gm,* further investigation using the WT strain from which it was derived, H37Rv, was necessary to determine whether the susceptibility of *Gm* to members of MTBC is specific to the pathogenicity of each strain or a generic response to infectious dose.

In Chapter 5, the interaction of *Gm*-H37Rv was evaluated in CL3. The design of the model was adjusted to reflect the chronic nature of TB, by reducing the infectious dose to 10^6 CFU and

extending the study duration to 192 h. H37Rv was more virulent than BCG *lux* or SAMTB *lux* at both 10^6 and 10^7 CFU infectious doses, indicating that *Gm* survival reflected the pathogenicity of the each MTBC strain and not a generic response to infectious dose. The formation of granuloma-like structures over time was most evident with H37Rv out of all the mycobacterial - *Gm* models established, and the loss of ZN reactivity in such structures was recorded more frequently at an earlier stage of infection. Non-replicative intracellular bacilli (ILI formation) were lacking in the circulating haemocyte population as with SAMTB *lux*. The use of *Gm* as a screen for comparative *MTB* virulence was demonstrated using H37Rv WT and two isogenic mutants Δ*phop* and Δ*dosR*, known to be attenuated in mammalian models. Infection with either mutant led to substantial changes in virulence in *Gm* when compared to the WT, and virulence reverted to that of WT once the deletion was complemented. In *Gm*, Δ*phop* was attenuated as predicted, whereas Δ*dosR* unexpectedly resulted in hypervirulence. Differences in phenotypic outcome for Δ*dosR* likely originated from overactivation of virulence during the acute stage of infection, which was similarly observed in SCID mice, indicating that an adaptive immune response is required for correcting/controlling Δ*dosR* infection.

Having successfully established and characterised the three *Gm*-MTBC infection models, in Chapter 6 these models were evaluated as a screen for anti-mycobacterial compounds. All clinically relevant first- and second-line compounds examined were non-toxic to *Gm*; and treatment generally improved survival outcome in all models, relative to the control. INH and RIF were the most effective at reducing *in vivo* mycobacterial burden. ETH and MOX showed activity but only when used at a higher than recommended dosage. PZA, which targets Pan biosynthesis, lacked any substantial activity in all models, even at a higher than recommended

dosages, likely due to the abundance of Pan in *Gm*. The efficacy of INH, RIF, ETH and MOX in *Gm* is in agreement with results previously reported in mammalian models. The efficacy of antimycobacterial compounds did not improve when administered in combination or after repeated dosing in the BCG *lux* and SAMTB *lux* models. The differences in model design between *Gm*-BCG *lux*/SAMTB *lux* and H37Rv (i.e., incubation period, infectious dosage, and length of infection prior to treatment) did not appear to influence overall treatment outcome. The use of *Gm*-FluorBCG as a live fluorescence *in vivo* screen, that lacks the need for larval termination to measure efficacy was demonstrated as proof-of-concept, with treated larvae showing a clear reduction in FluorBCG YFP fluorescence following treatment.

In Chapter 7, the innate immune response of *Gm* to BCG *lux* infection was characterised using proteomics and transcriptomics (gene expression). A total of 146 SSDA proteins were identified, from the cell free haemolymph of infected larvae, relative to the control. Amongst these were proteins associated with phagocytosis (hemolin and β-actin), granuloma-like structure formation (Hdd11, hemolin and β-actin), PPO cascade (PPAE and serpins), PRR (PGRPs and β-1,3-glucan recognition protein), and AMPs (cecropins and gloverin). BCG *lux* proteins were also detected over the course of infection, and were mostly associated with intracellular adaptation and survival, indicating that *Gm* induces intracellular stress as seen in other infection models. Immunisation with a non-lethal dose of BCG *lux*, protected larvae from a lethal dose, reducing the rate of larval mortality relative to the non-immunised control. Proteomic analysis of immunised larvae identified that abundance of hemolin, cecropin A and lysozyme, increased in response to immunisation, which may act to enhance antimycobacterial responses at the point of infection. Gene expression analysis of a selection of innate immune genes, revealed the induction of innate immune gene expression, the level

of which positively correlated with the infectious dose. However, correlation between protein abundance and gene expression was poor. Nevertheless, as an indicator of protein presence, gene expression correlated well, especially with the progression of infection.

By designing, conducting, and analysing the data generated in *Gm*, key limitations or 'gaps in our knowledge' were identified. As a model in its infancy, *Gm* currently lacks a fully annotated genome, although a fully sequenced genome (Lange et al., 2018a) and a scaffold assembly-level annotation is available on NCBI (ASM364042v2). Nevertheless, transcriptomics and proteomic analysis can be carried out using the more comprehensively annotated genomes/protein database of other lepidoptera (butterfly/moth) or diptera (fly) genomes (Vogel et al., 2011); although reliance on non-host data limits the depth of the analysis. Through personal communication, I am aware that multiple groups, both national and international, are currently making progress on generating a fully annotated genome for *Gm*. The generation of such data is critical for the continued uptake of this model, and to enable more comprehensive *Gm*-MTBC (and other pathogen) studies to be conducted. Comprehensive knowledge of the genome is essential for generation of transgenic mutants, which have proven to be a valuable asset to determine key aspects of host immunity to infection in established models (Swearengen, 2018).

Another gap in our knowledge is the *Gm* innate immune system. Our current understanding of insect innate immunology relies on data primarily generated in the fruit fly (Sheehan et al., 2018b). Through microscopy at least five haemocyte sub-types have been described in *Gm*, however only the functions of plasmatocytes and granulocytes have been described in detail (Dubovskiy et al., 2016b). As for the remaining three sub-types: prohaemocytes,

spherulocytes and oenocytoids, their contribution to the innate immune response remains speculative (Hillyer, 2016; Stączek et al., 2020). Historically, the extensive collection of commercially available immunological and molecular tools (e.g., Abs and probes) have allowed isolation and detailed characterisation of immunological cell types, complex immunological assays, and the generation of quantitative data. *Gm* is currently limited by the lack of such tools. While *Gm* monoclonal Abs has been generated in the past (Mullet et al., 1993), no additional Abs have been described in the past 20 years. More detailed study of *Gm*-MTBC interactions will require tools which can: 1) easily identify haemocyte sub-types; and 2) allow for a comprehensive characterisation of the host response.

While these gaps in our knowledge limit our current application of *Gm* in research, the capabilities of this model will continue to improve over time with innovative research approaches within the *Gm* community. For example, the innate immune system can further be characterised via single cell transcriptomic analysis of haemocytes. Unlike the broad view of *Gm* innate immunity generated via whole organisms (Vogel et al., 2011), tissues (Sheehan et al., 2020b) or cell free haemolymph (Sheehan et al., 2018a), single cell data will identify groups with a transcriptomically distinct signature, corresponding to haemocyte sub-types, and provide a highly specific view of *Gm* innate immune responses under both uninfected and infected conditions. While such analysis is currently constricted to the data generated from other insects, the identification of transcripts will only improve with the availability of a fully annotated *Gm* genome. Generation of a single cell haemocyte transcriptome is crucial for comparison against a similarly generated dataset from mammalian or human *MTB* activated neutrophils and macrophages.

For characterisation of haemocyte activity, groups of sub-types can be isolated via centrifuge density gradient separation (Anggraeni & Ratcliffe, 1991; Mead et al., 1986), which could further be purified into single sub-types using fluorescence-activated single cell sorting (Browne et al., 2015). The isolated haemocyte sub-types will be used to modify the *ex vivo Gm* granuloma-like structure model, to evaluate the role of each subtype in the formation of such structures. I hypothesise that the formation of granuloma-like structures is dependent on a select few sub-types. Furthermore, using sub-type specific transcriptomic signatures as template, DNA/RNA probes could be generated to study the cellular composition of granuloma-like structures developed *in vivo* and *ex vivo*, through fluorescence *in situ* hybridisation (Kwon et al., 2021). Moreover, such DNA/RNA probes, could be capable of accurately measuring the changes to haemocyte population over the course of infection, and be used as an alternative for Abs (Young et al., 2020). Additionally, using the transcriptomic data, sub-type specific innate immune genes could be identified, and confirmed by gene knockdown assays carried out via RNA inhibitors (Grizanova et al., 2021). I hypothesise that inhibition of such genes will lead to adverse outcomes for larvae infected with mycobacteria. The use of RNA inhibitors may be of interest to supress expression of Hdd11 to observe its effect on the development of granuloma-like structures *in vivo* and *ex vivo*. The generation of single cell transcriptomic data, methodology to isolate sub-types, and generation of probes and inhibitors could greatly enhance our capacity to conduct more complex studies. Thereby elevating the status of *Gm* as an infection model, not only in the field of TB, but in the broader research community.

Another aspect that will require further investigation is the loss of ZN reactivity in populations of mycobacteria found within granuloma-like structures, as seen in the H37Rv and SAMTB *lux*-

Gm models. Evidence that such loss of ZN reactivity is associated with a non-replicative phenotype could be provided by conducting Ab-based mycobacterial staining, reactivity to which is retained by non-replicative bacilli (Vilchèze & Kremer, 2017). Other factors associated with the non-replicative phenotype can be evaluated using staining techniques such as lipophilic Nile red to visualise the accumulation of ILI within mycobacteria (Vilchèze & Kremer, 2017). Similarly, the granuloma-like structures could be dissected out of the larvae and processed for TEM. However, as the granuloma-like structures contain a dense mass of mycobacteria, penetration of the epoxy resin throughout the structure is likely to be challenging, leading to sample breakage as previously seen for large aggregates of mycobacteria in the haemocyte TEM samples. Proteomic analysis of mycobacterial responses (as well as *Gm* response) during varying stages of granuloma-like structure formation will also give substantial information regarding the host-pathogen interaction taking place within this model, as previously carried out for *M. mycetomatis* infection in *Gm* (Sheehan et al., 2020b).

Finally, to further develop the use of *Gm*-MTBC models as a screen for antimycobacterial compounds, efficacy of novel compounds (e.g., synthetic AMPs) could be assessed in parallel to mammalian studies, to comprehensively evaluate the use of *Gm* as a pre-screen. The lack of PK/PD data for antimycobacterial compounds in *Gm* could possibly be resolved by applying a metabolomics approach, through isolation of drug metabolites and monitoring their abundance over time (Alseekh et al., 2021). The availability of such data would be vital for relative comparison against drug studies in existing TB models. The pilot *Gm*-FluorBCG live drug screening model will continue to be developed. A parallel medium-throughput screening system using 24 well plates or custom larvae holders could enhance screening efficacy, where fluorescence measurement could be automated to give hourly drug efficacy readout.

The data presented in this Thesis highlighted the value of *Gm* as an alternative TB model underlining its potential in reducing animal usage in areas of TB research such as drug testing and comparative *MTB* virulence screening, which currently relies on the use of mammalian infection models. Such application of *Gm*, not only in TB but in the broader field of infectious disease has the potential to substantially reduce animal usage, of which in 2020 alone, more than 37800 animals were used for translational and applied infectious disease research (Home Office UK, 2020).

In conclusion, the results presented in this project support the hypothesis that *Gm* is a reproducible, low-cost, and ethically more acceptable model for TB, which is capable of mimicking key aspects of disease, can be used to assess comparative MTB virulence, and has the potential to be utilised as a medium throughput drug screen. The adoption and continued development of this TB model has the potential to substantially reduce/replace the use of animals in TB research. Nevertheless, I acknowledge that *Gm* is as a model still in its infancy and limitations do exist, such as the lack of a fully annotated genome and the limited knowledge of *Gm* innate immunity. However, researchers are actively addressing these limitations and it can be anticipated that *Gm* will continue its rapid adoption as a valuable host for infectious disease research.

Chapter 9
Bibliography

Aathmanathan VS, Jothi N, Prajapati VK & Krishnan M (2018) Investigation of immunogenic properties of hemolin from silkworm, *Bombyx mori* as carrier protein: An immunoinformatic approach. *Scientific Reports* 8, 6957.

Agarwal S, Sharma A, Bouzeyen R, Deep A, Sharma H, Mangalaparthi KK, Datta KK, Kidwai S, Gowda H, Gowda H, Varadarajan R, Sharma RD, Thakur KG & Singh R (2020) VapBC22 toxin-antitoxin system from *Mycobacterium tuberculosis* is required for pathogenesis and modulation of host immune response. *Science Advances* 6(23), eaba6944.

Aguilo N, Uranga S, Marinova D, Monzon M, Badiola J & Martin C (2016) MTBVAC vaccine is safe, immunogenic and confers protective efficacy against *Mycobacterium tuberculosis* in newborn mice. *Tuberculosis* 96, 71–74.

Alahari A, Trivelli X, Guérardel Y, Dover LG, Besra GS, Sacchettini JC, Reynolds RC, Coxon GD & Kremer L (2007) Thiacetazone, an antitubercular drug that inhibits cyclopropanation of cell wall mycolic acids in mycobacteria. *PLoS ONE* 2(12), e1343.

Alaridah N, Lutay N, Tenland E, Rönnholm A, Hallgren O, Puthia M, Westergren-Thorsson G & Godaly G (2017) Mycobacteria manipulate G-protein-coupled receptors to increase mucosal Rac1 expression in the lungs. *Journal of Innate Immunity* 9, 318–329.

Almeida DV, Tyagi S, Li S, Wallengren K, Pym AS, Ammerman NC, Bishai WR & Grosset JH (2014) Revisiting anti-tuberculosis activity of pyrazinamide in mice. *Mycobacterial diseases* 4(2), 145.

Alseekh S, Aharoni A, Brotman Y, Contrepois K, D'Auria J, Ewald J, C. Ewald J, Fraser PD, Giavalisco P, Hall RD, Heinemann M, Link H, Luo J, Neumann S, Nielsen J, Perez de Souza L, Saito K, Sauer U, Schroeder FC, Schuster S, Siuzdak G, Skirycz A, Sumner LW, Snyder MP, Tang H, Tohge T, Wang Y, Wen W, Wu S, Xu G, Zamboni N & Fernie AR (2021) Mass spectrometry-based metabolomics: a guide for annotation, quantification and best reporting practices. *Nature Methods* 18(7), 747–756.

Altaf M, Miller CH, Bellows DS & O'Toole R (2010) Evaluation of the *Mycobacterium smegmatis* and BCG models for the discovery of *Mycobacterium tuberculosis* inhibitors. *Tuberculosis* 90, 333–337.

Andreu N, Zelmer A, Fletcher T, Elkington PT, Ward TH, Ripoll J, Parish T, Bancroft GJ, Schaible U, Robertson BD & Wiles S (2010) Optimisation of bioluminescent reporters for use with mycobacteria. *PLoS ONE* 5(5), e10777.

Anggraeni T & Ratcliffe NA (1991) Studies on cell-cell co-operation during phagocytosis by purified haemocyte populations of the wax moth, *Galleria mellonella*. *Journal of Insect Physiolology* 37(6), 453–460.

Arrese EL & Soulages JL (2010) Insect Fat Body: Energy, Metabolism, and Regulation. *Annual Review of Entomology* 55, 225.

Asai M, Li Y, Singh Khara J, Gladstone CA, Robertson BD, Langford PR & Newton SM (2019a) Use of the invertebrate *Galleria mellonella* as an infection model to study the *Mycobacterium tuberculosis* complex. *Journal of Visualized Experiments* (148), e59703.

Asai M, Li Y, Singh Khara J, Robertson BD, Langford PR & Newton SM (2019b) *Galleria mellonella*: an infection model for screening compounds against the *Mycobacterium tuberculosis* complex. *Frontiers in Microbiology* 10, 2630.

Asai M, Li Y, Spiropoulos J, Cooley W, Everest D, Robertson BD, Langford PR & Newton SM (2020) A novel biosafety level 2 compliant tuberculosis infection model using a Δ*leuD*Δ*panCD* double auxotroph of *Mycobacterium tuberculosis* H37Rv and *Galleria mellonella*. *Virulence* 11(1), 811–824.

Asai M, Sheehan G, Li Y, Robertson BD, Kavanagh K, Langford PR & Newton SM (2021) Innate immune responses of *Galleria mellonella* to *Mycobacterium bovis* BCG challenge identified using proteomic and molecular approaches. *Frontiers in Cellular and Infection Microbiology* 11, 619981.

Ashburner M & Roote J (2007) Maintenance of a *Drosophila* laboratory: General procedures. *Cold Spring Harbor Protocols*, pdb.ip35.

Asis A, Savoretti F, Cabruja M, Gramajo H & Gago G (2021) Characterization of key enzymes involved in triacylglycerol biosynthesis in mycobacteria. *Scientific Reports* 11(1), 1–13.

Asmar S & Drancourt M (2015) Rapid culture-based diagnosis of pulmonary tuberculosis in developed and developing countries. *Frontiers in Microbiology* 6, 1184.

Astarie-Dequeker C, Guyader L le, Malaga W, Seaphanh F, Chalut C, Lopez A & Guilhot C (2009) Phthiocerol dimycocerosates of *M. tuberculosis* participate in macrophage invasion by inducing changes in the organization of plasma membrane lipids. *PLoS Pathogens* 5(2), e1000289.

Astvad KMT, Meletiadis J, Whalley S & Arendrup MC (2017) Fluconazole pharmacokinetics in *Galleria mellonella* larvae and performance evaluation of a bioassay compared to liquid chromatography-tandem mass spectrometry for hemolymph specimens. *Antimicrobial Agents and Chemotherapy* 61(10), e00895-17.

Avdesh A, Chen M, Martin-Iverson MT, Mondal A, Ong D, Rainey-Smith S, Taddei K, Lardelli M, Groth DM, Verdile G & Martins RN (2012) Regular care and maintenance of a Zebrafish (*Danio rerio*) laboratory: An introduction. *Journal of Visualized Experiments* (69), e4196.

Bahal RK, Mathur S, Chauhan P & Tyagi AK (2018) An attenuated quadruple gene mutant of *Mycobacterium tuberculosis* imparts protection against tuberculosis in guinea pigs. *Biology Open* 7(1), bio029546.

Barberis I, Bragazzi NL, Galluzzo L & Martini M (2017) The history of tuberculosis: From the first historical records to the isolation of Koch's bacillus. *Journal of Preventive Medicine and Hygiene* 58(1), E9–E12.

Barnoy S, Gancz H, Zhu Y, Honnold CL, Zurawski DV & Venkatesan MM (2017) The *Galleria mellonella* larvae as an *in vivo* model for evaluation of *Shigella* virulence. *Gut Microbes* 8(4), 335–350.

Be NA, Klinkenberg LG, Bishai WR, Karakousis PC & Jain SK (2011) Strain-dependent CNS dissemination in guinea pigs after *Mycobacterium tuberculosis* aerosol challenge. *Tuberculosis* 91(5), 386–389.

Becker K, Bluhm A, Casas-Vila N, Dinges N, Dejung M, Sayols S, Kreutz C, Roignant JY, Butter F & Legewie S (2018) Quantifying post-transcriptional regulation in the development of *Drosophila melanogaster*. *Nature Communications* 9, 4970.

Bergin D, Murphy L, Keenan J, Clynes M & Kavanagh K (2006) Pre-exposure to yeast protects larvae of *Galleria mellonella* from a subsequent lethal infection by *Candida albicans* and is mediated by the increased expression of antimicrobial peptides. *Microbes and Infection* 8(8), 2105–2112.

Bergin D, Reeves EP, Renwick J, Wientjes FB & Kavanagh K (2005) Superoxide production in *Galleria mellonella* hemocytes: identification of proteins homologous to the NADPH oxidase complex of human neutrophils. *Infection and Immunity* 73(7), 4161–4170.

Bergman P, Raqib R, Rekha RS, Agerberth B & Gudmundsson GH (2020) Host directed therapy against infection by boosting innate immunity. *Frontiers in Immunology* 11, 1209.

Bhatt A, Fujiwara N, Bhatt K, Gurcha SS, Kremer L, Chen B, Chan J, Porcelli SA, Kobayashi K, Besra GS & Jacobs WR (2007) Deletion of *kasB* in *Mycobacterium tuberculosis* causes loss of acid-fastness and subclinical latent tuberculosis in immunocompetent mice. *Proceedings of the National Academy of Sciences of the United States of America* 104(12), 5157–5162.

Bisht D & Meena L (2019) Adhesion molecules facilitate host-pathogen interaction & mediate *Mycobacterium tuberculosis* pathogenesis. *The Indian Journal of Medical Research* 150(1), 23–32.

Blevins SM & Bronze MS (2010) Robert Koch and the “golden age” of bacteriology. *International Journal of Infectious Diseases* 14(9), e744–e751.

Blokpoel MCJ, O’Toole R, Smeulders MJ & Williams HD (2003) Development and application of unstable GFP variants to kinetic studies of mycobacterial gene expression. *Journal of Microbiological Methods* 54(2), 203–211.

Bokhari H, Ali A, Noreen Z, Thomson N & Wren BW (2017) *Galleria mellonella* is low cost and suitable surrogate host for studying virulence of human pathogenic *Vibrio cholerae*. *Gene* 628, 1–7.

Borkute RR, Woelke S, Pei G & Dorhoi A (2021) Neutrophils in tuberculosis: cell biology, cellular networking and multitasking in host defense. *International Journal of Molecular Sciences* 22(9), 4801.

von Both U, Berk M, Agapow PM, Wright JD, Git A, Hamilton MS, Goldgof G, Siddiqui N, Bellos E, Wright VJ, Coin LJ, Newton SM & Levin M (2018) *Mycobacterium tuberculosis* exploits a molecular off switch of the immune system for intracellular survival. *Scientific Reports* 8(1), 661.

Bouté M, Carreras F, Rossignol C, Doz E, Winter N & Epardaud M (2017) The C3HeB/FeJ mouse model recapitulates the hallmark of bovine tuberculosis lung lesions following *Mycobacterium bovis* aerogenous infection. *Veterinary Research* 48(1), 73.

Bouz G & al Hasawi N (2018) The zebrafish model of tuberculosis - no lungs needed. *Critical Reviews in Microbiology* 44(6), 779–792.

Brodin P, Majlessi L, Marsollier L, Jonge MI de, Bottai D, Demangel C, Hinds J, Neyrolles O, Butcher PD, Leclerc C, Cole ST & Brosch R (2006) Dissection of ESAT-6 system 1 of *Mycobacterium tuberculosis* and impact on immunogenicity and virulence. *Infection and Immunity* 74(1), 98.

Brodl E, Winkler A & Macheroux P (2018) Molecular mechanisms of bacterial bioluminescence. *Computational and Structural Biotechnology Journal* 16, 564.

Brosch R, Gordon S, Garnier T, Eiglmeier K, Frigui W, Valenti P, Santos S dos, Duthoy S, Lacroix C, Garcia-Pelayo C, Inwald JK, Golby P, Garcia JN, Hewinson RG, Behr MA, Quail MA, Churcher C, Barrell BG, Parkhill J & Cole ST (2007) Genome plasticity of BCG and impact on vaccine efficacy. *Proceedings of the National Academy of Sciences of the United States of America* 104(13), 5596–5601.

Broset E, Martín C & Gonzalo-Asensio J (2015) Evolutionary landscape of the *Mycobacterium tuberculosis* complex from the viewpoint of PhoPR: Implications for virulence regulation and application to vaccine development. *mBio* 6(5), e01289-15.

Browne N, Heelan M & Kavanagh K (2013) An analysis of the structural and functional similarities of insect hemocytes and mammalian phagocytes. *Virulence* 4(7), 597–603.

Browne N, Surlis C, Maher A, Gallagher C, Carolan JC, Clynes M & Kavanagh K (2015) Prolonged pre-incubation increases the susceptibility of *Galleria mellonella* larvae to bacterial and fungal infection. *Virulence* 6(5), 458–465.

Bucsan AN, Mehra S, Khader SA & Kaushal D (2019) The current state of animal models and genomic approaches towards identifying and validating molecular determinants of *Mycobacterium tuberculosis* infection and tuberculosis disease. *Pathogens and Disease* 77(4), ftz037.

Bunnell TM, Burbach BJ, Shimizu Y & Ervasti JM (2011) β-Actin specifically controls cell growth, migration, and the G-actin pool. *Molecular Biology of the Cell* 22(21), 4047–4058.

Bussi C & Gutierrez MG (2019) *Mycobacterium tuberculosis* infection of host cells in space and time. *FEMS Microbiology Reviews* 43(4), 341–361.

Calderon VE, Valbuena G, Goez Y, Judy BM, Huante MB, Sutjita P, Johnston RK, Estes DM, Hunter RL, Actor JK, Cirillo JD & Endsley JJ (2013) A humanized mouse model of tuberculosis. *PLoS ONE* 8(5), e63331.

Camacho LR, Constant P, Raynaud C, Lanéelle MA, Triccas JA, Gicquel B, Daffé M & Guilhot C (2001) Analysis of the phthiocerol dimycocerosate locus of *Mycobacterium tuberculosis*: evidence that this lipid is involved in the cell wall permeability barrier. *Journal of Biological Chemistry* 276(23), 19845–19854.

Cambier CJ, Falkow S & Ramakrishnan L (2014) Host evasion and exploitation schemes of *Mycobacterium tuberculosis*. *Cell* 159(7), 1497–1509.

Cambier CJ, Takaki KK, Larson RP, Hernandez RE, Tobin DM, Urdahl KB, Cosma CL & Ramakrishnan L (2013) Mycobacteria manipulate macrophage recruitment through coordinated use of membrane lipids. *Nature* 505(7482), 218–222.

Cameron GR (1934) Inflammation in the caterpillars of Lepidoptera. *The Journal of Pathology and Bacteriology* 38(3).

Cao X & Jiang H (2017) An analysis of 67 RNA-seq datasets from various tissues at different stages of a model insect, *Manduca sexta*. *BMC Genomics* 18, 796.

Card R, Vaughan K, Bagnall M, Spiropoulos J, Cooley W, Strickland T, Davies R & Anjum MF (2016) Virulence characterisation of *Salmonella enterica* isolates of differing antimicrobial resistance recovered from UK livestock and imported meat samples. *Frontiers in Microbiology* 7, 640.

Caron E & Hall A (1998) Identification of two distinct mechanisms of phagocytosis controlled by different Rho GTPases. *Science* 282(5394), 1717–1721.

Carroll P, Schreuder LJ, Muwanguzi-Karugaba J, Wiles S, Robertson BD, Ripoll J, Ward TH, Bancroft GJ, Schaible UE & Parish T (2010) Sensitive detection of gene expression in mycobacteria under replicating and non-replicating conditions using optimized far-red reporters. *PLoS one* 5(3), e9823.

Carvalho C, Gaspar A, Knight A & Vicente L (2019) Ethical and scientific pitfalls concerning laboratory research with non-human primates, and possible solutions. *Animals* 9(1), 12.

Cé R, Silva RC, Trentin DS, Marchi JGB de, Paese K, Guterres SS, Macedo AJ & Pohlmann AR (2020) *Galleria mellonella* larvae as an *in vivo* model to evaluate the toxicity of polymeric nanocapsules. *Journal of nanoscience and nanotechnology* 20(3), 1486–1494.

Chadwick J (1967) Some aspects of immune responses in insects. *In Vitro* 3, 120–128.

Champion OL, Wagley S & Titball RW (2016) *Galleria mellonella* as a model host for microbiological and toxin research. *Virulence* 7(7), 840–845.

Chandler CIR (2019) Current accounts of antimicrobial resistance: Stabilisation, individualisation and antibiotics as infrastructure. *Palgrave Communications* 5(1), 1–13.

Charlet D, Mostowy S, Alexander D, Sit L, Wiker HG & Behr MA (2005) Reduced expression of antigenic proteins MPB70 and MPB83 in *Mycobacterium bovis* BCG strains due to a start codon mutation in *sigK*. *Molecular Microbiology* 56(5), 1302–1313.

Chen RY & Keddie BA (2021) The *Galleria mellonella*-enteropathogenic *Escherichia coli* model system: characterization of pathogen virulence and insect immune responses. *Journal of Insect Science* 21(4), 7–8.

Cheng Y, Liepert LD, Waller J, Leevy M & Schorey JS (2017) A novel method for intratracheal injection of infectious agents into mice. *Laboratory Animals* 51(5), 530–533.

Clark S, Hall Y & Williams A (2015) Animal models of tuberculosis: Guinea pigs. *Cold Spring Harbor Perspectives in Medicine* 5(5), a018572.

Clay J (1935) The inheritance of acquired immunity. *Journal of Experimental Biology* 12(1), 49–51.

Clemmensen HS, Knudsen NPH, Rasmussen EM, Winkler J, Rosenkrands I, Ahmad A, Lillebaek T, Sherman DR, Andersen PL & Aagaard C (2017) An attenuated *Mycobacterium tuberculosis* clinical strain with a defect in ESX-1 secretion induces minimal host immune responses and pathology. *Scientific Reports* 7(1), 1–13.

Coates CJ, Lim J, Harman K, Rowley AF, Griffiths DJ, Emery H & Layton W (2019) The insect, *Galleria mellonella*, is a compatible model for evaluating the toxicology of okadaic acid. *Cell biology and toxicology* 35(3), 219–232.

Converse PJ, Karakousis PC, Klinkenberg LG, Kesavan AK, Ly LH, Allen SS, Grosset JH, Jain SK, Lamichhane G, Manabe YC, McMurray DN, Nuermberger EL & Bishai WR (2009) Role of the *dosR-dosS* two-component regulatory system in *Mycobacterium tuberculosis* virulence in three animal models. *Infection and Immunity* 77(3), 1230–1237.

Cook GM, Berney M, Gebhard S, Heinemann M, Cox RA, Danilchanka O & Niederweis M (2009) Physiology of mycobacteria. *Advances in Microbial Physiology* 55, 81–319.

Cook SM & McArthur JD (2013) Developing *Galleria mellonella* as a model host for human pathogens. *Virulence* 4(5), 350–353.

Cools F, Torfs E, Aizawa J, Vanhoutte B, Maes L, Caljon G, Delputte P, Cappoen D & Cos P (2019) Optimization and characterization of a *Galleria mellonella* larval infection model for virulence studies and the evaluation of therapeutics against *Streptococcus pneumoniae*. *Frontiers in Microbiology* 10.

Cooper D & Eleftherianos I (2017) Memory and specificity in the insect immune system: Current perspectives and future challenges. *Frontiers in Immunology* 8(MAY), 539.

Coors ME, Glover JJ, Juengst ET & Sikela JM (2010) The ethics of using transgenic non-human primates to study what makes us human. *Nature Reviews Genetics* 11(9), 658–662.

Correa W, Manrique-Moreno M, Behrends J, Patiño E, Marella C, Peláez-Jaramillo C, Garidel P, Gutsmann T, Brandenburg K & Heinbockel L (2014a) *Galleria mellonella* native and analogue peptides Gm1 and Δ*gm1. II*) anti-bacterial and anti-endotoxic effects. *Biochimica et Biophysica Acta - Biomembranes* 1838(10), 2739–2744.

Correa W, Manrique-Moreno M, Patiño E, Peláez-Jaramillo C, Kaconis Y, Gutsmann T, Garidel P, Heinbockel L & Brandenburg K (2014b) *Galleria mellonella* native and analogue peptides Gm1 and Δ*gm1. I*) biophysical characterization of the interaction mechanisms with bacterial model membranes. *Biochimica et Biophysica Acta - Biomembranes* 1838(10), 2728–2738.

Cox J, Neuhauser N, Michalski A, Scheltema RA, Olsen JV & Mann M (2011) Andromeda: a peptide search engine integrated into the MaxQuant environment. *Journal of Proteome Research* 10(4), 1794–1805.

Cronan MR, Beerman RW, Rosenberg AF, Saelens JW, Johnson MG, Oehlers SH, Sisk DM, Jurcic Smith KL, Medvitz NA, Miller SE, Trinh LA, Fraser SE, Madden JF, Turner J, Stout JE, Lee S & Tobin DM (2016) Macrophage epithelial reprogramming underlies mycobacterial granuloma formation and promotes infection. *Immunity* 45(4), 861–876.

Cronan MR, Matty MA, Rosenberg AF, Blanc L, Pyle CJ, Espenschied ST, Rawls JF, Dartois V & Tobin DM (2018) An explant technique for high-resolution imaging and manipulation of mycobacterial granulomas. *Nature Methods* 15, 1098–1107.

Cronan MR & Tobin DM (2014) Fit for consumption: Zebrafish as a model for tuberculosis. *DMM Disease Models and Mechanisms* 7(7), 777–784.

Cutuli MA, Petronio Petronio G, Vergalito F, Magnifico I, Pietrangelo L, Venditti N & di Marco R (2019) *Galleria mellonella* as a consolidated *in vivo* model hosts: New developments in antibacterial strategies and novel drug testing. *Virulence* 10(1), 527–541.

Cuvertino S, Stuart HM, Chandler KE, Roberts NA, Armstrong R, Bernardini L, Bhaskar S, Callewaert B, Clayton-Smith J, Davalillo CH, Deshpande C, Devriendt K, Digilio MC, Dixit A, Edwards M, Friedman JM, Gonzalez-Meneses A, Joss S, Kerr B, Lampe AK, Langlois S, Lennon R, Loget P, Ma DYT, McGowan R, des Medt M, O'Sullivan J, Odent S, Parker MJ, Pebrel-Richard C, Petit F, Stark Z, Stockler-Ipsiroglu S, Tinschert S, Vasudevan P, Villa O, White SM, Zahir FR, Woolf AS & Banka S (2017) ACTB loss-of-function mutations result in a pleiotropic developmental disorder. *American Journal of Human Genetics* 101(6), 1021–1033.

Cytryńska M, Mak P, Zdybicka-Barabas A, Suder P & Jakubowicz T (2007) Purification and characterization of eight peptides from *Galleria mellonella* immune hemolymph. *Peptides* 28, 533–546.

Dalton JP, Uy B, Okuda KS, Hall CJ, Denny WA, Crosier PS, Swift S & Wiles S (2017) Screening of anti-mycobacterial compounds in a naturally infected zebrafish larvae model. *Journal of Antimicrobial Chemotherapy* 72(2), 421–427.

Daniel J, Maamar H, Deb C, Sirakova T & Kolattukudy P (2011) *Mycobacterium tuberculosis* uses host triacylglycerol to accumulate lipid droplets and acquires a dormancy-like phenotype in lipid-loaded macrophages. *PLoS Pathogens* 7(6), e1002093.

Darrah PA, Zeppa JJ, Maiello P, Hackney JA, Wadsworth MH, Hughes TK, Pokkali S, Swanson PA, Grant NL, Rodgers MA, Kamath M, Causgrove CM, Laddy DJ, Bonavia A, Casimiro D, Lin PL, Klein E, White AG, Scanga CA, Shalek AK, Roederer M, Flynn JAL & Seder RA (2020) Prevention of tuberculosis in macaques after intravenous BCG immunization. *Nature* 577(7788), 95–102.

Davis JM, Clay H, Lewis JL, Ghori N, Herbomel P & Ramakrishnan L (2002) Real-time visualization of mycobacterium-macrophage interactions leading to initiation of granuloma formation in zebrafish embryos. *Immunity* 17(6), 693–702.

Davis JM & Ramakrishnan L (2009) The role of the granuloma in expansion and dissemination of early tuberculous infection. *Cell* 136(1), 37–49.

Deb C, Lee C, Dubey V, Daniel J, Abomoelak B, Sirakova T, Pawar S, Rogers L & Kolattukudy P (2009) A novel *in vitro* multiple-stress dormancy model for *Mycobacterium tuberculosis* generates a lipid-loaded, drug-tolerant, dormant pathogen. *PLoS ONE* 4(6), e6077.

Derrick SC, Evering TH, Sambandamurthy VK, Jalapathy KV, Hsu T, Chen B, Chen M, Russell RG, Junqueira-Kipnis AP, Orme IM, Porcelli SA, Jacobs WR & Morris SL (2007) Characterization of the protective T-cell response generated in CD4-deficient mice by a live attenuated *Mycobacterium tuberculosis* vaccine. *Immunology* 120(2), 192–206.

Dhar N & McKinney JD (2010) *Mycobacterium tuberculosis* persistence mutants identified by screening in isoniazid-treated mice. *Proceedings of the National Academy of Sciences of the United States of America* 107(27), 12275–12280.

Dheda K, Limberis JD, Pietersen E, Phelan J, Esmail A, Lesosky M, Fennelly KP, te Riele J, Mastrapa B, Streicher EM, Dolby T, Abdallah AM, Ben-Rached F, Simpson J, Smith L, Gumbo T, van Helden P, Sirgel FA, McNerney R, Theron G, Pain A, Clark TG & Warren RM (2017) Outcomes, infectiousness, and transmission dynamics of patients with extensively drug-resistant tuberculosis and home-discharged patients with programmatically incurable tuberculosis: a prospective cohort study. *The Lancet Respiratory Medicine* 5(4), 269–281.

Ding Y, Raterink R, Marín-Juez R, Veneman WJ, Egbers K, van den Eeden S, Haks MC, Joosten SA, Ottenhoff THM, Harms AC, Alia A, Hankemeier T & Spaink HP (2020) Tuberculosis causes highly conserved metabolic changes in human patients, mycobacteria-infected mice and zebrafish larvae. *Scientific Reports* 10(1), 1–13.

Dinh H, Semenec L, Kumar SS, Short FL & Cain AK (2021) Microbiology's next top model: *Galleria* in the molecular age. *Pathogens and Disease* 79(2), ftab006.

Dionne M, Ghori N & Schneider D (2003) *Drosphila melonagaster* is a genetically tractable model host for *Mycobacterium marinum*. *Infection and Immunity* 71(6), 3540–3550.

Dionne M, Pham L, Shirasu-Hiza M & Schneider D (2006) Akt and FOXO dysregulation contribute to infection-induced wasting in *Drosophila*. *Current Biology* 16(20), 1977–1985.

Dockrell HM & Smith SG (2017) What have we learnt about BCG vaccination in the last 20 years? *Frontiers in Immunology* 8, 1134.

Driver E, Ryan G, Hoff D, Irwin S, Basaraba R, Kramnik I & Lenaerts A (2012) Evaluation of mouse model forming necrotic granulomas using C3HeB/FeJ mice, for the testing of *Mycobacterium tuberculosis* drugs. *Antimicrobial Agents and Chemotherapy* 56(6), 3181–3195.

Dubnau E, Chan J, Mohan VP & Smith I (2005) Responses of *Mycobacterium tuberculosis* to growth in the mouse lung. *Infection and immunity* 73(6), 3754–3757.

Dubovskiy IM, Grizanova EV, Whitten MMA, Mukherjee K, Greig C, Alikina T, Kabilov M, Vilcinskas A, Glupov VV & Butt TM (2016a) Immuno-physiological adaptations confer wax moth *Galleria mellonella* resistance to *Bacillus thuringiensis*. *Virulence* 7(8), 860–870.

Dubovskiy I, Kryukova N, Glupov V & Ratcliffe N (2016b) Encapsulation and nodulation in insects. *Invertebrate Survival Journal* 13(1), 230–246.

Durieux M, Melloul É, Jemel S, Roisin L, Dardé M, Guillot J, Dannaoui É & Botterel F (2021) *Galleria mellonella* as a screening tool to study virulence factors of *Aspergillus fumigatus*. *Virulence* 12(1), 818–834.

Ehlers S & Schaible UE (2013) The granuloma in tuberculosis: dynamics of a host-pathogen collusion. *Frontiers in Immunology* 3, 411.

Ehrt S, Guo XV, Hickey CM, Ryou M, Monteleone M, Riley LW & Schnappinger D (2005) Controlling gene expression in mycobacteria with anhydrotetracycline and Tet repressor. *Nucleic acids research* 33(2), e21.

Eleftherianos I, Gökçen F, Felföldi G, Millichap PJ, Trenczek TE, Ffrench-Constant RH & Reynolds SE (2007) The immunoglobulin family protein hemolin mediates cellular immune responses to bacteria in the insect *Manduca sexta*. *Cellular Microbiology* 9(5), 1137–1147.

Eleftherianos I, Marokhazi J, Millichap PJ, Hodgkinson AJ, Sriboonlert A, Ffrench-Constant RH & Reynolds SE (2006) Prior infection of *Manduca sexta* with non-pathogenic *Escherichia coli* elicits immunity to pathogenic *Photorhabdus luminescens*: Roles of immune-related proteins shown by RNA interference. *Insect Biochemistry and Molecular Biology* 36(6), 517–525.

Engel P & Moran NA (2013) The gut microbiota of insects – diversity in structure and function. *FEMS Microbiology Reviews* 37(5), 699–735.

Entrican G, Lunney JK, Wattegedera SR, Mwangi W, Hope JC & Hammond JA (2020) The veterinary immunological toolbox: past, present, and future. *Frontiers in Immunology* 11, 1651.

Entwistle FM & Coote PJ (2018) Evaluation of greater wax moth larvae, *Galleria mellonella*, as a novel *in vivo* model for non-tuberculosis mycobacteria infections and antibiotic treatments. *Journal of Medical Microbiology* 67(4), 585–597.

Eoh H & Rhee KY (2013) Multifunctional essentiality of succinate metabolism in adaptation to hypoxia in *Mycobacterium tuberculosis*. *Proceedings of the National Academy of Sciences of the United States of America* 110(16), 6554–6559.

Esteves PJ, Abrantes J, Baldauf HM, BenMohamed L, Chen Y, Christensen N, González-Gallego J, Giacani L, Hu J, Kaplan G, Keppler OT, Knight KL, Kong XP, Lanning DK, le Pendu J, de Matos AL, Liu J, Liu S, Lopes AM, Lu S, Lukehart S, Manabe YC, Neves F, McFadden G, Pan R, Peng X, de Sousa-Pereira P, Pinheiro A, Rahman M, Ruvoën-Clouet N, Subbian S, Tuñón MJ, van der Loo W, Vaine M, Via LE, Wang S & Mage R (2018) The wide utility of rabbits as models of human diseases. *Experimental and Molecular Medicine* 50(5), 1–10.

Etna MP, Giacomini E, Pardini M, Severa M, Bottai D, Cruciani M, Rizzo F, Calogero R, Brosch R & Coccia EM (2015) Impact of *Mycobacterium tuberculosis* RD1-locus on human primary dendritic cell immune functions. *Scientific Reports* 5(1), 1–14.

Finke MD (2015) Complete nutrient content of four species of commercially available feeder insects fed enhanced diets during growth. *Zoo Biology* 34(6), 554–564.

Fitts DA (2011) Ethics and animal numbers: Informal analyses, uncertain sample sizes, inefficient replications, and type I errors. *Journal of the American Association for Laboratory Animal Science* 50(4), 445–453.

Flajnik MF & Kasahara M (2009) Origin and evolution of the adaptive immune system: genetic events and selective pressures. *Nature Reviews Genetics* 11(1), 47–59.

Flynn JL, Gideon HP, Mattila JT & Lin P ling (2015) Immunology studies in non-human primate models of tuberculosis. *Immunological Reviews* 264(1), 60–73.

Fogel N (2015) Tuberculosis: A disease without boundaries. *Tuberculosis* 95(5), 527–531.

Fonseca KL, Rodrigues PNS, Olsson IAS & Saraiva M (2017) Experimental study of tuberculosis: From animal models to complex cell systems and organoids. *PLoS Pathogens* 13(8), e1006421.

Fontán P, Aris V, Ghanny S, Soteropoulos P & Smith I (2008) Global transcriptional profile of *Mycobacterium tuberculosis* during THP-1 human macrophage infection. *Infection and Immunity* 76(2), 725.

Forastiero A, Bernal-Martínez L, Mellado E, Cendejas E & Gomez-Lopez A (2015) *In vivo* efficacy of voriconazole and posaconazole therapy in a novel invertebrate model of

Aspergillus fumigatus infection. *International Journal of Antimicrobial Agents* 46(5), 511–517.

Foreman TW, Mehra S, Lackner AA & Kaushal D (2017) Translational research in the nonhuman primate model of tuberculosis. *Institute for Laboratory Animal Research Journal* 58(2), 151–159.

Franco NH & Olsson IAS (2014) Scientists and the 3Rs: attitudes to animal use in biomedical research and the effect of mandatory training in laboratory animal science. *Laboratory Animals* 48(1), 50–60.

Frigui W, Bottai D, Majlessi L, Monot M, Josselin E, Brodin P, Garnier T, Gicquel B, Martin C, Leclerc C, Cole ST & Brosch R (2008) Control of *M. tuberculosis* ESAT-6 secretion and specific T cell recognition by PhoP. *PLoS Pathogens* 4(2), e33.

Fuchs BB, Chaturvedi S, Rossoni RD, de Barros PP, Torres-Velez F, Mylonakis E & Chaturvedi V (2018) *Galleria mellonella* experimental model for bat fungal pathogen *Pseudogymnoascus destructans* and human fungal pathogen *Pseudogymnoascus pannorum*. *Virulence* 9, 1539–1547.

Fuchs BB, O'Brien E, Khoury JBE & Mylonakis E (2010) Methods for using *Galleria mellonella* as a model host to study fungal pathogenesis. *Virulence* 1(6), 475–482.

Fursov MV, Shitikov EA, Lagutkin DA, Fursova AD, Ganina EA, Kombarova TI, Grishenko NS, Rudnitskaya TI, Bespiatykh DA, Kolupaeva NV, Firstova VV, Domotenko LV, Panova AE, Vinokurov AS, Gushchin VA, Tkachuk AP, Vasilyeva IA, Potapov VD & Dyatlov IA (2021) MDR and pre-XDR clinical *Mycobacterium tuberculosis* Beijing strains: assessment of virulence and host cytokine response in mice infectious model. *Microorganisms* 9(8), 1792.

Gandhe AS, John SH & Nagaraju J (2007) Noduler, a novel immune up-regulated protein mediates nodulation response in Insects. *The Journal of Immunology* 179(10), 6943–6951.

Garnier T, Eiglmeier K, Camus JC, Medina N, Mansoor H, Pryor M, Duthoy S, Grondin S, Lacroix C, Monsempe C, Simon S, Harris B, Atkin R, Doggett J, Mayes R, Keating L, Wheeler PR, Parkhill J, Barrell BG, Cole ST, Gordon SV & Hewinson RG (2003) The complete genome sequence of *Mycobacterium bovis*. *Proceedings of the National Academy of Sciences of the United States of America* 100(13), 7877–7882.

Gautam US, Mehra S & Kaushal D (2015) In-vivo gene signatures of *Mycobacterium tuberculosis* in C3HeB/FeJ mice. *PLoS ONE* 10(8), e0135208.

Gengenbacher M & Kaufmann SHE (2012) *Mycobacterium tuberculosis*: Success through dormancy. *FEMS Microbiology Review* 36(3), 514–532.

Ghazaei C (2018) *Mycobacterium tuberculosis* and lipids: Insights into molecular mechanisms from persistence to virulence. *Journal of Research in Medical Sciences* 23, 63.

Glaziou P, Floyd K & Raviglione M (2018) Trends in tuberculosis in the UK. *Thorax* 73(8), 702–703.

Gonzalo-Asensio J, Malaga W, Pawlik A, Astarie-Dequeker C, Passemar C, Moreau F, Laval F, Daffé M, Martin C, Brosch R & Guilhot C (2014) Evolutionary history of tuberculosis shaped by conserved mutations in the PhoPR virulence regulator. *Proceedings of the National Academy of Sciences of the United States of America* 111(31), 11491–11496.

Gonzalo-Asensio J, Mostowy S, Harders-Westerveen J, Huygen K, Hernández-Pando R, Thole J, Behr M, Gicquel B & Martín C (2008) PhoP: a missing piece in the intricate puzzle of *Mycobacterium tuberculosis* virulence. *PLoS ONE* 3(10), e3496.

Gopal P, Nartey W, Ragunathan P, Sarathy J, Kaya F, Yee M, Setzer C, Manimekalai MSS, Dartois V, Grüber G & Dick T (2017) Pyrazinoic acid inhibits mycobacterial coenzyme A biosynthesis by binding to aspartate decarboxylase PanD. *ACS Infectious Diseases* 3(11), 807–819.

Gopal P, Yee M, Sarathy J, Liang Low J, Sarathy JP, Kaya F, Dartois V, Gengenbacher M & Dick T (2016) Pyrazinamide resistance is caused by two distinct mechanisms: Prevention of coenzyme a depletion and loss of virulence factor synthesis. *ACS Infectious Diseases* 2(9), 616–626.

Grizanova EV, Coates CJ, Butt TM & Dubovskiy IM (2021) RNAi-mediated suppression of insect metalloprotease inhibitor (IMPI) enhances *Galleria mellonella* susceptibility to fungal infection. *Developmental and Comparative Immunology* 122, 104126.

Grygorcewicz B, Roszak M, Golec P, Śleboda-taront D, Łubowska N, Górska M, Jursa-kulesza J, Rakoczy R, Wojciuk B & Dołęgowska B (2020) Antibiotics act with vB_AbaP_AGC01 phage against *Acinetobacter baumannii* in human heat-inactivated plasma blood and *Galleria mellonella*. *International Journal of Molecular Sciences* 21(12), 1–14.

Guleria I, Teitelbaum R, McAdam R, Kalpana G, Jacobs Jr W & Bloom B (1996) Auxotrophic vaccines for tuberculosis. *Nature Medicine* 2(3), 334–337.

Gunatilake M (2019) Zebrafish, *Danio Rerio* as a replacement alternative model useful in CKDu experiments (H Kojima, T Seidle, & H Spielmann, Ed. by). Springer, Singapore.

Gupta CM, Ambaru B & Bajaj R (2020) Emerging functions of actins and actin binding proteins in trypanosomatids. *Frontiers in Cell and Developmental Biology* 8, e587685.

Gygi SP, Rochon Y, Franza BR & Aebersold R (1999) Correlation between protein and mRNA abundance in yeast. *Molecular and Cellular Biology* 19, 1720–1730.

Gygli SM, Borrell S, Trauner A & Gagneux S (2017) Antimicrobial resistance in *Mycobacterium tuberculosis*: mechanistic and evolutionary perspectives. *FEMS Microbiology Reviews* 41(3), 354–373.

Harris SA, Meyer J, Satti I, Marsay L, Poulton ID, Tanner R, Minassian AM, Fletcher HA & McShane H (2014) Evaluation of a human BCG challenge model to assess

antimycobacterial immunity induced by BCG and a candidate tuberculosis vaccine, MVA85A, alone and in combination. *The Journal of Infectious Diseases* 209(8), 1259–1268.

Hillion M, Bernhardt J, Busche T, Rossius M, Maaß S, Becher D, Rawat M, Wirtz M, Hell R, Röckert C, Kalinowski J & Antelmann H (2017) Monitoring global protein thiol-oxidation and protein S-mycothiolation in *Mycobacterium smegmatis* under hypochlorite stress. *Scientific Reports* 7, 1195.

Hillyer JF (2016) Insect immunology and hematopoiesis. *Developmental & Comparative Immunology* 58, 102–118.

Hinson JM, Bradsher RW & Bodner SJ (1981) Gram-stain neutrality of *Mycobacterium tuberculosis*. *American Review of Respiratory Disease* 123(4), 365–366.

Hollande AC (1930) La digestion des bacilles tuberculeux par les leucocytes du sang des chenilles. *Archives de Zoologie Expérimentale et Générale : Histoire Naturelle, Morphologie, Histologie, Évolution des Animaux* 70, 231–280.

Home Office UK (2020) Annual Statistic of Scientific Procedures on Living Animals Great Britain 2020 . UK Government, London.

Hondalus MK, Bardarov S, Russell R, Chan J, Jacobs WR & Bloom BR (2000) Attenuation of and protection induced by a leucine auxotroph of *Mycobacterium tuberculosis*. *Infection and Immunity* 68(5), 2888–2898.

Howe K, Clark MD, Torroja CF, Torrance J, Berthelot C, Muffato M, Collins JE, Humphray S, McLaren K, Matthews L, McLaren S, Sealy I, Caccamo M, Churcher C, Scott C, Barrett JC, Koch R, Rauch GJ, White S, Chow W, Kilian B, Quintais LT, Guerra-Assunção JA, Zhou Y, Gu Y, Yen J, Vogel JH, Eyre T, Redmond S, Banerjee R, Chi J, Fu B, Langley E, Maguire SF, Laird GK, Lloyd D, Kenyon E, Donaldson S, Sehra H, Almeida-King J, Loveland J, Trevanion S, Jones M, Quail M, Willey D, Hunt A, Burton J, Sims S, McLay K, Plumb B, Davis J, Clee C, Oliver K, Clark R, Riddle C, Eliott D, Threadgold G, Harden G, Ware D, Mortimer B, Kerry G, Heath P, Phillimore B, Tracey A, Corby N, Dunn M, Johnson C, Wood J, Clark S, Pelan S, Griffiths G, Smith M, Glithero R, Howden P, Barker N, Stevens C, Harley J, Holt K, Panagiotidis G, Lovell J, Beasley H, Henderson C, Gordon D, Auger K, Wright D, Collins J, Raisen C, Dyer L, Leung K, Robertson L, Ambridge K, Leongamornlert D, McGuire S, Gilderthorp R, Griffiths C, Manthravadi D, Nichol S, Barker G, Whitehead S, Kay M, Brown J, Murnane C, Gray E, Humphries M, Sycamore N, Barker D, Saunders D, Wallis J, Babbage A, Hammond S, Mashreghi-Mohammadi M, Barr L, Martin S, Wray P, Ellington A, Matthews N, Ellwood M, Woodmansey R, Clark G, Cooper J, Tromans A, Grafham D, Skuce C, Pandian R, Andrews R, Harrison E, Kimberley A, Garnett J, Fosker N, Hall R, Garner P, Kelly D, Bird C, Palmer S, Gehring I, Berger A, Dooley CM, Ersan-Ürün Z, Eser C, Geiger H, Geisler M, Karotki L, Kirn A, Konantz J, Konantz M, Oberländer M, Rudolph-Geiger S, Teucke M, Osoegawa K, Zhu B, Rapp A, Widaa S, Langford C, Yang F, Carter NP, Harrow J, Ning Z, Herrero J, Searle SMJ, Enright A, Geisler R, Plasterk RHA, Lee C, Westerfield M, de Jong PJ, Zon LI, Postlethwait JH, Nüsslein-Volhard C, Hubbard

TJP, Crollius HR, Rogers J & Stemple DL (2013) The zebrafish reference genome sequence and its relationship to the human genome. *Nature* 496(7446), 498–503.

Hsu T, Hingley-Wilson SM, Chen B, Chen M, Dai AZ, Morin PM, Marks CB, Padiyar J, Goulding C, Gingery M, Eisenberg D, Russell RG, Derrick SC, Collins FM, Morris SL, King CH & Jacobs WR (2003) The primary mechanism of attenuation of bacillus Calmette–Guérin is a loss of secreted lytic function required for invasion of lung interstitial tissue. *Proceedings of the National Academy of Sciences of the United States of America* 100(21), 12420–12425.

Huan Y, Kong Q, Mou H & Yi H (2020) Antimicrobial peptides: Classification, design, application and research progress in multiple fields. *Frontiers in Microbiology* 11, e2559.

Ignasiak K & Maxwell A (2017) *Galleria mellonella* (greater wax moth) larvae as a model for antibiotic susceptibility testing and acute toxicity trials. *BMC Research Notes* 10(1), 428.

Iseman MD (2002) Tuberculosis therapy: past, present and future. *European Respiratory Journal, Supplement* 20(36), 87s–94s.

Jackson SK, Stark JM, Taylor S & Harwood JL (1989) Changes in phospholipid fatty acid composition and triacylglycerol content in mouse tissues after infection with bacille Calmette-Guérin. *British Journal of Experimental Pathology* 70(4), 441.

Jiang J, Gu J, Zhang L, Zhang C, Deng X, Dou T, Zhao G & Zhou Y (2015) Comparing *Mycobacterium tuberculosis* genomes using genome topology networks. *BMC Genomics* 16(1), 1–10.

Jijie R, Mihalache G, Balmus IM, Strungaru SA, Baltag ES, Ciobica A, Nicoara M & Faggio C (2021) Zebrafish as a screening model to study the single and joint effects of antibiotics. *Pharmaceuticals* 14(6), 578.

Jiravanichpaisal P, Lee BL & Söderhäll K (2006) Cell-mediated immunity in arthropods: Hematopoiesis, coagulation, melanization and opsonization. *Immunobiology* 211(4), 213–236.

Johansen MD, Herrmann J-L & Kremer L (2020) Non-tuberculous mycobacteria and the rise of *Mycobacterium abscessus*. *Nature Reviews Microbiology* 18(7), 392–407.

Jønsson R, Struve C, Jenssen H & Krogfelt KA (2017) The wax moth *Galleria mellonella* as a novel model system to study enteroaggregative *Escherichia coli* pathogenesis. *Virulence* 8(8), 1894–1899.

Jorjão AL, Oliveira LD, Scorzoni L, Figueiredo-Godoi LMA, Cristina A. Prata M, Jorge AOC & Junqueira JC (2018) From moths to caterpillars: Ideal conditions for *Galleria mellonella* rearing for *in vivo* microbiological studies. *Virulence* 9(1), 383–389.

Jung J, Sajjadian SM & Kim Y (2019) Hemolin, an immunoglobulin-like peptide, opsonizes nonself targets for phagocytosis and encapsulation in *Spodoptera exigua*, a lepidopteran insect. *Journal of Asia-Pacific Entomology* 22(3), 947–956.

Kaito C, Murakami K, Imai L & Furuta K (2020) Animal infection models using non-mammals. *Microbiology and Immunology* 64(9), 585–592.

Kalsy M, Tonk M, Hardt M, Dobrindt U, Zdybicka-Barabas A, Cytrynska M, Vilcinskas A & Mukherjee K (2020) The insect antimicrobial peptide cecropin A disrupts uropathogenic *Escherichia coli* biofilms. *npj Biofilms and Microbiomes* 6(1), 1–8.

Kampmann B, Gaora PÓ, Snewin VA, Gares M, Young DB & Levin M (2000) Evaluation of human antimycobacterial immunity using recombinant reporter mycobacteria. *The Journal of Infectious Diseases* 182(3), 895–901.

Kampmann B, Tena GN, Mzazi S, Eley B, Young DB & Levin M (2004) Novel human in vitro system for evaluating antimycobacterial vaccines. *Infection and Immunity* 72(11), 6401–6407.

Kampmann B, Tena-Coki GN, Nicol MP, Levin M & Eley B (2006) Reconstitution of antimycobacterial immune responses in HIV-infected children receiving HAART. *AIDS* 20(7), 1011–1018.

Kanabalan RD, Lee LJ, Lee TY, Chong PP, Hassan L, Ismail R & Chin VK (2021) Human tuberculosis and *Mycobacterium tuberculosis* complex: A review on genetic diversity, pathogenesis and omics approaches in host biomarkers discovery. *Microbiological Research* 246, 126674.

Kanetsuna F (1980) Effect of lysozyme on mycobacteria. *Microbiology and Immunology* 24(12), 1151–1162.

Kapoor N, Pawar S, Sirakova TD, Deb C, Warren WL & Kolattukudy PE (2013) Human granuloma *in vitro* model, for TB dormancy and resuscitation. *PLoS ONE* 8(1), e53657.

Kar R, Nangpal P, Mathur S, Singh S & Tyagi AK (2017) *bioA* mutant of *Mycobacterium tuberculosis* shows severe growth defect and imparts protection against tuberculosis in guinea pigs. *PLoS ONE* 12(6), e0179513.

Kato-Maeda M, Shanley CA, Ackart D, Jarlsberg LG, Shang S, Obregon-Henao A, Harton M, Basaraba RJ, Henao-Tamayo M, Barrozo JC, Rose J, Kawamura LM, Coscolla M, Fofanov VY, Koshinsky H, Gagneux S, Hopewell PC, Ordway DJ & Orme IM (2012) Beijing sublineages of *Mycobacterium tuberculosis* differ in pathogenicity in the guinea pig. *Clinical and Vaccine Immunology* 19(8), 1227–1237.

Kaur D, Brennan PJ & Crick DC (2004) Decaprenyl diphosphate synthesis in *Mycobacterium tuberculosis*. *Journal of Bacteriology* 186(22), 7564–7570.

Kavanagh K & Fallon JP (2010) *Galleria mellonella* larvae as models for studying fungal virulence. *Fungal Biology Reviews* 24(1–2), 79–83.

Kavanagh K & Reeves EP (2004) Exploiting the potential of insects for in vivo pathogenicity testing of microbial pathogens. *FEMS Microbiology Reviews* 28(1), 101–112.

Kay S, Edwards J, Brown J & Dixon R (2019) *Galleria mellonella* infection model identifies both high and low lethality of *Clostridium perfringens* toxigenic strains and their response to antimicrobials. *Frontiers in Microbiology* 10, 1281.

Keshavjee S & Farmer PE (2012) Tuberculosis, drug resistance, and the history of modern medicine. *New England Journal of Medicine* 367(10), 931–936.

Khara JS, Mojsoska B, Mukherjee D, Langford PR, Robertson BD, Jenssen H, Ee PLR & Newton SM (2020) Ultra-short antimicrobial peptoids show propensity for membrane activity against multi-drug resistant *Mycobacterium tuberculosis*. *Frontiers in Microbiology* 11, 417.

Killiny N (2018) Generous hosts: Why the larvae of greater wax moth, *Galleria mellonella* is a perfect infectious host model? *Virulence* 9(4), 860–865.

Kirubakar G, Schäfer H, Rickerts V, Schwarz C & Lewin A (2020) Mutation on lysX from Mycobacterium avium hominissuis impacts the host-pathogen interaction and virulence phenotype. *Virulence* 11(1), 132–144.

Kloezen W, Poppel M van H, Fahal AH & van de Sande WWJ (2015) A *Madurella mycetomatis* grain model in *Galleria mellonella* larvae. *PLoS Neglected Tropical Diseases* 9(7), e0003926.

Knight GM, McQuaid CF, Dodd PJ & Houben RMGJ (2019) Global burden of latent multidrug-resistant tuberculosis: trends and estimates based on mathematical modelling. *The Lancet Infectious Diseases* 19(8), 903–912.

Koch R (1882) Die Atiologic der Tuberkulose. *Berliner Klinische Wochenschrift* 15, 221–230.

Koyuncu D, Niazi MKK, Tavolara T, Abeijon C, Ginese ML, Liao Y, Mark C, Specht A, Gower AC, Restrepo BI, Gatti DM, Kramnik I, Gurcan M, Yener B & Beamer G (2021) CXCL1: A new diagnostic biomarker for human tuberculosis discovered using diversity outbred mice. *PLoS Pathogens* 17(8), e1009773.

Kramnik I & Beamer G (2016) Mouse models of human TB pathology: Roles in the analysis of necrosis and the development of host-directed therapies. *Seminars in Immunopathology* 38(2), 221–237.

Krezdorn J, Adams S & Coote PJ (2014) A *Galleria mellonella* infection model reveals double and triple antibiotic combination therapies with enhanced efficacy versus a multidrug-resistant strain of *Pseudomonas aeruginosa*. *Journal of Medical Microbiology* 63(7), 945–955.

Kubica G, Kim T & Dunbar F (1972) Designation of strain H37Rv as the neotype of *Mycobacterium tuberculosis*. *International Journal of Systematic and Evolutionary Microbiology* 22(2), 99–106.

Kumar D, Bansal G, Narang A, Basak T, Abbas T & Dash D (2016a) Integrating transcriptome and proteome profiling: Strategies and applications. *Proteomics* 16, 2533–2544.

Kumar VA, Goyal R, Bansal R, Singh N, Sevalkar RR, Kumar A & Sarkar D (2016b) EspR-dependent ESAT-6 protein secretion of *Mycobacterium tuberculosis* requires the presence of virulence regulator PhoP. *The Journal of Biological Chemistry* 291(36), 19030.

Kwadha CA, Ong'amo GO, Ndegwa PN, Raina SK & Fombong AT (2017) The biology and control of the greater wax moth, *Galleria mellonella*. *Insects* 8(2), 61.

Kwon H, Mohammed M, Franzén O, Ankarklev J & Smith RC (2021) Single-cell analysis of mosquito hemocytes identifies signatures of immune cell subtypes and cell differentiation. *eLife* 10, e66192.

Laga AC, Milner DA & Granter SR (2014) Utility of acid-fast staining for detection of mycobacteria in cutaneous granulomatous tissue reactions. *American Journal of Clinical Pathology* 141(4), 584–586.

Lange A, Beier S, Huson DH, Parusel R, Iglauer F & Frick JS (2018a) Genome sequence of *Galleria mellonella* (greater wax moth). *Genome Announcements* 6(2), e01220-17.

Lange A, Schäfer A, Bender A, Steimle A, Beier S, Parusel R & Frick JS (2018b) *Galleria mellonella*: A novel invertebrate model to distinguish intestinal symbionts from pathobionts. *Frontiers in Immunology* 9, 2114.

Lapointe JF, Dunphy GB & Mandato CA (2012) Hemocyte–hemocyte adhesion and nodulation reactions of the greater wax moth, *Galleria mellonella* are influenced by cholera toxin and its B-subunit. *Results in Immunology* 2, 54–65.

Lavin RC, Johnson Calvin, Ahn Y-O, Kremiller KM, Sherwood Matthew, Patel JS, Pan Y, Russo R, MacGilvary NJ, Giacalone D, Kevorkian YL, Zimmerman MD, Glickman JF, Freundlich JS & Tan S (2021) Targeting *Mycobacterium tuberculosis* response to environmental cues for the development of effective antitubercular drugs. *PLoS Biology* 19(7), e3001355.

Lay G, Poquet Y, Salek-Peyron P, Puissegur M-P, Botanch C, Bon H, Levillain F, Duteyrat J-L, Emile J-F & Altare F (2007) Langhans giant cells from *M. tuberculosis*-induced human granulomas cannot mediate mycobacterial uptake. *The Journal of Pathology* 211(1), 76–85.

Le CF, Fang CM & Sekaran SD (2017) Intracellular targeting mechanisms by antimicrobial peptides. *Antimicrobial Agents and Chemotherapy* 61(4), e02340-16.

Lee BY, Clemens DL, Silva A, Dillon BJ, Maslesa-Galić S, Nava S, Ho CM & Horwitz MA (2018) Ultra-rapid near universal TB drug regimen identified via parabolic response surface platform cures mice of both conventional and high susceptibility. *PLoS ONE* 13(11), e0207469.

Lee E, Jeong KW, Lee J, Shin A, Kim JK, Lee J, Lee DG & Kim Y (2013) Structure-activity relationships of cecropin-like peptides and their interactions with phospholipid membrane. *BMB Reports* 46(5), 282–287.

Lee E, Shin A & Kim Y (2015) Anti-inflammatory activities of cecropin A and its mechanism of action. *Archives of Insect Biochemistry and Physiology* 88(1), 31–44.

Lee A, Xie YL, Barry CE & Chen RY (2020) Current and future treatments for tuberculosis. *The British Medical Journal* 368, m216.

van Leeuwen LM, van der Sar AM & Bitter W (2015) Animal models of tuberculosis: Zebrafish. *Cold Spring Harbor Perspectives in Medicine* 5(3), a018580.

Leggett HC, Cornwallis CK, Buckling A & West SA (2017) Growth rate, transmission mode and virulence in human pathogens. *Philosophical Transactions of the Royal Society B: Biological Sciences* 372(1719), 20160094.

Lei J, Sun LC, Huang S, Zhu C, Li P, He J, Mackey V, Coy DH & He QY (2019) The antimicrobial peptides and their potential clinical applications. *American Journal of Translational Research* 11(7), 3919–3931.

Leitão AB & Sucena É (2015) *Drosophila* sessile hemocyte clusters are true hematopoietic tissues that regulate larval blood cell differentiation. *eLife* 4, e06166.

Lekko YM, Ooi PT, Omar S, Mazlan M, Ramanoon SZ, Jasni S, Abdullah Jesse FF & Che-Amat A (2020) *Mycobacterium tuberculosis* complex in wildlife: review of current applications of antemortem and postmortem diagnosis. *Veterinary World* 13(9), 1822–1836.

Lenaerts AJ, Chapman PL & Orme IM (2004) Statistical limitations to the Cornell model of latent tuberculosis infection for the study of relapse rates. *Tuberculosis* 84(6), 361–364.

Lerner TR, Borel S & Gutierrez MG (2015) The innate immune response in human tuberculosis. *Cellular Microbiology* 17(9), 1277–1285.

Lewis KN, Liao R, Guinn KM, Hickey MJ, Smith S, Behr MA & Sherman DR (2003) Deletion of RD1 from *Mycobacterium tuberculosis* mimics bacille Calmette-Guérin attenuation. *The Journal of Infectious Diseases* 187(1), 117–123.

Li D, Li L, Ma Y, Zhuang Y, Li D, Shen H, Wang X, Yang F, Ma Y & Wu D (2017) Dopamine-assisted fixation of drug-loaded polymeric multilayers to osteoarticular implants for tuberculosis therapy. *Biomaterials Science* 5(4), 730–740.

Li D, Scherfer C, Korayem AM, Zhao Z, Schmidt O & Theopold U (2002) Insect hemolymph clotting: Evidence for interaction between the coagulation system and the prophenoloxidase activating cascade. *Insect Biochemistry and Molecular Biology* 32(8), 919–928.

Li Y, Spiropoulos J, Cooley W, Singh Khara J, Gladstone CA, Asai M, Bossé JT, Robertson BD, Newton SM & Langford PR (2018) *Galleria mellonella* - a novel infection model for the *Mycobacterium tuberculosis* complex. *Virulence* 9(1), 1126–1137.

Li Q, Wang D, Lv S & Zhang Y (2014) Comparative proteomics and expression analysis of five genes in *Epicauta chinensis* larvae from the first to fifth instar. *PLoS ONE* 9(2), e89607.

Lin Q, Su G, Wu A, Chen D, Yu B, Huang Z, Luo Y, Mao X, Zheng P, Yu J, Luo J & He J (2019) *Bombyx mori* gloverin A2 alleviates enterotoxigenic *Escherichia coli*-induced inflammation and intestinal mucosa disruption. *Antimicrobial Resistance and Infection Control* 8(1), 1–11.

Liu Y, Beyer A & Aebersold R (2016) On the dependency of cellular protein levels on mRNA abundance. *Cell* 165, 535–550.

Liu M, Huang M, Huang L, Biville F, Zhu D, Wang M, Jia R, Chen S, Zhao X, Yang Q, Wu Y, Zhang S, Huang J, Tian B, Chen X, Liu Y, Zhang L, Yu Y, Pan L, Rehman MU & Cheng A (2019) New perspectives on *Galleria mellonella* larvae as a host model using *Riemerella anatipestifer* as a proof of concept. *Infection and Immunity* 87(8), e0079-19.

Liu J, Tran V, Leung AS, Alexander DC & Zhu B (2009) BCG vaccines: their mechanisms of attenuation and impact on safety and protective efficacy. *Human Vaccines* 5(2), 78.

Loh JM, Adenwalla N, Wiles S & Proft T (2013) *Galleria mellonella* larvae as an infection model for group A streptococcus. *Virulence* 4(5), 419–428.

Lu A, Zhang Q, Zhang J, Yang B, Wu K, Xie W, Luan YX & Ling E (2014) Insect prophenoloxidase: The view beyond immunity. *Frontiers in Physiology* 5, e252.

Lurie MB (1964) Resistance to Tuberculosis. Harvard University Press, Cambridge.

Ly A & Liu J (2020) Mycobacterial virulence factors: Surface-exposed lipids and secreted proteins. *International Journal of Molecular Sciences* 21(11), 3985.

Malhotra V, Sharma D, Ramanathan VD, Shakila H, Saini DK, Chakravorty S, Das TK, Li Q, Silver RF, Narayanan PR & Tyagi JS (2004) Disruption of response regulator gene, *devR*, leads to attenuation in virulence of *Mycobacterium tuberculosis*. *FEMS Microbiology Letters* 231(2), 237–245.

Mallassez L & Vignal W (1883) Tuberculose zoologique. *Archives de Physiologie Normale et Pathologique* 2, 369–412.

Manabe YC, Dannenberg AM, Tyagi SK, Hatem CL, Yoder M, Woolwine SC, Zook BC, Pitt MLM & Bishai WR (2003) Different strains of *Mycobacterium tuberculosis* cause various spectrums of disease in the rabbit model of tuberculosis. *Infection and Immunity* 71(10), 6004–6011.

Manabe YC, Kesavan AK, Lopez-Molina J, Hatem CL, Brooks M, Fujiwara R, Hochstein K, Pitt MLM, Tufariello JA, Chan J, McMurray DN, Bishai WR, Dannenberg AM & Mendez S

(2008) The aerosol rabbit model of TB latency, reactivation and immune reconstitution inflammatory syndrome. *Tuberculosis* 88(3), 187–196.

Manca C, Tsenova L, Barry CE, Bergtold A, Freeman S, Haslett PA, Musser JM, Freedman VH & Kaplan G (1999) *Mycobacterium tuberculosis* CDC1551 induces a more vigorous host response in vivo and in vitro, but is not more virulent than other clinical isolates. *Journal of Immunology* 162(11), 6740–6746.

Martin C, Williams A, Hernandez-Pando R, Cardona PJ, Gormley E, Bordat Y, Soto CY, Clark SO, Hatch GJ, Aguilar D, Ausina V & Gicquel B (2006) The live *Mycobacterium tuberculosis phoP* mutant strain is more attenuated than BCG and confers protective immunity against tuberculosis in mice and guinea pigs. *Vaccine* 24(17), 3408–3419.

Martineau AR, Newton SM, Wilkinson KA, Kampmann B, Hall BM, Nawroly N, Packe GE, Davidson RN, Griffiths CJ & Wilkinson RJ (2007a) Neutrophil-mediated innate immune resistance to mycobacteria. *Journal of Clinical Investigation* 117(7), 1988–1994.

Martineau AR, Wilkinson KA, Newton SM, Floto RA, Norman AW, Skolimowska K, Davidson RN, Sørensen OE, Kampmann B, Griffiths CJ & Wilkinson RJ (2007b) IFN-γ- and TNF-independent vitamin D-inducible human suppression of mycobacteria: The role of cathelicidin LL-37. *The Journal of Immunology* 178(11), 7190–7198.

Masten AR (1935) Sunlight in tuberculosis. *Diseases of the Chest* 1(7), 8–23.

Matty MA, Knudsen DR, Walton EM, Beerman RW, Cronan MR, Pyle CJ, Hernandez RE & Tobin DM (2019) Potentiation of P2RX7 as a host-directed strategy for control of mycobacterial infection. *eLife* 8, e39123.

Maurer E, Hörtnagl C, Lackner M, Grässle D, Naschberger V, Moser P, Segal E, Semis M, Lass-Flörl C & Binder U (2019) *Galleria mellonella* as a model system to study virulence potential of mucormycetes and evaluation of antifungal treatment. *Medical Mycology* 57(3), 351–362.

McDermott W & Tompsett R (1954) Activation of pyrazinamide and nicotinamide in acidic environments in vitro. *American Review of Tuberculosis* 70(4), 748–754.

Mead, G. P. Ratcliffe, N. A. Renwrantz LR (1986) The separation of insect haemocyte type on Percoll Gradients; methodology and problems. *Journal of Insect Physiolology* 32(2), 167–177.

Medzhitov R, Preston-Hurlburt P & Janeway CA (1997) A human homologue of the *Drosophila* Toll protein signals activation of adaptive immunity. *Nature* 388(6640), 394–397.

Meehan CJ, Goig GA, Kohl TA, Verboven L, Dippenaar A, Ezewudo M, Farhat MR, Guthrie JL, Laukens K, Miotto P, Ofori-Anyinam B, Dreyer V, Supply P, Suresh A, Utpatel C, van Soolingen D, Zhou Y, Ashton PM, Brites D, Cabibbe AM, de Jong BC, de Vos M, Menardo F, Gagneux S, Gao Q, Heupink TH, Liu Q, Loiseau C, Rigouts L, Rodwell TC, Tagliani E, Walker TM, Warren RM, Zhao Y, Zignol M, Schito M, Gardy J, Cirillo DM, Niemann S,

Comas I & van Rie A (2019) Whole genome sequencing of *Mycobacterium tuberculosis*: current standards and open issues. *Nature Reviews Microbiology* 17(9), 533–545.

Mehra S, Foreman TW, Didier PJ, Ahsan MH, Hudock TA, Kissee R, Golden NA, Gautam US, Johnson A-M, Alvarez X, Russell-Lodrigue KE, Doyle LA, Roy CJ, Niu T, Blanchard JL, Khader SA, Lackner AA, Sherman DR & Kaushal D (2015) The DosR regulon modulates adaptive immunity and is essential for *Mycobacterium tuberculosis* persistence. *American Journal of Respiratory and Critical Care Medicine* 191(10), 1185–1196.

Meir M, Grosfeld T & Barkan D (2018) Establishment and validation of *Galleria mellonella* as a novel model organism to study *Mycobacterium abscessus* infection, pathogenesis, and treatment. *Antimicrobial Agents and Chemotherapy* 62(4), e02539-17.

Metalnikov S (1920) L'immunité naturelle et acquise chez la chenille de *Galleria mellonella*. *Annales de l'Institut Pasteur* 34, 888–909.

Metalnikov S (1928) L'infection microbietine et vimmunite chez la mite des abeilles *Galleria mellonella*. *Nature* 121, 822–823.

Mikonranta L, Mappes J, Kaukoniitty M & Freitak D (2014) Insect immunity: oral exposure to a bacterial pathogen elicits free radical response and protects from a recurring infection. *Frontiers in Zoology* 11(1), 1–7.

Miller FR (1932) The induced development of non-acid-fast forms of *Bacillus tuberculosis* and other mycobacteria. *The Journal of Experimental Medicine* 56(3), 411–424.

Mishra AK, Driessen NN, Appelmelk BJ & Besra GS (2011) Lipoarabinomannan and related glycoconjugates: Structure, biogenesis and role in *Mycobacterium tuberculosis* physiology and host-pathogen interaction. *FEMS Microbiology Reviews* 35(6), 1126–1157.

Mishra BB, Lovewell RR, Olive AJ, Zhang G, Wang W, Eugenin E, Smith CM, Phuah JY, Long JE, Dubuke ML, Palace SG, Goguen JD, Baker RE, Nambi S, Mishra R, Booty MG, Baer CE, Shaffer SA, Dartois V, McCormick BA, Chen X & Sassetti CM (2017) Nitric oxide prevents a pathogen-permissive granulocytic inflammation during tuberculosis. *Nature Microbiology* 2, 17072.

Mizrahi V & Warner DF (2019) Expanding the anti-TB arsenal. *Science* 363(6426), 457–458.

Mostowy S, Tsolaki AG, Small PM & Behr MA (2003) The in vitro evolution of BCG vaccines. *Vaccine* 21(27–30), 4270–4274.

Mourik BC, de Knegt GJ, Verbon A, Mouton JW, Bax HI & de Steenwinkel JEM (2017) Assessment of bactericidal drug activity and treatment outcome in a mouse tuberculosis model using a clinical Beijing strain. *Antimicrobial Agents and Chemotherapy* 61(10), e00696-17.

Mourik BC, de Steenwinkel JEM, de Knegt GJ, Huizinga R, Verbon A, Ottenhoff THM, van Soolingen D & Leenen PJM (2019) *Mycobacterium tuberculosis* clinical isolates of the

Beijing and East-African Indian lineage induce fundamentally different host responses in mice compared to H37Rv. *Scientific Reports* 9(1), 1–11.

Mouton JM, Heunis T, Dippenaar A, Gallant JL, Kleynhans L & Sampson SL (2019) Comprehensive characterization of the attenuated double auxotroph *Mycobacterium tuberculosis* Δ*leuD*Δ*panCD* as an alternative to H37Rv. *Frontiers in Microbiology* 10, 1922.

Moya-Andérico L, Vukomanovic M, Cendra M del M, Segura-Feliu M, Gil V, del Río JA & Torrents E (2021) Utility of *Galleria mellonella* larvae for evaluating nanoparticle toxicology. *Chemosphere* 266, 129235.

Mullet H, Ratcliffe N & Rowley A (1993) The generation and characterisation of anti-insect blood cell monoclonal antibody. *Journal of Cell Science* 105, 93–100.

Murray JF (2004) A century of tuberculosis. *American Journal of Respiratory and Critical Care Medicine* 169(11), 1181–1186.

Nakhleh J, el Moussawi L & Osta MA (2017) The melanization response in insect immunity. *Advances in Insect Physiology* 52, 83–109.

Nappi AJ & Christensen BM (2005) Melanogenesis and associated cytotoxic reactions: Applications to insect innate immunity. *Insect Biochemistry and Molecular Biology* 35(5), 443–459.

Nascimento MTC, Silva KP, Garcia MCF, Medeiros MN, Machado EA, Nascimento SB & Saraiva EM (2018) DNA extracellular traps are part of the immune repertoire of *Periplaneta americana*. *Developmental and Comparative Immunology* 84.

Neilson JW, Pierce SA & Maier RM (1999) Factors Influencing expression of *luxCDABE* and *nah* genes in *Pseudomonas putida* RB1353(NAH7, pUTK9) in dynamic systems. *Applied and Environmental Microbiology* 65(8), 3473–3482.

Nemeth J, Olson GS, Rothchild AC, Jahn AN, Mai D, Duffy FJ, Delahaye JL, Srivatsan S, Plumlee CR, Urdahl KB, Gold ES, Aderem A & Diercks AH (2020) Contained *Mycobacterium tuberculosis* infection induces concomitant and heterologous protection. *PLoS Pathogens* 16(7), e1008655.

Newton SM, Mackie SL, Martineau AR, Wilkinson KA, Kampmann B, Fisher C, Dutta S, Levin M, Wilkinson RJ & Pasvol G (2008) Reduction of chemokine secretion in response to mycobacteria in infliximab-treated patients. *Clinical and Vaccine Immunology* 15(3), 506–512.

Newton S, Martineau A & Kampmann B (2011) A functional whole blood assay to measure viability of mycobacteria, using reporter-gene tagged BCG or M.Tb (BCG *lux*/M.Tb *lux*). *Journal of Visualized Experiments* (55), e3332.

Nguyen TVA, Anthony RM, Cao TTH, Bañuls AL, Nguyen VAT, Vu DH, Nguyen NV & Alffenaar JWC (2020) Delamanid resistance: Update and clinical management. *Clinical Infectious Diseases* 71(12), 3252–3259.

Nikonenko B v, Samala R, Einck L & Nacy CA (2004) Rapid, simple in vivo screen for new drugs active against *Mycobacterium tuberculosis*. *Antimicrobial Agents and Chemotherapy* 48(12), 4550–4555.

Nimmo C, Millard J, Brien K, Moodley S, van Dorp L, Lutchminarain K, Wolf A, Grant AD, Balloux F, Pym AS, Padayatchi N & O'Donnell M (2020) Bedaquiline resistance in drug-resistant tuberculosis HIV co-infected patients. *European Respiratory Journal* 55(6), 1902383.

Nuermberger EL, Yoshimatsu T, Tyagi S, Bishai WR & Grosset JH (2004) Paucibacillary tuberculosis in mice after prior aerosol immunization with *Mycobacterium bovis* BCG. *Infection and Immunity* 72(2), 1065–1071.

Nunoi H, Yamazaki T, Tsuchiya H, Kato S, Malech HL, Matsuda I & Kanegasaki S (1999) A heterozygous mutation of β-actin associated with neutrophil dysfunction and recurrent infection. *Proceedings of the National Academy of Sciences of the United States of America* 96(15), 8693–8698.

Oatway WH & Steenken W (1936) The pathogenesis and fate of tubercle produced by dissociated variants of tubercle bacilli. *The Journal of Infectious Diseases* 59(3), 306–325.

Oh C-T, Moon C, Choi TH, Kim BS & Jang J (2013) *Mycobacterium marinum* infection in *Drosophila melanogaster* for antimycobacterial activity assessment. *Journal of Antimicrobial Chemotherapy* 68(3), 601–609.

Oñate-Garzón J, Manrique-Moreno M, Trier S, Leidy C, Torres R & Patiño E (2017) Antimicrobial activity and interactions of cationic peptides derived from *Galleria mellonella* cecropin D-like peptide with model membranes. *Journal of Antibiotics* 70, 238–245.

O'Neill J (2016) Tackling drug-resistant infections globally: final report and recommendations. Wellcome Trust, London.

Ordas A, Raterink RJ, Cunningham F, Jansen HJ, Wiweger MI, Jong-Raadsen S, Bos S, Bates RH, Barros D, Meijer AH, Vreeken RJ, Ballell-Pages L, Dirks RP, Hankemeier T & Spaink HP (2015) Testing tuberculosis drug efficacy in a zebrafish high-throughput translational medicine screen. *Antimicrobial Agents and Chemotherapy* 59(2), 753–762.

Orme IM & Collins FM (1983) Protection against *Mycobacterium tuberculosis* infection by adoptive immunotherapy requirement for T cell-deficient recipients. *Journal of Experimental Medicine* 158(1), 74–83.

O'Toole RF & Gautam SS (2017) Limitations of the *Mycobacterium tuberculosis* reference genome H37Rv in the detection of virulence-related loci. *Genomics* 109(5–6), 471–474.

Pagán AJ & Ramakrishnan L (2018) The formation and function of granulomas. *Annual Review of Immunology* 36, 639–665.

Pai M, Behr MA, Dowdy D, Dheda K, Divangahi M, Boehme CC, Ginsberg A, Swaminathan S, Spigelman M, Getahun H, Menzies D & Raviglione M (2016) Tuberculosis. *Nature Reviews Disease Primers* 2, 16076.

Painter H, Prabowo SA, Cia F, Stockdale L, Tanner R, Willcocks S, Reljic R, Fletcher HA & Zelmer A (2020) Adaption of the *ex vivo* mycobacterial growth inhibition assay for use with murine lung cells. *Scientific Reports* 10, 3311.

Parasa VR, Muvva JR, Rose JF, Braian C, Brighenti S & Lerm M (2017) Inhibition of tissue matrix metalloproteinases interferes with *Mycobacterium tuberculosis*-induced granuloma formation and reduces bacterial load in a human lung tissue model. *Frontiers in Microbiology* 8, 2370.

Parish T, Smith DA, Kendall S, Casali N, Bancroft GJ & Stoker NG (2003) Deletion of two-component regulatory systems increases the virulence of *Mycobacterium tuberculosis*. *Infection and Immunity* 71(3), 1134–1140.

Péan CB, Schiebler M, Tan SWS, Sharrock JA, Kierdorf K, Brown KP, Maserumule MC, Menezes S, Pilátová M, Bronda K, Guermonprez P, Stramer BM, Andres Floto R & Dionne MS (2017) Regulation of phagocyte triglyceride by a STAT-ATG2 pathway controls mycobacterial infection. *Nature Communications* 8(1), 1–11.

Peleg AY, Jara S, Monga D, Eliopoulos GM, Moellering RC & Mylonakis E (2009) *Galleria mellonella* as a model system to study *Acinetobacter baumannii* pathogenesis and therapeutics. *Antimicrobial Agents and Chemotherapy* 53(6), 2605–2609.

Peña JC & Ho W-Z (2016) Non-human primate models of tuberculosis. *Microbiology Spectrum* 4(4), TBTB2-0007–2016.

Peng X, Knouse JA & Hernon KM (2015) Rabbit models for studying human infectious diseases. *Comparative Medicine* 65(6), 499–507.

Perdoni F, Falleni M, Tosi D, Cirasola D, Romagnoli S, Braidotti P, Clementi E, Bulfamante G & Borghi E (2014) A histological procedure to study fungal infection in the wax moth *Galleria mellonella*. *European Journal of Histochemistry* 58(3), 258–262.

Pereira TC, Barros PP de, de Oliveira Fugisaki LR, Rossoni RD, Ribeiro F de C, Menezes RT de, Junqueira JC & Scorzoni L (2018) Recent advances in the use of *Galleria mellonella* model to study immune responses against human pathogens. *Journal of Fungi* 4(4), E128.

Pereira MF & Rossi CC (2020) Overview of rearing and testing conditions and a guide for optimizing *Galleria mellonella* breeding and use in the laboratory for scientific purposes. *APMIS* 128(12), 607–620.

Pérez E, Samper S, Bordas Y, Guilhot C, Gicquel B & Martín C (2001) An essential role for *phoP* in *Mycobacterium tuberculosis* virulence. *Molecular Microbiology* 41(1), 179–187.

Peterson ND, Rosen BC, Dillon NA & Baughn AD (2015) Uncoupling environmental pH and intrabacterial acidification from pyrazinamide susceptibility in *Mycobacterium tuberculosis*. *Antimicrobial Agents and Chemotherapy* 59(12), 7320–7326.

Petronio GP, Cutuli MA, Magnifico I, Venditti N, Pietrangelo L, Vergalito F, Pane A, Scapagnini G & di Marco R (2020) In vitro and in vivo biological activity of berberine chloride against uropathogenic *E. coli* strains using *Galleria mellonella* as a host model. *Molecules* 25(21), 5010.

Peyron P, Vaubourgeix J, Poquet Y, Levillain F, Botanch C, Bardou F, Daffé M, Emile J-F, Marchou B, Cardona P-J, Chastellier C de & Altare F (2008) Foamy macrophages from tuberculous patients' granulomas constitute a nutrient-rich reservoir for *M. tuberculosis* persistence. *PLOS Pathogens* 4(11), e1000204.

Pham LN, Dionne MS, Shirasu-Hiza M & Schneider DS (2007) A specific primed immune response in *Drosophila* is dependent on phagocytes. *PLoS Pathogens* 3(3), e26.

Podell BK, Ackart DF, Obregon-Henao A, Eck SP, Henao-Tamayo M, Richardson M, Orme IM, Ordway DJ & Basaraba RJ (2014) Increased severity of tuberculosis in guinea pigs with type 2 diabetes: A model of diabetes-tuberculosis comorbidity. *American Journal of Pathology* 184(4), 1104–1118.

Polsfuss S, Hofmann-Thiel S, Merker M, Krieger D, Niemann S, Rüssmann H, Schönfeld N, Hoffmann H & Kranzer K (2019) Emergence of low-level delamanid and bedaquiline resistance during extremely drug-resistant tuberculosis treatment. *Clinical Infectious Diseases* 69(7), 1229–1231.

Posner E (1971) The early years of chest radiology in Britain. *Thorax* 26(3), 239.

Pym AS, Brodin P, Brosch R, Huerre M & Cole ST (2002) Loss of RD1 contributed to the attenuation of the live tuberculosis vaccines *Mycobacterium bovis* BCG and *Mycobacterium microti*. *Molecular Microbiology* 46(3), 709–717.

Pype C, Verbueken E, Saad MA, Casteleyn CR, van Ginneken CJ, Knapen D & van Cruchten SJ (2015) Incubation at 32.5°C and above causes malformations in the zebrafish embryo. *Reproductive Toxicology* 56, 56–63.

Quigley J, Hughitt VK, Velikovsky CA, Mariuzza RA, El-Sayed NM & Briken V (2017) The cell wall lipid PDIM contributes to phagosomal escape and host cell exit of *Mycobacterium tuberculosis*. *mBio* 8(2), e00148-17.

Ragunathan P, Cole M, Latka C, Aragaw WW, Hegde P, Shin J, Subramanian Manimekalai MS, Rishikesan S, Aldrich CC, Dick T & Grüber G (2021) *Mycobacterium tuberculosis* PanD structure-function analysis and identification of a potent pyrazinoic acid-derived enzyme inhibitor. *ACS Chemical Biology* 16(6), 1030–1039.

Ramage HR, Connolly LE & Cox JS (2009) Comprehensive functional analysis of *Mycobacterium tuberculosis* toxin-antitoxin systems: implications for pathogenesis, stress responses, and evolution. *PLoS Genetics* 5(12), e1000767.

Ramarao N, Nielsen-Leroux C & Lereclus D (2012) The insect *Galleria mellonella* as a powerful infection model to investigate bacterial pathogenesis. *Journal of Visualized Experiments* (70), e4392.

Ratnatunga CN, Lutzky VP, Kupz A, Doolan DL, Reid DW, Field M, Bell SC, Thomson RM & Miles JJ (2020) The rise of non-tuberculosis mycobacterial lung disease. *Frontiers in Immunology* 11, 303.

Reid MJA, Arinaminpathy N, Bloom A, Bloom BR, Boehme C, Chaisson R, Chin DP, Churchyard G, Cox H, Ditiu L, Dybul M, Farrar J, Fauci AS, Fekadu E, Fujiwara PI, Hallett TB, Hanson CL, Harrington M, Herbert N, Hopewell PC, Ikeda C, Jamison DT, Khan AJ, Koek I, Krishnan N, Motsoaledi A, Pai M, Raviglione MC, Sharman A, Small PM, Swaminathan S, Temesgen Z, Vassall A, Venkatesan N, van Weezenbeek K, Yamey G, Agins BD, Alexandru S, Andrews JR, Beyeler N, Bivol S, Brigden G, Cattamanchi A, Cazabon D, Crudu V, Daftary A, Dewan P, Doepel LK, Eisinger RW, Fan V, Fewer S, Furin J, Goldhaber-Fiebert JD, Gomez GB, Graham SM, Gupta D, Kamene M, Khaparde S, Mailu EW, Masini EO, McHugh L, Mitchell E, Moon S, Osberg M, Pande T, Prince L, Rade K, Rao R, Remme M, Seddon JA, Selwyn C, Shete P, Sachdeva KS, Stallworthy G, Vesga JF, Vilc V & Goosby EP (2019) Building a tuberculosis-free world: The Lancet commission on tuberculosis. *Lancet* 393, 1331–1384.

Renwick J, Reeves E, Wientjes F & Kavanagh K (2007) Translocation of proteins homologous to human neutrophil p47phox and p67phox to the cell membrane in activated hemocytes of *Galleria mellonella*. *Developmental and Comparative Immunology* 31(4), 347–359.

Rigotto Caruso G, Tonani L, Marcato PD & von Zeska Kress MR (2021) Phenothiazinium photosensitizers associated with silver nanoparticles in enhancement of antimicrobial photodynamic therapy. *Antibiotics* 10(5), 569.

Ritz N & Curtis N (2009) Mapping the global use of different BCG vaccine strains. *Tuberculosis* 89(4), 248–251.

Ritz N, Tebruegge M, Connell TG, Sievers A, Robins-Browne R & Curtis N (2009) Susceptibility of *Mycobacterium bovis* BCG vaccine strains to antituberculous antibiotics. *Antimicrobial Agents and Chemotherapy* 53(1), 316–318.

Rohde KH, Abramovitch RB & Russell DG (2007) *Mycobacterium tuberculosis* invasion of macrophages: linking bacterial gene expression to environmental cues. *Cell Host & Microbe* 2(5), 352–364.

la Rosa S, Casey P, Hill C, Diep D, Nes I & Brede D (2013) *In vivo* assessment of growth and virulence gene expression during commensal and pathogenic lifestyles of *luxABCDE*-tagged *Enterococcus faecalis* strains in murine gastrointestinal and intravenous infection models. *Applied and Environmental Microbiology* 79(13), 3986–3997.

Rougerie P, Miskolci V & Cox D (2013) Generation of membrane structures during phagocytosis and chemotaxis of macrophages: Role and regulation of the actin cytoskeleton. *Immunological Reviews* 256(1), 222–239.

Rousseau C, Winter N, Pivert E, Bordat Y, Neyrolles O, Avé P, Huerre M, Gicquel B & Jackson M (2004) Production of phthiocerol dimycocerosates protects *Mycobacterium tuberculosis* from the cidal activity of reactive nitrogen intermediates produced by macrophages and modulates the early immune response to infection. *Cellular Microbiology* 6(3), 277–287.

Roy R (2017) Protection from *Mycobacterium tuberculosis* infection: Learning from exposed but uninfected children. Imperial College London, PhD Thesis.

Russell DG, Cardona P-J, Kim M-J, Allain S & Altare F (2009) Foamy macrophages and the progression of the human tuberculosis granuloma. *Nature Immunology* 10(9), 943–948.

Rustad TR, Harrell MI, Liao R & Sherman DR (2008) The enduring hypoxic response of *Mycobacterium tuberculosis*. *PLoS ONE* 3(1), e1502.

Ryan GJ, Shapiro HM & Lenaerts AJ (2014) Improving acid-fast fluorescent staining for the detection of mycobacteria using a new nucleic acid staining approach. *Tuberculosis* 94(5), 511–518.

Sadd BM & Schmid-Hempel P (2006) Insect immunity shows specificity in protection upon secondary pathogen exposure. *Current Biology* 16(12), 1206–1210.

Sakula A (1983) BCG: Who were Calmette and Guerin? *Thorax* 38(11), 806–812.

Sambandamurthy VK, Derrick SC, Jalapathy KV, Chen B, Russell RG, Morris SL & Jacobs WR (2005) Long-term protection against tuberculosis following vaccination with a severely attenuated double lysine and pantothenate auxotroph of *Mycobacterium tuberculosis*. *Infection and Immunity* 73(2), 1196–1203.

Sambandamurthy VK, Wang X, Chen B, Russell RG, Derrick S, Collins FM, Morris SL & Jacobs WR (2002) A pantothenate auxotroph of *Mycobacterium tuberculosis* is highly attenuated and protects mice against tuberculosis. *Nature Medicine* 8(10), 1171–1174.

Sampson SL, Dascher CC, Sambandamurthy VK, Russell RG, Jacobs WR, Bloom BR & Hondalus MK (2004) Protection elicited by a double leucine and pantothenate auxotroph of *Mycobacterium tuberculosis* in guinea pigs. *Infection and Immunity* 72(5), 3031–3037.

Sampson SL, Mansfield KG, Carville A, Magee DM, Quitugua T, Howerth EW, Bloom BR & Hondalus MK (2011) Extended safety and efficacy studies of a live attenuated double leucine and pantothenate auxotroph of *Mycobacterium tuberculosis* as a vaccine candidate. *Vaccine* 29(29–30), 4839–4847.

Santucci P, Bouzid F, Smichi N, Poncin I, Kremer L, Chastellier C de, Drancourt M & Canaan S (2016) Experimental models of foamy macrophages and approaches for dissecting the

mechanisms of lipid accumulation and consumption during dormancy and reactivation of tuberculosis. *Frontiers in Cellular and Infection Microbiology* 6, 122.

Scanga CA & Flynn JL (2014) Modeling tuberculosis in nonhuman primates. *Cold Spring Harbor Perspectives in Medicine* 4(12), a018564.

Schnappinger D, Ehrt S, Voskuil MI, Liu Y, Mangan JA, Monahan IM, Dolganov G, Efron B, Butcher PD, Nathan C & Schoolnik GK (2003) Transcriptional adaptation of *Mycobacterium tuberculosis* within macrophages: insights into the phagosomal environment. *The Journal of Experimental Medicine* 198(5), 704.

Schwanhüusser B, Busse D, Li N, Dittmar G, Schuchhardt J, Wolf J, Chen W & Selbach M (2011) Global quantification of mammalian gene expression control. *Nature* 473, 337–342.

Seiler P, Ulrichs T, Bandermann S, Pradl L, Jörg S, Krenn V, Morawietz L, Kaufmann SHE & Aichele P (2003) Cell-wall alterations as an attribute of *Mycobacterium tuberculosis* in latent infection. *The Journal of Infectious Diseases* 188(9), 1326–1331.

Sette CS, Wachholz PA, Masuda PY, da Costa Figueira RBF, de Oliveira Mattar FR & Ura DG (2015) *Mycobacterium marinum* infection: a case report. *Journal of Venomous Animals and Toxins Including Tropical Diseases* 21(1), 7.

Sharrock A, Ruthe A, Andrews ESV, Arcus VA & Hicks JL (2018) VapC proteins from *Mycobacterium tuberculosis* share ribonuclease sequence specificity but differ in regulation and toxicity. *PLoS ONE* 13(8), e0203412.

Sheehan G, Clarke G & Kavanagh K (2018a) Characterisation of the cellular and proteomic response of *Galleria mellonella* larvae to the development of invasive aspergillosis. *BMC Microbiology* 18, 63.

Sheehan G, Dixon A & Kavanagh K (2019) Utilization of *Galleria mellonella* larvae to characterize the development of *Staphylococcus aureus* infection. *Microbiology* 165(8), 863–875.

Sheehan G, Farrell G & Kavanagh K (2020a) Immune priming: the secret weapon of the insect world. *Virulence* 11(1), 238–246.

Sheehan G, Garvey A, Croke M & Kavanagh K (2018b) Innate humoral immune defences in mammals and insects: The same, with differences? *Virulence* 9(1), 1625–1639.

Sheehan G & Kavanagh K (2018) Analysis of the early cellular and humoral responses of *Galleria mellonella* larvae to infection by *Candida albicans*. *Virulence* 9(1), 163–172.

Sheehan G, Konings M, Lim W, Fahal A, Kavanagh K & van de Sande WJ (2020b) Proteomic analysis of the processes leading to *Madurella mycetomatis* grain formation in *Galleria mellonella* larvae. *PLoS Neglected Tropical Diseases* 14(4), e0008190.

Sheehan G, Margalit A, Sheehan D & Kavanagh K (2021) Proteomic profiling of bacterial and fungal induced immune priming in *Galleria mellonella* larvae. *Journal of Insect Physiology* 131, 104213.

Shrivastava P & Bagchi T (2013) IL-10 modulates *in vitro* multinucleate giant cell formation in human tuberculosis. *PLoS ONE* 8(10), e77680.

Sigle LT & Hillyer JF (2016) Mosquito hemocytes preferentially aggregate and phagocytose pathogens in the periostial regions of the heart that experience the most hemolymph flow. *Developmental and Comparative Immunology* 55, 90–101.

Simeone R, Sayes F, Lawarée E & Brosch R (2021) Breaching the phagosome, the case of the tuberculosis agent. *Cellular Microbiology* 23(7), e13344.

Singh V & Seed T (2021) How necessary are animal models for modern drug discovery? *Expert opinion on drug discovery* 16(12), 1–7.

Singhal N, Sharma P, Kumar M, Joshi B & Bisht D (2012) Analysis of intracellular expressed proteins of *Mycobacterium tuberculosis* clinical isolates. *Proteome Science* 10, 14.

Sirakova TD, Dubey VS, Deb C, Daniel J, Korotkova TA, Abomoelak B & Kolattukudy PE (2006) Identification of a diacylglycerol acyltransferase gene involved in accumulation of triacylglycerol in *Mycobacterium tuberculosis* under stress. *Microbiology* 152, 2717–2725.

Skowronek P, Wójcik Ł & Strachecka A (2021) Fat body—multifunctional insect tissue. *Insects* 12(6), 547.

Smith CM, Proulx MK, Olive AJ, Laddy D, Mishra BB, Moss C, Gutierrez NM, Bellerose MM, Barreira-Silva P, Phuah JY, Baker RE, Behar SM, Kornfeld H, Evans TG, Beamer G & Sassetti CM (2016) Tuberculosis susceptibility and vaccine protection are independently controlled by host genotype. *mBio* 7(5), e01516-16.

Snewin VA, Gares M, Ógaora P, Hasan Z, Brown IN & Young DB (1999) Assessment of immunity to mycobacterial infection with luciferase reporter constructs. *Infection and Immunity* 67(9), 4586–4593.

Sonawane AR, Platig J, Fagny M, Chen CY, Paulson JN, Lopes-Ramos CM, DeMeo DL, Quackenbush J, Glass K & Kuijjer ML (2017) Understanding tissue-specific gene regulation. *Cell Reports* 21(4), 1077–1088.

de Sousa Abreu R, Penalva LO, Marcotte EM & Vogel C (2009) Global signatures of protein and mRNA expression levels. *Molecular BioSystems* 5, 1512–1526.

Sousa J, Cá B, Maceiras AR, Simões-Costa L, Fonseca KL, Fernandes AI, Ramos A, Carvalho T, Barros L, Magalhães C, Chiner-Oms Á, Machado H, Veiga MI, Singh A, Pereira R, Amorim A, Vieira J, Vieira CP, Bhatt A, Rodrigues F, Rodrigues PNS, Gagneux S, Castro AG, Guimarães JT, Bastos HN, Osório NS, Comas I & Saraiva M (2020) *Mycobacterium*

tuberculosis associated with severe tuberculosis evades cytosolic surveillance systems and modulates IL-1β production. *Nature Communications* 11(1), 1–14.

Sousa PS, Silva IN, Moreira LM, Veríssimo A & Costa J (2018) Differences in virulence between *Legionella pneumophila* isolates from human and non-human sources determined in *Galleria mellonella* infection model. *Frontiers in Cellular and Infection Microbiology* 8, 97.

Sridevi JP, Anantaraju HS, Kulkarni P, Yogeeswari P & Sriram D (2014) Optimization and validation of *Mycobacterium marinum*-induced adult zebrafish model for evaluation of oral anti-tuberculosis drugs. *International Journal of Mycobacteriology* 3(4), 259–267.

Stączek S, Zdybicka-Barabas A, Wiater A, Pleszczyńska M & Cytryńska M (2020) Activation of cellular immune response in insect model host *Galleria mellonella* by fungal α-1,3-glucan. *Pathogens and Disease* 78(9), ftaa062.

Stinear TP, Seemann T, Harrison PF, Jenkin GA, Davies JK, Johnson PDR, Abdellah Z, Arrowsmith C, Chillingworth T, Churcher C, Clarke K, Cronin A, Davis P, Goodhead I, Holroyd N, Jagels K, Lord A, Moule S, Mungall K, Norbertczak H, Quail MA, Rabbinowitsch E, Walker D, White B, Whitehead S, Small PLC, Brosch R, Ramakrishnan L, Fischbach MA, Parkhill J & Cole ST (2008) Insights from the complete genome sequence of *Mycobacterium marinum* on the evolution of *Mycobacterium tuberculosis*. *Genome Research* 18(5), 729–741.

Swearengen JR (2018) Choosing the right animal model for infectious disease research. *Animal Models and Experimental Medicine* 1(2), 100–108.

Tabouret G, Astarie-Dequeker C, Demangel C, Malaga W, Constant P, Ray A, Honoré N, Bello NF, Perez E, Daffé M & Guilhot C (2010) *Mycobacterium leprae* phenolglycolipid-1 expressed by engineered *M. bovis* BCG modulates early interaction with human phagocytes. *PLOS Pathogens* 6(10), e1001159.

Tailleux L, Waddell SJ, Pelizzola M, Mortellaro A, Withers M, Tanne A, Castagnoli PR, Gicquel B, Stoker NG, Butcher PD, Foti M & Neyrolles O (2008) Probing host pathogen cross-talk by transcriptional profiling of both *Mycobacterium tuberculosis* and Infected human dendritic cells and macrophages. *PLoS ONE* 3(1), e1403.

Takaki K, Cosma CL, Troll MA & Ramakrishnan L (2012) An in vivo platform for rapid high-throughput antitubercular drug discovery. *Cell Reports* 2, 175–184.

Talbot EA & Raffa BJ (2014) *Mycobacterium tuberculosis* (Y Tang & A Sails, Ed. by). Elsevier Ltd, San Diego.

Talip BA, Sleator RD, Lowery CJ, Dooley JSG & Snelling WJ (2013) An update on global tuberculosis (TB). *Infectious Diseases: Research and Treatment* 6, 39–50.

Tarshis MS & Weed WA (1953) Lack of significant in vitro sensitivity of *Mycobacterium tuberculosis* to pyrazinamide on three different solid media. *American review of tuberculosis* 67(3), 391–395.

Tena GN, Young DB, Eley B, Henderson H, Nicol MP, Levin M & Kampmann B (2003) Failure to control growth of mycobacteria in blood from children infected with human immunodeficiency virus and its relationship to T cell function. *The Journal of Infectious Diseases* 187(10), 1544–1551.

Thieme L, Hartung A, Makarewicz O & Pletz MW (2020) *In vivo* synergism of ampicillin, gentamicin, ceftaroline and ceftriaxone against *Enterococcus faecalis* assessed in the *Galleria mellonella* infection model. *Journal of Antimicrobial Chemotherapy* 75(8), 2173–2181.

Thomas RJ, Hamblin KA, Armstrong SJ, Müller CM, Bokori-Brown M, Goldman S, Atkins HS & Titball RW (2013) *Galleria mellonella* as a model system to test the pharmacokinetics and efficacy of antibiotics against *Burkholderia pseudomallei*. *International Journal of Antimicrobial Agents* 41(4), 330–336.

Tiberi S, Muñoz-Torrico M, Duarte R, Dalcolmo M, D'Ambrosio L & Migliori GB (2018) New drugs and perspectives for new anti-tuberculosis regimens. *Revista Portuguesa de Pneumologia (English Edition)* 24(2), 86–98.

Tkhilaishvili T, Wang L, Tavanti A, Trampuz A & di Luca M (2020) Antibacterial efficacy of two commercially available bacteriophage formulations, staphylococcal bacteriophage and PYO bacteriophage, against methicillin-resistant *Staphylococcus aureus* : prevention and eradication of biofilm formation and control of a systemic infection of *Galleria mellonella* larvae. *Frontiers in Microbiology* 11, 110.

Tobin DM & Ramakrishnan L (2008) Comparative pathogenesis of *Mycobacterium marinum* and *Mycobacterium tuberculosis*. *Cellular Microbiology* 10(5), 1027–1039.

Torres-Juarez F, Cardenas-Vargas A, Montoya-Rosales A, González-Curiel I, Garcia-Hernandez MH, Enciso-Moreno JA, Hancock REW & Rivas-Santiago B (2015) LL-37 immunomodulatory activity during *Mycobacterium tuberculosis* infection in macrophages. *Infection and Immunity* 83(12), 4495–4503.

Trevijano-Contador N & Zaragoza O (2018) Immune response of *Galleria mellonella* against human fungal pathogens. *Journal of Fungi* 5(1), 3.

Tsai CJ-Y, Loh JMS & Proft T (2016) *Galleria mellonella* infection models for the study of bacterial diseases and for antimicrobial drug testing. *Virulence* 7(3), 214–229.

Tsenova L, Fallows D, Kolloli A, Singh P, O'Brien P, Kushner N, Kaplan G & Subbian S (2020) Inoculum size and traits of the infecting clinical strain define the protection level against *Mycobacterium tuberculosis* infection in a rabbit model. *European Journal of Immunology* 50(6), 858–872.

Tsukamura M (1991) Some observations on the mechanism of bactericidal activity of Tween 80 on mycobacteria. *Kekkaku* 66(2), 75–79.

Tucker EW, Pokkali S, Zhang Z, DeMarco VP, Klunk M, Smith ES, Ordonez AA, Penet MF, Bhujwalla Z, Jain SK & Kannan S (2016) Microglia activation in a pediatric rabbit model of tuberculous meningitis. *Disease Models and Mechanisms* 9(12), 1497–1502.

Turner RD, Tweed CD, Shukla J & Bothamley GH (2015) BCG and infection with *Mycobacterium tuberculosis*. *Thorax* 70(3), 286–286.

Tweed CD, Crook AM, Amukoye EI, Dawson R, Diacon AH, Hanekom M, McHugh TD, Mendel CM, Meredith SK, Murphy ME, Murthy SE, Nunn AJ, Phillips PPJ, Singh KP, Spigelman M, Wills GH & Gillespie SH (2018) Toxicity associated with tuberculosis chemotherapy in the REMoxTB study. *BMC Infectious Diseases* 18(1), 1–11.

Tzelepis I, Kapsetaki SE, Panayidou S & Apidianakis Y (2013) *Drosophila melanogaster*: a first step and a stepping-stone to anti-infectives. *Current Opinion in Pharmacology* 13(5), 763–768.

Uren C, Hoal EG & Möller M (2020) *Mycobacterium tuberculosis* complex and human coadaptation: A two-way street complicating host susceptibility to TB. *Human Molecular Genetics* 30(2), 146–153.

Uusi-Mäkelä M & Rämet M (2018) Hijacking host angiogenesis to drive mycobacterial growth. *Cell Host and Microbe* 24(4), 465–466.

Via LE, Savic R, Weiner DM, Zimmerman MD, Prideaux B, Irwin SM, Lyon E, O'Brien P, Gopal P, Eum S, Lee M, Lanoix JP, Dutta NK, Shim TS, Cho JS, Kim W, Karakousis PC, Lenaerts A, Nuermberger E, Barry CE & Dartois V (2015) Host-mediated bioactivation of pyrazinamide: Implications for efficacy, resistance, and therapeutic alternatives. *ACS Infectious Diseases* 8(1), 203–214.

Vilchèze C & Kremer L (2017) Acid-fast positive and acid-fast negative *Mycobacterium tuberculosis*: The Koch paradox. *Microbiology Spectrum* 5(2), TBTB2-0003–2015.

Vilcinskas A & Wedde M (2002) Insect inhibitors of metalloproteinases. *IUBMB Life* 54, 339–343.

Vinogradova T, Dogonadze M, Zabolotnykh N, Badleeva M, Yarusova I, Vyazovaya A, Gerasimova A, Zhdanova S, Vitovskaya M, Solovieva N, Pasechnik O, Ogarkov O & Mokrousov I (2021) Extremely lethal and hypervirulent *Mycobacterium tuberculosis* strain cluster emerging in far east, Russia. *Emerging Microbes and Infections* 10(1), 1691–1701.

Vogel H, Altincicek B, Glöckner G & Vilcinskas A (2011) A comprehensive transcriptome and immune-gene repertoire of the lepidopteran model host *Galleria mellonella*. *BMC Genomics* 12, 308.

Vogel C, de Sousa Abreu R, Ko D, Le SY, Shapiro BA, Burns SC, Sandhu D, Boutz DR, Marcotte EM & Penalva LO (2010) Sequence signatures and mRNA concentration can explain two-thirds of protein abundance variation in a human cell line. *Molecular Systems Biology* 6, 400.

Wade MM & Zhang Y (2004) Anaerobic incubation conditions enhance pyrazinamide activity against *Mycobacterium tuberculosis*. *Journal of Medical Microbiology* 53(8), 769–773.

Wagar LE, Difazio RM & Davis MM (2018) Advanced model systems and tools for basic and translational human immunology. *Genome Medicine* 10(1), 1–14.

Wang D, Eraslan B, Wieland T, Hallström B, Hopf T, Zolg DP, Zecha J, Asplund A, Li L hua, Meng C, Frejno M, Schmidt T, Schnatbaum K, Wilhelm M, Ponten F, Uhlen M, Gagneur J, Hahne H & Kuster B (2019a) A deep proteome and transcriptome abundance atlas of 29 healthy human tissues. *Molecular Systems Biology* 15, e8503.

Wang Y, Jiang H, Cheng Y, An C, Chu Y, Raikhel AS & Zou Z (2017) Activation of *Aedes aegypti* prophenoloxidase-3 and its role in the immune response against entomopathogenic fungi. *Insect Molecular Biology* 26(5), 552–563.

Wang R, Kreutzfeldt K, Botella H, Vaubourgeix J, Schnappinger D & Ehrt S (2019b) Persistent *Mycobacterium tuberculosis* infection in mice requires PerM for successful cell division. *eLife* 8, e49570.

Wang F, Sambandan D, Halder R, Wang J, Batt SM, Weinrick B, Ahmad I, Yang P, Zhang Y, Kim J, Hassani M, Huszar S, Trefzer C, Ma Z, Kaneko T, Mdluli KE, Franzblau S, Chatterjee AK, Johnson K, Mikusova K, Besra GS, Fütterer K, Jacobs WR & Schultz PG (2013) Identification of a small molecule with activity against drug-resistant and persistent tuberculosis. *Proceedings of the National Academy of Sciences of the United States of America* 110(27), E2510-2517.

Wang X, Zhang Y, Zhang R & Zhang J (2019c) The diversity of pattern recognition receptors (PRRs) involved with insect defense against pathogens. *Current Opinion in Insect Science* 33, 105–110.

Waters WR, Palmer MV, Nonnecke BJ, Thacker TC, Scherer CFC, Estes DM, Hewinson RG, Vordermeier HM, Barnes SW, Federe GC, Walker JR, Glynne RJ, Hsu T, Weinrick B, Biermann K, Larsen MH, Jacobs WR & Jr. (2009) Efficacy and immunogenicity of *Mycobacterium bovis* Δ*RD1* against aerosol *M. bovis* infection in neonatal calves. *Vaccine* 27(8), 1209.

Wedde M, Weise C, Nuck R, Altincicek B & Vilcinskas A (2007) The insect metalloproteinase inhibitor gene of the lepidopteran *Galleria mellonella* encodes two distinct inhibitors. *Biological Chemistry* 8(1), 119–127.

Whitten MMA, Tew IF, Lee BL & Ratcliffe NA (2004) A novel role for an insect apolipoprotein (apolipophorin III) in β-1,3-glucan pattern recognition and cellular encapsulation reactions. *The Journal of Immunology* 172(4), 2177–2185.

Wijesinghe GK, Maia FC, de Oliveira TR, de Feiria SNB, Joia F, Barbosa JP, Boni GC, Sardi J de CO, Rosalen PL & Höfling JF (2020) Effect of *Cinnamomum verum* leaf essential oil on virulence factors of *Candida* species and determination of the *in-vivo* toxicity with *Galleria mellonella* model. *Memorias do Instituto Oswaldo Cruz* 115(8), 1–13.

Wilkinson CF & Brattsten LB (1972) Microsomal Drug Metabolizing Enzymes in Insects. *Drug Metabolism Review* 1(1), 153–227.

Williams MJ, Kana BD & Mizrahi V (2011) Functional analysis of molybdopterin biosynthesis in mycobacteria identifies a fused molybdopterin synthase in *Mycobacterium tuberculosis*. *Journal of Bacteriology* 193(1), 98–106.

Williams A & Orme IM (2016) Animal models of tuberculosis: an overview. *Microbiology Spectrum* 4(4), TBTB2-004–2015.

Wittwer D, Franchini A, Ottaviani E & Wiesner A (1999) Presence of IL-1 and TNF-Like molecules in *Galleria mellonella* (Lepidoptera) haemocytes and in an insect cell line from *Estigmene acraea* (Lepidoptera). *Cytokine* 11(9), 637–642.

Wojda I (2017) Immunity of the greater wax moth *Galleria mellonella*. *Insect Science* 24(3), 342–357.

Wojda I, Staniec B, Sułek M & Kordaczuk J (2020) The greater wax moth *Galleria mellonella*: biology and use in immune studies. *Pathogens and Disease* 78(9), ftaa057.

World Health Organization (2010) Guidelines for treatment of tuberculosis. WHO Press, Geneva.

World Health Organization (2014) Companion handbook to the WHO guidelines for the programmatic management of drug-resistant tuberculosis. WHO Press, Geneva.

World Health Organization (2017) Guidelines for treatment of drug-susceptible tuberculosis and patient care (2017 update). WHO Press, Geneva.

World Health Organization (2018) Latent tuberculosis infection updated and consolidated guidelines for programmatic management. WHO Press, Geneva.

World Health Organization (2020) Global Tuberculosis Report 2020. WHO Press, Geneva.

Wrońska AK & Boguś MI (2020) Heat shock proteins (HSP 90, 70, 60, and 27) in *Galleria mellonella* (Lepidoptera) hemolymph are affected by infection with *Conidiobolus coronatus* (Entomophthorales). *PLoS ONE* 15(2), e0228556.

Wu Q, Patočka J & Kuča K (2018) Insect antimicrobial peptides, a mini review. *Toxins* 10(11), 461.

Wu G, Zhao Z, Liu C & Qiu L (2014) Priming *Galleria mellonella* (Lepidoptera: Pyralidae) larvae with heat-killed bacterial cells induced an enhanced immune protection against *Photorhabdus luminescens* TT01 and the role of innate immunity in the process. *Journal of Economic Entomology* 107(2), 559–569.

Yam KC, D'Angelo I, Kalscheuer R, Zhu H, Wang J-X, Snieckus V, Ly LH, Converse PJ, Jr. WRJ, Strynadka N & Eltis LD (2009) Studies of a ring-cleaving dioxygenase illuminate the role of cholesterol metabolism in the pathogenesis of *Mycobacterium tuberculosis*. *PLoS Pathogens* 5(3), e1000344.

Yang HJ, Wang D, Wen X, Weiner DM & Via LE (2021) One size fits all? Not in *in vivo* modeling of tuberculosis chemotherapeutics. *Frontiers in Cellular and Infection Microbiology* 11, 613149.

Yi HY, Chowdhury M, Huang YD & Yu XQ (2014) Insect antimicrobial peptides and their applications. *Applied microbiology and biotechnology* 98(13), 5807–5822.

Young AP, Jackson DJ & Wyeth RC (2020) A technical review and guide to RNA fluorescence in situ hybridization. *PeerJ* 8, e8806.

Yu XQ & Kanost MR (2002) Binding of hemolin to bacterial lipopolysaccharide and lipoteichoic acid. An immunoglobulin superfamily member from insects as a pattern-recognition receptor. *European Journal of Biochemistry* 269(7), 1827–1834.

Yuan H, Chang H, Zhao L, Yang C & Huang Y (2019) Sex- and tissue-specific transcriptome analyses and expression profiling of olfactory-related genes in *Ceracris nigricornis* Walker (Orthoptera: Acrididae). *BMC Genomics* 20, 808.

Yuan T & Sampson NS (2018) Hit generation in TB drug discovery: From genome to granuloma. *Chemical Reviews* 118(4), 1887–1916.

Yuan T, Werman JM & Sampson NS (2021) The pursuit of mechanism of action: Uncovering drug complexity in TB drug discovery. *RSC Chemical Biolology* 2, 440.

Yue S, Jie J, Xie L, Li Y, Zhang J, Lai X, Xie J, Guo X & Zhai Y (2020) Antimicrobial peptide CAMA-syn expressed in pulmonary epithelium by recombination adenovirus inhibited the growth of intracellular bacteria. *The Journal of Gene Medicine* 22(3), e3149.

Zdybicka-Barabas A, Stączek S, Pawlikowska-Pawlęga B, Mak P, Luchowski R, Skrzypiec K, Mendyk E, Wydrych J, Gruszecki WI & Cytryńska M (2019) Studies on the interactions of neutral *Galleria mellonella* cecropin D with living bacterial cells. *Amino Acids* 51, 175–191.

Zhai W, Wu F, Zhang Y, Fu Y & Liu Z (2019) The immune escape mechanisms of *Mycobacterium Tuberculosis*. *International Journal of Molecular Sciences* 20(2), 340.

Zhan L, Tang J, Sun M & Qin C (2017) Animal models for tuberculosis in translational and precision medicine. *Frontiers in Microbiology* 8, 717.

Zhang S, Chen J, Shi W, Liu W, Zhang W & Zhang Y (2013a) Mutations in *panD* encoding aspartate decarboxylase are associated with pyrazinamide resistance in *Mycobacterium tuberculosis*. *Emerging Microbes and Infections* 2, e35.

Zhang T, Li SY & Nuermberger EL (2012) Autoluminescent *Mycobacterium tuberculosis* for rapid, real-time, non-invasive assessment of drug and vaccine efficacy. *PLoS ONE* 7(1), e29774.

Zhang L, Ru H, Chen F, Jin C, Sun R, Fan X, Guo M, Mai J, Xu W, Lin Q & Liu J (2016) Variable virulence and efficacy of BCG vaccine strains in mice and correlation with genome polymorphisms. *Molecular Therapy* 24(2), 398.

Zhang Y, Shi W, Zhang W & Mitchison D (2013b) Mechanisms of pyrazinamide action and resistance. *Microbiology Spectrum* 2(4), 12.

Zhang Y, Wade MM, Scorpio A, Zhang H & Sun Z (2003) Mode of action of pyrazinamide: disruption of *Mycobacterium tuberculosis* membrane transport and energetics by pyrazinoic acid. *Journal of Antimicrobial Chemotherapy* 52(5), 790–795.

Zhao J, Lai L, Ji W & Zhou Q (2019) Genome editing in large animals: Current status and future prospects. *National Science Review* 6(3), 402–420.

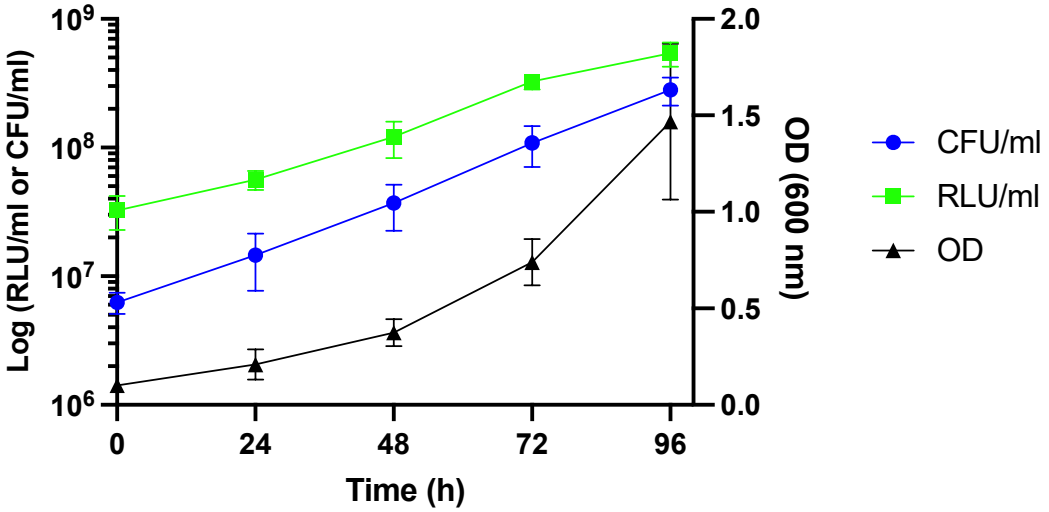
Zheng H, Colvin CJ, Johnson BK, Kirchhoff PD, Wilson M, Jorgensen-Muga K, Larsen SD & Abramovitch RB (2016) Inhibitors of *Mycobacterium tuberculosis* DosRST signaling and persistence. *Nature Chemical Biology* 13(2), 218–225.

Zheng H, Williams JT, Aleiwi B, Ellsworth E & Abramovitch RB (2020) Inhibiting *Mycobacterium tuberculosis* DosRST signaling by targeting response regulator DNA binding and sensor kinase heme. *ACS Chemical Biology* 15(1), 62.

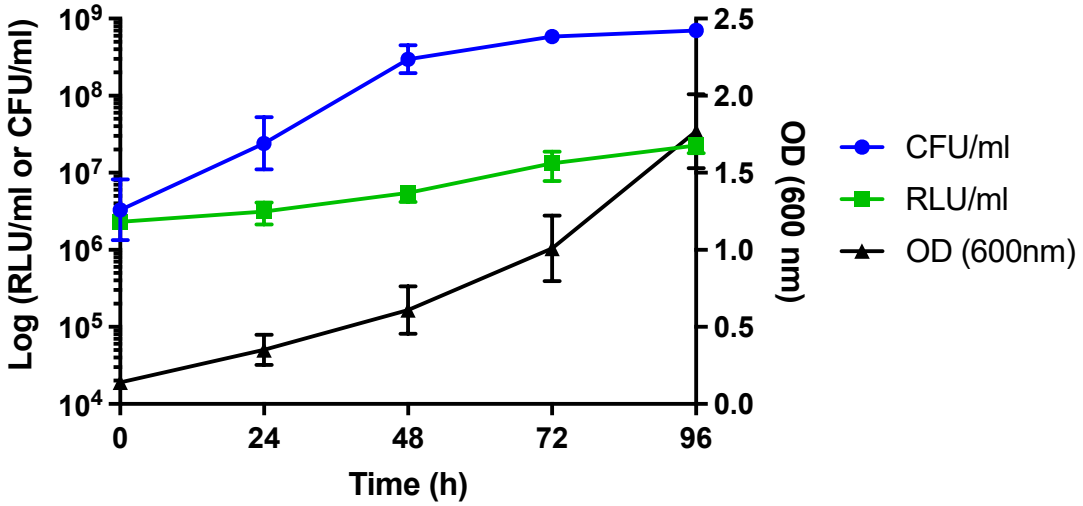
Zimmerman M, Lestner J, Prideaux B, O'Brien P, Dias-Freedman I, Chen C, Dietzold J, Daudelin I, Kaya F, Blanc L, Chen PY, Park S, Salgame P, Sarathy J & Dartois V (2017) Ethambutol partitioning in tuberculous pulmonary lesions explains its clinical efficacy. *Antimicrobial Agents and Chemotherapy* 61(9), e00924-17.

Appendix

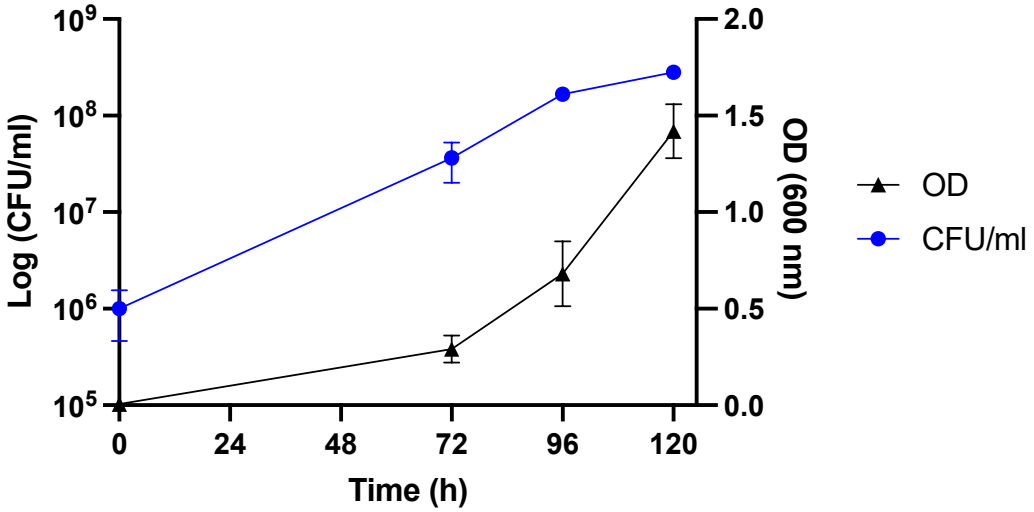
Supplementary Figures



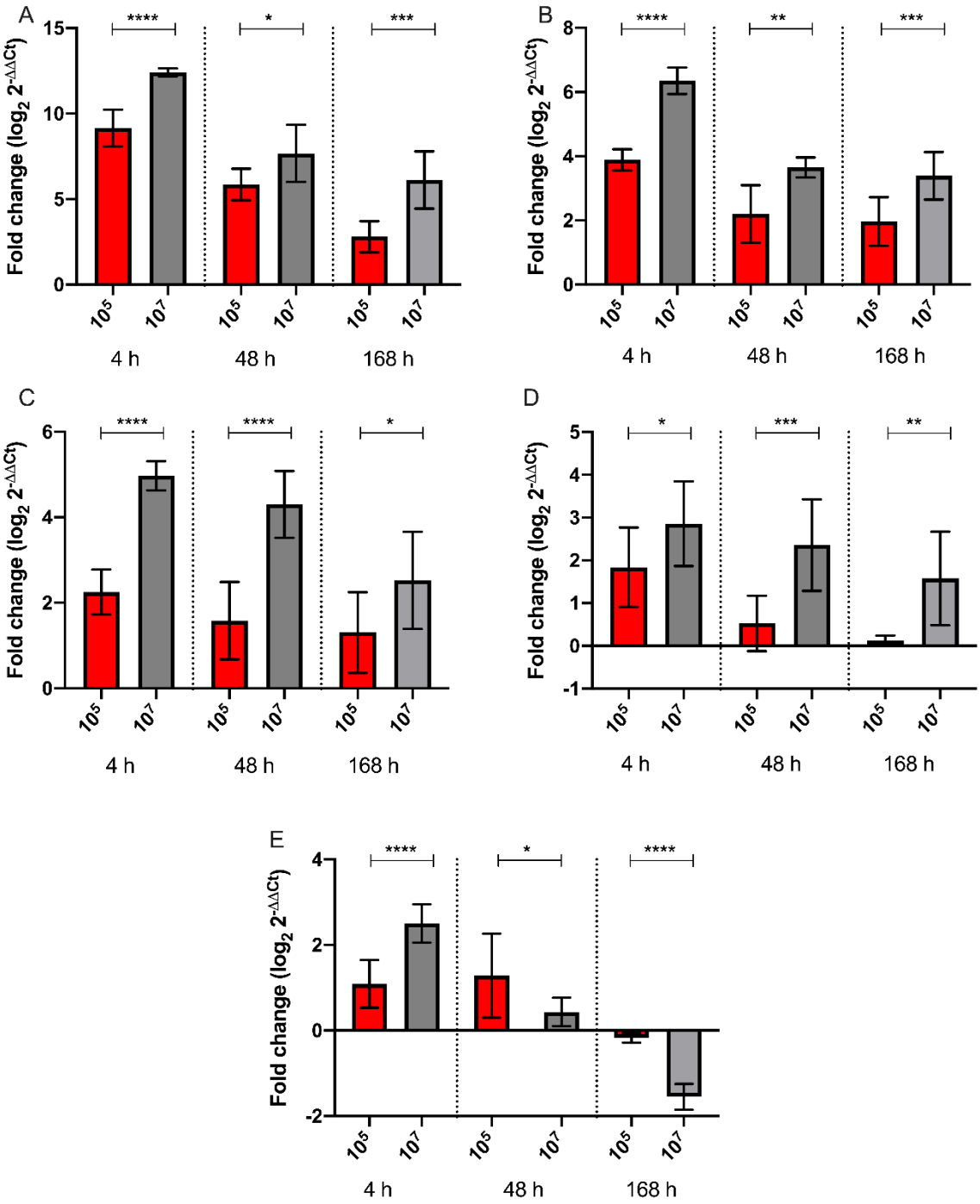
Supplementary Figure 2.1: *In vitro* growth curve of BCG *lux*. The growth of BCG *lux* in Middlebrook 7H9 broth was measured using luminescence (RLU/ml), CFU/ml and OD every 24 h for a 96 h time course. Plotted are the means of three independent experiments and the error bars represents the SD of the mean.



Supplementary Figure 2.2: *In vitro* growth curve of SAMTB *lux*. The growth of SAMTB *lux* in Middlebrook 7H9 broth (supplemented with Leu and Pan) was measured using luminescence (RLU/ml), CFU/ml and OD every 24 h for a 96 h time course. Plotted are the means of two independent experiments and the error bars represents the SD of the mean.



Supplementary Figure 2.3: *In vitro* growth curve of H37Rv. The growth of H37Rv in Middlebrook 7H9 broth was measured using CFU/ml and OD over 120 h. Plotted are the means of two independent experiments and the error bars represents the SD of the mean.



Supplementary Figure 7.1: Comparison of *G. mellonella* innate immune gene expression between low and high dose BCG *lux* infection. Relative gene expression of (A) *gloverin*, (B) *cecropin*, (C) *hemolin*, (D), *Hdd11* and (E) *IMPI* was measured by qPCR (ΔΔCT) using naïve larvae as control and ubiquitin as the house keeping gene. Plotted are the mean of three independent repeats, each consisting of three technical repeats. Error bars represent the SD. Level of gene expression between high and low dose BCG *lux* infection groups were compared at each time point using Mann-Whitney U-test: $p< 0.05$ (*), $p < 0.01$ (**), $p < 0.001$ (***) and $p < 0.0001$ (****).

Supplementary Tables

Supplementary Table 7.1: Proteins which are increased in abundance in *G. mellonella* larval haemolymph following infection with BCG *lux* (1x10^7 CFU) at 4 h post-infection relative to the 0 h control.

p value	Fold change (+)	GI number	Protein name	Peptides	Sequence coverage [%]	Score
0.003166	3.49	157927723	Beta actin	11	54.1	277.07
0.023588	2.20	186703381	Hemolin	7	50.7	323.31
0.016673	1.58	219552448	Arginine kinase	8	62.5	201.49

Supplementary Table 7.2: Proteins which are decreased in abundance in *G. mellonella* larval haemolymph following infection with BCG *lux* (1x10^7 CFU) at 4 h post-infection relative to the 0 h control.

p value	Fold change (-)	GI number	Protein name	Peptides	Sequence coverage [%]	Score
0.000121	2.37	225031010	Tubulin alpha chain	3	46.2	26.541
0.009208	1.82	229002332	Protein associated with transcription activator MBF2	3	14.5	114.37
0.02304	1.65	169646838	Heat shock protein 25.4	13	48	237.16

Supplementary Table 7.3: Proteins which are increased in abundance in *G. mellonella* larval haemolymph following infection with BCG *lux* (1x10^7 CFU) at 48 h post-infection relative to the 0 h control.

p value	Fold change (+)	GI Number	Protein names	Peptides	Sequence coverage [%]	Score
4.97E-05	145.25	156630481	Cecropin-D-like peptide	2	14.5	46.071
4.46E-05	66.41	112984054	Yellow-d	18	44.7	323.31
0.000311	56.27	110649240	Gloverin	2	28.8	18.817
5.49E-05	55.73	186703381	Hemolin	7	50.7	323.31
0.001092	47.51	116087	Cecropin-A (Alt. Cecropin-C)	1	8.5	9.783
0.011076	39.12	23208535	Peptidoglycan recognition-like protein B	13	34	231.94
4.51E-05	37.41	55139149	Hemolin	18	58	323.31
0.003829	22.85	110347843	Protease inhibitor-like protein	2	40	31.579
0.000188	19.60	112983052	Chemosensory protein 7 (Alt. Chemosensory protein 11)	7	27.7	169.29
0.009535	18.28	74873244	Hdd11	9	60.7	323.31
0.000104	16.78	154240658	Peptidoglycan recognition protein-D	7	22	120.85
0.004092	14.05	45594226	Serpin-4B	4	70	68.718
0.028322	14.04	56718390	Prophenol oxidase activating enzyme 3	17	42.1	210.04
0.005167	11.47	33860163	Inducible metalloproteinase inhibitor protein	8	33.2	67.368
0.000123	10.10	112983994	Peptidoglycan recognition protein	13	57.9	306.89
0.014612	9.93	25989211	Prophenol oxidase activating factor 3	7	53.6	102.38
0.01252	9.06	112702923	Peptidoglycan-recognition protein-LB	2	60.5	41.555
0.022459	8.72	23208526	6tox	6	17	36.001
0.032869	7.07	1705742	Hyphancin-3E (Alt. Cecropin-A1/Hyphancin-IIIE	1	4.7	18.42
0.047493	5.88	22901764	Kunitz-like protease inhibitor	3	23.8	62.084
0.016888	5.86	226342884	Serpin-11	13	39.2	166.87
1E-04	5.16	125629089	Gustatory receptor	2	14.9	24.41
0.000461	4.98	157927723	Beta actin	11	54.1	277.07
0.000708	4.59	183979237	Transgelin	6	21.1	169.94
0.001639	4.08	52782700	Beta-1,3-glucan recognition protein	2	12.7	43.006
0.0004	2.95	157704337	Hdd1	6	56.9	146.94

0.002815	2.58	52782700	Beta-1,3-glucan recognition protein	2	14.5	39.877
0.017544	2.33	110826028	Esterase	3	8.1	32.225
0.000655	2.32	156968291	Uncharacterized protein	16	35.2	244.53
0.011504	2.28	158289805	AGAP010733-PA	12	38.1	130.56
0.010426	2.26	27733415	Serpin 3a (Alt. Serpin 3b)	11	12.8	243.76
0.00195	2.15	73671225	Superoxide dismutase	3	57.8	312.25
0.009242	1.76	114649525	Beta-1,3-glucan recognition protein	14	37	163.22
0.024575	1.76	220902980	Carboxylic ester hydrolase	6	36.2	158.78
0.000161	1.74	170036627	Gelsolin (Alt. Gelsolin precursor)	22	35.8	323.31
6.84E-05	1.72	189181680	Carboxylic ester hydrolase	19	49.1	323.31
0.021036	1.52	242004672	Uncharacterized protein	10	51.9	205.8

Supplementary Table 7.4: Proteins which are decreased in abundance in *G. mellonella* larval haemolymph following infection with BCG *lux* (1x10^7 CFU) at 48 h post-infection relative to the 0 h control.

p value	Fold change (-)	GI Number	Protein names	Peptides	Sequence coverage [%]	Score
0.004211	22.90	229002332	Protein associated with transcription activator MBF2	3	14.5	114.37
0.0273	14.68	109119903	GAPDH	13	51.2	192.01
0.002301	9.39	121308868	Serine proteinase	9	25.4	96.748
0.009875	6.84	112983816	GAPDH	8	38.8	67.248
0.004925	5.96	116782397	Uncharacterized protein	8	16.9	84.718
0.023861	4.74	145286562	Lysozyme-like protein 1	3	9.2	48.058
0.003929	4.69	77415676	Uncharacterized protein	15	32.2	323.31
0.005601	4.30	114052174	Aminoacylase	6	20.1	38.514
0.016362	2.78	116791778	Uncharacterized protein	22	51.8	323.31
0.010089	2.48	164459610	Putative hydroxypyruvate isomerase	13	33.3	109.06
1.9E-05	2.07	153791206	Scolexin	15	28.2	323.31
0.035455	2.03	183979239	Similar to CG10638-PA	4	28.8	145.1
0.03539	1.87	46396271	27 kDa hemolymph protein	13	59.6	323.31
0.037852	1.74	114052174	Aminoacylase	6	17.8	52.484
0.018555	1.66	134103857	Cationic peptide CP8	6	29.2	323.31
0.001004	1.53	112983062	Lipopolysaccharide binding protein	13	47.7	173.12
0.007223	1.52	158515746	Juvenile hormone binding protein	15	41.7	323.31

Supplementary Table 7.5: Proteins which are increased in abundance in *G. mellonella* larval haemolymph following infection with BCG *lux* (1x10^7 CFU) at 168 h post-infection relative to the 0 h control.

p value	Fold Change (+)	GI Number	Protein Name	Peptides	Sequence coverage [%]	Score
0.00019	310.09	74873244	Hdd11	9	60.7	323.31
1.3E-05	87.75	186703381	Hemolin	7	50.7	323.31
6.37E-05	80.31	112984054	Yellow-d	18	44.7	323.31
5.38E-05	54.42	156630481	Cecropin-D-like peptide	2	14.5	46.071
7.84E-05	48.11	55139149	Hemolin	18	58	323.31
0.001611	42.22	112983052	Chemosensory protein 7 (Alt. Chemosensory protein 11)	7	27.7	169.29
3.6E-05	41.13	154240658	Peptidoglycan recognition protein-D	7	22	120.85
2.05E-05	26.60	183979237	Transgelin	6	21.1	169.94
0.016753	25.55	23208535	Peptidoglycan recognition-like protein B	13	34	231.94
0.01404	24.64	56718390	Prophenol oxidase activating enzyme 3	17	42.1	210.04
0.0047	23.40	110347843	Protease inhibitor-like protein	2	40	31.579
0.002981	20.92	45594226	Serpin-4B	4	70	68.718
0.000752	18.60	157927723	Beta actin	11	54.1	277.07
0.0039	16.29	116087	Cecropin-A (Cecropin-C)	1	8.5	9.783
0.000134	16.07	158962507	Chemosensory protein	6	23.3	93.297
0.02326	15.23	158962511	Chemosensory protein	5	16.7	110.2
0.003987	15.10	226342884	Serpin-11	13	39.2	166.87
0.016175	14.34	23208546	Heat shock 23	6	25.6	52.216
0.008751	14.00	25989211	Prophenol oxidase activating factor 3	7	53.6	102.38
0.005683	11.01	33860163	Inducible metalloproteinase inhibitor protein	8	33.2	67.368
0.015931	10.84	4090964	Hdd1	9	14.4	102.23
0.007629	10.67	112702923	Peptidoglycan-recognition protein-LB	2	60.5	41.555
0.000281	10.67	112983994	Peptidoglycan recognition protein	13	57.9	306.89
0.017641	10.31	156254836	Serpin-2	8	23.6	91.985
0.000207	10.02	157704337	Hdd1	6	56.9	146.94
0.028818	7.68	148298796	Thioredoxin	5	21.8	48.041
0.007352	7.61	110649240	Gloverin	2	28.8	18.817
0.001212	7.40	112984088	Yellow-fb	7	23.7	84.78
0.013799	7.09	110347794	Gloverin-like protein	5	23.2	102.62

0.038579	7.07	189181680	Carboxylic ester hydrolase	8	49.1	138.97
0.005899	6.49	110826028	Esterase	3	8.1	32.225
0.008522	5.61	112983342	Tubulin beta chain	7	17.3	48.989
0.024206	4.91	112983414	Heat shock protein 21.4	5	15	80.094
0.019645	4.11	45594226	serpin-4B	3	36	26.047
0.014155	4.06	170578347	Immunoglobulin I-set domain containing protein	2	35.2	14.72
0.01201	4.00	39579195	Odorant-binding protein (Alt. pheromone binding protein 4)	3	8.9	21.382
0.000321	3.49	219552448	Arginine kinase	8	62.5	201.49
0.000429	3.40	158289805	AGAP010733-PA	12	38.1	130.56
0.000956	3.40	39579195	Odorant-binding protein (Alt. pheromone binding protein 4)	5	19.5	41.671
0.004217	2.97	73671225	Superoxide dismutase	3	57.8	312.25
0.000545	2.93	156968291	Uncharacterized protein	16	35.2	244.53
0.004998	2.72	162462783	Carboxylic ester hydrolase	17	30.4	323.31
0.013369	2.68	220902980	Carboxylic ester hydrolase	6	36.2	158.78
0.007705	2.57	27733415	Serpin 3a (Alt. Serpin 3b)	11	12.8	243.76
4.6E-05	2.55	189181680	Integument esterase 2 precursor	19	49.1	323.31
0.004825	2.47	52782700	Beta-1,3-glucan recognition protein	2	14.5	39.877
0.001052	2.45	15146043	Alpha-crystallin	8	30.9	136.8
0.013933	2.09	225031010	Tubulin alpha chain	3	46.2	26.541
0.006553	2.02	162462783	Heat shock protein 25.4	6	12	51.116
0.04006	1.62	169646838	heat shock protein 25.4 precursor	13	48	237.16
0.02193	1.59	239938036	Beta-galactosidase	20	33.5	323.31

Supplementary Table 7.6: Proteins which are decreased in abundance in *G. mellonella* larval haemolymph following infection with BCG *lux* (1x10^7 CFU) at 168 h post-infection relative to the 0 h control.

p value	Fold change (-)	GI Number	Protein name	Peptides	Sequence coverage [%]	Score
0.013035	47.43	158515746	Juvenile hormone binding protein	11	52.1	227.09
0.003962	29.23	229002332	Protein associated with transcription activator MBF2	3	14.5	114.37
0.021672	20.83	9087198	Fibrohexamerin	13	18.1	245.2

0.000215	11.23	164459610	Putative hydroxypyruvate isomerase	13	33.3	109.06
0.045961	9.58	46396271	27 kDa hemolymph protein	8	24.7	78.91
0.002178	9.14	121308868	Serine proteinase	9	25.4	96.748
0.005229	8.52	183979239	Similar to CG10638-PA	4	28.8	145.1
0.000253	7.70	112983816	GAPDH	8	38.8	67.248
0.000958	6.98	116791778	Uncharacterized protein	22	51.8	323.31
0.000725	4.60	46396271	27 kDa hemolymph protein	13	59.6	323.31
0.007426	3.96	77415676	Uncharacterized protein	15	32.2	323.31
0.012093	3.82	114052174	Aminoacylase	6	17.8	52.484
0.002862	3.76	18140733	Twelve cysteine protein 1	9	43.4	163.18
0.017969	3.42	182509208	Carboxylic ester hydrolase	11	39.8	86.532
0.001288	3.41	114051866	Isocitrate dehydrogenase	12	29.7	111.81
0.000103	2.98	158515746	Juvenile hormone binding protein	15	41.7	323.31
0.016866	2.90	114051325	Phosphoribosylaminoimidazole carboxylase	6	14.3	43.745
0.022998	2.68	156630460	Anionic antimicrobial peptide 2	8	32.9	323.31
0.010865	2.67	134103857	Cationic peptide CP8	6	29.2	323.31
0.035097	2.57	153791847	Nucleoside diphosphate kinase	10	51.7	67.351
0.019017	2.49	56462286	Putative protease inhibitor 4	6	23.2	137.05
0.003218	2.44	229002332	Hypothetical protein	5	22.1	106.19
0.003107	1.90	153791206	Scolexin	15	28.2	323.31
0.04044	1.89	170035237	Aliphatic nitrilase	13	42.3	234.5
0.002963	1.87	114050871	Carboxylesterase	24	62	323.31
0.010259	1.79	116782397	Uncharacterized protein	13	37.4	323.31
0.008458	1.78	237874122	Multicystatin and procathepsin F precursor	7	48.3	168.16
0.010043	1.75	70609810	Transferrin	58	55.1	323.31
0.024724	1.75	229002332	Hypothetical protein	8	52.2	122.75
0.034435	1.75	112983070	BCP inhibitor	6	21	323.31
0.046289	1.74	34921426	Serine protease inhibitor dipetalogastin (Dipetalin)	13	28.8	323.31
0.00101	1.68	2498144	Apolipophorins (Alt. Apolipophorin II/Apolipophorin I)	12	85.9	323.31
0.006845	1.61	183979392	Uncharacterized protein	29	56.3	323.31
0.001263	1.57	229002332	Uncharacterized protein	9	42.4	175.39
0.046218	1.51	116245495	General odorant-binding protein 68	12	44.1	172.16

Supplementary Table 7.7: BCG *lux* proteins detected in hemolymph over a 168 h time course.

LFQ Intensity Value				Uniprot Identifier	Protein Name
0 h	4 h BCG	48 h BCG	168 h BCG		
0	0	2.96E+08	0	A0A0H3MDY6	Diacylglycerol O-acyltransferase
0	0	8.89E+07	0	A0A0H3MBF9	Uncharacterized protein
0	0	8.04E+07	0	A0A0H3M719	Possible molybdopterin biosynthesis protein MoeW
0	0	2.31E+07	0	A0A0H3M8U8	Probable acyl-CoA dehydrogenase FadE23
0	0	1.33E+07	0	A1KPT4	Lysine--tRNA ligase
0	0	9.24E+06	0	A0A0H3MB41	Uncharacterized protein
0	6.46E+08	0	0	A0A0H3M2K9	Ribonuclease VapC (RNase VapC) (Toxin VapC)
0	3.98E+07	0	0	A0A0H3M9E6	Possible cell division transmembrane protein FtsK
0	2.94E+07	0	0	A1KFW3	2,3-bisphosphoglycerate-dependent phosphoglycerate mutase
0	1.56E+07	0	0	A0A0H3M591	Heat shock protein HspX
0	1.05E+07	0	0	A0A0H3MJ06	Diacylglycerol O-acyltransferase
0	8.85E+06	0	0	A1KNQ0	Adenosylhomocysteinase
0	5.96E+06	0	0	A0A0H3MEF1	Possible transmembrane protein
0	0	0	3.07E+09	A0A0G2Q9J3	DUF4143 domain-containing protein
			3.48E+08	A0A0H3M2D4	Possible conserved transmembrane protein

Supplementary Table 7.8: Proteins which are increased in abundance in *G. mellonella* larval haemolymph at 48 h post-immunisation with BCG *lux* (1x10^5 CFU) relative to the 0 h control.

p value	Fold Change	GI Number	Protein Name	Peptides	Sequence coverage [%]	Score
0.018523	25.69	23208535	Peptidoglycan recognition-like protein B	13	34	231.94
0.024315	13.81	15214063	Lysozyme (Alt. 1,4-beta-N-acetylmuramidase)	3	13.3	24.686
0.000471	9.28	112983052	Chemosensory protein 7 (Alt. Chemosensory protein11)	7	27.7	169.29
0.013977	8.74	116087	Cecropin-A (Alt. Cecropin-C)	1	8.5	9.783
0.00165	8.49	112984054	Yellow-d	18	44.7	323.31
0.002902	5.58	112983994	Peptidoglycan recognition protein	13	57.9	306.89
0.016571	4.11	186703381	Hemolin	7	50.7	323.31
0.024725	3.76	55139149	Hemolin	18	58	323.31
0.000594	2.49	124527	Insecticyanin-B (Alt. INS-b/Blue biliprotein)	9	44.7	323.31
0.004963	1.99	73671225	Superoxide dismutase	3	57.8	312.25
0.005084	1.80	170036627	Gelsolin (Alt. Gelsolin precursor)	22	35.8	323.31
0.046278	1.78	112983070	BCP inhibitor	6	21	323.31
0.018521	1.69	112983653	Bombyrin	9	25.8	323.31
0.00492	1.67	116245495	General odorant-binding protein 68	12	44.1	172.16
0.01396	1.58	85726208	Imaginal disc growth factor-like protein	14	59.6	323.31
0.008092	1.54	116782397	Uncharacterized protein	13	37.4	323.31

Supplementary Table 7.9: Proteins which are decreased in abundance in *G. mellonella* larval haemolymph at 48 h post-immunisation with BCG *lux* (1x10^5 CFU) relative to the 0 h control.

p value	Fold Change	GI Number	Protein Name	Peptides	Sequence coverage [%]	Score
0.000989	49.44	2498144	Apolipophorins (Alt. Apolipophorin II/Apolipophorin I)	3	22.1	21.829
0.033365	9.30	109119903	GAPDH	13	51.2	192.01
0.033417	9.18	9087198	Fibrohexamerin	13	18.1	245.2
0.010375	6.28	112983816	GAPDH	8	38.8	67.248
0.048224	6.17	182509208	Carboxylic ester hydrolase	11	39.8	86.532
0.02423	3.31	229002332	Uncharacterized protein	3	14.5	114.37
0.031538	3.15	91080563	alpha-N-acetylglucosaminidase isoform X2	5	11.6	57.332
0.039932	2.78	45553223	HDC11369	2	11.9	32.194
0.040995	2.58	162462783	Carboxylic ester hydrolase	5	33.4	155.29

0.004256	2.24	49532918	Cellular retinoic acid binding protein	13	31.5	106.16
0.022777	2.14	384243	arylphorin	20	57.1	323.31
0.000212	1.82	153791847	Nucleoside diphosphate kinase	10	51.7	67.351
0.017359	1.75	91084741	Apolipoprotein D-like Protein	13	38.7	323.31
0.004462	1.50	114052174	Aminoacylase	6	17.8	52.484

VIRULENCE
2018, VOL. 9, NO. 1, 1126–1137
https://doi.org/10.1080/21505594.2018.1491255

Taylor & Francis
Taylor & Francis Group

RESEARCH PAPER

OPEN ACCESS Check for updates

Galleria mellonella - a novel infection model for the *Mycobacterium tuberculosis* complex

Yanwen Li[a], John Spiropoulos[b], William Cooley[b], Jasmeet Singh Khara[a,c], Camilla A Gladstone[a], Masanori Asai[a], Janine T Bossé[a], Brian D Robertson[d], Sandra M Newton[a], and Paul R Langford[a]

[a]Section of Paediatric Infectious Diseases and Allergy, Department of Medicine, Imperial College London, London, UK; [b]Department of Pathology, Animal and Plant Health Agency, Addlestone, UK; [c]Department of Pharmacy, National University of Singapore, Singapore; [d]MRC Centre for Molecular Bacteriology and Infection, Department of Medicine, Imperial College London, London, UK

ABSTRACT

Animal models have long been used in tuberculosis research to understand disease pathogenesis and to evaluate novel vaccine candidates and anti-mycobacterial drugs. However, all have limitations and there is no single animal model which mimics all the aspects of mycobacterial pathogenesis seen in humans. Importantly mice, the most commonly used model, do not normally form granulomas, the hallmark of tuberculosis infection. Thus there is an urgent need for the development of new alternative *in vivo* models. The insect larvae, *Galleria mellonella* has been increasingly used as a successful, simple, widely available and cost-effective model to study microbial infections. Here we report for the first time that *G. mellonella* can be used as an infection model for members of the *Mycobacterium tuberculosis* complex. We demonstrate a dose-response for *G. mellonella* survival infected with different inocula of bioluminescent *Mycobacterium bovis* BCG *lux*, and demonstrate suppression of mycobacterial luminescence over 14 days. Histopathology staining and transmission electron microscopy of infected *G. mellonella* phagocytic haemocytes show internalization and aggregation of *M. bovis* BCG *lux* in granuloma-like structures, and increasing accumulation of lipid bodies within *M. bovis* BCG *lux* over time, characteristic of latent tuberculosis infection. Our results demonstrate *that G. mellonella* can act as a surrogate host to study the pathogenesis of mycobacterial infection and shed light on host-mycobacteria interactions, including latent tuberculosis infection.

ARTICLE HISTORY
Received 8 February 2018
Accepted 12 June 2018

KEYWORDS
Galleria mellonella; mycobacteria; tuberculosis; *Mycobacterium bovis* BCG *lux*; granuloma; infection model; haemocytes; host-pathogen interactions; *Mycobacterium tuberculosis* complex

Background

Mycobacterium tuberculosis is a highly successful human pathogen that currently infects a third of the world's population, causing 9 million new cases of tuberculosis and 1.5 million deaths annually [1]. The close association of tuberculosis with the human immunodeficiency virus (HIV) pandemic, and the rising problem of multi-drug and extreme drug resistance have created difficulties for tuberculosis control programs worldwide [2,3]. There is thus an urgent need for a greater understanding of host and *M. tuberculosis* interactions, improved vaccines to prevent infection, and novel therapies to shorten the duration of treatment and target latent tuberculosis infection (LTBI), however this has in part been hampered by the current inadequate, costly and time-consuming *in vivo* infection models for tuberculosis. Animal models currently used in tuberculosis research include non-human primates (e.g. macaques), guinea pigs, rabbits, cattle, pigs, mice and zebrafish [4]. However working with such animals is difficult as the pathogenesis and progression of *M. tuberculosis* infection is complex and there is no single animal model that mimics all the aspects of pathogenesis in humans [5,6]. Mice are the most commonly used species (because of cost, availability of inbred lines, reproducibility of infection and availability of immunological reagents) [7], but granulomas and regions of hypoxia characteristic of LTBI, are not commonly seen in the lungs and no single mouse tuberculosis model can reflect the mechanistically and morphologically diverse forms of human tuberculosis [8]. The animal models most closely resembling human *M. tuberculosis* infection are non-human primates e.g. the macaque [9,10]. However ethical, cost, and practical considerations limit widespread use [6]. To overcome these issues there is an urgent need for a rapid, well-characterized, low-cost, high-throughput model that mimics the key features of *M. tuberculosis* pathogenesis to further understand host-pathogen interactions, that can also be used to screen

CONTACT Sandra M Newton s.newton@imperial.ac.uk
Supplementary data for this article can be accessed here.

© 2018 The Author(s). Published by Informa UK Limited, trading as Taylor & Francis Group.
This is an Open Access article distributed under the terms of the Creative Commons Attribution License (http://creativecommons.org/licenses/by/4.0/), which permits unrestricted use, distribution, and reproduction in any medium, provided the original work is properly cited.

novel drug candidates and assess the efficacy of vaccine candidates in early stage development.

Galleria mellonella insect larvae have increasingly been used as a surrogate to study host-pathogen interactions in a range of micro-organisms including Gram-positive and Gram-negative bacteria and fungi [11–14], and as a rapid model to screen novel antimicrobial drug candidates [15]. *G. mellonella* has a wide range of advantages that have made it a successful infection model. These include its sophisticated innate immune system, comprised of cellular and humoral defenses, that shares a high degree of structural and functional similarity to that of vertebrates [16,17], and its ability to discriminate between bacterial and fungal pathogens as identified by the repertoire of immune defense peptides [18]. *G. mellonella* are also easy to manipulate due to their large size (2–3 cm), allowing easy infection and collection of tissue/haemolymph for analysis. They are easy to maintain at 37°C making them well-suited to studying human pathogens, and precise infection studies can be performed by injection without anaesthesia for testing the efficacy of small quantities of antimicrobial agents. In addition, *G. mellonella* are ethically more acceptable than the use of vertebrates meaning larger group sizes can be used to enhance reproducibility [11,15,19,20].

Here we report the use of *G. mellonella* as a novel infection model for members of the *M. tuberculosis*-complex. Due to safety and practical considerations when using *M. tuberculosis* as an experimental organism, we have carried out this study using the non-pathogenic, luminescent reporter vaccine strain, *M. bovis* BCG *lux* [21], which has been well characterized and validated in a wide range of *in vitro* and *in vivo* models and clinical studies (e.g. liquid broth, human whole blood and cells, mouse) and has the advantage of faster measurement of mycobacterial viability [22–32]. Over a time-course we have assessed the survival of *G. mellonella* larvae in response to infection with different inocula of *M. bovis* BCG *lux*, and monitored the survival of *M. bovis* BCG *lux* by measuring bioluminescence and correlating with CFU. Furthermore we have undertaken histopathology staining and transmission electron microscopy (TEM) analysis of *M. bovis* BCG *lux* infected *G. mellonella* to look at bacteria inside phagocytic haemocytes and study the pathogenesis and progression of mycobacterial infection. Our results demonstrate that this mycobacteria-*G. mellonella* infection model can be used to study mycobacterial pathogenesis, particularly in the context of granuloma formation, and has the potential to be used in the assessment of novel vaccine candidates and anti-mycobacterial agents. The availability of this novel mycobacterial infection model also has the potential to significantly reduce the number of experimental animals used in some areas of tuberculosis research.

Results

Survival analysis of G. mellonella following infection with M. bovis BCG lux

G. mellonella survival (n = ≥ 10 per group), in response to differing inocula of *M. bovis* BCG *lux* infection (up to 2×10^7 CFU per larva) was determined over a 96 h period. Larvae that did not show any movement in response to touch were considered dead.

G. mellonella, infected with doses of 1×10^5 or 1×10^6 CFU *M. bovis* BCG *lux*, survived 100% (Figure 1 and Supplementary Table 1) as did the 'pricked' (empty needle injection) and 'uninfected' (PBS-Tween 80) control

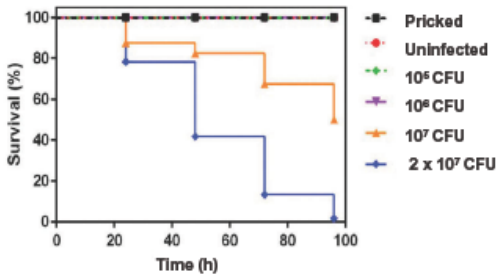


Figure 1. Effect of varying inoculum dose of *M. bovis* BCG *lux* on the survival of *G. mellonella* larvae following incubation at 37°C for 96 h. Healthy larva (n = ≥ 10 per group) infected with differing inocula of *M, bovis* BCG *lux* (up to 2×10^7 CFU per larva), were examined for survival by response to touch at 24 h intervals over a period of 96 h. Control groups (n = 10 larvae per group) included an uninfected group inoculated with 10 µl PBS-Tween 80, and a 'pricked' larval group (empty needle injection). Larvae were incubated at 37°C in the dark and monitored on a daily basis. Larvae that did not show any movement in response to touch were considered dead. Data are pooled from at least two independent experiments with a minimum of 10 larvae per group per run.

groups. This demonstrated that neither the needle injection nor the 0.05% Tween 80 used to prevent mycobacterial clumping, had any effect on *G. mellonella* survival. At higher doses of *M. bovis* BCG *lux* (1×10^7 and 2×10^7 CFU), a concentration-dependent effect on survival was observed. 50% *G. mellonella* survival was observed using a dose of 1×10^7 CFU *M. bovis* BCG *lux* per larva at 96 h, however there was less than 1% survival using a dose of 2×10^7 CFU per larva at this time-point. A time period of 96 h was used to measure larval survival, as at approximately 1 week of incubation at 37 C some of the larva in the 'pricked' and 'uninfected' groups started to pupate as they entered the next stage of the life cycle. Other observations of mycobacterial infected larvae compared to uninfected larvae over time, were a slight darkening in color and reduced flexibility and size, characteristic of the organism wasting.

M. bovis BCG lux survival in *G. mellonella* over time

The survival of *M. bovis* BCG *lux* (dose, 1×10^7 CFU) within *G. mellonella* was determined over a 2 week time-course to further validate *G. mellonella* as an infection model for mycobacteria. Here we investigated the recovery of *M. bovis* BCG *lux* by luminescence measurement over time (0, 24, 48, 72, 96, 168 and 366 h) from homogenized larvae (n = 5 per time-point) to assess the ability of the immune system of *G. mellonella* to control mycobacterial growth. Only live, non-melanized larvae were used for homogenization.

When *G. mellonella* were inoculated with a dose of 1×10^7 CFU per larva there was approximately a 1 log reduction in *M. bovis* BCG *lux* luminescence between 0 and 168 h, with a further steady decrease in bacterial numbers until the end of the time-course at 366 h (Figure 2). When we measured live *G. mellonella* uninfected crude extracts for background luminescence, very low levels were detected ranging from 5000–8000 RLU/ml indicating this did not have any impact on mycobacterial luminescence.

In addition to the luminescence measurement of mycobacteria, we also plated homogenized samples (n = 4 larva per time-point) for CFU quantification at the corresponding time-points up to 168 h on to Middlebrook 7H11 agar, containing hygromycin as an antibiotic selection marker and piperacillin which inhibited the growth of contaminating *G. mellonella* bacterial flora. Contamination from the normal bacterial flora of *G. mellonella* has been observed in other studies [33,34] but a recent paper by Entwistle & Coote [35] demonstrated that the antibiotic piperacillin was able to inhibit *G. mellonella* contaminating bacterial flora but did not inhibit the growth of non-tuberculous mycobacteria. We undertook a minimum inhibitory concentration (MIC) assay to assess the inhibitory concentration of piperacillin against *M. bovis* BCG *lux* at doubling concentrations ranging from 1280 – 10 μg/ml. The MIC of piperacillin against *M. bovis* BCG *lux* was 160 μg/ml. A concentration of 10 μg/ml was found to inhibit the growth of contaminating *G. mellonella* bacterial flora and hence was added to agar plates for *M.*

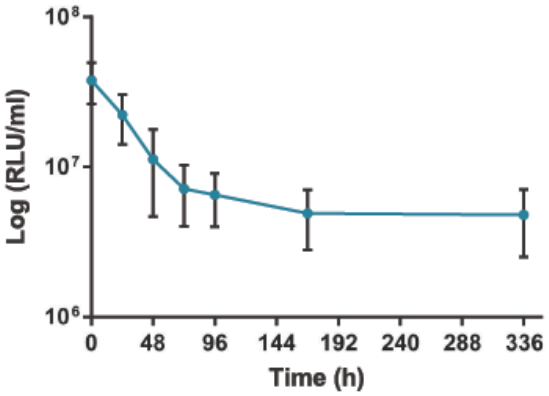


Figure 2. Recovery of *M. bovis* BCG *lux* (dose 1×10^7 CFU per larva) by luminescence measurement (RLU/ml) over a 2 week time-course from homogenized infected larvae. At least 30 larvae were infected with 10 μl of 1×10^7 CFU *M. bovis* BCG *lux*. The survival of *M. bovis* BCG *lux* within live *G. mellonella* was determined by luminescence measurement over time (24, 48, 72, 96, 168, 366 h) from the lysates of 5 homogenized larvae to assess the ability of the immune system of *G. mellonella* to control mycobacterial growth. Data are pooled from three independent experiments with 5 larvae per time-point per run. Error bars show standard deviation of the mean.

bovis BCG *lux* CFU quantification. We found that the RLU:CFU ratio was consistent over the time-course with an average ratio of 4:1 (range 2:1 to 5:1) (data not shown).

Histopathological analysis of M. bovis BCG lux infection of G. mellonella larvae

Granulomas in the human host, are highly dynamic and characteristic cellular structures that are the hallmark of tuberculosis and not only contain and control infection but also provide a niche for mycobacteria to survive. However, not all animal models form such structures in response to mycobacterial infection.

G. mellonella has an innate immune system comprised of cellular and humoral defenses including phagocytosis of pathogens by haemocytes (a similar cell type to human macrophages and neutrophils) [36] and the production of antimicrobial peptides, complement-like proteins and reactive oxygen and nitrogen species for killing ingested pathogens, all found within the haemolymph of *G. mellonella* [16]. Here we undertook both histopathology and TEM to follow the progression of *M. bovis* BCG *lux* infection, assess the impact of infection on larval tissues and determine whether granulomas are induced in this model of infection.

Histopathology analysis of sectioned larvae infected with *M. bovis* BCG *lux*, and stained using both H&E and ZN (acid-fast), demonstrated that at 24 h post-challenge, rod-shaped acid-fast bacilli (stained pink) were visible and many were co-localized with host cells (stained blue) (Figure 3(A)), presumably haemocytes. We also observed isolation and compartmentalization of bacilli within granuloma-like structures (Figure 3(B-D)). At 48 h post-challenge acid-fast amorphous material began to appear, most likely representing the by-product of destroyed acid-fast bacteria (Figure 3(D)). At subsequent time-points the acid-fast amorphous material within the granuloma-like structures increased, whilst individual bacilli were observed less frequently. By 168 h, the amorphous acid-fast material was the main structure associated with the granuloma-like structures, although occasionally a small number of individual bacilli were also observed (Figure 3(E)). Staining serial sections with H&E demonstrated that the bacilli in the granuloma-like structures were co-localized with host cells (Figure 3(F,G)). In the center of the granuloma-like structures necrotic host cells were evident (Figure 3(F-H)) and in some cases brown pigmented material which co-localized with the amorphous acid-fast material was detected (Figure 3(H)). Although using histology it was not possible to demonstrate that the bacilli were internalized, haemolymph smears stained with ZN appeared to demonstrate intracellular location of *M. bovis* BCG *lux* bacilli in individual host cells (Figure 3(I)) and in cell aggregates (Figure 3(J)), which have the appearance of granuloma-like structures. These structures were located in the haemocoel presumably surrounded by haemolymph, which was not possible to demonstrate in histological sections. Sometimes the granulomas were in contact with the fat body and infrequently with other internal organs (Figure 3(K, L)). No ZN positive bacilli were identified in uninfected (pricked) larvae or in larvae challenged with PBS (Supplementary Figure 1).

Phagocytosis of M. bovis BCG lux infected haemocytes in vivo

To assess phagocytosis of *M. bovis* BCG *lux* (dose 1×10^7 CFU) by *G. mellonella* haemocytes over a time-course of 2 weeks, TEM was undertaken on haemolymph samples extracted from infected *G. mellonella* (n = 3) at 24, 48, 72, 96, 144 and 366 h post-infection. Both *M. bovis* BCG *lux* inoculum (A) and uninfected *G. mellonella* at 96 h (n = 3) (Supplementary Figure 2(A)) served as controls. TEM (Figure 4), over the time-course, identified ultrastructurally internalized *M. bovis* BCG *lux* into cells from 24 h (Figure 4(B-H)). From 24 h to 366 h, aggregations of bacilli, typical of that found in granulomas was evident. TEM was able to confirm the histopathological findings suggesting that bacteria invade or are phagocytosed by haemocytes and multiply within to form aggregate-like structures. An increase in lipid material within *M. bovis* BCG *lux* during the time-course was also observed. Images of uninfected haemocytes, compared to *M. bovis* BCG *lux* infected haemocytes, at 96 h post-infection are shown in Supplementary Figure 2(A-B).

Discussion

The use of invertebrates, such as *Caenorhabditis elegans*, *Drosophila melanogaster* and *G. mellonella*, as models for infection studies have been widely reported as they are considerably cheaper, ethically less contentious than mammals, and although insects lack an acquired immune system they do possess a complex innate immune system [37]. Furthermore *D. melanogaster* has been used as an infection model for *M. abscessus* and *M. marinum*, particularly to study the pathogenesis and metabolic consequences of mycobacterial infection [38–41]. The larvae of *G. mellonella* have been widely used to study host-pathogen interactions for a range of microbes, including fungi, bacteria

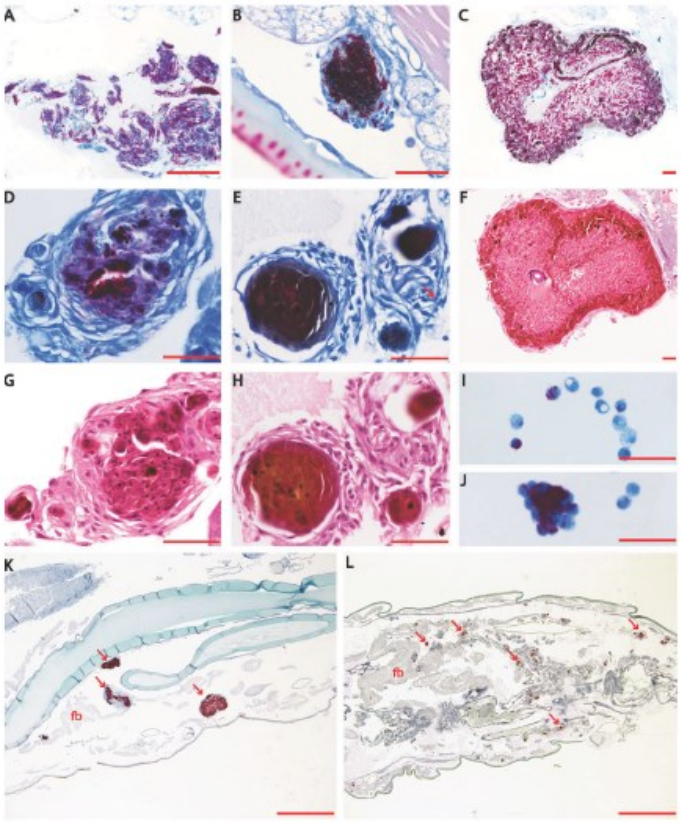


Figure 3. Histopathological analysis of *M. bovis* BCG *lux* infection of *G. mellonella* larvae (1×10^7 CFU per larva) over a time-course of 2 weeks. Both *M. bovis* BCG *lux* infected and uninfected (pricked and PBS challenged) larvae (n = 3 per group) were fixed by injecting 100 µl of buffered formalin with an insulin syringe in to the last left pro-leg at each time-point (0, 24, 48, 72, 96 h for uninfected and infected larvae, and additional time-points of 144 and 336 h were also included for infected larvae). Samples were embedded in paraffin wax, sectioned at 4 µm and then stained with haematoxylin and eosin (H&E) and Ziehl-Neelsen (ZN) stain for acid fast bacteria. Individual bacilli are discernible arranged loosely (A, 24 h post challenge) or organized in early granuloma-like structures (B, 24 h post challenge). Large well-defined granuloma-like structure containing individual bacilli (C, 72 h post challenge) and a granuloma-like structure (D, 96 h post challenge) with individual bacilli and amorphous acid fast-material (arrow). At subsequent stages of infection the acid fast material within the granuloma like structures was predominantly amorphous (E, 366 h post challenge) although individual bacilli may still be detected (arrow). Within the granuloma-like structures host cells are undergoing necrosis (F-H) and brown pigment may be associated with the necrotic areas (H). Haemolymph smears show that the bacilli are co-localized with individual cells (I) or cell aggregates (J) which most likely represent granuloma-like structures. Sections K and L (72 and 144 h post infection respectively) provide lower magnification images showing that the granulomas are dispersed in the haemocoel and they can be associated with the fat body (arrows indicate some characteristic granulomas). In Section K, the granulomas are similar to the ones shown in Sections B and C where individual bacilli can be identified. In Section L the granulomas are similar to the compact granulomas shown in Section E. Sections A-E, K, L, and smears I and J are stained with ZN. Sections F-H are stained with H&E and demonstrate the same structures shown in C-E respectively in adjacent planes (serial sections). Scale bar in images A-J represents 50 µm; in images K and L it represents 1000 µm; fb, fat body.

and viruses [11–13,42–45], but little has been reported using mycobacteria [35,46–48], for which new *in vivo* infection models are greatly needed. Here we have demonstrated that this simple invertebrate model shows promise as a novel infection model for the *M. tuberculosis* complex.

Over 1000 articles have been published on the use of *G. mellonella* as a surrogate host infection model for

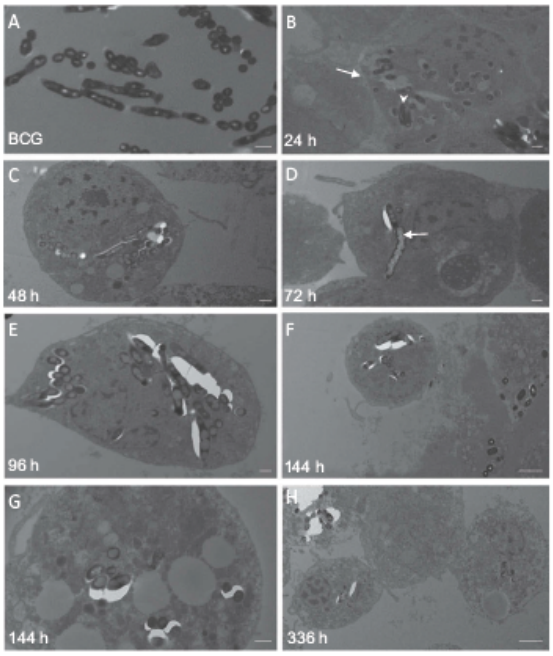


Figure 4. Transmission electron microscopy (TEM) of *M. bovis* BCG *lux* infected haemocytes (dose 1×10^7 CFU per larva) *in vivo from G. mellonella* over a time-course from 24 h to 336 h. Haemolymph was extracted from the haemocoel of *G. mellonella* (n = 10) at 24 h intervals post-infection by puncturing the larvae in the last left pro-leg using a sterile needle. Haemolymph was pooled, processed and analyzed using a Tecnai bioTWIN transmission electron microscope. *M. bovis* BCG *lux* inoculum alone served as a control (A). Further figures (B-H) show the haemolymph contains haemocytes (arrow, B) and the time-course study showed the ultrastructure of initial internalization of BCG *lux* into cells at 24 h (arrowhead, B). From 24 h to 366 h, aggregation of bacilli, typical to that found in granulomas was evident. TEM confirmed that over the time-course the bacteria invade or are phagocytosed by haemocytes and multiply within to form aggregations of bacilli, typical of those found in granulomas. There is also an increase in lipid material within *M. bovis* BCG *lux* during the time-course (arrow, D). Scale bar represents 500 nm (A-E, G) and 2 µm (F, H).

studying the pathogenesis of micro-organisms, with more than 200 publications in 2014–2015 alone [15]. Advantages of using this insect larva include, no ethical implications, wide availability of larvae from commercial suppliers, low cost, simple housing and easy maintenance at 37°C, which also mimics the human host, large size (20–30 mm) allowing easy manipulation without the need for anaesthesia, precision injection into the haemocel through the last pro-leg, and the availability of host tissue/haemolymph for experimental analysis [11,15,19,20]. In addition, a good correlation has been established between the pathogenicity of several micro-organisms in *G. mellonella* with vertebrate models of infection [49]. Moreover, *G. mellonella* has an innate immune system, comprised of cellular and humoral defenses, that share a high degree of structural and functional similarity to that of vertebrates [16], and has been shown to discriminate between bacterial and fungal pathogens as judged by the repertoire of immune defense peptides [18]. A transcriptomic study of *G. mellonella* larvae found a large repertoire of immune effectors, many shared with mammals [50]. Hence bacteria can elicit an immune response in *G. mellonella* that is species-specific and is attractive for studying the pathogenesis of micro-organisms. This model also has the benefits of allowing infection experiments to be undertaken in a controlled manner with precise time-course measurements, analysis of changes in host-pathogen transcriptome, proteome and biochemistry, and far greater group sizes and numbers of replicates (n = 20 minimum per group) compared to animal studies (e.g. mouse n = 5 per group), enhancing reproducibility.

In this study we set out to evaluate the use of *G. mellonella* as an infection model for *M. bovis* BCG *lux*, a luminescent derivative of the vaccine strain that has

the advantages of faster measurement of mycobacterial viability (luminescence requires co-factors only found in living metabolically active cells) compared to the slow growing *M. tuberculosis* with a doubling time of approximately 24 h [21,22,24]. Additionally, *M. bovis* BCG *lux* requires containment level (CL) 2, rather than CL3 laboratories. This organism has been very well-characterized and utilized in a wide range of clinical and non-clinical studies [21,24,27–32,51]. For example, differences in *M. bovis* BCG *lux* RLU measurements have been shown to reflect changes in the immune response in human whole blood and cellular models, including differences between tuberculin-positive and -negative individuals [23], changes induced by HIV infection and following antiretroviral treatment [25,26], changes in mycobacterial growth limitation induced by vaccines [24] and Vitamin D supplementation *in vitro* and in a clinical trial [29–31], and differences in gene expression in immune biological pathways compared to *M. tuberculosis* [32]. In addition we have also evaluated luminescent mycobacteria in the mouse model [27]. Hence the use of *M. bovis* BCG *lux* in *in vivo* studies as a model organism for *M. tuberculosis* lends further benefit to *in vivo* assays using *G. mellonella*.

To characterize the infection model we first assessed the virulence of *M. bovis* BCG *lux* in *G. mellonella* using a range of doses, and determined survival of both host and mycobacteria over a 96 h time-course of infection. All *G. mellonella* survived at infection doses of 1×10^5 and 1×10^6 CFU of *M. bovis* BCG *lux*, whereas at higher doses a concentration-dependent effect was observed. A dose of 1×10^7 CFU was therefore selected for further time-kill, histopathology and TEM studies and would be suitable for testing drug treatments using this model.

The observation of 'wasting' in mycobacteria infected larvae, compared to uninfected, is consistent with the clinical feature of tuberculosis in humans and animals and warrants further investigation. This has also been described by Dionne and Schnieder in the *D. melanogaster* model of *M. marinum* infection [39].

Due to differences between bacterial species, strains, growth rates, pathogenicity and inocula used to infect *G. mellonella* and also time-points for larval survival measurements, comparing larval survival between bacterial species is difficult with, ideally, side by side experiments under the same conditions being carried out. However, at the 96 h time point with an equivalent dose of 1×10^7 CFU of *M. bovis* BCG *lux* or *M. fortuitum* NCTC 10394 [35], 50% and no larvae respectively, survived. Comparative survival may reflect differences in the mechanism(s) of pathogenicity or that *M. fortuitum* NCTC 10394 is a faster growing species.

We also assessed survival of *M. bovis* BCG *lux* over time-course of 366 h using a dose of 1×10^7 CFU per larva and observed approximately a 1 log reduction in luminescence between time-points 0 and 168 h post-infection which continued to steadily decrease until the end of the time-course, indicating persistent viable mycobacterial infection. Whilst *G. mellonella* larvae do not possess an adaptive immune system they do display an innate immune system similar to humans with many analogous functions including, phagocytosis of pathogens by haemocytes [17,34,52–54], a similar cell type to human macrophages and neutrophils [36]. They also produce antimicrobial peptides, complement-like proteins and reactive oxygen and nitrogen species for killing ingested pathogens, all found within the haemolymph, a biological fluid similar to mammalian blood [15,16,18]. We speculate that death of infected larvae with higher *M. bovis* BCG *lux* doses (10^7 and 10^6 CFU per larvae) occurs despite no increase in mycobacterial growth, as a result of an overwhelming *G. mellonella* immune response at the site of infection. Further investigation of the molecular and functional immune mechanisms and specific cells involved in suppression of mycobacterial luminescence will be the subject of future work.

Luminescence measurement has been shown to be a measure of mycobacterial metabolic activity, related to viability [21,22,24,33]. We also isolated and enumerated mycobacterial CFU from infected *G. mellonella* at the same respective time-points as luminescence measurements up to 168 h to determine the correlation between RLU and CFU in the *G. mellonella* model. *G. mellonella* homogenized larvae were plated on to Middlebrook 7H11 agar, specific for mycobacterial growth, incorporating hygromycin as an antibiotic selection marker for the *lux* reporter and piperacillin to inhibit the growth of contaminating bacterial flora from *G. mellonella*. We found the MIC of piperacillin against *M. bovis* BCG *lux* to be 160 μg/ml and whilst inhibiting the growth of *G. melonella* bacterial flora, it did not inhibit the growth of *M. bovis* BCG *lux* at the concentration used (10 μg/ml). We found that the RLU: CFU ratio for *M. bovis* BCG *lux* correlated well at each time-point over the time-course with an average RLU: CFU ratio of 4:1 which is also consistent with the RLU: CFU 3:1 ratio in liquid broth culture. These findings highlight that although luminescence is a measure of metabolic activity in *M. bovis* BCG *lux*, it correlates with CFU *in vivo* in the *G. mellonella* model over time and further highlights the benefit of using this luminescent reporter organism.

Similarly the experiments of Meir *et al.* [48] showed that there was correlation between *lux* RLU and CFU with the fast growing non-tuberculous *M. abscessus* in the background of *G. mellonella*, as has also been shown with other bacteria e.g. *Enterococcus faecalis* [55].

The hallmark of tuberculosis infection in humans is the granuloma; a highly organized and dynamic cellular structure where mycobacteria reside in a non-replicating dormant state known as LTBI [6]. Several types can be found in humans including the caseous, non-necrotizing, and fibrotic granulomas [56]. However studying mechanisms underlying latency and reactivation of tuberculosis is hampered by the limitations of current animal models [57]. Furthermore the design of new drugs which penetrate granulomas to target LTBI in particular, is an urgent priority for any treatment control program [58]. Recently the zebrafish tuberculosis model, using *M. marinum*, has been used to mimic aspects of LTBI due to its small size, rapid reproduction, formation of granulomas and advanced genetic tools, making it a suitable animal model for large-scale screening of novel therapeutic agents in early-stage preclinical studies. However, zebrafish are anatomically and physiologically different to humans and lack the clinical manifestations and symptoms of tuberculosis disease and moreover they cannot be infected with the pathogenic human strain *M. tuberculosis* [4,59–62].

Granuloma-like structure formation in *G. mellonella* has been shown for the pathogenic fungal infections *Paracoccidioides lutzii* and *Histoplasma capsulatum* [34]. Hence, we undertook both histopathology staining and TEM to visually assess the progression of infection and examine the changes in host tissue and induction of granuloma-like formations in response to infection. Our data show that *M. bovis* BCG *lux* challenged larvae induce granuloma-like structures to sequester the bacteria as early as 24 h following infection, and inside these formations the bacilli lose their characteristic morphology forming amorphous acid-fast bodies by 48 h. Analysis of infected phagocytic haemocytes, extracted from *G. mellonella* larvae, show internalization and aggregation of *M. bovis* BCG *lux* in granuloma-like structures, with increasing accumulation of lipid bodies within *M. bovis* BCG *lux* over time. The accumulation of lipid bodies, in the form of triacylglycerides (TAGs), is evident in *M. tuberculosis* residing within lipid-rich foamy macrophages in human granulomas [63,64], and is proposed to serve as a source of carbon and energy representing a hallmark of persistent and non-dividing mycobacteria, labelled the drug tolerant, 'fat and lazy' bacilli [63,65]. It is therefore no surprise using this infection model, that mycobacteria are highly likely sourcing lipid rich material within their granuloma-like structures from their fatty *G. mellonella* host. These granuloma-like structures are formed in response to challenge with *M. bovis* BCG *lux*, which is an attenuated *M. bovis* strain. It would be of significant interest to study the response of *G. melonella* larvae to pathogenic mycobacterium (e.g. *M. tuberculosis, M. bovis*) as the vast majority of data in mammals derives from exposure to these species.

Whilst further investigation is required into the nature and composition of both the granuloma-like structures formed in response to *M. bovis* BCG *lux* infection, and the intracellular mycobacterial lipid bodies, our results are highly encouraging that *G. mellonella* represent an organism capable of forming such pathological features of tuberculosis, which are highly desirable for a novel tuberculosis infection model. In addition a range of mycobacterial strains, mutants classes (e.g. lipids, metabolism, persistence, stress) and reporters (e.g. luminesence and fluorescence), to assess host-pathogen interactions and characterize mechanisms of pathogenicity, could be used in this model.

In summary, this is, to our knowledge, the first report of *G. mellonella* larvae being used as a suitable infection model for a member of the *M. tuberculosis*-complex. Importantly we show that *G. mellonella* replicates features of the pathogenesis of tuberculosis through the induction of granuloma–like structures characteristic of LTBI, and the inclusion of lipid bodies within mycobacteria over time, characteristic of persistent infection. Further evaluation of this model has the potential to markedly reduce the use of more expensive and time-consuming animal models for evaluating mycobacterial host pathogenicity, the toxicity and efficacy of novel anti-mycobacterial agents and novel vaccine candidates *in vivo* [66]. The characterization and optimization of this model with both non-pathogenic, and pathogenic drug-sensitive and drug-resistant *M. tuberculosis* isolates will form the basis of future studies.

Materials and methods

M. bovis BCG lux growth conditions

M. bovis BCG *lux* (Montreal vaccine strain) was a kind gift from Professor Young's lab (Imperial College London), transformed with the luminescent reporter plasmid construct pSMT1 carrying the *luxAB* genes from *Vibrio harveyi* [21]. *M. bovis* BCG *lux* were grown shaking at 220 rpm and 37°C until mid-log phase in Middlebrook 7H9 broth (Difco, MI) medium containing 0.2% glycerol (Sigma-Aldrich), 0.05%

Tween 80 (Sigma-Aldrich), 10% ADC enrichment (Difco, MI) and 50 μg/ml hygromycin (Roche) as an antibiotic selection marker. Frozen aliquots were prepared in 15% glycerol and stored at −80°C until further use. Mycobacterial colony forming unit enumeration (CFU)/ml was determined by serial dilution on 7H11 agar (Difco, Detroit, MI) containing 0.5% glycerol, 10% oleic acid-albumin-dextrose-catalase (Difco, MI) enrichment and 50 μg/ml hygromycin. *M. bovis* BCG *lux* luminescence was measured after addition of decanal (Sigma) substrate (1% v/v in ethanol), as relative light units (RLU)/ml in a luminometer (Berthold Technologies) and correlated with CFU/ml counts. A ratio of 3 RLU correlated to 1 CFU in liquid broth culture as previously described [22].

Optimization and preparation of M. bovis BCG lux inoculum

Prior to infection experiments, a vial of mycobacteria was defrosted and grown in liquid medium (as described above) to mid-log phase for 72 h with *M. bovis* BCG *lux* growth monitored by luminescent measurements on a daily basis [22]. Cultures were centrifuged at 3880 g for 10 minutes, supernatant decanted and the cell pellet was resuspended in phosphate buffered saline (PBS) (Sigma-Aldrich) containing 0.05% (v \v) Tween 80 (PBS-Tween 80) and washed a further twice. PBS-Tween 80 was found to prevent mycobacterial clumping particularly when achieving dense concentrations of mycobacterial inoculum (e.g. 10^9 RLU/ml). The washed cell pellet was diluted in PBS-Tween 80 and the required mycobacterial inoculum measured by luminescence, resulting in a homogenous suspension. The inoculum dose was verified by plating on to Middlebrook 7H11 agar.

In vivo virulence assays of G. mellonella infected with M. bovis BCG lux

Final instar larvae of *G. mellonella* were obtained from Livefoods Direct Ltd, Sheffield, UK and stored in wood shavings in the dark at 19°C. Healthy larvae were identified by their cream colour, without dark discolouration, the ability to right themselves if turned on their backs, a body weight of approximately 250 mg and body length of 2–3 cm, and were used in infection experiments within 3 days of delivery. For experimental use healthy larvae were counted into 25 cm Petri dishes containing a layer of filter paper. Once selected, no food was made available. Larvae displaying signs of death (no movement when touched) were discarded along with those undergoing pupation.

Prior to each experiment, larvae were surface disinfected with ethanol, and at least 10 larvae per group were injected with 10 μl of a *M. bovis* BCG *lux* suspension in PBS-Tween 80. Doses, between 1×10^5 and 2×10^7 CFU, were injected via the last left pro-leg into the haemocoel using a SGE 25 μl microvolume syringe. Control groups (n = 10 larvae) included an uninfected group inoculated with 10 μl PBS-Tween 80, and a 'pricked' larval group (empty needle injection). Larvae were maintained in petri dishes containing a base layer of filter paper at 37°C in the dark. All larvae were monitored on a daily basis and melanization and survival were recorded. Larvae that did not show any movement in response to touch were considered dead. Data are pooled from at least two independent experiments with a minimum of 10 larvae per run. Kaplan-Meier survival curves of *G. mellonella* in response to pricked, uninfected and *M. bovis* BCG *lux* infection were plotted to display percentage survival over time.

Recovery of M. bovis BCG lux from G. mellonella over time

At least 30 larvae were infected with a 10 μl dose of 1×10^7 CFU as described above. At 24, 48, 72, 96, 168 and 366 h, five live larvae per time-point (no melanization) were disinfected by wiping down with 70% ethanol and homogenized in PBS-Tween 80 using a FastPrep-24 5G (MP Biomedicals) with sterile metal beads. Mycobacterial luminescence (RLU/ml) was measured in the homogenized lysate as described above. The mean RLU/ml of *M. bovis* BCG *lux* survival in *G. mellonella* was determined over 366 h. In addition, CFU enumeration was also determined in homogenized lysate by plating serial dilutions in duplicate on to Middlebrook 7H11 agar plates containing 50 μg/ml hygromycin as an antibiotic selection marker and 10 μg/ml piperacillin (Sigma) to inhibit the growth of *G. mellonella* bacterial flora. The mean CFU/ml of *M. bovis* BCG *lux* survival in *G. mellonella* was determined at each time-point over 168 h.

To determine CFU enumeration of the inoculating *M. bovis* BCG *lux*, 100 μl of mycobacterial inoculum was plated on to Middlebrook 7H11 agar plates, containing 50 μg hygromycin.

Minimum inhibitory concentration (MIC) assay of piperacillin

The MIC of piperacillin was determined against *M. bovis* BCG *lux*. Two-fold serial dilutions of piperacillin ranging from 1280 to 10 μg/ml were prepared in Middlebrook 7H9 broth and 100 μl of each concentration was combined with an equal volume of log-phase mycobacterial culture diluted to ~ 10^6 CFU/ml in a 96

well plate. Growth media containing mycobacteria only was used as the positive control and growth media alone as the negative control. For each concentration and control was performed in triplicate. Plates were incubated in a rocking incubator at 20 rpm at 37°C for 7 days. The MIC was defined as the lowest concentration at which no mycobacterial growth was observed visually or spectrophotometrically using a plate reader (Molecular Devices, UK) at an optical density 595 nm. Each MIC experiment was performed in triplicate.

To determine the concentration of piperacillin required to inhibit the growth of *G. mellonella* bacterial flora, 50 µl homogenized larvae (n = 5 larva) was plated on to Middlebrook 7H11 agar plates containing a range of concentrations of piperacillin (10, 20, 40 µg/ml). Agar plates without piperacillin were used as the positive control. Plates were incubated at 37°C for up to 2 weeks to check for growth of *G. mellonella* bacterial flora.

Time course, histopathology and transmission electron microscopy (TEM) analysis of M. bovis BCG lux recovered from G. mellonella

The time-course study was undertaken to investigate the progress of *M. bovis* BCG *lux* infection (dose 1×10^7 CFU) within *G. mellonella* infected larvae, and assess the impact of infection on *G. mellonella* internal tissue. Three larvae per time-point per group were used for histopathology analysis and at least ten larvae per time-point for TEM. The time-course ran for 96 h post-infection, with time-points at 0 h and then every 24 h intervals. In addition, some infected larvae were sacrificed and processed at 144 h and 336 h after inoculation.

For histopathological analysis, infected and uninfected (control group) larvae were fixed by injecting 100 µl of buffered formalin with an insulin syringe into the last left proleg. Larvae were kept in 40 ml formalin at room temperature. Subsequently, each larva was cut into two parts along the midline. Both parts were kept and processed for histology (Sakura Tissue-Tek VIP), embedded in paraffin wax (Thermo Scientific HistoStar embedding center), sectioned at 4 µm using a Leica RM2135 microtome, and then stained with haematoxylin and eosin (H&E), and Ziehl-Neelsen (ZN) stain, a specific stain for acid fast bacteria. The tissue slides were examined under a light microscope (Nikon Eclipse 80i) and photographed using a digital camera (Nikon DS-Ri1) attached to a computer equipped with NIS-Elements BR imaging software.

For TEM, at least 10 larvae per time-point (0, 24, 48, 72, 96, 144, 366 h) per group were used for haemolymph extraction. Haemolymph was collected from the haemocoel by puncturing the larvae in the last left proleg using a sterile needle. Haemolymph was carefully squeezed out of the larvae by applying gentle pressure, pooled into 50 ml of 1% formaldehyde and kept at room temperature for 2 h. Cells were then centrifuged and the cell pellet was re-suspended in 4% glutaraldehyde buffer and stored at 2–8C. An aliquot of the cells was then placed onto positively charged slides for ZN staining. The remaining cells were post-fixed with 1% osmium tetroxide (OsO4). After dehydration and embedding of the samples, ultra-thin (70–90 nm) sections were mounted on to grids and stained with uranyl acetate (0.5% w/v) and lead citrate (3% w/v) prior to examination using a Tecnai bioTWIN transmission electron microscope.

Acknowledgments

We thank Mr Tony Strickland for histological processing and staining of the specimens and Mr David Everest for preparation of the TEM samples.

Disclosure statement

No potential conflict of interest was reported by the authors.

Funding

This work was supported by grants from the Biotechnology and Biological Sciences Research Centre (BBSRC) [BB/P001262/1] to PRL and YL, and the National Centre for the Replacement, Refinement and Reduction of Animals in Research (NC3Rs) [NC/R001596/1] to PRL, SMN, BDR and YL.

Abbreviations

ADC:	Albumin Dextrose Catalase
CFU:	Colony Forming Units
G. mellonella:	*Galleria mellonella*
H&E:	Haematoxylin and Eosin
LTBI:	Latent tuberculosis infection
M. bovis:	*Mycobacterium bovis*
M. bovis BCG *lux:*	*Mycobacterium bovis* BCG *lux*
M. tuberculosis:	*Mycobacterium tuberculosis*
OADC:	Oleic Acid, Albumin, Dextrose, Catalase
OsO_4:	Osmium tetroxide
PBS:	Phosphate Buffered Saline
RLU:	Relative Light Units
TAGs:	Triacylglycerides
TEM:	Transmission Electron Microscopy
ZN:	Ziehl Neelsen

ORCID

Janine T Bossé http://orcid.org/0000-0002-8491-4779
Sandra M Newton http://orcid.org/0000-0001-6545-9558
Paul R Langford http://orcid.org/0000-0002-6368-4724

References

1. W.H.O. Global tuberculosis report. 2016. Switzerland: W.H.O Press.
2. Dheda K, Gumbo T, Maartens G, et al. The epidemiology, pathogenesis, transmission, diagnosis, and management of multidrug-resistant, extensively drug-resistant, and incurable tuberculosis. Lancet Respir Med. 2017;5:291–360.
3. Bell LCK, Noursadeghi M. Pathogenesis of HIV-1 and *Mycobacterium tuberculosis* co-infection. Nat Rev Microbiol. 2017;16:80–90.
4. Zhan L, Tang J, Sun M, et al. Animal models for tuberculosis in translational and precision medicine. Front Microbiol. 2017;8:717.
5. Gumbo T, Lenaerts AJ, Hanna D, et al. Non-clinical models for anti-tuberculosis drug development: a landscape analysis. J Infect Dis. 2015;211(Suppl 3):S83–95.
6. Cadena AM, Fortune SM, Flynn JL. Heterogeneity in tuberculosis. Nat Rev Immunol. 2017;17:691–702.
7. Flynn JL. Lessons from experimental *Mycobacterium tuberculosis* infections. Microbes Infect. 2006;8:1179–1188.
8. Kramnik I, Beamer G. Mouse models of human TB pathology: roles in the analysis of necrosis and the development of host-directed therapies. Semin Immunopathol. 2016;38:221–237.
9. Flynn JL, Gideon HP, Mattila JT, et al. Immunology studies in non-human primate models of tuberculosis. Immunol Rev. 2015;264:60–73.
10. Pena JC, Ho WZ. Monkey models of tuberculosis: lessons learned. Infect Immun. 2015;83:852–862.
11. Cook SM, McArthur JD. Developing *Galleria mellonella* as a model host for human pathogens. Virulence. 2013;4:350–353.
12. Binder U, Maurer E, Lass-Florl C. *Galleria mellonella*: an invertebrate model to study pathogenicity in correctly defined fungal species. Fungal Biol. 2016;120:288–295.
13. Borman AM. Of mice and men and larvae: *Galleria mellonella* to model the early host-pathogen interactions after fungal infection. Virulence. 2017;9:9–12.
14. Jander G, Rahme LG, Ausubel FM. Positive correlation between virulence of *Pseudomonas aeruginosa* mutants in mice and insects. J Bacteriol. 2000;182:3843–3845.
15. Tsai CJ, Loh JM, Proft T. *Galleria mellonella* infection models for the study of bacterial diseases and for antimicrobial drug testing. Virulence. 2016;7:214–229.
16. Wojda I. Immunity of the greater wax moth *Galleria mellonella*. Insect Sci. 2017;24:342–357.
17. Wu G, Liu Y, Ding Y, et al. Ultrastructural and functional characterization of circulating hemocytes from *Galleria mellonella* larva: cell types and their role in the innate immunity. Tissue Cell. 2016;48:297–304.
18. Mak P, Zdybicka-Barabas A, Cytrynska M. A different repertoire of *Galleria mellonella* antimicrobial peptides in larvae challenged with bacteria and fungi. Dev Comp Immunol. 2010;34:1129–1136.
19. Lopez Hernandez Y, Yero D, Pinos-Rodriguez JM, et al. Animals devoid of pulmonary system as infection models in the study of lung bacterial pathogens. Front Microbiol. 2015;6:38.
20. Ramarao N, Nielsen-Leroux C, Lereclus D. The insect *Galleria mellonella* as a powerful infection model to investigate bacterial pathogenesis. J Vis Exp. 2012;70:e4392.
21. Snewin V, Gares MP, Gaora PO, et al. Assessment of immunity to mycobacterial infection with luciferase reporter constructs. Infect Immun. 1999;67:4586–4593.
22. Newton S, Martineau A, Kampmann B. A functional whole blood assay to measure viability of mycobacteria, using reporter-gene tagged BCG or M.Tb (BCG *lux*/M. Tb *lux*). J Vis Exp. 2011;55:e3332.
23. Kampmann B, Gaora PO, Snewin VA, et al. Evaluation of human anti-mycobacterial immunity using recombinant reporter mycobacteria. J Infect Dis. 2000;182:895–901.
24. Kampmann B, Tena GN, Mzazi S, et al. Novel human *in vitro* system for evaluating antimycobacterial vaccines. Infect Immun. 2004;72:6401–6407.
25. Kampmann B, Tena-Coki GN, Nicol MP, et al. Reconstitution of anti-mycobacterial immune responses in HIV-infected children receiving HAART. AIDS. 2006;20:1011–1018.
26. Tena GN, Young DB, Eley B, et al. Failure to control growth of mycobacteria in blood from children infected with human immunodeficiency virus and its relationship to T cell function. J Infect Dis. 2003;187:1544–1551.
27. Andreu N, Zelmer A, Fletcher T, et al. Optimisation of bioluminescent reporters for use with mycobacteria. PLoS One. 2010;5:e10777.
28. Newton SM, Mackie SL, Martineau AR, et al. Reduction of chemokine secretion in response to mycobacteria in infliximab-treated patients. Clin Vaccine Immunol. 2008;15:506–512.
29. Martineau AR, Newton SM, Wilkinson KA, et al. Neutrophil-mediated innate immune resistance to mycobacteria. J Clin Invest. 2007;117:1988–1994.
30. Martineau AR, Wilkinson KA, Newton SM, et al. IFN-gamma- and TNF-independent vitamin D-inducible human suppression of mycobacteria: the role of cathelicidin LL-37. J Immunol. 2007;178:7190–7198.
31. Martineau AR, Wilkinson RJ, Wilkinson KA, et al. A single dose of vitamin D enhances immunity to mycobacteria. Am J Resp Crit Care. 2007;176:208–213.
32. von Both U, Berk M, Agapow PM, et al. *Mycobacterium tuberculosis* exploits a molecular off switch of the immune system for intracellular survival. Sci Rep. 2018;8:661.
33. Jarosz J. Gut flora of *Galleria mellonella* suppressing ingested bacteria. J Invertebr Pathol. 1979;34:192–198.
34. Thomaz L, Garcia-Rodas R, Guimaraes AJ, et al. *Galleria mellonella* as a model host to study *Paracoccidioides lutzii* and *Histoplasma capsulatum*. Virulence. 2013;4:139–146.
35. Entwistle FM, Coote PJ. Evaluation of greater wax moth larvae, *Galleria mellonella*, as a novel *in vivo* model for non-tuberculosis *Mycobacteria* infections and antibiotic treatments. J Med Microbiol. 2018;67:585–597.
36. Browne N, Kavanagh K. Developing the potential of using *Galleria mellonella* larvae as models for studying brain infection by *Listeria monocytogenes*. Virulence. 2013;4:271–272.
37. Freires IA, Sardi JC, de Castro RD, et al. Alternative animal and non-animal models for drug discovery and

development: bonus or burden? Pharm Res. 2017;34:681–686.
38. Dionne MS, Ghori N, Schneider DS. *Drosophila melanogaster* is a genetically tractable model host for *Mycobacterium marinum*. Infect Immun. 2003;71:3540–3550.
39. Dionne MS, Pham LN, Shirasu-Hiza M, et al. *Akt* and *foxo* dysregulation contribute to infection-induced wasting in *Drosophila*. Curr Biol. 2006;16:1977–1985.
40. Oh CT, Moon C, Choi TH, et al. *Mycobacterium marinum* infection in *Drosophila melanogaster* for antimycobacterial activity assessment. J Antimicrob Chemother. 2013;68:601–609.
41. Oh CT, Moon C, Jeong MS, et al. *Drosophila melanogaster* model for *Mycobacterium abscessus* infection. Microbes Infect. 2013;15:788–795.
42. Buyukguzel E, Tunaz H, Stanley D, et al. Eicosanoids mediate *Galleria mellonella* cellular immune response to viral infection. J Insect Physiol. 2007;53:99–105.
43. Garzon S, Charpentier G, Kurstak E. Morphogenesis of the nodamura virus in the larvae of the lepidopteran *Galleria mellonella* (L.). Arch Virol. 1978;56:61–76.
44. Ozkan S, Coutts RH. *Aspergillus fumigatus* mycovirus causes mild hypervirulent effect on pathogenicity when tested on *Galleria mellonella*. Fungal Genet Biol. 2015;76:20–26.
45. Dalton JP, Uy B, Swift S, et al. A novel restraint device for injection of *Galleria mellonella* larvae that minimizes the risk of accidental operator needle stick injury. Front Cell Infect Microbiol. 2017;7:99.
46. Rwegasila E, Mubofu EB, Nyandoro SS, et al. Preparation, characterization and *in vivo* antimycobacterial studies of panchovillin-chitosan nanocomposites. Int J Mol Sci. 2016;17:E1559.
47. Erasto P, Omolo J, Sunguruma R, et al. Evaluation of antimycobacterial activity of higenamine using *Galleria mellonella* as an *in vivo* infection model. Nat Prod Bioprospect. 2018;8:63–69.
48. Meir M, Grosfeld T, Barkan D. Establishment and validation of *Galleria mellonella* as a novel model organism to study *Mycobacterium abscessus* infection, pathogenesis and treatment. Antimicrob Agents Chemother. 2018;62:e02539-17.
49. Harding CR, Schroeder GN, Reynolds S, et al. *Legionella pneumophila* pathogenesis in the *Galleria mellonella* infection model. Infect Immun. 2012;80:2780–2790.
50. Vogel H, Altincicek B, Glockner G, et al. A comprehensive transcriptome and immune-gene repertoire of the lepidopteran model host *Galleria mellonella*. BMC Genomics. 2011;12:308.
51. Khara JS, Wang Y, Ke XY, et al. Anti-mycobacterial activities of synthetic cationic alpha-helical peptides and their synergism with rifampicin. Biomaterials. 2014;35:2032–2038.
52. Tomiotto-Pellissier F, Cataneo AHD, Orsini TM, et al. *Galleria mellonella* hemocytes: A novel phagocytic assay for *Leishmania* (*Viannia*) *braziliensis*. J Microbiol Methods. 2016;131:45–50.
53. Harding CR, Schroeder GN, Collins JW, et al. Use of *Galleria mellonella* as a model organism to study *Legionella pneumophila* infection. J Vis Exp. 2013;81:e50964.
54. Card R, Vaughan K, Bagnall M, et al. Virulence characterisation of *Salmonella enterica* isolates of differing antimicrobial resistance recovered from UK livestock and imported meat samples. Front Microbiol. 2016;7:640.
55. La Rosa SL, Casey PG, Hill C, et al. In vivo assessment of growth and virulence gene expression during commensal and pathogenic lifestyles of *luxABCDE*-tagged *Enterococcus faecalis* strains in murine gastrointestinal and intravenous infection models. Appl Environ Microbiol. 2013;79:3986–3997.
56. Barry CE 3rd, Boshoff HI, Dartois V, et al. The spectrum of latent tuberculosis: rethinking the biology and intervention strategies. Nat Rev Microbiol. 2009;7:845–855.
57. Meijer AH. Protection and pathology in TB: learning from the zebrafish model. Semin Immunopathol. 2016;38:261–273.
58. Nuermberger EL. Preclinical efficacy testing of new drug candidates. Microbiol Spectr. 2017;5:TBTB2-0034–2017.
59. Meijer AH, Spaink HP. Host-pathogen interactions made transparent with the zebrafish model. Curr Drug Targets. 2011;12:1000–1017.
60. Myllymaki H, Bauerlein CA, Ramet M. The zebrafish breathes new life into the study of tuberculosis. Front Immunol. 2016;7:196.
61. van der Vaart M, van Soest JJ, Spaink HP, et al. Functional analysis of a zebrafish *myd88* mutant identifies key transcriptional components of the innate immune system. Dis Model Mech. 2013;6:841–854.
62. Hammaren MM, Oksanen KE, Nisula HM, et al. Adequate Th2-type response associates with restricted bacterial growth in latent mycobacterial infection of zebrafish. PLoS Pathog. 2014;10:e1004190.
63. Santucci P, Bouzid F, Smichi N, et al. Experimental models of foamy macrophages and approaches for dissecting the mechanisms of lipid accumulation and consumption during dormancy and reactivation of tuberculosis. Front Cell Infect Microbiol. 2016;6:122.
64. Russell DG, Cardona PJ, Kim MJ, et al. Foamy macrophages and the progression of the human tuberculosis granuloma. Nat Immunol. 2009;10:943–948.
65. Prosser G, Brandenburg J, Reiling N, et al. The bacillary and macrophage response to hypoxia in tuberculosis and the consequences for T cell antigen recognition. Microbes Infect. 2017;19:177–192.
66. Desbois AP, Coote PJ. Utility of greater wax moth larva (*Galleria mellonella*) for evaluating the toxicity and efficacy of new antimicrobial agents. Adv Appl Microbiol. 2012;78:25–53.

jove Journal of Visualized Experiments www.jove.com

Video Article

Use of the Invertebrate *Galleria mellonella* as an Infection Model to Study the *Mycobacterium tuberculosis* Complex

Masanori Asai*[1], Yanwen Li*[1], Jasmeet Singh Khara[1,2], Camilla A. Gladstone[1], Brian D. Robertson[3], Paul R. Langford*[1], Sandra M. Newton*[1]

[1]Section of Pediatric Infectious Diseases and Allergy, Department of Medicine, Imperial College London

[2]Department of Pharmacy, National University of Singapore

[3]MRC Centre for Molecular Bacteriology and Infection, Department of Medicine, Imperial College London

*These authors contributed equally

Correspondence to: Sandra M. Newton at s.newton@imperial.ac.uk

URL: https://www.jove.com/video/59703
DOI: doi:10.3791/59703

Keywords: Immunology and Infection, Issue 148, *Galleria mellonella*, mycobacteria, tuberculosis, *Mycobacterium bovis* BCG *lux*, infection model, host-pathogen interactions, *Mycobacterium tuberculosis* complex, hemocytes

Date Published: 6/30/2019

Citation: Asai, M., Li, Y., Khara, J.S., Gladstone, C.A., Robertson, B.D., Langford, P.R., Newton, S.M. Use of the Invertebrate *Galleria mellonella* as an Infection Model to Study the *Mycobacterium tuberculosis* Complex. *J. Vis. Exp.* (148), e59703, doi:10.3791/59703 (2019).

Abstract

Tuberculosis is the leading global cause of infectious disease mortality and roughly a quarter of the world's population is believed to be infected with *Mycobacterium tuberculosis*. Despite decades of research, many of the mechanisms behind the success of *M. tuberculosis* as a pathogenic organism remain to be investigated, and the development of safer, more effective antimycobacterial drugs are urgently needed to tackle the rise and spread of drug resistant tuberculosis. However, the progression of tuberculosis research is bottlenecked by traditional mammalian infection models that are expensive, time consuming, and ethically challenging. Previously we established the larvae of the insect *Galleria mellonella* (greater wax moth) as a novel, reproducible, low cost, high-throughput and ethically acceptable infection model for members of the *M. tuberculosis* complex. Here we describe the maintenance, preparation, and infection of *G. mellonella* with bioluminescent *Mycobacterium bovis* BCG *lux*. Using this infection model, mycobacterial dose dependent virulence can be observed, and a rapid readout of in vivo mycobacterial burden using bioluminescence measurements is easily achievable and reproducible. Although limitations exist, such as the lack of a fully annotated genome for transcriptomic analysis, ontological analysis against genetically similar insects can be carried out. As a low cost, rapid, and ethically acceptable model for tuberculosis, *G. mellonella* can be used as a pre-screen to determine drug efficacy and toxicity, and to determine comparative mycobacterial virulence prior to the use of conventional mammalian models. The use of the *G. mellonella*-mycobacteria model will lead to a reduction in the substantial number of animals currently used in tuberculosis research.

Video Link

The video component of this article can be found at https://www.jove.com/video/59703/

Introduction

Tuberculosis (TB) is a major threat to global public health with 9 million new cases per year and 1.5 million deaths[1]. In addition, it is estimated that one quarter of the world's population is infected with the causative agent of the disease, *Mycobacterium tuberculosis* (*Mtb*). Amongst the infected population, 5−10% will develop active TB disease over their lifetime. Furthermore, the emergence and spread of multi-drug resistant (MDR) and extensively-drug (XDR) resistant *Mtb* poses a serious threat to disease control, with 123 countries reporting at least one XDR case[1]. Treatment of TB requires a cocktail of at least four anti-mycobacterial drugs, of which isoniazid and rifampicin are prescribed for a minimum duration of six months; treatment is often associated with complex side effects and toxicities. Protection from the only licensed vaccine against TB, *Mycobacterium bovis* Bacillus Calmette-Guérin (BCG), is variable[2]. An incomplete understanding of the pathogenesis of TB significantly hampers the development of new therapeutic and vaccination strategies.

For decades animal infection models have been vital for TB research to understand the basic pathogenesis and host response to infection, and to evaluate novel anti-mycobacterial agents, immuno-therapeutics and new vaccine candidates[3,4]. However, research using animal infection models of TB is notoriously difficult as the pathogenesis and progression of TB infection are complex, and there is no single animal model that mimics the full spectrum and important features of the disease[5,6]. Furthermore, animal experiments are expensive, time consuming to undertake and require full ethical justification. Nevertheless, animal infection models of TB have been described in non-human primates (e.g., macaques), guinea pigs, rabbits, cattle, pigs, mice and zebrafish, with each having their limitations[3,4]. The murine model is the most commonly used model due to cost, availability of inbred lines, reproducibility of infection and abundance of immunological reagents. However, they do not typically form granulomas associated with areas of hypoxia that are characteristic of latent tuberculosis infection (LTBI)[6]. Guinea pigs are highly susceptible to *Mtb* infection, with pathology and early granuloma formation similar to those in humans, and are widely used in vaccine testing; yet the lack of immunological reagents hampers their use as an infection model[7]. Zebrafish are suitable for large-scale screening in early-stage preclinical studies due to their small size, rapid reproduction and advanced genetic tools, but are anatomically and physiologically different to humans and are only susceptible to *Mycobacterium marinum* infection[3]. The animal models most closely resembling human *Mtb* infection are non-human

Copyright © 2019 Creative Commons Attribution 3.0 License

primates (e.g., the macaque), but they are expensive and have significant ethical and practical considerations which considerably limits their use[8].

The insect larva of the greater wax moth or honeycomb moth, *Galleria mellonella*, have become increasingly popular as an infection model for a variety of bacterial and fungal pathogens[9], and as a screen for novel antimicrobial drug candidates[10]. *G. mellonella* is a successful invertebrate model due to its sophisticated innate immune system (comprised of cellular and humoral defenses) that shares a high degree of structural and functional similarity to that of vertebrates[11]. This includes immune mechanisms such as the phagocytosis of pathogens by hemocytes (functionally similar to mammalian macrophage and neutrophils)[12,13], the production and circulation of anti-microbial peptides (AMPs) and complement-like proteins within the hemolymph (analogous to mammalian blood) of *G. mellonella*[11]. Other advantages[5,14,15] of *G. mellonella* larvae as a model include 1) their large size (20−30 mm) which allows for easy manipulation and infection, as well as the collection of tissue and hemolymph for analyses, 2) easy maintenance at 37 °C, compatible for studying human pathogens, 3) precise infection by injection without the need for anesthesia, 4) efficacy of antimicrobial agents can be assessed utilizing less drug for evaluation, 5) lack of ethical constraints compared to the use of mammals, 6) large group sizes can be used compared to animal models allowing greater reproducibility, and 7) shorter times for infection experiments are required.

In a recent study, we demonstrated that *G. mellonella* can be used as a novel infection model for studying the pathogenesis of infection by bioluminescent *M. bovis* BCG *lux*, a genetically modified version of the vaccine strain and member of the *Mtb* complex (MTBC)[16]. While *G. mellonella* has previously been used as an infection model for non-tuberculous mycobacteria (NTM), mainly *M. marinum* and *Mycobacterium abscessus*[17,18], studies using MTBC are limited to that of Li et al.[16]. Bioluminescent non-pathogenic mycobacterial strains, which can be used at containment level (CL) 2 as a surrogate for *Mtb*, offer the advantages of safety and practicality over pathogenic mycobacteria. Following infection with BCG *lux*, larvae begin to develop early granuloma-like structures, which could provide valuable insight into the role of innate immunity in the establishment of TB infection[16]. In addition, this simple invertebrate infection model has the potential to provide a rapid, low-cost, and reliable evaluation of TB pathogenesis incorporating controlled challenge and multiple replicates for reproducibility. Furthermore, the model has the potential to be used to screen novel anti-TB drug and vaccine candidates in early development, reducing the overall number of animals in experimentation. The ability to measure changes in host and pathogen structure, transcriptome and proteome to determine drug targets and assess mechanisms of action of novel drugs and therapeutic vaccines, are also advantageous.

Here we describe the experimental protocols for the preparation of a bioluminescent *M. bovis* BCG *lux* inoculum and *G. mellonella* larvae for mycobacterial infection, as well as the determination of both larval and mycobacterial survival in response to infection.

Protocol

NOTE: All work described below are to be carried out in a CL2 laboratory within a class 2 microbiological safety cabinet (MSC) following local health and safety guidelines.

1. Preparation *of M. bovis* BCG *lux* for Infection

1. Defrost a frozen 1.2 mL glycerol (15%) stock of *M. bovis* BCG *lux*, the Montreal vaccine strain transformed with the shuttle plasmid pSMT1 carrying the *luxAB* genes from *Vibrio harveyi* encoding the luciferase enzyme[19].
2. Inoculate 15 mL of Middlebrook 7H9 broth containing 0.2% glycerol, 10% albumin, dextrose, catalase (ADC) enrichment and 50 µg/mL hygromycin with a defrosted 1.2 mL aliquot of BCG *lux*, in a labelled 250 mL Erlenmeyer flask.
3. Place the flask in a sealed biosafety container and incubate at 37 °C in an orbital shaker incubator at 220 rpm for 72 h (or until the culture reaches the mid-log phase of growth).
4. Check the growth of BCG *lux* culture by preparing 1:10 dilutions of the culture in luminometer tubes using phosphate buffered saline (PBS, pH 7.4, 0.01 M phosphate buffer, 0.0027 M potassium chloride and 0.137 M sodium chloride) in duplicate. Vortex, and load the luminometer tubes into the luminometer and measure the bioluminescence (relative light unit [RLU]/mL) using n-decyl aldehyde as the substrate (1% v/v in absolute ethanol)[20].
   NOTE: The ratio of RLU/colony forming units (CFU) was previously determined to be 3:1 when BCG *lux* was grown in vitro in Middlebrook 7H9 broth[20].
5. Centrifuge the culture at 2,175 x *g* for 10 min at room temperature to pellet the cells and discard the supernatant into an appropriate disinfectant with known mycobactericidal activity. Dispose all culture waste with disinfectants appropriate for mycobacteria following local guidelines.
6. Wash the cell pellet twice in PBS containing 0.05% polysorbate 80 (PBS-T) to prevent bacterial clumping.
7. Following the final wash, decant waste supernatant, resuspend the mycobacterial cell pellet in PBS-T and dilute the mycobacterial suspension to the desired cell density using RLU measurements.
8. Prepare ten-fold serial dilutions of the inoculum in 24-well plates using PBS-T. Plate out 10 µL onto Middlebrook 7H11 agar plates (0.5% glycerol, 50 µg/mL hygromycin, 10% oleic acid, albumin, dextrose, catalase [OADC]) in duplicate to enumerate inoculum CFU counts.

2. Preparation of *G. mellonella* Larvae

1. Purchase last instar larvae from appropriate sources and maintain the larvae in the dark at 18 °C upon arrival and use within 1 week of purchase. Alternatively, larvae can be self-reared following the protocol of Jojão et al.[21]. For purchased larvae, discard any dead, discolored or pupating larvae prior to storage.
   NOTE: Pupating larvae are morphologically distinguishable to the last instar larvae.
2. Identify and select healthy larvae for experimentation, based on uniform cream color with little to no discoloration (melanization), size (2−3 cm in length), weight (approximately 250 mg), displaying a high level of motility, and possessing the ability to right themselves when turned over.

Copyright © 2019 Creative Commons Attribution 3.0 License

3. Carefully count the healthy larvae (minimum of 20−30 per group) into a Petri dish (94/15 mm) lined with a layer of filter paper (94/15 mm) using blunt-end tweezers to minimize contamination and store at room temperature in the dark until use.

3. Infecting *G. mellonella* with BCG *lux*

1. Minimize the clutter within the MSC to reduce the risk of contamination and needle stick injury.
2. Prepare the injection platform by taping a circular filter paper (94 mm) to a flat raised surface. Soft or hard surfaces can be used and is entirely dependent on user preference, e.g., pipette box lids or a nylon scouring sponge.
3. Sterilize a 25 µL microsyringe (25 G) by aspirating 3 volumes of 70% ethanol and further rinse with 3 volumes of sterile PBS-T.
4. Aspirate 10 µL of BCG *lux* inoculum (prepared in section 1) or PBS-T into the sterilized 25 µL microsyringe. Use a separate syringe for PBS-T negative control.
   NOTE: Resuspend the BCG *lux* inoculum following 10 injections to ensure uniform cell suspension.
5. Use tweezers to pick up one larva and place onto the injection platform.
6. On the platform, flip the larva on to its back and immobilize by securing the head and tail with the tweezers. Locate the last left proleg counting down from the head of the larva and carefully insert the tip of the needle (5−6 mm) at a 10−20° angle to the horizontal plane.
   NOTE: Short and narrow tweezers allow for easy immobilization with minimum larval stress. Pay attention not to over penetrate which may puncture the gut and cause non-BCG *lux* specific melanization or death.
7. Count the infected larvae into a Petri dish lined with a layer of filter paper, a single 90 mm Petri dish can accommodate up to 30 larvae.
8. Store the Petri dish containing the larvae in a vented or non-sealed dark box inside an incubator at 37 °C with 5% CO_2.

4. Monitoring the Survival of *G. mellonella* Following Infection

1. Over the time course, monitor the survival of the larvae every 24 h. Larvae are considered dead when they fail to move in response to touch.

5. Measuring the In Vivo Burden of BCG *lux* in *G. mellonella*

1. At each time point, randomly select five infected larvae previously prepared in section 3 and gently sterilize the larval surfaces using cotton bud swabs soaked in 70% ethanol.
   NOTE: This step is important when plating larval homogenate for mycobacterial CFU enumeration as non-sterilized larvae can lead to contamination.
2. Place the larvae individually into 2 mL lysing matrix tubes containing 800 µL of sterile PBS.
3. Homogenize the larvae using a homogenizer for 60 s at 6.0 m/s.
4. Centrifuge the lysing tubes at 3,500 x *g* for 5 s to remove homogenate from the lids, and carefully decant the homogenate into sterile luminometer tubes individually.
   NOTE: For CFU enumeration (step 5.7), ensure to reserve 100 µL of homogenate in a sterile 1.5 mL reaction tube.
5. Recover any remaining homogenate by washing the lysing matrix tubes with 1 mL of PBS-T and pipette into the corresponding luminometer tubes.
6. Vortex the luminometer tubes and measure the bioluminescence of the homogenates previously described in step 1.4.
7. Prepare ten-fold serial dilutions of the homogenate in 24-well culture plates using PBS-T. Plate out 10 µL of the dilution onto Middlebrook 7H11 agar plates containing 0.5% glycerol, 50 µg/mL hygromycin, 10% OADC and 20 µg/mL piperacillin, to determine the RLU/CFU ratio of BCG *lux* following in vivo infection.
   NOTE: Piperacillin eliminates native *G. mellonella* microbiota with minimal growth inhibition of BCG *lux*[16].

6. Statistical Analysis

1. Plot the Kaplan-Meier survival curve using data collected and carry out the Mantel-Cox (Log-rank) test to determine the significance of the result, where *p < 0.05, **p < 0.01, ***p < 0.001, and ****p < 0.0001.

Representative Results

Here we present representative data that can be obtained using the *G. mellonella* — BCG *lux* infection model and highlight the benefits of *G. mellonella* as an infection model for members of the MTBC (**Figure 1**). Experimental procedures with key technical points are outlined in **Figure 2**.

Copyright © 2019 Creative Commons Attribution 3.0 License

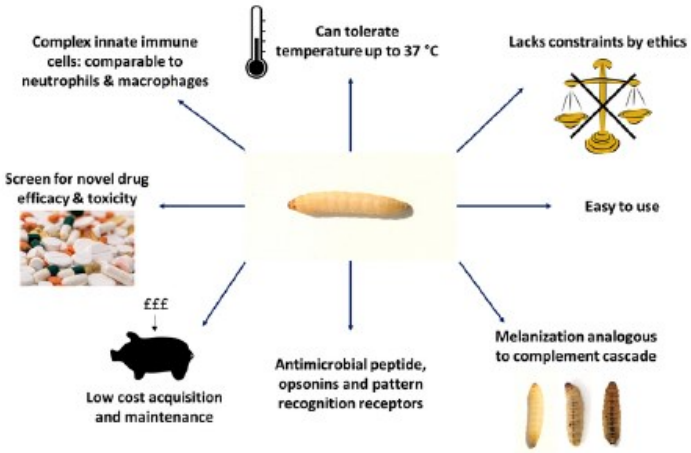


Figure 1: The benefits of *G. mellonella* as an infection model. This figure has been adapted from Kavanagh and Sheehan[22]. Please click here to view a larger version of this figure.

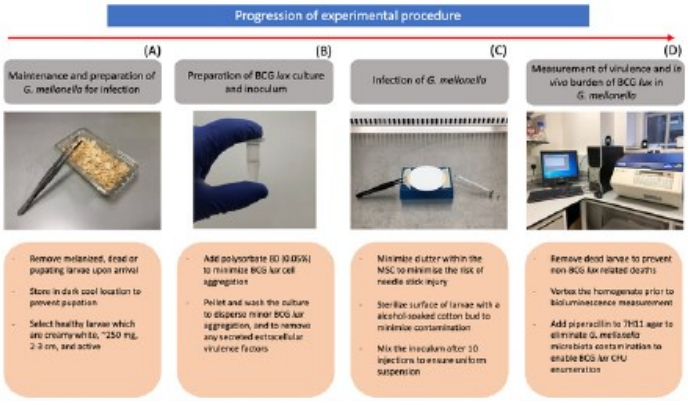


Figure 2: Outline of experimental procedures. (**A**) Maintenance and preparation of *G. mellonella* for infection with *M. bovis* BCG *lux*. (**B**) Preparation of BCG *lux* culture and inoculum for infection. (**C**) Infection of *G. mellonella* with BCG *lux*. (**D**) Measurement of virulence and in vivo burden of BCG *lux* in *G. mellonella* larvae. Please click here to view a larger version of this figure.

BCG *lux* dose dependent virulence was observed in *G. mellonella* larvae over a 96 h incubation period (**Figure 3**), and the lethal dose required for 50% larval mortality (LD_{50}) was determined to be 1 x 10^7 CFU. The survival distribution reflecting the virulence of the BCG *lux* doses tested was significantly different ($p < 0.0001$). Control groups injected with a 10 µL dose of PBS-T or those simply pricked simulating needle injuries, did not affect larval health or lead to an increase in mortality as determined by observational checks on motility and melanization at different time points.

Copyright © 2019 Creative Commons Attribution 3.0 License

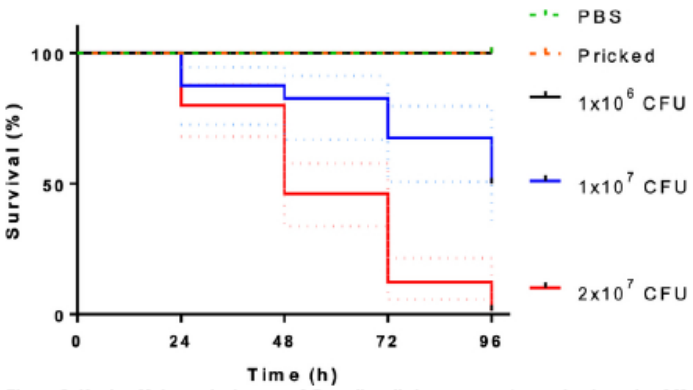


Figure 3: Kaplan-Meir survival curve of *G. mellonella* in response to varying inocula of *M. bovis* BCG *lux*. Healthy larvae (n ≥ 10 per group), were infected with varying doses of BCG *lux*. Larvae were incubated at 37 °C and monitored for survival every 24 h for up to 96 h. The uninfected group was injected with PBS, and a pricked group (insertion of needle only) demonstrated the effect of needle injury on larval health. The means of two independent experiments are shown, with 95% confidence interval, represented as dotted lines in corresponding color to the inoculum. This figure has been adapted from Li et al.[15]. Please click here to view a larger version of this figure.

All larvae infected with BCG *lux* displayed physiological changes over time and, for larvae infected with a 2 x 10^7 CFU dose of BCG *lux*, melanization of the larval dorsal line was observed from 48 h post infection (pi), and systematic melanization was observed from 96 h pi (**Figure 4**). Furthermore, the motility of the larvae reduced with the severity of melanization and the ability of larvae to pupate was lost upon infection in comparison with uninfected controls.



Figure 4: Melanization of *G. mellonella* in response to infection with *M. bovis* BCG *lux*. Healthy larvae at 0 h were infected with a 2 x 10^7 CFU dose of BCG *lux*. At 48 h and 96 h pi, melanization along the larval dorsal line and systematic melanization, respectively, was observed.

Survival of BCG *lux* within the *G. mellonella* larvae was determined over 2 weeks through bioluminescence measurement of larval homogenates. Infection with a 1 x 10^7 CFU dose of BCG *lux* resulted in an initial decline of BCG *lux* bioluminescence from 0–72 h pi. However, from 72–144 h pi, the bioluminescence of BCG *lux* plateaued, indicating the establishment of persistent infection (**Figure 5**).

Copyright © 2019 Creative Commons Attribution 3.0 License

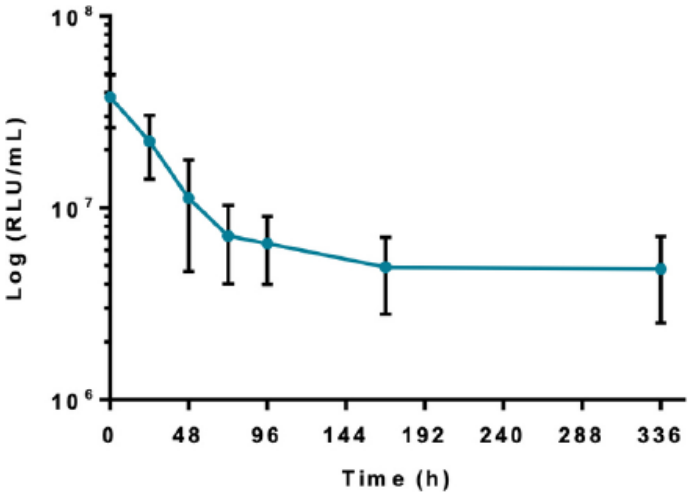


Figure 5: In vivo burden of *M. bovis* BCG *lux* in *G. mellonella* quantified using bioluminescence (relative light unit, RLU/mL) over a two week time course. Healthy larvae (n = 30) were infected with 1 x 10^7 CFU dose of BCG *lux*. In vivo burden was quantified by homogenizing five larvae at each time point (0, 24, 48, 72, 96, 168, 336 h), and measuring the bioluminescence of the homogenate. The means of three independent experiments are shown, and the error bars represent the standard deviation of the mean. This figure has been reprinted from Li et al.[16]. Please click here to view a larger version of this figure.

As the rapid and reproducible quantification of in vivo mycobacterial growth in these studies was determined by the measurement of bioluminescence, the ratio of RLU and CFU should also be determined in vivo. In our particular infection system, the in vivo ratio of RLU and CFU ranged from 2:1-5:1, with an average of 4:1 over the 168-h time course (**Figure 6**).

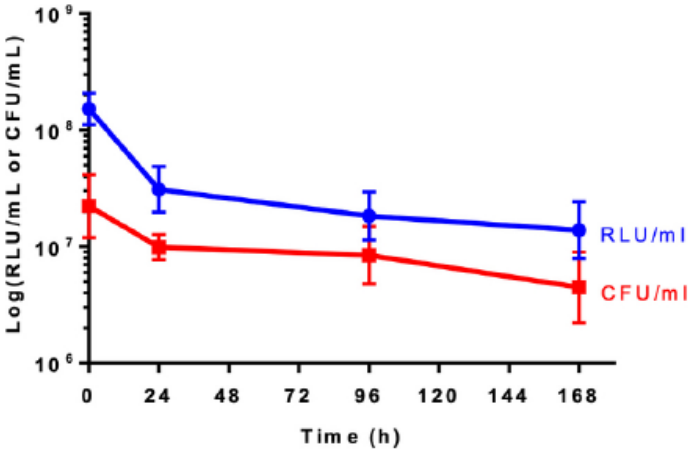


Figure 6: Determining the in vivo RLU/CFU ratio of *M. bovis* BCG *lux* in *G. mellonella*. Healthy larvae (n = 30) were infected with 1 x 10^7 CFU dose of BCG *lux*. At each time point (0, 24, 96 and 168 h), four infected/control (PBS-T) larvae were homogenized, and the homogenates were measured for bioluminescence and plated out onto 7H11 agar to enumerate CFU counts. The means of two independent experiments are shown and the error bars represent the standard deviation of the mean. Please click here to view a larger version of this figure.

Discussion

The use of *G. mellonella* as an infection model has been established for a number of bacterial and fungal pathogens for the study of virulence, host-pathogen interaction, and as a screen for novel therapeutics[10,22]. The following discussion is based on the experimental procedure for the use of *G. mellonella* as an infection model for the MTBC.

Copyright © 2019 Creative Commons Attribution 3.0 License

The health of the naïve larvae prior to experimentation can have a considerable impact on the outcome of the experiment. Therefore, it is vital that any discolored and/or injured larvae are removed upon arrival and are not used for any experimentation. If a large number of larvae are found dead within the same container upon arrival, it is advisable to discard the batch as pre-existing infections may be the cause of death. When possible perform experiments using the larvae as close to the day of purchase/arrival. Before use ensure to store the larvae at 18 °C to prevent pupation and to maximize the number of larvae available for experimentation. Healthy larvae can be used for up to 7 days following delivery/purchase. Following infection, ensure to remove any dead larvae from the Petri dish as, for reasons yet unknown, the presence of dead larvae appears to increase the rate of mortality in the sample population. For users of self-reared larvae, it is important to be aware of biological variability in comparison to purchased larvae, as variance in diet and growth conditions can have an impact on larval immunity[21,23]. Inter-experimental variabilities can be limited by keeping the source, if purchased, or the feed and growth conditions of the reared larvae consistent between experimentation. In all experiments, the inclusion of 'blank' and 'pricked' negative controls are essential; the blank control is an indicator of contamination or toxicity of the suspension matrix (PBS-T or media broth), and the pricked control mimics the effect of the needle injury on larval health. Furthermore, these controls normalize any biological variation between batches of larvae, ensuring reproducibility and accuracy between experiments.

For injection of *G. mellonella* larvae, the use of a 25 G needle is recommended as larger gauge needles can cause excessive bleeding and sharper smaller gauge needles can easily puncture the gut of the larvae, leading to larval mortality and false positive results. Conventional methods of needle injection typically immobilize the larvae by hand, which increases the risk of needle injury. By using tweezers to immobilize the larvae, the risk of needle stick injury is significantly reduced as the hand is not in close proximity to the needle at any point during infection. Alternatively, larvae could be immobilized by cooling. However, cold shock at 12 °C for 15 min prior to infection has been documented to enhance the innate immune response to infection. Therefore, the analysis of the results obtained via cooling should carefully consider its impact[24]. Using our technique, medium throughput of injection (2−3 larvae per minute) can be achieved with user practice; this is comparable to the speed of conventional injection from our experience (3−4 larvae per min). Furthermore, our method can be adapted for higher throughput injection by utilizing a pedal operated injection platform comprised of an infusion pump with a disposable syringe connected to a 25 G butterfly cannula.

The preparation of BCG *lux* inoculum is based on the rapid estimation of CFU using RLU of the mycobacterial culture[20]. In our experience with broth culture, the ratio of RLU to CFU is 3:1[20], contrasting with BCG *lux* growing in *G. mellonella* where the RLU to CFU ratio is 5:1[20]. Mycobacterial cell aggregation or 'clumping' commonly seen in dense cultures can have an impact on the RLU measurements, as clumping can result in unreliable bioluminescence measurements. As such, the use of clumped mycobacterial culture for inoculum preparation is not recommended. However, the addition of polysorbate 80 to the growth media minimizes cell clumping without altering the growth of BCG *lux*.[16] Any minor cell clumping can be resolved by washing the culture with PBS-T and is vital for preparing an accurate inoculum using RLU as the readout. Furthermore, the PBS-T wash is vital for removing any extracellular virulence factor secreted during growth. Mycobacterial strain and passage number should also be taken into consideration, as this can impact the severity of mycobacterial aggregation[25]. In all cases, the inoculum should be enumerated by CFU on 7H11 agar plates to ensure that the correct CFU was prepared by bioluminescence measurement. Additionally, the RLU/CFU ratio in vivo should be determined with new bioluminescent reporter or stocks, as the ratio will likely vary.

G. mellonella holds several advantages over conventional models of TB infection, including cheaper acquisition and maintenance costs, ease of infection and research throughput, especially in combination with bioluminescent strains[16]. The lack of ethical constraints allows for greater sample size (minimum of 20−30 larvae per group) in comparison to mammalian models, giving greater confidence and reliability in the results obtained[26,27]. However, there are a number of limitations in the use of *G. mellonella* as an infection model. As an invertebrate, they naturally lack adaptive immunity making them unsuitable for antigenicity or immunological studies[10]. Cellular innate immune responses of *G. mellonella* are comprised of a number of hemocyte types, and plasmatocytes and granulocytes have been reported to function similarly to mammalian phagocytes (neutrophils and macrophages)[12]. However, the role and mechanisms of these cell types remain under characterized, and direct comparative studies between mammalian and insect phagocytes are yet to be carried out. Furthermore, the lack of an annotated *G. mellonella* genome hinders the analysis of the host response to infection, and this is currently reliant on gene ontology analysis against transcriptomic libraries of other invertebrates, such as *Drosophila melanogaster* and *Bombyx mori*[28].

As a TB infection model, *G. mellonella* holds a promising future with its ability to develop granuloma-like structures in response to BCG *lux* infection[16], which are vital pathophysiological hallmarks of TB infection and are a key feature in the development of LTBI. Future work will aim to characterize this model with a particular interest in the formation of granuloma-like structures using reference, clinical and mutant *Mtb* isolates under CL3 conditions. Additionally, we anticipate that it may also be useful for novel anti-mycobacterial agent screening, as a similar *G. mellonella* model was used for NTMs[18], but this remains to be determined. The adoption of this model has the ability to significantly reduce the number of animals used within the TB research community, while simultaneously accelerating in vivo TB research output under ethically more acceptable conditions.

Disclosures

The authors have nothing to disclose.

Acknowledgments

This project was supported by grants from the Biotechnology and Biological Science Research Council (BBSRC), awarded to PRL and YL (BB/P001262/1), and the National Center for the Replacement, Refinement and Reduction of Animals in Research (NC3Rs) awarded to PRL, SMN, BDR, and YL (NC/R001596/1).

References

1. World Health Organization. *Global tuberculosis report 2018*. Geneva. (2018).

Copyright © 2019 Creative Commons Attribution 3.0 License

2. Colditz, G.A. et al. Efficacy of BCG Vaccine in the prevention of tuberculosis: meta-analysis of the published literature. *The Journal of the American Medical Association.* **271** (9), 698-702 (1994).
3. Meijer, A.H., Spaink, H.P. Host-pathogen interactions made transparent with the zebrafish model. *Current Drug Targets.* **12** (7), 1000-1017 (2011).
4. Zhan, L., Tang, J., Sun, M., Qin, C. Animal models for tuberculosis in translational and precision medicine. *Frontiers in Microbiology.* **8**, 717 (2017).
5. Gumbo, T., Lenaerts, A.J., Hanna, D., Romero, K., Nuermberger, E. Nonclinical models for antituberculosis drug development: a landscape analysis. *Journal of Infectious Diseases.* **211** (Suppl 3), S83-95 (2015).
6. Williams, A., Orme, I.M. Animal models of tuberculosis: an overview. *Microbiology Spectrum.* **4** (4), TBTB2-004-2015 (2016).
7. Myllymäki, H., Niskanen, M., Oksanen, K.E., Rämet, M. Animal models in tuberculosis research - where is the beef? *Expert Opinion in Drug Discovery.* **10** (8), 871-883 (2015).
8. Flynn, J.L., Gideon, H.P., Mattila, J.T., Lin, P.L. Immunology studies in non-human primate models of tuberculosis. *Immunological Reviews.* **264** (1), 60-73 (2015).
9. Cook, S.M., McArthur, J.D. Developing *Galleria mellonella* as a model host for human pathogens. *Virulence.* **4** (5), 350-353 (2013).
10. Tsai, C.J.-Y., Loh, J.M.S., Proft, T. *Galleria mellonella* infection models for the study of bacterial diseases and for antimicrobial drug testing. *Virulence.* **7** (3), 214-229 (2016).
11. Wojda, I. Immunity of the greater wax moth *Galleria mellonella*. *Insect Science.* **24** (3), 342-357 (2017).
12. Browne, N., Heelan, M., Kavanagh, K. An analysis of the structural and functional similarities of insect hemocytes and mammalian phagocytes. *Virulence.* **4** (7), 597-603 (2013).
13. Arteaga Blanco, L.A. et al. Differential cellular immune response of *Galleria mellonella* to *Actinobacillus pleuropneumoniae*. *Cell and Tissue Research.* **370** (1), 153-168 (2017).
14. López Hernández, Y., Yero, D., Pinos-Rodríguez, J.M., Gibert, I. Animals devoid of pulmonary system as infection models in the study of lung bacterial pathogens. *Frontiers in Microbiology.* **6**, 38 (2015).
15. Ramarao, N., Nielsen-Leroux, C., Lereclus, D. The Insect *Galleria mellonella* as a powerful infection model to investigate bacterial pathogenesis. *Journal of Visualized Experiments.* (70), e4392 (2012).
16. Li, Y. et al. *Galleria mellonella* - a novel infection model for the *Mycobacterium tuberculosis* complex. *Virulence.* **9** (1), 1126-1137 (2018).
17. Meir, M., Grosfeld, T., Barkan, D. Establishment and validation of *Galleria mellonella* as a novel model organism to study *Mycobacterium abscessus* infection, pathogenesis, and treatment. *Antimicrobial Agents and Chemotherapy.* **62** (4), e02539-17 (2018).
18. Entwistle, F.M., Coote, P.J. Evaluation of greater wax moth larvae, *Galleria mellonella*, as a novel in vivo model for non-tuberculosis mycobacteria infections and antibiotic treatments. *Journal of Medical Microbiology.* **67** (4), 585-597 (2018).
19. Snewin, V.A., Gares, M., Ógaora, P., Hasan, Z., Brown, I.N., Young, D.B. Assessment of immunity to mycobacterial infection with luciferase reporter constructs. *Infection and Immunity.* **67** (9), 4586-4593 (1999).
20. Newton, S., Martineau, A., Kampmann, B. A functional whole blood assay to measure viability of mycobacteria, using reporter-gene tagged BCG or M.Tb (BCG *lux*/M.Tb *lux*). *Journal of Visualized Experiments.* (55), e3332-e3332 (2011).
21. Jorjão, A.L. et al. From moths to caterpillars: Ideal conditions for *Galleria mellonella* rearing for in vivo microbiological studies. *Virulence.* **9** (1), 383-389 (2018).
22. Kavanagh, K., Sheehan, G. The use of *Galleria mellonella* larvae to identify novel antimicrobial agents against fungal species of medical interest. *Journal of Fungi.* **4** (3), 113 (2018).
23. Champion, O., Titball, R., Bates, S. Standardization of *G. mellonella* larvae to provide reliable and reproducible results in the study of fungal pathogens. *Journal of Fungi.* **4** (3), 108 (2018).
24. Wojda, I., Taszlow, P., Jakubowicz, T. The effect of cold shock on the immune response of the greater wax moth *Galleria mellonella* after infection with entomopathogenic bacteria *Bacillus thuringiensis*. *Journal of Maria Curie-Sklodowska University.* **69** (2), 7-18 (2015).
25. Nascimento, I.P., Leite, L.C.C. The effect of passaging in liquid media and storage on *Mycobacterium bovis* - BCG growth capacity and infectivity. *FEMS Microbiology Letters.* **243** (1), 81-86 (2005).
26. De Groote, M.A. et al. Comparative studies evaluating mouse models used for efficacy testing of experimental drugs against *Mycobacterium tuberculosis*. *Antimicrobial Agents and Chemotherapy.* **55** (3), 1237-1247 (2011).
27. Grosset, J. et al. Modeling early bactericidal activity in murine tuberculosis provides insights into the activity of isoniazid and pyrazinamide. *Proceedings of the National Academy of Sciences U.S.A.* **109** (37), 15001-15005 (2012).
28. Vogel, H., Altincicek, B., Glöckner, G., Vilcinskas, A. A comprehensive transcriptome and immune-gene repertoire of the lepidopteran model host *Galleria mellonella*. *BMC Genomics.* **12**, 308 (2011).

Copyright © 2019 Creative Commons Attribution 3.0 License

frontiers in Microbiology

ORIGINAL RESEARCH
published: 20 November 2019
doi: 10.3389/fmicb.2019.02630

Galleria mellonella: An Infection Model for Screening Compounds Against the *Mycobacterium tuberculosis* Complex

Masanori Asai[1†], Yanwen Li[2†], Jasmeet Singh Khara[1,2], Brian D. Robertson[3], Paul R. Langford[1†] and Sandra M. Newton[1†]*

[1]Section of Paediatric Infectious Diseases, Department of Infectious Disease, Imperial College London, London, United Kingdom, [2]Department of Pharmacy, National University of Singapore, Singapore, Singapore, [3]MRC Centre for Molecular Bacteriology and Infection, Department of Infectious Disease, Imperial College London, London, United Kingdom

OPEN ACCESS

Edited by:
Thomas Dick,
Hackensack Meridian Health,
United States

Reviewed by:
Andreas Vilcinskas,
University of Giessen, Germany
Siouxsie Wiles,
The University of Auckland,
New Zealand

***Correspondence:**
Sandra M. Newton
s.newton@imperial.ac.uk

[†]These authors have contributed equally to this work

Specialty section:
This article was submitted to Antimicrobials, Resistance and Chemotherapy, a section of the journal Frontiers in Microbiology

Received: 25 July 2019
Accepted: 29 October 2019
Published: 20 November 2019

Citation:
Asai M, Li Y, Khara JS, Robertson BD, Langford PR and Newton SM (2019) Galleria mellonella: An Infection Model for Screening Compounds Against the Mycobacterium tuberculosis Complex. Front. Microbiol. 10:2630. doi: 10.3389/fmicb.2019.02630

Drug screening models have a vital role in the development of novel antimycobacterial agents which are urgently needed to tackle drug-resistant tuberculosis (TB). We recently established the larvae of the insect *Galleria mellonella* (greater wax moth) as a novel infection model for the *Mycobacterium tuberculosis* complex. Here we demonstrate its use as a rapid and reproducible screen to evaluate antimycobacterial drug efficacy using larvae infected with bioluminescent *Mycobacterium bovis* BCG *lux*. Treatment improved larval survival outcome and, with the exception of pyrazinamide, was associated with a significant reduction in *in vivo* mycobacterial bioluminescence over a 96 h period compared to the untreated controls. Isoniazid and rifampicin displayed the greatest *in vivo* efficacy and survival outcome. Thus *G. mellonella*, infected with bioluminescent mycobacteria, can rapidly determine *in vivo* drug efficacy, and has the potential to significantly reduce and/or replace the number of animals used in TB research.

Keywords: *Galleria mellonella*, tuberculosis, infection model, *Mycobacterium tuberculosis* complex, drug screening, antimycobacterial agents, mycobacteria

INTRODUCTION

In 2017 alone, there were 1.6 million deaths from tuberculosis (TB), the leading global cause of infectious disease mortality (World Health Organization, 2018). It is estimated that approximately a quarter of the world's population is infected with *Mycobacterium tuberculosis* (MTB), the causative agent of TB. While the majority of these individuals are non-symptomatic and non-contagious carriers of latent TB infection (LTBI), 5–10% will develop symptomatic and highly contagious active disease over their lifetime (Pai et al., 2016; World Health Organization, 2018). Treatment of TB typically requires the use of four antimycobacterial drugs for a minimum duration of 6 months, which is associated with toxicity and/or unpleasant side effects. Treatment of TB has also become increasingly challenging with the rise and spread of multidrug (MDR) and extensively drug-resistant (XDR) TB (Fogel, 2015). Treatment challenges will likely worsen due to the limited arsenal of antimycobacterial drugs available, with only two novel antimycobacterial drugs, bedaquiline

and delamanid, being approved by the Food and Drug Administration (FDA) in the past four decades (Tiberi et al., 2019). Alarmingly, spontaneous resistance to bedaquiline and delamanid has already been reported in a number of studies (Bloemberg et al., 2015; Hoffmann et al., 2016). In 2015, the World Health Organization commissioned a global campaign to end TB, which aims to achieve a reduction in deaths and incidence of 95 and 90%, respectively, by 2035 (World Health Organization, 2018). However, despite global efforts, the progress of the End TB strategy has been bottlenecked by insufficient funding (Reid et al., 2019). One of the fundamental pillars of the End TB strategy is to intensify research and innovation, such as the research and development of novel, more effective, and safer antimycobacterial therapeutics. Based on the current trajectory, by 2050, MDR and XDR-TB alone will account for 2.5 million deaths each year (Reid et al., 2019). To minimize a further rise of MDR and XDR-TB and avoid catastrophic numbers of AMR TB mortality, there is an urgent need for the development of new anti-TB agents with novel mechanisms of action.

Animal infection models play a vital role in facilitating the advancement in TB research from pathogenesis to drug development (Zhan et al., 2017). Paradoxically, they are also one of the greatest bottlenecks in TB drug development, with all models being limited by financial sustainability, ethical regulation, research throughput, and physiological capacity to mimic TB disease (Zhan et al., 2017). For example, conventional murine models do not typically develop necrotic granulomas, which are observed in humans. While guinea pigs are able to develop human-like necrotic granulomas, there is a lack in abundance of immunological tools and their larger size increases maintenance costs (Zhan et al., 2017). Furthermore, large numbers of animals are used to screen candidate therapeutic compounds with promising activity *in vitro*, which often do not translate *in vivo* (Tsai et al., 2016). Additionally, some animal models (e.g., mice and non-human primates) can display significant biological variability within and between experiments, which is further influenced by the limited sample size as a consequence of ethical regulations (Fitts, 2011; Zhan et al., 2017). These problems underline the need for a novel, higher throughput, large-scale, drug screening infection model for TB.

We recently determined that the insect *Galleria mellonella* (*G. mellonella*, greater wax moth) can be used as a novel infection model for members of the *Mycobacterium tuberculosis* complex (MTBC) (Li et al., 2018) using *M. bovis* BCG *lux* (BCG *lux*), a vaccine strain incorporating a bioluminescence reporter plasmid (Snewin et al., 1999). BCG *lux* has been extensively validated and characterized under both *in vivo* (mice) and *in vitro* (broth, human whole blood, cell line) conditions and its bioluminescence can be used as a rapid measurement of mycobacterial viability (Kampmann et al., 2000, 2004, 2006; Tena et al., 2003; Martineau et al., 2007a,b,c; Newton et al., 2008, 2011; Andreu et al., 2010; Von Both et al., 2018). BCG *lux* was able to establish a persistent infection over a 2-week time-course with bacteria being internalized by phagocytic hemocytes (functionally similar to neutrophils and macrophages), and the presence of granuloma-like structures. Changes in mycobacterial phenotype within hemocytes were observed with the accumulation of lipid fat bodies, a hallmark of mycobacterial cells in LTBI (Li et al., 2018). Furthermore, *G. mellonella* has been widely used as an infection model to study a large range of pathogens, which include Gram-positive bacteria, e.g., *Streptococcus pyogenes*, *Staphylococcus aureus*, and *Clostridium perfringens* (Desbois and Coote, 2011; Loh et al., 2013; Kay et al., 2019); Gram-negative bacteria, e.g., *Legionella pneumophila*, *Pseudomonas aeruginosa*, and *Escherichia coli* (Harding et al., 2012; Alghoribi et al., 2014; Andrejko et al., 2014); and fungal pathogens, e.g., *Candida albicans* (Sheehan and Kavanagh, 2018). In this report, we demonstrate that *G. mellonella* larvae can also act as a surrogate host to evaluate the efficacy of antimycobacterial therapeutic agents, with the potential to be used as a low-cost, highly reproducible, ethically more acceptable and higher throughput, pre-screening model for drug testing against mycobacteria compared to conventional animal models.

MATERIALS AND METHODS

Mycobacteria, Growth, and Inoculum Preparation

M. bovis BCG *lux* (Montréal vaccine strain), transformed with the plasmid pSMT1 containing the *luxAB* genes of *Vibrio harveyi*, was kindly donated by Professor Young's lab (Snewin et al., 1999). Mid-log phase cultures of BCG *lux* were prepared in Middlebrook 7H9 broth (Difco, US), supplemented with 0.2% glycerol (Sigma-Aldrich, UK), 0.05% polysorbate 80 (Sigma-Aldrich, UK) and 10% albumin dextrose catalase (ADC) as described previously (Li et al., 2018). The bioluminescence of a BCG *lux* culture was measured by a luminometer (Berthold Technologies, DE) using decanal (Sigma-Aldrich, UK) as the substrate (1% v/v in absolute ethanol). Bioluminescence was quantified as relative light units (RLU/ml), which was previously correlated to colony forming units (CFU/ml) at a ratio of 3:1, and is used to rapidly quantify bacterial abundance. BCG *lux* inocula were prepared at 1×10^8 or 1×10^9 CFU/ml in PBS-Tween 80 (PBS-T, 0.05%) (Li et al., 2018).

Preparation of Antibiotics

Antibiotics were purchased from Sigma-Aldrich. Concentrations were prepared according to the recommended adult human dosages, at a relative body/mass concentration for the larvae (200 mg). First-line drugs: isoniazid (5 mg/kg, INH), rifampicin (10 mg/kg, RIF), pyrazinamide (25 mg/kg, PZA), and ethambutol (15 mg/kg, ETH); and the second-line drug moxifloxacin (6.7 mg/kg, MOX) were used. Relative to mammalian models, these treatment doses are equal to/or lower than what is typically used in mice (Mourik et al., 2017; Lee et al., 2018).

G. mellonella Acquisition, Infection, and Drug Treatment

G. mellonella larvae were purchased from Livefoods Direct Ltd. (Sheffield, UK). Healthy larvae were defined as those possessing a uniform cream color that lack discoloration (melanization), high motility with the ability to right themselves when turned over, 250 mg in weight, and 2–3 cm in length (Li et al., 2018). Larval surfaces were decontaminated using 70% ethanol and 10 µl of BCG *lux* was injected into the hemocoel via the last left proleg using a micro syringe (SGE Analytical Sciences, AU). Infected larvae were counted into 25-cm petri dishes lined with filter paper, and incubated in the dark at 37°C. For treatment, a 10 µl dose of a single drug type or drug combination was injected directly into the hemocoel via the last left proleg 1 h post-infection. Where multiple dosing was undertaken, an additional 10 µl dose was injected 24 h post-infection.

Survival Assay

Survival of infected larvae ($n = 20$ per group) following treatment was recorded every 24 h for 96 h. Larvae were considered dead when they failed to respond to touch. The control groups were infected larvae treated with 10 µl of PBS-T. Kaplan-Meier survival curves were plotted using data pooled from a minimum of two independent experiments.

Measurement of *in vivo* BCG *lux* Bioluminescence

Larvae ($n = 30$ per group) were infected. At each time point (0–96 h), four larvae were randomly selected and individually homogenized in PBS-T with six 1/8-inch metal beads in a 2 ml lysing tube (MP Biomedical, USA). The RLU of the homogenate was measured using a luminometer to quantify the internal mycobacterial bioluminescence. *In vivo* drug efficacy was determined using two or typically three independent experiments. *In vivo* RLU:CFU was determined to be 4:1 (Li et al., 2018). Homogenate of uninfected larvae was measured to determine background bioluminescence, which was approximately 5,000 RLU/ml.

Total Hemocyte Count

Larvae ($n = 20$ per group) were injected with 10 µl of PBS-T, INH, or RIF. At 2, 4, and 24 h post-injection, five larvae from each group were bled through needle puncture of the posterior abdomen (approximately 3 drops/60 µl per larva) using a 30 Gauge needle and their hemolymph was pooled into an ice cold Eppendorf to prevent coagulation. Bleeding is a terminal procedure. A volume of 200 µl of the pooled hemolymph was diluted in to PBS containing citrate buffer and 0.37% mercaptoethanol to further prevent coagulation and melanization. Hemolymph mixtures were centrifuged at 1,000 g for 10 min and the cell pellet resuspended in PBS. Then, 10 µl of the cell suspension was further diluted 1:1 with 0.4% trypan blue solution and total hemocyte count (THC) was determined using a hemocytometer. THCs were determined using three independent experiments.

Minimum Inhibitory Concentration Assay

The *in vitro* minimal inhibitory concentration (MIC), which is defined as the minimal concentration of antimycobacterial drug required to inhibit the growth of BCG *lux*, was determined for this study. A volume of 100 µl of antimycobacterial drugs, prepared in Middlebrook 7H9 broth, was seeded in triplicate into a 96-well plate. Additional 100 µl aliquots of mid-log BCG *lux* at a dilution of 1×10^6 CFU/ml were seeded into each well of the 96-well plate. The positive control consisted of bacterial culture alone; and the negative control consisted of broth alone. The plates were incubated at 37°C in a rocking incubator at 20 rpm for 1 week. Following incubation, optical density of each well was measured in a spectrophotometric plate reader (Molecular Device, UK) at 520 nm. MIC was determined through two independent experiments.

Statistical Analysis

The datasets were tested for normality using D'Agostino-Pearson omnibus. Data were then analyzed using the non-parametric Kruskal-Wallis test, followed by the Dunn's multiple comparison test, or Mann-Whitney test. All statistical analyses were carried out using Prism 8 (Graphpad Software Inc., UK).

RESULTS

All infected larvae in the control groups showed physiological changes including melanization, reduction in mobility and activity, and observational wasting. Treatment of larvae infected with a lethal dose of BCG *lux*, previously defined as 1×10^7 CFU (Li et al., 2018), using first- or second-line antimycobacterial drugs, resulted in improved survival outcome at all time points over the 96 h time-course with all drugs tested, when compared to the untreated control group (**Figure 1**). Larvae treated with RIF and INH had the greatest overall survival (100 and 95%, respectively) after 96 h of incubation. By similarly treating healthy naïve larvae with antibiotics alone, we demonstrated that the drug dosages did not result in cytotoxic activity leading to larval mortality (**Supplementary Figure S1**).

Furthermore, we demonstrated that an increase or decrease in BCG *lux* bioluminescence in larval lysates can be used to rapidly determine antimycobacterial drug efficacy, when compared to bioluminescence of non-treated infected larvae. In most treatment groups (INH, RIF, ETH, and MOX), we measured a substantial reduction in mycobacterial bioluminescence over the 96 h (**Figure 2**). INH showed the greatest reduction in mycobacterial bioluminescence, and hence inhibitory activity, at each time point between 24 and 96 h ($p < 0.0001$), with approximately a 1-log or 94% reduction at 96 h compared to the control (**Figure 2**). Comparison of the mean RIF, ETH, and MOX bioluminescence against the PBS control at 96 h revealed a reduction in mycobacterial bioluminescence of approximately 61%. PZA

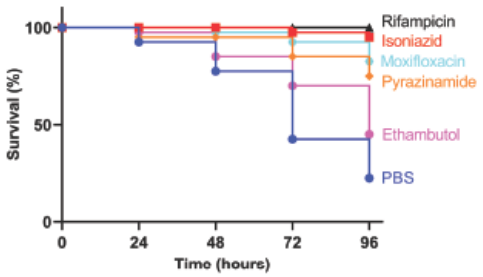


FIGURE 1 | Kaplan-Meier survival curves of *Galleria mellonella* larvae infected with *Mycobacterium bovis* BCG *lux* and treated with first- or second-line antimycobacterial drugs. Larvae (n = 20, per group) were infected with 1 × 10^7 CFU of *M. bovis* BCG *lux*. Following infection, larvae were treated with a single 10 µl dose of isoniazid (5 mg/kg), rifampicin (10 mg/kg), pyrazinamide (25 mg/kg), ethambutol (15 mg/kg), or moxifloxacin (6.7 mg/kg). Control groups consisted of infected larvae, treated with a 10 µl dose of PBS-Tween 80 (0.05%). Survival was monitored every 24 h over a period of 96 h. Data are pooled from a minimum of two independent experiments.

was the least effective drug with no more than 26% reduction in mean bioluminescence when compared to the control at any given time point. Despite substantial changes in mycobacterial bioluminescence for most drugs, only INH showed a significant reduction in bioluminescence, with RIF, ETH, and MOX showing only a trend in bioluminescence reduction (**Figure 2**). The use of three varying concentrations of INH (5, 0.5, and 0.05 mg/ml), or RIF (10, 0.1, and 0.01 mg/ml), demonstrated that the drug efficacy observed was dose-dependent (**Figure 3**). *In vitro* MICs of antimycobacterial drug were determined as follows: INH (0.24 µg/ml), RIF (0.004 µg/ml), PZA (>31.3 µg/ml), ETH (0.98 µg/ml), and MOX (0.015 µg/ml).

Synergism of dual (INH/RIF and RIF/ETH) and triple (RIF, ETH, and MOX) drug combination therapy was similarly investigated (**Figure 4**). Use of INH/RIF resulted in a significant reduction in BCG *lux* bioluminescence at 24 h over treatment with RIF alone ($p < 0.05$). Throughout the 96 h time-course, INH/RIF did not improve drug efficacy over the standalone use of INH. RIF in dual (RIF/ETH and RIF/MOX) combination did not yield improved performance over the use of RIF alone. However, triple (RIF/ETH/MOX) combination led to significant

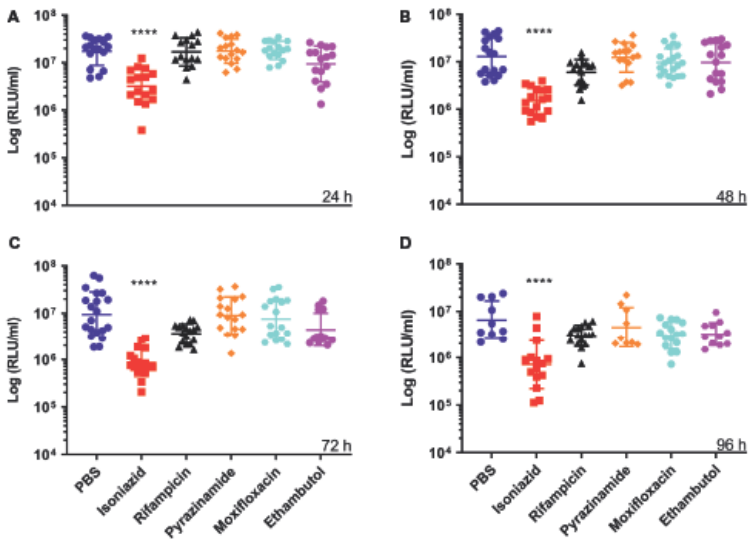


FIGURE 2 | The effect of antimycobacterial drug treatment on the reduction of *Mycobacterium bovis* BCG *lux* bioluminescence within *Galleria mellonella* larvae over 96 h. Larvae (n = 30 per group) were each infected with 1 × 10^7 CFU of *M. bovis* BCG *lux*. At 1 h post-infection, larvae were treated with a single 10 µl dose of isoniazid (5 mg/kg), rifampicin (10 mg/kg), pyrazinamide (25 mg/kg), ethambutol (15 mg/kg), and moxifloxacin (6.7 mg/kg). Control groups consisted of infected larvae similarly treated with a 10 µl dose of PBS-Tween 80 (0.05%). From each group, four larvae were homogenized at **(A)** 24 h, **(B)** 48 h, **(C)** 72 h, and **(D)** 96 h post-infection; and BCG *lux* luminescence of the homogenate was measured using a luminometer and expressed as relative light units (RLU/ml). Data are pooled from a minimum of three independent experiments. Error bars represent the standard deviation of the geometric mean. Kruskal-Wallis test with Dunn's multiple comparison was carried out against the control. ****$p < 0.0001$.

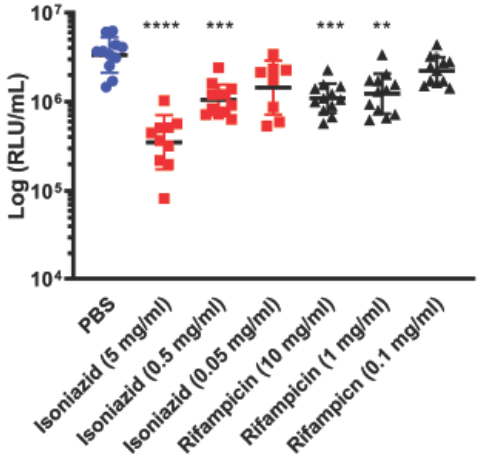


FIGURE 3 | The effect of isoniazid or rifampicin concentration on the reduction of *Mycobacterium bovis* BCG *lux* bioluminescence within *Galleria mellonella*. Larvae (n = 30 per group) were each infected with 1×10^7 CFU of *M. bovis* BCG *lux*. At 1 h post-infection, larvae were treated with a single 10 µl dose of isoniazid (5, 0.5, and 0.05 mg/kg) or rifampicin (10, 1, and 0.01 mg/kg). Control groups consisted of infected larvae similarly treated with a 10 µl dose of PBS-Tween 80 (0.05%). From each group, four larvae were homogenized 96 h post-infection and BCG *lux* luminescence of the homogenate was measured using a luminometer and expressed as relative light units (RLU/ml). Data are pooled from a minimum of three independent experiments. Error bars represent the standard deviation of the geometric mean. Kruskal-Wallis test with Dunn's multiple comparison was carried out against the PBS control. $^{**}p < 0.01$, $^{***}p < 0.001$, $^{****}p < 0.0001$.

improvement in drug efficacy at 96 h ($p < 0.05$) over the standalone use of RIF. Furthermore, in triple combination, both ETH and MOX showed significant improvements in drug efficacy by 96 h (**Figure 4**). We then determined whether multiple doses of either INH or RIF further reduced BCG *lux* bioluminescence in infected larvae over the course of the 96 h treatment period (**Figure 5**). There was no significant reduction in bioluminescence with multiple compared to single dosing of RIF over 96 h. For INH, multiple dosing showed little to no difference between 24 and 48 h in BCG *lux* bioluminescence compared to single dosing; however, between 48 and 96 h, there was a trend in improvement and a significant reduction at 96 h ($p < 0.01$).

Previous studies using *G. mellonella* reported activation of innate immunity or immune priming as a result of drug dosing (Entwistle and Coote, 2018; Sheehan and Kavanagh, 2018). Immune priming in our model was investigated by measuring the changes in number of circulating hemocytes in naïve larvae following treatment with INH or RIF. We observed no significant changes in the abundance of circulating hemocytes when compared against the PBS-treated control (**Figure 6**).

DISCUSSION

A number of studies have employed *G. mellonella* infection models using bacterial, viral, and fungal pathogens, to determine drug efficacy, dosing, and toxicity (Tsai et al., 2016). *G. mellonella* has thus proven to be a promising *in vivo* infection model, allowing rapid exploratory testing of novel compounds and treatment regimens without ethical constraints, prior to testing in conventional mammalian models (Tsai et al., 2016; Kavanagh and Sheehan, 2018) Furthermore, this model has the capacity to significantly reduce the number of animals used annually in drug pilot studies.

MTB animal research is limited by the prerequisite for containment level (CL) 3 animal facilities, with the associated maintenance costs and ethics (Fonseca et al., 2017). Therefore, to provide a more accessible *in vivo* TB research model, we established the *G. mellonella*-mycobacteria infection model as described previously, with the ability to undertake measurements of changes in host/pathogen interactions, transcriptome, and proteome (Li et al., 2018). Here we have further assessed the potential of *G. mellonella* as a drug screening model by evaluating the efficacy of standard antimycobacterial drugs.

Treatment of BCG *lux* infected larvae led to increased larvae survival and a reduction in BCG *lux* bioluminescence *in vivo*. INH and RIF proved to be the most effective first-line antimycobacterial drugs, which is comparable with studies in mice (Nikonenko et al., 2004; Driver et al., 2012), ETH and MOX showed a trend but non-significant reduction in bioluminescence. The antimycobacterial activity of each drug appeared to be time-dependent, which likely reflects the mode of action and thus the speed of mycobacterial inhibitory activity. In contrast, PZA consistently resulted in the highest bioluminescence of the treated groups and failed to reduce BCG *lux* bioluminescence at any time point, which is likely attributable to its intrinsic resistance to PZA due to deletion of *pncA*. This gene encodes for pyrazinamidase, essential for the conversion of PZA to "active drug," pyrazinoic acid (POA) (Ritz et al., 2009). While treatment with PZA lead to no more than 26% reduction in *in vivo* bioluminescence at any given point over the 96 h time-course, survival outcome of the PZA-treated group was substantially higher (75% survival) when compared to the PBS-treated control (22.5% survival). Despite the use of PZA as a core drug in the treatment of TB, the precise mechanism and target of the pro-drug remains elusive and still remains a topic of research (Shi et al., 2019). A study by Via and colleagues demonstrated that a substantial quantity of PZA is converted into POA by the host (Via et al., 2015). Recently, PanD (aspartate decarboxylase), involved in Coenzyme A biosynthesis, was identified as a target of POA (Gopal et al., 2017). If PZA is converted into POA by *G. mellonella*, this could account for the low-level efficacy in bioluminescence and improvement in survival outcome. However, PanD inhibition could be circumvented by BCG *lux* as *G. mellonella* are reared using vitamin B_5 (pantothenate)-rich diet (Finke, 2015), and the presence of exogenous pantothenate has been described to revert this resistance (Gopal et al., 2016). Additionally, POA resistance has also been associated with mutations in phthiocerol dimycocerosate (PDIM) biosynthesis genes *mas* and *ppsA-E* (Gopal et al., 2016),

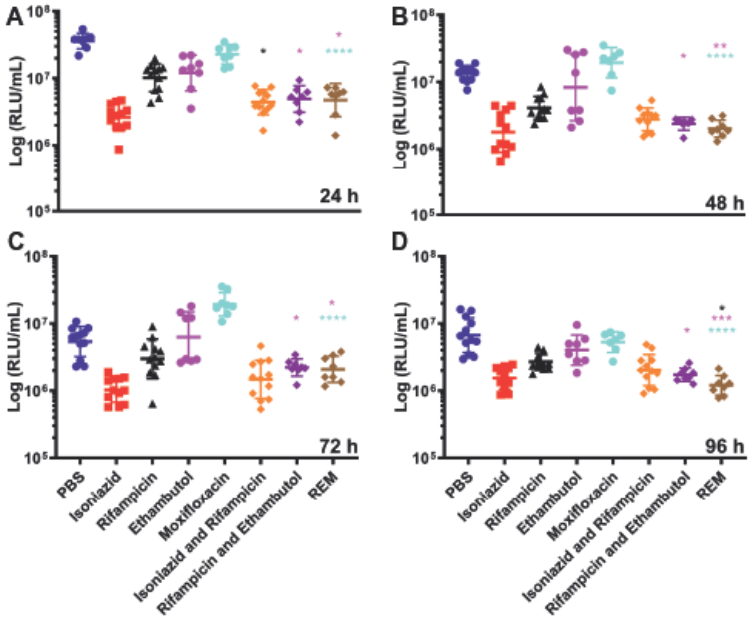


FIGURE 4 | The effect of combined dosing of antimycobacterial drugs on the reduction of *Mycobacterium bovis* BCG *lux* bioluminescence within *Galleria mellonella* larvae over 96 h. Larvae (n = 30 per group) were each infected with 1 × 10^7 CFU of *M. bovis* BCG *lux*. At 1 h post-infection, larvae were treated with a single 10 µl dose of isoniazid (5 mg/kg), rifampicin (10 mg/kg), isoniazid and rifampicin (5 and 10 mg/kg, respectively), rifampicin and ethambutol (10 and 15 mg/kg, respectively) and rifampicin, ethambutol and moxifloxacin (REM) (10, 15, and 6.7 mg/kg, respectively). Control groups consisted of infected larvae similarly treated with a 10 µl dose of PBS-Tween 80 (0.05%). From each group, four larvae were homogenized at **(A)** 24 h, **(B)** 48 h, **(C)** 72 h, and **(D)** 96 h post-infection; and *M. bovis* BCG *lux* luminescence of the homogenate was measured using a luminometer and expressed as relative light units (RLU/ml). Data are pooled from a minimum of two independent experiments. Error bars represent the standard deviation of the geometric mean. Kruskal-Wallis test with Dunn's multiple comparison was carried out between the combination drug and mono drugs therapy groups. *$p < 0.05$, **$p < 0.01$, ***$p < 0.001$, ****$p < 0.0001$, asterisk color correlates to treatment group.

suggesting a potential anti-virulent activity by PZA/POA. Therefore we speculate that host-mediated bioactivation of PZA to POA and/ or the interference with the production of PDIM by PZA/POA may potentially have led to increased survival outcome. This will be a subject for further investigation. The treatment of TB typically requires the use of a combination of antimycobacterial drugs, administered on multiple occasions (World Health Organization, 2010). We therefore investigated multiple drug dosing and combination drug therapy, using the *G. mellonella* model. Both combined, and multiple dosing, showed a trend in improved antimycobacterial activity over monotherapy and single dosing. The lack of a significant reduction in BCG *lux* luminescence with combination drug therapy over the use of single drug was not surprising, as the primary aim of combined drug therapy is to minimize the risk of drug resistance development (World Health Organization, 2010). Further work will determine the usage of *G. mellonella* for screening novel antimycobacterial agents and their synergistic activities with frontline drugs. Additionally, we observed a drug dose-dependent efficacy at three varying doses of INH and RIF, which clearly highlights the sensitivity of this model to changes in drug dosing. Therefore, we suggest that researchers should test various doses of their drugs of interest to determine the optimum dose. There is little information on the pharmacokinetics and pharmacodynamics of antibiotics in *G. mellonella* (Thomas et al., 2013), and no data to our knowledge with antimycobacterial drugs. Further studies are warranted and likely to increase the uptake of the *G. mellonella*-mycobacterial model.

The use of BCG over *Mycobacterium smegmatis* as a surrogate for MTB was rationalized by its genetic similarity. BCG shares >99.99% genetic similarity to MTB, while *M. smegmatis* shares roughly 70% of its genome with MTB (Garnier et al., 2003; Mohan et al., 2015; Yuan and Sampson, 2018). Furthermore, when 2,000 compounds were screened against MTB, BCG, and *M. smegmatis*, approximately 80% of compounds that were active in BCG showed efficacy against MTB, while only 50% of the compounds that were active in *M. smegmatis* displayed efficacy against MTB (Altaf et al., 2010). Therefore, BCG appears to be a more superior surrogate mycobacterial organism for drug screening against MTB when compared to *M. smegmatis*.

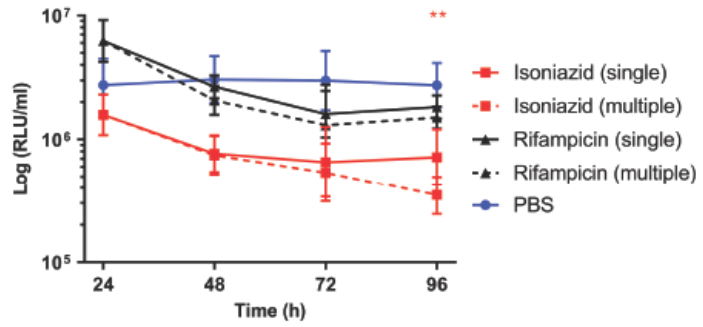


FIGURE 5 | The effect of multiple dosing of isoniazid and rifampicin on the reduction of *Mycobacterium bovis* BCG *lux* bioluminescence within *Galleria mellonella* larvae over 96 h. Larvae ($n = 30$ per group) were each infected with 1×10^7 CFU of *M. bovis* BCG *lux*. For multiple dosing, isoniazid (5 mg/kg) or rifampicin (10 mg/kg) was administered at both 1 h post-infection and 24 h post-infection. Control groups consisted of infected larvae similarly treated with a 10 µl dose/doses of PBS-Tween 80 (0.05%). From each group, four larvae were homogenized at 24, 48, 72, and 96 h post-infection. *M. bovis* BCG *lux* luminescence of the homogenate was measured using a luminometer and expressed as relative light units (RLU/ml). Data are pooled from a minimum of two independent experiments. Error bars represent the standard deviation of the geometric mean. Mann-Whitney test was carried out between single and multiple dosing of each drug type. $^{**}p < 0.01$, asterisk color correlates to treatment group.

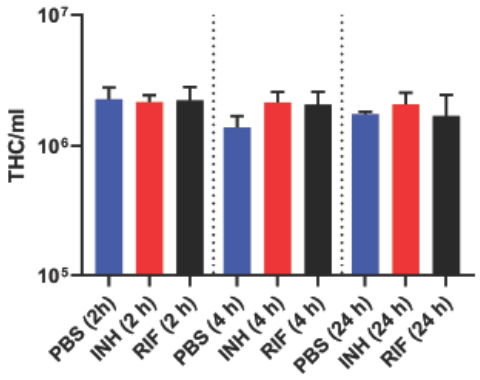


FIGURE 6 | Measurement of total circulating hemocyte density following injection of antimycobacterial drug over 24 h. Naïve healthy *Galleria mellonella* larvae ($n = 20$, per group) were treated with a single 10 µl dose of isoniazid (5 mg/kg) or rifampicin (10 mg/kg). Control groups consisted of larvae, treated with a 10 µl dose of PBS-Tween 80 (0.05%). At 2, 4, and 24 h post-treatment, five larvae from each group were bled, pooled, and the number of total hemocytes (THC) per ml was determined. Data are pooled from a minimum of three independent experiments. Error bars represent the standard deviation of the geometric mean. Kruskal-Wallis test with Dunn's multiple comparison was carried out against the PBS control.

Drug efficacies for non-tuberculous mycobacteria (NTM) such as *Mycobacterium marinum*, *Mycobacterium aurum*, *Mycobacterium fortuitum*, and *Mycobacterium abscessus* have been reported in the *G. mellonella* model. However, comparisons between mycobacterial species are challenging as the drug efficacies and susceptibilities of NTM are different to those observed for the MTBC (Entwistle and Coote, 2018; Meir et al., 2018).

The innate immune system of *G. mellonella* is highly sensitive to external factors ranging from thermal, physical, and chemical stress (Browne et al., 2014; Sheehan and Kavanagh, 2018). Browne et al. highlighted that innate immune priming can occur in response to thermal stress, leading to a transient increase in circulating hemocyte density and production of antimicrobial peptides in anticipation of infection. A similar priming response can also occur in response to antibiotic treatment (Entwistle and Coote, 2018; Sheehan and Kavanagh, 2018). However, in our *G. mellonella* model, the use of INH and RIF, the most efficacious drugs, led to non-significant minor or no changes in circulating hemocyte density when compared to the PBS-treated control. Regardless of our observation, the possibility of immune priming should be explored when testing any new drugs in this model, as this may influence the outcome of the experiment. Antimicrobial peptides (AMP) are additional immune factors that should be taken into consideration when using this model for drug screening. Approximately 20 putative AMP have thus far been identified in *G. mellonella* (Pereira et al., 2018). Synergism of *G. mellonella* AMP with antibiotics has not yet been described. However a number of studies have reported synergism between AMP of other invertebrate and antibiotics, e.g., AMP of *Apis mellifera* with vancomycin (Akbari et al., 2019) or AMP of *Aedes aegypti* with tetracycline (Zheng et al., 2017). As such, the production and abundance of host AMP and the potential synergism with conventional antibiotics for treatment of TB will be investigated in the near future as a separate proteomic study.

The establishment of infection prior to treatment in a host organism is an important factor to consider when defining the true efficacy of the drugs tested *in vivo*, and the time required for the establishment of infection can vary between models, e.g., establishment of infection in mouse model will generally

take longer than those seen in *Drosophila melanogaster* (fruit fly) or *Danio rerio* (zebrafish) (Dionne et al., 2003; Myllymäki et al., 2016; Zhan et al., 2017). Additionally, the incubation period following infection can be altered to further mimic types of infection, e.g., active TB infection or LTBI in certain models. For this particular study, 1 h post-infection was chosen as a point of treatment for two reasons. Firstly, a previous study has shown that phagocytosis of mycobacteria occurs within 1 h post-infection demonstrated through the Fluorescein isothiocyanate (FITC) labeled non-tuberculous mycobacteria (NTM) phagocytic assay using similar inocula density (3×10^7 CFU) (Entwistle and Coote, 2018). Secondly, the standard procedure for the treatment of *G. mellonella* following infection is typically 30 min to 2 h post-infection (Tsai et al., 2016). Nonetheless, we do acknowledge the potential merits of extended incubation prior to treatment. For example, Meir and colleagues (Meir et al., 2018) started treatment of *M. abscessus* infected *G. mellonella* at 24 and 48 h post-infection. However, this required the use of a low dose of bacterial inocula (1×10^3 CFU) to accommodate the required incubation period. A potential downside of the use of extended incubation time prior to treatment may be the possible accumulation or time-dependent induction of AMP within the hemocoel (Sheehan et al., 2019). In future studies, the effect of treatment timing on drug efficacy will be evaluated.

As briefly mentioned above, other non-mammalian infection models such as *D. melanogaster* and *D. rerio* have similarly been used for antimycobacterial drug screening (Dionne et al., 2003; Oh et al., 2013; Ordas et al., 2015). However, both the fruit fly and zebrafish are biologically incompatible with the MTBC and require the use of *M. marinum* as a surrogate organism for MTB (Myllymäki et al., 2015; Zhan et al., 2017). In contrast, both MTBC and NTM species can be used with *G. mellonella* (Entwistle and Coote, 2018; Meir et al., 2018), providing a broader variety of compatible mycobacterial species for use when screening antimycobacterial compounds. While *M. marinum* and MTBC share significant similarities in the expression of virulence factors and other physiological properties (Tobin and Ramakrishnan, 2008), antimycobacterial drug efficacy against NTM does not always lead to efficacy in MTBC. Furthermore, the ability to study mycobacterial responses under human physiological conditions (e.g., 37°C) during drug treatment using MTBC is highly desirable, as temperature can affect mycobacterial physiology (Flentie et al., 2016). Infection of both *D. melanogaster* and *D. rerio* typically requires the use of a costly microinjector, where bacterial inocula/drugs are delivered through a glass capillary tube under microscopy due to their size. For novice users, this method of infection can be difficult and training and familiarity with the technique become essential for throughput and experimental outcome (Benard et al., 2012; Khalil et al., 2015). For infection of *D. rerio*, recent advances now allow for a non-invasive natural method of infection through bathing (Dalton et al., 2017). In comparison, the BCG *lux-G. mellonella* infection model requires minimal training, the prerequisite of infection is an inexpensive micro syringe alone, and the size of *G. mellonella* (2–3 cm) makes handling and manipulation of the larvae during injection effortless (Asai et al., 2019).

CONCLUSION

In conclusion, this proof-of-principle study has shown that *G. mellonella* combined with the use of a bioluminescent reporter mycobacterial species allows for the rapid determination of efficacy of antimycobacterial agents and drug regimens. There are a number of advantages over pre-existing non-mammalian infection models, such as relative ease of infection for novice users and the ability to utilize MTBC over NTM. The successful uptake of this model as a drug screen within the TB research community could accelerate drug development while significantly reducing and replacing the use of animal models in TB drug research and development.

DATA AVAILABILITY STATEMENT

The datasets generated for this study are available on request to the corresponding author.

AUTHOR CONTRIBUTIONS

MA, YL, and JK contributed to acquisition, analysis, and interpretation of data for the work. MA wrote the first draft. All authors contributed to the conception and design of the work and to manuscript revision, and read and approved the submitted and final version.

FUNDING

This work was supported by the Biotechnology and Biological Sciences Research Council (BBSRC) (BB/P001262/1 to PL and YL) and the National Centre for the Replacement, Refinement and Reduction of Animals in Research (NC3Rs) (NC/R001596/1 to PL, SN, BR, and YL).

SUPPLEMENTARY MATERIAL

The Supplementary Material for this article can be found online at: https://www.frontiersin.org/articles/10.3389/fmicb.2019.02630/full#supplementary-material

REFERENCES

Akbari, R., Hakemi-Vala, M., Pashaie, F., Bevalian, P., Hashemi, A., and Bagheri, K. P. (2019). Highly synergistic effects of melittin with conventional antibiotics against multidrug-resistant isolates of *Acinetobacter baumannii* and *Pseudomonas aeruginosa*. *Microb. Drug Resist.* 25, 193–202. doi: 10.1089/mdr.2018.0016

Alghoribi, M. F., Gibreel, T. M., Dodgson, A. R., Beatson, S. A., and Upton, M. (2014). *Galleria mellonella* infection model demonstrates high lethality of ST69 and ST127 uropathogenic *Escherichia coli*. *PLoS One* 9:e101547. doi: 10.1371/journal.pone.0101547

Altaf, M., Miller, C. H., Bellows, D. S., and O'Toole, R. (2010). Evaluation of the *Mycobacterium smegmatis* and BCG models for the discovery of

Mycobacterium tuberculosis inhibitors. *Tuberculosis* 90, 333–337. doi: 10.1016/j.tube.2010.09.002

Andrejko, M., Zdybicka-Barabas, A., and Cytryńska, M. (2014). Diverse effects of *Galleria mellonella* infection with entomopathogenic and clinical strains of *Pseudomonas aeruginosa*. *J. Invertebr. Pathol.* 115, 14–25. doi: 10.1016/j.jip.2013.10.006

Andreu, N., Zelmer, A., Fletcher, T., Elkington, P. T., Ward, T. H., Ripoll, J., et al. (2010). Optimisation of bioluminescent reporters for use with mycobacteria. *PLoS One* 5:e10777. doi: 10.1371/journal.pone.0010777

Asai, M., Li, Y., Singh Khara, J., Gladstone, C. A., Robertson, B. D., Langford, P. R., et al. (2019). Use of the invertebrate *Galleria mellonella* as an infection model to study the *Mycobacterium tuberculosis* complex. *J. Vis. Exp.* e59703. doi: 10.3791/59703

Benard, E. L., van der Sar, A. M., Ellett, F., Lieschke, G. J., Spaink, H. P., and Meijer, A. H. (2012). Infection of zebrafish embryos with intracellular bacterial pathogens. *J. Vis. Exp.* e3781. doi: 10.3791/3781

Bloemberg, G. V., Keller, P. M., Stucki, D., Trauner, A., Borrell, S., Latshang, T., et al. (2015). Acquired resistance to bedaquiline and delamanid in therapy for tuberculosis. *N. Engl. J. Med.* 373, 1986–1988. doi: 10.1056/NEJMc1505196

Browne, N., Surlis, C., and Kavanagh, K. (2014). Thermal and physical stresses induce a short-term immune priming effect in *Galleria mellonella* larvae. *J. Insect Physiol.* 63, 21–26. doi: 10.1016/j.jinsphys.2014.02.006

Dalton, J. P., Uy, B., Okuda, K. S., Hall, C. J., Denny, W. A., Crosier, P. S., et al. (2017). Screening of anti-mycobacterial compounds in a naturally infected zebrafish larvae model. *J. Antimicrob. Chemother.* 72, 421–427. doi: 10.1093/jac/dkw421

Desbois, A. P., and Coote, P. J. (2011). Wax moth larva (*Galleria mellonella*): an *in vivo* model for assessing the efficacy of antistaphylococcal agents. *J. Antimicrob. Chemother.* 66, 1785–1790. doi: 10.1093/jac/dkr198

Dionne, M., Ghori, N., and Schneider, D. (2003). *Drosphila melonagaster* is a genetically tractable model host for *Mycobacterium marinum*. *Infect. Immun.* 71, 3540–3550. doi: 10.1128/IAI.71.6.3540-3550.2003

Driver, E., Ryan, G., Hoff, D., Irwin, S., Basaraba, R., Kramnik, I., et al. (2012). Evaluation of mouse model forming necrotic granulomas using C3HeB/FeJ mice, for the testing of *Mycobacterium tuberculosis* drugs. *Antimicrob. Agents Chemother.* 56, 3181–3195. doi: 10.1128/AAC.00217-12

Entwistle, F. M., and Coote, P. J. (2018). Evaluation of greater wax moth larvae, *Galleria mellonella*, as a novel *in vivo* model for non-tuberculosis mycobacteria infections and antibiotic treatments. *J. Med. Microbiol.* 67, 585–597. doi: 10.1099/jmm.0.000696

Finke, M. D. (2015). Complete nutrient content of four species of commercially available feeder insects fed enhanced diets during growth. *Zoo Biol.* 34, 554–564. doi: 10.1002/zoo.21246

Fitts, D. A. (2011). Ethics and animal numbers: informal analyses, uncertain sample sizes, inefficient replications, and type I errors. *J. Am. Assoc. Lab. Anim. Sci.* 50, 445–453.

Flentie, K., Garner, A. L., and Stallings, C. L. (2016). *Mycobacterium tuberculosis* transcription machinery: ready to respond to host attacks. *J. Bacteriol.* 18, 1360–1373. doi: 10.1128/JB.00935-15

Fogel, N. (2015). Tuberculosis: a disease without boundaries. *Tuberculosis* 95, 527–531. doi: 10.1016/j.tube.2015.05.017

Fonseca, K. L., Rodrigues, P. N. S., Olsson, I. A. S., and Saraiva, M. (2017). Experimental study of tuberculosis: from animal models to complex cell systems and organoids. *PLoS Pathog.* 13:e1006421. doi: 10.1371/journal.ppat.1006421

Garnier, T., Eiglmeier, K., Camus, J. C., Medina, N., Mansoor, H., Pryor, M., et al. (2003). The complete genome sequence of *Mycobacterium bovis*. *Proc. Natl. Acad. Sci. U. S. A.* 100, 7877–7882. doi: 10.1073/pnas.1130426100

Gopal, P., Nartey, W., Ragunathan, P., Sarathy, J., Kaya, F., Yee, M., et al. (2017). Pyrazinoic acid inhibits mycobacterial coenzyme A biosynthesis by binding to aspartate decarboxylase PanD. *ACS Infect. Dis.* 3, 807–819. doi: 10.1021/acsinfecdis.7b00079

Gopal, P., Yee, M., Sarathy, J., Liang Low, J., Sarathy, J. P., Kaya, F., et al. (2016). Pyrazinamide resistance is caused by two distinct mechanisms: prevention of coenzyme a depletion and loss of virulence factor synthesis. *ACS Infect. Dis.* 2, 616–626. doi: 10.1021/acsinfecdis.6b00070

Harding, C. R., Schroeder, G. N., Reynolds, S., Kosta, A., Collins, J. W., Mousnier, A., et al. (2012). *Legionella pneumophila* pathogenesis in the *Galleria mellonella* infection model. *Infect. Immun.* 80, 2780–2790. doi: 10.1128/IAI.00510-12

Hoffmann, H., Kohl, T. A., Hofmann-Thiel, S., Merker, M., Beckert, P., Jaton, K., et al. (2016). Delamanid and bedaquiline resistance in *Mycobacterium tuberculosis* ancestral Beijing genotype causing extensively drug-resistant tuberculosis in a tibetan refugee. *Am. J. Respir. Crit. Care Med.* 193, 337–340. doi: 10.1164/rccm.201502-0372LE

Kampmann, B., Gaora, P. Ó., Snewin, V. A., Gares, M., Young, D. B., and Levin, M. (2000). Evaluation of human antimycobacterial immunity using recombinant eporter mycobacteria. *J. Infect. Dis.* 182, 895–901. doi: 10.1086/315766

Kampmann, B., Tena, G. N., Mzazi, S., Eley, B., Young, D. B., and Levin, M. (2004). Novel human *in vitro* system for evaluating antimycobacterial vaccines. *Infect. Immun.* 72, 6401–6407. doi: 10.1128/IAI.72.11.6401-6407.2004

Kampmann, B., Tena-Coki, G. N., Nicol, M. P., Levin, M., and Eley, B. (2006). Reconstitution of antimycobacterial immune responses in HIV-infected children receiving HAART. *AIDS* 20, 1011–1018. doi: 10.1097/01.aids.0000222073.45372.ce

Kavanagh, K., and Sheehan, G. (2018). The use of *Galleria mellonella* larvae to identify novel antimicrobial agents against fungal species of medical interest. *J. Fungi* 4:113. doi: 10.3390/jof4030113

Kay, S., Edwards, J., Brown, J., and Dixon, R. (2019). *Galleria mellonella* infection model identifies both high and low lethality of *Clostridium perfringens* toxigenic strains and their response to antimicrobials. *Front. Microbiol.* 10:1281. doi: 10.3389/fmicb.2019.01281

Khalil, S., Jacobson, E., Chambers, M. C., and Lazzaro, B. P. (2015). Systemic bacterial infection and immune defense phenotypes in *Drosophila melanogaster*. *J. Vis. Exp.* e52613. doi: 10.3791/52613

Lee, B. Y., Clemens, D. L., Silva, A., Dillon, B. J., Maslesa-Galić, S., Nava, S., et al. (2018). Ultra-rapid near universal TB drug regimen identified via parabolic response surface platform cures mice of both conventional and high susceptibility. *PLoS One* 13:e0207469. doi: 10.1371/journal.pone.0207469

Li, Y., Spiropoulos, J., Cooley, W., Singh Khara, J., Gladstone, C. A., Asai, M., et al. (2018). *Galleria mellonella* - a novel infection model for the *Mycobacterium tuberculosis* complex. *Virulence* 9, 1126–1137. doi: 10.1080/21505594.2018.1491255

Loh, J. M. S., Adenwalla, N., Wiles, S., and Proft, T. (2013). *Galleria mellonella* larvae as an infection model for group A streptococcus. *Virulence* 4, 419–428. doi: 10.4161/viru.24930

Martineau, A. R., Newton, S. M., Wilkinson, K. A., Kampmann, B., Hall, B. M., Nawroly, N., et al. (2007a). Neutrophil-mediated innate immune resistance to mycobacteria. *J. Clin. Invest.* 117, 1988–1994. doi: 10.1172/JCI31097

Martineau, A. R., Wilkinson, K. A., Newton, S. M., Floto, R. A., Norman, A. W., Skolimowska, K., et al. (2007b). IFN-γ- and TNF-independent vitamin D-inducible human suppression of mycobacteria: the role of cathelicidin LL-37. *J. Immunol.* 178, 7190–7198. doi: 10.4049/jimmunol.179.12.8569-c

Martineau, A. R., Wilkinson, R. J., Wilkinson, K. A., Newton, S. M., Kampmann, B., Hall, B. M., et al. (2007c). A single dose of vitamin D enhances immunity to mycobacteria. *Am. J. Respir. Crit. Care Med.* 176, 208–213. doi: 10.1164/rccm.200701-007OC

Meir, M., Grosfeld, T., and Barkan, D. (2018). Establishment and validation of *Galleria mellonella* as a novel model organism to study *Mycobacterium abscessus* infection, pathogenesis, and treatment. *Antimicrob. Agents Chemother.* 62:e02539-17. doi: 10.1128/AAC.02539-17

Mohan, A., Padiadpu, J., Baloni, P., and Chandra, N. (2015). Complete genome sequences of a Mycobacterium smegmatis laboratory strain (MC2 155) and isoniazid-resistant (4XR1/R2) mutant strains. *Genome Announc.* 3:e01520-14. doi: 10.1128/genomeA.01434-15

Mourik, B. C., De Knegt, G. J., Verbon, A., Mouton, J. W., Bax, H. I., and De Steenwinkel, J. E. M. (2017). Assessment of bactericidal drug activity and treatment outcome in a mouse tuberculosis model using a clinical Beijing strain. *Antimicrob. Agents Chemother.* 61, e00696–e00617. doi: 10.1128/AAC.00696-17

Myllymäki, H., Bäuerlein, C. A., and Rämet, M. (2016). The zebrafish breathes new life into the study of tuberculosis. *Front. Immunol.* 7:196. doi: 10.3389/fimmu.2016.00196

Myllymäki, H., Niskanen, M., Oksanen, K. E., and Rämet, M. (2015). Animal models in tuberculosis research – where is the beef? *Expert Opin. Drug Discovery* 10, 871–883. doi: 10.1517/17460441.2015.1049529

Newton, S., Martineau, A., and Kampmann, B. (2011). A functional whole blood assay to measure viability of mycobacteria, using reporter-gene tagged BCG or M.Tb (BCG *lux*/M.Tb *lux*). *J. Vis. Exp.* e3332. doi: 10.3791/3332

Newton, S. M., Mackie, S. L., Martineau, A. R., Wilkinson, K. A., Kampmann, B., Fisher, C., et al. (2008). Reduction of chemokine secretion in response to mycobacteria in infliximab-treated patients. *Clin. Vaccine Immunol.* 15, 506–512. doi: 10.1128/CVI.00401-07

Nikonenko, B. V., Samala, R., Einck, L., and Nacy, C. A. (2004). Rapid, simple *in vivo* screen for new drugs active against *Mycobacterium tuberculosis*. *Antimicrob. Agents Chemother.* 48, 4550–4555. doi: 10.1128/AAC.48.12.4550-4555.2004

Oh, C. T., Moon, C., Choi, T. H., Kim, B. S., and Jang, J. (2013). *Mycobacterium marinum* infection in *Drosophila melanogaster* for antimycobacterial activity assessment. *J. Antimicrob. Chemother.* 68, 601–609. doi: 10.1093/jac/dks425

Ordas, A., Raterink, R. J., Cunningham, F., Jansen, H. J., Wiweger, M. I., Jong-Raadsen, S., et al. (2015). Testing tuberculosis drug efficacy in a zebrafish high-throughput translational medicine screen. *Antimicrob. Agents Chemother.* 52, 753–762. doi: 10.1128/AAC.03588-14

Pai, M., Behr, M. A., Dowdy, D., Dheda, K., Divangahi, M., Boehme, C. C., et al. (2016). Tuberculosis. *Nat. Rev. Dis. Prim.* 2:16076. doi: 10.1038/nrdp.2016.76

Pereira, T. C., de Barros, P. P., de Oliveira Fugisaki, L. R., Rossoni, R. D., de Ribeiro, F. C., de Menezes, R. T., et al. (2018). Recent advances in the use of *Galleria mellonella* model to study immune responses against human pathogens. *J. Fungi* 4:E128. doi: 10.3390/jof4040128

Reid, M. J. A., Arinaminpathy, N., Bloom, A., Bloom, B. R., Boehme, C., Chaisson, R., et al. (2019). Building a tuberculosis-free world: the lancet commission on tuberculosis. *Lancet* 393, 1331–1384. doi: 10.1016/S0140-6736(19)30024-8

Ritz, N., Tebruegge, M., Connell, T. G., Sievers, A., Robins-Browne, R., and Curtis, N. (2009). Susceptibility of *Mycobacterium bovis* BCG vaccine strains to antituberculous antibiotics. *Antimicrob. Agents Chemother.* 53, 316–318. doi: 10.1128/AAC.01302-08

Sheehan, G., Dixon, A., and Kavanagh, K. (2019). Utilization of *Galleria mellonella* larvae to characterize the development of *Staphylococcus aureus* infection. *Microbiology* 165, 863–875. doi: 10.1099/mic.0.000813

Sheehan, G., and Kavanagh, K. (2018). Analysis of the early cellular and humoral responses of *Galleria mellonella* larvae to infection by *Candida albicans*. *Virulence* 9, 163–172. doi: 10.1080/21505594.2017.1370174

Shi, W., Cui, P., Niu, H., Zhang, S., Tønjum, T., Zhu, B., et al. (2019). Introducing RpsA point mutations Δ438A and D123A into the chromosome of *Mycobacterium tuberculosis* confirms their role in causing resistance to pyrazinamide. *Antimicrob. Agents Chemother.* 63:e02681-18. doi: 10.1128/AAC.02681-18

Snewin, V. A., Gares, M., Ógaora, P., Hasan, Z., Brown, I. N., and Young, D. B. (1999). Assessment of immunity to mycobacterial infection with luciferase reporter constructs. *Infect. Immun.* 67, 4586–4593.

Tena, G. N., Young, D. B., Eley, B., Henderson, H., Nicol, M. P., Levin, M., et al. (2003). Failure to control growth of mycobacteria in blood from children infected with human immunodeficiency virus and its relationship to T cell function. *J. Infect. Dis.* 187, 1544–1551. doi: 10.1086/374799

Thomas, R. J., Hamblin, K. A., Armstrong, S. J., Müller, C. M., Bokori-Brown, M., Goldman, S., et al. (2013). *Galleria mellonella* as a model system to test the pharmacokinetics and efficacy of antibiotics against *Burkholderia pseudomallei*. *Int. J. Antimicrob. Agents* 41, 330–336. doi: 10.1016/j.ijantimicag.2012.12.009

Tiberi, S., Munoz-Torrico, M., Duarte, R., Dalcolmo, M., S'Ambrosio, L., and Migliori, G. B. (2019). New drugs and perspectives for new anti-tuberculosis regimens. *Pulmonology* 24, 86–98. doi: 10.1016/j.rppnen.2017.10.009

Tobin, D. M., and Ramakrishnan, L. (2008). Comparative pathogenesis of *Mycobacterium marinum* and *Mycobacterium tuberculosis*. *Cell. Microbiol.* 10, 1027–1039. doi: 10.1111/j.1462-5822.2008.01133.x

Tsai, C. J.-Y., Loh, J. M. S., and Proft, T. (2016). *Galleria mellonella* infection models for the study of bacterial diseases and for antimicrobial drug testing. *Virulence* 7, 214–229. doi: 10.1080/21505594.2015.1135289

Via, L. E., Savic, R., Weiner, D. M., Zimmerman, M. D., Prideaux, B., Irwin, S. M., et al. (2015). Host-mediated bioactivation of pyrazinamide: implications for efficacy, resistance, and therapeutic alternatives. *ACS Infect. Dis.* 8, 203–214. doi: 10.1021/id500028m

Von Both, U., Berk, M., Agapow, P. M., Wright, J. D., Git, A., Hamilton, M. S., et al. (2018). *Mycobacterium tuberculosis* exploits a molecular off switch of the immune system for intracellular survival. *Sci. Rep.* 8:661. doi: 10.1038/s41598-017-18528-y

World Health Organization (2010). *Guidelines for treatment of tuberculosis*. 4th Edn. Geneva: World Health Organization.

World Health Organization (2018). *Global tuberculosis report 2018*. Geneva: World Health Organization.

Yuan, T., and Sampson, N. S. (2018). Hit generation in TB drug discovery: from genome to granuloma. *Chem. Rev.* 118, 1887–1916. doi: 10.1021/acs.chemrev.7b00602

Zhan, L., Tang, J., Sun, M., and Qin, C. (2017). Animal models for tuberculosis in translational and precision medicine. *Front. Microbiol.* 8:717. doi: 10.3389/fmicb.2017.00717

Zheng, Z., Tharmalingam, N., Liu, Q., Jayamani, E., Kim, W., Fuchs, B. B., et al. (2017). Synergistic efficacy of *Aedes aegypti* antimicrobial peptide cecropin A2 and tetracycline against *Pseudomonas aeruginosa*. *Antimicrob. Agents Chemother.* 61:e00686-17. doi: 10.1128/AAC.00686-17

Conflict of Interest: The authors declare that the research was conducted in the absence of any commercial or financial relationships that could be construed as a potential conflict of interest.

Copyright © 2019 Asai, Li, Khara, Robertson, Langford and Newton. This is an open-access article distributed under the terms of the Creative Commons Attribution License (CC BY). The use, distribution or reproduction in other forums is permitted, provided the original author(s) and the copyright owner(s) are credited and that the original publication in this journal is cited, in accordance with accepted academic practice. No use, distribution or reproduction is permitted which does not comply with these terms.

VIRULENCE
2020, VOL. 11, NO. 1, 811–824
https://doi.org/10.1080/21505594.2020.1781486

Taylor & Francis
Taylor & Francis Group

RESEARCH PAPER

OPEN ACCESS Check for updates

A novel biosafety level 2 compliant tuberculosis infection model using a ΔleuDΔpanCD double auxotroph of *Mycobacterium tuberculosis* H37Rv and *Galleria mellonella*

Masanori Asai[a,*], Yanwen Li[a,*], John Spiropoulos[b], William Cooley[b], David Everest[b], Brian D. Robertson[c], Paul R. Langford[a], and Sandra M. Newton[a]

[a]Section of Paediatric Infectious Disease, Department of Infectious Disease, Imperial College London, London, UK; [b]Department of Pathology, Animal and Plant Health Agency, Addlestone, UK; [c]MRC Centre for Molecular Bacteriology and Infection, Department of Infectious Disease, Imperial College London, London, UK

ABSTRACT

Mammalian infection models have contributed significantly to our understanding of the host-mycobacterial interaction, revealing potential mechanisms and targets for novel antimycobacterial therapeutics. However, the use of conventional mammalian models such as mice, are typically expensive, high maintenance, require specialized animal housing, and are ethically regulated. Furthermore, research using *Mycobacterium tuberculosis* (MTB), is inherently difficult as work needs to be carried out at biosafety level 3 (BSL3). The insect larvae of *Galleria mellonella* (greater wax moth), have become increasingly popular as an infection model, and we previously demonstrated its potential as a mycobacterial infection model using *Mycobacterium bovis* BCG. Here we present a novel BSL2 complaint MTB infection model using *G. mellonella* in combination with a bioluminescent *ΔleuDΔpanCD* double auxotrophic mutant of MTB H37Rv (SAMTB *lux*) which offers safety and practical advantages over working with wild type MTB. Our results show a SAMTB *lux* dose dependent survival of *G. mellonella* larvae and demonstrate proliferation and persistence of SAMTB *lux* bioluminescence over a 1 week infection time course. Histopathological analysis of *G. mellonella*, highlight the formation of early granuloma-like structures which matured over time. We additionally demonstrate the drug efficacy of first (isoniazid, rifampicin, and ethambutol) and second line (moxifloxacin) antimycobacterial drugs. Our findings demonstrate the broad potential of this insect model to study MTB infection under BSL2 conditions. We anticipate that the successful adaptation and implementation of this model will remove the inherent limitations of MTB research at BSL3 and increase tuberculosis research output.

ARTICLE HISTORY
Received 17 December 2019
Revised 19 May 2020
Accepted 7 June 2020

KEYWORDS
Galleria mellonella; tuberculosis; infection model; *Mycobacterium tuberculosis* complex; drug screening; antimycobacterial agents; mycobacteria; auxotrophic

Introduction

Mycobacterium tuberculosis (MTB) is the causative agent of tuberculosis (TB), the leading cause of global infectious disease mortality. In 2018, there were 10 million cases and 1.6 million deaths from TB [1]. One quarter of the world's population have latent TB infection (LTBI), of which 10% will go on to develop active disease over their lifetime [1]. Treatment of TB is challenging, especially with the rise of drug resistant TB and the lack of efficacious treatments [2]. Only three new drugs have been approved by the US Food and Drug Administration (FDA) in almost five decades [3,4]. Furthermore, preventative measures are limited with only one FDA approved vaccine, Bacillus Calmette-Guérin (BCG), which has variable efficacy [5]. The World Health Organization (WHO) target to end the global TB epidemic by 2035 [1], which is a highly improbable goal taking into account current progress [2]. In order to end the global TB epidemic, significant advancement in research is needed to develop novel treatments, preventative measures and diagnostic tools.

Animal infection models have played a substantial role in TB research leading to an increased understanding of host-bacterial interactive biology, and are crucial for novel therapeutic and vaccine development [6–8]. The mouse, rabbit, guinea pig, non-human primate and zebrafish (*Danio rerio*) have all been used [6]. However, each model has limitations with no single model being able to replicate all aspects of the disease. For example, the widely used mouse strains (C57BL/6 and BALB/c)

CONTACT Sandra M. Newton s.newton@imperial.ac.uk

*Both authors contributed equally in different aspects of the project and the order has been discussed and approved by all authors

This article has been republished with minor changes. These changes do not impact the academic content of the article.

Supplemental data for this article can be accessed here.

© 2020 Informa UK Limited, trading as Taylor & Francis Group
This is an Open Access article distributed under the terms of the Creative Commons Attribution License (http://creativecommons.org/licenses/by/4.0/), which permits unrestricted use, distribution, and reproduction in any medium, provided the original work is properly cited.

do not develop necrotic granulomas, a hallmark phenotype of LTBI [9]. Rabbits and guinea pigs do develop human-like necrotic granulomas, but the lack of immunological reagents limits their use [6]. Most mammalian models are not naturally susceptible to mycobacteria and are time consuming. Additionally, such models require specialized biological containment (biological safety level 3, BSL3), are expensive, and require ethical approval. These limitations highlight the need for alternative infection models that can accelerate our understanding of TB biology and the development of novel therapeutics.

Over the past decade, the insect larva of *Galleria mellonella* (greater wax moth) has become a popular model to study the pathogenesis of Gram-negative and Gram-positive bacteria, and fungal pathogens [10,11]. Additionally, the model has been used for rapid drug efficacy testing [10,12,13]. The popularity of *G. mellonella* stems from its complex innate immune system, which shares high structural and functional similarity to that in mammals. *G. mellonella* has many advantages over conventional models: 1) larval maintenance does not require specialized housing: 2) last instar larvae do not need feeding: 3) no specialized equipment is required: 4) their size (2–3 cm) permits easy handling and precise dosing of pathogen and/or drugs: 5) they can be incubated at 37°C (optimum temperature for human pathogens); and 6) ethics permission is not required [14]. In previous studies using *Mycobacterium bovis* BCG as a surrogate for MTB, we demonstrated that *G. mellonella* can be used to study members of the MTB complex (MTBC) [14,15], including screening of antimycobacterial agents [14].

A recent publication described a BSL2 compliant, severely attenuated double auxotrophic Δ*leuC*Δ*panCD* strain of MTB H37Rv (SAMTB) [16]. Compared to H37Rv (wild-type, WT), SAMTB had comparable *in vitro* and intracellular growth, and immunogenicity, making it a suitable surrogate for WT MTB [16]. In this study, we have characterized a novel BSL2 compliant SAMTB-*G. mellonella* infection model, and show its potential to accelerate TB research.

Materials and methods

Bacterial growth conditions

The double auxotrophic *M. tuberculosis* H37Rv Δ*leuD* Δ*panCD* mutant (SAMTB) was kindly provided by Professor William Jacobs Jr. of Albert Einstein College of Medicine. SAMTB was transformed into an autoluminescent mutant (SAMTB *lux*), using the plasmid vector pMV306, carrying the full *lux* operon of *Photorhabdus luminescens* [17]. The use of pMV306 was chosen for its stability, as the plasmid is chromosomally integrated. The resistance status of SAMTB *lux* is similar to that of WT *M. tuberculosis* H37Rv [16], with additional resistance to kanamycin and hygromycin for Δ*leuD*Δ*panCD* and pMV306 selection respectively. SAMTB *lux* was cultured in Middlebrook 7H9 broth (BD, UK), supplemented with glycerol (0.2%) [Sigma-Aldrich, UK], albumin dextrose catalase (ADC 10%) [USBio, USA], polysorbate-80 (0.05%) [Sigma-Aldrich, UK], leucine (25 μg/ml) [Sigma-Aldrich, UK) and calcium pantothenate (24 μg/ml) [Sigma-Aldrich, UK]. The broth was further supplemented with hygromycin (50 μg/ml) and kanamycin (20 μg/ml) for pMV306 selection. For enumeration of colony forming unit (CFU)/ml, SAMTB *lux* was serially diluted ten-fold and each dilution was plated onto 7H11 agar (BD Difco, UK) supplemented with oleic albumin dextrose catalase (OADC 10%) [BD, UK], glycerol (0.5%), leucine (25 μg/ml) and calcium pantothenate (24 μg/ml), hygromycin (50 μg/ml) and kanamycin (20 μg/ml). SAMTB *lux* cultures were grown at 37°C with agitation (220 rpm) to mid-log phase and CFU enumeration was determined on agar plates incubated at 37°C with 5% CO_2 for 2 weeks. Growth of SAMTB *lux* was monitored through measurements of turbidity (OD 600 nm) and bioluminescence (relative light units, RLU) using a luminometer (Berthold Technologies, DE), where the RLU:CFU ratio had been determined to be 0.03:1 (Supplementary Figure 1). This ratio was maintained throughout the 96 h incubation, with the exception to 24 h, likely as a result of metabolic adjustment during the lag phase of growth.

G. mellonella maintenance

Last-instar *G. mellonella* larvae were purchased from Livefoods Direct Ltd, UK. Healthy larvae were defined by their uniform cream color, lack of melanization, body length (2–3 cm), weight (~250 mg), and high level of motility with the ability to right themselves when turned over. Dead, melanized or pupating larvae were discarded prior to storage at 18°C. Larvae were not fed prior to storage or during infection. Larvae were stored for no longer than 1 week before experimentation.

Preparation of mycobacterial inocula and infection of *G. mellonella*

All experiments with SAMTB were performed in a BSL2 laboratory. Mid-log phase SAMTB *lux* culture was pelleted for 10 min at 2175 g at room temperature.

The cell pellet was washed twice with phosphate buffered saline (PBS) [Sigma-Aldrich, UK], containing 0.05% polysorbate-80 (PBS-T). Following the final wash, the cell pellet was resuspended to the desired inoculum density using RLU and OD measurements, with the CFU being enumerated for each inoculum on agar plates. Healthy larvae were selected and infected with SAMTB *lux* as previously described [14]. Briefly, each larva was injected with a 10 µl dose of SAMTB *lux* ($2x10^7$ CFU) using a micro-syringe (SGE Analytical Science, AU), via the last left pro-leg directly into the hemocoel. Infected larvae were counted into a Petri dish (94 mm), lined with a layer of filter paper (n = 30, per group/Petri dish), and incubated in a vented box at 37°C in the dark. Heated treated inocula comprised, $2×10^7$ CFU heated at 85°C for 1 h.

Treatment of infected *G. mellonella* using antimycobacterial compounds

All antibiotics were purchased from Sigma-Aldrich, UK and prepared following the manufacturer's guidelines. Isoniazid (INH, 5 mg/kg), rifampicin (RIF, 10 mg/kg), ethambutol (ETH, 15 mg/kg), pyrazinamide (PZA, 25 mg/kg), moxifloxacin (MOX, 6.7 mg/kg) and bedaquiline (BDQ, 5.7 mg/kg) were used at recommended clinical dosages for adults following WHO guidelines [18], relative to the body weight of the larvae. Larvae were subjected to mono, dual (RIF/ETH) or triple (RIF/ETH/MOX) drug combination treatment in a single or double injection schedule. Treatment was carried out as previously described [13]. Briefly, larvae were treated 1 h post-infection via injection into the last left pro-leg; and for multiple dosing, a second dose was injected 24 h post-infection.

Minimum inhibitory concentration (MIC) assay

Mid-log phase SAMTB *lux* culture was diluted to 10^6 CFU/ml in fresh 7H9 broth supplemented with leucine and pantothenate. Kanamycin and hygromycin were omitted as they are non-essential for growth. All drugs were diluted in 7H9 to provide serial 1:1 dilutions ranging from 16 µg/ml to 0.125 µg/ml. One hundred microliters of SAMTB *lux* was seeded into the wells of a 96 well plate in triplicates. A further 100 µl of the drug dilutions were added to these wells in triplicates. Positive controls were SAMTB *lux* alone and negative controls were broth only. Only the inner wells of the plate were used for the assay to prevent evaporation; the outer ring of wells were filled with water to reduce the edge effect. The lidded plates were transferred to an airtight container lined with moistened paper towels to minimize evaporation. The plates were incubated at 37°C with agitation (20 rpm) for 1 week and the OD of the wells (520 nm) were read in a plate reader (Molecular Devices, UK). The MIC, defined as the minimum concentration of antibiotics required to inhibit the growth of SAMTB *lux*, was determined using two independent experiments.

In vivo virulence assay of SAMTB *lux* in *G. mellonella*

Larvae (n = 30 per group) were challenged with varying SAMTB *lux* inocula. Larval survival was recorded every 24 h, over a 96 h time course. Larvae were considered dead when they failed to respond to touch. Larvae which were pricked (to mimic needle injury) or PBS injected, were used as controls. Survival of larvae were plotted as a Kaplan-Meier survival curve from a minimum of two experimental repeats. Pupae were removed from the sample groups and omitted from the analysis.

Measurement of *in vivo* survival of SAMTB *lux* in *G. mellonella* and relative drug efficacy

Larvae were infected with $2×10^7$ CFU of SAMTB *lux* and relative changes in the *in vivo* mycobacterial loads were measured using bioluminescence over a one week time course. At each timepoint (0, 24, 48, 76, 92 and 168 h), five larvae were randomly selected and individually homogenized with 800 µl of PBS-T in a 2 ml lysis tube with six 1/8 inch metal beads (MP Biomedicals, US), using the FastPrep-24 5 G instrument (MP Biomedicals, US). Samples were homogenized at machine setting 6.0 m/s for 1 minute. The bioluminescence of the homogenate was measured using a luminometer. The survival of SAMTB *lux in vivo* was determined using data pooled from a minimum of three experimental repeats. The homogenates were plated onto 7H11 agar to enumerate the CFU to determine RLU:CFU ratio *in vivo*: 7H11 agar was further supplemented with piperacillin (20 µg/ml) to inhibit the growth of *G. mellonella* flora as previously described [15].

Total hemocyte count (THC)

Larvae (n = 5, per group) were bled through puncture of the last right pro leg using a sterile 30 gauge needle (Terumo, Japan) and three drops of hemolymph (approximately 60 µl) were collected into an ice cold 1.5 ml Eppendorf tube. Hemolymph from each larva were pooled (40 µl/larva, total 200 µl) and diluted with ice cold PBS containing 0.37% of mercaptoethanol

(Sigma-Aldrich, UK)). Diluted hemolymph was stained 1:1 with 0.4% trypan blue (Thermo Fisher, UK), and hemocytes counted using an automated hemocytometer (Thermo Fisher, UK). Bleeding of larvae is a terminal procedure. Larvae were bled at 2, 4, 24, 48 h post-infection. Data were pooled from three independent repeats, each with two technical repeats.

Histopathological, confocal microscopy and transmission electron microscopy (TEM) analysis of SAMTB *lux* infection in *G. mellonella*

G. mellonella larvae were infected with SAMTB *lux* ($2x10^7$ CFU) for histopathological and TEM time course analysis, performed as previously described [15]. For histopathology, three larvae were fixed and stored in buffered formalin at 0, 24, 48 and 168 h post-infection. Uninfected healthy larvae were fixed and stored as controls. Each larva was cut into half along the dorsal line, and both halves were processed for histology (Sakura Tissue-Tek VIP) by embedding in paraffin wax (Thermo Scientific Histostar Embedding Center), and sectioning (4 µm) using a Leica RM2135 before being transferred onto a glass slide, for hematoxylin and eosin (H&E) or Ziehl-Neelsen (ZN) staining. Slides were examined using light microscopy (Nikon Eclipse 80i), and images captured using the NIS-Elements BR imagine software and a Nikon DS-Ri1 camera. For TEM analysis, infected *G. mellonella* larvae (n = 10 per timepoint) at 1, 24, and 168 h post-infection, were bled through needle puncture and their hemolymph pooled into an ice cold 2 ml Eppendorf tube, washed with ice cold PBS, and centrifuged at 800 g for 10 min. The pelleted cells were resuspended in 3% glutaraldehyde (v/v in PBS) and fixed for 10 min, pelleted at 800 g, and stored at 4°C. Subsequently, the cell pellet was post-treated with 1% osmium tetroxide (0.1 M phosphate buffer), dehydrated (in a graded series of alcohol up to 100%), embedded (in epoxy resin, Araldite), cut into 70–90 nm ultra-thin sections, which were mounted onto a grid, stained with 0.5% uranyl acetate (w/v) and 3% lead citrate (w/v), and examined on a Tecnai bioTWIN transmission electron microscope. For confocal microscopy, larvae were infected with SAMTB *lux* ($2x10^7$ CFU) and hemolymph were bled through needle puncture at 1 h and 168 h post-infection. Three larvae were bled at each timepoint and pooled (approx. 40 µl/larva) with 700 µl of PBS. The cell suspension was mixed and 200 µl layered onto a 4-well Millicell® EZ SLIDE (Merck, UK) with a further 200 µl of PBS. The cells were incubated at room temperature for 30 min to allow for cell adhesion and washed twice with PBS to removed non-adherent cells. The slides were fixed with 3% formaldehyde for 15 min and washed twice with PBS. SYBR gold (Thermo Fisher, UK) was used to stain SAMTB *lux* bacilli, using the method previously described by Lenaerts and colleagues [19]. SlowFade Gold with 4′,6-diamidino-2-phenylindole (DAPI, Thermo fisher, UK), was used to counterstain the nucleus and mount the slides for imaging on a Leica SP8 inverted confocal microscope.

Statistical analysis

The experimental data were analyzed using Prism 8 (Graphpad Software Inc, UK). Where appropriate, the non-parametric Kruskal–Wallis test with Dunn's multiple comparison test or Mann-Whitney test was used.

Results

G. mellonella survival is SAMTB *lux* dose-dependent

G. mellonella larvae (n = 30 per group) were challenged with a range of SAMTB *lux* inocula and survival monitored over 96 h. Survival was dose-dependent, with higher inocula correlating with increased larval mortality ($p < 0.0001$) (Figure 1). The LD_{50} (dose required to achieve 50% killing) was $2.5x10^7$ CFU. There was no death using PBS-T as the mock infection or with the

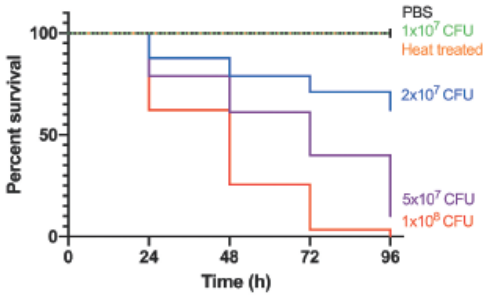


Figure 1. Kaplan-Meier survival curves of *G. mellonella* challenged with a range of SAMTB *lux* inocula over a 96 h time course.

G. mellonella larvae (n = 30/group) were infected with 1×10^7–10^8 CFU of SAMTB *lux*. Infected larvae were stored in a dark box and incubated at 37°C. Survival was recorded every 24 h for a period of 96 h. Larvae were considered dead when they failed to move in response to touch. All SAMTB *lux* doses were statistically different from each other ($P < 0.0001$, Mantle-Cox test with Holm-Sidak correction) at each timepoint. Data were pooled from three independent experiments.

pricked (simulated injection injury) control group (Figure 1, pricked not shown). SAMTB *lux* virulence is dependent on viability since heat-treated bacteria ($2x10^7$ CFU) did not kill larvae (Figure 1). Physiological changes in infected larvae ($2x10^7$ CFU) were monitored over 96 h. Infection led to gradual melanization over time, initially manifesting at the dorsal line 48 h post-infection, which became systemic by 168 h post-infection. Additionally, larval motility decreased as the infection progressed. Pupation was observed in larval groups inoculated with PBS, heat-killed and $1x10^7$ CFU SAMTB *lux*. No pupation was observed in larval groups inoculated with $2x10^7$, $5x10^7$ and $1x10^8$ CFU.

SAMTB *lux* proliferates in *G. mellonella*

Larvae were infected with SAMTB *lux* ($2x10^7$ CFU) and the changes in *in vivo* load of SAMTB *lux* were monitored over a 168 h time course using bioluminescence (RLU) of the larval homogenates. SAMTB *lux* bioluminescence increased by approximately 0.75 log RLU over 168 h, demonstrating that the bacterium can survive and proliferate within larvae (Figure 2). Post-infection, there was an initial rise in bioluminescence (0.25 log RLU) between 0–24 h; an increase of 0.1 log RLU between 24–96 h; and a 0.4 log RLU increase between 96–168 h. Background bioluminescence of the larval

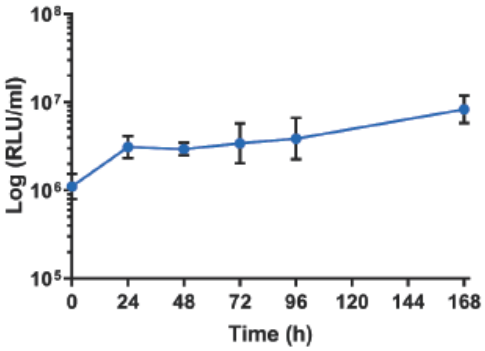


Figure 2. *In vivo* proliferation of SAMTB *lux* in *G. mellonella* larvae over a 168 h time course.

G. mellonella larvae ($n \leq 30$) were infected with $2x10^7$ CFU of SAMTB *lux* and at each timepoint (0, 24, 48, 72, 96 and 168 h), four larvae were individually homogenized, and the bioluminescence (RLU/ml) of the homogenate was measured to quantify the relative abundance of SAMTB *lux in vivo*. Data are pooled from three independent experiments. The means of each group are plotted, and the error bars represent the standard deviation of the mean.

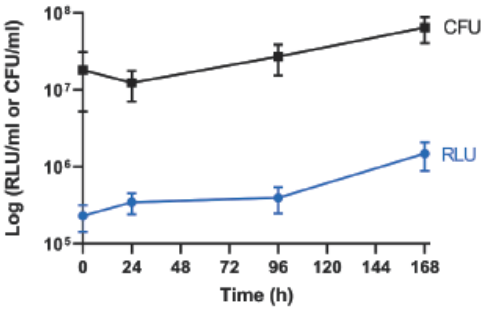


Figure 3. Recovery of SAMTB *lux* from larval homogenate over a 168 h time course.

Larvae were infected with $2x10^7$ CFU of SAMTB *lux*. At 0, 24, 96 and 168 h post-infection, four larvae were homogenized and plated onto Middlebrook 7H11 agar containing additional growth supplements (leucine and pantothenate) as well as piperacillin (20 µg/ml) to prevent contamination from larval microbiota. Data are pooled from two independent experiments.

homogenates was low (5000–8000 RLU/ml) with no impact on SAMTB *lux* bioluminescence. The RLU:CFU ratio *in vivo* was determined to be 0.02:1 over a 168 h time course (Figure 3). This ratio was used as the baseline to rapidly quantify relative *in vivo* SAMTB *lux* load. There was a gradual increase, in both the RLU and CFU counts *in vivo* over the 168 h time course, with the exception of the 24 h timepoint, where there was a slight drop in CFU counts relative to the rise in RLU.

Granuloma-like structures develop in *G. mellonella* in response to SAMTB *lux* infection

Histological sections from larvae infected with SAMTB *lux* ($2x10^7$ CFU) were stained with H&E or ZN to visualize host-SAMTB *lux* interaction. As early as 24 h post-infection, acid fast bacilli were organized in foci that were surrounded by host cells to form granuloma-like structures (Figure 4a-c). In these structures individual bacilli formed foci of variable bacterial density, with some granuloma-like structures containing compact clusters of acid fast amorphous material. H&E staining of the same section correlated to these structures as deep red/dark brown or black color formations for compact acid fast structures, and golden brown for areas containing high numbers of individual bacilli. Dispersed individual bacilli were not detectable in H&E sections (Figure 4b-d). The morphology of the granuloma-like structures varied considerably

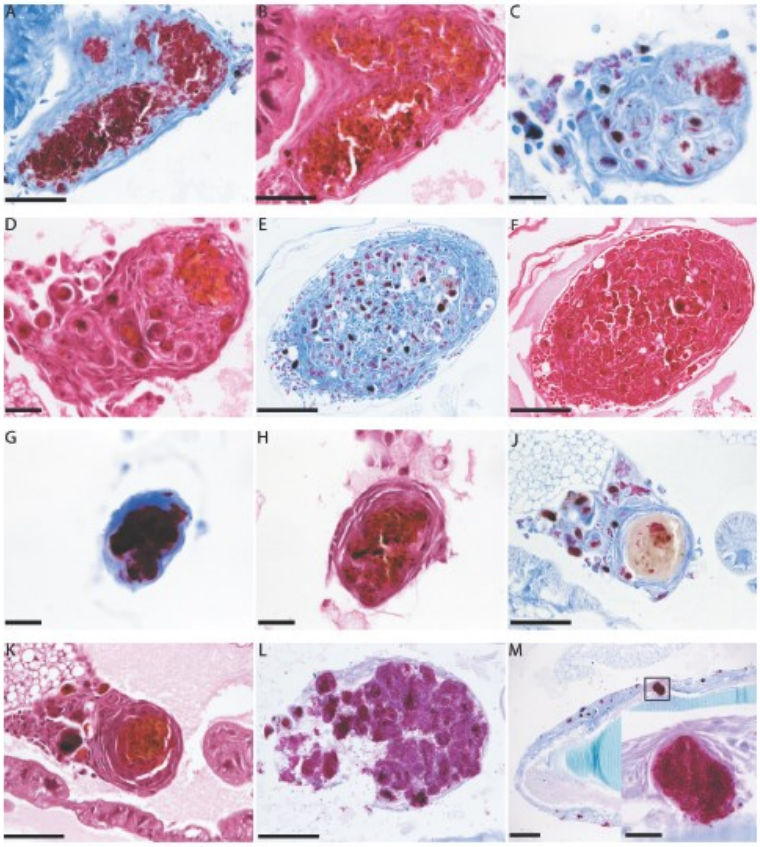


Figure 4. Histological analysis of *G. mellonella*-SAMTB *lux* interaction over time.

Histological sections of *G. mellonella* infected with SAMTB *lux* stained with Ziehl-Neelsen (ZN) or hematoxylin and eosin (H&E). (A) At 24 h post infection, large numbers of individual and densely organized bacilli were stained with ZN. (B) The H&E section of the same granuloma-like structure shows host cells occupying spaces which, in the ZN section, are filled with bacilli. Loss of eosinophilia from the H&E section gives rise to a brown pigmentation which co-localizes with clumping of bacilli in the ZN section. (C) As early as 24 h post-infection, granuloma-like structures may contain independent colonies of bacilli and compact ZN reactive amorphous material. (D) The H&E section of the same structure shown in C; loss of eosinophilia coincides with the existence of a large colony of bacilli. (E-F) At 168 h post-infection, granuloma-like structures containing compact ZN positive substances and individual bacilli or colonies of bacilli, were observed. At 48 h post-infection, (G) ZN and (H) H&E staining, show a single compact granuloma with a ZN reactive core. Such granuloma-like structures can be observed as single entities or can be included in formations that include multiple compact ZN positive structures similar to panels C-F. (J-K) Granuloma-like structure at 168 h post-infection, stained with ZN and H&E respectively, shows a single compact granuloma structure. However, the ZN affiliation of the amorphous central core has been abolished to a large extend implying breakdown of the structures that bind to the ZN dye. (L) Swarms of ZN positive bacilli form a granuloma-like structure. Part of the granuloma wall is impaired allowing access of bacteria to the surrounding hemolymph. (M) shows bacilli invading and forming colonies in internal organs of a larva. There is no evident host reaction to invading bacilli. The inset shows a larger magnification of the rectangle enclosed structure which shows abundant proliferation of bacilli. Scale bar in A, B, J, K and L represents 50 µm; in C, D, G, H and the M inset, scale bar represents 20 µm; while in E, F and M the scale bar represents 100 µm.

throughout all stages of infection with a mixture of individually identifiable bacilli and dense bodies with high affinity for ZN staining (Figure 4e–f), and discreet dense material composed almost exclusively of acid fast material (Figure 4g–h). Some of these densely packed structures at 168 h post-infection lost their affinity for the ZN stain (Figure 4j), although they remained compact (Figure 4k). Dissemination of prolific SAMTB *lux* bacilli were visualized at 168 h post-infection (Figure 4l). Occasionally bacilli appeared to migrate from the hemolymph to the internal organs (Figure 4m); within the resolution limits of light microscopy no host reaction was evident. In ZN labeled sections individual bacilli, not associated with host cells, were also identified within the hemolymph at all stages of the infection. As the infection progressed from 24 to 168 h, granuloma-like structures containing SAMTB *lux* bacilli were more numerous and found present throughout the body of the larvae (Figure 5a,b).

Innate immune cells of *G. mellonella* rapidly internalize SAMTB *lux* following infection

Confocal microscopy and TEM was carried out on hemolymph from infected larvae to visualize hemocyte–SAMTB *lux* interaction. Confocal microscopy visualized the association of SAMTB *lux* bacilli with hemocytes at 1 h post-infection (Figure 6a) and 168 h post-infection (Figure 6b), with the later timepoint showing a nodule like structure containing a number of central SAMTB *lux* clusters surrounded by hemocytes. TEM further confirmed that SAMTB *lux* had been internalized by hemocytes as early as 1 h post-infection (Figure 7a,b). There is clear evidence of early phagocytosis associated with interaction and formation of membrane invaginations. SAMTB are also clearly internalized at all timepoints up to and including 168 h post-infection (Figure 7c,d). Structural references of SAMTB *lux* alone, in different geometric orientations, are provided in Figure 7(f,g). TEM confirmed the histopathological findings, suggesting that SAMTB *lux* invades and/or is phagocytosed by hemocytes and multiplies within to form aggregate-like structures.

SAMTB *lux* infection induce a transient increase in circulating hemocyte counts

A significant increase in *G. mellonella* hemocyte counts was found at both 2 and 4 h for both the PBS injected

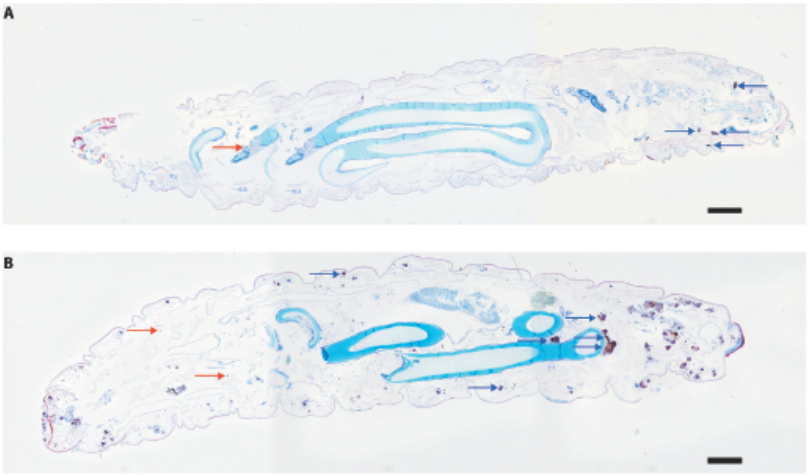


Figure 5. Cross sectional view of whole larvae infected with SAMTB *lux*.

Histological sections of whole *G. mellonella* larvae infected with SAMTB *lux* 24 h (A) and 168 h (B) post challenge showing multiple granuloma-like structures. Blue arrows indicate formations where there is an abundance of active bacilli which may be also accompanied by more consolidated structures similar to those presented in Figure4 (a,c,e,l). Red arrows show formations that are similar to those presented in Figure 4(g). Scale bar represents 1000 µm.

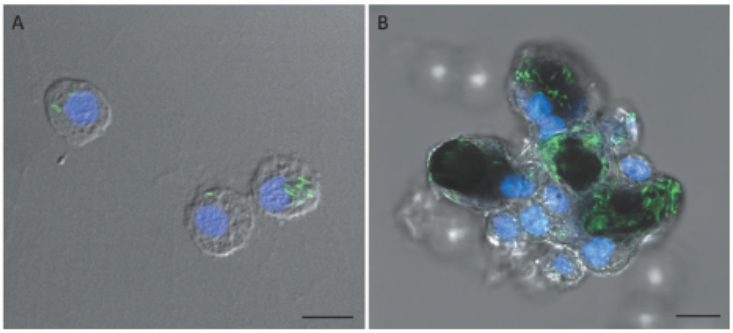


Figure 6. SAMTB *lux* associates with hemocytes following infection.
Confocal microscopy was carried out on hemocytes extracted from *G. mellonella* larvae infected with SAMTB *lux* ($2x10^7$ CFU) at (a) 1 h and (b) 168 h post-infection. Early association between hemocyte and SAMTB *lux* was seen at 1 h post-infection (a). Aggregates of hemocytes in an early granuloma like structure surrounding multiple clusters of SAMTB *lux* was observed at 168 h post-infection (b). These images are a superimposition of DAPI (nucleus, blue), SYBR gold (SAMTB *lux*, green) and differential interference contrast (DIC) image. Scale bars represents 10 µm.

larvae ($p < 0.05$ and $p < 0.05$ each timepoint, respectively) and SAMTB *lux* infected larvae ($p < 0.0001$ and $p < 0.01$, respectively for each timepoint) when compared to naïve larvae (Figure 8). However, hemocyte counts rapidly normalized to the level of naïve larvae by 24 h for both groups. Additionally, hemocyte counts were significantly higher in SAMTB *lux* infected compared to PBS treated larvae at 2 h ($p < 0.01$). However, by 4 h there was no significant difference in hemocyte counts between the two groups.

The *G. mellonella* – SAMTB *lux* infection model can be used to screen for drug efficacy

SAMTB *lux* infected *G. mellonella* larvae were treated with first-line, INH, RIF, PZA and ETH; and second-line, MOX and BDQ antibiotics at recommended adult clinical dosage relative to larval weight, to evaluate the use of this *in vivo* model as a drug screen. The *in vitro* MIC of the antibiotics against SAMTB *lux* were: INH (0.25 µg/ml), RIF (< 0.125 µg/ml), BDQ (< 0.125 µg/ml), ETH (0.5 µg/ml), PZA (> 16 µg/ml), and MOX (0.25 µg/ml). Drug efficacy was determined by comparing the change in the *in vivo* bioluminescence of SAMTB *lux* between the treated and mock treated (PBS-T) control over a 96 h time course. Treatment led to significant reductions in SAMTB *lux* bioluminescence for INH ($P < 0.0001$) and RIF ($p < 0.01$) treated larvae, but not for BDQ, ETH, MOX and PZA 96 h post-treatment at the recommended adult clinical dose relative to the larvae body weight (Figure 9, Supplementary Figure 2). When treated with a ten-fold higher dose of ETH, MOX or PZA, a significant reduction in SAMTB *lux* bioluminescence was observed for MOX (x10) at all timepoints (with $P < 0.0001$ by 96 h post-infection); while ETH (x10) showed a trend in the reduction of SAMTB *lux* bioluminescence, with significant reduction at 96 h post-treatment ($p < 0.05$) when compared to the control (Figure 9). No significant changes in RLU were detected in PZA (x10) treated larvae when compared to the control. Due to their substantial bioluminescence reducing activity on SAMTB *lux*, INH and RIF were further screened at three different doses, which demonstrated a clear dose-dependent effect (Figure 10). The effects of single and dual dosing for RIF was tested. INH was not used in multiple drug combination studies as any further improvements in drug efficacy, and hence reduced bioluminescence, were likely to result in RLU measurements indistinguishable from background bioluminescence of larval homogenates (~5000 RLU). Dual RIF treatment did not improve drug efficacy over single dose treatment, as both single and dual dosing achieved similar levels of drug efficacy over the 96 h time course (Figure 11a). Furthermore, the use of RIF in combination with ETH and/or MOX, (both of which did not show any significant antimycobacterial activity in this model against SAMTB *lux*) at clinically recommended dosages for adult TB treatment relative to larval body mass (Supplementary Figure 2), was tested

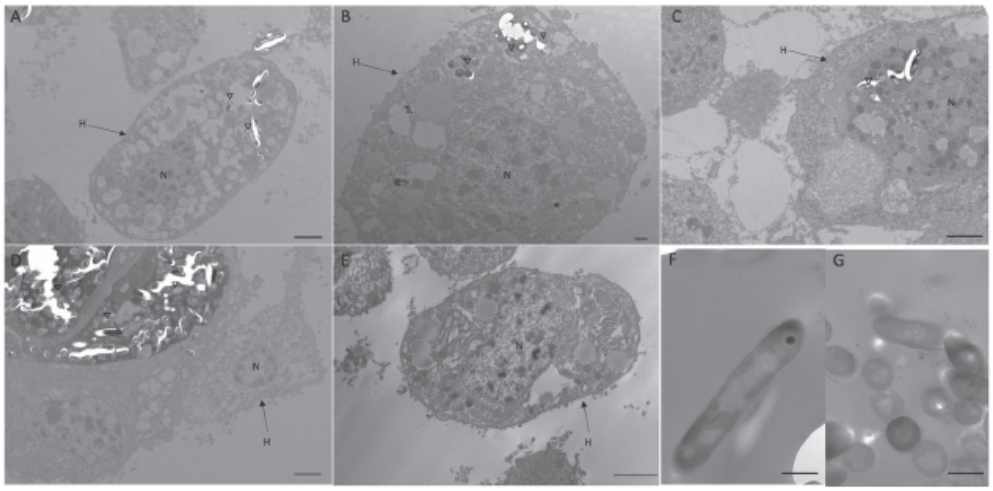


Figure 7. Interaction between SAMTB *lux* and phagocytic hemocytes.

Transmission electron microscopy (TEM) was carried out on hemocytes extracted from *G. mellonella* larvae infected with SAMTB *lux* ($2x10^7$ CFU) at: (a, b) 1 h (c) 24 h and (d) 168 h post infection. (e) shows healthy non-infected hemocytes. (f, g) show SAMTB *lux* bacilli in various geometric orientations. Internalization of SAMTB *lux* was observed as early as 1 h post-infection and presence of the bacilli persisted 24 h post-infection (A-C). By 168 h post-infection, aggregates of SAMTB *lux* bacilli, surrounded by hemocytes in an early granuloma-like structure, could be observed under TEM (D). H = hemocytes, N = nucleus, inverted triangles indicate SAMTB *lux*. Scale bars represent (a, c-e): 2 µm, (b, f, g): 500 nm.

with RIF as a dual (RIF/ETH) and triple (RIF/ETH/MOX) combination treatment. Both dual and triple combination treatments resulted in improved drug efficacy over the use of either ETH or MOX alone (Figure 11b). However, no improvement was seen over the use of RIF alone.

Discussion

We sought to determine whether *G. mellonella* could be used as a surrogate host for SAMTB *lux* thereby allowing experiments to be performed at BSL2. Virulence of SAMTB *lux* in *G. mellonella* was dependent on viability and inoculum size. The LD_{50} dose of SAMTB *lux* ($2.5x10^7$ CFU) was of a similar order of magnitude to that of BCG ($1x10^7$ CFU) [15]. In immunocompromised SCID mice SAMTB was considered attenuated compared to BCG or wild-type MTB H37Rv, since BCG-infected mice had lower survival outcome compared to those challenged with SAMTB [20]. In *G. mellonella*, SAMTB *lux*, unlike BCG [15], proliferated. Our results are in contrast with those in guinea pigs and mice where SAMTB or the single auxotrophic MTB mutant (Δ*leuD*) did not replicate [20,21]. We speculate that SAMTB was unable to replicate as there was insufficient availability of leucine and pantothenate in these hosts to overcome the auxotrophy. In *G. mellonella*, leucine comprised 4.91% of the total metabolome detected [22], and common insect feed for rearing *G. mellonella* typically contains 10.8 g/kg of leucine and 32.8 mg/kg of pantothenic acid [23]. While larvae were not fed during the experiments, we speculate that the residual abundance of leucine and pantothenate allowed auxotrophic SAMTB *lux* to proliferate *in vivo*. Furthermore, the abundance of these amino acids, likely contributed to the initial increase RLU 24 h post-infection as SAMTB *lux* metabolism adapted to this nutrient rich environment.

Histological analysis identified that the interaction between *G. mellonella* larvae and SAMTB *lux* was similar to that of BCG *lux* [15]. However, unlike BCG infection where most bacilli were contained and eventually digested into acid fast amorphous masses by the innate immune system, some SAMTB *lux* bacilli appear to replicate uninhibited within smaller granuloma-like foci, with such structures increasing in number and size over time. Furthermore, clusters of SAMTB *lux* bacilli were found at 168 h, suggesting that the initial containment within granuloma-like structures was overcome by rapidly multiplying bacteria. These observations agree with *in vivo* proliferation of SAMTB *lux* between

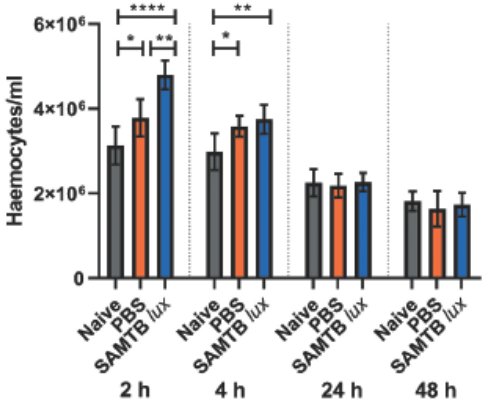


Figure 8. Changes in hemocyte counts in SAMTB *lux* infected larvae.

Total number of circulating hemocytes of naïve, PBS-T injected and SAMTB *lux* infected ($2x10^7$ CFU) larvae were determined at 2, 4, 24 and 48 h post-injection. Five larvae were bled (approximately 60 µl of hemolymph/larva) and diluted in PBS containing 0.37% of mercaptoethanol. Hemocytes were stained 1:1 with trypan blue (0.4%) and counted in a hemocytometer. Data are pooled from three independent experiments, each with two technical repeats. Plotted are the means of each group and the error bars represent the standard deviation of the mean. PBS and SAMTB *lux* infected larvae were compared to the naïve control using one-way ANOVA with Dunnett's multiple comparison test. * $P < 0.05$, ** $P < 0.01$, *** $P < 0.001$, **** $P < 0.0001$.

96 and 168 h post-infection. While the cellular composition of *G. mellonella* granuloma-like structures is unknown, it is likely that they contain a mixture of hemocyte sub-types: plasmatocytes, granular cells, and oenocytoids. These hemocytes are integral components of phagocytosis, nodulation (co-ordinated adherence or internalization of bacteria), and melanization [24]. Confocal microscopy clearly showed an association of SAMTB *lux* bacilli with hemocytes at 1 h post-infection, which developed into nodules resembling early granuloma-like structures at 168 h post-infection. As images lacked cytoskeletal staining, the geometric location of the bacilli in relationship to the hemocyte could not be identified. However, TEM visualized rapid internalization of SAMTB *lux* 1 h post-infection, which is in line with prior reports of phagocytic activity against non-tuberculous mycobacteria (NTM) [25], and the SAMTB *lux*-hemocyte association seen from the confocal microscopy images. Presence of internalized SAMTB *lux* bacilli within hemocytes were observed throughout the 168 h time course with aggregation of internal bacilli, similar to those observed in the BCG *lux* infection [15] and that of the confocal microscopy image seen at the same timepoint. However, unlike BCG *lux* infection, SAMTB *lux* bacilli did not accumulate lipid bodies with progression of the infection, likely reflecting the proliferative nature of SAMTB *lux* in comparison to BCG *lux*. Future studies will characterize the interaction between the hemocytes and MTB, including cellular signals (e.g. apoptosis/necrosis) or lysosomal activity following infection.

Characterization of the *G. mellonella* innate immune response revealed that infection with SAMTB *lux* resulted in a temporary increase in circulating hemocyte numbers at 2 and 4 h post-infection, which normalized to the basal level of naïve larvae by 24 h. Larval response to mycobacterial infection were previously characterized by Entwistle and Coote [25] using NTM (*M. marinum* and *M. fortuitum*) at a similarly lethal dose. Unlike our study, NTM infection led to an increase in circulating hemocyte numbers throughout the 48 h time course, when compared to the naïve and PBS controls [25]. The transient rise in our study is likely a basal response to fluid injection, rather than a specific response to SAMTB *lux*, as no significant difference between the PBS injected and SAMTB *lux*-infected control groups was identified 4 h post-infection. Infection with fast-growing bacterial pathogens, e.g. *Legionella pneumophila* and *Staphylococcus aureus*, led to 3–6 fold increases in hemocyte counts [26,27]. We speculate that a greater rate of bacterial replication may be associated with an increase in circulating hemocyte counts.

Treatment of SAMTB *lux* infected larvae with INH and RIF resulted in rapid reduction in SAMTB *lux*

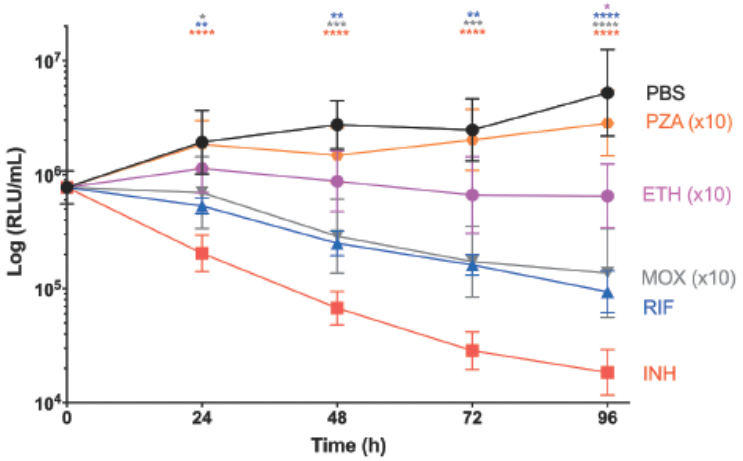


Figure 9. The effect of first-line and second-line antibiotics on the reduction of SAMTB *lux* bioluminescence within *G. mellonella* over a 96 h time course.

Larvae (n = 30/group) were infected with 2×10^7 CFU of SAMTB *lux*. At 1 h post-infection, larvae were treated with a single dose of INH (5 mg/kg), RIF (10 mg/kg), and BDQ (5.7 mg/kg) at the recommended clinical dosage relative to the larval body weigh; while PZA (250 mg/kg), ETH (150 mg/kg), MOX (67 mg/kg) were used at concentrations ten-folds higher than the recommended dosage. Control groups were injected larvae mock treated with PBS-T. At 0, 24, 48, 72, and 96 h post-infection, four larvae from each group were individually homogenized and the bioluminescence (RLU/ml) of the homogenates was measured to determine the relative drug efficacies. Data are pooled from three independent experiments. Plotted are the mean of each group and the error bars represent the standard deviation of the mean. Non-parametric Kruskal-Wallis test with Dunn's multiple comparison was carried out against the PBS-T injected control for all treatment groups. * $P < 0.05$, ** $P < 0.01$, *** $P < 0.001$, **** $P < 0.0001$.

bioluminescence. This was unsurprising as both drugs are highly effective antimycobacterials *in vitro* and *in vivo* [28,29]. Despite *in vitro* activity, BDQ, ETH and MOX did not result in a significant reduction in SAMTB *lux* bioluminescence at the standard dosage. Similar observations were made for larvae infected with BCG, where treatment with ETH and MOX or PZA had no efficacy [13]. However, the use of ETH or MOX at a ten-fold higher concentration than that of the clinically recommended dosage, resulted in significant reduction in SAMTB *lux* bioluminescence. This induction of drug efficacy *in vivo* is a clear indication that this model is sensitive to drug dosage, underlining the importance of testing a range of drug doses. This is important as our knowledge of the pharmacokinetic (PK) and pharmacodynamic (PD) properties of antibiotics in *G. mellonella* is currently limited [30]. PZA was inactive *in vitro* and *in vivo* at both standard and ten-fold higher concentrations. PZA was expected to be inactive against SAMTB *lux* as it lacks *panD* which synthesizes the enzyme aspartate decarboxylase, a known target of pyrazinoic acid [31]: this is evident from the lack of efficacy when used at a ten-fold higher concentration to that of the standard dosage. Repeated dosing of RIF alone or in combination with ETH, or ETH and MOX at the standard dosage, did not reduce SAMTB *lux* bioluminescence any further than RIF alone. Combination drug therapy is the gold standard for the treatment of TB. However, the primary use of a cocktail of antimycobacterials is to minimize the development of drug resistant TB during the lengthy treatment period and not for synergistic activities [18]. Further PK/PD research is required to maximize the use of *G. mellonella* in screening for novel antibiotics.

The use of RLU as a read-out of mycobacterial viability within *G. mellonella* is advantageous and allows for the rapid evaluation of drug efficacy, acting as a pre-screen for candidate compounds prior to mammalian testing. Such application would greatly increase the number of compounds that could be tested at a fraction of the cost and time of conventional *in vivo* studies. Furthermore, pre-screening would significantly reduce the number of mammals that are often used as antimicrobial activities do not always

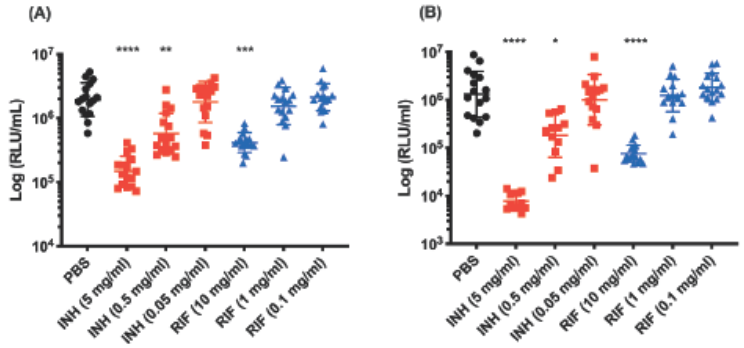


Figure 10. The effect of INH and RIF concentration on the reduction of SAMTB *lux* bioluminescence within *G. mellonella*.

Larvae (n = 30/group) were infected with 2×10^7 CFU of SAMTB *lux*. At 1 h post-infection, larvae were treated with a single dose of INH (5 mg/kg) or RIF (10 mg/kg). Control groups were injected larvae mock treated with PBS-T. At (A) 24 h and (B) 96 h post-infection, four larvae from each group were individually homogenized and the bioluminescence (RLU/ml) of the homogenate was measured to determine relative drug efficacy. Data are pooled from two independent experiments. Plotted are the mean for each group and the error bars represent the standard deviation of the mean. Non-parametric Kruskal-Wallis test with Dunn's multiple comparison was carried out against the PBS-T control for all treatment groups. * $P < 0.05$, ** $P < 0.01$, *** $P < 0.001$, **** $P < 0.0001$.

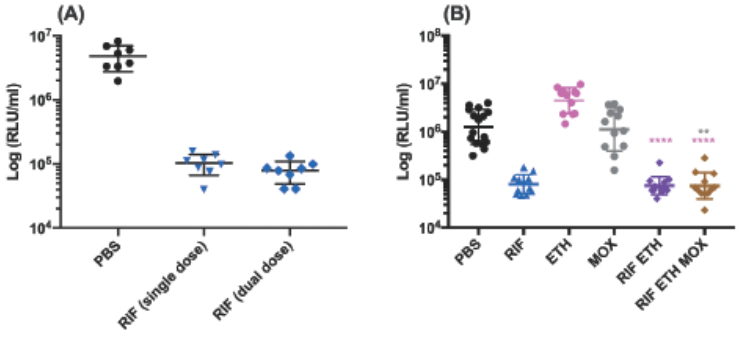


Figure 11. The effect of RIF multiple dosing and RIF combination drug therapy on the reduction of SAMTB *lux* bioluminescence within *G. mellonella*.

Larvae (n = 30/group) were infected with 2×10^7 CFU of SAMTB *lux*. (a) At 1 h post-infection, larvae were treated with a single dose of RIF (10 mg/kg) and for dual dosing an additional dose was given 24 h post-infection. (b) At 1 h post-infection, larvae were treated with a single dose of RIF (10 mg/kg), ETH (15 mg/kg), MOX (6.7 mg/kg) or in combination as RIF/ETH or RIF/ETH/MOX. At 96 h post-infection, four larvae from each group were individually homogenized and the bioluminescence (RLU/ml) of the homogenate was measured to determine relative drug efficacy. The efficacy of dual RIF dosing was compared to single dosing using the Mann-Whitney test. As for combination drug therapy, the efficacy of each drug combination was compared to their respective single drug type efficacy using a non-parametric Kruskal-Wallis test with Dunn's multiple comparison. For combination drug therapy, the color of * correlates to the color of the single drug type. * $P < 0.05$, ** $P < 0.01$, *** $P < 0.001$, **** $P < 0.0001$.

correlate between *in vitro* and *in vivo* conditions. However, it is important to note that RLU alone cannot determine the mechanism behind the antimycobacterial activity (i.e. bactericidal/bacteriostatic effects), as RLU production is a measure of the metabolic activity of SAMTB *lux* [32]. Therefore, RLU simply serves as a rapid measure of drug efficacy, that does not rely on time consuming CFU enumeration. A more

comprehensive study into the antimycobacterial activity of candidate compounds is essential during mammalian studies.

D. rerio is a popular non-mammalian TB infection model, as it is genetically tractable, high throughput, financially sustainable, and is ethically more acceptable than conventional mammalian counterparts (with the exception of adult zebrafish) [33]. Limitations of *D. rerio* include the use of *M. marinum* due to biological incompatibility (cannot be incubated at 37°C) [6,34], and the need for specialized rearing facilities and regular maintenance [35]. In contrast, *G. mellonella* can be incubated at 37°C and requires no specialized facility or maintenance, making the study of the MTBC easier and more accessible to the wider research community. Incubation temperature is a key factor as this can affect mycobacterial physiology [36], and the ability to study virulence at human temperatures is highly beneficial. A current limitation of *G. mellonella* is the lack of a fully annotated genome. However, an extensive transcriptomic database [37], and an unannotated genome [38] are available. A fully annotated genome and the development of methods to genetically manipulate *G. mellonella*, as described for other Lepidoptera [39], will facilitate uptake of the BSL2-compliant SAMTB *lux* infection model.

In conclusion, this study demonstrates the use of *G. mellonella* as an infection model for MTB, which lacks both the conventional ethical limitations associated with the use of mammalian infection models, and the need for BSL3 facilities. Infection of *G. mellonella* with SAMTB *lux* led to the proliferation of the bacilli *in vivo* and the formation of granuloma-like structures. Furthermore, this model can be used as a drug screen for antimycobacterial agents. Further optimization and characterization of the model will be carried out in the future, with specific focus on the proteomic, metabolomic and cellular response to infection. The successful uptake of this model in the MTB research community could significantly increase research throughput, while considerably reducing the number of mammalian models used in research.

Disclosure statement

Authors have no conflict of interest to declare.

Funding

This work was supported by the Biotechnology and Biological Sciences Research Council (BBSRC) [BB/P001262/1 to P.R. L. and Y.L] and the National Centre for the Replacement, Refinement and Reduction of Animals in Research (NC3Rs) [NC/R001596/1 to P.R.L., S.M.N., B.D.R. and Y.L].

ORCID

John Spiropoulos http://orcid.org/0000-0003-0119-8920
Brian D. Robertson http://orcid.org/0000-0001-5785-5307
Sandra M. Newton http://orcid.org/0000-0001-6545-9558

References

[1] World Health Organization. Global Tuberculosis Report 2019. Geneva: WHO Press; 2019.
[2] Reid MJA, Arinaminpathy N, Bloom A, et al. Building a tuberculosis-free world: the Lancet Commission on tuberculosis. Lancet. 2019;393:1331–1384.
[3] TB Alliance. Pretomanid and BPaL [Internet]. 2019. https://www.tballiance.org/access/pretomanid-and-bpal-regimen[Accessed 10 December 2019]
[4] Esposito S, Bianchini S, Blasi F. Bedaquiline and delamanid in tuberculosis. Expert Opin Pharmacother. 2015;16:2319–2330.
[5] Dockrell HM, Smith SG. What have we learnt about BCG vaccination in the last 20 years? Front Immunol. 2017;8:1134.
[6] Zhan L, Tang J, Sun M, et al. Animal models for tuberculosis in translational and precision medicine. Front Microbiol. 2017;8:717.
[7] Williams A, Orme IM. Animal models of tuberculosis: an overview. Microbiol Spectr. 2016;4:TBTB2-004–2015.
[8] Fonseca KL, Rodrigues PNS, Olsson IAS, et al. Experimental study of tuberculosis: from animal models to complex cell systems and organoids. PLoS Pathog. 2017;13:e1006421.
[9] Orme IM. The mouse as a useful model of tuberculosis. Tuberculosis. 2003;83:112–115.
[10] Tsai CJ-Y, Loh JMS, Proft T. *Galleria mellonella* infection models for the study of bacterial diseases and for antimicrobial drug testing. Virulence. 2016;7:214–229.
[11] Pereira TC, Barros PPD, de Oliveira Fugisaki LR, et al. Recent advances in the use of *Galleria mellonella* model to study immune responses against human pathogens. J Fungi. 2018;4:E128.
[12] Cutuli MA, Petronio Petronio G, Vergalito F, et al. *Galleria mellonella* as a consolidated *in vivo* model hosts: new developments in antibacterial strategies and novel drug testing. Virulence. 2019;10:527–541.
[13] Asai M, Li Y, Singh Khara J, et al. *Galleria mellonella*: an infection model for screening compounds against the *Mycobacterium tuberculosis* complex. Front Microbiol. 2019;10:2630.
[14] Asai M, Li Y, Singh Khara J, et al. Use of the invertebrate *Galleria mellonella* as an infection model to study the *Mycobacterium tuberculosis* complex. J Vis Exp. 2019;(148):e59703.
[15] Li Y, Spiropoulos J, Cooley W, et al. *Galleria mellonella* - a novel infection model for the *Mycobacterium tuberculosis* complex. Virulence. 2018;9:1126–1137.
[16] Mouton JM, Heunis T, Dippenaar A, et al. Comprehensive characterization of the attenuated double

auxotroph *Mycobacterium tuberculosis* Δ*leuD*Δ*panCD* as an alternative to H37Rv. Front Microbiol. 2019;10:1922.
[17] Andreu N, Fletcher T, Krishnan N, et al. Rapid measurement of antituberculosis drug activity *in vitro* and in macrophages using bioluminescence. J Antimicrob Chemother. 2012;67:404–414.
[18] World Health Organization. Guidelines for treatment of tuberculosis. 4th ed. Geneva: WHO Press; 2010.
[19] Ryan GJ, Shapiro HM, Lenaerts AJ. Improving acid-fast fluorescent staining for the detection of mycobacteria using a new nucleic acid staining approach. Tuberculosis. 2014;94:511–518.
[20] Sampson SL, Dascher CC, Sambandamurthy VK, et al. Protection elicited by a double leucine and pantothenate auxotroph of *Mycobacterium tuberculosis* in guinea pigs. Infect Immun. 2004;72:3031–3037.
[21] Hondalus MK, Bardarov S, Russell R, et al. Attenuation of and protection induced by a leucine auxotroph of *Mycobacterium tuberculosis*. Infect Immun. 2000;68:2888–2898.
[22] Killiny N. Generous hosts: why the larvae of greater wax moth, *Galleria mellonella* is a perfect infectious host model? Virulence. 2018;9:860–865.
[23] Finke MD. Complete nutrient content of four species of commercially available feeder insects fed enhanced diets during growth. Zoo Biol. 2015;34:554–564.
[24] Wojda I. Immunity of the greater wax moth *Galleria mellonella*. Insect Sci. 2017;24:342–357.
[25] Entwistle FM, Coote PJ. Evaluation of greater wax moth larvae, *Galleria mellonella*, as a novel *in vivo* model for non-tuberculosis mycobacteria infections and antibiotic treatments. J Med Microbiol. 2018;67:585–597.
[26] Sheehan G, Dixon A, Kavanagh K. Utilization of *Galleria mellonella* larvae to characterize the development of *Staphylococcus aureus* infection. Microbiology. 2019;165:863–875.
[27] Harding CR, Schroeder GN, Reynolds S, et al. *Legionella pneumophila* pathogenesis in the *Galleria mellonella* infection model. Infect Immun. 2012;80:2780–2790.
[28] Driver E, Ryan G, Hoff D, et al. Evaluation of mouse model forming necrotic granulomas using C3HeB/FeJ mice, for the testing of *Mycobacterium tuberculosis* drugs. Antimicrob Agents Chemother. 2012;56:3181–3195.
[29] Nikonenko BV, Samala R, Einck L, et al. Rapid, simple *in vivo* screen for new drugs active against *Mycobacterium tuberculosis*. Antimicrob Agents Chemother. 2004;48:4550–4555.
[30] Thomas RJ, Hamblin KA, Armstrong SJ, et al. *Galleria mellonella* as a model system to test the pharmacokinetics and efficacy of antibiotics against *Burkholderia pseudomallei*. Int J Antimicrob Agents. 2013;41:330–336.
[31] Gopal P, Nartey W, Ragunathan P, et al. Pyrazinoic acid inhibits mycobacterial coenzyme A biosynthesis by binding to aspartate decarboxylase PanD. ACS Infect Dis. 2017;3:807–819.
[32] Andreu N, Zelmer A, Fletcher T, et al. Optimisation of bioluminescent reporters for use with mycobacteria. PLoS One. 2010;5:e10777.
[33] Myllymäki H, Bäuerlein CA, Rämet M. The zebrafish breathes new life into the study of tuberculosis. Front Immunol. 2016;7:196.
[34] Myllymäki H, Niskanen M, Oksanen KE, et al. Animal models in tuberculosis research – where is the beef? Expert Opin Drug Discov. 2015;10:871–883.
[35] Avdesh A, Chen M, Martin-Iverson MT, et al. Regular care and maintenance of a Zebrafish (*Danio rerio*) laboratory: an introduction. J Vis Exp. 2012;(69):e4196.
[36] Flentie K, Garner AL, Stallings CL. *Mycobacterium tuberculosis* transcription machinery: ready to respond to host attacks. J Bacteriol. 2016;18:1360–1373.
[37] Vogel H, Altincicek B, Glöckner G, et al. A comprehensive transcriptome and immune-gene repertoire of the lepidopteran model host *Galleria mellonella*. BMC Genomics. 2011;12:308.
[38] Lange A, Beier S, Huson DH, et al. Genome sequence of *Galleria mellonella* (greater wax moth). Genome Announc. 2018;6:e01220–17.
[39] Xu H, O'Brochta DA. Advanced technologies for genetically manipulating the silkworm *Bombyx mori*, a model lepidopteran insect. Proc R Soc B Biol Sci. 2015;282:20150487.

frontiers in Cellular and Infection Microbiology

ORIGINAL RESEARCH
published: 09 February 2021
doi: 10.3389/fcimb.2021.619981

Innate Immune Responses of *Galleria mellonella* to *Mycobacterium bovis* BCG Challenge Identified Using Proteomic and Molecular Approaches

Masanori Asai[1†], *Gerard Sheehan*[2,3†], *Yanwen Li*[1†], *Brian D. Robertson*[4], *Kevin Kavanagh*[2], *Paul R. Langford*[1*†] *and Sandra M. Newton*[1*†]

[1] Section of Paediatric Infectious Disease, Department of Infectious Disease, Imperial College London, London, United Kingdom, [2] SSPC Pharma Research Centre, Department of Biology, Maynooth University, Maynooth, Ireland, [3] Institute of Microbiology and Infection, School of Biosciences, University of Birmingham, Birmingham, United Kingdom, [4] MRC Centre for Molecular Bacteriology and Infection, Department of Infectious Disease, Imperial College London, London, United Kingdom

OPEN ACCESS

Edited by:
Christopher Lupfer,
Missouri State University,
United States

Reviewed by:
Ivan Dubovskiy,
Novosibirsk State Agrarian University, Russia
Andreas Vilcinskas,
University of Giessen, Germany
Krishnendu Mukherjee,
University Hospital Münster, Germany

***Correspondence:**
Sandra M. Newton
s.newton@imperial.ac.uk
Paul R. Langford
p.langford@imperial.ac.uk

[†]These authors have contributed equally to this work

Specialty section:
This article was submitted to Microbes and Innate Immunity, a section of the journal Frontiers in Cellular and Infection Microbiology

Received: 22 October 2020
Accepted: 04 January 2021
Published: 09 February 2021

Citation:
Asai M, Sheehan G, Li Y, Robertson BD, Kavanagh K, Langford PR and Newton SM (2021) Innate Immune Responses of Galleria mellonella to Mycobacterium bovis BCG Challenge Identified Using Proteomic and Molecular Approaches. Front. Cell. Infect. Microbiol. 11:619981. doi: 10.3389/fcimb.2021.619981

The larvae of the insect *Galleria mellonella*, have recently been established as a non-mammalian infection model for the *Mycobacterium tuberculosis* complex (MTBC). To gain further insight into the potential of this model, we applied proteomic (label-free quantification) and transcriptomic (gene expression) approaches to characterise the innate immune response of *G. mellonella* to infection with *Mycobacterium bovis* BCG *lux* over a 168 h time course. Proteomic analysis of the haemolymph from infected larvae revealed distinct changes in the proteome at all time points (4, 48, 168 h). Reverse transcriptase quantitative PCR confirmed induction of five genes (*gloverin*, *cecropin*, *IMPI*, *hemolin*, and *Hdd11*), which encoded proteins found to be differentially abundant from the proteomic analysis. However, the trend between gene expression and protein abundance were largely inconsistent (20%). Overall, the data are in agreement with previous phenotypic observations such as haemocyte internalization of mycobacterial bacilli (hemolin/β-actin), formation of granuloma-like structures (Hdd11), and melanization (phenoloxidase activating enzyme 3 and serpins). Furthermore, similarities in immune expression in *G. mellonella*, mouse, zebrafish and *in vitro* cell-line models of tuberculosis infection were also identified for the mechanism of phagocytosis (β-actin). Cecropins (antimicrobial peptides), which share the same α-helical motif as a highly potent peptide expressed in humans (h-CAP-18), were induced in *G. mellonella* in response to infection, giving insight into a potential starting point for novel antimycobacterial agents. We believe that these novel insights into the innate immune response further contribute to the validation of this cost-effective and ethically acceptable insect model to study members of the MTBC.

Keywords: *Galleria mellonella*, *Mycobacterium bovis* BCG, tuberculosis, innate immunity, *in vivo* model, proteomics, gene expression

INTRODUCTION

Tuberculosis (TB) is the leading cause of global infectious disease mortality, with a quarter of the world's population believed to be infected with the causative agent, *Mycobacterium tuberculosis* (MTB) (World Health Organization [WHO], 2020). A large majority of this population will live with a non-contagious and asymptomatic infection known as latent TB infection. Amongst these individuals, 5%–10% will develop active TB disease over their lifetime, serving as a reservoir for future transmission and infection (WHO, 2020). WHO is currently working to end the global TB epidemic by 2035. The first milestone goal is set for 2020, which will be missed by substantial margins (Reid et al., 2019). In order to meet the next milestone goal in 2035, significant advancement and increase in TB research output is needed to further understand the disease, and to identify novel mechanisms, drug targets and biomarkers, and the subsequent development of much needed tools to end the TB epidemic.

Animal infection models (e.g., mice, guinea pigs, macaques) have played an essential role in our current understanding of TB disease (Williams and Orme, 2016; Zhan et al., 2017). There are a wide variety of animal models used for TB research, but each comes with their limitations (Zhan et al., 2017). For example, in the most widely used mouse (C57Bl/6 and BALB/c) models, necrotic granulomas, a hallmark of TB, do not form (Orme, 2003). However, the ability to comprehensively study the immune response to infection, makes them useful despite their limitations. Furthermore, the use of animals is resource intensive, time consuming, requires the use of specialized animal facilities and is associated with ethical constraints, leading to a bottleneck in the research pipeline (Williams and Orme, 2016; Zhan et al., 2017). Over the past decade, the larvae of the insect, *Galleria mellonella* (Greater wax moth) have become increasingly popular as an infection model to study bacterial [e.g., *Klebsiella pneumoniae* (Insua et al., 2013), *Escherichia coli* (Alghoribi et al., 2014), *Staphylococcus aureus* (Sheehan et al., 2019)] and fungal [e.g., *Candida albicans* (Kelly and Kavanagh, 2011), *Aspergillus fumigatus* (Sheehan et al., 2018a) and *Madurella mycetomatis* (Sheehan et al., 2020b)] pathogens. Additionally the use of non-mammalian models, such as *G. mellonella*, in research is driven by the movement to reduce, replace and refine (3Rs) the use of vertebrate animals in scientific experimentation (Graham and Prescott, 2015). This insect model offers a number of advantages over conventional mammalian models: 1) low acquisition and maintenance costs, 2) accessibility, requiring minimal training and without the need for specialized equipment and facilities, 3) can tolerate incubation at 37°C, 4) no ethical constraints, 5) study of innate immunity in isolation from adaptive immunity, and 6) rapid infection cycle which allows for mid to high throughput data generation (Asai et al., 2019a). Furthermore pre-existing, non-mammalian infection models such as *Drosophila melanogaster* (fruit flies) and *Danio rerio* (zebrafish), are often incompatible with human pathogens, and require specialized facilities and equipment for infection and maintenance (Avdesh et al., 2012; Siva-Jothy et al., 2018).

Although the invertebrate *G. mellonella* lacks adaptive immunity, its innate immune system is complex and shares functional and anatomical similarities to those found in mammals (Wojda, 2017). The innate immune response of *G. mellonella* is broadly differentiated into two categories, cellular and humoral responses (Hillyer, 2016). The cellular response is driven by innate immune cells known as haemocytes (analogous to blood cells) (Pereira et al., 2018). At least six types of haemocytes have been identified in *G. mellonella*, with plasmatocytes and granulocytes being the most common types and the primary drivers of cellular functions such as phagocytosis, nodulation and encapsulation (Pereira et al., 2018). The humoral response is activated upon the detection of invading pathogens, through recognition of pathogen/damage associated molecular patterns (PAMPs/DAMPs) using pattern recognition receptors (PRRs), e.g., Toll-like receptors, β-1,3-glucan and IL-1R, and inducing signalling cascades, e.g., IMD, JNK, JAK-STAT pathways (Sheehan et al., 2018b). This leads to the expression and production of antimicrobial peptides (AMPs), mainly within the fat body (liver-like tissue), NADPH oxidase complex dependent production of reactive oxygen/nitrogen species (ROS/RNS) and hydrogen peroxide, which are secreted into the haemolymph found in the haemocoel (analogous to blood/blood vessel) (Sheehan et al., 2018b). The phenoloxidase (PO) cascade is responsible for modulation of melanization, which is a key process to localize and control infection through melanin deposition and production of phenolic compounds (Hillyer, 2016). The PO cascade system shares similarities with the mammalian complement cascade, e.g., both are initiated in response to pathogen recognition and are tightly regulated by proteases and protease inhibitors. However, they do differ in their final stages, i.e., melanization in insects and induction of cell lysis in mammals (Sheehan et al., 2018b).

Studies have demonstrated that *G. mellonella* is a viable host for mycobacterial species including both members of the MTB complex (MTBC), including MTB (Li et al., 2018; Asai et al., 2019a; Asai et al., 2019b; Asai et al., 2020), and non-tuberculous mycobacteria (NTM) (Entwistle and Coote, 2018; Meir et al., 2018; Kirubakar et al., 2020). Previously we established a *G. mellonella* – *Mycobacterium bovis* BCG *lux* model, characterised by establishment of intracellular and non-replicative but persistent infection, development of granuloma-like structures within the infected larvae, and a shift to a non-replicative lipid-rich BCG phenotype (Li et al., 2018). In addition, we demonstrated its capability as a rapid drug screen for antimycobacterial compounds, giving results within 96 h following infection (Asai et al., 2019b). We have employed BCG as a surrogate for MTB, due to its compliance with

Abbreviations: AMP, Antimicrobial peptides; BCG, Bacillus Calmette-Guérin; IMPI, Insect metalloproteinase inhibitor; LFQ, Label free quantification; MTB, *Mycobacterium tuberculosis*; MTBC, *Mycobacterium tuberculosis* complex; NTM, Non-tuberculous mycobacterium; PAMP/DAMP, Pathogen/damage associated molecular patterns; PPR, Pattern recognition receptors; PO, Phenoloxidase; ROS, Reactive oxygen species; RT-qPCR, Reverse transcriptase quantitative PCR; TB, Tuberculosis.

containment level (CL)/biosafety level (BSL) two facilities, thereby enabling researchers lacking specialized facilities (CL3/BSL3) to undertake TB research. While other surrogate mycobacteria exist, such as *Mycobacterium smegmatis*, BCG is considered to be superior due to its genetic similarity (>99.9% vs 70%) with MTB (Altaf et al., 2010). Furthermore, BCG has widely been used for *in vitro*/*ex vivo* mycobacterial growth inhibition assays (MGIAs) to study the immune mechanisms of mycobacterial control, proving to be a valuable organism in mycobacterial research (Roy et al., 2019; Tanner et al., 2019; Painter et al., 2020). Methodologies such as histopathology, transmission electron microscopy, bioluminescence, *ex vivo* haemocyte assays, and larval survival studies have typically been used to study the innate immune response to mycobacterial infection in *G. mellonella* (Li et al., 2018; Asai et al., 2019a; Asai et al., 2019b; Sheehan et al., 2019). However, greater knowledge of the larval innate immune system in response to mycobacterial infection is needed to further characterise and expand its potential as a model organism. In this study, and for the first time to our knowledge, we present a proteomic and reverse transcriptase quantitative PCR (RT-qPCR) analysis of the innate immune response of *G. mellonella* to infection with a member of the MTBC over a time course of 168 h.

METHODS

Mycobacteria Culture Conditions

M. bovis BCG *lux*, is a genetically modified bioluminescent Montréal vaccine strain which has been transformed with the shuttle plasmid vector pSMT1 expressing the *luxAB* genes of *Vibrio harveyi* (Snewin et al., 1999; Newton et al., 2011). BCG *lux* was cultured in Middlebrook 7H9 media (BD Difco, UK) supplemented with 0.2% glycerol (Sigma-Aldrich, UK), 0.05% polysorbate-80 (Sigma-Aldrich, UK) and 10% albumin dextrose catalase (BD Difco, UK), 50 μg/ml of hygromycin (Roche, UK), and incubated at 37°C in an orbital shaker. For enumeration of colony forming units (CFU), 10-fold serial dilutions of BCG *lux* were plated onto Middlebrook 7H11 agar (BD Difco, UK) supplemented with 0.5% glycerol, 10% oleic acid albumin dextrose catalase (BD Difco, UK), 50 μg/ml of hygromycin, and statically incubated at 37°C. The bioluminescence, relative light unit (RLU)/ml of BCG *lux*, was measured using a luminometer (Berthold Technologies, DE) and 1% decanal (Sigma-Aldrich) as the substrate. RLU was used as a relative and rapid estimation of CFU at a ratio of 3:1/4:1 *in vitro* and *in vivo*, respectively, as previously determined (Li et al., 2018).

G. mellonella Maintenance

Last instar *G. mellonella* larvae were purchased from Livefoods Direct, UK. Upon arrival, larvae were examined, and melanized or dead larvae were removed prior to storage in the dark at 18°C. Larvae were used within a week of arrival and were not fed during this period or throughout the experiment. Healthy larvae of approximately equal size (2–3 cm), weight (250 mg), motility and colour were picked for experimentation and acclimatised to room temperature before experimentation.

G. mellonella Infection With BCG *lux*

Mid-log phase BCG *lux* was prepared and injection of healthy *G. mellonella* larvae were carried out as previously described (Asai et al., 2019a). *G. mellonella* larvae were injected with 10 μl of BCG *lux* inoculum (1×10^5, 1×10^7 or 2×10^7 CFU) *via* the last left proleg of the larva. Injection is the preferred method over feeding, as dosing of BCG *lux* can be more accurately controlled. Infected larvae were transferred to a Petri dish lined with filter paper and incubated in a vented box at 37°C in the dark. N = 30 larvae were infected for each experimental group, unless otherwise stated, and each experiment consisted of three biological replicates (N = 90). The negative infection controls were naïve larvae, mock infected with phosphate-buffered saline (PBS), with tween (0.05%, PBS-T). Survival of the infected larvae were recorded for up to 1-week post infection (pi). Larvae were considered dead when they failed to respond to touch. Where appropriate, a t-test was carried out to determine statistical significance.

Determination of BCG *lux* Load in *G. mellonella*

The survival of BCG *lux in vivo*, over a one week-time course was determined at 0, 24, 48, 72, 96, and 168 h pi. Five larvae were individually homogenized and the RLU of the homogenate was measured using a luminometer as previously described (Asai et al., 2019a). Background bioluminescence of the homogenate was previously reported as approximately 5,000 RLU/ml.

Preparation of Larval Haemolymph for Proteomic Analysis

Collection of haemolymph for proteomic analysis was carried out using our previously established protocol (Sheehan and Kavanagh, 2018; Sheehan et al., 2018a; Sheehan et al., 2019; Sheehan et al., 2020b). Briefly, larval haemolymph was collected at 4, 48, and 168 h pi for proteomic analysis. Larvae were punctured between the head and the thorax using a sterile 30-gauge needle. Haemolymph from 10 larvae was pooled (three drops [approximately 60 μl]/larva) into a sterile 1.5 ml reaction tube containing a few pellets of N-phenylthiourea on ice to prevent melanization. The haemolymph was centrifuged at 10,000 x g for 10 min to pellet the cells, and 30 μl of the cell free haemolymph was transferred into a fresh 1.5 ml reaction tube containing 270 μl of PBS. Three independent samples were collected. Haemolymph from uninfected naive larvae was collected as a reference control.

Label-Free Quantification (LFQ) Proteomics of Larval Haemolymph

Cell free haemolymph proteins (75 μg) were processed for proteomics using previously described and established protocols (Sheehan and Kavanagh, 2018; Sheehan et al., 2018a; Sheehan et al., 2019; Sheehan et al., 2020b). Protein identification from MS/MS data was performed using the Andromeda search engine in MaxQuant (v 1.2.2.5; http://maxquant.org/), correlating the data against the six-frame translation of the expressed sequence tags (EST) contigs for *G. mellonella*, with

the addition of the proteomes of insect species *Hyalophora cecropia, Manduca sexta, Bombyx mori* (Vogel et al., 2011), and a proteomic database of *M. bovis* BCG (Brosch et al., 2007). The MS proteomic data and MaxQuant search output files were deposited to the ProteomeXchange Consortium *via* PRIDE partner repository with the dataset identifier PXD015250.

Data processing, statistical analysis, and graph generation were conducted using Persus (v 1.5.5.3). LFQ intensities were $\log_2$ transformed and one-way analysis of variance (ANOVA) and t-tests were carried out between the naïve reference and 4, 48, and 168 h BCG *lux* pi larval haemolymph samples. Significance was determined using p-value of 0.05 as a cut-off and Benjamini-Hochberg correction (Benjamini and Hochberg, 1995) was applied for false discovery rate. Proteins with non-existent values (absence or low abundance) were expressed as the imputation of the zero-value using a number close to the lowest value of the range of proteins plus or minus the standard deviation. Once imputed, these proteins were included in the analysis of total differentially expressed groups.

Reverse Transcriptase Quantitative PCR (RT-qPCR)

To quantify gene expression in *G. mellonella* larvae infected with BCG *lux*, five larvae were individually homogenized using a Ribolyser in a 2 ml lysing tube containing 900 µl of TRIzol (Thermo Fisher Scientific, UK) and six 1/8-inch metal beads (MP Biomedical, USA) at 4, 48 and 168 h pi. The lysate was processed to extract RNA using an RNeasy Mini Kit (Qiagen, UK) following the manufacturer's instructions. RNA of five larvae were pooled and cDNA was synthesised using the QuantiTect Reverse Transcription kit (Qiagen, UK), using 1 µg gDNA treated RNA as recommended by the manufacturer's protocol. Real-time quantitative PCR (RT-qPCR) was carried out using the QuantiFast SYBR® Green RT-PCR kit (Qiagen, UK) on a StepOne Plus real-time PCR system (Thermo Fisher Scientific, UK) targeting genes using primers in **Table 1**. The primer sequences for *gloverin*, *cecropin*, *hemolin*, insect metalloproteinase inhibitor (*IMPI*) and *ubiquitin* genes were acquired from prior publications (Dubovskiy et al., 2016; Lange et al., 2018b). The primer sequences for *Hdd11* were designed using NCBI primer-BLAST and their specificity were checked against the *G. mellonella* genome. Specificity of all PCR amplicons were confirmed by agarose gel electrophoresis and staining. All PCR amplicons were sequenced and blasted against the *G. mellonella* nucleotide database (NCBI), which returned expected matches [NCBI ascension number: XM_026892927 (ubiquitin), XM_026898304 (cecropin), XM_026893524 (hemolin), XM_031907851 (Hdd11), XM_026909162 (gloverin), XM_031913565 (IMPI)]. Fold changes for each gene, relative to the naïve control at t = 0 h, are shown using the comparative CT (ΔΔCt) method using *ubiquitin* as the house keeping gene. Gene expression was determined using three independent experiments, and each sample was run in triplicate. The Mann-Whitney U test was used for statistical analyses.

TABLE 1 | List of primers used in this study.

Gene	Primer sequence (5'-3')	Reference
Gloverin F	GTGTTGAGCCCGTATGGGAA	Lange et al. 2018b
Gloverin R	CCGTGCATCTGCTTGCTAAC	Lange et al., 2018b
Cecropin F	CTGTTCGTGTTCGCTTGTGT	Lange et al. 2018b
Cecropin R	GTAGCTGCTTCGCCTACCAC	Lange et al., 2018b
Hemolin F	CTCCCTCACGGAGGACAAAC	Lange et al., 2018b
Hemolin R	GCCACGCACATGTATTCACC	Lange et al., 2018b
IMPI F	TAGTAAGCAGTAGCATAGTCC	Dubovskiy et al., 2016
IMPI R	GCCATCTTCACAGTAGCA	Dubovskiy et al., 2016
Hdd11 F	TCGGCTTGTGAGTTCGTTGT	This study
Hdd11 R	GGCACTAGAAGGAGCACCAC	This study
Ubiquitin F	TCAATGCAAGTAGTCCGGTTC	Lange et al., 2018b
Ubiquitin R	CCAGTCTGCTGCTGATAAACC	Lange et al., 2018b

RESULTS

Larval Survival Following Infection With BCG *lux*

As previous work focused on larval and BCG *lux* survival over a time course of 96 h (Li et al., 2018; Asai et al., 2019a; Asai et al., 2019b), larval survival was determined over a longer 168 h time course for this proteomic and transcriptomic analysis (**Figure 1**). Larvae were considered dead when they failed to respond to touch. Larval survival decreased with increasing BCG *lux* inoculum density, where 2 x 10^7, 1 x 10^7, and 1 x 10^5 CFU resulted in 0, ~50 and 100% survival at 96 h pi, respectively. By 168 h pi, larvae infected with 1 x 10^7 and 1 x 10^5 CFU had ~15% and 100% survival, respectively. The PBS-T group displayed no fatalities, suggesting that neither injection procedure nor PBS-T induced adverse effects on survival outcome of the larvae. However, by 168 h pi some larvae in the 1 x 10^5 CFU and PBS-T groups began to pupate, entering their next stage of life cycle. These larvae were removed from the group and were omitted from the study. Over the course of infection larvae began to melanize at 48 h pi, which progressed steadily to extensive melanization at 96 h - 168 h pi. Larvae immunized with 1 x 10^5 CFU BCG *lux*, 48 h prior to infection with 2 x 10^7 CFU BCG *lux*, displayed a significant improvement in survival outcome at 96 h pi (t-test, $p < 0.01$) compared to those non-immunized (30% vs 3% respectively, **Figure 2**).

Survival of BCG *lux* Within *G. mellonella*

The survival of BCG *lux* (1 x 10^7 CFU) within *G. mellonella* was monitored over a 168 h time course, where bioluminescence of the larval homogenate was used as a rapid and validated method of quantifying changes in mycobacterial load *in vivo* (**Figure 3**). While previous data are available (Li et al., 2018), survival was repeated to ensure consistency with the survival curve for these experiments. The bioluminescence of BCG *lux* steadily decreased over the first 72 h of infection as the bacteria likely succumbed to the initial larval innate immune response. However, between 72 and 168 h pi, the reduction in bioluminescence became more gradual and plateaued by 168 h pi. These observations, consistent with our previous data (Li et al., 2018), indicate that by 72 to 96 h pi, BCG *lux* had evaded the larval innate immune response and established a persistent infection. Survival of BCG *lux* (1 x 10^5 CFU) was monitored similarly; at this lower dose RLU continued

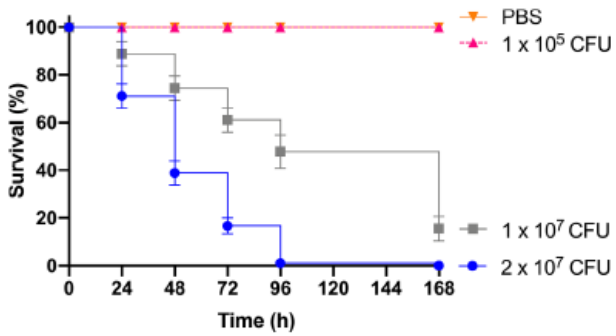


FIGURE 1 | Survival curve of *G. mellonella* over a 168 h time course following infection with varying BCG *lux* inocula. Data represent three independent experiments, n=30 for each experimental group. Plotted are the mean and the standard deviation of the mean.

to decline until 96 h, where a slight increase in RLU was observed at 168 h pi (**Supplementary Figure 1**).

Analysis of *G. mellonella* Proteome Following Infection With BCG *lux*

LFQ proteomic analysis was carried out on larval cell free haemolymph extracted from BCG *lux* (1 x 10^7 CFU) infected larvae at 4, 48, and 168 h pi, and the proteomic profiles were compared to that of 0 h control (naïve larvae). A total of 2013 peptides were identified representing 185 proteins with two or more peptide matches, of which 104 proteins were found at all time points. A number of differentially abundant proteins

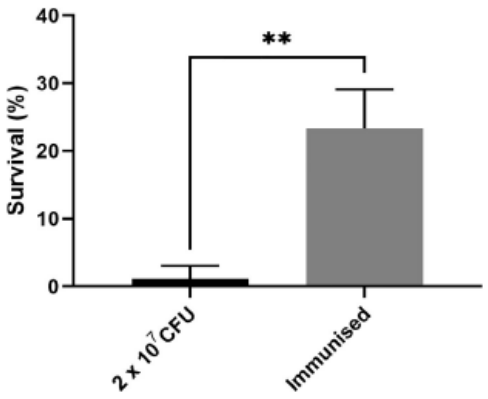


FIGURE 2 | Survival of *G. mellonella* 96 h post infection immunized with a non-lethal dose of BCG *lux* 48 h pre infection. Data represent three independent experiments n = 30, n = 10 for each experimental repeat. Plotted are the mean and the standard deviation of the mean. ** = $p < 0.01$.

(ANOVA, $p < 0.05$), with a fold change of > ± 1.5 were found, i.e., 6 at 4 h pi, 54 at 48 h pi, and 86 at 168 h pi, and a total 11 proteins were deemed exclusive (LFQ signal found in all replicates of a given time point). These exclusive proteins were used in statistical analysis following imputation of the zero value as described in the methodology. Principal component analysis (PCA) of filtered proteins clearly distinguished the proteome of each time point, and clustered independent replicates of each time point together (**Figure 4**). The full list of differentially abundant proteins is available in **Supplementary Tables 1–6**.

At 4 h pi with BCG *lux*, β-actin (+3.5 fold), hemolin (+2.2 fold) and arginine kinase (+1.6 fold) were found differentially more abundant in larval haemolymph compared to 0 h. Tubulin alpha chain (-2.4 fold), and heat shock protein 25.4 (-1.7 fold) were differentially less abundant in the larval haemolymph compared to 0 h (**Figure 5A**).

Larval proteins, which increased in relative abundance 48 h pi when compared to 0 h were cecropin-D-like peptide (+145.2 fold), gloverin (+56.3 fold), hemolin (+55.7 fold), cecropin-A (+47.5 fold), putative defence protein Hdd11 (+18.3 fold), serpin-4B (+14 fold), prophenoloxidase activating enzyme 3 (+14 fold), insect metalloproteinase inhibitor (+11.5 fold), serpin-11 (+5.9 fold), transgelin (+4.6 fold), Hdd-1 like protein (+2.9 fold), serpin-3a (+2.3 fold). Proteins which decreased in relative abundance 48 h pi were GAPDH (-14.7 fold), serine proteinase (-9.4 fold), lysozyme-like protein 1 (-4.74 fold), scolexin (-2.1 fold), and 27 kDa haemolymph protein (-1.9 fold) (**Figure 5B**).

Larval proteins which were increased in relative abundance at 168 h pi when compared to 0 h were putative defence protein Hdd11 (+310.1 fold), hemolin (+87.8 fold), cecropin-D-like peptide (+54.42 fold), chemosensory protein 7 (+42.2 fold), transgelin (+26.6 fold), prophenoloxidase activating enzyme 3 (+24.6 fold), serpin-4B (+20.9 fold), cecropin-A (+16.3 fold), serpin-11 (+15.1 fold), hdd1 (+10.8 fold), serpin-2 (+10.3 fold), gloverin (+7.61 fold), serpin-3a (+2.6 fold). Proteins which decreased in relative abundance 169 h pi were 27 kDa haemolymph protein (-9.6 fold), serine proteinase (-9.1 fold),

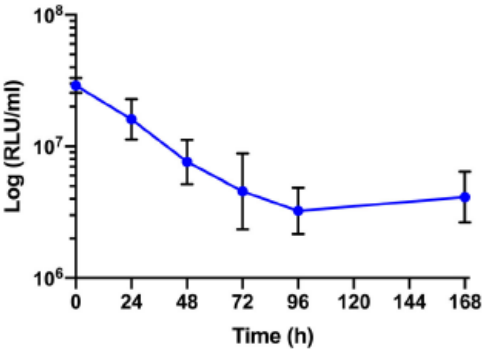


FIGURE 3 | *In vivo* survival of BCG *lux* in *G. mellonella*. Changes in BCG *lux* bioluminescence (relative light units, RLU) within *G. mellonella* following infection (1 x 10^7 CFU) over a 168 h time course. Data represent three independent experiments each with five technical replicates. Plotted are the mean and the standard deviation of the mean. RLU : CFU is approximately 4:1 as previously described by Li et al., 2018.

GAPDH (-7.7 fold), scolexin (-1.9 fold), and apolipophorin (-1.7 fold) (**Figure 5C**).

BCG *lux* Proteins Detected in *G. mellonella* Haemolymph

LFQ proteomics analysis additionally identified 15 BCG *lux* proteins within the haemolymph of the infected larvae during the 168 h time course. At 4 h pi, ribonuclease VapC, 2,3 bisphosphoglycerate-dependent phosphoglycerate mutase, diacylglycerol O-acyltransferase, and adenosylhomocysteinase were detected. At 48 h pi, molybdopterin, acyl-CoA dehydrogenase (FadE23), and an uncharacterised protein containing an undecaprenyl diphosphate synthase domain were detected. However, no proteins with a known function associated with virulence, intracellular metabolism or survival, were detected at 168 h pi. A list of detected BCG *lux* proteins is available in **Supplementary Table 7**. The relative abundance of these proteins could not be determined, and these data are qualitative observations.

G. mellonella Gene Expression Following BCG *lux* Infection

G. mellonella larvae were challenged with high (1 x 10^7 CFU) and low (1x10^5 CFU) doses of BCG *lux*. Over a 168 h time course, the expression of five genes of the *G. mellonella* innate immune system were measured at 4, 48, and 168 h pi, *via* RT-qPCR using the ΔΔCt method, *ubiquitin* as the housekeeping gene, and naïve non-infected larvae as the reference. Expression of the house keeping gene *ubiquitin* and four others encoding proteins that were differentially expressed in the proteomic analysis, i.e., *hemolin*, *IMPI*, *gloverin*, and *cecropin*, were measured. *Hemolin*, and its encoded protein, was found to be differentially abundant at all time points, *IMPI*, and its encoded protein, was found in relatively consistent abundance at 48 and 168 h pi, as was *Hdd11* and its encoded protein, which is of interest as it is involved in the formation of granuloma-like structures, which are a hallmark of TB infection (Sheehan et al., 2020b). For all five genes tested, the high dose BCG *lux* infection induced greater gene expression/suppression at all time points when compared to the low dose (**Supplementary Figure 2**). While none were statistically significant, all genes displayed a trend of reduction of gene expression over time. *Gloverin* and *cecropin* encode AMPs induced in *G. mellonella* in response to a number of bacterial and fungal pathogens (Tsai et al., 2016). The gene expression for the AMPs, *gloverin*, and *cecropin*, in response to high dose infection, significantly decreased between 4 h and 48 h pi ($p < 0.0001$). However, the level of gene expression was lower but of similar levels between 48 and 168 h pi for both genes (**Figures 6A, B**). For low dose expression *gloverin*, expression continued to decrease significantly between 4, 48, and 168 h pi ($p < 0.0001$), while *cecropin* mirrored high dose infection but at significantly lower levels of gene expression (**Figures 6A, B**, **Supplementary Figures 2A, B**). For the *hemolin* gene, high dose infection induced

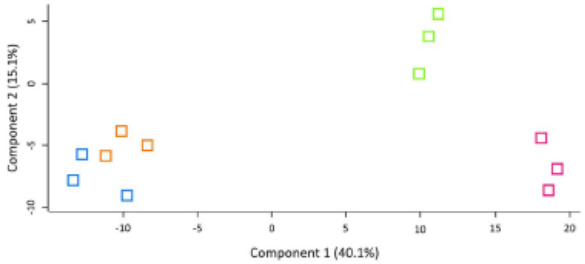


FIGURE 4 | Principal component analysis (PCA) of *G. mellonella* haemolymph proteomic profiles following infection with BCG *lux* inoculum (1 x 10^7 CFU) after 0 h (blue), 4 h (orange), 48 h (green), and 168 h (pink). Number of larvae/time point/replicate n=10. PCA of three replicates included in label free quantification analysis with a clear distinction between each time point.

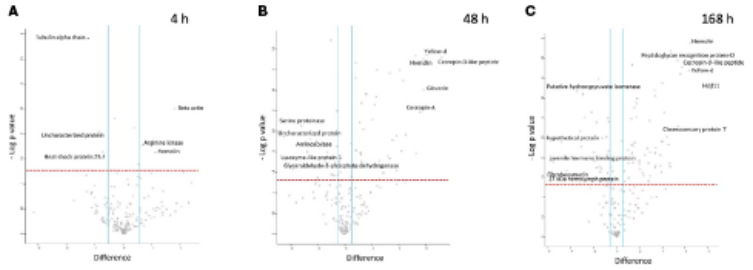


FIGURE 5 | Proteomic responses of *G. mellonella* larvae following infection by BCG *lux* (1 x 10^7 CFU) after 4 h **(A)**, 48 h **(B)**, and 168 h **(C)**. Volcano plots represent protein intensity difference (- log2 mean intensity difference) and significance in differences (- log P-value) based on a two-sided t-test. Proteins above the red dashed line are considered statistically significant (p value < 0.05) and those to the right and left of the vertical blue lines indicate relative fold changes > ± 1.5. These plots are based upon post imputed data. Each independent experiment consists of pooled haemolymph collected from 10 larvae. Data represent 3 independent experiments.

statistically significant reduction in gene expression between 48 and 168 h pi (**Figure 6C**) ($p < 0.01$). No significant reduction in gene expression was observed in low dose infection. High dose infection resulted in statistically significant higher levels of gene expression at all time points when compared to low dose infection (**Supplementary Figure 2C**) ($P < 0.001$ for 4 and 48 h pi and $P < 0.05$ for 168 h pi). For *Hdd11*, high dose infection induced greater levels of gene expression with a trend of reduction for all time points (**Figure 6D** and **Supplementary Figure 2D**). Finally, for the *IMPI* gene, induction of gene expression followed high dose infection and thereafter steadily decreased over time (**Figure 6E**), with apparent suppression between 48 and 168 h pi ($p < 0.0001$). Low dose infection led to a sustained level of gene induction between 4 and 48 h pi, and a reduced substantial gene suppression between 48 and 168 h pi ($p < 0.01$).

DISCUSSION

Previously we described, using survival curves, bacterial counts, and electron microscopy, a BCG *lux* - *G. mellonella* infection model for the MTBC complex (Li et al., 2018; Asai et al., 2019a; Asai et al., 2019b). The aim of this study was to increase our understanding of the host-bacterial interactive biology, focusing on innate immunity, through proteomic and gene expression analyses. To accommodate the increased incubation period in this study, larval survival and changes in BCG *lux* load *in vivo* over the 168 h time course were examined, which was consistent with expected observations extrapolated from our prior studies (Li et al., 2018; Asai et al., 2019a; Asai et al., 2019b). Using this established model of BCG persistence, we characterised the larval innate immune response to BCG *lux* (1 x 10^7 CFU) at 4 h, 48 h, and 168 h pi using LFQ proteomics. Distinct changes in larval proteome in response to infection at all three time points were found, with the least changes in differentially abundant proteins being at 4 h pi.

Hemolin, a member of the immunoglobulin super family (Eleftherianos et al., 2007), was found to be more abundant in the infected larvae at all time points with increasing abundance over time, 4 h (+2.2 fold) 48 h (+55.7 fold) and 168 h (+87.8 fold) pi. Hemolin aids haemocyte aggregation and phagocytosis of foreign cells through recognition of lipopolysaccharide (LPS) and lipoteichoic acid (LTA) of Gram-negative and -positive bacteria, as well as fungal β-1,3-glucan (Eleftherianos et al., 2007; Jung et al., 2019). Hemolin opsonizes microbial pathogens and binds to haemocytes, enhancing phagocytic uptake and eliminating invading pathogens (Aathmanathan et al., 2018). The interaction of hemolin with the structurally unique mycobacterial cell wall has not been described. However, as hemolin is able to recognize microbial molecular signatures, we speculate that *G. mellonella* hemolin may detect lipoglycans (noncanonical type V LTA) found in abundance on the mycobacterial cell wall (Mishra et al., 2011); this will be investigated in a future study.

As an intracellular pathogen, exploiting innate immune mechanisms to increase phagocytic uptake would be beneficial to mycobacteria. The increased abundance of β-actin at 4 h pi (+3.5 fold), may reflect the cytoskeletal redistribution and remodelling which takes place during phagocytosis (Rougerie et al., 2013). In line with this observation, infection of primary murine epithelial and lung cells with BCG has been shown to up-regulate actin redistribution (Alaridah et al., 2017). Studies of early granuloma structures in larval zebrafish found extensive reorganization of the actin cytoskeleton in granulomatous macrophages (Cronan et al., 2016). Therefore, the abundance of β-actin at 48 h and 168 h pi (+5.0 and +18.6 fold) may reflect haemocyte actin reorganization within developing granuloma-like structures. The presence and increasing abundance of β-actin in the cell-free haemolymph over time, likely reflects the equilibrium between live and dead host-cells in the granuloma-like structure (Cronan et al., 2018), with necrotic and/or lytic haemocytes likely releasing β-actin into the haemolymph.

AMPs were induced following infection with BCG *lux*. Cecropin A, cecropin-D-like protein, and gloverin were differentially more abundant than at 0 h at both 48 h and

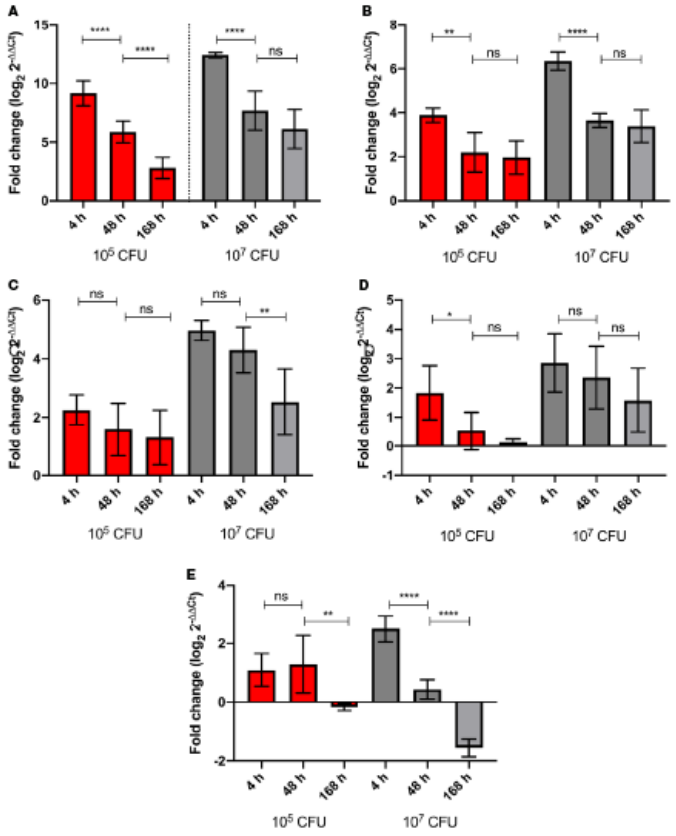


FIGURE 6 | Level of *G. mellonella* gene expression was measured by RT-qPCR from RNA of larvae challenged with either low dose (10^5 CFU, red) or high dose (10^7 CFU, grey) BCG *lux* at 4, 48, and 168 h pi. The comparative ΔΔCt method was used for relative quantification of **(A)** *gloverin*, **(B)** *cecropin*, **(C)** *hemolin*, **(D)** *Hdd11*, and **(E)** *IMPI* using *ubiquitin* as a housekeeping gene. Data represent three independent experiments, each with RNA extracted from five larvae, which was pooled. Each independent experiment consisted of three technical repeats. Bar charts represent changes in gene expression expressed as fold change. Comparison of gene expression with each infectious dose over time was carried out using the Mann-Whitney U test; where *,**,****, and ns signifies $p < 0.05$, 0.01, 0.0001 and non-significant, respectively.

168 h pi, but not at 4 h pi. Cecropins are amphipathic α-helical AMPs, reported to be effective against both Gram-positive and Gram-negative bacteria by permeating the bacterial cell wall (Zdybicka-Barabas et al., 2019). Gloverin is a glycine rich AMP efficacious against filamentous fungi and Gram-positive and Gram-negative bacteria (Wojda, 2017). As a relative comparison, gloverin (+121.7 fold), cecropin-D-like peptide (+73.7 fold), and cecropin-A (+10.56 fold) were also more abundant in larvae infected with 2 x 10^6 CFU of *S. aureus* 24 h pi (Sheehan et al., 2019). BCG *lux* infection led to increased expression of cecropin-D-like peptide (+145.2 fold), gloverin (+56.3 fold), and cecropin-A (+47.5 fold) at 48 h pi. Although variance in the infectious dose and time point complicates comparisons, the higher abundance of gloverin in response to a lower infectious dose of *S. aureus* may indicate that gloverin is preferentially expressed in the presence of Gram-positive bacteria, or alternatively the higher abundance of cecropin-D-like peptide may indicate BCG *lux* is a more potent inducer. In mammals, cathelicidins, cationic α-helical AMPs, are released by leukocytes in response to infection (Arranz-Trullén et al., 2017). The human cationic antimicrobial peptide 18 (h-CAP-18) is the leading AMP in TB therapeutics, with both bactericidal and immunomodulating activity (Arranz-Trullén et al., 2017). Immunomodulation of macrophages and neutrophils by LL-37,

a proteolyzed component of h-CAP-18, has been reported during infection, such as the promotion of autophagy in human monocytes (Arranz-Trullén et al., 2017). A previous report indicates that Cecropin-A induces immunomodulating activity in macrophages, regulating inflammatory responses (Lee et al., 2015a). If similar activities occur in phagocytic haemocytes, then increased abundance of hemolin and cytoskeletal actin could result from upregulation of autophagy-related activities. The production of synthetic cecropin-D-like peptides has been reported (Correa et al., 2014b; Correa et al., 2014a). Cytotoxicity of cecropin-D-like peptides, has previously been determined against erythrocytes with haemolysis of 2.3% at 115 μM (Oñate-Garzón et al., 2017). Cecropin-D-like peptides have shown antimicrobial activity against Gram-positive (*S. aureus*) and negative (*Pseudomonas aeruginosa* and *E. coli*) bacteria through permeabilization and disruption of the cell membrane (Cytryńska et al., 2007; Oñate-Garzón et al., 2017). Therefore, *in vitro* drug screening against mycobacteria using synthetic *G. mellonella* AMPs, may reveal promising antimycobacterial properties.

Hdd11 (homologous to Noduler) is associated with the formation of nodules or granuloma-like structures; facilitated by crosslinking pathogens and haemocytes by Hdd11 (Gandhe et al., 2007; Sheehan et al., 2020b). In line with published histopathology data from BCG *lux* infected *G. mellonella* larvae (Li et al., 2018), where numbers of granuloma-like structures increased over time, the abundance of Hdd11 within the haemolymph increased +18.3 and +310 fold compared to 0 h, as infection progressed at 48 h and 169 h pi, respectively. The fungal granulomatous disease, mycetoma, caused by *M. mycetomatis* has been modelled using *G. mellonella* larvae. In larvae infected with *M. mycetomatis*, Hdd11 was +533 fold more abundant within the haemolymph at 168 h pi when compared to 0 h (Sheehan et al., 2020b). Although Hdd11 levels are higher in *M. mycetomatis* infection, this indicates that BCG *lux* induces a similar granulomatous response. Formation of early granuloma in humans is tightly regulated by the interaction between matrix metalloproteinases (MMPs) and tissue inhibitors of MMPs (TIMPs) (Parasa et al., 2017). IMPI, found differentially abundant at 48 h and 168 h pi, is an insect metalloproteinase inhibitor, but has no structural similarities to vertebrate or invertebrate TIMPs (Vilcinskas and Wedde, 2002). IMPI does not inhibit host MMP activity, its primary function is to inhibit microbial metalloproteinases. However, IMPI can additionally regulate endogenous metalloproteinases involved in metamorphosis and thereby, depending on the life stage of the larvae, potentially impact on the larval tissue response to infection (Wedde et al., 2007). MMPs and TIMPs have been identified in fruit flies, and it is likely similar systems exist in *G. mellonella* (Vilcinskas and Wedde, 2002). The challenge remains in identifying these systems, as the publicly available genome of *G. mellonella* is yet to be fully annotated (Lange et al., 2018a).

Another key invertebrate innate immune response is melanization, modulated through the PO cascade (Dubovskiy et al., 2013). Proteins associated with the PO cascade were more abundant at 48 h pi (phenoloxidase activating enzyme 3, serpin-3a, serpin-4b, and serpin-11) and 168 h pi (phenoloxidase activating enzyme 3, serpin-2, serpin-3a, serpin-4b, and serpin-11), but not at 4 h pi. In contrast, larvae challenged with a lower infectious dose of *S. aureus* (2 x 10^6 CFU) induced more abundant levels of phenoloxidase activating enzyme 3 and serpin-4b by 6 h pi compared to the 0 h control (Sheehan et al., 2019). This may reflect the more virulent or rapid growth of *S. aureus*, as the rate of mortality was 90% by 72 h pi (Sheehan et al., 2019). Previous studies using the *G. mellonella* – BCG *lux* infection model, found slow gradual melanization over 96 h, with little to no melanization within the first 24 h (Asai et al., 2019a). Serpins, a class of protease inhibitor which negatively regulates the PO cascade (Lu et al., 2014), were detected in response to BCG *lux* infection. We speculate that the lack of abundant PO cascade proteins at 4 h pi and the rate of larval melanization, reflects the slow growth and persistence of BCG *lux* infection leading to host modulation of the PO cascade to prevent uncontrollable melanization.

While distinct changes in proteomic signatures over the time course were detected, changes specific to mycobacteria infection were not identified. Despite the lack of a BCG specific response, *G. mellonella* larvae immunized with a non-lethal dose of BCG *lux* (1x10^5 CFU), 48 h prior to infection with a lethal dose of BCG *lux* (2x10^7 CFU), resulted in improved survival outcome when compared to the non-immunized control. This observation, commonly referred to as immune priming, has widely been reported in invertebrate infection models (Bergin et al., 2006; Sadd and Schmid-Hempel, 2006; Pham et al., 2007; Sheehan et al., 2020a). The precise mechanism, of how a non-lethal exposure to a pathogen leads to protection/immunity, remains unclear with a number of mechanisms being suggested (Sheehan et al., 2020a). However, it is known that non-lethal exposure typically leads to an increase in the number of circulating haemocytes and the production of AMPs (Bergin et al., 2006). Moreover, it is unclear as to whether these responses are pathogen type/class specific or are more generalized. Therefore, future studies will focus on whether immunization with non-lethal BCG dose leads to primed protection against other mycobacterial species, Gram-positive/negative bacteria and fungi.

LFQ proteomics analysis identified BCG *lux* proteins within the larval haemolymph giving qualitative insight into the response of the larval innate immune system. Most proteins detected were associated with intracellular adaptations and survival. At 4 h pi, proteins were associated with metabolic changes. These included: ribonuclease VapC and 2,3 bisphosphoglycerate-dependent phosphoglycerate mutase, both of which have been associated with regulation of metabolism in response to intracellular conditions and glucogenesis (Hillion et al., 2017; Sharrock et al., 2018). Adenosylhomocysteinase catalyses the reversible processing of S-adenosylmethionine dependent methyltransferase reaction and is essential for *in vitro* growth, and was upregulated in lung tissues of MTB infected mice (Singhal et al., 2012). Diacylglycerol O-acyltransferase is involved in the accumulation of triacylglycerol in MTB under stress (Sirakova et al., 2006).

The presence of diacylglycerol O-acyltransferase is in agreement with the accumulation of lipid droplet structures in BCG *lux in vivo* in *G. mellonella* which have been observed using transmission electron microscopy (Li et al., 2018). At 48 h pi, proteins associated with intracellular survival were detected. Molybdoperin is induced in response to hypoxia and nitric oxide stress (Wang et al., 2013). Acyl-CoA dehydrogenase induced in response to cell envelope damage following oxidative and nitrosative stress, may have a role in recycling of fatty acids (Voskuil, 2013). An uncharacterised protein with an undecaprenyl diphosphate synthase domain, typically associated with cell wall synthesis was detected (Kaur et al., 2004). Abundance of this protein may be associated with thickening of the mycobacterial cell wall as a stress response to intracellular conditions (Ghazaei, 2018). Similar to 4 h pi, diacylglycerol O-acyltransferase was also detected at 48 h pi. These proteins in the haemolymph may be associated with MTB extracellular vesicles, as both diacylglycerol O-acyltransferase and acyl-CoA dehydrogenase have been detected in such structures. (Lee et al., 2015b). The presence of BCG *lux* proteins involved in intracellular adaptation and survival at 4 and 48 h pi indicate that the haemocytic environment is a mycobacterial stress-inducer.

The *G. mellonella* innate immune response to BCG *lux* was also investigated using RT-qPCR. The results show that infection with BCG *lux* at high (1×10^7 CFU) and low (1×10^5 CFU) doses, led to differential gene expression of innate immune genes, with higher dose infection inducing more substantial changes. Changes in gene expression were detected in *gloverin*, *cecropin*, *IMPI*, *hemolin*, and *Hdd11* regardless of infectious dose when compared to the 0 h control. Induction of expression was highest at 4 h pi, and thereafter decreased over the time course despite the presence of a persistent infection. Similar observations were made in an RT-qPCR study of *G. mellonella* innate immune responses to infection with *Riemerella anatipestifer*, a Gram-negative bacterium, where genes involved in innate immunity (e.g., encoding AMPs and opsonin), were highest at 4 h pi, and declined over time (Liu et al., 2019). In this study, the trend between the presence of protein and the corresponding mRNA improved over the course of infection, but the abundance of protein was largely inconsistent with gene expression signals, with only 20% in agreement between 48-168 h pi. Proteins induced by genes expression at 4 h pi were mostly undetected in the proteomic analysis with the exception to hemolin. The discrepancy between the two datasets may be attributed to the preparation of the samples. The proteomic study was carried out on cell free haemolymph, whereas the gene expression study was carried out on mRNA prepared from the whole larva. Gene expression studies in both humans (Sonawane et al., 2017) and insects, *Manduca sexta* (Cao and Jiang, 2017) and *Ceracris nigricornis* Walker (Yuan et al., 2019), have highlighted the importance of acknowledging tissue specific expression of genes. It is unknown whether the genes examined in this study are expressed globally or are tissue specific. Nevertheless, the comparison of proteomics and transcriptomics has been an ongoing subject of discussion. A study that compared the correlation of proteome and transcriptome across developmental stages of fruit flies (Becker et al., 2018) and *Epicauta chinensis* (blister beetle) (Li et al., 2014) reported a low correlation (20%–34%) between mRNA levels and protein expression. Becker et al. 2018 adjusted for the translational delay of mRNA into protein (~ 4-6 h) for a small subset of genes in fruit flies, which showed modest improvements (+2.4%). This supports the idea that there are lags between the initiation of gene expression and protein biosynthesis, possibly due to the basal mRNA state (steady, long/short-term), downstream gene regulation, post-transcriptional modification to mRNA, and/or availability of biosynthetic material (Liu et al., 2016). Studies have determined that the correlation between these two Omics approaches, are modest at best (40%) (Gygi et al., 1999; Kumar et al., 2016), with correlation decreasing with increasing biological complexity, i.e., single cellular to multi-cellular organisms (Gygi et al., 1999; De Sousa Abreu et al., 2009; Schwanhüusser et al., 2011; Kumar et al., 2016; Meir et al., 2018). Furthermore, a comparative proteomic and transcriptomic study of 29 human tissue types revealed that a number of protein molecules synthesised per highly abundant transcript were near quadratic (Wang et al., 2019). It is generally speculated that abundance of protein/gene is regulated at the translational level through enhanced translational efficiency and protein stability (Vogel et al., 2010). The presentation of both the gene expression and proteomic data in this paper is the first of its kind for *G. mellonella*. We acknowledge that the number of genes tested are limited and a more comprehensive analysis to determine a broader correlation between transcriptome and proteome of *G. mellonella* is warranted in the future. As proteomics investigates the presence/absence and relative abundance of a protein, it is a more reliable indicator of the state of the innate immune response of *G. mellonella* at a given time point.

In conclusion, to our knowledge, this is the first report of the innate immune response of *G. mellonella* to mycobacterial infection using molecular transcriptomic and proteomic approaches. The proteomic profiles were unique over the course of infection. Responses were similar to those in *G. mellonella* infected with fungal granulomatous infectious disease. BCG *lux* proteins were detected, associated with intracellular survival and metabolism in vertebrate hosts, indicating that *G. mellonella* induces similar stress responses. RT-qPCR confirmed the proteomic analysis. However, gene expression and protein abundance was not always in agreement, and careful comparison of data should be made in future studies. Several targets for further studies, such hemolin as an opsonising agent and cecropin as an antimycobacterial agent, were identified and will be further investigated. While this study focused on the host response to infection, future studies will evaluate the mycobacterial response to humoral innate immunity of *G. mellonella*. The data presented here provide a vital insight into the *G. mellonella* – mycobacterial infection model and highlights its value for accelerating in TB research.

DATA AVAILABILITY STATEMENT

The datasets presented in this study can be found in online repositories. The names of the repository/repositories and accession number(s) can be found in the article/ **Supplementary Material**.

AUTHOR CONTRIBUTIONS

MA, GS, YL, BR, KK, PL, and SN conceptualized the study. MA drafted the manuscript. MA, GS, and YL carried out the experimental procedures. MA and GS carried out experimental analysis. MA, GS, YL, BR, KK, PR, and SN reviewed, edited, and approved the manuscript for submission. All authors contributed to the article and approved the submitted version.

FUNDING

This work was supported by grants from the Biotechnology and Biological Sciences Research Centre (BBSRC) [BB/P001262/1] to PL and YL, and the National Centre for the Replacement, Refinement and Reduction of Animals in Research (NC3Rs) [NC/R001596/1] to PL, SN, BR, and YL. GS is the recipient of a Maynooth University doctoral studentship. The Q-exactive mass spectrometer was funded under the Science Foundation Ireland (SFI) Research Infrastructure Call 2012, [12/RI/2346] (3). This publication emanated from research supported in part by a research grant from the SFI and is co-funded under the European Regional Development Fund [12/RC/2275_P2].

SUPPLEMENTARY MATERIAL

The Supplementary Material for this article can be found online at: https://www.frontiersin.org/articles/10.3389/fcimb.2021.619981/full#supplementary-material

REFERENCES

Aathmanathan, V. S., Jothi, N., Prajapati, V. K., and Krishnan, M. (2018). Investigation of immunogenic properties of Hemolin from silkworm, *Bombyx mori* as carrier protein: An immunoinformatic approach. *Sci. Rep.* 8, 6957. doi: 10.1038/s41598-018-25374-z

Alaridah, N., Lutay, N., Tenland, E., Rönnholm, A., Hallgren, O., Puthia, M., et al. (2017). Mycobacteria manipulate G-Protein-coupled receptors to increase mucosal Rac1 expression in the lungs. *J. Innate Immun.* 9, 318–329. doi: 10.1159/000453454

Alghoribi, M. F., Gibreel, T. M., Dodgson, A. R., Beatson, S. A., and Upton, M. (2014). *Galleria mellonella* infection model demonstrates high lethality of ST69 and ST127 uropathogenic *Escherichia coli*. *PLoS One* 9, e101547. doi: 10.1371/journal.pone.0101547

Altaf, M., Miller, C. H., Bellows, D. S., and O'Toole, R. (2010). Evaluation of the *Mycobacterium smegmatis* and BCG models for the discovery of *Mycobacterium tuberculosis* inhibitors. *Tuberculosis* 90, 333–337. doi: 10.1016/j.tube.2010.09.002

Arranz-Trullén, J., Lu, L., Pulido, D., Bhakta, S., and Boix, E. (2017). Host antimicrobial peptides: The promise of new treatment strategies against tuberculosis. *Front. Immunol.* 8, 1499. doi: 10.3389/fimmu.2017.01499

Asai, M., Li, Y., Singh Khara, J., Gladstone, C. A., Robertson, B. D., Langford, P. R., et al. (2019a). Use of the invertebrate *Galleria mellonella* as an infection model to study the *Mycobacterium tuberculosis* complex. *J. Vis. Exp.* 148, e59703. doi: 10.3791/59703

Asai, M., Li, Y., Singh Khara, J., Robertson, B. D., Langford, P. R., and Newton, S. M. (2019b). *Galleria mellonella*: an infection model for screening compounds against the *Mycobacterium tuberculosis* complex. *Front. Microbiol.* 10, 2630. doi: 10.3389/fmicb.2019.02630

Asai, M., Li, Y., Spiropoulos, J., Cooley, W., Everest, D., Robertson, B. D., et al. (2020). A novel biosafety level 2 compliant tuberculosis infection model using a *ΔleuDΔpanCD* double auxotroph of *Mycobacterium tuberculosis* H37Rv and *Galleria mellonella*. *Virulence* 11, 811–824. doi: 10.1080/21505594.2020.1781486

Avdesh, A., Chen, M., Martin-Iverson, M. T., Mondal, A., Ong, D., Rainey-Smith, S., et al. (2012). Regular care and maintenance of a Zebrafish (*Danio rerio*) laboratory: An introduction. *J. Vis. Exp.* 69, e4196. doi: 10.3791/4196

Becker, K., Bluhm, A., Casas-Vila, N., Dinges, N., Dejung, M., Sayols, S., et al. (2018). Quantifying post-transcriptional regulation in the development of *Drosophila melanogaster*. *Nat. Commun.* 9, 4970. doi: 10.1038/s41467-018-07455-9

Benjamini, Y., and Hochberg, Y. (1995). Controlling the false discovery rate: a practical and powerful approach to multiple testing. *J. R. Stat. Soc Ser. B* 57, 289–300. doi: 10.1111/j.2517-6161.1995.tb02031.x

Bergin, D., Murphy, L., Keenan, J., Clynes, M., and Kavanagh, K. (2006). Pre-exposure to yeast protects larvae of *Galleria mellonella* from a subsequent lethal infection by *Candida albicans* and is mediated by the increased expression of antimicrobial peptides. *Microbes Infect.* 8, 2105–2112. doi: 10.1016/j.micinf.2006.03.005

Brosch, R., Gordon, S. V., Garnier, T., Eiglmeier, K., Frigui, W., Valenti, P., et al. (2007). Genome plasticity of BCG and impact on vaccine efficacy. *Proc. Natl. Acad. Sci. U. S. A.* 104, 5596–5601. doi: 10.1073/pnas.0700869104

Cao, X., and Jiang, H. (2017). An analysis of 67 RNA-seq datasets from various tissues at different stages of a model insect, *Manduca sexta*. *BMC Genomics* 18, 796. doi: 10.1186/s12864-017-4147-y

Correa, W., Manrique-Moreno, M., Behrends, J., Patiño, E., Marella, C., Peláez-Jaramillo, C., et al. (2014a). *Galleria mellonella* native and analogue peptides Gm1 and ΔGm1. II) Anti-bacterial and anti-endotoxic effects. *Biochim. Biophys. Acta - Biomembr.* 1838, 2739–2744. doi: 10.1016/j.bbamem.2014.07.005

Correa, W., Manrique-Moreno, M., Patiño, E., Peláez-Jaramillo, C., Kaconis, Y., Gutsmann, T., et al. (2014b). *Galleria mellonella* native and analogue peptides Gm1 and ΔGm1. I) Biophysical characterization of the interaction mechanisms with bacterial model membranes. *Biochim. Biophys. Acta - Biomembr.* 1838, 2728–2738. doi: 10.1016/j.bbamem.2014.07.006

Cronan, M. R., Beerman, R. W., Rosenberg, A. F., Saelens, J. W., Johnson, M. G., Oehlers, S. H., et al. (2016). Macrophage epithelial reprogramming underlies mycobacterial granuloma formation and promotes infection. *Immunity* 45, 861–876. doi: 10.1016/j.immuni.2016.09.014

Cronan, M. R., Matty, M. A., Rosenberg, A. F., Blanc, L., Pyle, C. J., Espenschied, S. T., et al. (2018). An explant technique for high-resolution imaging and manipulation of mycobacterial granulomas. *Nat. Methods* 15, 1098–1107. doi: 10.1038/s41592-018-0215-8

Cytryńska, M., Mak, P., Zdybicka-Barabas, A., Suder, P., and Jakubowicz, T. (2007). Purification and characterization of eight peptides from *Galleria mellonella* immune hemolymph. *Peptides* 28, 533–546. doi: 10.1016/j.peptides.2006.11.010

De Sousa Abreu, R., Penalva, L. O., Marcotte, E. M., and Vogel, C. (2009). Global signatures of protein and mRNA expression levels. *Mol. Biosyst.* 5, 1512–1526. doi: 10.1039/b908315d

Dubovskiy, I. M., Whitten, M. M. A., Kryukov, V. Y., Yaroslavtseva, O. N., Grizanova, E. V., Greig, C., et al. (2013). More than a colour change: Insect melanism, disease resistance and fecundity. *Proc. R. Soc B Biol. Sci.* 280, 20130584. doi: 10.1098/rspb.2013.0584

Dubovskiy, I. M., Grizanova, E. V., Whitten, M. M. A., Mukherjee, K., Greig, C., Alikina, T., et al. (2016). Immuno-physiological adaptations confer wax moth *Galleria mellonella* resistance to *Bacillus thuringiensis*. *Virulence* 7, 860–870. doi: 10.1080/21505594.2016.1164367

Eleftherianos, I., Gökçen, F., Felföldi, G., Millichap, P. J., Trenczek, T. E., Ffrench-constant, R. H., et al. (2007). The immunoglobulin family protein Hemolin mediates cellular immune responses to bacteria in the insect *Manduca sexta*. *Cell. Microbiol.* 9, 1137–1147. doi: 10.1111/j.1462-5822.2006.00855.x

Entwistle, F. M., and Coote, P. J. (2018). Evaluation of greater wax moth larvae, *Galleria mellonella*, as a novel *in vivo* model for non-tuberculosis mycobacteria infections and antibiotic treatments. *J. Med. Microbiol.* 67, 585–597. doi: 10.1099/jmm.0.000696

Gandhe, A. S., John, S. H., and Nagaraju, J. (2007). Noduler, a novel immune up-regulated protein mediates nodulation response in insects. *J. Immunol.* 179, 6943–6951. doi: 10.4049/jimmunol.179.10.6943

Ghazaei, C. (2018). *Mycobacterium tuberculosis and* lipids: Insights into molecular mechanisms from persistence to virulence. *J. Res. Med. Sci.* 23, 63. doi: 10.4103/jrms.JRMS_904_17

Graham, M. L., and Prescott, M. J. (2015). The multifactorial role of the 3Rs in shifting the harm-benefit analysis in animal models of disease. *Eur. J. Pharmacol.* 795, 19–29. doi: 10.1016/j.ejphar.2015.03.040

Gygi, S. P., Rochon, Y., Franza, B. R., and Aebersold, R. (1999). Correlation between protein and mRNA abundance in yeast. *Mol. Cell. Biol.* 19, 1720–1730. doi: 10.1128/MCB.19.3.1720

Hillion, M., Bernhardt, J., Busche, T., Rossius, M., Maaß, S., Becher, D., et al. (2017). Monitoring global protein thiol-oxidation and protein S-mycothiolation in *Mycobacterium smegmatis* under hypochlorite stress. *Sci. Rep.* 7, 1195. doi: 10.1038/s41598-017-01179-4

Hillyer, J. F. (2016). Insect immunology and hematopoiesis. *Dev. Comp. Immunol.* 58, 102–118. doi: 10.1016/j.dci.2015.12.006

Insua, J. L., Llobet, E., Moranta, D., Pérez-Gutiérrez, C., Tomás, A., Garmendia, J., et al. (2013). Modeling *Klebsiella pneumoniae* pathogenesis by infection of the wax moth *Galleria mellonella*. *Infect. Immun.* 81, 3552–3565. doi: 10.1128/IAI.00391-13

Jung, J., Sajjadian, S. M., and Kim, Y. (2019). Hemolin, an immunoglobulin-like peptide, opsonizes nonself targets for phagocytosis and encapsulation in *Spodoptera exigua*, a lepidopteran insect. *J. Asia Pac. Entomol.* 22, 947–956. doi: 10.1016/j.aspen.2019.08.002

Kaur, D., Brennan, P. J., and Crick, D. C. (2004). Decaprenyl diphosphate synthesis in *Mycobacterium tuberculosis*. *J. Bacterial.* 186, 7564–7570. doi: 10.1128/JB.186.22.7564-7570.2004

Kelly, J., and Kavanagh, K. (2011). Caspofungin primes the immune response of the larvae of *Galleria mellonella* and induces a non-specific antimicrobial response. *J. Med. Microbiol.* 60, 189–196. doi: 10.1099/jmm.0.025494-0

Kirubakar, G., Schäfer, H., Rickerts, V., Schwarz, C., and Lewin, A. (2020). Mutation on *lysX* from *Mycobacterium avium hominissuis* impacts the host-pathogen interaction and virulence phenotype. *Virulence* 11, 132–144. doi: 10.1080/21505594.2020.1713690

Kumar, D., Bansal, G., Narang, A., Basak, T., Abbas, T., and Dash, D. (2016). Integrating transcriptome and proteome profiling: Strategies and applications. *Proteomics* 16, 2533–2544. doi: 10.1002/pmic.201600140

Lange, A., Beier, S., Huson, D. H., Parusel, R., Iglauer, F., and Frick, J. S. (2018a). Genome sequence of *Galleria mellonella* (greater wax moth). *Genome Announc.* 6, e01220–e01217. doi: 10.1128/genomeA.01220-17

Lange, A., Schäfer, A., Bender, A., Steimle, A., Beier, S., Parusel, R., et al. (2018b). *Galleria mellonella*: A novel invertebrate model to distinguish intestinal symbionts from pathobionts. *Front. Immunol.* 9, 2114. doi: 10.3389/fimmu.2018.02114

Lee, E., Shin, A., and Kim, Y. (2015a). Anti-inflammatory activities of cecropin A and its mechanism of action. *Arch. Insect Biochem. Physiol.* 88, 31–44. doi: 10.1002/arch.21193

Lee, J., Kim, S. H., Choi, D. S., Lee, J. S., Kim, D. K., Go, G., et al. (2015b). Proteomic analysis of extracellular vesicles derived from *Mycobacterium tuberculosis*. *Proteomics* 15, 3331–3337. doi: 10.1002/pmic.201500037

Li, Q., Wang, D., Lv, S., and Zhang, Y. (2014). Comparative proteomics and expression analysis of five genes in *Epicauta chinensis* larvae from the first to fifth instar. *PLoS One* 9, e89607. doi: 10.1371/journal.pone.0089607

Li, Y., Spiropoulos, J., Cooley, W., Singh Khara, J., Gladstone, C. A., Asai, M., et al. (2018). *Galleria mellonella* - a novel infection model for the *Mycobacterium tuberculosis* complex. *Virulence* 9, 1126–1137. doi: 10.1080/21505594.2018.1491255

Liu, Y., Beyer, A., and Aebersold, R. (2016). On the dependency of cellular protein levels on mRNA abundance. *Cell* 165, 535–550. doi: 10.1016/j.cell.2016.03.014

Liu, M., Huang, M., Huang, L., Biville, F., Zhu, D., Wang, M., et al. (2019). New perspectives on *Galleria mellonella* larvae as a host model using *Riemerella anatipestifer* as a proof of concept. *Infect. Immun.* 87, e0079–e0019. doi: 10.1128/IAI.00072-19

Lu, A., Zhang, Q., Zhang, J., Yang, B., Wu, K., Xie, W., et al. (2014). Insect prophenoloxidase: The view beyond immunity. *Front. Physiol.* 5, 252. doi: 10.3389/fphys.2014.00252

Meir, M., Grosfeld, T., and Barkan, D. (2018). Establishment and validation of *Galleria mellonella* as a novel model organism to study *Mycobacterium abscessus* infection, pathogenesis, and treatment. *Antimicrob. Agents Chemother.* 62, e02539–e02517. doi: 10.1128/AAC.02539-17

Mishra, A. K., Driessen, N. N., Appelmelk, B. J., and Besra, G. S. (2011). Lipoarabinomannan and related glycoconjugates: Structure, biogenesis and role in *Mycobacterium tuberculosis* physiology and host-pathogen interaction. *FEMS Microbiol. Rev.* 35, 1126–1157. doi: 10.1111/j.1574-6976.2011.00276.x

Newton, S., Martineau, A., and Kampmann, B. (2011). A functional whole blood assay to measure viability of mycobacteria, using reporter-gene tagged BCG or M.Tb (BCG *lux*/M.Tb *lux*). *J. Vis. Exp.* 55, e3332. doi: 10.3791/3332

Oñate-Garzón, J., Manrique-Moreno, M., Trier, S., Leidy, C., Torres, R., and Patiño, E. (2017). Antimicrobial activity and interactions of cationic peptides derived from *Galleria mellonella* cecropin D-like peptide with model membranes. *J. Antibiot. (Tokyo)* 70, 238–245. doi: 10.1038/ja.2016.134

Orme, I. M. (2003). The mouse as a useful model of tuberculosis. *Tuberculosis* 83, 112–115. doi: 10.1016/S1472-9792(02)00069-0

Painter, H., Prabowo, S. A., Cia, F., Stockdale, L., Tanner, R., Willcocks, S., et al. (2020). Adaption of the *ex vivo* mycobacterial growth inhibition assay for use with murine lung cells. *Sci. Rep.* 10, 3311. doi: 10.1038/s41598-020-60223-y

Parasa, V. R., Muvva, J. R., Rose, J. F., Braian, C., Brighenti, S., and Lerm, M. (2017). Inhibition of tissue matrix metalloproteinases interferes with *Mycobacterium tuberculosis*-induced granuloma formation and reduces bacterial load in a human lung tissue model. *Front Microbiol.* 8, 2370. doi: 10.3389/fmicb.2017.02370

Pereira, T. C., de Barros, P. P., de Oliveira Fugisaki, L. R., Rossoni, R. D., de Ribeiro, F. C., de Menezes, R. T., et al. (2018). Recent advances in the use of *Galleria mellonella* model to study immune responses against human pathogens. *J. Fungi* 4, E128. doi: 10.3390/jof4040128

Pham, L. N., Dionne, M. S., Shirasu-Hiza, M., and Schneider, D. S. (2007). A specific primed immune response in *Drosophila* is dependent on phagocytes. *PLoS Pathog.* 3, e26. doi: 10.1371/journal.ppat.0030026

Reid, M. J. A., Arinaminpathy, N., Bloom, A., Bloom, B. R., Boehme, C., Chaisson, R., et al. (2019). Building a tuberculosis-free world: The Lancet Commission on tuberculosis. *Lancet* 393, 1331–1384. doi: 10.1016/S0140-6736(19)30024-8

Rougerie, P., Miskolci, V., and Cox, D. (2013). Generation of membrane structures during phagocytosis and chemotaxis of macrophages: Role and regulation of the actin cytoskeleton. *Immunol. Rev.* 256, 222–239. doi: 10.1111/imr.12118

Roy, R. B., Sambou, B., Uhia, I., Roetynck, S., Robertson, B. D., and Kampmann, B. (2019). An auto-luminescent fluorescent BCG whole blood assay to enable evaluation of paediatric mycobacterial responses using minimal blood volumes. *Front. Pediatr.* 7, 151. doi: 10.3389/fped.2019.00151

Sadd, B. M., and Schmid-Hempel, P. (2006). Insect immunity shows specificity in protection upon secondary pathogen exposure. *Curr. Biol.* 16, 1206–1210. doi: 10.1016/j.cub.2006.04.047

Schwanhüusser, B., Busse, D., Li, N., Dittmar, G., Schuchhardt, J., Wolf, J., et al. (2011). Global quantification of mammalian gene expression control. *Nature* 473, 337–342. doi: 10.1038/nature10098

Sharrock, A., Ruthe, A., Andrews, E. S. V., Arcus, V. A., and Hicks, J. L. (2018). VapC proteins from *Mycobacterium tuberculosis* share ribonuclease sequence specificity but differ in regulation and toxicity. *PLoS One* 13, e0203412. doi: 10.1371/journal.pone.0203412

Sheehan, G., Clarke, G., and Kavanagh, K. (2018a). Characterisation of the cellular and proteomic response of *Galleria mellonella* larvae to the development of invasive aspergillosis. *BMC Microbiol.* 18, 63. doi: 10.1186/s12866-018-1208-6

Sheehan, G., Garvey, A., Croke, M., and Kavanagh, K. (2018b). Innate humoral immune defences in mammals and insects: The same, with differences? *Virulence* 9, 1625–1639. doi: 10.1080/21505594.2018.1526531

Sheehan, G., Dixon, A., and Kavanagh, K. (2019). Utilization of *Galleria mellonella* larvae to characterize the development of *Staphylococcus aureus* infection. *Microbiology* 165, 863–875. doi: 10.1099/mic.0.000813

Sheehan, G., Farrell, G., and Kavanagh, K. (2020a). Immune priming: the secret weapon of the insect world. *Virulence* 11, 238–246. doi: 10.1080/21505594.2020.1731137

Sheehan, G., Konings, M., Lim, W., Fahal, A., Kavanagh, K., and Van de Sande, W. J. (2020b). Proteomic analysis of the processes leading to *Madurella mycetomatis* grain formation in *Galleria mellonella* larvae. *PLoS Negl. Trop. Dis.* 14, e0008190. doi: 10.1371/journal.pntd.0008190

Sheehan, G., and Kavanagh, K. (2018). Analysis of the early cellular and humoral responses of *Galleria mellonella* larvae to infection by *Candida albicans*. *Virulence* 9, 163–172. doi: 10.1080/21505594.2017.1370174

Singhal, N., Sharma, P., Kumar, M., Joshi, B., and Bisht, D. (2012). Analysis of intracellular expressed proteins of *Mycobacterium tuberculosis* clinical isolates. *Proteome Sci.* 10, 14. doi: 10.1186/1477-5956-10-14

Sirakova, T. D., Dubey, V. S., Deb, C., Daniel, J., Korotkova, T. A., Abomoelak, B., et al. (2006). Identification of a diacylglycerol acyltransferase gene involved in accumulation of triacylglycerol in *Mycobacterium tuberculosis* under stress. *Microbiology* 152, 2717–2725. doi: 10.1099/mic.0.28993-0

Siva-Jothy, J. A., Prakash, A., Vasanthakrishnan, R. B., Monteith, K. M., and Vale, P. F. (2018). Oral bacterial infection and shedding in *Drosophila melanogaster*. *J. Vis. Exp.* 135, e57676. doi: 10.3791/57676

Snewin, V. A., Gares, M., Ógaora, P., Hasan, Z., Brown, I. N., and Young, D. B. (1999). Assessment of immunity to mycobacterial infection with luciferase reporter constructs. *Infect. Immun.* 67, 4586–4593. doi: 10.1128/IAI.67.9.4586-4593.1999

Sonawane, A. R., Platig, J., Fagny, M., Chen, C. Y., Paulson, J. N., Lopes-Ramos, C. M., et al. (2017). Understanding tissue-specific gene regulation. *Cell Rep.* 21, 1077–1088. doi: 10.1016/j.celrep.2017.10.001

Tanner, R., Smith, S. G., van Meijgaarden, K. E., Giannoni, F., Wilkie, M., Gabriele, L., et al. (2019). Optimisation, harmonisation and standardisation of the direct mycobacterial growth inhibition assay using cryopreserved human peripheral blood mononuclear cells. *J. Immunol. Methods* 469, 1–10. doi: 10.1016/j.jim.2019.01.006

Tsai, C. J.-Y., Loh, J. M. S., and Proft, T. (2016). *Galleria mellonella* infection models for the study of bacterial diseases and for antimicrobial drug testing. *Virulence* 7, 214–229. doi: 10.1080/21505594.2015.1135289

Vilcinskas, A., and Wedde, M. (2002). Insect inhibitors of metalloproteinases. *IUBMB Life* 54, 339–343. doi: 10.1080/15216540216040

Vogel, C., De Sousa Abreu, R., Ko, D., Le, S. Y., Shapiro, B. A., Burns, S. C., et al. (2010). Sequence signatures and mRNA concentration can explain two-thirds of protein abundance variation in a human cell line. *Mol. Syst. Biol.* 6, 400. doi: 10.1038/msb.2010.59

Vogel, H., Altincicek, B., Glöckner, G., and Vilcinskas, A. (2011). A comprehensive transcriptome and immune-gene repertoire of the lepidopteran model host *Galleria mellonella*. *BMC Genomics* 12, 308. doi: 10.1186/1471-2164-12-308

Voskuil, MI (2013). *Mycobacterium tuberculosis* cholesterol catabolism requires a new class of acyl coenzyme a dehydrogenase. *J. Bacteriol.* 195, 4319–4321. doi: 10.1128/JB.00867-13

Wang, F., Sambandan, D., Halder, R., Wang, J., Batt, S. M., Weinrick, B., et al. (2013). Identification of a small molecule with activity against drug-resistant and persistent tuberculosis. *Proc. Natl. Acad. Sci. U. S. A.* 110, E2510–E2517. doi: 10.1073/pnas.1309171110

Wang, D., Eraslan, B., Wieland, T., Hallström, B., Hopf, T., Zolg, D. P., et al. (2019). A deep proteome and transcriptome abundance atlas of 29 healthy human tissues. *Mol. Syst. Biol.* 15, e8503. doi: 10.15252/msb.20188503

Wedde, M., Weise, C., Nuck, R., Altincicek, B., and Vilcinskas, A. (2007). The insect metalloproteinase inhibitor gene of the lepidopteran *Galleria mellonella* encodes two distinct inhibitors. *Biol. Chem.* 8, 119–127. doi: 10.1515/BC.2007.013

Williams, A., and Orme, I. M. (2016). Animal models of tuberculosis: an overview. *Microbiol. Spectr.* 4, TBTB2-004–2015. doi: 10.1128/microbiolspec.TBTB2-0004-2015

Wojda, I. (2017). Immunity of the greater wax moth *Galleria mellonella*. *Insect Sci.* 24, 342–357. doi: 10.1111/1744-7917.12325

World Health Organization (2020). *Global Tuberculosis Report 2019* (Geneva: WHO Press).

Yuan, H., Chang, H., Zhao, L., Yang, C., and Huang, Y. (2019). Sex- And tissue-specific transcriptome analyses and expression profiling of olfactory-related genes in *Ceracris nigricornis* Walker (Orthoptera: Acrididae). *BMC Genomics* 20, 808. doi: 10.1186/s12864-019-6208-x

Zdybicka-Barabas, A., Stączek, S., Pawlikowska-Pawlęga, B., Mak, P., Luchowski, R., Skrzypiec, K., et al. (2019). Studies on the interactions of neutral *Galleria mellonella* cecropin D with living bacterial cells. *Amino Acids* 51, 175–191. doi: 10.1007/s00726-018-2641-4

Zhan, L., Tang, J., Sun, M., and Qin, C. (2017). Animal models for tuberculosis in translational and precision medicine. *Front. Microbiol.* 8, 717. doi: 10.3389/fmicb.2017.00717

Conflict of Interest: The authors declare that the research was conducted in the absence of any commercial or financial relationships that could be construed as a potential conflict of interest.

Copyright © 2021 Asai, Sheehan, Li, Robertson, Kavanagh, Langford and Newton. This is an open-access article distributed under the terms of the Creative Commons Attribution License (CC BY). The use, distribution or reproduction in other forums is permitted, provided the original author(s) and the copyright owner(s) are credited and that the original publication in this journal is cited, in accordance with accepted academic practice. No use, distribution or reproduction is permitted which does not comply with these terms.

Permission summary table for third party copyright work

Page No.	Type of work:	Name of work	Source of work	Copyright holder and contact	permission requested on	I have permission yes /no	Permission note
30	figure	Fig. 1. Pathogenic lifecycle of *M. tuberculosis*	Host Evasion and Exploitation Schemes of Mycobacterium tuberculosis - Cell (2014), vol 159 (7), 1497-1509.	© 2014 Elsevier Inc. Published by Elsevier Inc customercare@copyright.com	20.12.21	yes	Licensed under Elsevier licence (No. 5213041355670)
53	Table	Table 1. Summary of similarities between insect hemocytes and human neutrophils	An analysis of the structural and functional similarities of insect hemocytes and mammalian phagocytes – Virulence (2013), vol 4 (7), 597-603.	© 2013 Landes Bioscience. Published by Taylor & Francis Group permissionrequest@tandf.co.uk	20.12.21	yes	We will be pleased to grant the permission without fee on the condition that you acknowledge the original source of publication and insert a reference to the Journal's web site: www.tandfonline.com

ELSEVIER LICENSE
TERMS AND CONDITIONS

Jan 17, 2022

This Agreement between Mr. Masanori Asai ("You") and Elsevier ("Elsevier") consists of your license details and the terms and conditions provided by Elsevier and Copyright Clearance Center.

License Number	5213041355670
License date	Dec 20, 2021
Licensed Content Publisher	Elsevier
Licensed Content Publication	Cell
Licensed Content Title	Host Evasion and Exploitation Schemes of Mycobacterium tuberculosis
Licensed Content Author	C.J. Cambier,Stanley Falkow,Lalita Ramakrishnan
Licensed Content Date	Dec 18, 2014
Licensed Content Volume	159
Licensed Content Issue	7
Licensed Content Pages	13
Start Page	1497
End Page	1509
Type of Use	reuse in a thesis/dissertation
Portion	figures/tables/illustrations

Number of figures/tables/illustrations	1
Format	electronic
Are you the author of this Elsevier article?	No
Will you be translating?	No
Title	Galleria mellonella: an infection model for the Mycobacterium tuberculosis complex’
Institution name	Imperial College London
Expected presentation date	Feb 2022
Portions	Figure 1
Requestor Location	Mr. Masanori Asai [redacted] Attn: Mr. Masanori Asai
Publisher Tax ID	GB 494 6272 12
Total	0.00 GBP
Terms and Conditions	

INTRODUCTION

1. The publisher for this copyrighted material is Elsevier. By clicking "accept" in connection with completing this licensing transaction, you agree that the following terms and conditions apply to this transaction (along with the Billing and Payment terms and conditions established by Copyright Clearance Center, Inc. ("CCC"), at the time that you opened your Rightslink account and that are available at any time at http://myaccount.copyright.com).

GENERAL TERMS

2. Elsevier hereby grants you permission to reproduce the aforementioned material subject to the terms and conditions indicated.

3. Acknowledgement: If any part of the material to be used (for example, figures) has appeared in our publication with credit or acknowledgement to another source, permission must also be sought from that source. If such permission is not obtained then that material may not be included in your publication/copies. Suitable acknowledgement to the source must be made, either as a footnote or in a reference list at the end of your publication, as follows:

"Reprinted from Publication title, Vol /edition number, Author(s), Title of article / title of chapter, Pages No., Copyright (Year), with permission from Elsevier [OR APPLICABLE SOCIETY COPYRIGHT OWNER]." Also Lancet special credit - "Reprinted from The Lancet, Vol. number, Author(s), Title of article, Pages No., Copyright (Year), with permission from Elsevier."

4. Reproduction of this material is confined to the purpose and/or media for which permission is hereby given.

5. Altering/Modifying Material: Not Permitted. However figures and illustrations may be altered/adapted minimally to serve your work. Any other abbreviations, additions, deletions and/or any other alterations shall be made only with prior written authorization of Elsevier Ltd. (Please contact Elsevier's permissions helpdesk here). No modifications can be made to any Lancet figures/tables and they must be reproduced in full.

6. If the permission fee for the requested use of our material is waived in this instance, please be advised that your future requests for Elsevier materials may attract a fee.

7. Reservation of Rights: Publisher reserves all rights not specifically granted in the combination of (i) the license details provided by you and accepted in the course of this licensing transaction, (ii) these terms and conditions and (iii) CCC's Billing and Payment terms and conditions.

8. License Contingent Upon Payment: While you may exercise the rights licensed immediately upon issuance of the license at the end of the licensing process for the transaction, provided that you have disclosed complete and accurate details of your proposed use, no license is finally effective unless and until full payment is received from you (either by publisher or by CCC) as provided in CCC's Billing and Payment terms and conditions. If full payment is not received on a timely basis, then any license preliminarily granted shall be deemed automatically revoked and shall be void as if never granted. Further, in the event that you breach any of these terms and conditions or any of CCC's Billing and Payment terms and conditions, the license is automatically revoked and shall be void as if never granted. Use of materials as described in a revoked license, as well as any use of the materials beyond the scope of an unrevoked license, may constitute copyright infringement and publisher reserves the right to take any and all action to protect its copyright in the materials.

9. Warranties: Publisher makes no representations or warranties with respect to the licensed material.

10. Indemnity: You hereby indemnify and agree to hold harmless publisher and CCC, and their respective officers, directors, employees and agents, from and against any and all claims arising out of your use of the licensed material other than as specifically authorized pursuant to this license.

11. No Transfer of License: This license is personal to you and may not be sublicensed, assigned, or transferred by you to any other person without publisher's written permission.

12. No Amendment Except in Writing: This license may not be amended except in a writing signed by both parties (or, in the case of publisher, by CCC on publisher's behalf).

13. Objection to Contrary Terms: Publisher hereby objects to any terms contained in any purchase order, acknowledgment, check endorsement or other writing prepared by you, which terms are inconsistent with these terms and conditions or CCC's Billing and Payment terms and conditions. These terms and conditions, together with CCC's Billing and Payment terms and conditions (which are incorporated herein), comprise the entire agreement between you and publisher (and CCC) concerning this licensing transaction. In the event of any conflict between your obligations established by these terms and conditions and those established by CCC's Billing and Payment terms and conditions, these terms and conditions shall control.

14. Revocation: Elsevier or Copyright Clearance Center may deny the permissions described in this License at their sole discretion, for any reason or no reason, with a full refund payable to you. Notice of such denial will be made using the contact information provided by you. Failure to receive such notice will not alter or invalidate the denial. In no event will Elsevier or Copyright Clearance Center be responsible or liable for any costs, expenses or damage incurred by you as a result of a denial of your permission request, other than a refund of the amount(s) paid by you to Elsevier and/or Copyright Clearance Center for denied permissions.

LIMITED LICENSE

The following terms and conditions apply only to specific license types:

15. **Translation**: This permission is granted for non-exclusive world **English** rights only unless your license was granted for translation rights. If you licensed translation rights you may only translate this content into the languages you requested. A professional translator must perform all translations and reproduce the content word for word preserving the integrity of the article.

16. **Posting licensed content on any Website**: The following terms and conditions apply as follows: Licensing material from an Elsevier journal: All content posted to the web site must maintain the copyright information line on the bottom of each image; A hyper-text must be included to the Homepage of the journal from which you are licensing at http://www.sciencedirect.com/science/journal/xxxxx or the Elsevier homepage for books at http://www.elsevier.com; Central Storage: This license does not include permission for a scanned version of the material to be stored in a central repository such as that provided by Heron/XanEdu.

Licensing material from an Elsevier book: A hyper-text link must be included to the Elsevier homepage at http://www.elsevier.com . All content posted to the web site must maintain the copyright information line on the bottom of each image.

Posting licensed content on Electronic reserve: In addition to the above the following clauses are applicable: The web site must be password-protected and made available only to bona fide students registered on a relevant course. This permission is granted for 1 year only. You may obtain a new license for future website posting.

17. **For journal authors:** the following clauses are applicable in addition to the above:

Preprints:

A preprint is an author's own write-up of research results and analysis, it has not been peer-reviewed, nor has it had any other value added to it by a publisher (such as formatting, copyright, technical enhancement etc.).

Authors can share their preprints anywhere at any time. Preprints should not be added to or enhanced in any way in order to appear more like, or to substitute for, the final versions of

articles however authors can update their preprints on arXiv or RePEc with their Accepted Author Manuscript (see below).

If accepted for publication, we encourage authors to link from the preprint to their formal publication via its DOI. Millions of researchers have access to the formal publications on ScienceDirect, and so links will help users to find, access, cite and use the best available version. Please note that Cell Press, The Lancet and some society-owned have different preprint policies. Information on these policies is available on the journal homepage.

Accepted Author Manuscripts: An accepted author manuscript is the manuscript of an article that has been accepted for publication and which typically includes author-incorporated changes suggested during submission, peer review and editor-author communications.

Authors can share their accepted author manuscript:

- immediately
  - via their non-commercial person homepage or blog
  - by updating a preprint in arXiv or RePEc with the accepted manuscript
  - via their research institute or institutional repository for internal institutional uses or as part of an invitation-only research collaboration work-group
  - directly by providing copies to their students or to research collaborators for their personal use
  - for private scholarly sharing as part of an invitation-only work group on commercial sites with which Elsevier has an agreement
- After the embargo period
  - via non-commercial hosting platforms such as their institutional repository
  - via commercial sites with which Elsevier has an agreement

In all cases accepted manuscripts should:

- link to the formal publication via its DOI
- bear a CC-BY-NC-ND license - this is easy to do
- if aggregated with other manuscripts, for example in a repository or other site, be shared in alignment with our hosting policy not be added to or enhanced in any way to appear more like, or to substitute for, the published journal article.

Published journal article (JPA): A published journal article (PJA) is the definitive final record of published research that appears or will appear in the journal and embodies all value-adding publishing activities including peer review co-ordination, copy-editing, formatting, (if relevant) pagination and online enrichment.

Policies for sharing publishing journal articles differ for subscription and gold open access articles:

Subscription Articles: If you are an author, please share a link to your article rather than the full-text. Millions of researchers have access to the formal publications on ScienceDirect, and so links will help your users to find, access, cite, and use the best available version.

Theses and dissertations which contain embedded PJAs as part of the formal submission can be posted publicly by the awarding institution with DOI links back to the formal publications on ScienceDirect.

If you are affiliated with a library that subscribes to ScienceDirect you have additional private sharing rights for others' research accessed under that agreement. This includes use for classroom teaching and internal training at the institution (including use in course packs and courseware programs), and inclusion of the article for grant funding purposes.

Gold Open Access Articles: May be shared according to the author-selected end-user license and should contain a CrossMark logo, the end user license, and a DOI link to the formal publication on ScienceDirect.

Please refer to Elsevier's posting policy for further information.

18. **For book authors** the following clauses are applicable in addition to the above: Authors are permitted to place a brief summary of their work online only. You are not allowed to download and post the published electronic version of your chapter, nor may you scan the printed edition to create an electronic version. **Posting to a repository:** Authors are permitted to post a summary of their chapter only in their institution's repository.

19. **Thesis/Dissertation**: If your license is for use in a thesis/dissertation your thesis may be submitted to your institution in either print or electronic form. Should your thesis be published commercially, please reapply for permission. These requirements include permission for the Library and Archives of Canada to supply single copies, on demand, of the complete thesis and include permission for Proquest/UMI to supply single copies, on demand, of the complete thesis. Should your thesis be published commercially, please reapply for permission. Theses and dissertations which contain embedded PJAs as part of the formal submission can be posted publicly by the awarding institution with DOI links back to the formal publications on ScienceDirect.

Elsevier Open Access Terms and Conditions

You can publish open access with Elsevier in hundreds of open access journals or in nearly 2000 established subscription journals that support open access publishing. Permitted third party re-use of these open access articles is defined by the author's choice of Creative Commons user license. See our open access license policy for more information.

Terms & Conditions applicable to all Open Access articles published with Elsevier:

Any reuse of the article must not represent the author as endorsing the adaptation of the article nor should the article be modified in such a way as to damage the author's honour or reputation. If any changes have been made, such changes must be clearly indicated.

The author(s) must be appropriately credited and we ask that you include the end user license and a DOI link to the formal publication on ScienceDirect.

If any part of the material to be used (for example, figures) has appeared in our publication with credit or acknowledgement to another source it is the responsibility of the user to ensure their reuse complies with the terms and conditions determined by the rights holder.

Additional Terms & Conditions applicable to each Creative Commons user license:

CC BY: The CC-BY license allows users to copy, to create extracts, abstracts and new works from the Article, to alter and revise the Article and to make commercial use of the Article (including reuse and/or resale of the Article by commercial entities), provided the user gives appropriate credit (with a link to the formal publication through the relevant DOI), provides a link to the license, indicates if changes were made and the licensor is not represented as endorsing the use made of the work. The full details of the license are available at http://creativecommons.org/licenses/by/4.0.

CC BY NC SA: The CC BY-NC-SA license allows users to copy, to create extracts, abstracts and new works from the Article, to alter and revise the Article, provided this is not done for commercial purposes, and that the user gives appropriate credit (with a link to the formal publication through the relevant DOI), provides a link to the license, indicates if changes were made and the licensor is not represented as endorsing the use made of the

work. Further, any new works must be made available on the same conditions. The full details of the license are available at http://creativecommons.org/licenses/by-nc-sa/4.0.

CC BY NC ND: The CC BY-NC-ND license allows users to copy and distribute the Article, provided this is not done for commercial purposes and further does not permit distribution of the Article if it is changed or edited in any way, and provided the user gives appropriate credit (with a link to the formal publication through the relevant DOI), provides a link to the license, and that the licensor is not represented as endorsing the use made of the work. The full details of the license are available at http://creativecommons.org/licenses/by-nc-nd/4.0. Any commercial reuse of Open Access articles published with a CC BY NC SA or CC BY NC ND license requires permission from Elsevier and will be subject to a fee.

Commercial reuse includes:

- Associating advertising with the full text of the Article
- Charging fees for document delivery or access
- Article aggregation
- Systematic distribution via e-mail lists or share buttons

Posting or linking by commercial companies for use by customers of those companies.

20. **Other Conditions**:

v1.10

Questions? customercare@copyright.com or +1-855-239-3415 (toll free in the US) or +1-978-646-2777.

RE: kvir20:An analysis of the structural and functional similarities of insect hemocytes and mammalian phagocytes

Academic UK Non Rightslink <permissionrequest@tandf.co.uk>

Wed 02/02/2022 14:48

To: Asai, Masanori <m.asai16@imperial.ac.uk>

This email from permissionrequest@tandf.co.uk originates from outside Imperial. Do not click on links and attachments unless you recognise the sender. If you trust the sender, add them to your safe senders list to disable email stamping for this address.

Dear Sir/Madam

Thank you for your correspondence requesting permission to reproduce content from a Taylor & Francis Group content from our Journal in your thesis to be posted on your University's repository.

We will be pleased to grant the permission without fee on the condition that you acknowledge the original source of publication and insert a reference to the Journal's web site: www.tandfonline.com

This permission does not cover any third party copyrighted work which may appear in the material requested. Please ensure you have checked all original source details for the rights holder.

Please note that this licence **does not allow you to post our content on any third-party websites.**

Please note permission does not provide access to our article, if you are affiliated to an institution and your institution holds a subscription to the content you are requesting you will be able to view the article free of charge, if your institution does not hold a subscription or you are not affiliated to an institution that has a subscription then you will need to purchase this for your own personal use as we do not provide our articles free of charge for research.

Thank you for your interest in our Journal.

With best wishes,

Journal Permissions
Journals, Taylor & Francis Group
Permissions e-mail: permissionrequest@tandf.co.uk
Web: www.tandfonline.com

4 Park Square, Milton Park, Abingdon, OX14 4RN
☎ +44 (0)20 8052 0600

Taylor & Francis is a trading name of Informa UK Limited,
registered in England under no. 1072954
Before printing, think about the environment.

Information Classification: General

From: Masanori Asai <m.asai16@imperial.ac.uk>
Sent: 20 December 2021 13:21
To: Academic UK Non Rightslink <permissionrequest@tandf.co.uk>
Subject: kvir20:An analysis of the structural and functional similarities of insect hemocytes and mammalian phagocytes

Permissions Request

Type of use: Academic
Article title: An analysis of the structural and functional similarities of insect hemocytes and mammalian phagocytes
Article DOI: 10.4161/viru.25906
Author name: Niall Browne, Michelle Heelan & Kevin Kavanagh
Journal title: Virulence
Volume number: 4
Issue number: 7
Year of publication: 2013
Name: Masanori Asai
Street address: [redacted]
Town: London
Postcode/ZIP code: [redacted]
Country: United Kingdom
Email: m.asai16@imperial.ac.uk
Telephone: [redacted]
Intended use: To be used in your Thesis?
Are you requesting the full article?: No
Extract and number of words: Table 1 for reproduction in thesis
Details of figure/table: Table 1
Which University?: Imperial College London
Title of your Thesis?: Galleria mellonella: an infection model for the Mycobacterium tuberculosis complex
University repository URL: TBA
Is this a “Closed” or “Open” deposit?: open
Additional comments: Looking to reproduce Table 1 from Browne et al. Once accepted, the thesis will be deposited in to Imperial's institutional repository (http://spiral.imperial.ac.uk), under CC-BY-NC-4.0